

Copyright
by
David Torres
2011

**The Dissertation Committee for David Enrique Torres López Certifies that
this is the approved version of the following dissertation:**

**Enhancing the Productivity of Volatile Oil Reservoirs Using
Fluorinated Chemical Treatments**

Committee:

Mukul M. Sharma, Supervisor

Gary A. Pope, Co-Supervisor

Gary T. Rochelle

Roger T. Bonnecaze

Benny D. Freeman

**Enhancing the Productivity of Volatile Oil Reservoirs Using Fluorinated
Chemical Treatments**

by

David Enrique Torres López, B. S.; M. S.

Dissertation

Presented to the Faculty of the Graduate School of

The University of Texas at Austin

in Partial Fulfillment

of the Requirements

for the Degree of

Doctor of Philosophy

The University of Texas at Austin

August 2011

Dedication

To God for giving me the gift of life and his unconditional love

and

To my family for their support, loyalty, care, patience and love; specially my parents for raising me as a good human being and an honest citizen, and for teaching me that hard working is the right way to reach big goals.

Acknowledgements

I would like to specially acknowledge Dr. Mukul M. Sharma and Dr. Gary A. Pope, my research and dissertation advisors, for their knowledge, support, encouragement, and guidance of my project. The opportunity given to me to be part of their research group opened the door to unique engineering ways of thinking and exposed me to higher academic, scientific and industrial environments. Experiencing their professional approach to develop this and other works has been a great experience that has helped me to develop as a professional engineer. I am also very thankful to my committee members Dr. Gary Rochelle, Dr. Roger Bonnecaze and Dr. Benny D. Freeman for their time and effort to serve on my committee and review my dissertation.

Thank you to our lab manager Harry Linnemeyer for his valuable help and support in solving all of the technical issues while performing experiments and for his time spend to offer suggestions and comments intended to improve the quality of the research. His contribution to this dissertation is also very important.

Furthermore, the friendship and help of my laboratory colleagues Harry Linnemeyer, Corey McCulley, Mohabbat Ahmadi, Syed Gilani, Lionel Ribeiro, Mac Pedlow and other members of Dr. Sharma and Dr. Pope's group made of the time spent in this project a great and very pleasant experience. I would like to thank all my friends in Austin who have always supported me during my graduate studies.

I also want to acknowledge the laboratory and technical support provided by Tony Bermudez[†], Glen Baum, Gary Miscoe and the help from our undergraduate colleagues Briklynd Briggs, Muchlis Krueng, Botong Wang, Alexander Vyssotski, Mustafa Haque and Dhruv Sharma. Thank you to Dr. Stephanie Freeman, Dr. Hugo Celio and M.S. Hassan Dehghanpour for their guidance and help with the analysis performed with HPLC XPS and CT Scan respectively. Thanks to M.S. Jongsoo Wang for his help performing the numerical simulations presented in this dissertation.

Thanks to the staff of the Chemical Engineering and Petroleum Engineering Department for their help, support and guidance during my PhD studies. Especially to Dr. Isaac Sanchez, “T” Stockman, Kay Costales, Jin K. Lee and Johanna L. Castillo.

I appreciate the financial and technical support provided by 3M, especially to Jim Baran and Doug Johnson, for their advice and for providing most of the surfactants used in this research.

I would like to express my profound gratitude to Mexican Council of Science and Technogy (CONACyT) for the provided financial support making possible my studies at The University of Texas at Austin. The support has giving me not only the opportunity of graduate school education, but also the opportunity to better serve my country and society.

Finally, I am grateful to all of my family members for their support, loyalty, care, patience and love.

Enhancing the Productivity of Volatile Oil Reservoirs Using Fluorinated Chemical Treatments

Publication No. _____

David Enrique Torres López, PhD

The University of Texas at Austin, 2011

Supervisor: Mukul M. Sharma and Gary A. Pope

Many producing volatile oil reservoirs experience a significant decrease in well deliverability when the bottom-hole pressure of the well falls below the bubble point pressure. This is due to the liberation of a gas phase which resides in the pore space and blocks the flow of the oil phase. This situation is known as "gas blocking". This occurs because the presence of two or three immiscible phases (gas, oil and water) results in a reduction of the oil saturation and a decrease in the oil relative permeability. The main objective of this research was to develop an effective and durable chemical treatment method to improve and/or restore the productivity of volatile oil wells undergoing "gas blocking". The treatment method is based on the use of fluorinated surfactants in tailored solvents to increase the oil relative permeability by changing the wettability of the rock's surface. High-temperature high-pressure (HTHP) core flood experiments were used to evaluate the uses of fluorinated surfactants under reservoir conditions. Analytical tools such as X-ray photoelectron spectroscopy (XPS), high-performance liquid chromatography (HPLC) and computerized axial tomography (CT Scan) were also used

to interpret the experimental results. High-pressure high-temperature (HPHT) coreflood tests showed that the treatments improved the oil and gas relative permeability in both sandstone and limestone cores. This was observed for synthetic volatile oil mixtures with gas-oil ratios (GOR) in the range of 4000 to 13,000 scf/STB at low capillary numbers (Nc) on the order of 1×10^{-5} to 1×10^{-6} and for PVT ratios greater than 0.5. The fluorinated chemical treatments were effective in the presence of connate water over the temperature range of 155°F to 275°F. Wettability alteration was measured using contact angle and imbibition rate tests. Results from analytical tools showed that fluorinated surfactants were uniformly adsorbed along the core and the surfactant desorption after treatment was low (10 ppm or less). The gas saturation decreased following treatment and both the oil and gas relative permeability increased. Numerical simulations using the measured relative permeability data were used to estimate the gain in productivity for treated wells. The proposed fluorinated chemical treatments could be used as a preventive treatment or for a damaged well that has already been producing below the bubble point to increase oil production rates and recoverable reserves.

Table of Contents

List of Tables	xiv
List of Figures	xxx
Chapter 1: Introduction	1
1.1 Objectives of this research	4
1.2 Chapters summary	5
Chapter 2: Literature Review	11
2.1 Petrophysical concepts and definitions	11
2.1.1 Wettability.....	11
2.1.2 Capillary Pressure	14
2.1.3 Permeability	15
2.1.3.1 Relative Permeability.....	16
2.2 Phase behavior of near critical fluids.....	17
2.2.1 Volatile oil reservoirs.....	20
2.2.2 Gas blocking and productivity decline in volatile oil reservoirs	21
2.3 Studies on relative permeability and critical saturation for near critical fluids in porous media.....	23
2.4 Proposed solutions to improve oil and gas production	27
2.5 Fluorinated treatment solution to alter wettability.....	28
2.5.1 Fluorinated surfactants.....	32
Chapter 3: Coreflood Experimental Apparatus, Procedures, and Calculations	41
3.1 Coreflood experimental apparatus	41
3.1.1 Accumulators	43
3.1.2 Back pressure regulators	43
3.1.3 Balances	43
3.1.4 Computer equipment and software	44
3.1.5 Core holders	44
3.1.5.1 Stainless steel core holder	44

3.1.5.2 Aluminum core holder	45
3.1.6 Sample collector.....	45
3.1.7 Oven.....	45
3.1.8 Pressure regulators	45
3.1.9 Pressure transducers.....	46
3.1.9.1 Gauge pressure transducers.....	46
3.1.9.2 Differential pressure transducers	46
3.1.10 Pumps.....	46
3.1.10.1 Booster pump.....	47
3.1.10.2 Continuous flow pump.....	47
3.1.10.3 Hydraulic manual pump.....	47
3.1.10.4 Vacuum pump.....	47
3.1.11 Valves	47
3.1.12 Tubing	48
3.2 experimental procedures for core flood experiments.....	48
3.2.1 Core and fluid preparation	48
3.2.1.1 Core preparation.....	48
3.2.1.2 Gas, liquid and brine preparation.....	49
3.2.1.3 Synthetic volatile oil preparation	50
3.2.1.4 Chemical treatment preparation.....	51
3.2.2 General experimental procedure for core flood experiments	51
3.2.2.1 Initial gas flood to measure gas permeability on dry core.....	52
3.2.2.2 Establishing initial water saturation.....	52
3.2.2.3 Gas flood to measure gas permeability at S_{wi}	53
3.2.2.4 Pre-treatment two-phase volatile oil flood.....	53
3.2.2.5 Chemical treatment flood.....	54
3.2.2.6 Post-treatment two-phase volatile oil flood	54
3.2.2.7 Final gas flood to verify gas permeability	55
3.3 Calculations.....	55
3.3.1 Flow rate	56

3.3.2 Absolute and relative permeability	58
3.3.3 Capillary number	60
3.3.4 Improvement Factor	61
3.3.5 Phase behavior calculations	62
3.3.5.1 PVT software	62
3.3.5.2 Equations of state	63
3.3.5.3 PVT Diagrams	66
Chapter 4: Selection and Formulation of the Fluorinated Chemical Treatments ..	80
4.1 Phase behavior studies for the selection of solvent delivery system for the chemical treatment	81
4.1.1 Characteristics of the solvent formulation	81
4.1.2 Solubility and compatibility tests	82
4.2 Screening tests for surfactants	83
4.2.1 Drop and imbibition rate tests	84
4.2.2 XPS analysis	85
4.3 Results and discussion	87
Chapter 5: Chemical Treatment of Sandstones	103
5.1 effect of surfactant type	104
5.2 effect of temperature	108
5.3 effect of capillary number	110
5.4 Effect of PVT ratio	113
5.4.1 The improvement factor – PVT ratio correlation	115
5.5 effect of low permeability	117
5.6 Summary and conclusions	118
Chapter 6: Chemical Treatment of Carbonate Rocks	162
6.1 Effect of anionic surfactant	163
6.2 Effect of capillary number	165
6.3 Effect of PVT ratio	166
6.4 Effect of low permeability	166
6.5 Summary and conclusions	166

Chapter 7: Evaluation of the Chemical Treatment Performance	177
7.1 X-ray photoelectron spectroscopy for fluorine measurements	177
7.1.2 Analytical procedure	178
7.1.2 Fluorine content along treated cores	179
7.2 High-performance liquid chromatography for surfactant adsorption and desorption measurements	181
7.2.1 Analytical procedure	182
7.2.2 Adsorption and desorption of the surfactant	183
7.3 Computerized axial tomography for fluid saturation measurements	184
7.3.1 Analytical procedure and calculations	185
7.3.2 Oil and gas saturations	187
7.3.3 Changes in oil and gas relative permeability	189
7.4 Summary and conclusions	190
Chapter 8: Numerical Simulations of Volatile Oil Reservoirs Treated with Fluorinated Chemical Treatments	207
8.1 STARS reservoir simulator	207
8.2 Reservoir model	208
8.3 Fluid characterization	208
8.4 Rock-fluid properties model	209
8.5 Initialization	209
8.6 Simulation results	210
8.6.1 Base case model	210
8.6.2 Effect of the treated near wellbore zone volume	211
8.7 Summary and conclusions	213
Chapter 9: Summary, Conclusions, and Future work	223
9.1 Summary	223
9.2 Conclusions	226
9.3 Future work	229
Appendix A	230
Appendix A.1: Experiment #134	231

Appendix A.2: Experiment #141	241
Appendix A.3: Experiment#146	251
Appendix A.4: Experiment#148	261
Appendix A.5: Experiment#158	271
Appendix A.6: Experiment#176	280
Appendix A.7: Experiment #181	291
Appendix A.8: Experiment #185	301
Appendix A.9: Experiment #189	311
Appendix A.10: Experiment #192	321
Appendix A.11: Experiment #196	331
Appendix A.12: Experiment #198	340
Appendix A.13: Experiment #200	349
Appendix A.14: Experiment #210	358
Appendix A.15: Experiment #221	367
Appendix A.16: Experiment #224	375
Appendix A.17: Experiment #225	385
Appendix A.18: Experiment #228	395
Appendix A.19: Experiment #229	405
Appendix A.20: Experiment #231	415
Appendix A.21: Experiment #234	429
Appendix A.22: Experiment #235	441
Appendix B.....	453
References.....	459
Vita	467

List of Tables

Table 2.1 Composition of Gas Condensate, Volatile Oil and Black Oil mixture illustrated in Figure 2.5 (Pedersen 2007).....	35
Table 2.2 Volatile oil definitions found in literature	35
Table 3.1 Grain density values provided by TerraTek (rock supplier for different outcrops)	67
Table 3.2 Composition of brines used to establish S_{wi}	67
Table 3.3 Composition of volatile oil mixtures used for corefloods at different experimental temperatures	67
Table 4.1 List of candidate fluorinated surfactants with different chemistries.....	93
Table 4.2 Parameters used for XPS analysis	93
Table 4.3 Elements analyzed in XPS according to the type of rock.....	94
Table 4.4 Fluorinated surfactants used for wettability alteration	94
Table 4.5 Solubility and sample appearance of L-20294 in different pure solvents and solvent mixtures at different concentrations and temperatures.....	94
Table 4.6 Solubility and sample appearance of F-CX in different solvent mixtures at different concentrations, solvent ratios and temperatures.....	95
Table 4.7 Solubility and sample appearance for L-18961 in the different solvent mixtures at different ratios, concentrations, and temperatures	96
Table 4.8 Solubility and sample appearance for L-19446#1 in a solvent mixture of 2BE-EtOH (70-30 wt %) at different concentrations and temperatures	96
Table 4.9 Composition of brines used for sandstone and limestone cores	96

Table 4.10 Compatibility of FC-X (2 wt%) in 2BE-EtOH (70-30 wt%) with Brine 1	96
Table 4.11 Compatibility of L-20294 (2 wt%) in 2BE-EtOH (70-30 wt%) with Brine 1.....	97
Table 4.12 Compatibility of L-18961 (1 wt%) in 2BE-EtOH-IPA (60-30-10 wt%) with Brine 1.....	97
Table 4.13 Compatibility of L-19973 #9 (2 wt%) in 2BE-EtOH (70-30 wt%) with Brine 1.....	97
Table 4.14 Compatibility of L-19446#1 (2 wt%) in 2BE-EtOH (70-30 wt%) with Brine 2.....	98
Table 4.15 Composition of chemical treatments used for core flood experiments	98
Table 5.1 Experimental conditions of core flood experiments performed for treatment of sandstones.....	120
Table 5.2 Summary of conditions for Experiments # 141, #146, #158 and #192	121
Table 5.3 Summary of results for the effect of surfactant type on treatment of Berea sandstone (Experiments #141, #146, #158 and #192).....	121
Table 5.5 Summary of results for the effect of temperature on treatment of Berea sandstone with surfactant L-18961 (Experiments #158, #176 and #189)	122
Table 5.6 Summary of conditions for Experiments # 210, #228 and #229	123
Table 5.7 Summary of results for the effect of temperature on treatment of Berea sandstone with surfactant FC-X (Experiments #210, #228 and #229)	123
Table 5.8 Summary of conditions for Experiment # 148.....	124
Table 5.9 Summary of results for the effect of increasing capillary number (Experiment #148).....	124

Table 5.10 Summary of conditions for Experiment # 176.....	125
Table 5.11 Summary of results for the effect of increasing capillary number (Experiment #176)	125
Table 5.12 Summary of conditions for Experiment # 210.....	126
Table 5.13 Summary of results for the effect of increasing capillary number (Experiment # 210)	126
Table 5.14 PVT ratio and improvement factors by surfactant type for experiments performed on Berea sandstone.....	127
Table 5.15 Summary of conditions for Experiment # 196 and #198.....	128
Table 5.16 Summary of results for the effect of rock permeability (Experiment # 196 & #198).....	128
Table 5.17 Summary of HPHT core flood experiments for treatment of sandstones	129
Table 6.1 Summary of conditions for Experiment # 181.....	168
Table 6.2 Summary of results for Experiment # 181.....	168
Table 6.3 Summary of conditions for Experiment # 185.....	168
Table 6.4 Summary of results for Experiment # 185.....	169
Table 7.1 XPS Fluorine content analysis along the core for core flood experiments	193
Table 7.2 HPLC Measurements	193
Table 7.3 Summary of conditions for Experiments #231, #234 and #235	195
Table 7.4 Summary of results for Experiment #231, #234 and #235	195
Table 7.5 Gas and oil phase composition for volatile oil mixture 1 at 75°F and 850 psia.....	196
Table 7.6 Saturations and relative permeabilities for Experiment # 235.....	196
Table 8.1 Reservoir grid length in the radial direction	215

Table 8.2 Reservoir model parameters	215
Table 8.3 EOS parameters used in WINPROP	215
Table 8.4 Initialization reservoir parameters	216
Table A.1.1 Core properties (Exp #134).....	234
Table A.1.2 Fluid properties and conditions for nitrogen gas permeability (Exp #134)	234
Table A.1.3 Nitrogen flood results (Exp #134)	234
Table A.1.4 Fluid properties and conditions for methane gas permeability (Exp #134)	234
Table A.1.5 Methane flood results (Exp #134).....	235
Table A.1.6 Fluid properties and conditions for methane gas permeability at S_{wi} (Exp #134)	235
Table A.1.7 Methane flood results at S_{wi} (Exp #134).....	235
Table A.1.8 Volatile oil properties at BPR-1 and BPR-2 pressures (Exp #134).....	235
Table A.1.9 Fluid properties and conditions for final methane gas permeability (Exp #134)	236
Table A.1.10 Final methane flood results (Exp #134).....	236
Table A. 1.11 Pre and post-treatment volatile oil flood results and measured improvement factors (Exp #134)	236
Table A.2.1 Core properties (Exp #141).....	244
Table A.2.2 Fluid properties and conditions for initial gas permeability (Exp #141)	244
Table A.2.3 Initial methane flood results (Exp #141)	244
Table A.2.4 Fluid properties and conditions for methane gas permeability at S_{wi} (Exp #141)	244

Table A.2.5 Methane flood results at S_{wi} (Exp #141).....	245
Table A.2.6 Volatile oil properties at BPR-1 and BPR-2 pressures (Exp #141).	245
Table A.2.7 Fluid properties and conditions for final methane gas permeability (Exp #141)	245
Table A.2.8 Final methane flood results (Exp #141).....	245
Table A.2.9 Pre and post-treatment volatile oil flood results and measured improvement factors (Exp #141)	246
Table A.3.1 Core properties (Exp #146).....	254
Table A.3.2 Fluid properties and conditions for initial gas permeability (Exp #146)	254
Table A. 3.3 Initial methane flood results (Exp #146)	254
Table A.3.4 Fluid properties and conditions for methane gas permeability at S_{wi} (Exp #146)	254
Table A.3.5 Methane flood results at S_{wi} (Exp #146).....	255
Table A.3.6 Volatile oil properties at BPR-1 and BPR-2 pressures (Exp #146).	255
Table A.3.7 Fluid properties and conditions for final gas permeability (Exp #146)	255
Table A.3.8 Final methane flood results (Exp #146).....	255
Table A.3.9 Pre and post-treatment volatile oil flood results and measured improvement factors (Exp #146)	256
Table A.4.1 Core properties (Exp #148).....	264
Table A.4.2 Fluid properties and conditions for initial gas permeability (Exp #148)	264
Table A.4.3 Initial methane flood results (Exp #148)	264
Table A.4.4 Fluid properties and conditions for methane gas permeability at S_{wi} (Exp #148)	264

Table A.4.5 Methane flood results at S_{wi} (Exp #148).....	265
Table A.4.6 Volatile oil properties at BPR-1 and BPR-2 pressures (Exp #148).	265
Table A.4.7 Fluid properties and conditions for final gas permeability (Exp #148)	265
Table A.4.8 Final methane flood results (Exp #148).....	266
Table A.4.9 Pre and post-treatment volatile oil flood results and measured improvement factors (Exp #148)	266
Table A.5.1 Core properties (Exp #158).....	274
Table A.5.2 Fluid properties and conditions for initial gas permeability (Exp #158)	274
Table A.5.3 Initial methane flood results (Exp #158)	274
Table A.5.4 Fluid properties and conditions for methane gas permeability at S_{wi} (Exp #158)	274
Table A.5.5 Methane flood results at S_{wi} (Exp #158).....	275
Table A.5.6 Volatile oil properties at BPR-1 and BPR-2 pressures (Exp #158).	275
Table A.5.7 Fluid properties and conditions for final gas permeability (Exp #158)	275
Table A.5.8 Final methane flood results (Exp #158).....	276
Table A.5.9 Pre and post-treatment volatile oil flood results and measured improvement factors (Exp #158)	276
Table A.6.1 Core properties (Exp #176).....	283
Table A.6.2 Fluid properties and conditions for initial gas permeability (Exp #176)	283
Table A.6.3 Initial methane flood results (Exp #176)	283
Table A.6.4 Fluid properties and conditions for methane gas permeability at S_{wi} (Exp #176)	283
Table A.6.5 Methane flood results at S_{wi} (Exp #176).....	284

Table A.6.6 Volatile oil properties at BPR-1 and BPR-2 pressures (Exp #176)	284
Table A.6.7 Fluid properties and conditions for final gas permeability (Exp #176)	284
Table A.6.8 Final methane flood results (Exp #176)	285
Table A.6.9 Pre and post-treatment volatile oil flood results and measured improvement factors (Exp #176)	285
Table A. 7.1 Core properties (Exp #181)	294
Table A.7.2 Fluid properties and conditions for initial gas permeability (Exp #181)	294
Table A.7.3 Initial methane flood results (Exp #181)	294
Table A.7.4 Fluid properties and conditions for methane gas permeability at S_{wi} (Exp #181)	294
Table A.7.5 Methane flood results at S_{wi} (Exp #181)	295
Table A.7.6 Volatile oil properties at BPR-1 and BPR-2 pressures (Exp #181)	295
Table A.7.7 Fluid properties and conditions for final gas permeability (Exp #181)	295
Table A.7.8 Final methane flood results (Exp #181)	296
Table A.7.9 Pre and post-treatment volatile oil flood results and measured improvement factors (Exp #181)	296
Table A. 8.1 Core properties (Exp #185)	304
Table A.8.2 Fluid properties and conditions for initial gas permeability (Exp #185)	304
Table A.8.3 Initial methane flood results (Exp #185)	304
Table A.8.4 Fluid properties and conditions for methane gas permeability at S_{wi} (Exp #185)	304
Table A.8.5 Methane flood results at S_{wi} (Exp #185)	305
Table A.8.6 Volatile oil properties at BPR-1 and BPR-2 pressures (Exp #185)	305

Table A.8.7 Fluid properties and conditions for final gas permeability (Exp #185)	305
Table A.8.8 Final methane flood results (Exp #185)	305
Table A.8.9 Pre and post-treatment volatile oil flood results and measured improvement factors (Exp #185)	306
Table A. 9.1 Core properties (Exp #189)	314
Table A.9.2 Fluid properties and conditions for initial gas permeability (Exp #189)	314
Table A.9.3 Initial methane flood results (Exp #189)	314
Table A.9.4 Fluid properties and conditions for methane gas permeability at S_{wi} (Exp #189)	314
Table A.9.5 Methane flood results at S_{wi} (Exp #189)	315
Table A.9.6 Volatile oil properties at BPR-1 and BPR-2 pressures (Exp #189)	315
Table A.9.7 Fluid properties and conditions for final gas permeability (Exp #189)	315
Table A.9.8 Final methane flood results (Exp #189)	316
Table A.9.9 Pre and post-treatment volatile oil flood results and measured improvement factors (Exp #189)	316
Table A. 10.1 Core properties (Exp #192)	324
Table A.10.2 Fluid properties and conditions for initial gas permeability (Exp #192)	324
Table A.10.3 Initial methane flood results (Exp #192)	324
Table A.10.4 Fluid properties and conditions for methane gas permeability at S_{wi} (Exp #192)	324
Table A.10.5 Methane flood results at S_{wi} (Exp #192)	325
Table A.10.6 Volatile oil properties at BPR-1 and BPR-2 pressures (Exp #192)	325

Table A.10.7 Fluid properties and conditions for final gas permeability (Exp #192)	325
.....	325
Table A.10.8 Final methane flood results (Exp #192).....	325
Table A.10.9 Pre and post-treatment volatile oil flood results and measured	
improvement factors (Exp #192)	326
Table A. 11.1 Core properties (Exp #196).....	334
Table A.11.2 Fluid properties and conditions for initial gas permeability (Exp #196)	
.....	334
Table A.11.3 Initial methane flood results (Exp #196)	334
Table A.11.4 Fluid properties and conditions for methane gas permeability at S_{wi}	
(Exp #196)	334
Table A.11.5 Methane flood results at S_{wi} (Exp #196).....	335
Table A.11.6 Volatile oil properties at BPR-1 and BPR-2 pressures (Exp #196)	335
Table A.11.7 Fluid properties and conditions for final gas permeability (Exp #196)	
.....	335
Table A.11.8 Final methane flood results (Exp #196).....	335
Table A.11.9 Pre and post-treatment volatile oil flood results and measured	
improvement factors (Exp #196)	336
Table A. 12.1 Core properties (Exp #198).....	343
Table A.12.2 Fluid properties and conditions for initial gas permeability (Exp #198)	
.....	343
Table A.12.3 Initial methane flood results (Exp #198)	343
Table A.12.4 Fluid properties and conditions for methane gas permeability at S_{wi}	
(Exp #198)	343
Table A.12.5 Methane flood results at S_{wi} (Exp #198).....	344

Table A.12.6 Volatile oil properties at BPR-1 and BPR-2 pressures (Exp #198)	344
Table A.12.7 Fluid properties and conditions for final gas permeability (Exp #198)	344
Table A.12.8 Final methane flood results (Exp #198)	344
Table A.12.9 Pre and post-treatment volatile oil flood results and measured improvement factors (Exp #198)	345
Table A.13.1 Core properties (Exp #200)	352
Table A.13.2 Fluid properties and conditions for initial gas permeability (Exp #200)	352
Table A.13.3 Initial methane flood results (Exp #200)	352
Table A.13.4 Fluid properties and conditions for methane gas permeability at S_{wi} (Exp #200)	352
Table A.13.5 Methane flood results at S_{wi} (Exp #200)	353
Table A.13.6 Volatile oil properties at BPR-1 and BPR-2 pressures (Exp #200)	353
Table A.13.7 Fluid properties and conditions for final gas permeability (Exp #200)	353
Table A.13.8 Final methane flood results (Exp #200)	354
Table A.13.9 Pre and post-treatment volatile oil flood results and measured improvement factors (Exp #200)	354
Table A.14.1 Core properties (Exp #210)	361
Table A.14.2 Fluid properties and conditions for initial gas permeability (Exp #210)	361
Table A.14.3 Initial methane flood results (Exp #210)	361
Table A.14.4 Fluid properties and conditions for methane gas permeability at S_{wi} (Exp #210)	361

Table A.14.5 Methane flood results at S_{wi} (Exp #210).....	362
Table A.14.6 Volatile oil properties at BPR-1 and BPR-2 pressures (Exp #210)	362
Table A.14.7 Fluid properties and conditions for final gas permeability (Exp #210)	362
Table A.14.8 Final methane flood results (Exp #210).....	363
Table A.14.9 Pre and post-treatment volatile oil flood results and measured improvement factors (Exp #210)	363
Table A.15.1 Core properties (Exp #221).....	370
Table A.15.2 Fluid properties and conditions for initial gas permeability (Exp #221)	370
Table A.15.3 Initial methane flood results (Exp #221)	370
Table A.15.4 Fluid properties and conditions for methane gas permeability at S_{wi} (Exp #221)	370
Table A.15.5 Methane flood results at S_{wi} (Exp #221).....	371
Table A.15.6 Volatile oil properties at BPR-1 and BPR-2 pressures (Exp #221)	371
Table A.15.7 Pre and post-treatment volatile oil flood results and measured improvement factors (Exp #221)	371
Table A.16.1 Core properties (Exp #224).....	378
Table A.16.2 Fluid properties and conditions for initial gas permeability (Exp #224)	378
Table A.16.3 Initial methane flood results (Exp #224)	378
Table A.16.4 Fluid properties and conditions for methane gas permeability at S_{wi} (Exp #224)	378
Table A.16.5 Methane flood results at S_{wi} (Exp #224).....	379
Table A.16.6 Volatile oil properties at BPR-1 and BPR-2 pressures (Exp #224)	379

Table A.16.7 Fluid properties and conditions for final gas permeability (Exp #224)	379
Table A.16.8 Final methane flood results (Exp #224)	379
Table A.16.9 Pre and post-treatment volatile oil flood results and measured improvement factors (Exp #224)	380
Table A.17.1 Core properties (Exp #225)	388
Table A.17.2 Fluid properties and conditions for initial gas permeability (Exp #225)	388
Table A.17.3 Initial nitrogen flood results (Exp #225)	388
Table A.17.4 Fluid properties and conditions for nitrogen gas permeability at S_{wi} (Exp #225)	388
Table A.17.5 Methane flood results at S_{wi} (Exp #225)	389
Table A.17.6 Volatile oil properties at BPR-1 and BPR-2 pressures (Exp #225)	389
Table A.17.7 Fluid properties and conditions for final gas permeability (Exp #225)	389
Table A.17.8 Final nitrogen flood results (Exp #225)	389
Table A.17.9 Pre and post-treatment volatile oil flood results and measured improvement factors (Exp #225)	390
Table A.18.1 Core properties (Exp #228)	398
Table A.18.2 Fluid properties and conditions for initial gas permeability (Exp #228)	398
Table A.18.3 Initial nitrogen flood results (Exp #228)	398
Table A.18.4 Fluid properties and conditions for nitrogen gas permeability at S_{wi} (Exp #228)	398
Table A.18.5 Nitrogen flood results at S_{wi} (Exp #228)	399

Table A.18.6 Volatile oil properties at BPR-1 and BPR-2 pressures (Exp #228)	399
Table A.18.7 Fluid properties and conditions for final gas permeability (Exp #228)	399
Table A.18.8 Final methane flood results (Exp #228)	400
Table A.18.9 Pre and post-treatment volatile oil flood results and measured improvement factors (Exp #228)	400
Table A.19.1 Core properties (Exp #229)	408
Table A.19.2 Fluid properties and conditions for initial gas permeability (Exp #229)	408
Table A.19.3 Initial nitrogen flood results (Exp #229)	408
Table A.19.4 Fluid properties and conditions for nitrogen gas permeability at S_{wi} (Exp #229)	408
Table A.19.5 Nitrogen flood results at S_{wi} (Exp #229)	409
Table A.19.6 Volatile oil properties at BPR-1 and BPR-2 pressures (Exp #229)	409
Table A.19.7 Fluid properties and conditions for final gas permeability (Exp #229)	409
Table A.19.8 Final nitrogen flood results (Exp #229)	410
Table A.19.9 Pre and post-treatment volatile oil flood results and measured improvement factors (Exp #229)	410
Table A.20.1 Core properties (Exp #231)	419
Table A.20.2 Fluid properties and conditions for initial gas permeability (Exp #231)	419
Table A.20.3 Initial methane flood results (Exp #231)	419
Table A.20.4 Composition of saturated gas (Exp #231)	419
Table A.20.5 Composition of saturated oil (Exp #231)	420

Table A.20.6 Fluid properties and conditions for methane gas permeability after initial core cleaning (Exp #231).....	420
Table A.20.7 Methane flood results after initial core cleaning (Exp #231)	420
Table A.20.8 Volatile oil properties at BPR-1 and BPR-2 pressures (Exp #231)	421
Table A.20.9 Fluid properties and conditions for saturated gas flood to measure S_{or} before treatment (Exp #231)	421
Table A.20.10 Saturated gas flood results before treatment (Exp #231).....	421
Table A.20.11 Fluid properties and conditions for saturated gas flood to measure S_{or} after treatment (Exp #231).....	421
Table A.20.12 Saturated gas flood results after treatment (Exp #231).....	422
Table A.20.13 Fluid properties and conditions for final gas permeability (Exp #231)	422
Table A.20.14 Final nitrogen flood results (Exp #231)	422
Table A.20.15 Pre and post-treatment volatile oil flood results and measured improvement factors (Exp #231)	423
Table A.21.1 Core properties (Exp #234).....	433
Table A.21.2 Fluid properties and conditions for initial gas permeability (Exp #234)	433
Table A.21.3 Initial nitrogen flood results (Exp #234).....	433
Table A.21.4 Composition of saturated gas (Exp #234).....	433
Table A.21.5 Composition of saturated oil (Exp #234).....	434
Table A.21.6 Fluid properties and conditions for nitrogen gas permeability after initial core cleaning (Exp #234).....	434
Table A.21.7 Nitrogen flood results after initial core cleaning (Exp #234)	434
Table A.21.8 Volatile oil properties at BPR-1 and BPR-2 pressures (Exp #234)	435

Table A.21.9 Fluid properties and conditions for saturated gas flood to measure S_{or} before treatment (Exp #234)	435
Table A.21.10 Saturated gas flood results before treatment (Exp #234).....	435
Table A.21.11 Fluid properties and conditions for saturated gas flood to measure S_{or} after treatment (Exp #234).....	435
Table A.21.12 Saturated gas flood results after treatment (Exp #234).....	436
Table A.21.13 Fluid properties and conditions for final gas permeability (Exp #234)	436
Table A.21.14 Final nitrogen flood results (Exp #234)	436
Table A.21.15 Pre and post-treatment volatile oil flood results and measured improvement factors (Exp #234)	437
Table A.22.1 Core properties (Exp #235).....	445
Table A.22.2 Fluid properties and conditions for initial gas permeability (Exp #235)	445
Table A.22.3 Initial nitrogen flood results (Exp #235).....	445
Table A.22.4 Composition of saturated gas (Exp #235).....	445
Table A.22.5 Composition of saturated oil (Exp #235).....	446
Table A.22.6 Fluid properties and conditions for nitrogen gas permeability after initial core cleaning (Exp #235).....	446
Table A.22.7 Nitrogen flood results after initial core cleaning (Exp #235)	446
Table A.22.8 Volatile oil properties at BPR-1 and BPR-2 pressures (Exp #235)	446
Table A.22.9 Fluid properties and conditions for saturated gas flood to measure S_{or} before treatment (Exp #235)	447
Table A.22.10 Saturated gas flood results before treatment (Exp #235).....	447

Table A.22.11 Fluid properties and conditions for saturated oil flood to measure S_{gr} before treatment (Exp #235)	447
Table A.22.12 Saturated oil flood results before treatment (Exp #235).....	447
Table A.22.13 Fluid properties and conditions for saturated gas flood to measure S_{or} after treatment (Exp #235)	448
Table A.22.14 Saturated gas flood results after treatment (Exp #231).....	448
Table A.22.15 Fluid properties and conditions for saturated oil flood to measure S_{gr} after treatment (Exp #235)	448
Table A.22.16 Saturated oil flood results after treatment (Exp #235).....	448
Table A.22.17 Fluid properties and conditions for final gas permeability (Exp #235)	448
Table A.22.18 Final nitrogen flood results (Exp #235)	449
Table A.22.19 Pre and post-treatment volatile oil flood results and measured improvement factors (Exp #235)	449

List of Figures

Figure 1.1 World market energy use fuel type, 1990-2035 (quadrillion BTU) (U.S. Energy Information Administration 2010).....	8
Figure 1.2 World supply of primary energy by fuel type in millions of barrels of oil equivalent per day (mboe/d) (OPEC 2010)	8
Figure 1.3 Historic and projected gas demand in million tons of oil equivalent (mtoe) (OPEC 2010).....	9
Figure 1.4 Historic and projected oil demand in millions of barrels per day (mb/d) (OPEC 2010).....	9
Figure 1.5 Near wellbore schematic for a volatile oil reservoir with oil, gas and water production	10
Figure 1.6 Relative permeability curves for oil-gas system at different interfacial tensions	10
Figure 2.1 Wettability representation for an oil-water-solid system (Peters).....	36
Figure 2.2 Wettability representation for a gas-liquid system.....	36
Figure 2.3 Schematic for capillary desaturation curves. Correlation of residual wetting and non-wetting phase saturation with respect to capillary number (Lake 1989)	37
Figure 2.4 Imbibition and drainage relative permeability curves	37
Figure 2.5 Phase envelope of various types of reservoir fluids, (Pedersen 2007)	38
Figure 2.6 Phase diagram of a typical volatile oil with line of isothermal reduction of reservoir pressure, 123, and surface separator conditions (McCain 1990)	38

Figure 2.7 Gas saturation by region in a volatile oil well with BHP below the bubble point pressure (Sharifi and Ahmadi 2009).....	39
Figure 2.8 Residual oil saturation S_{or} variation with respect to wettability index Ia-h for Berea sandstone.....	39
Figure 2.9 Schematic of fluorinated surfactant adsorbed on the rock surface and molecule representation	40
Figure 3.1 High-temperature high-pressure core flood experimental apparatus schematic.....	68
Figure 3.2 Coreflood setup - equipment inside the oven.....	68
Figure 3.3 Coreflood experimental setup – equipment outside the oven	69
Figure 3.4 Schematic of isothermal gas expansion at BPR-1	69
Figure 3.5 Schematic of isothermal volatile oil flash around BPR-1	69
Figure 3.6 P-T diagram for volatile oil mixture 1.....	70
Figure 3.7 Interfacial tension and liquid volume % vs. pressure for volatile oil mixture 1 at 75°F.....	70
Figure 3.8 Gas and liquid phase densities vs. pressure for volatile oil mixture 1 at 75°F	71
Figure 3.9 Gas and liquid phase viscosities vs. pressure for volatile oil mixture 1 at 75°F	71
Figure 3.10 P-T diagram for volatile oil mixture 2.....	72
Figure 3.11 Interfacial tension and liquid volume % vs. pressure for volatile oil mixture 2 at 155°F.....	72
Figure 3.12 Gas and liquid phase densities vs. pressure for volatile oil mixture 2 at 155°F	73

Figure 3.13 Gas and liquid phase viscosities vs. pressure for volatile oil mixture 2 at 155°F	73
Figure 3.14 P-T diagram for volatile oil mixture 3.....	74
Figure 3.15 Interfacial tension and liquid volume % vs. pressure for volatile oil mixture 3 at 215°F.....	74
Figure 3.16 Gas and liquid phase densities vs. pressure for volatile oil mixture 3 at 215°F	75
Figure 3.17 Gas and liquid phase viscosities vs. pressure for volatile oil mixture 3 at 215°F	75
Figure 3.18 P-T diagram for volatile oil mixture 4.....	76
Figure 3.19 Interfacial tension and liquid volume % vs. pressure for volatile oil mixture 4 at 250°F.....	76
Figure 3.20 Gas and liquid phase densities vs. pressure for volatile oil mixture 4 at 250°F	77
Figure 3.21 Gas and liquid phase viscosities vs. pressure for volatile oil mixture 4 at 250°F	77
Figure 3.22 P-T diagram for volatile oil mixture 5.....	78
Figure 3.23 Interfacial tension and liquid volume % vs. pressure for volatile oil mixture 5 at 275°F.....	78
Figure 3.24 Gas and liquid phase densities vs. pressure for volatile oil mixture 5 at 275°F	79
Figure 3.25 Gas and liquid phase viscosities vs. pressure for volatile oil mixture 5 at 275°F	79
Figure 4.1 XPS Schematic (Bvcrist).....	99

Figure 4.2 XPS results for fluorine content on surface of treated chips with candidate fluorinated surfactants.....	99
Figure 4.3 Drop test on sandstone and limestone chips treated with FC-X and amine primer.....	100
Figure 4.4 XPS results for fluorine content on surface of treated chips with selected fluorinated surfactants.....	100
Figure 4.5 Examples of a clear single phase sample, sample with phase separation, with cloudiness and with solid precipitation, respectively, during compatibility analysis for the systems surfactant-solvents-brine ...	100
Figure 4.6 to 4.15 Drop and imbibition rate test for Berea	101
Figure 4.16 to 4.19 Drop and imbibition rate test for Limestone	102
Figure 5.1 Pressure drop across the core during injection of chemical treatment 2 (Experiment # 141)	132
Figure 5.2 Pre and post-treatment pressure drop during two-phase volatile oil floods at two different flow rates (Experiment # 141).....	132
Figure 5.3 Pressure drop across the core during injection of chemical treatment 1 (Experiment # 146)	133
Figure 5.4 Pre and post-treatment pressure drop during two-phase volatile oil floods at two different flow rates (Experiment # 146).....	133
Figure 5.5 Pressure drop across the core during injection of chemical treatment 3 (Experiment # 158)	134
Figure 5.6 Pre and post-treatment pressure drop during two-phase volatile oil floods (Experiment # 158)	134
Figure 5.7 Pressure drop across the core during injection of chemical treatment 4 (Experiment # 192)	135

Figure 5.8 Pre and post-treatment pressure drop during two-phase volatile oil floods at two different flow rates (Experiment # 192).....	135
Figure 5.9 Improvement factor achieved for different volatile oil floods (batches) on treated Berea sandstone with selected fluorinated surfactants (Experiments #141, #146, #158 & #192).....	136
Figure 5.10 Effect of temperature on surfactant adsorption on Berea sandstone surface for treatment solution containing 2 wt% FC-X (Bang 2007)	136
Figure 5.11 Pressure drop across the core during injection of chemical treatment 3 (Experiment # 176)	137
Figure 5.12 Pressure drop across the core during injection of chemical treatment 3 (Experiment # 189)	137
Figure 5.13 Pre and post-treatment pressure drop during two-phase volatile oil floods (Experiment # 176)	138
Figure 5.14 Pre and post-treatment pressure drop during two-phase volatile oil floods (Experiment # 189)	138
Figure 5.15 Pre and post-treatment gas and oil relative permeabilities versus temperature for Exp # 158, #176 and #189 treated with 1 wt% L-18961	139
Figure 5.16 Pressure drop across the core during injection of chemical treatment 1 (Experiment # 210)	139
Figure 5.17 Pressure drop across the core during injection of chemical treatment 1 (Experiment # 228)	140
Figure 5.18 Pressure drop across the core during injection of chemical treatment 1 (Experiment # 229)	140

Figure 5.19 Pre and post-treatment pressure drop during two-phase volatile oil floods (Experiment # 210)	141
Figure 5.20 Pre and post-treatment pressure drop during two-phase volatile oil floods (Experiment # 228)	141
Figure 5.21 Pre and post-treatment pressure drop during two-phase volatile oil floods (Experiment # 229)	142
Figure 5.22 Pre and post-treatment gas and oil relative permeabilities versus temperature for Exp #210, #228 and #229 treated with 2 wt% FC-X142	
Figure 5.23 Temperature effect on improvement factor	143
Figure 5.24 Gas relative permeability as a function of N_c (Bang 2007)	143
Figure 5.25 Capillary number effect on gas relative permeability before and after chemical treatment 2 wt% L-20294 (Experiment #148).....	144
Figure 5.26 Capillary number effect on gas relative permeability before and after chemical treatment 2 wt% L-20294 (Experiment #148).....	144
Figure 5.27 Pressure drop across the core during injection of chemical treatment 2 (Experiment # 148)	145
Figure 5.28 Pre and post-treatment pressure drop during two-phase volatile oil floods at 900 psig core pressure (Experiment # 148)	145
Figure 5.29 Pre and post-treatment pressure drop during two-phase volatile oil floods at 1600 psig core pressure (Experiment # 148)	146
Figure 5.30 Pre and post-treatment pressure drop during two-phase volatile oil floods at 2500 psig core pressure (Experiment # 148)	146
Figure 5.31 Pre and post-treatment pressure drop during two-phase volatile oil floods at 3100 psig core pressure (Experiment # 148)	147

Figure 5.32 Pre and post-treatment pressure drop during two-phase volatile oil floods at 3500 psig core pressure (Experiment # 148)	147
Figure 5.33 Capillary number effect on gas relative permeability before and after chemical treatment (Experiment #146, #141 & #192).....	148
Figure 5.34 Capillary number effect on improvement factor (Experiment #141, #146, #148 and #192)	149
Figure 5.35 Pressure drop across the core during injection of chemical treatment 1 (Experiment # 210)	149
Figure 5.36 Pre and post-treatment pressure drop during two-phase volatile oil floods at 800 psig core pressure (Experiment # 210)	150
Figure 5.37 Pre and post-treatment pressure drop during two-phase volatile oil floods at 1100 psig core pressure (Experiment # 210)	150
Figure 5.38 Pre and post-treatment pressure drop during two-phase volatile oil floods at 1500 psig core pressure (Experiment # 210)	151
Figure 5.39 Pre and post-treatment pressure drop during two-phase volatile oil floods at 2200 psig core pressure (Experiment # 210)	151
Figure 5.40 Pre and post-treatment pressure drop during two-phase volatile oil floods at 2900 psig core pressure (Experiment # 210)	152
Figure 5.41 Observed improvement factors and capillary numbers for different oil volume fractions (Experiment #148)	152
Figure 5.42 Observed improvement factors and capillary numbers for different oil volume fractions (Experiment #176)	153
Figure 5.43 Observed improvement factors and capillary numbers for different oil volume fractions (Experiment #210)	153

Figure 5.44 Observed improvement factors and PVT ratios for different oil volume fractions (Experiment #148)	154
Figure 5.45 Observed improvement factors and PVT ratios for different oil volume fractions (Experiment #176)	154
Figure 5.46 Observed improvement factors and PVT ratios for different oil volume fractions (Experiment #210)	155
Figure 5.47 IF vs PVT ratio for experiments treated with 2 wt% FC-X	155
Figure 5.48 IF vs PVT ratio for experiments treated with 1 wt% L-18961	155
Figure 5.49 IF vs PVT ratio for experiments treated with 2 wt% L-20294.....	156
Figure 5.50 IF vs PVT ratio for experiments treated with 2 wt% L-19973#9.....	156
Figure 5.51 Improvement factor - PVT ratio correlation for Berea sandstones treated with C ₄ fluorinated surfactants (initial improvement factor).....	157
Figure 5.52 Improvement factor - PVT ratio correlation for Berea sandstones treated with C ₄ fluorinated surfactants (final improvement factor).....	158
Figure 6.1 Pressure drop across the core during injection of chemical treatment 5 (Experiment # 181)	170
Figure 6.2 Pre and post-treatment pressure drop during two-phase volatile oil floods at 800 psi core pressure (Experiment # 181)	170
Figure 6.3 Pre and post-treatment pressure drop during two-phase volatile oil floods at 1500 psi core pressure (Experiment # 181)	171
Figure 6.4 Pre and post-treatment pressure drop during two-phase volatile oil floods at 2200 psi core pressure (Experiment # 181)	171
Figure 6.5 Pre and post-treatment pressure drop during two-phase volatile oil floods at 2900 psi core pressure (Experiment # 181)	172

Figure 6.6 Pressure drop across the core during injection of second chemical treatment 5 (Experiment # 181)	172
Figure 6.7 Pre and post-treatment pressure drop during two-phase volatile oil floods for 1 st and 2 nd chemical treatment at 800 psi and 1500 psi core pressures (Experiment # 181)	173
Figure 6.8 Pressure drop across the core during injection of chemical treatment 5 (Experiment # 185)	173
Figure 6.9 Pre and post-treatment pressure drop during two-phase volatile oil floods at three different flow rates (Experiment # 185).....	174
Figure 6.10 Capillary number effect on pre and post-treatment gas relative permeability (Experiment # 181).....	174
Figure 6.11 Capillary number effect on pre and post-treatment oil relative permeability (Experiment # 181).....	175
Figure 6.12 Capillary number effect on improvement factor (Experiments #181 & # 185)	175
Figure 6.13 Effect of PVT ratio on improvement factor for carbonate cores.....	176
Figure 6.14 Effect of core absolute permeability on improvement factor for carbonate cores	176
Figure 7.1 Core cuts for XPS analysis & direction of flood performance for case 1197	
Figure 7.2 Core cuts for XPS analysis & direction of flood performance for case 2197	
Figure 7.3 Fluorine content along Berea sandstone cores treated with different chemical treatments and experimental conditions	197
Figure 7.4 Fluorine content along Berea sandstone cores treated with different amounts of chemical treatment 1 (2 wt% FC-X) at 155°F temp (Exp #226)	198

Figure 7.5 Fluorine content along Berea sandstone cores treated with different chemical treatments at 155°F and case 1 for flood direction (Exp #141, #148, #189 & #224)	198
Figure 7.6 Fluorine content along Berea sandstone cores treated w/ chemical treatment 1 (2 wt% FC-X) at different temp and case 2 for flood direction (Exp #225, #228 & #229)	199
Figure 7.7 Fluorine content a along TCL core treated with chemical treatment 5 (2 wt% L-19446#1) at 155°F and case 2 for flood direction (Exp #185)	199
Figure 7.8 HPLC calibration curve for surfactant concentration.....	200
Figure 7.9 Surfactant concentration in chemical treatment effluent (Experiment # 224)	200
Figure 7.10 Surfactant mass in post-treatment volatile oil effluent (Experiment # 224)	201
Figure 7.11 Cumulative surfactant mass in post-treatment volatile oil effluent (Experiment #224)	201
Figure 7.12 Oil saturation (S_o) profile before and after treatment (Experiment #231)	202
Figure 7.13 Oil saturation (S_o) profile before and after 2nd treatment (Experiment #231)	202
Figure 7.14 Residual oil saturation (S_{or}) profile before and after 1 st & 2 nd treatment (Experiment #231)	203
Figure 7.15 Oil saturation (S_o) profile before and after treatment (Experiment #234)	203
Figure 7.16 Residual oil saturation (S_{or}) profile before and after treatment (Exp #234)	204

Figure 7.17 Oil saturation (S_o) profile before and after treatment (Experiment #235)	204
Figure 7.18 Residual oil saturation (S_{or}) profile before and after treatment (Exp #235)	205
Figure 7.19 Residual gas saturation (S_{gr}) profile before and after treatment (Exp #235)	205
Figure 7.20 Pre and post-treatment oil and gas relative permeability curves	206
Figure 8.1 Cylindrical reservoir model with refined grids near wellbore	217
Figure 8.2 P-T diagram for volatile oil mixture 2 generated with WINPROP	217
Figure 8.3 Liquid volume and produced gas with respect to pressure- CVD calculations using WINPROP	218
Figure 8.4 Simulation results for the reservoir depletion of the base case	218
Figure 8.5 Productivity index profile for the base case	219
Figure 8.6 Well bottom-hole pressure profile for non-treated and treated cases	219
Figure 8.7 Rate of produced gas versus well bottom-hole pressure for non-treated and treated cases	220
Figure 8.8 Cumulative oil vs. well-bottom hole pressure for non-treated and treated cases	220
Figure 8.9 Cumulative gas vs. well-bottom hole pressure for non-treated and treated cases	221
Figure 8.10 Oil Saturation profiles during reservoir depletion for a treated radius of 20 ft	221
Figure 8.11 Productivity index profile for the non-treated and treated cases	222
Figure 8.12 Productivity index for different radius of treated zone after 7 years of production	222

Figure A.1.1 Pressure drop across the core during the initial nitrogen flood at 75°F (Exp #134)	237
Figure A.1.2 Pressure drop across the core during the initial methane flood at 155°F (Exp #134)	237
Figure A.1.3 Pressure drop across the core during the methane flood at S_{wi} 20% (Exp #134)	238
Figure A.1.4 Pressure drop across the core during the pre-treatment two-phase volatile oil flood (Exp #134).....	238
Figure A.1.5 Pressure drop across the core during injection of chemical treatment 1 (Exp # 134)	239
Figure A.1.6 Pressure drop across the core during the post-treatment two-phase volatile oil flood (Exp #134).....	239
Figure A.1.7 Pressure drop across the core during injection of 2 nd chemical treatment 1 (Exp # 134)	240
Figure A.1.8 Pressure drop across the core during the post-2 nd treatment two-phase volatile oil flood (Exp #134).....	240
Figure A.2.3 Pressure drop across the core during the pre-treatment two-phase volatile oil flood (Exp #141).....	248
Figure A.2.4 Pressure drop across the core during injection of chemical treatment 2 (Exp # 141)	248
Figure A.2.5 Pressure drop across the core during the post-treatment two-phase volatile oil flood 1 (Exp #141).....	249
Figure A.2.6 Pressure drop across the core during the post-treatment two-phase volatile oil flood 2 (Exp #141).....	249

Figure A.2.7 Pressure drop across the core during the post-treatment two-phase volatile oil flood 3 (Exp #141).....	250
Figure A.2.8 Pressure drop across the core during the final methane flood (Exp #141)	250
Figure A. 3.1 Pressure drop across the core during the initial methane flood at 155°F (Exp #146)	257
Figure A. 3.2 Pressure drop across the core during the methane flood at S_{wi} of 20% (Exp #146)	257
Figure A. 3.3 Pressure drop across the core during the pre-treatment two-phase volatile oil flood (Exp #146).....	258
Figure A.3.4 Pressure drop across the core during injection of chemical treatment 1 (Exp # 146)	258
Figure A.3.5 Pressure drop across the core during the post-treatment two-phase volatile oil flood 1 (Exp #146).....	259
Figure A.3.6 Pressure drop across the core during the post-treatment two-phase volatile oil flood 2 (Exp #146).....	259
Figure A.3.7 Pressure drop across the core during the post-treatment two-phase volatile oil flood 3 (Exp #146).....	260
Figure A.3.8 Pressure drop across the core during the final methane flood at 155°F (Exp #146)	260
Figure A.4.1 Pressure drop across the core during the initial methane flood at 155°F (Exp #148)	267
Figure A.4.2 Pressure drop across the core during the methane flood at S_{wi} of 20% (Exp #148)	267

Figure A.4.3 Pressure drop across the core during the pre-treatment two-phase volatile oil flood (Exp #148).....	268
Figure A.4.4 Pressure drop across the core during injection of chemical treatment 2 (Exp # 148)	268
Figure A.4.5 Pressure drop across the core during the post-treatment two-phase volatile oil flood 1 (Exp #148).....	269
Figure A.4.6 Pressure drop across the core during the post-treatment two-phase volatile oil flood 2 (Exp #148).....	269
Figure A.4.7 Pressure drop across the core during the final methane flood at 155°F (Exp #148)	270
Figure A.5.1 Pressure drop across the core during the initial methane flood at 155°F (Exp #158)	277
Figure A.5.2 Pressure drop across the core during the methane flood at S_{wi} of 20% (Exp #158)	277
Figure A.5.3 Pressure drop across the core during the pre-treatment two-phase volatile oil flood (Exp #158).....	278
Figure A.5.4 Pressure drop across the core during injection of chemical treatment 3 (Exp # 158)	278
Figure A.5.5 Pressure drop across the core during the post-treatment two-phase volatile oil flood (Exp #158).....	279
Figure A.6.1 Pressure drop across the core during the initial methane flood at 155°F (Exp #176)	286
Figure A.6.2 Pressure drop across the core during the methane flood at S_{wi} of 20% (Exp #176)	286

Figure A.6.3 Pressure drop across the core during the pre-treatment two-phase volatile oil flood (Exp #176).....	287
Figure A.6.4 Pressure drop across the core during injection of chemical treatment 3 (Exp # 176)	287
Figure A.6.5 Pressure drop across the core during the post-treatment two-phase volatile oil flood (Exp #176).....	288
Figure A.6.6 Pressure drop across the core during injection of 2 nd chemical treatment 3 (Exp # 176)	288
Figure A.6.7 Pressure drop across the core during injection of 3 rd chemical treatment 3 (Exp # 176)	289
Figure A.6.8 Pressure drop across the core during the post-2 nd treatment two-phase volatile oil flood (Exp #176).....	289
Figure A.6.9 Pressure drop across the core during the post-3 rd treatment two-phase volatile oil flood (Exp #176).....	290
Figure A.6.10 Pressure drop across the core during the final methane flood at 155°F (Exp #176)	290
Figure A.7.1 Pressure drop across the core during the initial methane flood at 155°F (Exp #181)	297
Figure A.7.2 Pressure drop across the core during the methane flood at S_{wi} of 20% (Exp #181)	297
Figure A.7.3 Pressure drop across the core during the pre-treatment two-phase volatile oil flood (Exp #181).....	298
Figure A.7.4 Pressure drop across the core during injection of chemical treatment 5 (Exp # 181)	298

Figure A.7.5 Pressure drop across the core during the post-treatment two-phase volatile oil flood (Exp #181).....	299
Figure A.7.6 Pressure drop across the core during injection of 2 nd chemical treatment 5 (Exp # 181)	299
Figure A.7.7 Pressure drop across the core during the post-2 nd treatment two-phase volatile oil flood (Exp #181).....	300
Figure A.7.8 Pressure drop across the core during the final methane flood at 155°F (Exp #181)	300
Figure A.8.1 Pressure drop across the core during the initial methane flood at 155°F (Exp #185)	307
Figure A.8.2 Pressure drop across the core during the methane flood at S_{wi} of 20% (Exp #185)	307
Figure A.8.3 Pressure drop across the core during the pre-treatment two-phase volatile oil flood (Exp #185).....	308
Figure A.8.4 Pressure drop across the core during injection of chemical treatment 5 (Exp # 185)	308
Figure A.8.5 Pressure drop across the core during the post-treatment two-phase volatile oil flood (Exp #185).....	309
Figure A.8.6 Pressure drop across the core during the post-treatment two-phase volatile oil flood 2 (Exp #185).....	309
Figure A.8.7 Pressure drop across the core during the post- treatment two-phase volatile oil flood 3 (Exp #185).....	310
Figure A.8.8 Pressure drop across the core during the final methane flood at 155°F (Exp #185)	310

Figure A.9.1 Pressure drop across the core during the initial methane flood at 250°F (Exp #189)	317
Figure A.9.2 Pressure drop across the core during the methane flood at S_{wi} of 20% (Exp #189)	317
Figure A.9.3 Pressure drop across the core during the pre-treatment two-phase volatile oil flood (Exp #189).....	318
Figure A.9.4 Pressure drop across the core during injection of chemical treatment 3 (Exp # 189)	318
Figure A.9.5 Pressure drop across the core during the post-treatment two-phase volatile oil flood (Exp #189).....	319
Figure A.9.6 Pressure drop across the core during the post-treatment two-phase volatile oil flood 2 (Exp #189).....	319
Figure A.9.7 Pressure drop across the core during the final methane flood at 250°F (Exp #189)	320
Figure A.10.1 Pressure drop across the core during the initial methane flood at 155°F (Exp #192)	327
Figure A.10.2 Pressure drop across the core during the methane flood at S_{wi} of 20% (Exp #192)	327
Figure A.10.3 Pressure drop across the core during the pre-treatment two-phase volatile oil flood (Exp #192).....	328
Figure A.10.4 Pressure drop across the core during injection of chemical treatment 4 (Exp # 192)	328
Figure A.10.5 Pressure drop across the core during the post-treatment two-phase volatile oil flood (Exp #192).....	329

Figure A.10.6 Pressure drop across the core during the post-treatment two-phase volatile oil flood 2 (Exp #192).....	329
Figure A.10.7 Pressure drop across the core during the final methane flood at 155°F (Exp #192)	330
Figure A.11.1 Pressure drop across the core during the initial methane flood at 155°F (Exp #196)	337
Figure A.11.2 Pressure drop across the core during the methane flood at S_{wi} of 20% (Exp #196)	337
Figure A.11.3 Pressure drop across the core during the pre-treatment two-phase volatile oil flood (Exp #196).....	338
Figure A.11.4 Pressure drop across the core during injection of chemical treatment 4 (Exp # 196)	338
Figure A.11.5 Pressure drop across the core during the post-treatment two-phase volatile oil flood (Exp #196).....	339
Figure A.11.6 Pressure drop across the core during the final methane flood at 155°F (Exp #196)	339
Figure A.12.1 Pressure drop across the core during the initial methane flood at 155°F (Exp #198)	346
Figure A.12.2 Pressure drop across the core during the methane flood at S_{wi} of 20% (Exp #198)	346
Figure A.12.3 Pressure drop across the core during the pre-treatment two-phase volatile oil flood (Exp #198).....	347
Figure A.12.4 Pressure drop across the core during injection of chemical treatment 4 (Exp # 198)	347

Figure A.12.5 Pressure drop across the core during the post-treatment two-phase volatile oil flood (Exp #198).....	348
Figure A.12.6 Pressure drop across the core during the final methane flood at 155°F (Exp #198)	348
Figure A.13.1 Pressure drop across the core during the initial methane flood at 155°F (Exp #200)	355
Figure A.13.2 Pressure drop across the core during the methane flood at S_{wi} of 20% (Exp #200)	355
Figure A.13.3 Pressure drop across the core during the pre-treatment two-phase volatile oil flood (Exp #200).....	356
Figure A.13.4 Pressure drop across the core during injection of chemical treatment 3 (Exp # 200)	356
Figure A.13.5 Pressure drop across the core during the post-treatment two-phase volatile oil flood (Exp #200).....	357
Figure A.13.6 Pressure drop across the core during the final methane flood at 155°F (Exp #200)	357
Figure A.14.1 Pressure drop across the core during the initial methane flood at 155°F (Exp #210)	364
Figure A.14.2 Pressure drop across the core during the methane flood at S_{wi} of 20% (Exp #210)	364
Figure A.14.3 Pressure drop across the core during the pre-treatment two-phase volatile oil flood (Exp #210).....	365
Figure A.14.4 Pressure drop across the core during injection of chemical treatment 1 (Exp # 210)	365

Figure A.14.5 Pressure drop across the core during the post-treatment two-phase volatile oil flood (Exp #210).....	366
Figure A.14.6 Pressure drop across the core during the final methane flood at 155°F (Exp #210)	366
Figure A.15.1 Pressure drop across the core during the initial methane flood at 155°F (Exp #221)	372
Figure A.15.2 Pressure drop across the core during the methane flood at S_{wi} of 20% (Exp #221)	372
Figure A.15.3 Pressure drop across the core during the pre-treatment two-phase volatile oil flood (Exp #221).....	373
Figure A.15.4 Pressure drop across the core during injection of chemical treatment 1 (Exp # 221)	373
Figure A.15.5 Pressure drop across the core during the post-treatment two-phase volatile oil flood (Exp #221).....	374
Figure A.15.6 Pressure drop across the core during the post-treatment two-phase volatile oil flood 2 (Exp #221).....	374
Figure A.16.1 Pressure drop across the core during the initial methane flood at 155°F (Exp #224)	381
Figure A.16.2 Pressure drop across the core during the methane flood at S_{wi} of 20% (Exp #224)	381
Figure A.16.3 Pressure drop across the core during the pre-treatment two-phase volatile oil flood (Exp #224).....	382
Figure A.16.4 Pressure drop across the core during injection of chemical treatment 1 (Exp # 224)	382

Figure A.16.5 Pressure drop across the core during the post-treatment two-phase volatile oil flood (Exp #224).....	383
Figure A.16.6 Pressure drop across the core during the post-treatment two-phase volatile oil flood 2 (Exp #224).....	383
Figure A.16.7 Pressure drop across the core during the final methane flood at 155°F (Exp #224)	384
Figure A.17.1 Pressure drop across the core during the initial nitrogen flood at 75°F (Exp #225)	391
Figure A.17.2 Pressure drop across the core during the nitrogen flood at S_{wi} of 20% (Exp #225)	391
Figure A.17.3 Pressure drop across the core during the pre-treatment two-phase volatile oil flood (Exp #225).....	392
Figure A.17.4 Pressure drop across the core during injection of chemical treatment 1 (Exp # 225)	392
Figure A.17.5 Pressure drop across the core during the post-treatment two-phase volatile oil flood (Exp #225).....	393
Figure A.17.6 Pressure drop across the core during the post-treatment two-phase volatile oil flood 2 (Exp #225).....	393
Figure A.17.7 Pressure drop across the core during the final nitrogen flood at 155°F (Exp #225)	394
Figure A.18.1 Pressure drop across the core during the initial nitrogen flood at 75°F (Exp #228)	401
Figure A.18.2 Pressure drop across the core during the nitrogen flood at S_{wi} of 20% (Exp #228)	401

Figure A.18.3 Pressure drop across the core during the pre-treatment two-phase volatile oil flood (Exp #228).....	402
Figure A.18.4 Pressure drop across the core during injection of chemical treatment 1 (Exp # 228)	402
Figure A.18.5 Pressure drop across the core during the post-treatment two-phase volatile oil flood (Exp #228).....	403
Figure A.18.6 Pressure drop across the core during the post-treatment two-phase volatile oil flood 2 (Exp #228).....	403
Figure A.18.7 Pressure drop across the core during the final methane flood at 215°F (Exp #228)	404
Figure A.19.1 Pressure drop across the core during the initial nitrogen flood at 75°F (Exp #229)	411
Figure A.19.2 Pressure drop across the core during the nitrogen flood at S_{wi} of 20% (Exp #229)	411
Figure A.19.3 Pressure drop across the core during the pre-treatment two-phase volatile oil flood (Exp #229).....	412
Figure A.19.4 Pressure drop across the core during injection of chemical treatment 1 (Exp # 229)	412
Figure A.19.5 Pressure drop across the core during the post-treatment two-phase volatile oil flood (Exp #229).....	413
Figure A.19.6 Pressure drop across the core during the post-treatment two-phase volatile oil flood 2 (Exp #229).....	413
Figure A.19.7 Pressure drop across the core during the final nitrogen flood at 75°F (Exp #229)	414

Figure A.20.1 Pressure drop across the core during the initial nitrogen flood at 75°F (Exp #231)	424
Figure A.20.2 Pressure drop across the core during the methane flood after initial core cleaning (Exp #231).....	424
Figure A.20.3 Pressure drop across the core during the pre-treatment two-phase volatile oil flood (Exp #231).....	425
Figure A.20.4 Pressure drop across the core during injection of chemical treatment 1 (Exp # 231)	425
Figure A.20.5 Pressure drop across the core during the post-treatment two-phase volatile oil flood (Exp #231).....	426
Figure A.20.6 Pressure drop across the core during injection of second chemical treatment 1 (Exp # 231)	426
Figure A.20.7 Pressure drop across the core during the post-2 nd treatment two-phase volatile oil flood 1 and 2 (Exp #231).....	427
Figure A.20.8 Pressure drop across the core during the post-2 nd treatment two-phase volatile oil flood 3 (Exp #231).....	427
Figure A.20.9 Pressure drop across the core during the final nitrogen flood at 75°F (Exp #231)	428
Figure A.21.1 Pressure drop across the core during the initial nitrogen flood at 75°F (Exp #234)	438
Figure A.21.2 Pressure drop across the core during the nitrogen flood after initial core cleaning (Exp #234).....	438
Figure A.21.3 Pressure drop across the core during the pre-treatment two-phase volatile oil flood (Exp #234).....	439

Figure A.21.4 Pressure drop across the core during the post-treatment two-phase volatile oil flood (Exp #234).....	439
Figure A.21.5 Pressure drop across the core during the final nitrogen flood at 75°F (Exp #234)	440
Figure A.22.1 Pressure drop across the core during the initial nitrogen flood at 75°F (Exp #235)	450
Figure A.22.2 Pressure drop across the core during the nitrogen flood after initial core cleaning (Exp #235).....	450
Figure A.22.3 Pressure drop across the core during the pre-treatment two-phase volatile oil flood (Exp #235).....	451
Figure A.22.4 Pressure drop across the core during injection of chemical treatment 1 (Exp # 235)	451
Figure A.22.5 Pressure drop across the core during the post-treatment two-phase volatile oil flood (Exp #235).....	452
Figure A.22.6 Pressure drop across the core during the final nitrogen flood at 75°F (Exp #235)	452

Chapter 1: Introduction

Energy is vital to power houses, business, industries and transportation, and to produce the services that keep world economies functioning. Energy is produced from many types of sources. Among these are: a) renewable sources, such as wind, solar, geothermal, biomass and water (rain, tides, rivers), b) atomic-nuclear sources; such as fission and fusion, and c) fossil fuels; such as coal, oil and gas.

The availability of energy sources and the usage of the same have been fundamental for determining the course and development of human history. For example, the use of coal in the 18th and 19th centuries was fundamental for fueling the industrial revolution and in the 20th century the use of oil was the basis of the mobility revolution. In our time, these basic types of fuels are used to produce energy in various forms, particularly as electricity, allowing economic growth, technological development, and social progress. As a consequence of increased industrialization, the energy demand to satisfy human needs has continuously increased. In addition, the increase in human population and improvements in living conditions have further increased energy demand.

According to the U.S. Energy Information Administration (EIA) in the reference case presented in the International Energy Outlook 2010, the total world energy consumption will grow by 49% from 2007 to 2035. That is from 495 quadrillion British thermal units (Btu) in 2007 to 739 quadrillion Btu in 2035. Use of energy produced from all fuel sources will increase over the 2007-2035 projection period and the expectation is that fossil fuels will continue to supply much of the energy used worldwide (Figure 1.1).

Similar projections are illustrated in the World Oil Outlook 2010 prepared by the Organization of the Petroleum Exporting Countries (OPEC). Here, their reference case shows that world energy demand will increase by 40% in 2030 compared to today's

levels. Throughout the period to 2030, over 80% of the demand is expected to be supplied by fossil fuels (Figure 1.2). Figure 1.3 and Figure 1.4 show the historic and projected gas and oil demands respectively. It is observed that gas demand in developing countries is expected to grow rapidly and oil demand in countries outside of the Organization for Economic Cooperation and Development (OECD) will overtake OECD demand by 2016. These projections were done assuming a nominal oil price in the range of \$75-85/b over the years to 2020, reaching \$106/b by 2030. Thus, increasing volumes of natural gas and oil will be required to satisfy the world's energy demand in the future. This is a good back drop and justification for the intensive efforts to enhance the exploration and the production of hydrocarbon resources.

As the world runs out of easy-to-produce hydrocarbon resources the intensive demands for energy are forcing exploration and production to move into deeper geological formations. The discovery of volatile oil and gas condensate reservoirs which are typically found at greater depths is becoming increasingly common (Sanni and Gringarten 2008) and with this come new production challenges. Production of volatile oil and gas condensate reservoirs is different in many ways than production from oil or dry gas reservoirs. Oil reservoirs producing above their bubble point and dry gas reservoirs, are generally produced in a single-phase state; liquid or gas respectively. This is not the case for volatile oil and gas condensate fluids. During the production of these types of reservoirs, pressure depletion causes the formation of a second phase resulting in a two-phase flow regime. This along with other factors such as the nature of the fluid phases, the rock and reservoir properties, the pressure gradients imposed, can negatively impact the reservoir productivity.

In the specific case of production in volatile oil reservoirs, when the bottom-hole pressure of a producing well falls below the bubble point pressure, a significant amount of gas is liberated. The gas then resides in the pore space which blocks the flow of the oil phase; this is commonly referred to as "gas blocking". In volatile oil reservoirs, the formation of two fluid phases near the wellbore is usually a common problem that negatively impacts well deliverability. The presence of two immiscible phases; gas and liquid, results in a reduction of the liquid saturation and a decrease in the oil relative permeability. The oil relative permeability can decrease by an order of magnitude or more as gas saturation increases (Figure 1.5 and 1.6). Capillary forces due to the presence of two-phases promote the trapping of both the oil and the gas phase. The capillary pressure depends on the contact angle of the wetting phase which depends on the wetting state of the reservoir rock. The rock's wetting state is also known as rock wettability and its effect on the liquid trapped due to "gas blocking" is significant. In gas-liquid systems, high liquid fractions can be held by the porous media if it is strongly liquid wet due to the low mobility of this liquid phase (Tang and Firoozabadi 2000). These causes lead to lower oil production rates. Thus, the degree of liquid trapping will depend on different factors such as fluid properties, rock characteristics, pressure gradients and production rates.

To mitigate the effects of "gas blocking" and the consequent productivity decline, methods such as hydraulic fracturing and horizontal wells have been suggested. The use of these methods have been shown to increase well productivity and oil and gas recovery, even when two hydrocarbon fluid phases are already present (Sanni and Gringarten 2008). However, the use of these techniques is sometimes not feasible and is subject to economics. For example, if the reservoir is underlain by an aquifer, it may not be

advisable to fracture the well as it may connect the oil-bearing part of the reservoir with the aquifer. Complementary to these enhancing methods, the idea of using fluorinated chemical treatments to restore productivity has been proposed, and the first attempts to develop this technique for volatile oil reservoirs have been made (Bang 2007).

The use of fluorinated surfactants to mitigate the damage due to "condensate blocking" has been extensively investigated (Li and Firoozabadi 2000; Kumar 2006; Kumar et al. 2006; Bang 2007; Bang et al. 2008; Bang et al. 2009) . This is when the mobility of the gas phase is affected by the presence of the formation of a liquid phase due to production below the dew point. An advantage of this chemical treatment technique compared to the other methods mentioned above is that only the near wellbore region, the area where the hydrocarbon mixture exists as two phases, needs to be treated (Figure 1.5).

Hence, for both problems "gas blocking" and "condensate blocking", a similar scenario is faced; the formation of two-phase flow decreases well deliverability. However, any approach to enhance or restore well deliverability may be quite different in the two cases. Thus, performing a complete study of the application of fluorinated chemical treatments to treat "gas blocked" volatile oil reservoirs was the motivation for the present research work.

1.1 OBJECTIVES OF THIS RESEARCH

The main objective of this research was to develop a chemical technique to improve and/or restore the productivity of volatile oil wells undergoing "gas blocking". This was to be done by changing the rock wettability using fluorinated surfactants.

The goal is to develop a treatment that is effective, durable and environmentally friendly. Fluorinated surfactants have the ability to change the water and oil wettability of the formation from water/oil wet to neutral wet allowing oil, gas, and even water to flow more easily. Wettability alterations were indirectly observed as changes in oil and gas relative permeabilities. The use of fluorinated surfactants have been shown to work in the past for gas condensate wells that have “condensate blocking” problems (Butler et al. 2009). These fluorinated surfactants have worked for sandstone rocks and for limestone rocks with the aid of an amine primer (Bang 2007; Ahmadi et al. 2010). Although preliminary results for the applicability of this technique on volatile oil reservoirs had been obtained, a more intensive study was needed (Bang 2007). That study was done in this research, where this chemical technique was applied specifically to volatile oil reservoirs.

The research goals were obtained by performing high-temperature high-pressure (HTHP) core flood experiments to study the feasibility of this technique. The experiments were conducted using variable reservoir conditions. Analytical tools such as x-ray electron microscopy (XPS), high-performance liquid chromatography (HPLC) and computerized axial tomography (CAT Scan), as well as the use of computational simulations were also used to interpret the experimental results.

1.2 CHAPTERS SUMMARY

The dissertation is organized into nine chapters.

Chapter 1 reviews the world energy demand and justifies the importance of this research. It also describes the problem encountered in volatile oil reservoirs producing below bubble point, called “gas blocking”, and reviews the proposed solutions to mitigate

the problem. The chapter describes the objectives of this research the main goal being to enhance oil and gas relative permeability using chemical treatments that contain fluorinated surfactants.

Chapter 2 reviews the petrophysical concepts pertinent to this research and the previous studies relevant to the problem of “gas blocking”.

Chapter 3 explains the setup of the high-pressure high-temperature core flood experiments and describes all of its components. It also explains the general core flood experimental procedure that was followed and illustrates the calculations made to interpret the results.

Chapter 4 shows the methodology developed for the formulation of chemical treatments. This includes screening of fluorinated surfactants and solvent used to deliver the surfactant. The screening methodologies used; solubility, stability, compatibility tests, X-ray photoelectron spectroscopy (XPS) analysis, and contact angle and imbibition rate tests are described. The test results and final formulations are also presented.

Chapter 5 shows the results obtained for the experiments performed on sandstone cores using fluorinated chemical treatments. The chapter discusses the effect that surfactant type, experimental temperature, capillary number, PVT ratio and rock permeability have on the effectiveness of the chemical treatment to mitigate the “gas blocking problem” by enhancing the oil and gas relative permeabilities.

Chapter 6 shows preliminary results obtained for carbonate cores treated with fluorinated chemical treatments and explains the use of an anionic surfactant for treatment. The effects of capillary number and PVT ratio are also discussed.

Chapter 7 explains the analytical techniques that were used to evaluate the performance of fluorinated chemical treatments and shows the results. The analytical

techniques explained are X-ray photoelectron spectroscopy (XPS) for fluorine measurements on treated cores, high-performance liquid chromatography (HPLC) for surfactant adsorption and desorption measurements, and computerized axial tomography (CT Scan) for fluid saturation measurements in core flood experiments.

Chapter 8 presents the preliminary results of numerical simulations for the depletion of volatile oil reservoirs treated with fluorinated chemical treatments. The results for five cases with different treatment radii are compared to a non-treated case and the improvements in oil and gas production with respect to well-reservoir drawdown are shown.

Chapter 9 is a summary of the results and conclusions drawn from this research and provides recommendations for future work.

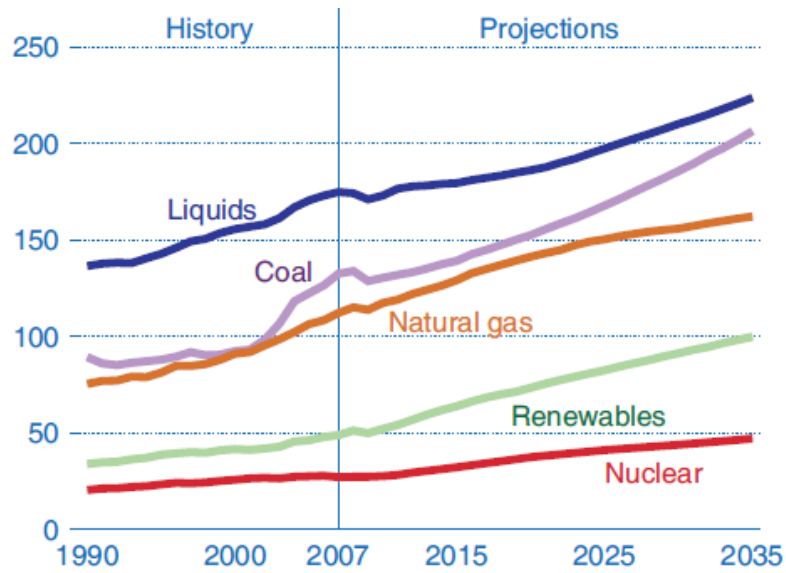


Figure 1.1 World market energy use fuel type, 1990-2035 (quadrillion BTU) (U.S. Energy Information Administration 2010)

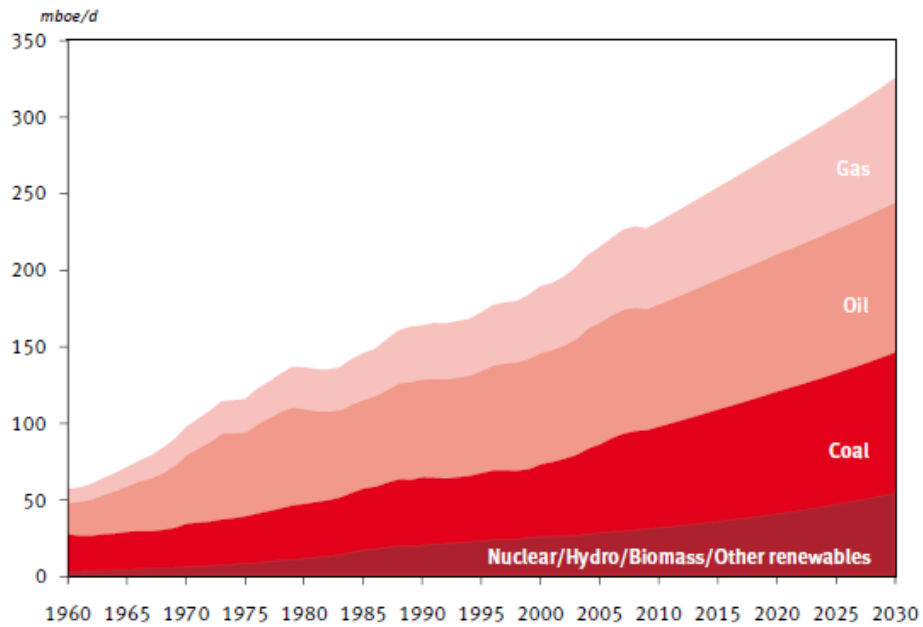


Figure 1.2 World supply of primary energy by fuel type in millions of barrels of oil equivalent per day (mboe/d) (OPEC 2010)

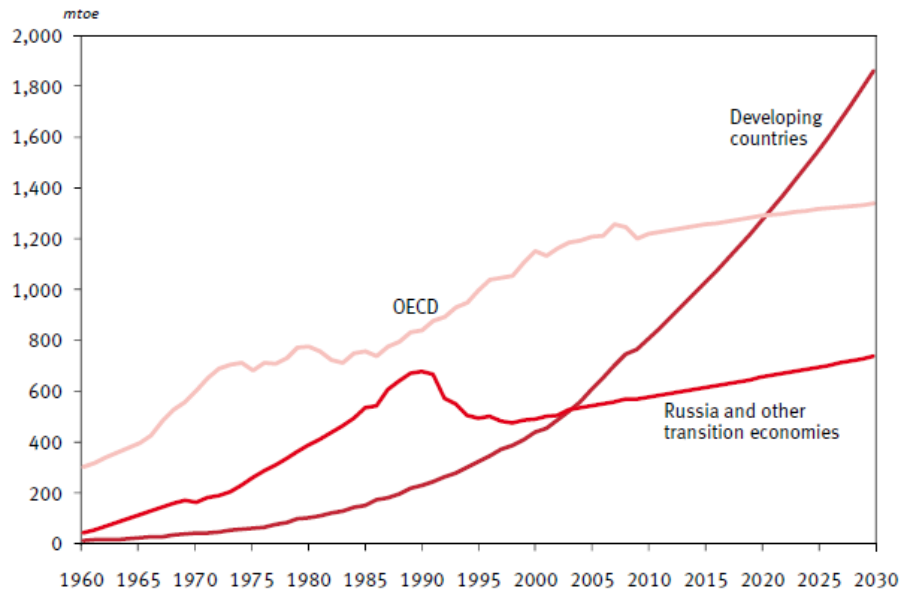


Figure 1.3 Historic and projected gas demand in million tons of oil equivalent (mtoe) (OPEC 2010)

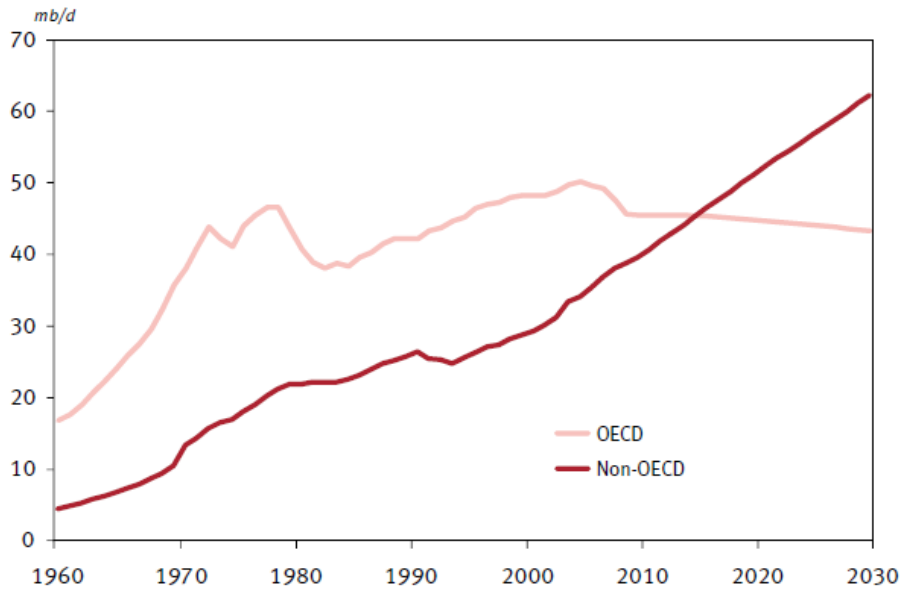


Figure 1.4 Historic and projected oil demand in millions of barrels per day (mb/d) (OPEC 2010)

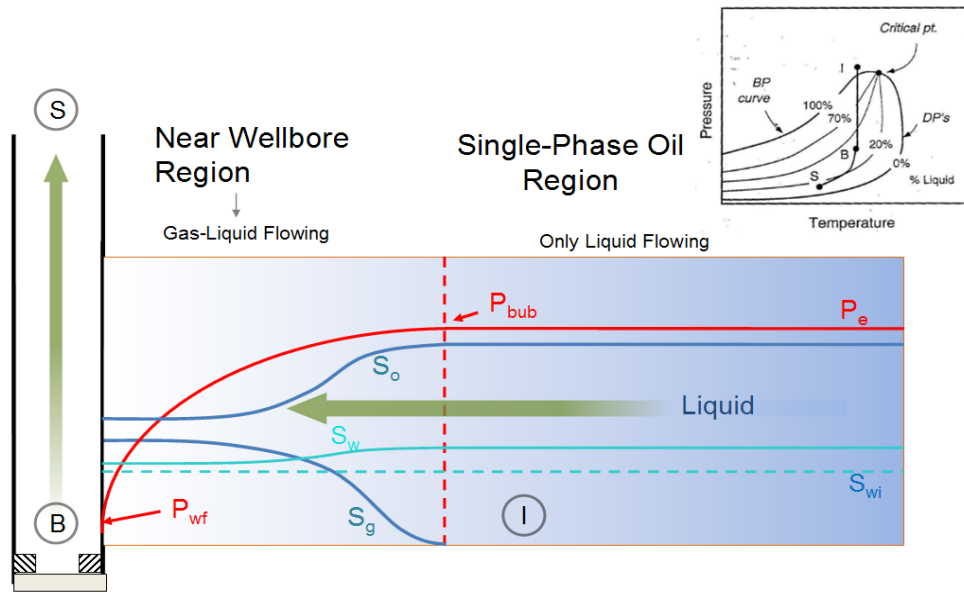


Figure 1.5 Near wellbore schematic for a volatile oil reservoir with oil, gas and water production

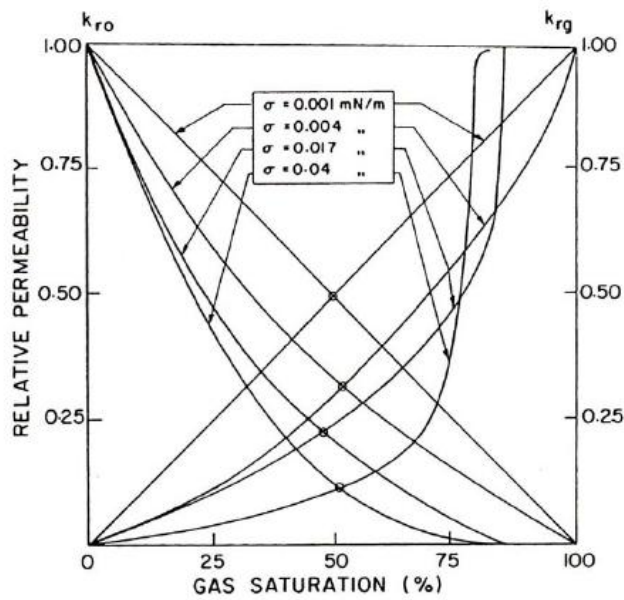


Figure 1.6 Relative permeability curves for oil-gas system at different interfacial tensions

Chapter 2: Literature Review

Having a clear understanding of the petrophysical concepts pertinent to this research such as wettability, capillarity and permeability; and also understanding the phase behavior of near critical fluids was fundamental for the conduct of this research. In this chapter, a review of these concepts has been undertaken as well as an extensive review of the studies relevant to the problem of “gas/condensate blocking”. This includes studies of the phenomena itself and methodologies to mitigate the damage caused during reservoir depletion.

2.1 PETROPHYSICAL CONCEPTS AND DEFINITIONS

The main objective of this research is to mitigate the damage in wells due to gas/condensate blocking using a chemical treatment. The treatment increases the relative permeability of the fluid phases by altering the wettability of the rock. Thus, the concepts of wettability, capillary pressure, permeability and relative permeability are most important and are briefly described below.

2.1.1 Wettability

Wettability is a measure of the tendency of a liquid to spread out on a solid surface. In the presence of other immiscible fluids the liquid that preferentially contacts the solid surface is known as the wetting fluid and the others are non-wetting fluids. The wetting fluid has a tendency to occupy the small pores and to contact the majority of the rock surface while the non-wetting fluid typically occupies the centers of the larger pores. In an oil or gas reservoir, the fluids are normally water, oil, and gas (usually a non-wetting fluid) and the solid surface is the reservoir rock (which could be silica for sandstone reservoirs and calcite for limestone reservoirs).

The degree of wetting by a fluid is defined and measured by the contact angle that the wetting fluid forms with the solid surface. Figure 2.1 illustrates water and oil, liquid phases, in contact with a solid surface. Here σ_{os} is the solid-oil interfacial tension, σ_{ow} is the oil-water interfacial tension and σ_{ws} is the water-solid interfacial tension. The Young-Dupre equation correlates the interfacial tensions and the contact angle at equilibrium. A force balance in the x direction can be written as,

$$\sigma_{os} - \sigma_{ws} = \sigma_{os} \cos\theta \quad (2.1)$$

A solid surface is considered water-wet when $\sigma_{ws} < \sigma_{os}$, therefore, $\theta < 90^\circ$. On the other hand a solid is called oil-wet when $\sigma_{ws} > \sigma_{os}$ or $\theta > 90^\circ$. The degree of wettability will depend on the difference between σ_{os} and σ_{ws} . Neutral or intermediate wettability is observed when σ_{os} is equal to σ_{ws} and the contact angle is 90° , implying that the solid has no preferential wettability for either fluid.

For a solid surface that is not liquid-wet (gas or oil), the liquid-solid interfacial tension σ_{LS} is higher than the gas-solid interfacial tension σ_{GS} , $\sigma_{LS} > \sigma_{GS}$, and the contact angle is $90^\circ \leq \theta \leq 180^\circ$. In this case, the cohesive forces of the liquid are stronger than the adhesive forces to the solid surface, and the liquid tends to bead-up (Figure 2.2).

It is also possible for areas with different wetting preferences to be present on a solid surface. This is referred to as fractional wettability and it is explained by the fact that the internal surface of reservoir rock is composed of many minerals with different surface chemistries and adsorption properties. Names such as heterogeneous, spotted and dalmation wettability have been used to define the fractional wettability of some reservoir rocks (Brown and Fatt 1956). A specific case of fractional wettability was defined by Salathiel (1973) as mixed wettability. Here, the oil-wet surfaces form continuous paths throughout the larger pores and the smaller pores remain water-wet and contain no oil.

Thus, a water-flood could displace more of the oil because it forms thin continuous films on the rock surface with small but finite conductivity even at low oil saturations. In these types of systems the oil saturation remaining after water flooding is less than that for water-wet or oil-wet reservoirs. The main difference between mixed and fractional wettability is that the latter implies neither specific locations for the oil-wet surfaces nor continuous oil-wet paths.

The wettability of gas and petroleum reservoirs spans the entire spectrum from water to oil-wet. Treiber and Owens (1972) evaluated the wettability of 30 sandstone and 25 carbonate reservoirs. They did it by measuring contact angles at reservoir temperatures using oil reservoir samples and synthetic brine. Their results showed that 27% of the reservoirs were preferentially water-wet, 66% were preferentially oil-wet and 6% were neutral wet. The actual wettability depends on many factors such as rock mineralogy, oil and brine composition and reservoir characteristics.

Wettability plays a decisive role on multiphase interactions. It will affect fluid distribution at the pore scale, the amount of residual wetting phase(s), the capillary pressure curve of the system and the displacement of the immiscible phases in the porous medium.

The effect of wettability on liquid accumulation in porous media can be explained by noting the well-established relationship between the residual liquid saturation and the capillary number (Figure 2.3). Here the capillary number is defined as the ratio of viscous forces to capillary forces (Chapter 3, Equation 3.14).

There are several methods to determine the wettability of a solid surface, either quantitatively or qualitatively. The quantitative methods are the contact angle method, the Amott method, the Amott-Harvey method and the combined Amott-USBM method.

The qualitative methods are imbibition rate, microscopic examination, capillary pressure curves and relative permeability/saturation relationship. The combined Amott-USBM method is the most accurate and the most time-consuming. However, all of these methods have been subject to criticism because of discrepancies in measurements from different sources and dates. Therefore, discretion should be used when using data from literature. In this work the contact angle method and imbibition rate tests were used to determine changes in wettability.

2.1.2 Capillary Pressure

Capillary pressure is the pressure difference at the interface of two immiscible fluids. This value depends on the curvature of the interface separating the two fluids with the pressure on the concave side of the interface is higher than that on the convex side.

The capillary pressure (no flowing phases) in a capillary tube of radius r is defined as,

$$P_c = \frac{2 \sigma \cos\theta}{r} \quad (2.2)$$

Here the pressure difference is proportional to the surface tension σ and contact angle θ , and inversely proportional to the radius r of the capillary.

The complexity of a porous medium, such as a reservoir rock, precludes the use of this equation for capillary pressure calculations. Therefore, to establish the relationship between capillary pressure and wetting phase saturation of a porous medium and a liquid wetting phase, laboratory experiments must be performed. In a drainage experiment, the capillary pressure increases with decreasing saturation of the wetting phase. The wetting fluid reached a residual saturation at high capillary pressures as shown in Figure 2.3. If

the wetting phase saturation is now increased by decreasing the saturation, an imbibition capillary pressure curve is obtained.

2.1.3 Permeability

An important flow characteristic of fluids in a porous medium such as hydrocarbons in oil and gas reservoirs, and groundwater in aquifers, is the concept of permeability. Permeability measures the porous medium's ability to transmit fluids.

Fluid flow through a porous medium can be described by Darcy's law which can be written for 1-dimensional flow as,

$$q = \frac{kA}{\mu} \frac{dP}{dx} \quad (2.3)$$

Where k is the permeability, A is the cross sectional area, μ is the viscosity, and dP/dx is the pressure gradient.

Darcy's equation can be applied only for low flow rates where the flow is laminar (Reynolds number less than one) and inertial effects are negligible.

The permeability illustrated in Equation 2.3 is the absolute permeability of the medium. This corresponds to the permeability value when the porous medium is completely saturated by a single phase non-reactive liquid. Deviations from Darcy's law occur due to Knudsen flow and due to inertial flow. At low mean pressures, the mean free path of the gas molecules is about the same size as the pores in the rocks. This results in an increase of gas slippage at the wall of the pores reducing the effect of molecule-wall collisions. It is possible to derive a correction for Knudsen flow from the kinetic theory of gases. This effect is important only for low pressure gas flow in low permeability porous media. In our experiments this condition is never met and so this correction factor does not need to be applied.

For high velocity fluid flow in porous media, as is the case of natural gas reservoirs, Darcy's original equation cannot be applied directly. For Reynolds numbers greater than 1 this non-Darcy flow is described by the Forchheimer equation,

$$-\frac{dP}{dx} = \frac{\mu v}{k} + \beta \rho v^2 \quad (2.4)$$

Where v is the velocity, ρ is the fluid density, and β is the inertia resistance factor (the beta factor).

And Reynolds number is,

$$Re = \rho q d / \mu \quad (2.5)$$

Where q is the specific discharge and d is some length dimension of the porous matrix, often the mean grain diameter.

The first term on the right side of equation 2.4 represents the viscous component of the pressure gradient or the Darcy flow component, and the second term adds the component of the pressure gradient due to inertial-turbulent forces produced when Reynolds numbers are above one and is termed the non-Darcy component. Firoozabadi and Katz (1979) performed studies to better understand the behavior of high-velocity flow through porous media and they showed that the velocity coefficient β decreases linearly with increasing permeability on a log-log scale i.e. $\beta = (1/k)^n$

2.1.3.1 Relative Permeability

The relative permeability term applies when two or more phases flow simultaneously through a porous media. For multiphase flow it will be necessary to know the permeability of each fluid in the presence of other immiscible fluids, or in other words, the relative permeability of each fluid.

Flow rate calculation of each individual phase is performed by using Darcy's law as shown in equation 2.6.

$$q_i = \frac{kk_{ri}A}{\mu_i} \frac{\partial P_i}{\partial x} + \rho_i g \sin\alpha \quad (2.6)$$

Where i represents water, oil or gas; α is angle of inclination with the horizontal, A is the cross sectional area of flow, μ_i , ρ_i and P_i are the viscosity, density and pressure of the i phase and g is gravity. Here, the product of relative permeability of the fluid phase k_{ri} times a selected base permeability k , corresponds to the effective permeability of the phase k_i .

Figure 2.4 illustrates imbibition and drainage relative permeability curves for a two-phase system. Imbibition relative permeability curves are used when a wetting phase displaces the non-wetting phase or a least-wetting phase and drainage relative permeability curves are used when the non-wetting phase displaces the wetting phase in the porous medium.

2.2 PHASE BEHAVIOR OF NEAR CRITICAL FLUIDS

Petroleum reservoirs are distinguished by the mixture-critical temperature relative to the reservoir temperature, T_{res} . Figure 2.5 illustrates the phase envelope of the various types of petroleum reservoir fluids and their corresponding critical points (critical temperature-pressure). The reservoir temperature does not change during production but the reservoir pressure decreases due to removal of hydrocarbons from the reservoir as shown in the Figure 2.6.

The dividing line between black oils and volatile oils (also called near critical oils) is rather arbitrary and the proximity of the reservoir temperature with the critical

temperature will help to define under what category the hydrocarbon mixture falls, but as pointed out by McCain (1990), the dividing line will be the point at which material balance equations begin to have intolerable inaccuracy and at this point the fluid is considered a volatile oil. Contrary to this, the distinction between volatile oils and gas condensate mixtures (also called retrograde gases) is clear and is delimited by the critical point.

Since the hydrocarbon fluids used in the present work are volatile oil mixtures, phase behavior studies previously performed are of special interest not only for volatile oil mixtures but also for near critical gas condensate mixtures. It is assumed that results and concepts achieved for gas condensates can also be applied to volatile oils.

Measured vapor-liquid equilibrium (VLE) and PVT data of multicomponent mixtures in the near-critical region (including the critical point) is very limited in the open literature. Data of this nature is valuable for understanding the characteristics of near-critical fluid phase behavior of complex mixtures and for thermodynamic modeling. In an effort to understand the phase behavior of near-critical reservoir fluid mixtures, Yang et al. (1997) experimentally studied the phase behavior of two highly asymmetric multicomponent mixtures, a ternary mixture of methane–n-butane–n-octane and a naturally occurring reservoir fluid mixture of a Chinese reservoir containing a C₇₊-fraction of about 9.9 mol% (in the range of rich gas condensate/light volatile oil) in the near critical region. By using a high precision PVT apparatus (manufactured by ROP France) they measured the VLE and PVT properties of these mixtures and compared them with the calculated values obtained using the Soave-Redlich-Kwong equation of state (SRK EOS) coupled with conventional quadratic mixing rules. They observed that the calculated bubble/dew point pressure and liquid percentage for the Chinese reservoir

were not satisfactory in the near critical region. Also, their results illustrate that near the critical point the relative volumetric amounts of gas and liquid change rapidly with pressure and temperature. Later, Yan et al. (2001) reported experimental measurements of near-critical phase behavior for five synthetic reservoir fluid mixtures where the C_{7+} fraction ranged from 6.67 to 11.15 mol%. Using constant composition expansion (CCE) in the range of 303 to 433 K, the compressibility factor in the single-phase region, the partial pressure–temperature (P – T) phase envelope, the total molar volume and liquid volume fraction in the two-phase region, and the critical point for each sample were measured.

Recent attempts to understand the behavior of volatile oil reservoirs have been performed using reservoir simulations. Sanni and Gringarten (2008) studied the factors that affect well deliverability in volatile oil reservoirs producing at flowing bottom-hole pressures below the bubble point pressure and evaluated vertical hydraulic fractures and horizontal wells to restore lost productivity caused by “gas blocking”. They modeled an actual well producing at a flowing bottom-hole pressure below the bubble point pressure using a one dimensional single well compositional simulator. Their results showed that the main factors mitigating well productivity of volatile oil reservoirs producing below the bubble point pressure are: end point relative permeability of the oil phase and fluid composition. Also they showed that contrary to what happens above the bubble point pressure, where productivity of volatile oil is controlled by viscosity, below the bubble point pressure productivity is controlled by fluid saturation. They observed that below the bubble point pressure, high gas saturation causes a relatively larger reduction in the productivity index of highly volatile oil reservoirs compared to the less volatile oil

reservoirs. The volatility of the hydrocarbon mixture is directly proportional to the amount of intermediate carbon number molecules (C_3 to C_6).

Sharifi and Ahmadi (2009) compared different well testing methods for volatile oil reservoirs. They claim that the two-phase pseudo-pressure method has good accuracy for the prediction of true permeability and mechanical skin on volatile and highly volatile oil reservoirs producing below bubble point. In their simulations, indication of a low liquid saturation zone produced by velocity stripping phenomena near wellbore was not observed.

2.2.1 Volatile oil reservoirs

A volatile oil reservoir is defined as a reservoir in which the reservoir temperature lies to the left of the critical point of the reservoir fluid (as previously shown in Figure 2.5). Volatile oils are also called high-shrinkage crude oils and near-critical oils. A phase diagram for volatile oil is shown in Figure 2.6. Volatile oils contain relatively fewer high carbon number molecules (C_{7+}) and more intermediate carbon number molecules (C_3 to C_6) compared to black oils. Table 2.1 shows the composition of the volatile oil, gas condensate and black oil illustrated in Figure 2.5

As one might expect, as the reservoir pressure decreases below its bubble point, a gas phase forms as small molecules vaporize from the liquid phase. High amounts of gas are formed with small pressure drops causing high liquid shrinkage immediately below the bubble point. This associated gas is very rich and behaves as a gas condensate releasing more liquid while expanding. The initial producing gas-oil ratio (GOR) for volatile oils is in the range of 2000 to 3300 scf/STB and the stock-tank oil gravity is approximately 40° API or higher and both increase during production while reservoir

pressure drops (McCain 1990). Table 2.2 summarizes some other definitions for volatile oil found in the literature.

2.2.2 Gas blocking and productivity decline in volatile oil reservoirs

In volatile oil reservoirs, when the bottom-hole pressure (BHP) falls below the bubble point pressure, the formation of a second phase (the gas phase) occurs in the near wellbore area, resulting in multiphase flow. Away from the well where the pressure is above the bubble point only the liquid phase (undersaturated oil) is present.

Three main regions can be identified in the reservoir as we move away from the well as illustrated in Figure 2.7. Region 1 is generated as the bottom-hole pressure falls below the bubble point pressure and the volume of gas liberated is high enough to exceed the residual gas saturation so that gas can flow. Hence, in this region near the wellbore, multiphase flow (gas and liquid) occurs. Region 2 follows region 1 and this is where the pressure first drops below the bubble point pressure, where the gas bubbles begin to form, the volume of gas liberated in this region is below the critical gas saturation resulting an immobile gas phase. In region 2 only the liquid phase flows. Finally away from the well, region 3 is where the pressure in the reservoir exceeds the bubble point and volatile oil exists only as mobile liquid phase. This region identification is similar to that for gas condensate reservoirs with the only difference that phases are reversed. It has been claimed that for gas condensate reservoirs there exists a fourth region in the very near vicinity of the well, where low interfacial tensions at high rates yield a decrease of liquid saturation and an increase of gas relative permeability. The increase in mobility of this zone has been called “velocity stripping” and its existence has been suggested from the results of laboratory core flood experiments and numerical simulations (Robert Mott, Cable, and Spearing 1999; Gringarten et al. 2000). However, these results have been

viewed with caution and for the case of volatile oil reservoirs Sharifi and M. Ahmadi (2009) reported no observation of this zone in either the saturation distribution or in the well test analysis.

Hence, the presence of two immiscible gas and liquid phases in the pores of the near-wellbore area, results in a reduction in the liquid saturation which in turns decreases the oil relative permeability causing lower mobility of the oil phase and liquid trapping. This phenomenon has been called "gas blocking". The wetting state of the reservoir rock will also have a significant impact on the liquid trapping caused by "gas blocking" since capillary pressure depends on the contact angle of the wetting phase. (G-Q Tang and Firoozabadi 2000e) show that for gas-liquid systems, high liquid fractions can be held by the porous media if it is strongly liquid wet. This results in low mobility of the liquid phase leading to lower oil production rates.

Thus, in volatile oil wells producing below the bubble point pressure, the formation of two fluid phases near the wellbore negatively impacts the well deliverability resulting in a decline in the well productivity. The degree of liquid trapping will depend on many factors such as fluid properties, rock characteristics, pressure gradients and production rates. Sanni and Gingarten (2008) claim that among the factors that affect well deliverability in volatile oil reservoirs producing below the bubble point pressure are the end point relative permeability of the oil phase and the fluid composition.

Similar to the phenomena described above is the behavior of gas-condensate reservoirs below the dew point where the liquid condensate phase accumulates around the well and reduces the mobility of gas (Afidick et al. 1994). This building up of the liquid condensate near the wellbore is known as "condensate banking" and leads to a reduction in gas relative permeability and loss in well productivity. Consequently, this phenomenon

is known as "condensate blocking" and as pointed by Ayyalasomayajula et al. (2005) this has been well documented for several fields and theoretical studies.

How sensitive a reservoir is to any of these phenomena and how they influence the production rate, depends on several factors. Some of these are: phase behavior, flow regime, interfacial forces between fluids, capillary number, reservoir heterogeneity, basic rock and fluid properties, wettability, gravitational forces and well type (well inclination, fractured or non-fractured).

2.3 STUDIES ON RELATIVE PERMEABILITY AND CRITICAL SATURATION FOR NEAR CRITICAL FLUIDS IN POROUS MEDIA

For near critical reservoir fluids the reduction in gas and oil permeability due to gas or condensate blocking (liquid saturation for two phase flow regime) have led to an extensive investigation for an accurate model for predicting gas and oil/condensate relative permeabilities. The gas and liquid relative permeabilities and the liquid residual (or critical) saturation are key parameters to evaluate the right strategy for recovery of hydrocarbons.

In the near wellbore area, where two phase flow is occurring, the physical properties of gas and oil phase are very similar, the pressure gradients in both flowing phases are large and the interfacial tension between oil and gas is low. Conventionally, relative permeability functions are used to describe multiphase flow in this region. Relative permeabilities are sensitive to flow regime (rates), liquid saturation and interfacial tension. Capillary number and non-Darcy effects must be considered in modeling of gas and oil/condensate flows. Relative permeabilities are rate sensitive and increase with increasing capillary number and are reduced by inertial, or non-Darcy, flow effects.

The best way to experimentally determine gas and oil/condensate relative permeabilities is by using a steady-state method because the two phase flow near the wellbore is essentially a steady-state flow process. Ham and Eilerts (1967) reported one of the earliest laboratory measurements of two phase flow of gas condensates and to evaluate effects of condensate saturation on the mobility of gas. The fluid system used was nitrogen and a separator liquid from a Gulf Coast condensate and the cores used were consolidated sandstone and low-permeability limestone. They showed that relative mobility and liquid-vapor volume ratio depend on pressure, saturation and slightly on velocity. They also showed that there is a minimum saturation (critical saturation) at which two phase flow begins, which is dependent on the porous medium, the pressure gradient and the fluid velocity.

For the case of gas condensate wells producing below the dew point, Gravier et al. (1986), Kalaydjian et al. (1996), and Li and Firoozabadi (2000) have shown experimentally that the critical condensate saturation ranges from 20-80%. Kalaydjian, Bourbiaux, and Lombard (1996) also showed that increasing the IFT increases critical liquid saturation and that critical condensate saturation is related to initial water saturation, keeping constant the total critical liquid saturation. Ali et al. (1997) indicated that the developed saturation in the region immediate to the wellbore is a function of the relative permeabilities, the characteristics of the rock, the characteristics of the fluid phase behavior and the degree of pressure drawdown, which is related to the rates of the fluid phases. Wang and Mohanty (1999) showed that the critical saturation at which liquid condensate flows is a function of pore geometry, water saturation and interfacial tension. Their results, obtained by using two structural pore-network models, indicated

that critical saturation reduces as connate water saturation increases and the gas-condensate interfacial tension decreases.

Thus, the effect of interfacial tension (IFT) on relative permeability has been intensively studied. Asar and Handy (1988) experimentally proved that the curvatures of the relative permeability curves approach to linearity and the irreducible gas and liquid saturations approach to zero as IFT decreases i.e. the fluids approach miscible conditions. They also observed that oil relative permeability decreases faster than the gas relative permeability with an increase in IFT. For low IFT values, less than 0.05mN/m, Haniff and Ali (1990) observed a significant reduction in residual saturation and improved flow rates for a methane-propane gas condensate system. They claim that below this IFT value, the capillary forces become negligible and a first order transition takes place, thus gravitational forces become significant.

Henderson et al. (1998) studied the steady-state relative permeability values over a wide range of condensate-to-gas ratios (CGR) while changing velocity and IFT. They did this for gas condensate fluids using sandstone cores in high pressure experiments. Their results showed that the relative permeability of both phases proved sensitive to flow rate and IFT, increasing with an increase in flow rate and decreasing with higher IFT values. All their experiments were conducted with Reynolds number indicating that flow was laminar. Hence, the observed effect of flow rate was contrary to what happens at non-Darcy flow, where the effective permeability decreases with increasing flow rate.

Blom et al. (2000) used a methanol/n-hexane mixture as the fluid system that exhibited a critical point at ambient conditions and their experimental results show a strong dependence of relative permeability on interfacial tension and superficial velocity, as well as a clear trend from curved relative permeability functions to straight lines with

increasing superficial velocity and capillary number, and decreasing IFT. They claim that near-miscible relative permeability functions come into play in the vicinity of the well bore, contrary to what happens if the relative permeability is a function of only IFT; and that capillary-number dependence of relative permeability is not the same for the wetting and non-wetting phase, the latter being affected at lower values of capillary number.

Mott et al. (2000) studied the effect of capillary number and inertial effects on relative permeabilities at high flow rates in steady-state gas-condensate core flood experiments. They observed that gas relative permeability increases with velocity at fixed IFT and decreases with velocity due to inertial flow at fixed capillary numbers.

Du et al. (2000) and Al-Anazi (2003) observed in laboratory core floods that condensate dropout can reduce the relative permeability by an order of magnitude and even more in the presence of high water saturation.

Pope et al. (2000) presented a relative permeability model for gas and liquid relative permeabilities as a function of capillary number where the relative permeability of each phase is calculated by interpolating between the measured value at low capillary number and a straight line corresponding to a very high capillary number. In their model the residual saturation of each phase is modeled as a function of trapping number. Bang et al. (2006) tested this model for gas condensate systems with the data gathered from their own experiments and from the literature. Their results showed that gas and oil relative permeabilities have a strong dependence on capillary numbers and the model adequately captures this dependence for both limestones and sandstone cores.

Kumar (2006) experimentally measured gas and condensate relative permeabilities over a wide range of capillary numbers (from 10^{-6} to 10^{-4}) for sandstone

and limestone rocks. The author expressed the relative permeability as a function of capillary number and k_{rg}/k_{ro} ratio and for capillary numbers higher than 10^{-4} a significant increase in relative permeability was observed. However, in this study the effects of non-Darcy flow were neglected and these effects can be significant for the high flow rates that were used to achieve high capillary numbers.

App and Burger (2009) addressed experimental measurements of relative permeabilities for a rich gas-condensate system using a live reservoir fluid. They developed correlations for gas and condensate relative permeabilities as function of capillary number and they observed that gas relative permeability increased around 20-fold from the low -to high-capillary-number flow regime.

2.4 PROPOSED SOLUTIONS TO IMPROVE OIL AND GAS PRODUCTION

To restore oil and gas production rates, after a decline due to "gas blocking" or "condensate blocking" several methods have been proposed. Changing the phase behavior of the volatile oil/gas condensate fluid or reducing the pressure drawdown and maintaining pressure above the bubble/dew point is one solution. Some other techniques are: gas re-injection, hydraulic fracturing, and volatile solvent injection (i.e. methanol).

Injection of undersaturated gas has been used to improve recovery from volatile oil reservoirs due to its efficiency for hydrocarbon vaporization. Thiebot and Sakthikumar (1991) suggested that injecting methane and nitrogen in a volatile oil reservoir can lead to an improvement in recovery efficiency. Their experiments on different outcrop quarries of the Parisian basin with different permeabilities showed fast and complete recoveries of light and intermediate components and appreciable amounts of heavy hydrocarbons by injection of these gases. As expected, methane recovered more of the heavy components than nitrogen.

Sanni and Gingarten (2008) modeled an actual volatile oil well producing at flowing bottomhole pressure below the bubble point pressure. Their one-dimensional single well compositional reservoir simulation with velocity dependent relative permeabilities functions of capillary number (N_c) and Forchheimer parameter (λ) proved that with *hydraulic fractures* and *horizontal wells* the impairment in productivity due to "gas blocking" can be lessened. They suggested that both should be employed in the early life of the well in order to delay the time when reservoir pressure falls below the bubble point pressure and improve ultimate recovery.

Volatile solvent injection has been used to mitigate the damage caused by condensate or water blocking in well deliverability. Du et al. (2000), Walker (2000) and Al-Anazi (2003) used methanol as the volatile solvent and experimentally observed that after solvent treatment the oil and gas relative permeability increases for a finite time period. The efficiency of this treatment is due to removal of condensate from the pores by miscible displacement. Thus, in the presence of high water saturation the treatment was more effective since the additional damage caused by water blocking was also eliminated. However, despite the benefit of possible permanent water removal, producing below the dew point causes the condensate to reform. Thus, in the present work the use of volatile solvents to deliver the intended chemical treatment follows the gains observed for condensate (oil phase) and water removal. The next section explains the objectives of the chemical treatment used in this research.

2.5 FLUORINATED TREATMENT SOLUTION TO ALTER WETTABILITY

The use of chemical treatments to modify the wettability of rocks in the near wellbore region from strongly water-wet or oil-wet to neutral wet has been studied for gas condensate wells. This treatment method could provide a long-term solution to the

problem of “gas blocking” in volatile oil wells producing below the bubble point pressure. Wettability alteration to intermediate or neutral wet decreases the capillary pressure that is holding the wetting (usually liquid) phases in the pore space, and reduces the total liquid saturation (oil + water) in the near wellbore region. The near wellbore region has a dominant influence on the productivity of non-fractured wells. Such treatments should also increase the mobility and recovery of oil/condensate from the reservoirs. The dependence of residual oil saturation on the wettability has been recognized since the early 90's. Jadhunandan and Morrow (1995), Owolabi and Watson (1993) and Chen et al. (2004) showed that a minimum for oil saturation is found when surface wettability is changed to intermediate or neutral-wet. Figure 2.8 shows the residual oil saturation (S_{or}) versus wettability index (I_{a-h}) for Berea sandstone. Here the minimum residual oil saturation is found near neutral-wettability. Wettability index varies from -1 (oil-wet) to +1 (water-wet) and 0 corresponds to neutral-wet. The authors measured the wettability index using the Amott-Harvey method.

It is in the last few years that major progress in the chemical alteration of rock wettability has been achieved in gas condensate wells.

Fluorinated chemical treatments have proven their efficacy by using surfactants with a fluorinated group that provide water and oil repellency and a functional group (epoxy, silanol, alkoxy, etc.) that binds to the rock surface for durable wettability alteration. Fluorinated chemistries accomplish this due to the high electronegativity of fluorine which allows fluorinated surfaces to repel both oil and water (as happens in the case of polytetrafluoroethylene (PTFE)). Figure 2.9 illustrates how the surfactant molecules are thought to either physically or chemically adsorb to the rock surface and produce the wettability alteration.

Li and Firoozabadi (2000) examined the alteration of rock wettability from liquid-wetting to intermediate gas-wetting for both gas-water and gas-oil systems. The treatment was conducted with the chemicals FC 754 and FC 722 (from 3M Corp.) at 24°C. The results showed irreversible changes in wetting in Berea and in chalk cores.

Seeking to make this process feasible for industry use, Tang and Firoozabadi (2000) looked for additional types of surfactants. Two polymers, FC-722 and FC-759, were studied; FC-759 is soluble in water and is 20 times less expensive than FC-722. The results demonstrated a significant increase in liquid-phase relative permeability for both chemicals. Because of the very high liquid mobility and reduced liquid saturation, the gas mobility also increased for a fixed pressure drop. Liquid injectivity tests revealed that the liquid-phase mobility increased significantly when the wettability of rocks was altered from strong liquid-wetting to intermediate gas-wetting. These results were effective for reservoirs at 90°C.

For high temperature gas-condensate reservoirs, around 130-150°C, Fahes and Firoozabadi (2005), proposed the use the chemicals 11-12P (from 3M). They altered wettability from liquid-wetting to intermediate gas-wetting at high reservoir temperatures.

Liu et al. (2006) enhanced gas productivity in real reservoir rock from the Dongpu gas-condensate reservoir that had a permeability of around 0.1 md. They used the use of chemical WA12, which is thermally stable at a temperature of 170°C, and is effective at high salinity (70,000 ppm TDS).

Surfactants in a methanol-water solvent mixture were evaluated to treat cores under reservoir conditions by Kumar et al. (2006). Several fluorosurfactants were evaluated and they were found to significantly improve the relative permeabilities of gas

and condensate after chemical treatment in both Berea and reservoir sandstones. The authors showed that a new nonionic polymeric fluoro-surfactant, FC4430, made also by 3M, gave the most positive results. The steady state gas and condensate relative permeabilities at 145 °F, 250 °F and 275 °F using different synthetic gas-condensate fluids increased by a factor on the order of 2. Their results proved the effectiveness of this method at high temperature and high flow rates with no connate water saturation..

Noh and Firoozabadi (2006) studied the effect of wettability on the inertial flow coefficient, β (Forchheimer equation 2.4), for two-phase gas-liquid flow. They concluded that another benefit from wettability alteration is the significant decrease in the high velocity coefficient in two-phase flow. The coefficient was measured as a function of liquid relative permeability. Results showed that when the liquid is strongly wetting, the high velocity coefficient increases some 270 fold in water-gas two phase flow. Its increase is much less pronounced when the wettability is altered from strongly liquid wetting to intermediate gas-wetting.

Forty one chemicals for altering the wettability of rocks from liquid wetting to gas wetting for the remediation of the damage caused by water blocking in gas wells were evaluated by Panga et al. (2006, 2007). The authors conducted three types of tests to evaluate the performance of these chemicals; contact angle measurements, imbibition tests and core flow tests. Only two chemicals, A5 and A6, were selected for core flood test and only the former showed a good uniform wettability alteration and improved water cleanup after treatment.

Bang et. al. (2008, 2009) moved to more complicated systems that included placing connate water in the core followed by a subsequent condensate flood. The treatment improved the gas and condensate relative permeabilities by a factor that ranged

from 2 to 4 times the original relative permeabilities on liquid blocked outcrop and reservoir sandstone rocks.

Ahmadi et al. (2010) performed a two-step chemical treatment to modify the wettability of Texas cream limestone (TCL) cores and measured the gas relative permeability values before and after treatment for a gas condensate system. A special amine primer was used to promote adsorption of the fluorinated molecules on the rock surface. Thus, the gas relative permeability increased about 80% after treatment compared to that before treatment. A considerable increase in gas relative permeability was also observed during unsteady displacement of water by methane. The authors performed this with high pressure high temperature (HPHT) core flood experiments at 175°F and 275°F.

Butler et.al (2009) reported the results for the first field trial using a fluorinated chemical treatment for a gas condensate well. After stimulation and seven months of production the well-produced an average of 3 barrels per day of condensate. Previously the zone had produced no condensate.

For volatile oil reservoirs, Bang (2007) performed the first core flood experiment using a volatile oil synthetic mixture in sandstone at low temperature. He showed that the oil and gas relative permeability increased by a factor of 3. However, no further work was done to prove the efficacy of this method for these types of reservoirs.

2.5.1 Fluorinated surfactants

Surfactants are surface active agents with the ability of lowering the surface tension of a liquid (liquid-gas interface), the interfacial tension between two liquids, or the interfacial between a liquid and a solid even at low concentrations. Their characteristic structure is usually amphiphilic, containing hydrophobic groups (the tails)

and hydrophilic groups (the heads). The surface tension or interfacial tension reduction is achieved by adsorbing at the liquid-gas, liquid-liquid or solid-liquid interface where molecules orient with the hydrophobic group away from the aqueous phase and the hydrophilic group towards the aqueous phase. The hydrophobic part is usually a hydrocarbon group, but surfactants containing oxygen, nitrogen, sulfur, silicon, and/or halogens are also used; the hydrophilic group is an ionic or highly polar group. Surfactants are classified based on the hydrophilic group (Rosen 2004) . Surfactants are classified as:

- Anionic. The hydrophilic part has a negative charge
- Cationic. The hydrophilic part has a positive charge
- Amphoteric / zwitterionic. Negative and positive charge may be present in the hydrophilic part; they can be anionic, cationic or nonionic in solution, depending on the acidity or pH of the aqueous phase.
- Nonionic. The hydrophilic part has no apparent ionic charge.

Fluorinated surfactants have fluorine atoms in the hydrophobic part of the molecule. The number of fluorine atoms present and their position in the surfactant's tail affect the properties of the surfactant. Fluorinated surfactants are classified as:

- Perfluorinated. All hydrogen atoms in the hydrophobic segment have been replaced by fluorine.
- Partially fluorinated. Hydrogen and fluorine atoms are present in the hydrophobic segment.

The hydrophobic part of fluorinated surfactants not only repels water but also repels oil. The fluorine atoms present in the molecule reduce the tendency for polarization of the surfactants' fluorinated molecular surface. This reduces the

susceptibility to London dispersion forces, which contributes to lipophilicity. Hence, attractive interactions resulting from fleeting dipoles are mitigated compared to hydrocarbon surfactants. The high stability of carbon-fluorine bond allows the molecule to resist hostile conditions such as high temperature and the presence of acids, bases, and reducing and oxidizing agents. Also, these molecules exhibit surface activity in organic systems.

Therefore, fluorinated surfactants perform much better as surface active agents compared to their hydrocarbon counterparts. Fluorinated surfactants can lower the surface tension of aqueous systems to below 20mN/m and prove effective at low concentrations, i.e. 10 ppm could drop the water surface tension to 40 mN/m (Kissa 2001).

Table 2.1 Composition of Gas Condensate, Volatile Oil and Black Oil mixture illustrated in Figure 2.5 (Pedersen 2007)

Component	Gas Condensate	Volatile Oil	Black Oil
	mole %	mole %	mole %
N ₂	0.53	0.46	0.04
CO ₂	3.3	3.63	0.69
C ₁	72.98	62.36	39.24
C ₂	7.68	8.9	1.59
C ₃	4.1	5.31	0.25
iC ₄	0.7	0.92	0.11
nC ₄	1.42	2.08	0.1
iC ₅	0.54	0.73	0.11
nC ₅	0.67	0.85	0.03
C ₆	0.85	1.05	0.2
C ₇	1.33	1.85	0.69
C ₈	1.33	1.75	1.31
C ₉	0.78	1.4	0.75
C ₁₀₊	3.79	8.71	54.89

Table 2.2 Volatile oil definitions found in literature

Author	Definition	API	GOR	Bo
Moses 1986	High shrinkage immediately below bubble point pressure. Shrinkage can go as high as 45%	$\geq 40^\circ$	2,000 - 3,500	≥ 2.0
Ahmed 1989	Higher gas production compared to black oil for same pressure drop. Greenish to orange color	45° to 55°	2,000 - 3,500	≈ 2.0
McCain 1990	Relatively fewer heavy molecules and more intermediates. Brown, orange or green color	$\geq 40^\circ$	2,000 - 3,300	≥ 2.0
Whitson et al. 2000	High GOR and high shrinkage to 50%	$\geq 35^\circ$	1,000 to 3,000	> 1.5

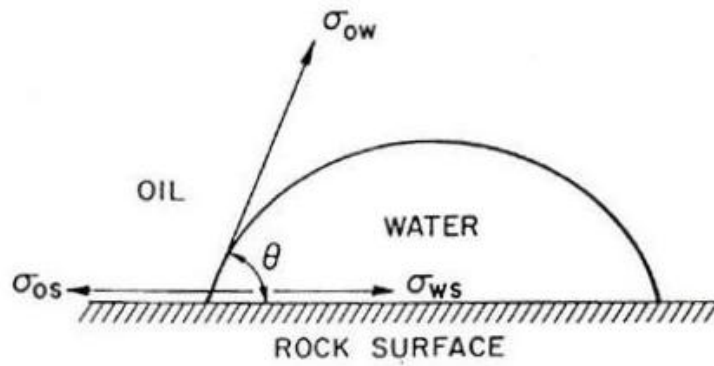


Figure 2.1 Wettability representation for an oil-water-solid system (Peters)

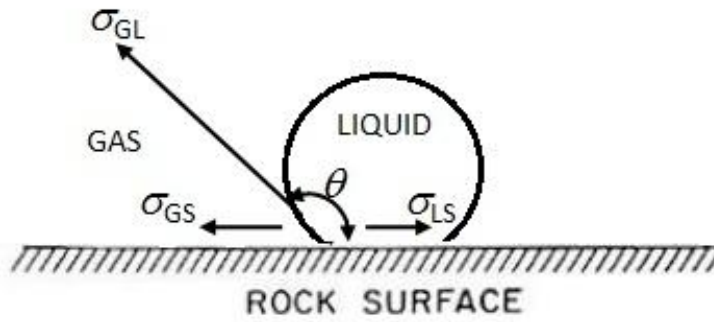


Figure 2.2 Wettability representation for a gas-liquid system

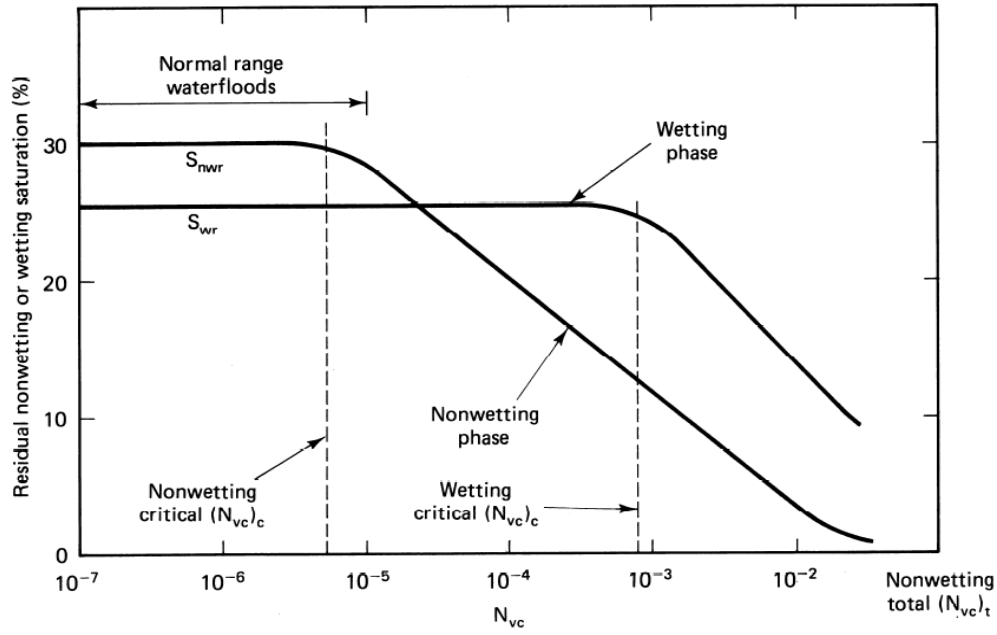


Figure 2.3 Schematic for capillary desaturation curves. Correlation of residual wetting and non-wetting phase saturation with respect to capillary number (Lake 1989)

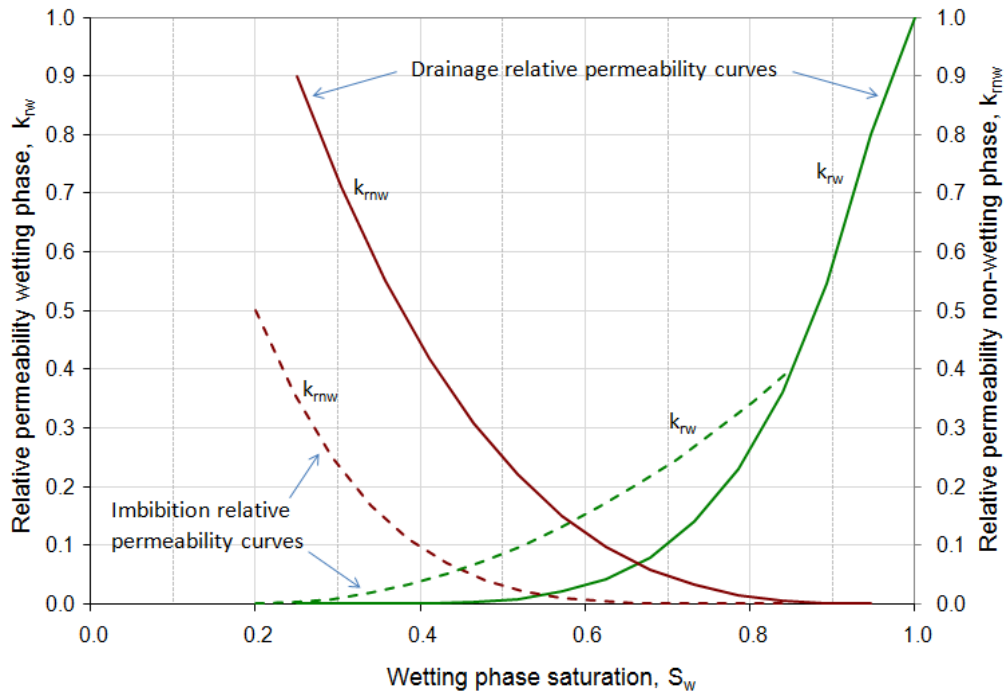


Figure 2.4 Imbibition and drainage relative permeability curves

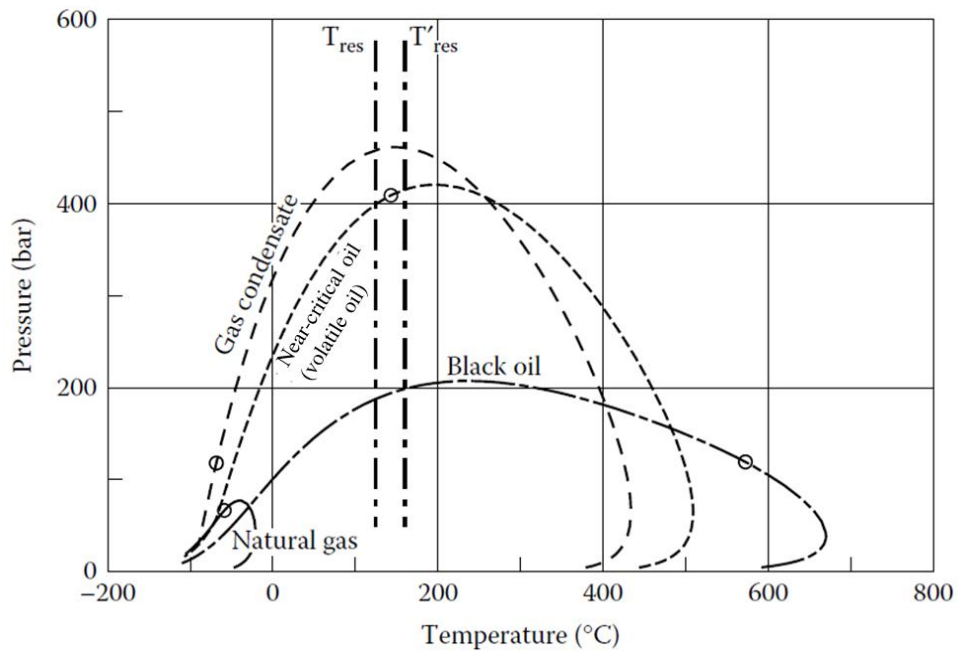


Figure 2.5 Phase envelope of various types of reservoir fluids, (Pedersen 2007)

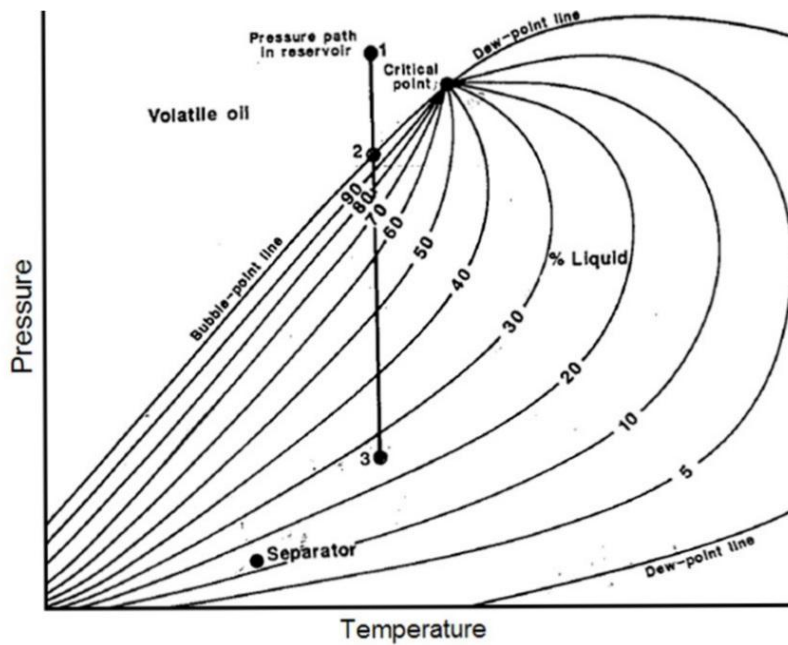


Figure 2.6 Phase diagram of a typical volatile oil with line of isothermal reduction of reservoir pressure, 123, and surface separator conditions (McCain 1990)

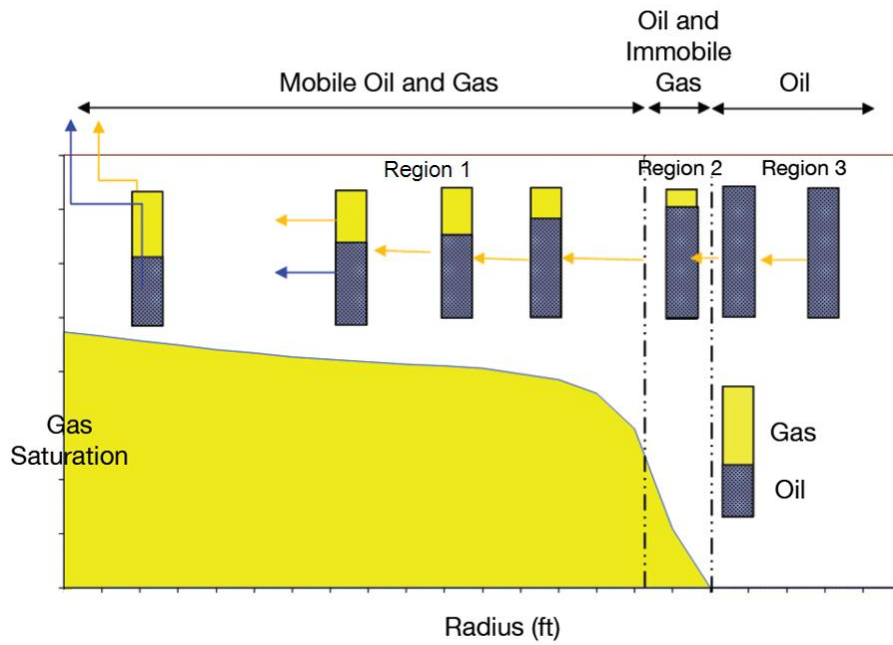


Figure 2.7 Gas saturation by region in a volatile oil well with BHP below the bubble point pressure (Sharifi and Ahmadi 2009)

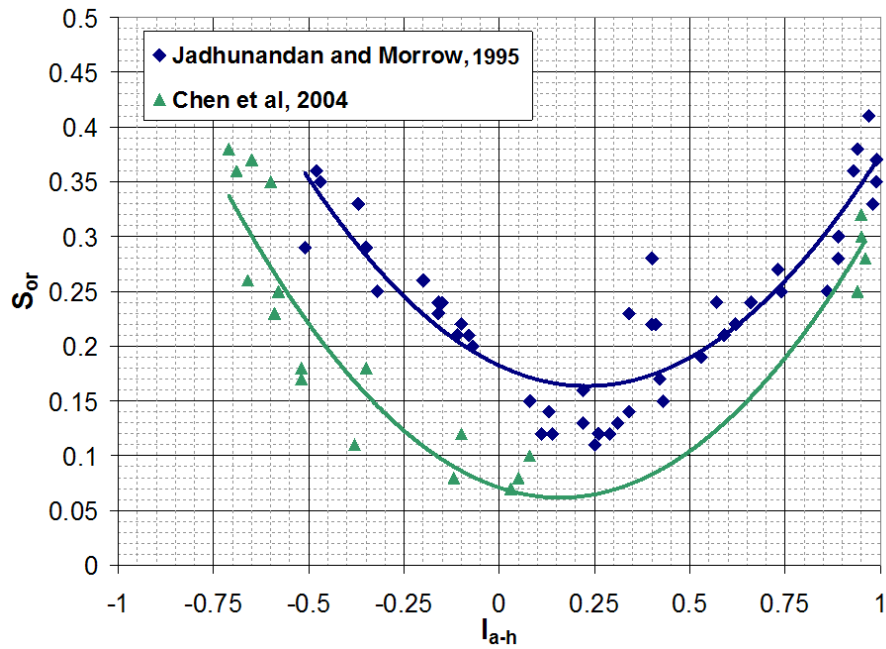


Figure 2.8 Residual oil saturation S_{or} variation with respect to wettability index I_{a-h} for Berea sandstone

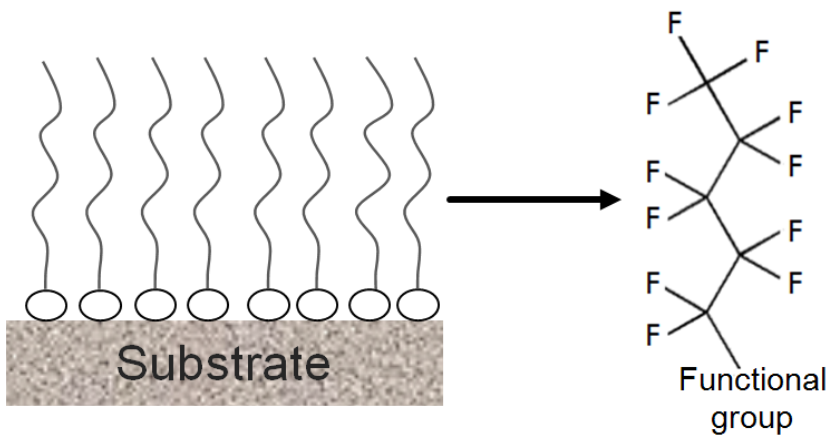


Figure 2.9 Schematic of fluorinated surfactant adsorbed on the rock surface and molecule representation

Chapter 3: Coreflood Experimental Apparatus, Procedures, and Calculations

To assess the effectiveness of a given treatment formulation, corefloods were conducted to measure changes in relative permeability to oil and gas before and after treatment. A dynamic fluid flashing method was used to simulate gas accumulation (gas blocking) in the near wellbore region shown in Figure 1.5. A schematic of the experimental apparatus is shown in Figure 3.1. The relative permeability is determined by measuring the steady-state pressure drop along the length of the core before and after treatment and using these values to calculate the relative permeabilities using Darcy's law.

This chapter describes in detail the core flood experimental apparatus and its components, as well as the experimental procedures and the calculations used for interpretation of the experimental results.

3.1 COREFLOOD EXPERIMENTAL APPARATUS

The core flood experimental apparatus used for this research is a high-temperature high-pressure (HTHP) apparatus. Figure 3.1 shows a schematic of the core flood experimental apparatus. Figure 3.2 and Figure 3.3 show the two main parts of the actual experimental set up. The former shows the equipment that simulates the reservoir conditions and the latter the equipment for controlling, measuring, and recording data such as temperature, pressure and effluent rates (volumetric and mass).

The equipment used to represent the reservoir conditions, specifically near the wellbore, consists of a core holder, back pressure regulators (BPRs), accumulators and oven. The first three components are placed inside the oven where high reservoir

temperatures can be achieved (up to 350°F). The core holder holds the core in place for fluid flow and also applies a confining pressure to the core (equivalent to the overburden pressure in a reservoir). This confining pressure is typically set about 1000 psi higher than the pressure of the fluids in the core. The core is kept in a vertical position to avoid gravity segregation during multiphase flow. The accumulators contain the fluids that will be injected through the core. A back pressure regulator (BPR-1) upstream from the core maintains a pressure above the core pressure and for near critical fluids a minimum of 500 psi above the bubble/dew point to ensure injection of a single phase fluid. The downstream back pressure regulator (BPR-2) regulates the pressure in the core and typically simulates the flowing bottom-hole pressure in a producing well, the pressure is set below the bubble point to simulate gas blocking and multiphase flow near the well bore. This BPR arrangement allows a dynamic flashing of the volatile oil downstream of BPR-1. Thus after the flash the hydrocarbons separate into two equilibrium phases (liquid and gas) at the specified BPR-2 pressure and oven temperature. The two phases flow through the core and after reaching the corresponding critical gas and liquid saturations they both begin to flow reaching a steady state condition. All of the components of the HTHP core flood apparatus are connected with stainless-steel tubing and valves to conduct and control the fluid flow at high pressure and temperature.

A dual-cylinder syringe pump is used to deliver the fluid at high pressure and constant rate through the core. The temperature in the oven is measured and controlled with a thermocouple that has an accuracy of $\pm 0.1^\circ\text{F}$. The pressure is measured with differential pressure transducers and for some experiments the mass of liquid effluent was measured with a digital balance. Pressure, temperature and effluent mass are displayed in real time and logged using Labview.

A description and specifications for each of the major components used in the coreflood experimental set up is given below.

3.1.1 Accumulators

Stainless steel accumulators with capacities of 1,000 cc, 1,500 cc and 2,000 cc. were used for these experiments. They were rated for pressures up to 5,000 psi at temperatures of 350°F. Pistons made from PEEK, with O-rings or Teflon spring loaded seals, were used to displace the injected fluids using water as the driving fluid.

3.1.2 Back pressure regulators

Dome loaded back pressure regulators (BPRs), model BPR-50 and BPR-100 from Temco Inc. were used. These were rated for 5,000 psi and 10,000 psi respectively and use a diaphragm to separate the dome from the lower section where the fluid flows through. The domes were pressurized with nitrogen. A BPR was located both upstream (BPR-1) and downstream (BPR-2) of the core as can be seen in Figure 3.1. The upstream BPR-1 was used to control the pressure of the fluid in the accumulator and allow its subsequent flash. The downstream BPR-2 was used to control the core pressure, defining the final state of the fluids after the flash.

3.1.3 Balances

Analytical and top-loading digital balances from Acculab, Mettler and Ohaus were used for these experiments. The balances were employed either for measuring the mass of liquid effluent, or for measuring the mass of components for the synthetic hydrocarbon mixtures (e.g. volatile oil), brines, chemical treatments, and liquid effluent mass. The mass of the liquid effluent was measured to provide evidence that the injected volatile oil was single-phase and thus at equilibrium as it was injected through the core.

The synthetic hydrocarbon mixtures were prepared on mass base resulting from a conversion from the desired molar composition.

3.1.4 Computer equipment and software

A Dell computer model PSW390 with processor Intel® Core™ 2 with Labview 8.0 software was used to display and record the data obtained from the core flood experiments. This data included BPR dome pressures, core inlet and outlet pressure, pressure drop across the cores (if necessary), confining pressure, pump pressure, pump flow rate, temperature, and effluent mass. The software Quizix pumpworks was used to operate the corresponding Quizix pump; e.g. defining operating mode, setting flow rates, adjusting pump parameters, etc.

3.1.5 Core holders

Hassler-type core holders were used for these experiments. Depending on the type of experiment either a stainless steel or an aluminum core holder was selected.

3.1.5.1 Stainless steel core holder

Stainless steel (SS-316) Hassler type core holders manufactured by Phoenix Instruments were used for the majority of the experiments. These core holders were rated for pressures up to 3,000 psi and temperatures up to 400°F. They can accommodate cores of one inch in diameter and up to 8.0 inches in length. A Viton sleeve was used to keep the core in place and isolated from the confining fluid. The core holders have three pressure taps at 2 inch intervals so that the pressure drop can be measured at multiple intervals.

3.1.5.2 Aluminum core holder

An Aluminum core holder wrapped with carbon fiber composite (model FCHR-1.0) from Temco Inc. was used for core flood experiments where x-ray CAT scanning was performed. CAT scanning was performed to observe changes in the liquid saturation profile along the core due to chemical treatment. In this core holder the core sample is held in a Viton sleeve by radial confining pressure. The aluminum core holder was rated for pressures up to 7,500 psi and 300°F.

3.1.6 Sample collector

Effluent sampling was performed using sample collectors from Spectrum Chromatography. The sample collector has racks that rotate and collect the sample in vials. An integrated programmable timer was used to set the times of sample collection. Only the liquid effluents were collected, for chemical treatment and volatile oil floods. Sampling allowed observation of effluents color and immiscible liquid or solid phases. Samples were also used for subsequent analysis to measure adsorption and desorption of the fluorinated surfactants.

3.1.7 Oven

Blue M mechanical industrial convection ovens were used for the HTHP coreflood experiments. The dimensions the ovens are 4'x4'x3'. The controller for the oven is a single set point STAT-350 from Lindberg and Blue M. These ovens are rated for temperatures up to 750°F.

3.1.8 Pressure regulators

Swagelok pressure regulator (KHR series) was used to control the confining pressure on the core. This model is rated for 10,000 psi and temperatures up to 212°F.

Tescom pressure regulators were used to control the pressures in the domes of the BPRs. These units are rated for 6,000 psi and 225°F. All the pressure regulators are spring loaded and were kept outside the oven.

3.1.9 Pressure transducers

Two different types of transducers were used based on the type of sensor and are described below.

3.1.9.1 Gauge pressure transducers

Two models of digital gauge pressure transducers were used. One from Mensor (model 2101) and the other from Heise (model ST-2H). The gauges had ranges of either 0 to 5000 psi or 0 – 10,000 psi. These were used to read the pressures of the inlet and outlet of the core, the net confining pressure on the core, and the dome pressure of the BPRs.

3.1.9.2 Differential pressure transducers

Differential pressure transducers were used to measure the pressure differential across the core, and core intervals. A Rosemount model 3051CD was used. They were capable of ranges from 0-3 psi up to 0-300 psi. The range used depended on the expected pressure drop during the flood. The accuracy is of 0.1% of the full range.

3.1.10 Pumps

Four different types of pumps: booster pump, continuous flow syringe pump, hydraulic pump and vacuum pump were used for the various tasks required to perform the HTHP core flood experiments.

3.1.10.1 *Booster pump*

A pneumatic gas booster pump (model DLE75-1) from Maxpro Technologies, Inc. was used to pressurize gases and load them into accumulators.

3.1.10.2 *Continuous flow pump*

A continuous flow dual cylinder pump model QX6000 from Quizix was used to inject the fluids at high pressure and constant rates throughout the core. The pump is rated for flow rate ranges from 0.001 to 3000 cc/hr with an accuracy of 0.1% and a maximum pressure of 6000 psi.

3.1.10.3 *Hydraulic manual pump*

A hydraulic manual pump (model P-39) manufactured by Enerpac was used to inject mineral oil in the annular space of the core holder to provide overburden pressure. The pump is rated for pressures up to 10,000 psi.

3.1.10.4 *Vacuum pump*

Vacuum pump (model 1VSF-10-M100X) from GAST was used to remove air from the accumulators and create negative pressures allowing loading of the synthetic hydrocarbon mixtures liquids before loading the gases. It was also used to induce a vacuum on the core before establishing initial water saturation and for core preparation.

3.1.11 Valves

Several stainless steel valves from Autoclave and HiP were used to control pressures, isolate sections, and set fluid flow paths. The valves were rated for pressures up to 15,000 psi.

3.1.12 Tubing

Stainless steel 1/8 inch diameter tubing was used to for all flow lines; the tubing was rated for pressures up to 10,200 psi.

3.2 EXPERIMENTAL PROCEDURES FOR CORE FLOOD EXPERIMENTS

All the experimental procedures relevant to conducting the HTHP core flood experiments are described in the sections below.

3.2.1 Core and fluid preparation

Before initiating the core floods the core and various fluids used for the experiment are to be prepared for flooding. The procedures used in preparing the core, liquids and gasses for injection, brine, volatile oil, and treatment solution are given in the following sections.

3.2.1.1 Core preparation

Three different types of cores were used for these experiment; Berea sandstone, Torrey Buff sandstone, and Texas cream limestone (TCL). They were prepared for core flood experiments using the following procedure.

Cylindrical cores with dimensions of 1 inch in diameter and 8 inches in length were drilled from an outcrop block. The cores were placed in an oven at 100°C to 130°C overnight to dry. Once the cores were dried, the exact dimensions and the mass of the core were measured and the pore volume and porosity were calculated. The pore volume and porosity were calculated using the grain densities reported in Table 3.1. The core was then wrapped with Teflon tape overlapping half of the strand of tape with each pass. This was followed by adding on a layer of aluminum foil and finally a piece of Teflon

heat-shrink tube. The core was then mounted into a Hassler-type core holder, confining pressure was applied and the core holder placed inside the oven for flooding and heating.

3.2.1.2 Gas, liquid and brine preparation

Fluids such as methane, nitrogen, brine, and solvents were injected during the core flood experiments. All of these, with the exception of brine, were prepared and loaded into accumulators before injection. The preparation procedure for the various fluids varies depending on whether it is a gas or liquid. The preparation procedures are described below.

Gaseous fluids were prepared as follows. First Viton O-rings were placed on the end-caps of the accumulator and a piston with its corresponding O-rings was placed inside the accumulator. In one side of the accumulator, water was poured in and the end-cap was put in place leaving no air in the water side. Next, a vacuum was applied on the gas-side of the accumulator to remove the air inside. After doing this, the accumulator was placed on a top-loading balance and the gaseous fluid(s) was (were) loaded using a booster pump until the desired pressure or mass of gas was reached. Finally, the accumulator loaded with gas was put in the oven for heating if required and injection.

For liquid fluid preparation the desired amount(s) of liquid(s) were weighed using a digital balance. Then, the O-rings were placed in the end-caps and a piston was placed into the accumulator, the liquid mixture was then loaded into the accumulator and the end-cap was placed taking care to bleed out all of the air. Next, the other side of the accumulator was filled with water and the cap screwed on. The loaded accumulator was then put in the oven for heating if required and injection.

To prepare brine a volumetric flask was partially filled with DI water. The mass of salt(s) was (were) weighed out using an analytical balance. The salt(s) was (were) then

poured into the flask and the flask was filled to volume with de-ionized water and mixed using a magnetic stir plate. Then brine was loaded in a burette for injection into the core to establish initial water saturation (S_{wi}). The brine injection procedure is described in more detail later in this chapter. Two types of brines were used for these experiments depending on the core used. Table 3.2 shows the composition of the brine 1, used for Berea sandstone and Torrey-Buff cores, and the composition of brine 2, used for TCL cores. In the formulation of brine 2, Ca^{++} ions were added to avoid dissolution/precipitation of calcium carbonate.

3.2.1.3 Synthetic volatile oil preparation

Five different types of synthetic volatile oil mixtures were used for these experiments. Each of them was specifically designed for different core flood conditions. The compositions of all of the different volatile oil mixtures are shown in Table 3.3.

The synthetic volatile oil preparation was as follows. First Viton O-rings were placed on the end-caps of the accumulator and a piston with Teflon spring loaded seals were placed inside the accumulator. In one side of the accumulator, water was poured in and the end-cap was put in place leaving no air in the water side. Next, a vacuum was applied on the other side of the accumulator to remove the air inside. The liquid components of the synthetic volatile oil mixture (C7+) were measured using a digital balance and then, with the aid of a burette connected to the vacuumed side of the accumulator were loaded into the accumulator. Next, the accumulator was placed on a top-loading balance and the gases were loaded using a booster pump until the desired mass was reached. The accumulator was then placed in the oven and the water side was connected to the Quizix pump. The mixture was heated and pressurized to the

experimental conditions. The accumulator was given a minimum of 16 hours to reach equilibrium. The accumulator was frequently rocked to ensure mixing of the components.

3.2.1.4 Chemical treatment preparation

The chemical treatment solution is made of two parts: the fluorinated surfactant and the solvent(s). The process for surfactant and solvent selection is described in Chapter 4. To prepare the treatment solution the desired amounts of surfactant and solvents are weighed using a digital balance. The components were poured into a beaker and mixed using a magnetic stirrer until complete dissolution of the surfactant was observed. The accumulator was prepared by putting O-rings were in the end-caps and placing a piston the accumulator. The chemical treatment solution was then loaded into one side of the accumulator and an end-cap was placed on making sure that all of the air had bleed out. Then, the other side of the accumulator was filled with water and capped. Finally the chemical treatment solution was placed in an oven for heating.

3.2.2 General experimental procedure for core flood experiments

All core flood experiments performed for this research were conducted in a experimental setup like the one shown in **Error! Reference source not found.** lthough each of the experiments had a particular goal and therefore were slightly different, all of them followed the same basic procedure. The procedure for the core flood experiments, is described below and include: initial gas flood to measure the permeability of the dry core, establishing initial water saturation (S_{wi}), gas flood to measure permeability at S_{wi} , pre-treatment two-phase volatile oil flood, chemical treatment flood, post-treatment two-phase volatile oil flood, and final gas flood to measure the final

permeability of the core after flooding. The specific conditions and procedures for each experiment are described in Appendix A.

3.2.2.1 Initial gas flood to measure gas permeability on dry core

The HTHP core flood apparatus was prepared for flooding as follows; the core was mounted in the core holder, the system was leak tested, it was heated to the experimental temperatures, and the back pressure regulators were set to the desired pressures. The downstream BPR (BPR-2) at the flowing bottom-hole pressure (BHP) and BPR-1 is set at a pressure above BPR-2. The gas flood was then conducted using a dry gas (e.g. methane or nitrogen). The dry gas was flowed through the core until a steady state pressure drop was observed. Multiple flow rates, typically five, were used and the pressure drop across the core for each flow rate was measured and recorded. The absolute gas permeability was calculated using the recorded pressure drops using Darcy's law. In some instances non-Darcy flow was observed in these cases the permeability was calculated using the Forchheimer equation (Equation 2.4) to account for the non-Darcy effects.

3.2.2.2 Establishing initial water saturation

To establish the initial water saturation (S_{wi}) in the core, the desired brine solution was prepared and was loaded into a graduated burette, then one of the following two methods for injection was followed.

For experiments when the brine was injected at room temperature, a vacuum was first applied on the core. A graduated burette loaded with brine was then connected to the core inlet the inlet valve was opened and the desired volume of brine was injected

into the core. The core was shut in for at least 3 hours to allow water the brine to distribute through the core.

For experiments when brine was injected at the experimental temperature a different procedure was used. A sample loop was made of 1/8" OD stainless steel tubing with valves at each end. A vacuum was applied to the loop which was then connected to a burette filled with brine and the desired amount of brine was then allowed to flow into the loop. The loop was pressurized with nitrogen to a pressure about 100-200 psi above the core pressure. The loop was placed in the oven and connected to the core inlet and allowed to heat to the experimental temperature. The coil inlet valve was opened allowing the brine to flow into the core. This was followed by a nitrogen flood to empty the loop and to help distribute brine through the core.

3.2.2.3 Gas flood to measure gas permeability at S_{wi}

A gas flood was conducted after establishing S_{wi} to measure the permeability to gas. The flood was conducted using five flow rates beginning with the highest rate in decreasing order. The highest rate was used first because this provided the highest pressure gradient and would give a more uniform distribution of the brine. The permeability was then calculated following the procedure used for the initial permeability flood taking into account non-Darcy effects when appropriate.

3.2.2.4 Pre-treatment two-phase volatile oil flood

To obtain baseline oil and gas relative permeabilities a flood with volatile oil was conducted. A synthetic volatile oil mixture was made and put in the oven to heat following the procedure previously outlined. The BPR pressures were adjusted if necessary so that BPR-1 set to a pressure that was a minimum of 500 psi above the

bubble point pressure of the synthetic volatile oil and BPR-2 was set at the well bottom-hole pressure. With this configuration the synthetic volatile oil mixture was pumped through BPR-1 as a single phase and was then flashed to the core at BPR-2 pressure. The BPR-2 pressure is below the bubble point so a gas phase forms. Therefore two equilibrium phases now exist, one gas and one liquid. The liquid and gas begin to build up in the core, and, after reaching their critical saturations, pseudo-steady two-phase flow was established. The required time to reach this pseudo-steady state depended on the core permeability, initial water saturation, injection rate, and liquid-gas ratio of the flowing phases. Finally, the steady pressure drop across the core was recorded and oil and gas relative permeabilities were calculated using Darcy's Equation 3.13. For some experiments this flood was performed for more than one flow rate.

3.2.2.5 Chemical treatment flood

The chemical treatment flood was performed by preparing the chemical treatment mixture (procedure explained above) and then injecting the treatment at a rate that provided a residence time in the core of not less than 3 minutes. The treatment was performed at the BHP by by-passing BPR-1, and the volume of injected treatment was between 10 and 20 PVs depending on the type of chemical used. For some experiments, samples of the treatment effluent were collected for further HPLC analysis. The core was shut in for a minimum of 15 hrs following injection.

3.2.2.6 Post-treatment two-phase volatile oil flood

The post-treatment volatile oil flood was conducted following the same procedure and conditions used for the pre-treatment volatile oil flood. The post-treatment oil and gas relative permeabilities were calculated using the steady state pressure drop and was

used to calculate the improvement factor (IF). The improvement factor is defined as the ratio of the post-treatment oil (or gas) relative permeability to the pre-treatment one. The IF was calculated for each of the flow rates used in the volatile oil floods. In experiments when the IF was ≥ 1.5 , another volatile oil flood was conducted to assess the durability of the chemical treatment.

3.2.2.7 Final gas flood to verify gas permeability

Finally, the single phase permeability was measured again with dry gas (nitrogen or methane) to check if the treatment had in any way damaged the core. This final gas flood was performed similarly to the initial gas flood. Gas was injected at the highest rate first until the pressure drop was stable and then the remaining flow rates were run. Because it is impractical to remove all of the liquid hydrocarbons from the core, a final permeability that was within 80% to 100% of the initial permeability was considered evidence that the core had not been damaged. Calculation of the final gas permeability also took into account non-Darcy effects.

3.3 CALCULATIONS

Interpretation of the results obtained with the data gathered from the HPHT core flood experiments requires a series of calculations. Calculation of flow rates, permeabilities, capillary numbers, improvement factors and thermodynamic properties were done. The methodology and assumptions used in making these calculations are given in the following sections.

3.3.1 Flow rate

During the HTHP core flood experiments, the flow rates of the injected fluids through the core were calculated. For the case of injected liquids, all of them were assumed incompressible and the pump flow rate was used as the liquid flow rate in the core. For gas injection the flow rate through the core was greater than the pump rate due to the expansion of gas as it is flashed through BPR-1. Figure 3.4 illustrates the schematic of the gas expansion as the gas passes through BPR-1.

Hence, a mass balance around BPR-1 was performed,

$$m_1 = m_2 \quad (3.1)$$

Where m_1 and m_2 are the mass gas flow rates before and after expansion, and from there the gas rate in the core q_g was calculated as in Equation 3.2;

$$q_g = q_{pump} \frac{\rho_1}{\rho_2} \quad (3.2)$$

Where q_{pump} is the pump flow rate, and ρ_1 and ρ_2 are the densities before and after expansion respectively. Thus the ratio of densities expresses the gas expansion.

For the two-phase volatile oil flood it was necessary to calculate both the gas and oil flow rates inside the core. This is because during injection the volatile oil mixture passes through three different set of conditions. Initially, the volatile oil mixture is above the bubble point pressure and only a single liquid phase exists. Then after passing BPR-1, the fluid goes to a second set of conditions as the pressure drops below the bubble point and the fluid flashes into two-phases; gas and liquid. Thus, two phases flow through the core and the liquid and gas built up in the pores until a critical saturation is reached and the two fluids flow simultaneously developing a pseudo-steady state flow. This set

of conditions is what simulates the two-phase flow in the near wellbore region and mimics the “gas blocking” problem. The third set of conditions is when the two-phase flow passes throughout BPR-2 and flashes again going to atmospheric pressure and room temperature conditions. The core conditions are the conditions of interest and where used to calculate the gas and oil flow rates. Figure 3.5 show a schematic of the mass balance used for this dynamic flash calculation.

The mass balance around BPR-1 is represented as follows,

$$m_1 = m_g + m_o \quad (3.3)$$

Similarly,

$$q_{pump}\rho_1 = q_g\rho_g + q_o\rho_o \quad (3.4)$$

Where m_1 and m_2 are the mass gas flow rates before and after expansion, ρ_1 is the density of the volatile oil before expansion (pressure above bubble point), ρ_g and ρ_o are the densities of gas and oil after expansion (pressure below bubble point) and q_g and q_o are the gas and oil flow rates in the core.

For steady state q_g and q_o can be defined as a function of the gas and oil volumetric fractions V_g and V_o respectively.

$$q_g = q_{core} \frac{V_g}{V_g + V_o} \quad (3.5)$$

$$q_o = q_{core} \frac{V_o}{V_g + V_o} \quad (3.6)$$

Hence, solving for q_o using eq. 3.5 and eq. 3.6 gives,

$$q_o = q_g \frac{V_o}{V_g} \quad (3.7)$$

Substituting eq. 3.7 into eq. 3.4 yields to,

$$q_{pump}\rho_1 = q_g\rho_g + q_g\rho_o\frac{V_o}{V_g} \quad (3.8)$$

Solving for q_g ,

$$q_g = \frac{q_{pump}\rho_1 V_g}{\rho_g V_g + \rho_o V_o} \quad (3.9)$$

And finally following similar solution for q_o ,

$$q_o = \frac{q_{pump}\rho_1 V_o}{\rho_g V_g + \rho_o V_o} \quad (3.10)$$

3.3.2 Absolute and relative permeability

As discussed in Chapter 2, Darcy's equation 2.3 describes the flow in porous media of Newtonian fluids at low velocities, where inertia effects are negligible. For fluids flowing at high velocities the Forchheimer's Equation 2.4 is used because it takes into account the increase in pressure gradient due to inertial-turbulent forces. To calculate the absolute permeability (k) using the Forchheimer equation (Equation 2.4) the right term was integrated from the inlet to the outlet of the core assuming linear pressure drop, obtaining;

$$\frac{P_{inlet} - P_{outlet}}{L} = \frac{\Delta P}{L} = \frac{\mu}{k}u + \beta\rho u^2 \quad (3.11)$$

where P_{inlet} and P_{outlet} are the pressure at the inlet and the outlet of the core and ΔP is the resulting pressure drop across the length of the core L .

Gas is injected at multiple flow rates and then $\Delta P/L$ is plotted with respect to velocity u , a quadratic regression equation is then obtained. Using the coefficients of the quadratic and linear term of the equation, the β factor and the absolute permeability of the core were calculated. This absolute permeability, k , is called the initial gas permeability at 100% gas saturation.

For multi-phase flow, the relative permeability k_{rj} of each phase j is defined as the ratio between the permeability of the j -phase k_j , and the absolute permeability k ;

$$k_{rj} = \frac{k_j}{k} \quad (3.12)$$

Using this concept and Darcy's law, the calculation of the relative permeability of each of the phases (gas and oil) in the core at steady-state during two-phase volatile oil flooding, was done using;

$$k_{rj} = \frac{q_j \mu_j L}{k A \Delta P_j} \quad (3.13)$$

For volatile oil fluids, the interfacial tension between phases is relatively small therefore the capillary pressure is negligible compared to the measured pressure drop across the core. Then, the pressure drop of all the phases is the same ($\Delta P = \Delta P_g = \Delta P_o$).

In this research, for the calculation of oil and gas relative permeability during two-phase flow, non-Darcy effects were neglected. This was due to the low flow rates used. Bang (2007), in his work for gas condensate reservoirs, studied the effect of non-Darcy flow on relative permeability for two-phase flow. He observed that the true gas

relative permeability is underestimated by almost a factor of 2 if it is calculated using the measured pressure drop and Darcy's law without taking into account non-Darcy flow effects. However, the error decreased with low gas velocities. The compressibility effects of the gas (or gas expansion effects) across the core were also neglected since the measured pressure drops across the core were relatively low.

3.3.3 Capillary number

Capillary number expresses the ratio of viscous to capillary forces. This number has an important effect on the relative permeabilities and fluid saturations where after certain threshold values relative permeabilities of oil and gas significantly increase and saturation of wetting and non-wetting phase decrease. From the different definitions available in the literature (Brownel and Katz 1947, Lake 1989, etc.) the capillary number used is as defined in equation 3.14.

$$N_c = 2.6784 * 10^{-7} \frac{k_g \Delta P}{\sigma L} \quad (3.14)$$

Where k_g is the single phase gas permeability (md), ΔP is the pressure drop across the core (psi), σ is the interfacial tension between gas and oil (dyne/cm), and L is the core length (in).

Interfacial tension is calculated as,

$$\sigma^{\beta/\theta} = P \rho_L - \rho_V \quad (3.14b)$$

Where β is a constant, which for most pure components has a value between 0.3 and 0.5, θ is a function of the actual density and the critical density $\theta = (\rho - \rho_c)/\rho_c$, ρ_L and ρ_V are the molar densities of the liquid and vapor phases, and P is the Parachor.

3.3.4 Improvement Factor

The improvement factor IF is defined as the ratio of the relative permeability of the j -phase after treatment to the relative permeability of the j -phase before treatment. The IF was the primary measure used to evaluate the effectiveness of the chemical treatment.

$$IF = \frac{k_{rj \text{ after treatment}}}{k_{rj \text{ before treatment}}} \quad (3.15)$$

Chopra and Carter (1986) recognized that for steady state flow, the ratio of relative permeabilities of gas to oil, can be expressed as a function of PVT ratio when non-Darcy flow is insignificant. Thus, under this condition and using equation 3.13, the ratio for gas to oil relative permeabilities is;

$$\frac{k_{rg}}{k_{ro}} = \frac{q_g \mu_g}{q_o \mu_o} \quad (3.16)$$

Substituting equation 3.7 into 3.16 yields to;

$$\frac{k_{rg}}{k_{ro}} = \frac{V_g \mu_g}{V_o \mu_o} = \frac{f_g \mu_g}{f_o \mu_o} = PVT \text{ Ratio} \quad (3.17)$$

Were f_g and f_o are the volumetric fractional flow of gas and oil respectively ($f_j = q_j / q_{core}$).

This relationship implies that the ratio of gas to oil relative permeability at a given core pressure is fixed and governed by the fluid properties only. In addition, this allows

for the comparison of the relative permeability before and after the treatment for any of the phases (oil or gas) to calculate the improvement factor.

3.3.5 Phase behavior calculations

Calculation of the thermodynamic properties of the fluids used in the core flood experiments were required to mathematically represent the fluids phase behavior. The calculated thermodynamic properties were volume, surface tension, density, and viscosity. All of these properties were calculated using Pen Robinson equations of state (PREOS) at the experimental conditions of temperature and pressure. The use of specialized thermodynamic software simplified time and effort for such calculations. The software, the equations of state (EOS) and the calculated properties are discussed and shown below.

3.3.5.1 PVT software

PVTSim, provided by Calsep Inc., was the PVT software used to calculate the thermodynamic properties of the various fluids. This software includes the original and modified forms of the EOS models by Soave-Redlich-Kwong and Peng-Robinson. Some of the main features offered by the software are:

- Calculation of many thermodynamic properties such as volume, surface tension, density, viscosity for a wide range of conditions.
- Different type of mixing rules allowing the use of polar and non-polar molecules.
- Ability to perform three-phase flashes and calculation of three-phase P-T phase diagrams. Where the algorithm used to calculate two and three-phase boundaries for the P-T phase diagrams was given by Lindeloff and Michelsen (2002).(Chopra and Carter 1986)

- Calculation of minimum miscibility pressure for gas injection
- Simulation of hydrates and asphaltenes
- EOS parameter regression to match experimental values measured through constant composition expansion (CCE), constant volume depletion (CVD) and other PVT experimental data

3.3.5.2 Equations of state

Equations of state (EOS) are used to show the relation between volume, pressure, and temperature for a single fluid or some mixture. One of the simpler equations of state is expressed by the ideal gas law. Although this EOS is used to predict the behavior of gases under many conditions, their results are approximations and can significantly deviate from actual values. These deviations obey to assumptions made such as; ideality of gases (no attractive or repulsive forces between molecules), particles with zero volume, perfectly elastic collisions, etc. Thus, EOS accounting for non-idealities have been proposed such as; the Van der Waals EOS, the Soave-Redlich-Kwong EOS, the Elliott-Suresh-Donohue EOS and the Peng-Robinson EOS.

The Peng-Robinson EOS (PREOS) is a cubic EOS developed by Peng and Robinson in 1976 and has been shown to accurately describe the phase behavior of hydrocarbons. The PREOS is also the most widely used EOS in compositional reservoir simulators and therefore it was used for this research work. The PREOS is the following;

$$P = \frac{RT}{V - b} - \frac{a(T)}{V(V + b) + b(V - b)} \quad (3.18)$$

Where P is pressure, R is the gas constant, T is temperature, V is the molar volume, and the other terms are expressed as;

$$a(T) = a_c \alpha(T) \quad (3.19)$$

$$a_c = \Omega_b \frac{R^2 T_c^2}{P_c} \quad (3.20)$$

$$\alpha(T) = 1 + m \left(1 - \frac{T}{T_c} \right)^{0.5} \quad (3.21)$$

$$b = \Omega_b \frac{RT_c}{P_c} \quad (3.22)$$

$$m = 0.37464 + 1.54226\omega - 0.269922\omega^2 \quad (3.23)$$

Where $\Omega_a = 0.45724$ and $\Omega_b = 0.0778$.

If the acentric factor of the species $\omega \leq 0.49$ then m is calculated using equation 3.23, else the correction made to PREOS in 1978 is used and m is calculated using equation 3.24. This corrected PREOS is known as PR48 EOS.

$$m = 0.379642 + \omega(1.48503 - 0.164423\omega + 0.01666\omega^2) \quad (3.24)$$

With Peneloux volume correction the PR78 EOS is expressed as follows;

$$P = \frac{RT}{V - b} - \frac{a(T)}{(V + c)(V + 2c + b) + (b + c)(V - b)} \quad (3.25)$$

Where c is the Peneloux volume correction defined as the difference between the Penloux molar volume and the molar volume calculated without Peneloux volume correction. In PVTsim, the parameter c is defined as the sum of a temperature independent volume correction c' and a temperature dependent volume correction c'' .

$$c = c' + c''(T - 288.15) \quad (3.26)$$

$$c'' = 0.50033 \frac{RT_c}{P_c} (0.25969 - Z_{RA}) \quad (3.27)$$

Where Z_{RA} is known as the Racket compressibility factor and is calculated as;

$$Z_{RA} = 0.29056 - 0.08775\omega \quad (3.28)$$

The most common mixing rules used for non-polar mixtures are the classical van der Waals mixing rules. These are based on the binary interaction parameter per pair. The parameters a , b and c for the mixture are calculated as;

$$a = \sum_{i=1}^N \sum_{j=1}^N z_i z_j a_{ij} \quad (3.29)$$

$$b = \sum_{i=1}^N z_i b_i \quad (3.30)$$

$$c = \sum_{i=1}^N z_i c_i \quad (3.31)$$

Where z_i and c_i are mole fractions, i and j component indices and

$$a_{ij} = \overline{a_i a_j} (1 - k_{ij}) \quad (3.32)$$

Where k_{ij} is the binary interaction parameter between component i and j .

PR78 EOS with Peneloux temperature dependent volume corrections and binary interactions of zero between components were the PREOS used. Bang (2005) showed that PVT properties of mixtures of pure hydrocarbon components can only be accurately calculated using zero binary interaction coefficients for van der Waal's mixing rule.

3.3.5.3 PVT Diagrams

Five different synthetic volatile oil mixtures were used for the HPHT core flood experiments the compositions are given in Table 3.3. These volatile oil mixtures 1 through 5 were used for the experimental temperatures of 75°F, 155°F, 215°F, 250°F and 275°F correspondingly. For each of the volatile oil mixtures, the corresponding P-T diagrams (phase envelopes), liquid volume fraction, interfacial tension (IFT), viscosity and density of gas and liquid phases for different pressures, are shown from Figure 3.6 P-T diagram for volatile oil mixture 1 to Figure 3.25. All of the calculations were performed with PVT Sim using flash calculations and CCE.

Table 3.1 Grain density values provided by TerraTek (rock supplier for different outcrops)

Core type	Grain density (g/cm ³)
Berea Sandstone	2.64 - 2.66
Torrey Buff Sandstone	2.68 - 2.72
Texas Cream Limestone	2.40 - 2.65

Table 3.2 Composition of brines used to establish S_{wi}

Component	Brine 1	Brine 2
	Concentration	
NaCl	25,000 ppm	25,000 ppm
CaCl ₂	0 ppm	250 ppm
H ₂ O	N/A	N/A

Table 3.3 Composition of volatile oil mixtures used for corefloods at different experimental temperatures

Component	Mixture 1	Mixture 2	Mixture 3	Mixture 4	Mixture 5
	Mole %				
Methane (C ₁)	78	75	73	71	69
Propane (C ₃)	13	12	11	12	12
n-Heptane (nC ₇)	6	9	11	10	13
n-Decane (nC ₁₀)	3	4	5	4	6
n-Dodecane (nC ₁₂)	0	0	0	3	0

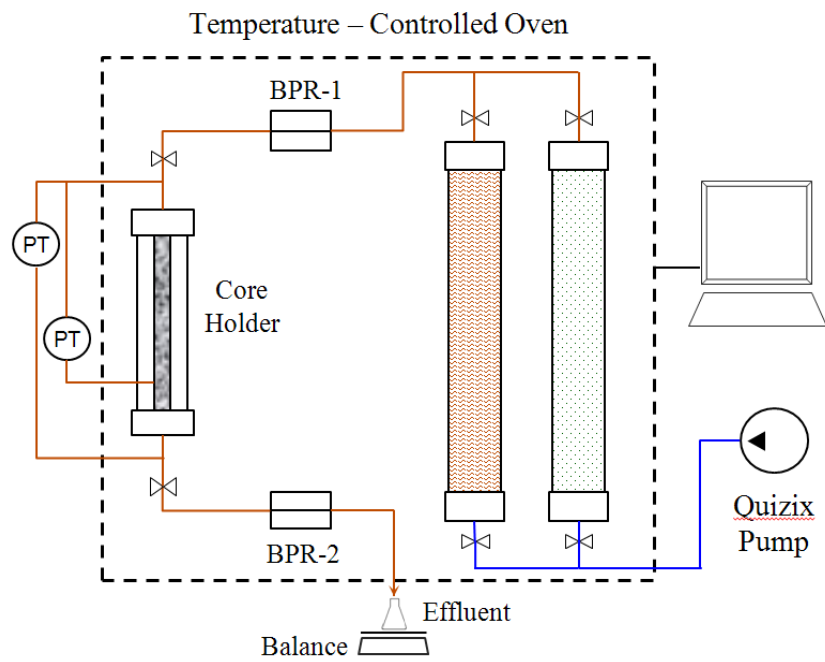


Figure 3.1 High-temperature high-pressure core flood experimental apparatus schematic

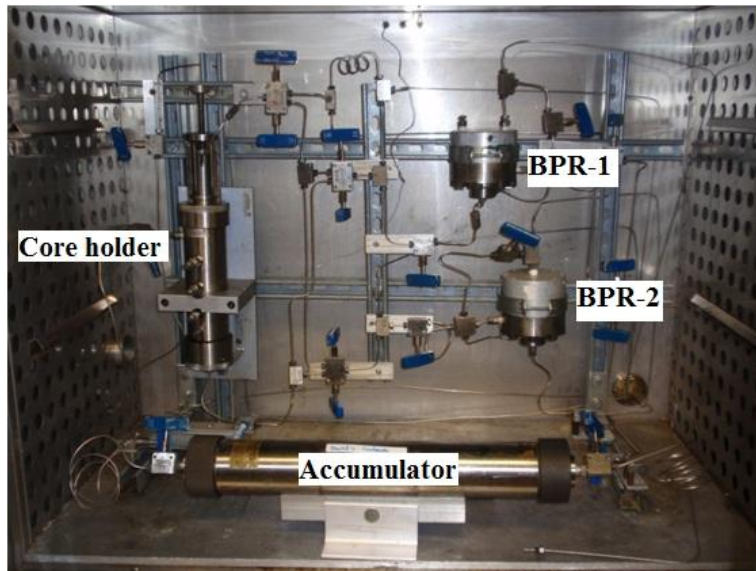


Figure 3.2 Coreflood setup - equipment inside the oven

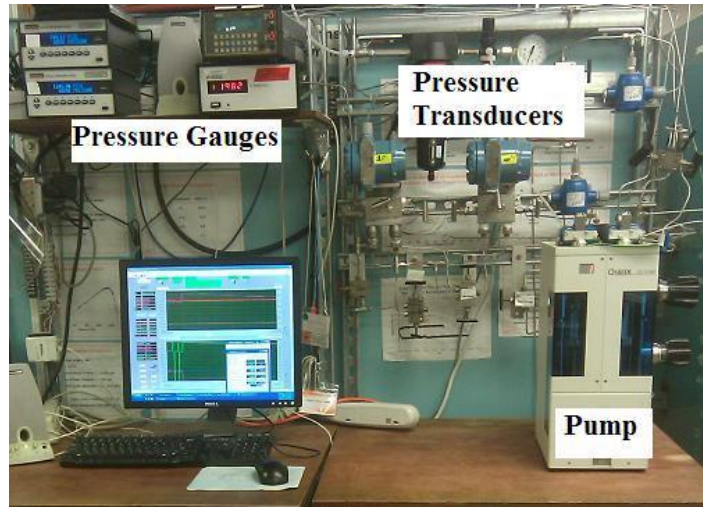


Figure 3.3 Coreflood experimental setup – equipment outside the oven

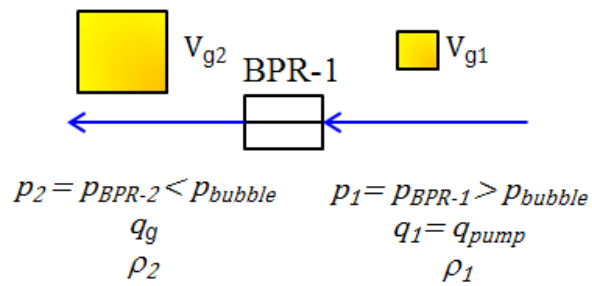


Figure 3.4 Schematic of isothermal gas expansion at BPR-1

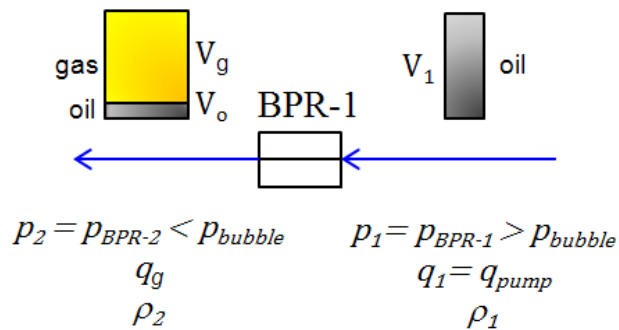


Figure 3.5 Schematic of isothermal volatile oil flash around BPR-1

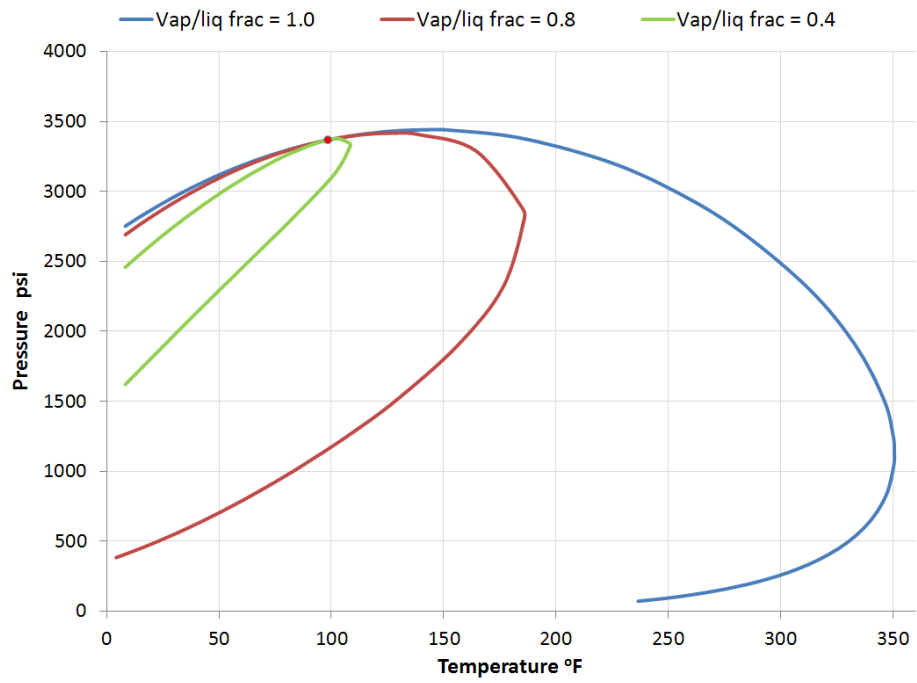


Figure 3.6 P-T diagram for volatile oil mixture 1

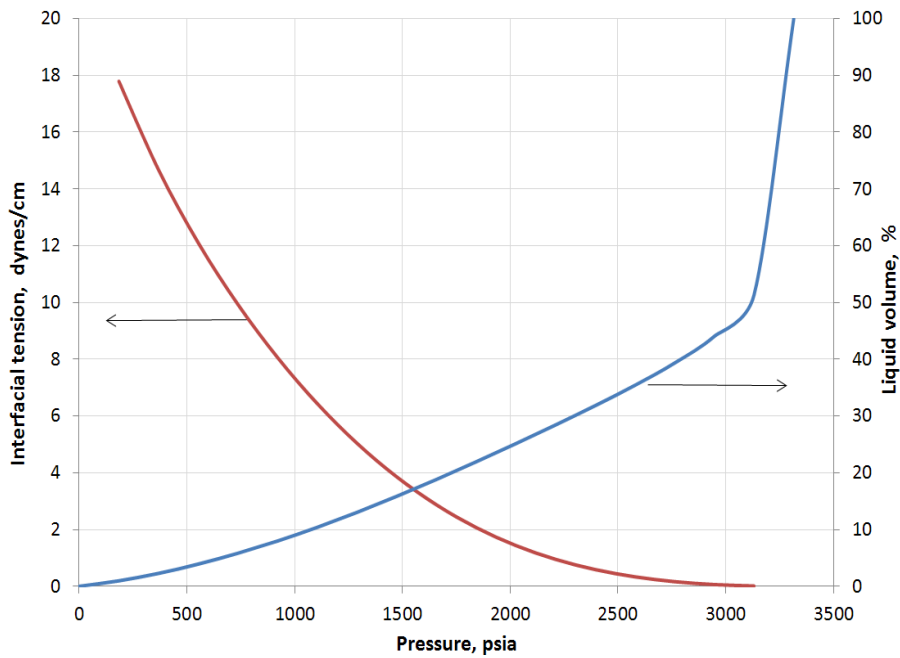


Figure 3.7 Interfacial tension and liquid volume % vs. pressure for volatile oil mixture 1 at 75°F

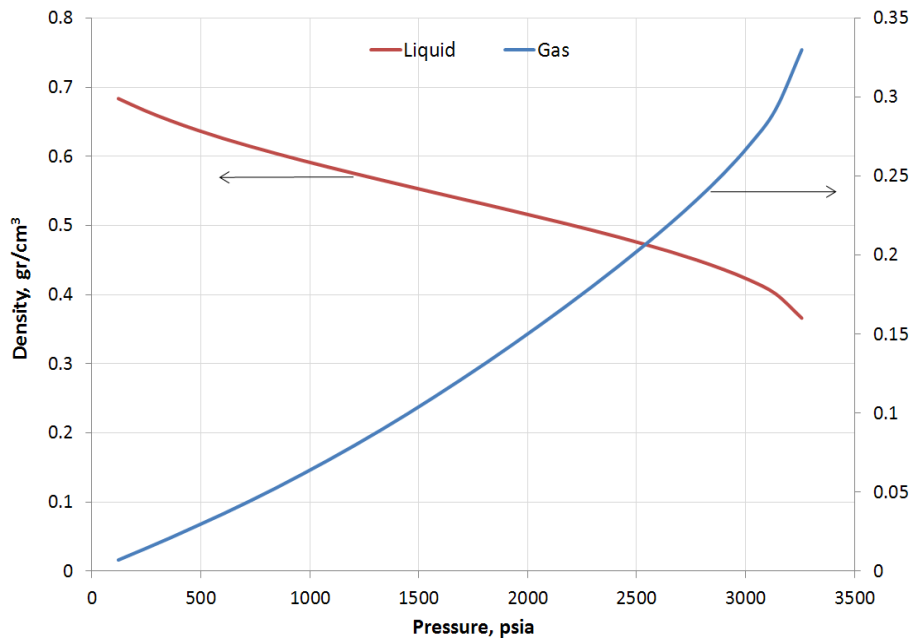


Figure 3.8 Gas and liquid phase densities vs. pressure for volatile oil mixture 1 at 75°F

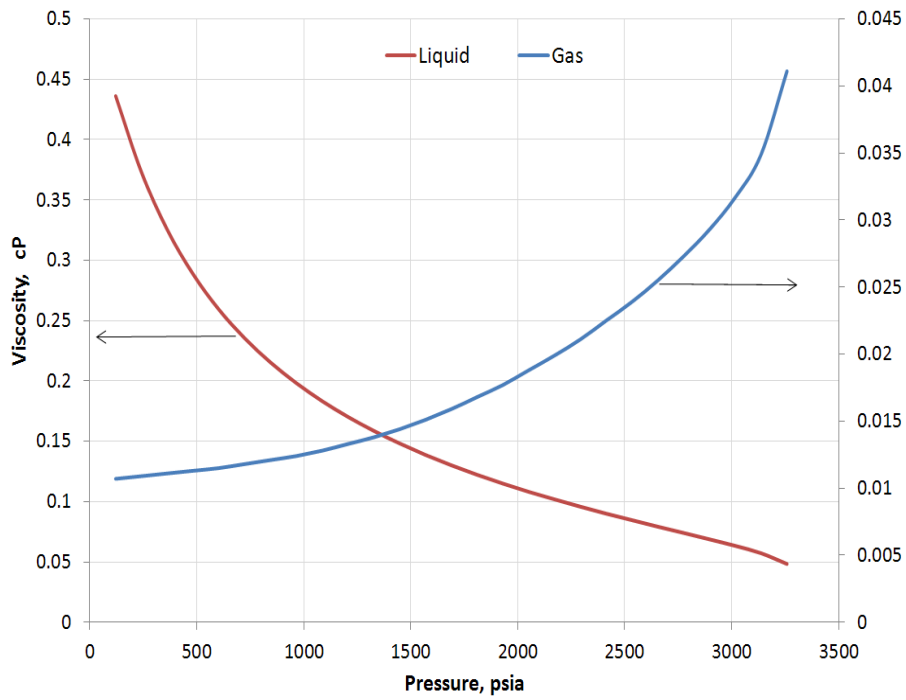


Figure 3.9 Gas and liquid phase viscosities vs. pressure for volatile oil mixture 1 at 75°F

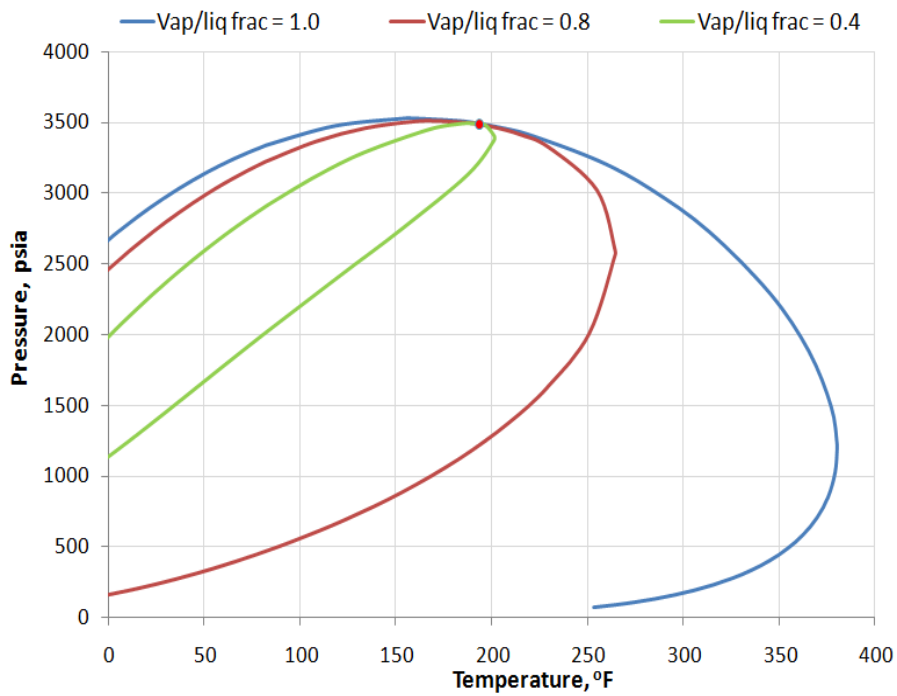


Figure 3.10 P-T diagram for volatile oil mixture 2

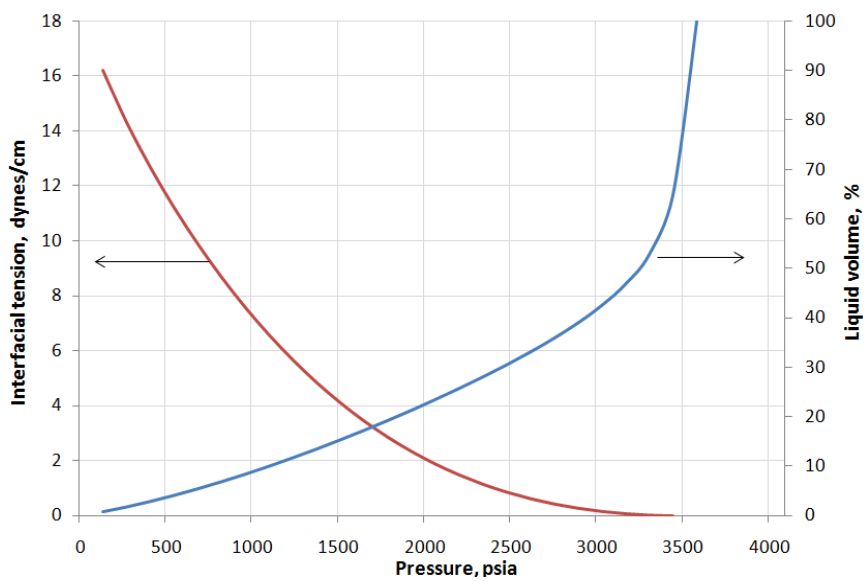


Figure 3.11 Interfacial tension and liquid volume % vs. pressure for volatile oil mixture 2 at 155°F

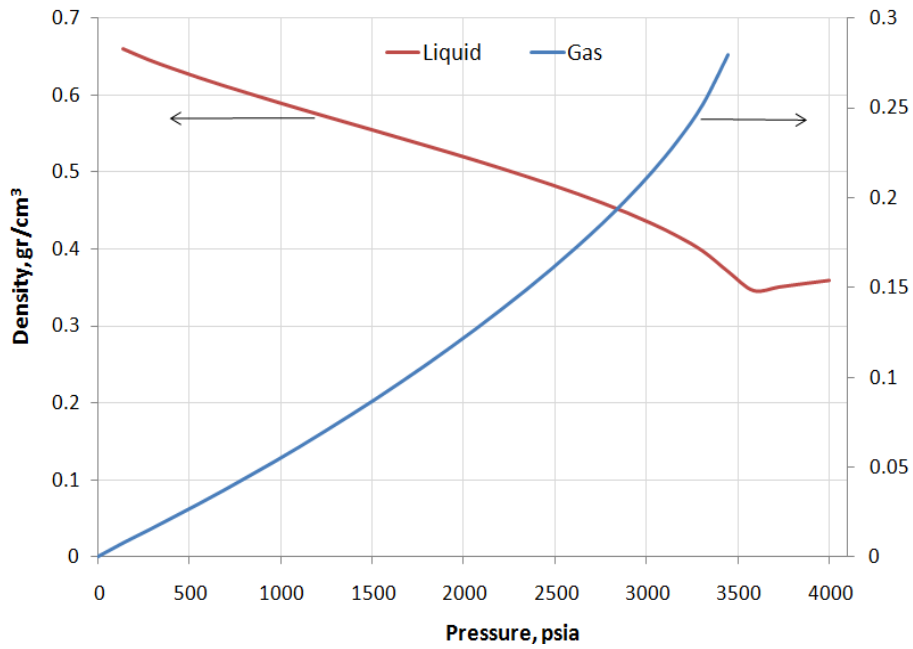


Figure 3.12 Gas and liquid phase densities vs. pressure for volatile oil mixture 2 at 155°F

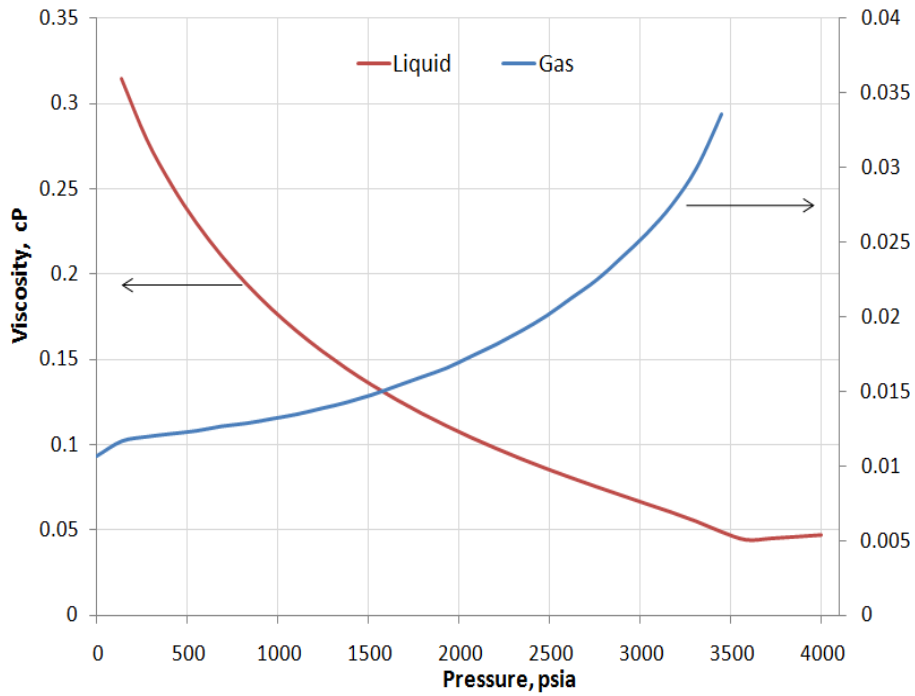


Figure 3.13 Gas and liquid phase viscosities vs. pressure for volatile oil mixture 2 at 155°F

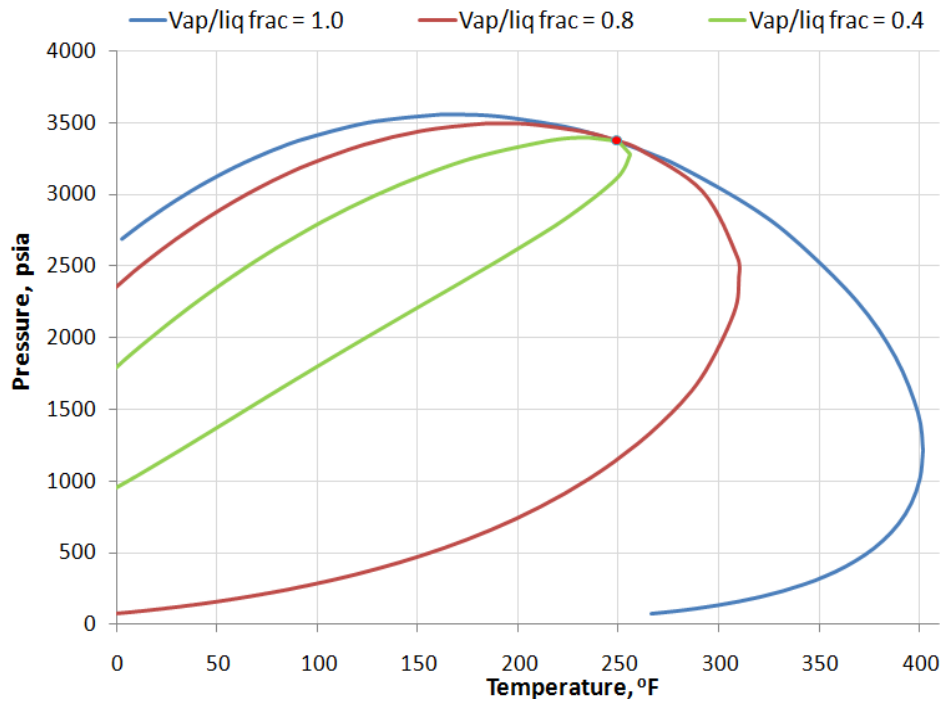


Figure 3.14 P-T diagram for volatile oil mixture 3

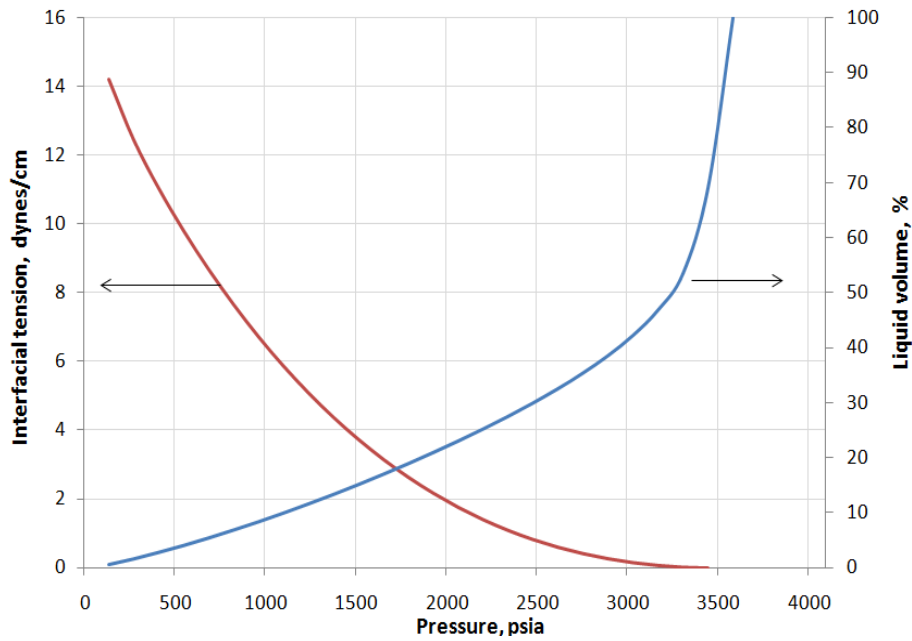


Figure 3.15 Interfacial tension and liquid volume % vs. pressure for volatile oil mixture 3 at 215°F

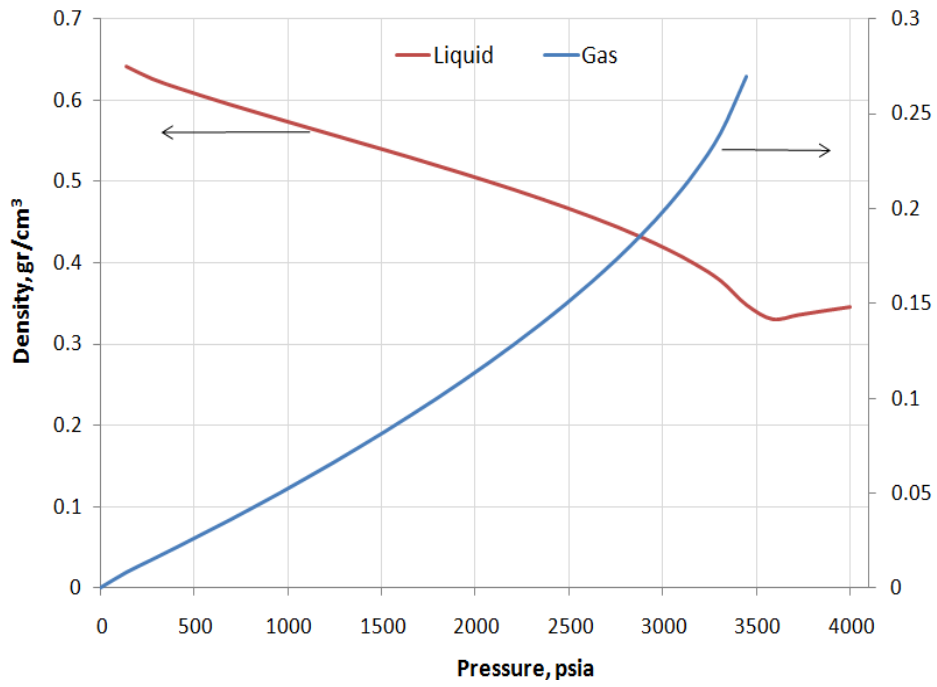


Figure 3.16 Gas and liquid phase densities vs. pressure for volatile oil mixture 3 at 215°F

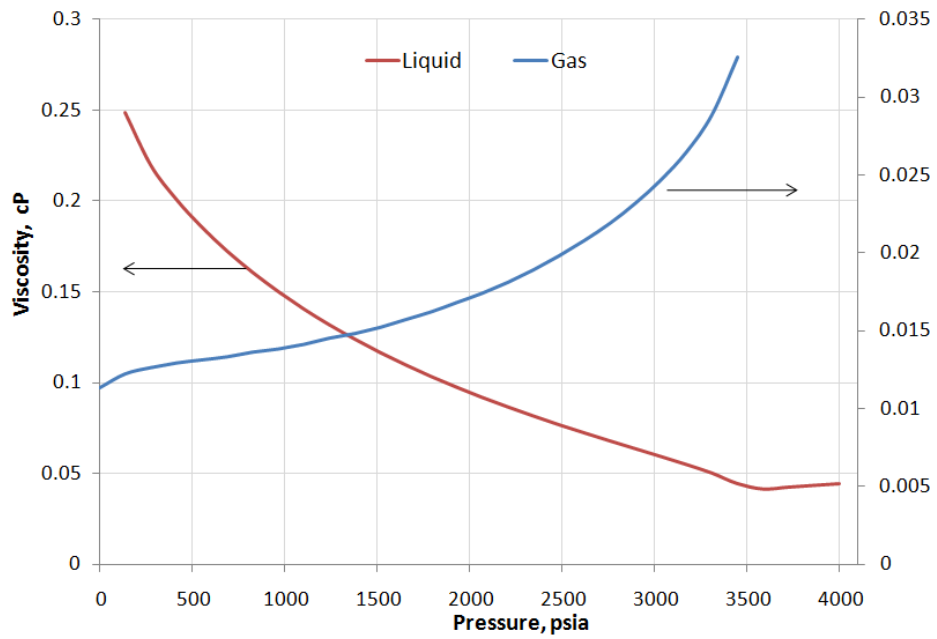


Figure 3.17 Gas and liquid phase viscosities vs. pressure for volatile oil mixture 3 at 215°F

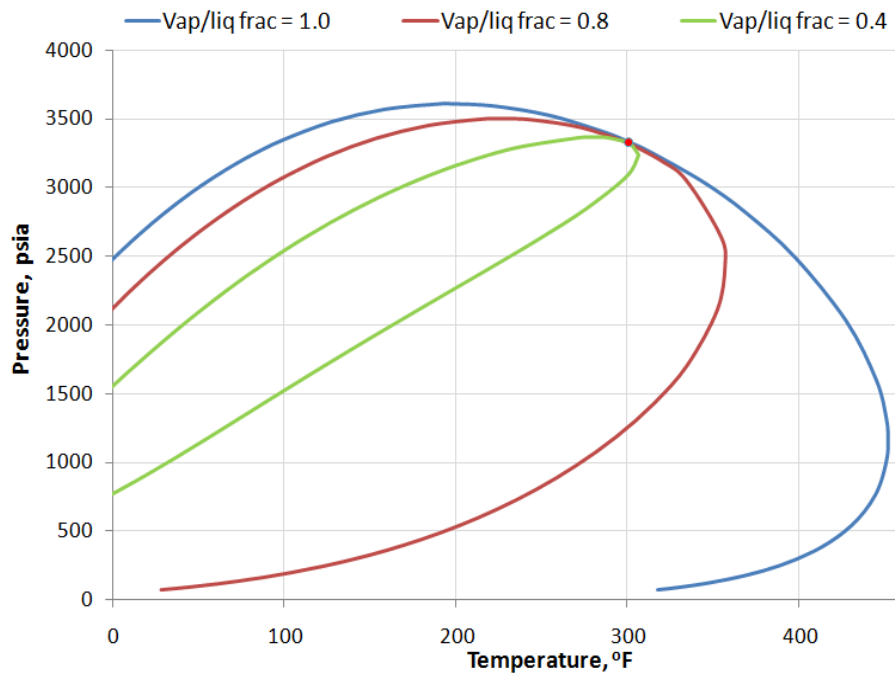


Figure 3.18 P-T diagram for volatile oil mixture 4

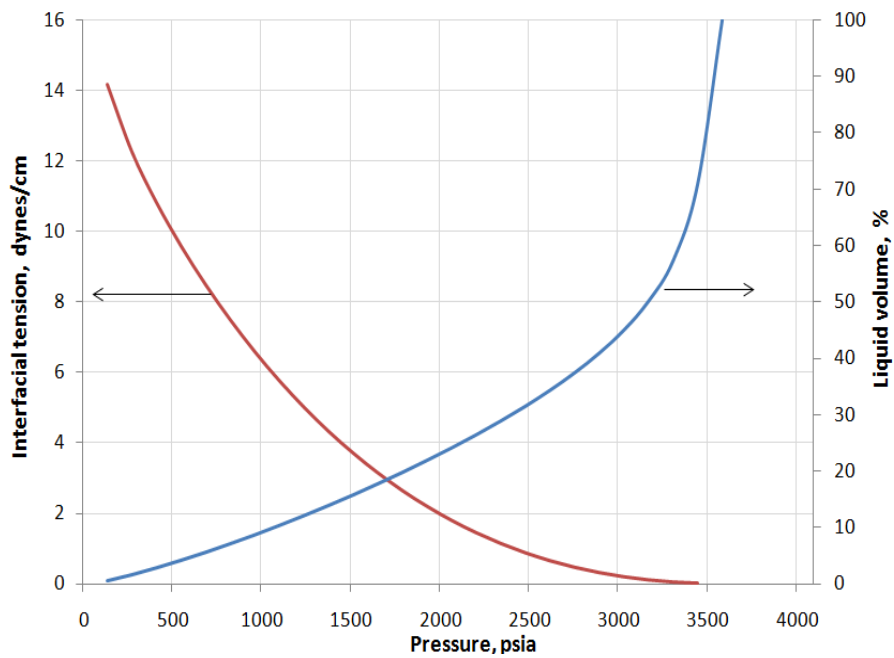


Figure 3.19 Interfacial tension and liquid volume % vs. pressure for volatile oil mixture 4 at 250°F

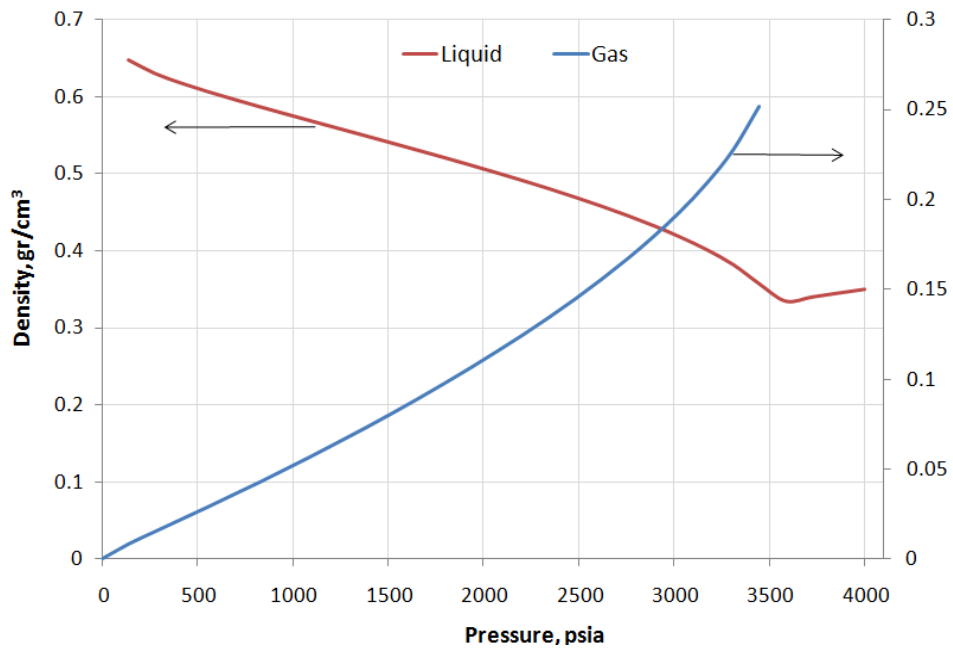


Figure 3.20 Gas and liquid phase densities vs. pressure for volatile oil mixture 4 at 250°F

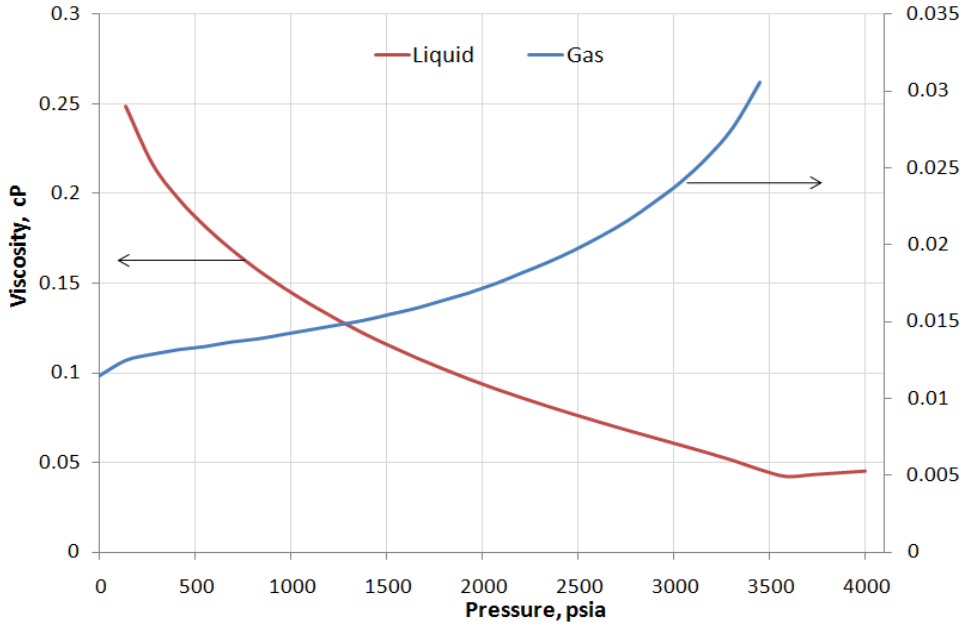


Figure 3.21 Gas and liquid phase viscosities vs. pressure for volatile oil mixture 4 at 250°F

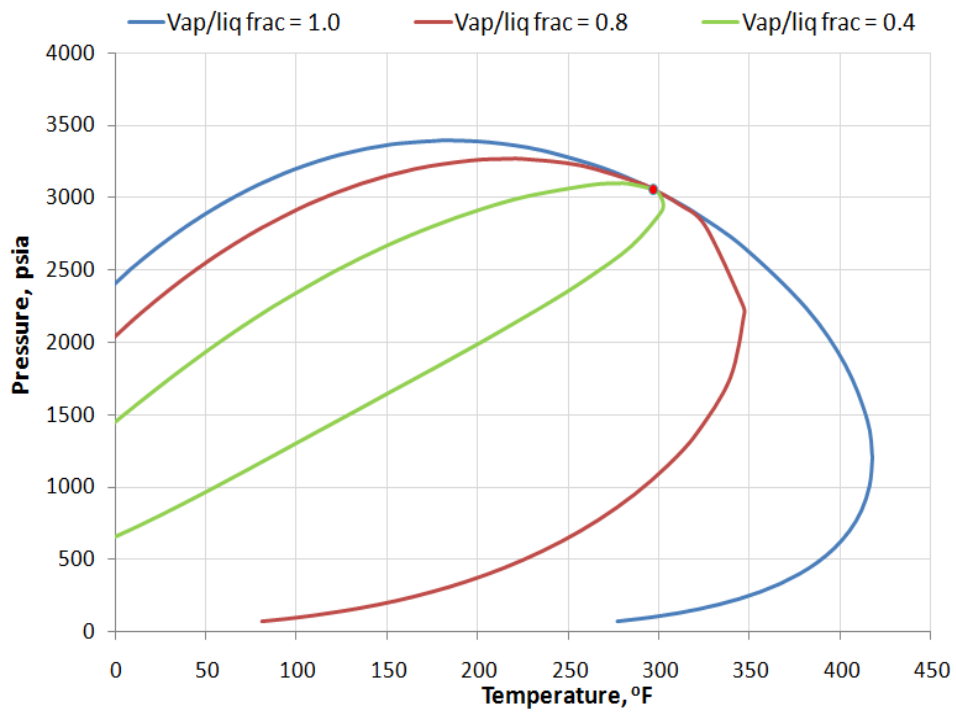


Figure 3.22 P-T diagram for volatile oil mixture 5

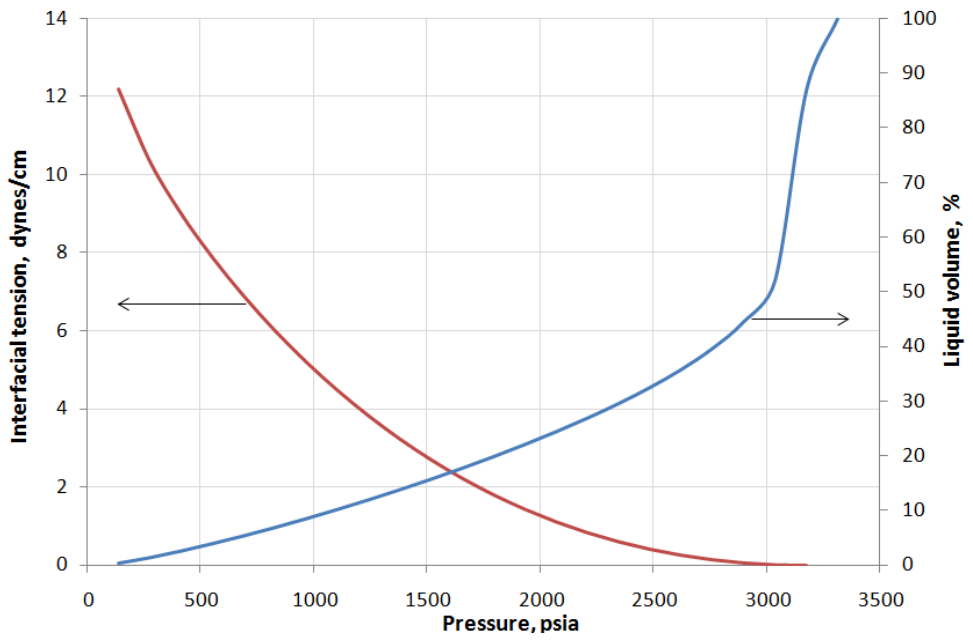


Figure 3.23 Interfacial tension and liquid volume % vs. pressure for volatile oil mixture 5 at 275°F

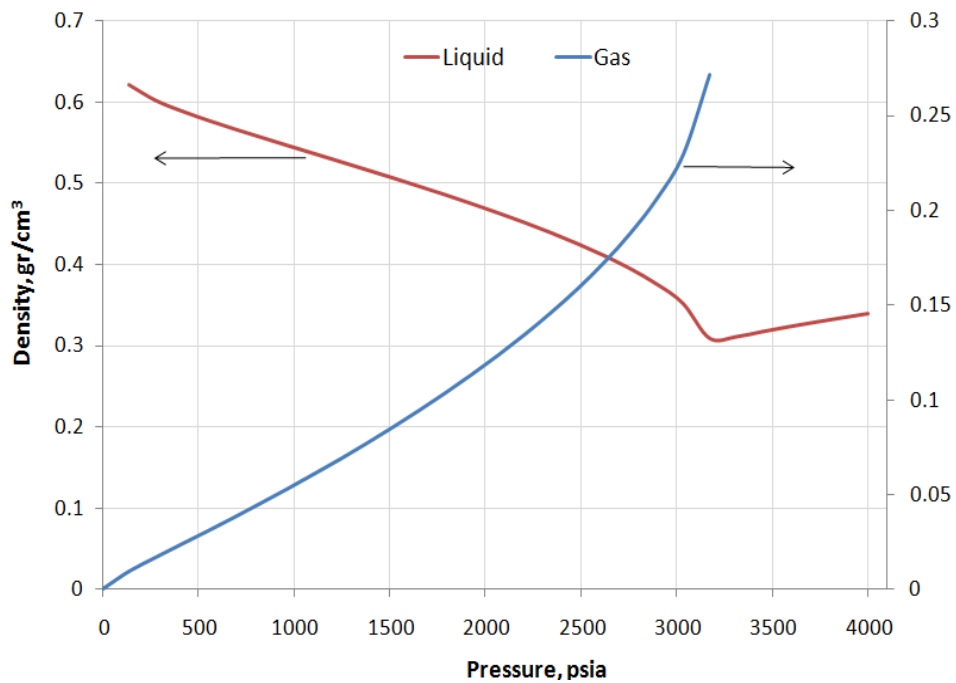


Figure 3.24 Gas and liquid phase densities vs. pressure for volatile oil mixture 5 at 275°F

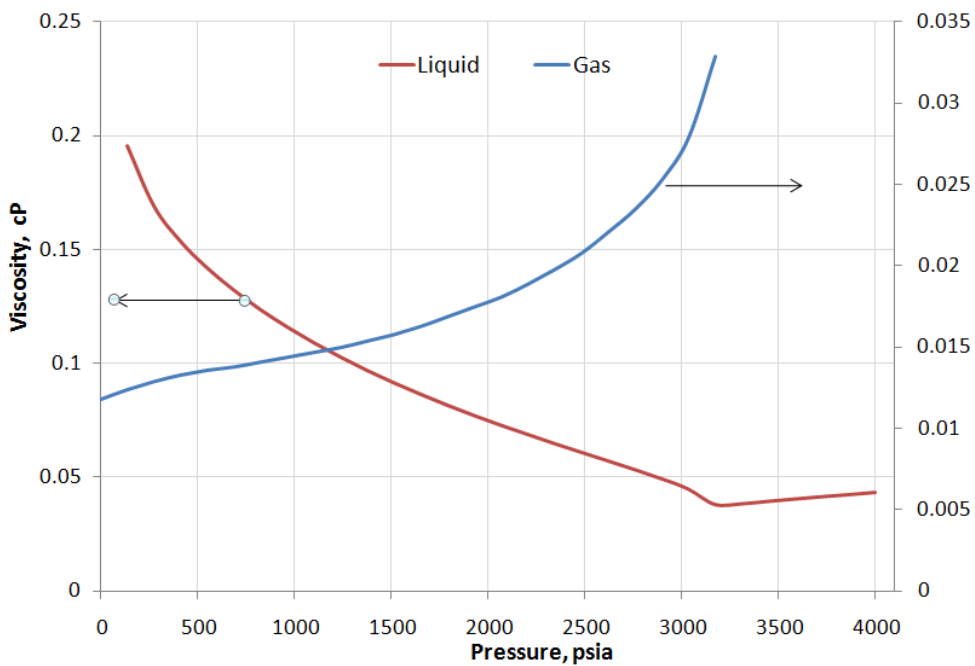


Figure 3.25 Gas and liquid phase viscosities vs. pressure for volatile oil mixture 5 at 275°F

Chapter 4: Selection and Formulation of the Fluorinated Chemical Treatments

The present research addressed the problem of “gas blocking” of volatile oil reservoirs, by means of rock wettability alteration using fluorinated chemical treatments. The fluorinated surfactant treatment had the purpose of altering the wettability of the rock surface from gas/oil wet to neutral wet. This resulted in an increase in the oil and gas relative permeability and thus reducing the effects of “gas blocking”. Chemical treatments were developed and tested using fluorinated surfactants and a solvent designed to deliver the surfactant to the rock surface. Surfactants and solvents were then first screened to select formulations.

Candidate surfactants were selected based on their ability to provide good repellency to oil and water. Two main features were sought in the molecular structure of the surfactants: a functional group to provide a strong interaction with the rock surface and consequently provide adequate and durable adsorption onto the rock, and a fluorinated tail to provide repellency to oil and water. Figure 2.8 is a schematic of the surfactant adsorbed to the rock surface. Surfactant adsorption could result from a number of different mechanisms: chemisorption (chemical bonding), physisorption (Van der Waal forces) and/or by hydrogen bonding.

There are a large number of potentially effective fluorinated surfactants available. Only chemicals that satisfied environmental concerns were considered. These were chemicals made from C_4 chemistry rather than C_{4+} chemistry. A list of the selected surfactants is given in Table 4.1. All of the selected surfactants had a C_4 fluorinated tail.

The treatment formulations were composed of a fluorinated surfactant and a solvent solution to deliver the surfactant to the rock. These formulations had to be stable

at high temperatures (up to 300°F) so that the surfactant could be delivered to the rock surface without damaging the core. In order for a formulation to be considered for use, a number of screening experiments were conducted to assess: surfactant solubility, temperature stability, and brine compatibility.

Once a chemical treatment formulation was found to meet the criteria developed for the above tests, additional screening studies were conducted to evaluate the chemicals potential as a wettability alteration agent. Drop tests, imbibition rate tests and XPS analysis were performed to provide a qualitative, assessment of the behavior of the chemical treatment formulation. Those formulations which were thought to be good candidates based on the above screening criteria were used for the core flood experiments reported in Chapter 5 and 6.

4.1 PHASE BEHAVIOR STUDIES FOR THE SELECTION OF SOLVENT DELIVERY SYSTEM FOR THE CHEMICAL TREATMENT

The phase behavior studies for selecting the solvent formulation involved a study of the solvents ability to solubilize the selected fluorinated surfactant and it's stability at high temperature and in the presence of brine. The viscosity and volatility were also considered because once the surfactant was delivered to the rock the solvent must easily flow back so as not to block the pores.

4.1.1 Characteristics of the solvent formulation

Selection of solvent formulations for screening was based on recommendations from the chemical manufacturer, from previous experience with the surfactants, and a trial and error process. An acceptable solvent formulation should meet the following list of characteristics:

1. **Solubility.** The solvent system could be either a single component or a mixture, and it had to solubilize the chemical at concentrations required for a successful treatment. The solution must also solubilize and remove residual oil so that the treatment chemical gets an adequate opportunity to contact the rock surface.
2. **Brine compatibility.** Because brine is present in most reservoirs, the solvent system had to be stable in the presence of various amounts of brine at reservoir salinities without precipitation of solids or phase separation.
3. **Thermal-stability.** The surfactant-solvent formulation should show stability at high temperatures (e.g. 300°F). Again, no phase separation, solid precipitation, or degradation of any of the components should be observed.
4. **Volatility and viscosity.** To avoid liquid blocking produced by the chemical treatment, the solvent mixture used should have a high volatility and a low viscosity. This was desired because when this type of treatment is to be injected in an actual well, it has to be produced back when the well is returned to production.

4.1.2 Solubility and compatibility tests

The solvent or mixture of solvents selected for the chemical treatment had to dissolve the fluorinated surfactant at concentrations deemed adequate for wettability alteration. Keeping the concentration of the surfactant within the limits where its performance is optimum was important since the fluorinated surfactant is the most expensive part of the treatment.

As mentioned before brine is present in most reservoirs, hence many different brine compositions as well as concentrations can be found. Thus, the solvents had to be stable at various brine salinities and saturations.

Solubility, compatibility and stability of the solvents with the fluorinated surfactant, brine and hydrocarbons (e.g. decane) were evaluated with solubility and compatibility tests. These simple tests helped to determine limits and working conditions of the chemical treatment systems.

The testing procedure consisted of dilution of the surfactant in the selected solvent formulation at different concentrations at room and experimental temperatures up to 300°F. The samples were aged for 1 hour and visual observations for phase separation and solid precipitation were made. Next, the selected solution was mixed with brine at different ratios and the mixtures were again evaluated for phase separation and solid precipitation, at room temperature and after aging for 1 hr at a prescribed high temperature. Then, for the final selected solution, low volumes of decane were added and the same evaluation procedure was again performed. The observation of more than one phase, a cloudy or opaque phase, or any trace of precipitated solids indicated instability of the solution and solvent reformulation and testing were performed until favorable results were obtained.

4.2 SCREENING TESTS FOR SURFACTANTS

To select a surfactant for a core flood experiment, it was necessary to perform screening tests on candidate surfactants. The screening tests consisted of: drop and imbibition rate tests, and XPS analysis. These tests provided information on the surfactant's ability to alter the rock wettability and allowed a visual observation of changes in contact angles for the rock-liquid interface, rates of adsorption of liquids into the rock matrix, and a measure of the relative concentrations of fluorine on the rock surface.

Preparation of the samples for these tests consisted of the following:

- Pieces of rock, 1 inch in diameter and about 3 millimeters in thickness, called chips, were cut.
- The chips were treated at ambient pressure and experimental temperature with the candidate chemical treatment formulation. They were kept in the treatment solution overnight.
- The samples were partially dried with air and rinsed with heptane for about 30 minutes.
- Finally, the samples were blow dried with air and they were placed in the oven over night for complete drying.

The description of the screening tests performed on the treated chips is described below.

4.2.1 Drop and imbibition rate tests

Drop and imbibition rate tests consisted of placing a drop of water (de-ionized) and a drop of oil (e.g. decane) onto the surface of pre and post-treated rock samples. The contact angle and the rate of imbibition into the rock matrix were observed. These tests provided information about the pre and post-treatment wettability of the rock. The wettability alteration was assessed by noting changes in the contact angle and the rate of imbibition. Higher contact angles in the gas-liquid interface and reductions in the rate of water and oil imbibed over a fixed period of time demonstrated that the fluorinated chemical is present on the rock. These tests were the first step performed in the process of chemical treatment selection.

4.2.2 XPS analysis

X-ray photoelectron spectroscopy (XPS) is a surface chemical analysis technique that can be used to analyze the surface chemistry of a material by measuring the elemental composition, chemical state and electronic state of the elements that exist within a material surface. Measuring the elemental composition is what drove the use of this technique as a screening test for selecting potential surfactants. The presence of the fluorine atoms in the surfactant's structure was used to trace the presence of the surfactant on the treated rock surface. In the past, XPS analysis was found to be a quick and easy technique to measure fluorine atoms (Brundle and Baker 1977; Briggs and Seah 1990). In the petroleum industry, the use of XPS analysis is not uncommon, XPS analysis has been used in the past for surface composition analysis of reservoir rocks where rock mineralogy and carbon content have been correlated with rock wettability states (Ramirez et al. 1986; Mitchell et al. 1990; Durand and Beccat 1998; Toledo et al. 1996).

A schematic describing the operating principle of XPS is given in Figure 4.1. XPS is based on the photoelectric effect which involves the emission or ejection of electrons of the surface of a material, in response of incident light. The energy contained within the incident light is absorbed by the electrons at the surface metals giving the electrons sufficient energy to be emitted from the material surface. In XPS tests, the method consists of irradiating a sample with monochromatic x-rays, resulting in the emission of photoelectrons whose energies are characteristic of the elements within the sampling volume. The analysis occurs at the top of the sample between 1-12 nm of the surface layers because the applied soft X-ray excitation cannot penetrate below the surface layers.

In XPS analysis a sample is placed under a beam of an X-ray source in an ultra-high vacuum (UHV) chamber. A hemispherical sector analyzer is used to detect electrons at

different energy levels. Al-K α ($h\nu = 1486.8$ eV) and Mg-K α ($h\nu = 1253.6$ eV) X-rays sources are the two most common anodes used. The ejected electron has a kinetic energy (KE) that is related to the energy of the incident beam ($h\nu$), the electron binding energy (BE), and the work function of the spectrometer (Φ). Thus, the binding energy of the electron can be calculated from

$$KE = h\nu - BE - \Phi \quad (4.1)$$

Where KE is the kinetic energy in electron volts (eV), $h\nu$ is the energy of the photon (incident beam) which is the product of the plank constant h ($6.62E-34$ J*s) times the frequency of radiation ν in Hertz (Hz), and Φ is as mentioned before, the work function of the spectrometer.

The resulting plot of the number of electrons detected versus the binding energy is known as the XPS spectrum. For the spectrum, each element has a characteristic set of peaks at characteristic binding energy values that directly identify each element that exists in an analyzed sample surface. The characteristic peaks corresponds to the electron configuration of the electrons with the atoms e.g., 1s, 2s, 2p, 3s etc. The number of detected electrons in each of the characteristic peaks is directly related to the amount of the element within the area (volume) irradiated (Mohanty 2007).

The x-ray photoelectron spectrometer used in this research was manufactured by Kratos Analytical Company. The analytical procedure started by loading samples of blanks (untreated rocks) and treated rocks (small pieces of the treated chips) into the XPS loading chamber overnight to induce an UHV. It was important to perform the analysis under these conditions because only the electrons emitted from the atoms close to the surface will have any chance of escaping the sample without colliding with another particle. Then the samples were transferred to the x-ray chamber where the analysis was

performed. The analytical software was programmed by selecting optimum positions for each of the samples (this is where the photo-emitted electrons are adequately captured by the analyzer), then selecting the elements to be analyzed and finally all the other parameters such as type of beam, energy level, etc. Table 4.2 shows the parameters used for XPS analysis and Table 4.3 shows the analyzed elements according to the type of sample rock. Finally, the XPS signals were processed and mass concentrations were measured.

The data collected from XPS analysis was the most quantitative method available to us for selecting candidate fluorinated surfactants. Surfactants that showed the highest content of fluorine on the surface of the rock were selected for core flow tests.

4.3 RESULTS AND DISCUSSION

Table 4.1 shows the list of the available candidate fluorinated surfactants. These surfactants had varied chemistries: functional groups and fluorinated tails. The functional groups consisted of ethylene oxide, epoxides, silanes, ionic compounds and amines. Perfluorinated and partially fluorinated surfactant tails of different carbon numbers were included. Initially, the idea of the more fluorine atoms in the surfactant structure the better the oil and water repellency and the consequently a higher degree of wettability alteration, was followed. Then, fluorinated tails with carbon chains as high as C₈'s, were studied. However, environmental concerns regarding bio-accumulation of fluorinated C₅ chains or above restricted the use of these surfactants to C₄ fluorinated carbon chains.

As mentioned before, XPS analysis was carried out to screen candidate surfactants by measuring the amount of fluorine on treated rock surfaces.

Table 4.2 lists all the parameters used for XPS analysis such as type of X-ray gun and type of charge neutralizer.

Table 4.3 lists the elements analyzed according to the type of rock being analyzed; Berea and Torrey Buff sandstones, and Texas cream limestone (TCL). The XPS results for fluorine content on the treated chips are given in Figure 4.2. The results are for Berea sandstone chips with the exception of the result for L-19446#1, which was used to treat the TCL chips. The fluorine content was reported in a mass basis and it was relative to the other analyzed elements. Fluorine content results provided a qualitative measurement of the surfactant's molecular adsorption onto the rock surface. Only the surfactants that exhibited the highest fluorine contents were selected for further tests and core flood experiments. For the case of the surfactant 474088, although it exhibited the highest fluorine content on the rock surface, it was rejected because it has C₈ chemistry which is environmentally unacceptable. For the case of FC-X, even though the fluorine content was rather low it was selected because it is already commercially available and it had been previously shown to provide good results for wettability alteration in gas condensate fluids and even volatile oils (only one experimental set of conditions for the volatile oil case) (Bang 2007). As reported by Ahmadi et al. (2010), the interaction of FC-X with limestone and sandstone rocks was enhanced by using a special amine primer used for multifunctional coatings (Lee et al. 2007). However, despite the significant increase of the fluorine content on the rock surface and the positive changes in wettability towards a neutral wetting state (Figure 4.2 and Figure 4.3); the use of an amine primer was rejected due to the complications of a two-step process and the cost implications.

Table 4.4 and Figure 4.4 show the selected surfactants used for wettability alteration in core flood experiments and the results for XPS analysis done on the treated chips with the selected surfactants.

The results of the screening tests for the selected surfactants are shown in Table 4.5 through Table 4.8. Table 4.5 shows the solubility results and sample appearance of the surfactant L-20294 in different types of pure solvents and solvent mixtures; it also shows the nomenclature used for solvents and for the degree of solubility and sample appearance. It can be observed that the solvent mixtures of PG-IPA (70-30 wt%) and 2BE-EtOH (70-30 wt%) adequately dissolve the surfactant up to concentrations as high as 4 wt% and 5 wt% accordingly, while pure IPA and EtOH required heating for complete dissolution. Table 4.6 shows the solubility of FC-X in different solvent mixtures at different concentrations, solvent ratios and temperatures. FC-X proved to be soluble and stable in mixtures of PG-IPA, PG-EtOH and 2BE-EtOH for different ratios and at temperatures as high as 275°F. Table 4.7 shows the solubility and sample appearance for L-18961 in the different solvent mixtures at different ratios, concentrations, and temperatures. 2BE-EtOH mixture required the addition of 10 wt% IPA for dissolution of the surfactant, and total dissolution was achieved only at temperatures above room temperature and surfactant concentrations ≤ 2 wt%. The same way, Table 4.8 shows the solubility of L-19446 #1. The surfactant was completely soluble in 2BE-EtOH (70-30 wt%) at concentrations and temperatures as high as 3 wt% and 175°F. Thus, the solvent mixture of 2BE-EtOH 70-30 wt%, was shown to be a good solvent system for the selected C₄ fluorinated surfactants, and required only a small amount of IPA for the specific case of L-18961, to obtain complete dissolution of the surfactant and a clear single phase.

For some of the fluorinated surfactants used in this work, additional results for the compatibility of these with different solvents at various ratios has been previously reported by Bang (2007), Ahmadi (2010) and McCulley (2011). Also, additional results for XPS analysis are reported by Gilani (2010).

After finding a suitable solvent formulation for the selected surfactants, an analysis of compatibility with brine was performed. Two different brines were used for this analysis (Table 4.9). Brine 1 was used for the treatment of sandstones (FC-X, L-20294, L-18961 and L-19973#9) and brine 2 for surfactants applied to limestones (L-19446#1). A rather arbitrary but representative salinity of reservoir brine of 25 000 ppm of NaCl was selected for brine compatibility analysis and is the same brine that was to be used for establishing water saturation in corefloods. CaCl_2 was added to in formulation of brine 2 to avoid ion exchange in limestone cores (carbonate rocks) that could lead to damages of the rock structure and consequently induce permeability changes. Table 4.10 through Table 4.14 show the results of the compatibility tests for each of the selected surfactants and specific solvent systems with either brine 1 or brine 2. The cloud point, or the point when surfactant or salt comes out of solution, for each of the surfactant-solvent-brine systems was observed. In general, below brine amounts of 40 wt% the systems were compatible and thermodynamically stable; there is no observed precipitation of solids or phase separation at temperatures as high as 275°F. Figure 4.5 shows the cases of samples that exhibited phase separation, cloudiness and precipitation of solids during compatibility analysis of surfactant-solvent system with brine.

The surfactants-solvent formulations tested for brine compatibility were also tested for oil miscibility with an oil phase; N-decane was used to represent the oil phase. All of the formulations were completely soluble up to 30 vol% of oil without exhibiting

cloudiness, solid precipitation or phase separation. No higher amounts of oil were tested. The final formulations approved for core flood experiments are summarized in Table 4.15. This table shows the composition of the chemical treatments and the assigned numbers for each of them.

Using the chemical treatments from Table 4.15 chips of Berea sandstone and TCL were treated for drop and imbibition rate tests. These simple tests complemented and reinforced the results of the XPS analysis. The imbibition times measured and the observed contact angles, helped to identify the candidate surfactants that are more suitable for rock wettability alteration. As explained above, for the drop and imbibition rate tests, a drop of water and a drop of n-decane (oil) were placed on the surface of the treated chips to qualitatively observe water and oil wettability respectively. Times for complete imbibition of such drops were measured, but measurements of the contact angle were only semi-quantitative due to the dynamic imbibition of the drops into the pores of the rock. For these measurements, the roughness of the rock surface and the drop size were neglected. The results are shown in Figure 4.6 through Figure 4.19, these figures show pictures taken immediately after the water or n-decane drops were placed on the chips). Figure 4.6 and Figure 4.7 illustrate the drop and imbibition rate results for Berea sandstone without any treatment. The water and n-decane drop imbibition times were 1.5 and 1 seconds respectively and the contact angles were close to zero for both drops resulting in almost instantaneous spreading on the rock surface. These results represented the initial conditions of the rock. Berea sandstone chips treated with FC-X (chemical treatment 1) increased imbibition times by a factor of 7 for water and 4 for oil. Also, as illustrated in Figure 4.8 and Figure 4.9, the contact angles increased to some value in between 30° and 60° for both water and oil. Berea sandstone chips treated with L-

20294 (chemical treatment 2) and L-18961 (chemical treatment 3) modified the wettability to complete non-water wettability; the water drop sited up on the chip's surfaces and contact angles in between 150° and 180° were observed and no imbibition occurred even after several minutes (Figure 4.10 and Figure 4.12). For the oil wettability, despite the enhancement towards non-oil wettability, the contact angles observed were between 30° and 60° and the imbibition times increased by a factor of 4 for the chip treated with L-20294 (Figure 4.11) and by a factor of 5 for the chip treated with L-18961 (Figure 4.13). The ionic surfactant L-19973#9 showed a less pronounced effect on wettability alteration of Berea sandstone chips compared to the non-ionic surfactants. The imbibition times increased by a factor 13 for water and by a factor of 3 for oil, and the contact angles were in between 20° and 60° (Figure 4.14 and Figure 4.15). For TCL, the results of the chips without treatment are shown in Figure 4.16 and Figure 4.17, imbibition times of 15 sec for water and 1.5 sec for oil were observed indicating that the initial state of the rock is towards the oil wettability side. TCL chips treated with the ionic surfactant L-19446#1 increased the imbibition times by a factor of 3 for water and 5 for oil and the contact angle observed was in between 30° and 60° for both water and oil (Figure 4.18 and Figure 4.19). For all the chemical treatments used, the observations of increasing imbibition times and increase in contact angles for both water and oil drop indicate that the wettability of both Berea and TCL have been modified.

Table 4.1 List of candidate fluorinated surfactants with different chemistries

Surfactant Id.	Provider	Type	Physical State at RT	Functional Group	Number of Carbons in Fluorinated Tail
474053	Aldrich	non ionic	liquid	epoxide	C ₅
474088	Aldrich	non ionic	liquid	epoxide	C ₈
3130-3-09	Synquest	non ionic	liquid	amine	C ₈
FC-X	3M	non ionic	liquid	ethylene oxide	C ₄
L-18961	3M	non ionic	solution	silane	C ₄
L-19446 #1	3M	ionic	solid	anionic calcium salt (carboxylate)	C ₄
L-19973 #9	3M	ionic	solution	cationic salt	C ₄
L-20294	3M	non ionic	solid	epoxide	C ₄
L-20836	3M	non ionic	liquid	epoxide	C ₄
L-20886	3M	non ionic	liquid	epoxide	C ₄

Table 4.2 Parameters used for XPS analysis

Analyzer	Spectrum analyzer mode Hybrid lens mode Pass energy = 20
X-Ray Gun	Filament = mono Al Emission = 10 mA Anode HT = 12 kV
Charge Neutralizer	Filament current = 1.8 A Filament bias = 1 V Charge balance = 2.7479 V

Table 4.3 Elements analyzed in XPS according to the type of rock

Rock	Type	Analyzed elements
Berea	sandstone	C 1s, F 1s, O 1s, Si 2p, Al 2p
Torrey Buff	sandstone	C 1s, F 1s, O 1s, Si 2p, Al 2p
Texas Cream Limestone (TCL)	limestone	C 1s, F 1s, O 1s, Ca 2p

Table 4.4 Fluorinated surfactants used for wettability alteration

Surfactant Id.	Type	Functional Group	Physical State at RT
FC-X	non ionic	ethylene oxide	liquid
L-20294	non ionic	epoxide	solid
L-18961	non ionic	silane	solution 15wt% active
L-19446 #1	ionic	anionic calcium salt (carboxylate)	solid
L-19973 #9	ionic	cationic salt	solution 2wt% active

Table 4.5 Solubility and sample appearance of L-20294 in different pure solvents and solvent mixtures at different concentrations and temperatures

Chemical wt%	Solvent, wt%	75°F	175°F	230°F	280°F
1	PG-IPA, 70-30	PD	TD, C	TD, C	TD, C
2	PG-IPA, 70-30	PD	TD, C	TD, C	TD, C
4	PG-IPA, 70-30	PD	TD, C	TD, C	TD, C
5	PG-IPA, 70-30	PD	PD, C	PD, C	PD, C
1	IPA	U	TD, C	TD, C	TD, C
2	IPA	U, H	TD, C	TD, C	-
1	EtOH	U, H	TD, C	TD, C	-
2	EtOH	U, H	TD, C	TD, C	-
5	EtOH	U, H	TD, C	TD, C	-
1	2BE-EtOH, 70-30	TD, C	TD, C	TD, C	TD, C
2	2BE-EtOH, 70-30	TD, C	TD, C	TD, C	TD, C

Continuation of Table 4.5

3	2BE-EtOH, 70-30	TD, C	TD, C	TD, C	TD, C
4	2BE-EtOH, 70-30	TD, C	TD, C	TD, C	TD, C
5	2BE-EtOH, 70-30	TD, C	TD, C	TD, C	TD, C
<i>Solvent nomenclature</i>					
PG	Propylene glycol				
IPA	Isopropyl alcohol				
EtOH	Ethanol				
2BE	2-Butoxyethanol				
<i>Solubility and appearance nomenclature</i>					
U	Undissolved				
PD	Partially dissolved				
TD	Totally dissolved				
C	Clear				
H	Hazy				

Table 4.6 Solubility and sample appearance of F-CX in different solvent mixtures at different concentrations, solvent ratios and temperatures

Chemical wt%	Solvent, wt%	75°F	275°F
2	PG	H	-
2	PG-EtOH, 90-10	H	-
2	PG-EtOH, 80-20	TD, C	TD, C
2	PG-EtOH, 70-30	TD, C	TD, C
2	PG-IPA, 90-10	H	-
2	PG-IPA, 80-20	TD, C	TD, C
2	PG-IPA, 70-30	TD, C	TD, C
1	2BE-EtOH, 70-30	TD, C	TD, C
2	2BE-EtOH, 70-30	TD, C	TD, C
3	2BE-EtOH, 70-30	TD, C	TD, C

Table 4.7 Solubility and sample appearance for L-18961 in the different solvent mixtures at different ratios, concentrations, and temperatures

Chemical wt%	Solvent, wt%	75°F	175°F
1	IPA	TD, C	TD, C
1	2BE-EtOH 70-30	H	H
1	2BE-EtOH-IPA 70-25-5	H	PD, C
1	2BE-EtOH-IPA, 60-30-10	PD	TD, C
2	2BE-EtOH-IPA, 60-30-10	PD	TD, C
3	2BE-EtOH-IPA, 60-30-10	PD	PD, C

Table 4.8 Solubility and sample appearance for L-19446#1 in a solvent mixture of 2BE-EtOH (70-30 wt %) at different concentrations and temperatures

Chemical wt%	Solvent, wt%	75°F	175°F
1	2BE-EtOH, 70-30	TD, C	TD, C
2	2BE-EtOH, 70-30	TD, C	TD, C
3	2BE-EtOH, 70-30	PD	TD, C

Table 4.9 Composition of brines used for sandstone and limestone cores

Component	Brine 1 g/L	Brine 2 g/L
Sodium Chloride, NaCl	25	25
Calcium Chloride, CaCl ₂	-	0.25

Table 4.10 Compatibility of FC-X (2 wt%) in 2BE-EtOH (70-30 wt%) with Brine 1

Brine, wt%	75°F	175°F	275°F
5	Clear, precipitate	Clear	Clear
10	Clear	Clear	Clear
20	Clear	Clear	Clear
30	Clear	Clear	Clear
40	Cloudy	Clear	Clear
50	Cloudy	Cloudy	Little Cloudy
60	Cloudy	Cloudy	Clear -2 Phase

Table 4.11 Compatibility of L-20294 (2 wt%) in 2BE-EtOH (70-30 wt%) with Brine 1

Brine, wt%	75°F	175°F	275°F
5	Clear	Clear	Clear
10	Clear	Clear	Clear
20	Clear	Clear	Clear
30	Clear	Clear	Clear
40	Clear	Clear	Clear
50	Clear	Clear	Clear
60	Clear	Clear	Cloudy

Table 4.12 Compatibility of L-18961 (1 wt%) in 2BE-EtOH-IPA (60-30-10 wt%) with Brine 1

Brine, wt%	75°F	175°F
5	Clear	Clear
10	Clear	Clear
15	Clear	Clear
20	Clear	Clear
25	Clear	Clear
30	Little Cloudy	Clear
35	Cloudy	Clear
40	Cloudy	Little Cloudy
50	Cloudy	Cloudy

Table 4.13 Compatibility of L-19973 #9 (2 wt%) in 2BE-EtOH (70-30 wt%) with Brine 1

Brine, wt%	75°F	175°F	275°F
5	Clear	Clear	Clear
10	Clear	Clear	Clear
20	Clear	Clear	Clear
30	Clear	Clear	Clear
40	Clear	Clear	Clear
50	Clear	Cloudy	Clear
60	Cloudy	Cloudy	Little Cloudy

Table 4.14 Compatibility of L-19446#1 (2 wt%) in 2BE-EtOH (70-30 wt%) with Brine 2

Brine, wt%	75°F	175°F
5	Clear	Clear
10	Clear	Clear
20	Clear	Clear
30	Clear	Clear
40	Clear	Clear
50	Clear	Clear

Table 4.15 Composition of chemical treatments used for core flood experiments

Chemical Treatment	Surfactant Id.	Surfactant wt%	Solvents, wt %
1	FC-X	2	2-Butoxyethanol / Ethanol, 70/28
2	L-20294	2	2-Butoxyethanol / Ethanol, 70/28
3	L-18961	1	2-Butoxyethanol / Ethanol / IPA, 60/30/9
4	L-19973 #9	2	2-Butoxyethanol / Ethanol, 70/28
5	L-19446 #1	2	2-Butoxyethanol / Ethanol, 70/28

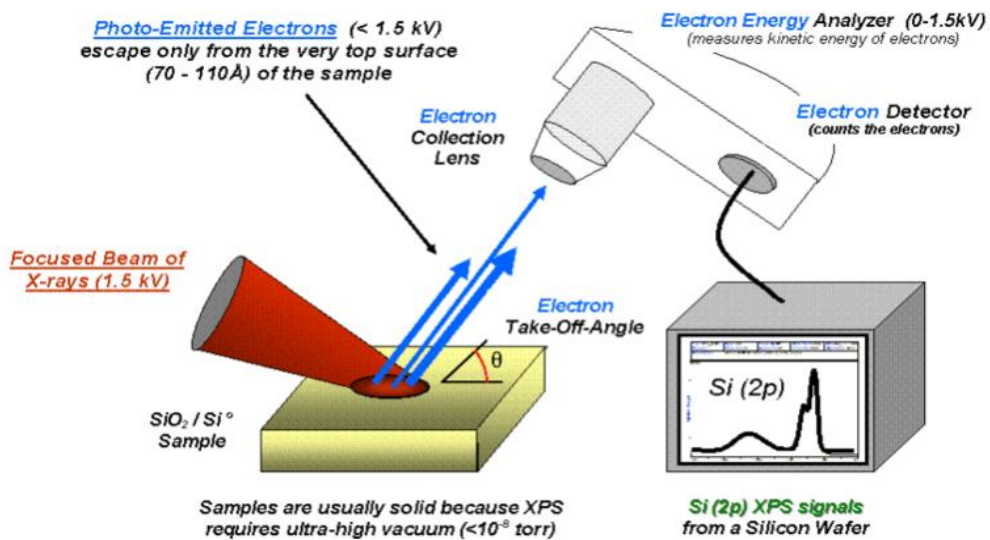


Figure 4.1 XPS Schematic (Bvcrist)

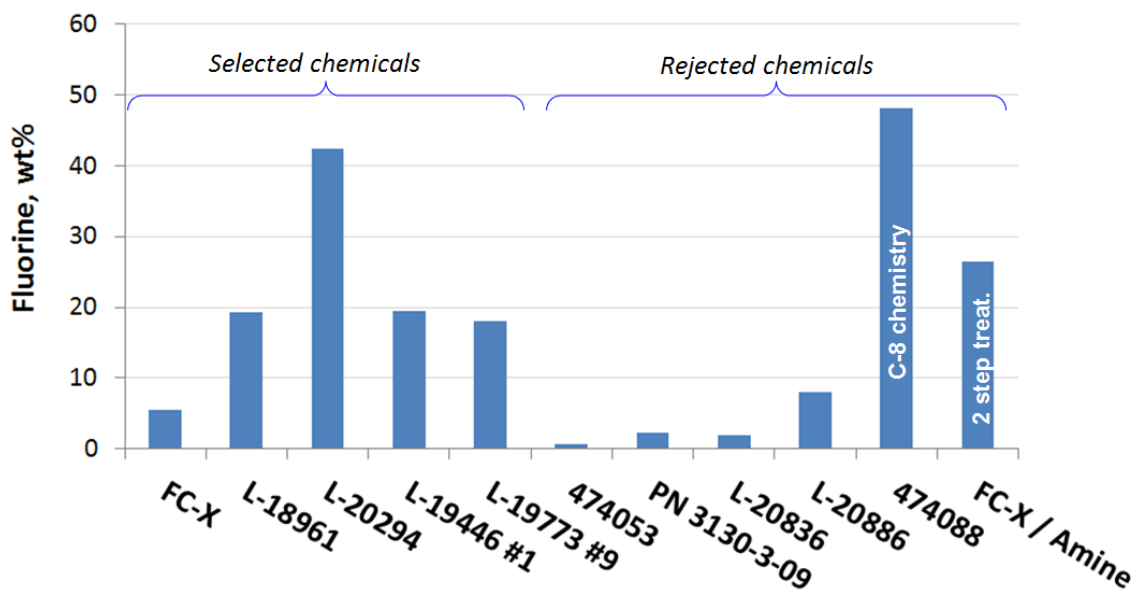


Figure 4.2 XPS results for fluorine content on surface of treated chips with candidate fluorinated surfactants

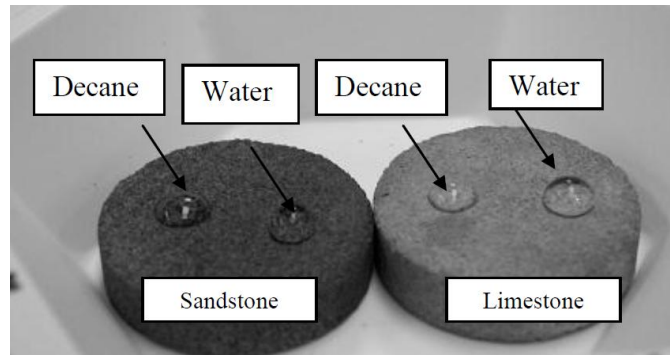


Figure 4.3 Drop test on sandstone and limestone chips treated with FC-X and amine primer

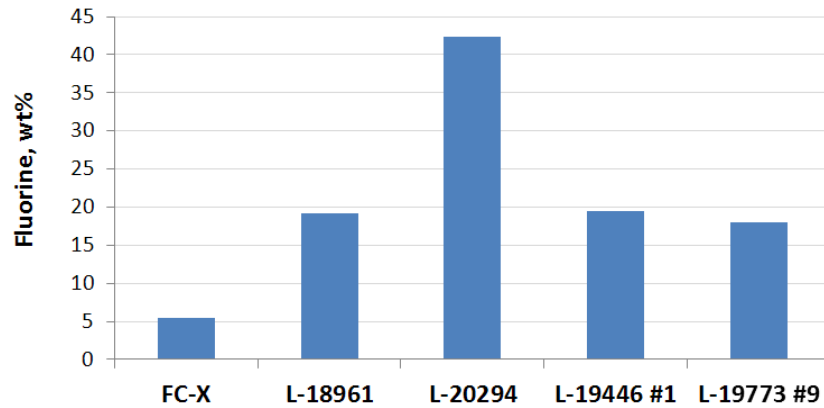


Figure 4.4 XPS results for fluorine content on surface of treated chips with selected fluorinated surfactants

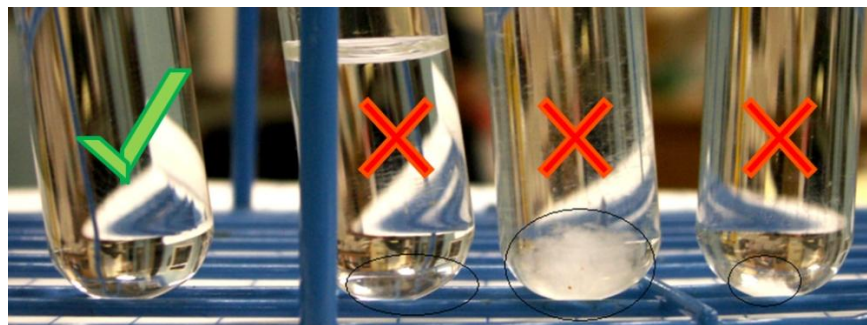


Figure 4.5 Examples of a clear single phase sample, sample with phase separation, with cloudiness and with solid precipitation, respectively, during compatibility analysis for the systems surfactant-solvents-brine

Water drop



Figure 4.6

Untreated Berea
sandstone

n-Decane drop



Figure 4.7

Time to complete imbibition ~1.5 sec

Time to complete imbibition ~ 1 sec

Berea sandstone
treated with
FC-X
(chem. treat. 1)



Figure 4.8

Time to complete imbibition ~ 10 sec



Figure 4.9

Time to complete imbibition ~ 4 sec

Berea sandstone
treated with
L-20294
(chem. treat. 2)

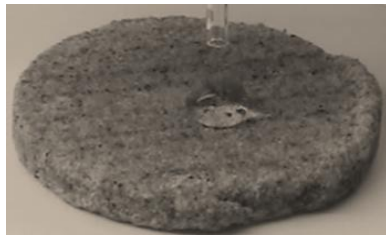


Figure 4.10

No imbibition even after several min



Figure 4.11

Time to complete imbibition ~ 4 sec

Berea sandstone
treated with
L-18961
(chem. treat. 3)



Figure 4.12

No imbibition even after several min

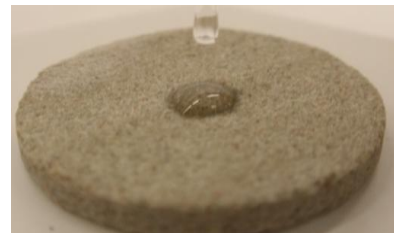


Figure 4.13

Time to complete imbibition ~ 5 sec

Berea sandstone
treated with
L-19973 #9
(chem. treat. 4)

Water drop



Figure 4.14

Time to complete imbibition ~20 sec

n-Decane drop

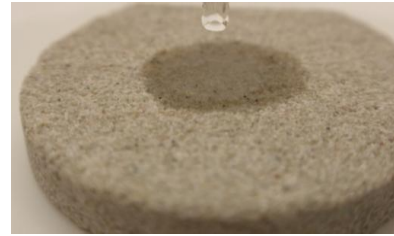


Figure 4.15

Time to complete imbibition ~3 sec

Untreated Texas
cream limestone
(TCL)



Figure 4.16

Time to complete imbibition ~15 sec



Figure 4.17

Time to complete imbibition ~1.5 sec

TCL
treated with
L-19446 # 1
(chem. treat. 5)



Figure 4.18

Time to complete imbibition ~40 sec



Figure 4.19

Time to complete imbibition ~8 sec

Chapter 5: Chemical Treatment of Sandstones

The most meaningful evaluation of the performance of fluorinate chemical treatments in mitigating “gas blocking” damage was done using high pressure high temperature (HTHP) core flood experiments. Using core flood experiments it is possible to study the actual behavior of fluids as they flow through the porous media under reservoir conditions. These experiments are the closest representation of reservoir conditions that can be achieved in the laboratory. Core flood experiments allow a calculation of the actual gas and oil relative permeabilities before and after and after treatment so that the effect that results from the fluorinated chemical treatment can be quantitatively measured.

The formulation of the chemicals treatments has been explained in detail in the previous chapter and the final formulations used for the HPHT core flood experiments are summarized in Table 4.15. Five chemical treatments were selected for core flood experiments; four of them were used for treating sandstones specifically Berea and Torrey Buff cores and the remaining chemical treatment was used to treat limestone, specifically Texas Cream Limestone (TCL) cores. In this chapter, the main results of these experiments are discussed as well as the observed effects that surfactant type, temperature, capillary number, PVT ratio and rock permeability can have on the outcome of sandstones treated with fluorinated surfactants. The results for treated limestone cores are discussed in Chapter 6. A detailed description of the HTHP core flood experimental set up and the general procedure for the experiments is in Chapter 3 and a schematic of the setup is shown in Figure 3.1. Variations in the general experimental procedures for each of the sandstone core flood experiments are noted in the following discussion and a detailed description of each of the core flood experiments is given in Appendix A. The

HPHT core flood experiments performed for the treatment of sandstones and the experimental conditions are summarized in Table 5.1. The sequence of the discussion of the experiments does not match the number of the experiment because not all of the chemicals were available from the beginning of this research, and it was during the research process that potential chemical treatments were identified, received, and studied.

5.1 EFFECT OF SURFACTANT TYPE

To find the best formulation to alter the wettability of sandstone rocks in volatile oil reservoirs, four different fluorinated chemical treatments were used to treat sandstone rocks; each of them using a different type of surfactant. The four surfactants chosen were FC-X (ethylene oxide), L-20294 (epoxide), L-18961 (silane) and L-19973#9 (an ionic carboxylate) (Table 4.4). All of them were assumed to have a similar type of C₄ fluorinated tail. These four chemicals were provided by 3M Company and disclosure of their molecular structure was not given. Thus, the study of the interaction of the surfactant with the treated sandstone rocks was limited to experimental observations of the behavior of each surfactant during core flood experiments and results from complementary analytical tools.

Four experiments were conducted to compare and to observe the behavior of the different selected surfactants (Experiments #141, #146, #158 and #192). The solvent used was common for all chemical treatments used: 2-butoxyethanol / ethanol (70/28), except for the case of chemical treatment 3, 2-butoxyethanol / ethanol / IPA (60/30/9) as shown in Table 4.15. All four experiments followed the general experimental procedure described in Section 3.2.2 and the experimental conditions are given in Table 5.2. These experiments were performed on Berea sandstone cores at 155°F. The composition of the synthetic

volatile oil mixture is given in Table 3.3. An initial water saturation of 20% was established following the procedures described in Section 3.2.2.2. This was done using synthetic brine 1 given in Table 4.9. In most of the cases, the gas relative permeability at S_{wi} was about 0.75 times the gas permeability in the dry core. Experiments #141, #146, #158 and #192 were performed using the chemical treatments numbers 2, 1, 3 and 4, respectively.

Bang (2007) measured about 3 to 3.5 mg of FC-X surfactant adsorption per gram of Berea sandstone. Based on this result, 660 to 770 mg of this surfactant were assumed to be adequate to treat a Berea core with a mass of 220 gr; this represents approximately 2 PV of chemical treatment with a surfactant concentration of 2 wt%. However, to be sure that maximum adsorption was obtained and that the rock surface was completely saturated with fluorinated surfactant, the mass of surfactant used to treat a core was increased 10 fold. For all the other surfactants shown in Table 4.4 surfactant adsorption values on Berea sandstone were not measured. For Experiments #141, #146 and #192, 20 PV of treatment at a surfactant concentration of 2 wt% was used for treating the cores, which is more than sufficient surfactant to satisfy adsorption assuming it is about the same as FC-X. The treatment rates were 110 to 120 cc/hr and the core was shut-in time for 12 to 15 hrs before conducting the post-treatment two-phase volatile oil flood. This flow rate was assumed to give enough residence time for the surfactant to adsorb based on the study by Bang (2007). He observed that shut-in times as short as 1 hour resulted in high improvement factors for two-phase gas condensate floods, and increasing this time to 15 hours resulted in a gain of only 15%. The relatively fast self-polymerization of the surfactant L-18961 used for Experiment # 158, which corresponds to chemical treatment 3, resulted in lower amounts of treatment used and shut-in time. For this

experiment, only 10 PV were injected and the core was shut-in for 2 hours only as suggested by the surfactant provider.

For experiment #141, the surfactant used was L-20294. Figure 5.1 illustrates the pressure drop between inlet and outlet of the core during injection of chemical treatment 2. The pressure drop reach a peak value of about 30 psi at 1 PV and then decreased to about 10 psi at about 3 PV. For the remaining injected pore volumes the pressure drop shows a slight increase. This type of pressure drop profile during treatment injection has been typically observed for this type of chemical treatments. Pre and post-treatment two-phase volatile oil floods were conducted at two flow rates, 680 and 1360 cc/hr, at 700 psig core pressure. For this pressure and for a temperature of 155°F, the PVT ratio for this synthetic fluid is 0.98. Figure 5.2 compares the pressure drop across the core during two-phase volatile oil injection before and after treatment. The treatment initially improved the gas and oil relative permeability (improvement factor) by a factor of 1.7 at 680 cc/hr and 1.6 at 1360 cc/hr.. After injection of about 730 PV of post treatment volatile oil injection, the improvement factor (IF) decreased to 1.5 and 1.4 at these same flow rates.

For Experiment # 146 the core was treated with surfactant FC-X. The pressure drop versus pore volumes injected of chemical treatment 1 is illustrated in Figure 5.3. No indications of plugging or rock damaging during chemical treatment injection were observed. The flow rates used for pre and post-treatment two-phase volatile oil floods were 460 and 920 cc/hr, the temperature 155°F and the core pressure 995 psig. PVT ratio was 0.79. About 600 PV of post-treatment two-phase volatile oil were injected and Figure 5.4 compares the pre and post-treatments pressure drops during two-phase volatile oil floods. The IF ranged from 1.4 to 1.3 for both flow rates.

Experiment # 158 used surfactant L-18961. The pressure drop data for injection of chemical treatment 3 is given in Figure 5.5. No plugging or abnormal pressure drop behavior was observed. For this experiment three flow rates were used for the two-phase volatile oil floods, but only the lowest rate is of interest for this section; 690 cc/hr at a core pressure of 800 psig and a temperature of 155°F. The PVT ratio was 0.85. After about 90 PV of post-treatment volatile oil injection an IF of 1.90 was obtained. The pressure drops for pre and post treatment two-phase volatile oil floods are compared in Figure 5.6.

Experiment # 192 tested surfactant L-19973#9. Figure 5.7 shows the pressure drop data in the core during injection of chemical treatment 4. As with the other chemical treatments, no plugging or abnormal behavior was observed. Two-phase volatile oil flood rates were used; 438 and 875 cc/hr at 155°F and 1040 psig core pressure. The PVT ratio for the synthetic volatile oil was 0.77. After about 550 PV of post-treatment volatile oil injection, the IF ranged from 1.8 to 1.6 for the low flow rate, and 1.5 to 1.4 for the high flow rate. Figure 5.8 compares the pre-treatment and post-treatment two-phase volatile oil floods.

The results for Experiments # 141, # 146, # 158 and # 192 are summarized in Table 5.3, and details for each of them are given in Appendixes A.2, A.3, A.5 and A.10 respectively. The pressure drop decreased in all of these experiments after treatment to change the wettability.

To test the durability of the treatment multiple post-treatment volatile oil floods were conducted for experiments #141 and #146. The improvement factor dropped slightly for the second flood and then remained constant at about 1.4 for the third. This suggests that the treatment will provide long term benefits.

Thus, under similar experimental conditions different chemical treatments with non-ionic and ionic polymeric C₄ fluorinated surfactants proved to increase relative permeability to oil and gas in sandstone. Improvement factor range was 1.3 to 1.9 (Figure 5.9).

5.2 EFFECT OF TEMPERATURE

Surfactant adsorption depends on surfactant structure and concentration, solvent composition, characteristics of the substrate's surface and temperature. Bang (2007) found that the adsorption of FC-X on Berea sandstone increased slightly with temperature (175°F to 250°F) (Figure 5.10). The solubility of FC-X decreases as temperature increases and eventually reaches a cloud point as expected for a non-ionic surfactant. The weaker interaction with the solvent as temperature increases would be expected to increase adsorption and make it more effective in changing the wettability of the mineral surfaces at higher temperatures. Experiments were done to determine the effect of temperature on the effectiveness of the surfactants L-18961 and FC-X used in this study. The range of testing temperatures was 155°F to 275°F which are typical reservoir temperatures.

Surfactant L-18961 was used for Experiment # 158 and # 176 at a temperature of 155°F, and for Experiment #189 at 250°F. Table 5.4 shows a summary of the experimental conditions for these experiments. The experimental procedure followed is the one described in Section 3.2.2, with the only variation that multiple core pressures were used. Multiple core pressures were used to test different volumetric gas to oil ratios. Detailed procedures for these experiments are given in Appendix A.5, A.6 and A.9. Figure 5.5, Figure 5.11 and Figure 5.12 show the pressure drop during injection of treatment solution for each of the experiments. The pressure drop for Experiment #189 is

less than half of that observed for the experiments #158 and #176. This is because the treatment solution viscosity is much lower at 250°F. Figure 5.6, Figure 5.13 and Figure 5.14 show the pressure drop during two-phase volatile oil injection before and after treatment. Lower pressure drops during volatile oil injection with increasing temperature were also observed. The gas to oil viscosity ratio varied from 0.06 at 155°F to 0.07 at 250°F, and the PVT ratio from 0.85 to 1. The initial improvement factor of oil and gas relative permeability was 1.8 at 155°F and 2.6 at 250°F. Figure 5.15 and Table 5.5 summarize the results for Experiments #158, #176 and #189.

FC-X was tested for temperature effects in Experiment # 210, # 228 and #229 at 155°F, 215°F and 275°F respectively. The experimental conditions are shown in Table 5.6. The experimental core flood procedure followed the general form and for each experiment the exact procedure and results are discussed in Appendixes A.14, A.18 and A.19. For Experiment #210 five different core pressures were used, but only the results obtained at 800 psia core pressure are of interest for this section. Results for injection of chemical treatment are shown in Figure 5.16, Figure 5.17 and Figure 5.18. For these experiments, it was also observed that treatment pressure drops decreased with increasing temperature and no plugging was observed. The results for two-phase volatile oil injection before and after treatment are shown in Figure 5.19, Figure 5.20, Figure 5.21. Pressure drops slightly decreased with increasing temperature. Using these pressure drops, oil and gas relative permeabilities before and after treatment were calculated and Figure 5.22 illustrates the changes of relative permeability with temperature before and after treatment. Oil relative permeability slightly decreases with increasing temperature, and the difference between the oil and gas relative permeability increases. Gas to oil viscosity ratio increased from 0.07 to 0.012 and PVT ratio increased from 0.9 to 1.5.

Improvement factors increased from 2.46 to 3.54 with increasing temperature. The results for Experiments #210, #228 and #229 are summarized in Table 5.7.

Experiments with L-18961 and FC-X indicate the improvement factor increases with temperature as shown in Figure 5.23. There are two possible reasons for this trend with temperature. The surfactants may be less soluble at higher temperature leading to higher adsorption on the mineral surfaces and the solvents are more volatile and less viscous at higher temperature, which makes them easier to remove from the core.

5.3 EFFECT OF CAPILLARY NUMBER

As explained in section 3.3.3, capillary number is an expression that relates the effect of viscous to capillary forces. Equation 3.14 shows the definition used in this research. When the viscous forces exceed the capillary forces, the residual saturations of wetting and non-wetting phases decrease and this leads to higher relative permeability values. The idea behind treating the reservoir rock with fluorinated chemicals is to modify the rock wettability to improve the oil and gas relative permeabilities. There is less potential for improvement from modifying the wettability as the capillary number increases to very high values because the cause of the low relative permeability values (residual saturations) has already been eliminated.

Bang (2007) corrected the gas relative permeability for non-Darcy effects at high Reynolds number using Equation (5.1):

$$k_{rg} = \frac{\mu_g u_g}{k \Delta P} (1 + N_{Re}) \quad (5.1)$$

Where μ_g and u_g are the gas viscosity and Darcy velocity, k is the gas permeability (same as absolute permeability), ΔP is the pressure drop across the rock, and N_{Re} is a modified Reynolds number (Mott et.al. 2000). Bang then correlated the

corrected gas relative permeability with the non-dimensional groups capillary number and PVT ratio. Figure 5.24 shows the gas relative permeability increases above a critical capillary number on the order of 10^{-5}

Results from Experiment #148 using synthetic volatile oil mixture shown in Figure 5.25 and Figure 5.26 indicate that volatile oils appear to follow this same trend. The observed threshold value was $N_c \sim 2 \times 10^{-5}$. The experimental conditions for this experiment are shown in Table 5.8. For this experiment, chemical treatment 2 was used (surfactant L-20294). Figure 5.27 illustrates the chemical treatment injection, no plugging or unusual behavior was observed. Data for the pressure drop at steady state was measured for five increasing core pressures; 900, 1600, 2500, 3100 and 3500 psi. Figure 5.28 to 5.32 show the injection of the pre and post treatment two-phase volatile oil floods for each of the core pressures. For each of the core pressures the volumetric gas to oil ratio was changed resulting in increasing capillary number and decreasing PVT ratio. The volumetric gas to oil ratio went from 12.2 to 0.6, the capillary number increased from 1.7×10^{-5} to 1×10^{-2} , the interfacial tension from 8.1 to 4×10^{-3} dyne/cm and the PVT ratio from 0.7 to 0.35. The injection flow rate of the single phase volatile oil mixture upstream of BPR-1 was kept constant. Table 5.9 shows the results and calculated improvement factors for each of the core pressures. As the core pressure was increased the capillary numbers increased from 1×10^{-5} to 1×10^{-3} . The improvement factors decreased from 1.4 to 0.7, as the capillary number increased. The loss of improvement factor with increasing capillary number confirms that the effect of fluorinated chemical treatment is diminished when flow is dominated viscous forces and not capillary forces. For these cases, the small variations in IF and the apparently null improvements ($IF < 1$)

observed may be due to experimental error that is inherent in complex experiments. Appendix A.4 compiles the experimental procedure and the results for Experiment #148.

In Figure 5.33 the capillary number effect on gas and oil relative permeability before and after chemical treatment for Experiment #146, #141 & #192 is also summarized. Only one PVT ratio is considered for each of the experiments. In this figure as well as in Figure 5.25Figure 5.26, it can be observed that the oil and gas relative permeability increase with capillary number. The results of these experiments are consistent with those shown before in that at capillary numbers of the order 2×10^{-5} and below a significant increase in relative permeability is observed. The capillary number decreases for a given PVT ratio after a successful chemical treatment due to the lower pressure drop.

Figure 5.34 shows the effect of capillary number on improvement factor for Experiment #141, #146, #148 & #192. In this figure, separate experiments using volatile oil mixture 2 but treated with different fluorinated surfactants (FC-X, L-20294 and L-19973#9) show a clear trend of decreasing improvement factor with increasing capillary number. There exists a threshold capillary number of about $N_c \sim 3.5 \times 10^{-5}$ where the chemical treatment is no longer effective. The same threshold capillary number was observed for Experiment #176, which followed the same procedure as Experiment #148, showing very similar results to the ones observed in Experiment #148 even though a different surfactant, L-18961, was used. Improvement factor decreased from 1.8 to 0.8 for capillary numbers from 1×10^{-5} to 5×10^{-5} . Experiment #176 is described in Appendix A.6. The experimental conditions and results are shown in Table 5.10 and Table 5.11.

Experiment #210 followed the same procedure as that used for Experiment #148 and #176; multiple core pressures of 800 psi, 1100 psi, 1500 psi, 2200 psi and 2900 psi

were used. However, for this experiment the capillary number was kept constant at a value of 1×10^{-5} . To obtain this value the single phase volatile oil flow rates were low for the experiments conducted at the higher core pressures. For the core pressure used, the volumetric gas to oil ratio decreased from 14.4 to 1.6, and the PVT ratio decreased from 0.9 to 0.54. Table 5.12 shows the experimental conditions of this experiment. FC-X was used to treat the core; the pressure drop versus pore volumes injected is illustrated in Figure 5.35. Nothing unusual was observed during the treatment injection. Figure 5.36 to 5.40 show the pre and post-treatment pressure drop during injection of two-phase volatile oil for each of the different core pressures used. The results and calculated improvement factors for each of the core pressures are summarized in Table 5.13. Improvement factor varied from 2.5 to 1.3 for a constant capillary number of about 1×10^{-5} . For this experiment IF was positive for all the floods at different core pressures. This indicates that the flow is dominated by capillary forces. Again, this is because capillary number was kept low. Complete experimental procedure and results for Experiment #210 are described in Appendix A.14.

For Experiments #148, #176 and #210, improvement factors and capillary numbers versus oil volume fractions are compared in Figure 5.41, Figure 5.42, Figure 5.43 respectively. For all the cases the improvement factor decreases with increasing capillary number. When the capillary number was kept constant an improvement was observed at all core pressures and volumetric fractions.

5.4 EFFECT OF PVT RATIO

As mentioned in Chapter 3, (Chopra and Carter 1986) recognized that for steady state flow, the gas/oil relative permeability ratio can be expressed as a function of PVT ratio. Later, Bang (2007) found this is true only when non-Darcy flow is insignificant or

when a correction is made for non-Darcy flow. The developed relationship previously expressed in Equation 3.7 implies that at a given core pressure, the ratio of gas to oil relative permeability is fixed and only the fluid properties define it assuming the temperature is also constant. Thus, relative permeability before and after treatment for any phase (oil or gas) can be compared, any observed difference being attributed to the chemical treatment.

From the results obtained in Experiment #148, #176 and #210, improvement factor and PVT ratios for different oil volume fractions are compared in Figure 5.44, Figure 5.45 and Figure 5.46. Comparison shows that both, the improvement factor and the PVT ratio, similarly decrease for increasing oil volume fractions at increasing capillary numbers and at constant low capillary number.

From Figure 5.47 through Figure 5.50, improvement factor versus PVT ratio is compared by type of chemical treatment for experiments performed on Berea sandstone cores with similar permeability and homogeneity. The permeability of these cores was within the range of 100 to 200 md. Table 5.14 summarizes improvement factors measured for different PVT ratios sorted by surfactant type for these various experiments. For all the chemical treatments, the improvement factor increases with increasing PVT ratio. Each of these experiments is explained in Appendix A. Two different IF values are used for the comparisons. Those that correspond to the improvement factor observed for the first post-treatment two-phase volatile flood, are called “initial improvement factor”, and those from for the second and/or third post-treatment two-phase volatile also called “final improvement factor”.

5.4.1 The improvement factor – PVT ratio correlation

To prove the relationship between PVT ratio and improvement factor, the results previously discussed (Table 5.14) were combined and correlated. The correlated results come from experiments that have in common the following characteristics: same type of core, similar permeability, treated with similar types and amounts of fluorinated chemicals, and flow rates within the same capillary number range. Experimental conditions such as temperature, pressure and hydrocarbon compositions define the fluid properties and are to be accounted for in the PVT ratio values.

Figure 5.51 shows the observed initial improvement factor as a function of PVT ratio and Figure 5.52 does the same but for final improvement factor. The results suggest a linear correlation between improvement factor and PVT ratio. The experimental correlation obtained for initial improvement factor for the set of experiment here discussed is as follows:

$$IF = 2.46 N_{PVT} - 0.09 \quad (5.2)$$

And for final improvement factor

$$IF = 1.89 N_{PVT} + 0.04 \quad (5.3)$$

Where N_{PVT} is the PVT ratio.

The correlations are for Berea sandstone cores with permeabilities in the range of 100 to 200 md, treated with 10 to 20 PV of 1 to 2 wt% fluorinated C4 chemical, and capillary numbers around 1×10^{-5} .

As shown in Figure 5.51, improvement factors obtained for gas condensate floods also seem to be in good agreement with the suggested correlation. The data for gas condensates plotted correspond to improvement factors obtained from Experiment # 192

(procedure described in Appendix A.10), and Experiment # 21 and #63 from Bang (2007).

Thus, the general form of this correlation can be resumed as

$$IF = a N_{PVT} + b \quad (5.4)$$

Where a and b are experimental constants for specific rock, fluorinated surfactant types, and capillary number range.

Substituting equation 3.17 into equation 5.4 gives

$$IF = a \frac{f_g \mu_g}{f_o \mu_o} + b \quad (5.5)$$

Where f_g and f_o are the volumetric fractional flows and μ_g and μ_o are the viscosities of gas and oil respectively, in other words: the fluid properties, for a given temperature and pressure.

Gas to oil viscosity ratio decreases with increasing PVT ratio therefore the increase in IF with PVT ratio is mainly driven by gas and oil saturations.

A mechanistic physical explanation of why the IF increases with PVT ratio may be due to the reason that higher PVT ratio is caused by higher gas volume which is higher gas saturation which implies higher residual gas saturation (Land 1968) which then provides more potential for improvement by reducing residual gas saturation by changing the wettability. Leading the reduction of residual gas saturation to higher oil saturation which in turns increases the oil relative permeability. The gas relative permeability increases as well since PVT ratio is constant before and after treatment.

5.5 EFFECT OF LOW PERMEABILITY

To evaluate the applicability of the fluorinated chemical treatment in lower permeability sandstones for volatile oil reservoirs, two experiments were performed; Experiment #196 and Experiment #198. In these experiments, Torrey Buff sandstone cores with a permeability of 1.1 and 2.7 md were used. For both of them, chemical treatment 4 (L-19973#9) showed an IF of 1.10 and 1.16 respectively. A summary of the experimental conditions is presented in Table 5.15 and the experiment description is shown in Appendix A.11 and A.12. Figure 5.53 and Figure 5.54 show the pressure drop across the core for chemical treatment 4 injection for both experiments. At low permeabilities, injection of the treatment resulted in very low injection rates, and high pressure drops. Pressure drops for two-phase volatile oil injection are shown in Figure 5.55 and Figure 5.56. For low-permeability cores pressure drops are high and oil and gas relative permeability increases slightly after chemical treatment. However, the small gains obtained in relative permeabilities due to the chemical treatment reduce the pressure drop significantly. The improvement factor was 1.1 for Experiment #196 and 1.2 for Experiment #198. Table 5.16 summarizes the results for these low permeability experiments.

Figure 5.57 compares the improvement factors obtained for the low permeability Experiment #196 and #198 with the result obtained for a higher permeability, Experiment #192. All these experiments were performed using chemical treatment 4. The effect of low permeability on improvement factor indicates that; for low permeabilities the improvement factor is smaller.

The lower improvement factor seen in lower permeability cores may be due to incomplete removal of the solvent. Solvents with greater volatility may be more effective and are being explored for these low permeability cores (McCulley 2011).

5.6 SUMMARY AND CONCLUSIONS

Several HPHT core flood experiments using sandstone cores, Berea and Torrey Buff, with initial water saturation and under reservoir conditions were treated with fluorinated surfactants. All the surfactants had a C₄ fluorinated chemistry. Steady-state gas and oil relative permeabilities were determined for pre and post-treatment two-phase volatile oil floods using measured steady state pressure drops. For sandstones, coreflood experimental results show that fluorinated surfactant treatments can improve the relative permeability of both oil and gas by factors as high as 3, at low capillary numbers on the order of 1×10^{-5} to 1×10^{-6} , and for volatile oils with GOR's in the range of 4000 to 13,000 scf/STB. Table 5.17 summarizes conditions and results for the HPHT volatile oil core floods performed on sandstones.

A linear correlation between the measured improvement factors and the PVT ratio was observed. . This correlation is a function of fluid properties and is specific for type of rock, permeability range, type and amount of chemical treatment, and capillary number range.

Additional conclusions are as follows:

- C₄ fluorinated surfactants with non-ionic and ionic functional groups were shown to work by altering the wettability of sandstone rocks.
- Fluorinated chemical treatments with surfactant concentrations ranging from 1 to 2 wt% in a 2-butoxyethanol/ethanol solvent improved gas and oil relative permeabilities of sandstones with initial water.
- The fluorinated chemical treatments proved their applicability at high temperatures.

- Temperature has a positive effect on the performance of fluorinated chemical treatments.
- Fluorinated chemical treatments are less effective above the critical capillary number of about $N_c \sim 3 \times 10^{-5}$ for Berea sandstone.
- For volatile oils, the improvement factor increases as the PVT ratio increases. This implies the treatment will work better in wells with high GORs where it is needed the most. The improvement factor was lower in low permeability sandstones. This may be due to the difficulty of displacing the solvent after the treatment.

Table 5.1 Experimental conditions of core flood experiments performed for treatment of sandstones

	<i>Rock Type</i>	k_g (md)	<i>Temperature</i> °F	<i>Core Pressure</i> (psia)	S_{wi} % w/ <i>Brine 1</i>	<i>Volatile Oil Mixture</i>	<i>Chemical Treat. Num</i>
Exp# 134	Berea	154	155	690	20	2	1
Exp# 141	Berea	189	155	700	20	2	2
Exp# 146	Berea	113	155	1000	20	2	1
Exp# 148	Berea	144	155	900,1600, 2500, 3100, 3500	20	2	2
Exp# 158	Berea	217	155	800,1500, 2200, 2900	20	2	3
Exp# 176	Berea	149	155	800, 1500, 2200, 2900	20	2	3
Exp# 189	Berea	211	250	800, 1500	20	4	3
Exp# 192	Berea	205	155	1000	20	2	4
Exp# 196	Torrey Buff	1.1	155	700	20	2	4
Exp# 198	Torrey Buff	2.7	155	700	20	2	4
Exp# 200	Berea	366	155	800, 1500, 2200, 2900	20	2	3
Exp# 210	Berea	178	155	800, 1100, 1500, 2200, 2900	20	2	1
Exp# 221	Berea	93	155	2915	20	2	1
Exp# 224	Berea	133	155	2220	20	2	1
Exp# 228	Berea	170	215	850	20	3	1
Exp# 229	Berea	193	275	850	20	5	1

Table 5.2 Summary of conditions for Experiments # 141, #146, #158 and #192

	Exp# 141	Exp# 146	Exp# 158	Exp# 192
<i>Rock type</i>	BEREA	BEREA	BEREA	BEREA
<i>k_g, md</i>	189	113	217	212
<i>S_{wi}%</i>	20	20	20	20
<i>Brine Salinity NaCl, ppm</i>	25,000	25,000	25,000	25,000
<i>Temperature, °F</i>	155	155	155	155
<i>Single-Phase Vol. Oil Pressure (BPR-1), psig</i>	4,475	4,435	4,460	4,455
<i>Two-Phase Vol. Oil Pressure (BPR-2), psig</i>	700	995	800	1040
<i>Volatile Oil Mixture</i>	2	2	2	2
<i>Chemical Treatment</i>	2	1	3	5
<i>Surfactant</i>	L-20294	FC-X	L-18961	L-19973#9

Table 5.3 Summary of results for the effect of surfactant type on treatment of Berea sandstone (Experiments #141, #146, #158 and #192)

	Exp# 141		Exp# 146		Exp#158	Exp# 192	
<i>Core pressure, psia</i>	700		995		800	1040	
<i>q_{gtot core}, cc/hr</i>	680	1359	460	920	689	438	875
<i>q_g, cc/hr</i>	643	1286	420	840	644	397	795
<i>q_o, cc/hr</i>	37	73	40	80	45	40	81
<i>Nc</i>	1.3E-05	2.4E-05	1.3E-05	2.3E-05	1.9E-05	2.5E-05	4.3E-05
<i>PVT Ratio</i>	0.98		0.79		0.85	0.77	
<i>Liquid Fraction</i>	5.40%		8.70%		6.50%	9.20%	9.20%
<i>k_{rg} Before Treatment</i>	0.035	0.039	0.031	0.036	0.029	0.017	0.020
<i>k_{ro} Before Treatment</i>	0.036	0.040	0.039	0.045	0.034	0.022	0.026
<i>Initial Improvement Factor *</i>	1.7	1.6	***	1.4	1.9	1.8	1.5
<i>PV of Vol. Oil Injected</i>	~ 730		~600		~ 90	~ 550	
<i>Final Improvement Factor **</i>	1.5	1.4	1.4	1.3	****	1.6	1.4

* Improvement factor obtained from injection of the first batch of volatile oil

** Improvement factor obtained from the last batch of volatile oil injected

*** During injection of the first batch of vol. oil, only one flow rate was used

**** No accurate data was obtained for injection of the second batch

Table 5.4 Summary of conditions for Experiments # 158, #176 and #189

	Exp# 158	Exp# 176	Exp# 189
<i>Rock type</i>	BEREA	BEREA	BEREA
<i>k_g, md</i>	217	149	212
<i>S_{wi}%</i>	20	20	20
<i>Brine Salinity NaCl, ppm</i>	25,000	25,000	25,000
<i>Temperature, °F</i>	155	155	250
<i>Single-Phase Vol. Oil Pressure (BPR-1), psig</i>	4,460	4350	4280
<i>Two-Phase Vol. Oil Pressure (BPR-2), psig</i>	800	805	780
<i>Volatile Oil Mixture</i>	2	2	4
<i>Chemical Treatment</i>	3	3	3
<i>Surfactant</i>	L-18961	L-18961	L-18961

Table 5.5 Summary of results for the effect of temperature on treatment of Berea sandstone with surfactant L-18961 (Experiments #158, #176 and #189)

	Exp#158	Exp# 176	Exp# 189
<i>Core pressure, psia</i>	800	805	780
<i>q_{gtot core}, cc/hr</i>	689	694	701
<i>q_g, cc/hr</i>	644	649	654
<i>q_o, cc/hr</i>	45	45	47
<i>Capillary Nc</i>	1.87E-05	1.76E-05	1.63E-05
<i>PVT Ratio</i>	0.85	0.85	1.01
<i>Viscosity Ratio μ_g/μ_o</i>	0.06	0.06	0.07
<i>Liquid Fraction</i>	6.5%	6.5%	6.7%
<i>k_{rg} Before Treatment</i>	0.029	0.031	0.042
<i>k_{ro} Before Treatment</i>	0.034	0.036	0.042
<i>Initial Improvement Factor</i>	1.9	1.8	2.6
<i>PV of Vol Oil Injected</i>	~ 90	~120	~310
<i>Final Improvement Factor</i>	*	*	2.1

* A second batch of a volatile oil was not injected

Table 5.6 Summary of conditions for Experiments # 210, #228 and #229

	Exp# 210	Exp# 228	Exp# 229
<i>Rock type</i>	BEREA	BEREA	BEREA
<i>k_g, md</i>	178	170	193
<i>S_{wi}%</i>	20	20	20
<i>Brine Salinity NaCl, ppm</i>	25,000	25,000	25,000
<i>Temperature, °F</i>	155	215	275
<i>Single-Phase Vol. Oil Pressure (BPR-1), psig</i>	4320	4350	4080
<i>Two-Phase Vol. Oil Pressure (BPR-2), psig</i>	810	850	855
<i>Volatile Oil Mixture</i>	2	3	5
<i>Chemical Treatment</i>	1	1	1
<i>Surfactant</i>	FC-X	FC-X	FC-X

Table 5.7 Summary of results for the effect of temperature on treatment of Berea sandstone with surfactant FC-X (Experiments #210, #228 and #229)

	Exp# 210	Exp# 228	Exp# 229
<i>Core pressure, psia</i>	810	850	850
<i>q_{g tot core}, cc/hr</i>	547	519	494
<i>q_g, cc/hr</i>	511	482	458
<i>q_o, cc/hr</i>	36	37	36
<i>Capillary Nc</i>	1.19E-05	1.51E-05	1.62E-05
<i>PVT Ratio</i>	0.92	1.11	1.50
<i>Viscosity Ratio μ_g/μ_o</i>	0.07	0.09	0.12
<i>Liquid Fraction</i>	6.6%	7.1%	7.2%
<i>k_{rg} Before Treatment</i>	0.034	0.032	0.038
<i>k_{ro} Before Treatment</i>	0.037	0.029	0.026
<i>Initial Improvement Factor</i>	2.5	2.6	3.5
<i>PV of Vol Oil Injected</i>	~150	~320	~330
<i>Final Improvement Factor</i>	*	2	3

* A second batch of a volatile oil was not injected

Table 5.8 Summary of conditions for Experiment # 148

	Exp# 148
<i>Rock type</i>	BEREA
<i>k_g, md</i>	144
<i>S_{wi}%</i>	20
<i>Brine Salinity NaCl, ppm</i>	25,000
<i>Temperature, °F</i>	155
<i>Single-Phase Vol. Oil Pressure (BPR-1), psig</i>	4300
<i>Two-Phase Vol. Oil Pressure (BPR-2), psig</i>	900, 1600, 2500, 3100 & 3500
<i>Volatile Oil Mixture</i>	2
<i>Chemical Treatment</i>	2
<i>Surfactant</i>	L-20294

Table 5.9 Summary of results for the effect of increasing capillary number (Experiment #148)

	Exp# 148				
<i>Core pressure, psia</i>	900	1600	2500	3100	3500
<i>q_{gtot core}, cc/hr</i>	608	329	213	177	162
<i>q_g, cc/hr</i>	562	275	148	101	58
<i>q_o, cc/hr</i>	46	54	64	76	104
<i>Capillary Nc</i>	1.73E-05	1.12E-05	3.51E-05	4.11E-05	1.02E-03
<i>PVT Ratio</i>	0.77	0.51	0.44	0.44	0.35
<i>Viscosity Ratio μ_g/μ_o</i>	0.06	0.10	0.19	0.33	0.63
<i>Liquid Fraction</i>	7.6%	16.3%	30.3%	42.9%	63.9%
<i>k_{rg} Before Treatment</i>	0.030	0.057	0.055	0.253	0.300
<i>k_{ro} Before Treatment</i>	0.040	0.113	0.127	0.570	0.846
<i>Initial Improvement Factor</i>	2.5	1.3	0.9	0.8	0.9
<i>PV of Vol Oil Injected</i>			~300		
<i>Final Improvement Factor</i>	1.3	1.4	1.1	0.7	0.9

Table 5.10 Summary of conditions for Experiment # 176

	Exp# 176
<i>Rock type</i>	BEREA
<i>k_g, md</i>	150
<i>S_{wi}%</i>	20
<i>Brine Salinity NaCl, ppm</i>	25,000
<i>Temperature, °F</i>	155
<i>Single-Phase Vol. Oil Pressure (BPR-1), psig</i>	4350
<i>Two-Phase Vol. Oil Pressure (BPR-2), psig</i>	800, 1500, 2200 & 2900
<i>Volatile Oil Mixture</i>	2
<i>Chemical Treatment</i>	3
<i>Surfactant</i>	L-18961

Table 5.11 Summary of results for the effect of increasing capillary number (Experiment #176)

	Exp# 176			
<i>Core pressure, psia</i>	805	1500	2200	2900
<i>q_{g tot core}, cc/hr</i>	694	353	240	188
<i>q_g, cc/hr</i>	649	300	180	116
<i>q_o, cc/hr</i>	45	53	61	71
<i>Capillary Nc</i>	1.00E-05	6.44E-06	2.55E-05	4.93E-05
<i>PVT Ratio</i>	0.85	0.53	0.44	0.44
<i>Viscosity Ratio μ_g/μ_o</i>	0.06	0.09	0.15	0.27
<i>Liquid Fraction</i>	6.5%	15.0%	25.2%	38.0%
<i>k_{rg} Before Treatment</i>	0.031	0.081	0.059	0.111
<i>k_{ro} Before Treatment</i>	0.036	0.154	0.132	0.251
<i>Initial Improvement Factor</i>	1.8	1.2	0.8	0.9
<i>PV of Vol Oil Injected</i>	~160			
<i>Final Improvement Factor</i>	*	*	*	*

* A second batch of a volatile oil was not injected

Table 5.12 Summary of conditions for Experiment # 210

	Exp# 210
<i>Rock type</i>	BEREA
k_g, md	178
$S_{wi}\%$	20
<i>Brine Salinity NaCl, ppm</i>	25,000
<i>Temperature, °F</i>	155
<i>Single-Phase Vol. Oil Pressure (BPR-1), psig</i>	4320
<i>Two-Phase Vol. Oil Pressure (BPR-2), psig</i>	800, 1100, 1500, 2200 & 2900
<i>Volatile Oil Mixture</i>	2
<i>Chemical Treatment</i>	1
<i>Surfactant</i>	FC-X

Table 5.13 Summary of results for the effect of increasing capillary number (Experiment # 210)

	Exp# 210				
<i>Core pressure, psia</i>	810	1100	1500	2200	2900
$q_{g\text{tot core}}, cc/hr$	547	442	305	128	31
$q_g, cc/hr$	511	398	260	96	19
$q_o, cc/hr$	36	44	46	32	12
<i>Capillary Nc</i>	1.19E-05	1.19E-05	1.19E-05	1.21E-05	1.08E-05
<i>PVT Ratio</i>	0.92	0.73	0.61	0.54	0.54
<i>Viscosity Ratio μ_g/μ_o</i>	0.07	0.08	0.11	0.18	0.33
<i>Liquid Fraction</i>	6.6%	9.9%	15.0%	25.2%	38.0%
k_{rg} Before Treatment	0.034	0.037	0.042	0.050	0.075
k_{ro} Before Treatment	0.037	0.051	0.069	0.094	0.140
<i>Initial Improvement Factor</i>	2.5	2.2	1.6	1.3	1.4
<i>PV of Vol Oil Injected</i>			~330		
<i>Final Improvement Factor</i>	2.4	2.1	1.0	1.0	1.0

Table 5.14 PVT ratio and improvement factors by surfactant type for experiments performed on Berea sandstone

<i>Surfactant</i>	<i>Experiment</i>	<i>PVT Ratio</i>	<i>Initial IF</i>	<i>Final IF</i>
FC-X	Exp# 146	0.71	1.4	1.4
		0.71	1.3	1.3
	Exp# 210	0.92	2.5	*
		0.73	2.2	*
		0.61	1.6	*
		0.54	1.3	*
		0.54	1.4	*
	Exp# 221	0.53	1.4	1.0
	Exp# 224	0.54	2.2	1.6
	Exp# 227	0.73	1.6	1.3
	Exp# 228	1.11	2.6	2.0
	Exp# 229	1.50	3.5	3.0
Exp# 21**	0.95***	1.93***	*	
Exp# 63**	0.95***	2.17***	*	
L-18961	Exp# 158	0.85	1.9	1.9
		0.52	0.9	0.9
		0.44	0.9	0.9
		0.44	0.7	0.7
	Exp# 176	0.85	1.8	1.8
		0.53	1.2	1.2
		0.44	0.8	0.8
		0.44	0.9	0.9
	Exp# 189	1.01	2.6	2.1
		0.59	0.9	0.9
L-20294	Exp# 141	0.98	1.7	1.7
		0.98	1.6	1.6
	Exp# 148	0.77	2.5	*
		0.51	1.3	*
		0.44	0.9	*
0.44	0.8	*		
L-19973#9	Exp# 192	0.77	1.8	1.6
		0.77	1.5	1.4
		1.00***	2.8***	*
		1.00***	2.1***	*

* Data not available - second flood was not performed

** Data for experiments from Bang (2007)

*** Results for two-phase gas condensate mixtures

Table 5.15 Summary of conditions for Experiment # 196 and #198

	Exp# 196	Exp# 198
<i>Rock type</i>	Torrey Buff	Torrey Buff
k_g , md	1.1	2.7
S_{wi} %	20	20
<i>Brine Salinity NaCl, ppm</i>	25000	25000
<i>Temperature, °F</i>	155	155
<i>Single-Phase Vol. Oil Pressure (BPR-1), psig</i>	4400	4392
<i>Two-Phase Vol. Oil Pressure (BPR-2), psig</i>	672	960
<i>Volatile Oil Mixture</i>	2	2
<i>Chemical Treatment</i>	4	4
<i>Surfactant</i>	L-19973#9	L-19973#9

Table 5.16 Summary of results for the effect of rock permeability (Experiment # 196 & #198)

	Exp# 196	Exp# 198
<i>Core pressure, psia</i>	672	670
$q_{g\text{tot core}}$, cc/hr	196	416
q_g , cc/hr	186	395
q_o , cc/hr	10	21
<i>Capillary Nc</i>	3.07E-06	5.07E-06
<i>PVT Ratio</i>	0.99	1.00
<i>Viscosity Ratio μ_g/μ_o</i>	0.05	0.05
<i>Liquid Fraction</i>	5.2%	5.2%
k_{rg} Before Treatment	0.044	0.057
k_{ro} Before Treatment	0.044	0.057
<i>Initial Improvement Factor</i>	1.1	1.2
<i>PV of Vol Oil Injected</i>	~850	~380
<i>Final Improvement Factor</i>	*	*

* A second batch of a volatile oil was not injected

Table 5.17 Summary of HPHT core flood experiments for treatment of sandstones

	Exp#134		Exp# 141		Exp# 146		Exp# 148				
Rock type	Berea		Berea		Berea		Berea				
k_g , md	169		189		113		144				
S_{wi} %	20		20		20		20				
Brine Salinity NaCl, ppm	25,000		25,000		25,000		25,000				
Volatile Oil Mixture	2		2		2		2				
Chemical Treatment	1		2		1		2				
Surfactant	FC-X		L-20294		FC-X		L-20294				
Temperature, °F	155		155		155		155				
BPR-1 Pressure, psig	4243		4,475		4,435		4300				
BPR-2 Pressure, psig	690		700		995		900	1600	2500	3100	3500
$q_{\text{tot core}}$, cc/hr	673	1345	680	1359	460	920	608	329	213	177	162
q_g , cc/hr	636	1273	643	1286	420	840	562	275	148	101	58
q_o , cc/hr	36	73	37	73	40	80	46	54	64	76	104
PVT Ratio	0.97		0.98		0.79		0.77	0.51	0.44	0.44	0.35
Viscosity Ratio μ_g/μ_o	0.06		0.06		0.06		0.06	0.10	0.19	0.33	0.63
Liquid Fraction	5.4%		5.4%		8.7%		7.6%	16.3%	30.3%	42.9%	63.9%
Capillary Nc	1.44E-05	2.52E-05	1.38E-05	2.46E-05	1.35E-05	2.36E-05	1.73E-05	1.12E-05	3.51E-05	4.11E-05	1.02E-03
k_{rg} Before Treatment	0.033	0.037	0.035	0.039	0.031	0.036	0.030	0.057	0.055	0.253	0.300
k_{ro} Before Treatment	0.034	0.039	0.036	0.040	0.039	0.045	0.040	0.113	0.127	0.570	0.846
k_{rg} After Treatment	0.038	0.043	0.060	0.063	0.046	0.050	0.075	0.076	0.051	0.205	0.272
k_{ro} After Treatment	0.039	0.044	0.062	0.066	0.065	0.070	0.097	0.150	0.117	0.460	0.769
Initial Improvement Factor	1.2	1.1	1.7	1.6	*	1.4	2.5	1.3	0.9	0.8	0.9
PV of Vol Oil Injected	~320		~ 730		~600		~300				
Final Improvement Factor	1.0	1.0	1.5	1.4	1.4	1.3	1.3	1.4	1.1	0.7	0.9

* Data not measured or a second batch of a volatile oil was not injected

Table 5.17 continuation...

	Exp#158				Exp# 176				Exp# 189		Exp# 192	
<i>Rock type</i>	Berea				Berea				Berea		Berea	
k_g , md	217				150				212		212	
S_{wi} %	20				20				20		20	
<i>Brine Salinity NaCl, ppm</i>	25,000				25,000				25,000		25,000	
<i>Volatile Oil Mixture</i>	2				2				4		2	
<i>Chemical Treatment</i>	3				3				3		5	
<i>Surfactant</i>	L-18961				L-18961				L-18961		L-19973#9	
<i>Temperature, °F</i>	155				155				250		155	
<i>BPR-1 Pressure, psig</i>	4260				4350				4280		4,455	
<i>BPR-2 Pressure, psig</i>	800	1500	2200	2900	805	1500	2200	2900	780	1460	1040	
$q_{g\text{tot core}}$, cc/hr	689	350	238	186	694	353	240	188	701	365	438	875
q_g , cc/hr	644	297	178	115	649	300	180	116	654	311	397	795
q_o , cc/hr	45	53	60	71	45	53	61	71	47	55	40	81
<i>PVT Ratio</i>	0.85	0.52	0.44	0.44	0.85	0.53	0.44	0.44	1.01	0.59	0.77	
<i>Viscosity Ratio μ_g/μ_o</i>	0.06	0.09	0.15	0.27	0.06	0.09	0.15	0.27	0.07	0.10	0.08	
<i>Liquid Fraction</i>	6.5%	15.0%	25.3%	38.2%	6.5%	15.0%	25.2%	38.0%	6.7%	15.0%	9.2%	9.2%
<i>Capillary Nc</i>	1.87E-05	7.03E-06	1.47E-05	5.26E-05	1.00E-05	6.44E-06	2.55E-05	4.93E-05	1.63E-05	6.81E-06	2.49E-05	4.28E-05
k_{rg} Before Treatment	0.029	0.086	0.081	0.099	0.031	0.081	0.059	0.111	0.042	0.105	0.017	0.020
k_{ro} Before Treatment	0.034	0.163	0.184	0.224	0.036	0.154	0.132	0.251	0.042	0.176	0.022	0.026
k_{rg} After Treatment	0.054	0.078	0.076	0.070	0.054	0.094	0.047	0.104	0.109	0.098	0.031	0.030
k_{ro} After Treatment	0.063	0.149	0.173	0.158	0.064	0.179	0.106	0.235	0.107	0.165	0.040	0.039
<i>Initial Improvement Factor</i>	1.9	0.9	0.9	0.7	1.8	1.2	0.8	0.9	2.6	*	1.8	1.5
<i>PV of Vol Oil Injected</i>	~ 130				~160				~490		~ 550	
<i>Final Improvement Factor</i>	*	*	*	*	*	*	*	*	2.1	0.9	1.6	1.4

* Data not measured or a second batch of a volatile oil was not injected

Table 5.17 continuation...

	Exp# 196	Exp# 198	Exp#200				Exp# 210					Exp #221	Exp #224	Exp# 228	Exp# 229
Rock type	Torrey Buff	Torrey Buff	Berea				Berea					Berea	Berea	Berea	Berea
k_g, md	1.1	2.7	366				178					93	134	170	193
$S_{wi}\%$	20	20	20				20					20	20	20	20
Brine Salinity NaCl, ppm	25000	25000	25,000				25,000					25,000	25,000	25,000	25,000
Volatile Oil Mixture	2	2	2				2					2	2	3	5
Chemical Treatment	4	4	1				1					1	1	1	1
Surfactant	L-19973#9	L-19973#9	FC-X				FC-X					FC-X	FC-X	FC-X	FC-X
Temperature, °F	155	155	155				155					155	155	215	275
BPR-1 Pressure, psig	4400	4392	4340				4320					4325	4320	4350	4080
BPR-2 Pressure, psig	672	670	800	1500	2200	2900	810	1100	1500	2200	2900	2915	2220	850	850
$q_{tot\ core}, cc/hr$	196	416	555	611	176	50	547	442	305	128	31	31	165	519	494
$q_g, cc/hr$	186	395	519	519	131	30	511	398	260	96	19	19	122	482	458
$q_o, cc/hr$	10	21	36	92	45	19	36	44	46	32	12	12	43	37	36
PVT Ratio	0.99	1.00	0.94	0.61	0.54	0.53	0.92	0.73	0.61	0.54	0.54	0.53	0.54	1.11	1.50
Viscosity Ratio μ_g/μ_o	0.05	0.05	0.07	0.11	0.19	0.34	0.07	0.08	0.11	0.18	0.33	0.35	0.19	0.09	0.12
Liquid Fraction	5.2%	5.2%	6.5%	15.1%	25.6%	39.0%	6.6%	9.9%	15.0%	25.2%	38.0%	39.3%	25.9%	7.1%	7.2%
Capillary Nc	3.07E-06	5.07E-06	1.98E-05	2.04E-05	2.13E-05	2.32E-05	1.19E-05	1.19E-05	1.19E-05	1.21E-05	1.08E-05	2.14E-05	3.00E-05	1.51E-05	1.62E-05
k_{rg} Before Treatment	0.044	0.057	0.021	0.050	0.041	0.061	0.034	0.037	0.042	0.050	0.075	0.044	0.028	0.032	0.038
k_{ro} Before Treatment	0.044	0.057	0.022	0.081	0.076	0.115	0.037	0.051	0.069	0.094	0.140	0.082	0.053	0.029	0.026
k_{rg} After Treatment	0.049	0.066	0.027	0.041	0.029	0.068	0.085	0.083	0.067	0.067	0.104	0.063	0.062	0.085	0.136
k_{ro} After Treatment	0.049	0.066	0.029	0.066	0.055	0.127	0.092	0.113	0.110	0.124	0.194	0.119	0.115	0.076	0.091
Initial Improvement Factor	1.1	1.2	1.3	0.8	0.7	1.1	2.5	2.2	1.6	1.3	1.4	1.4	2.18	2.6	3.5
PV of Vol Oil Injected	~850	~380	~200				~330					~60	~280	~320	~330
Final Improvement Factor	*	*	*	*	*	*	2.4	2.1	1.0	1.0	1.0	1.01	1.59	2	3

* Data not measured or a second batch of a volatile oil was not injected

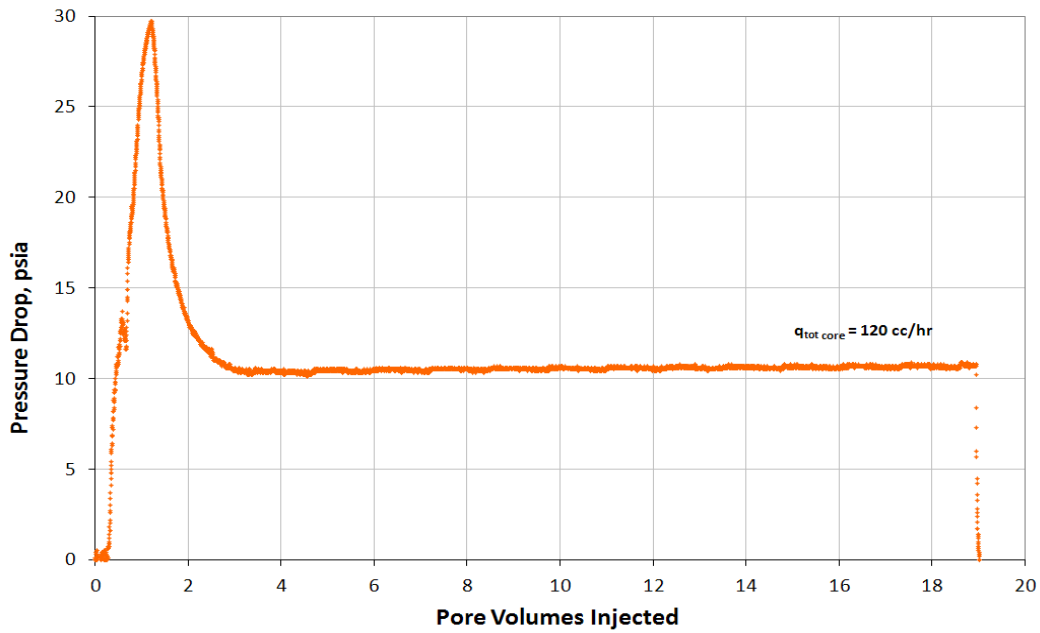


Figure 5.1 Pressure drop across the core during injection of chemical treatment 2 (Experiment # 141)

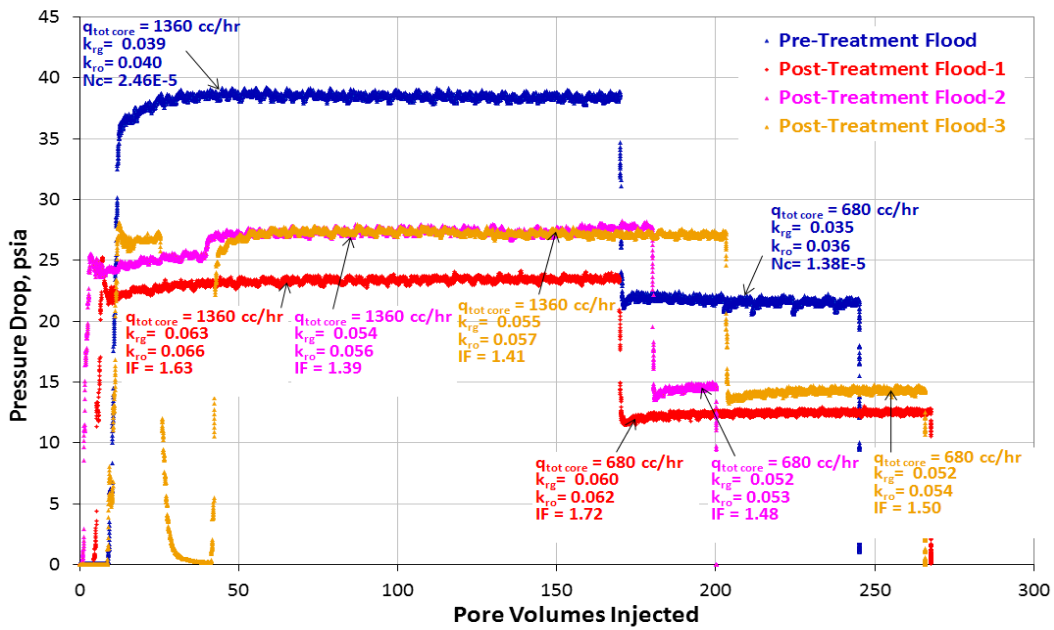


Figure 5.2 Pre and post-treatment pressure drop during two-phase volatile oil floods at two different flow rates (Experiment # 141)

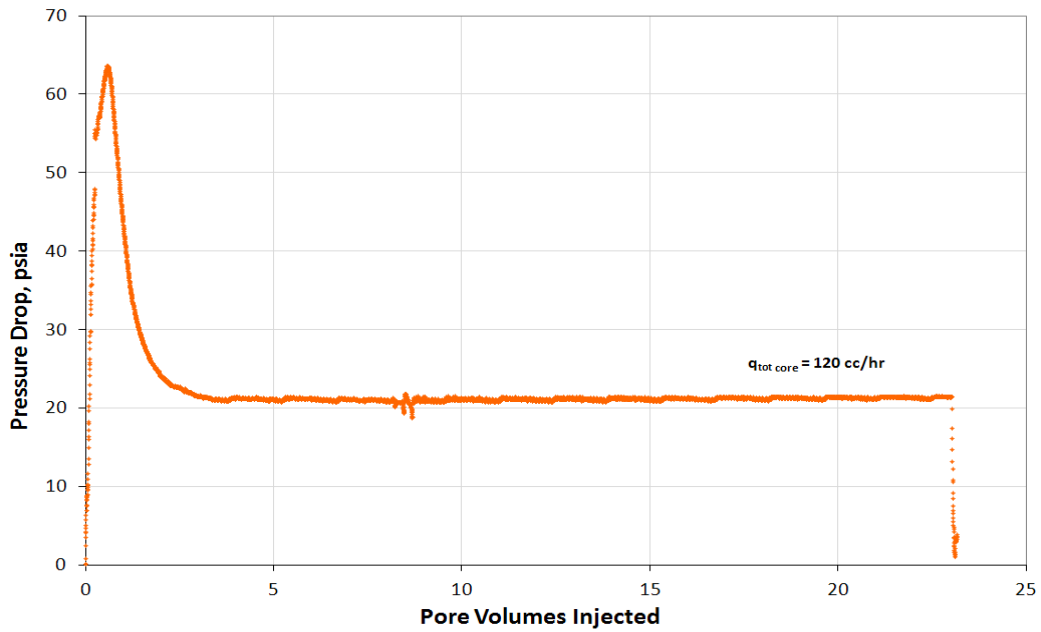


Figure 5.3 Pressure drop across the core during injection of chemical treatment 1 (Experiment # 146)

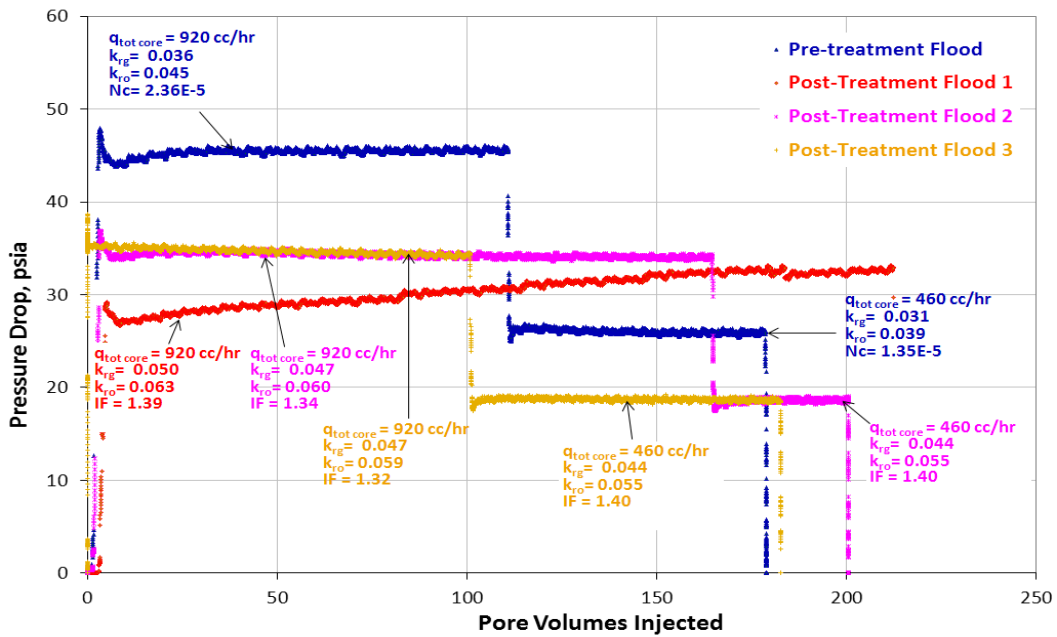


Figure 5.4 Pre and post-treatment pressure drop during two-phase volatile oil floods at two different flow rates (Experiment # 146)

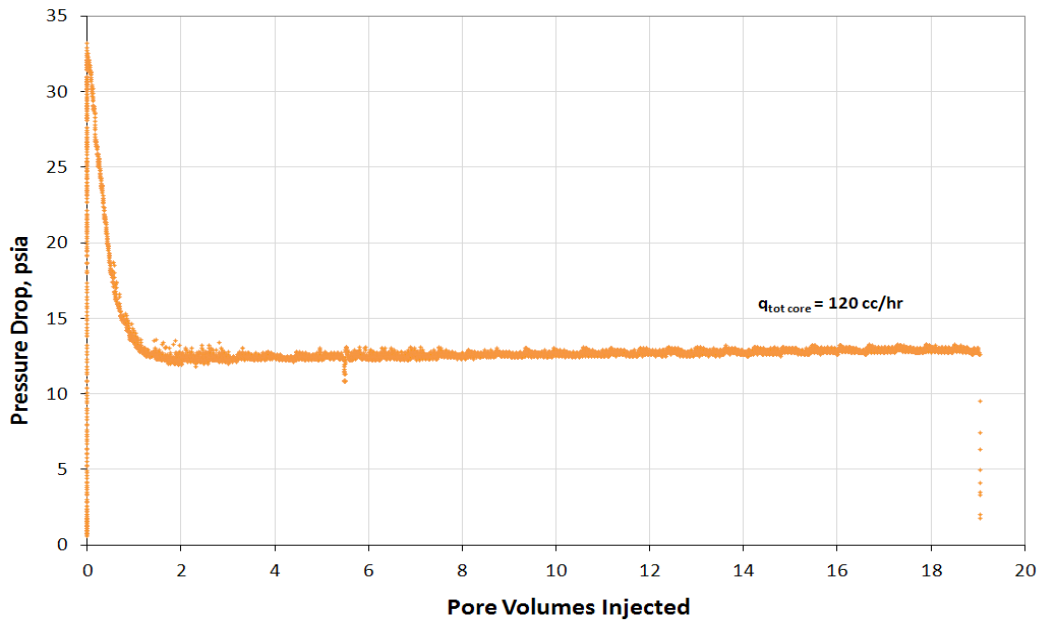


Figure 5.5 Pressure drop across the core during injection of chemical treatment 3 (Experiment # 158)

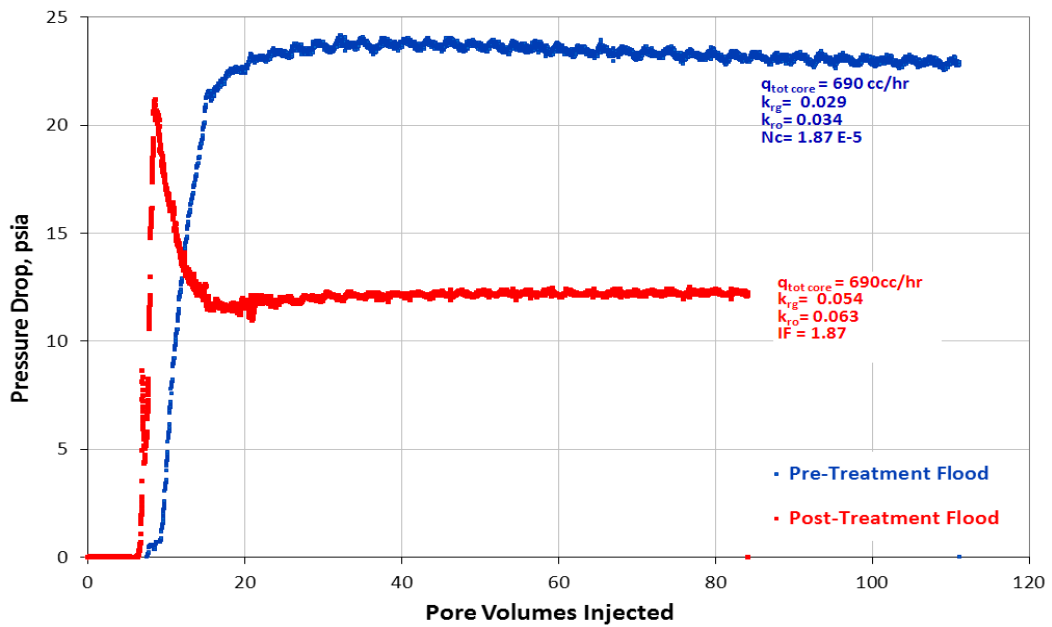


Figure 5.6 Pre and post-treatment pressure drop during two-phase volatile oil floods (Experiment # 158)

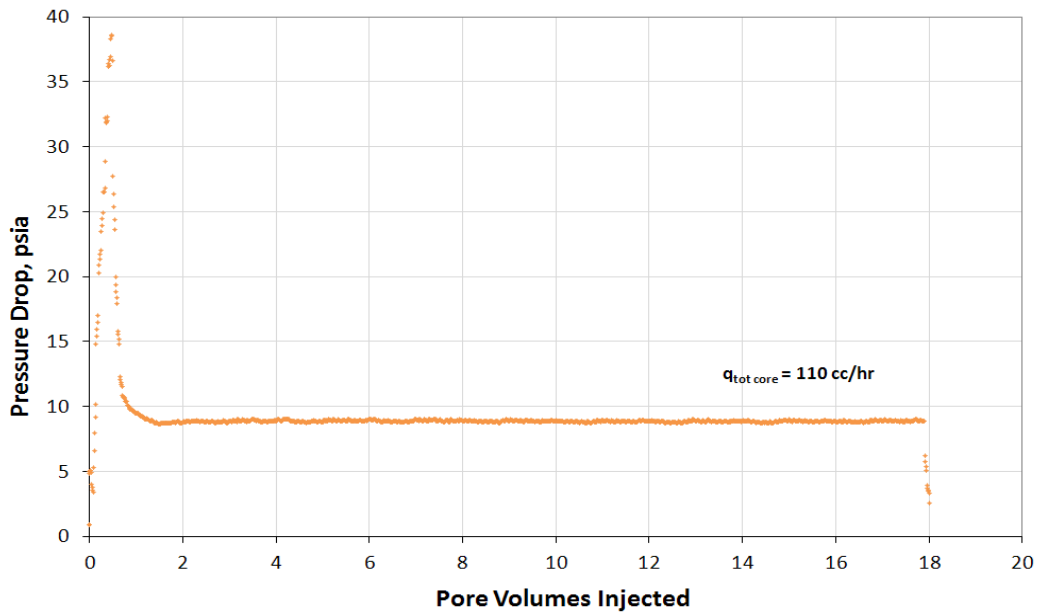


Figure 5.7 Pressure drop across the core during injection of chemical treatment 4 (Experiment # 192)

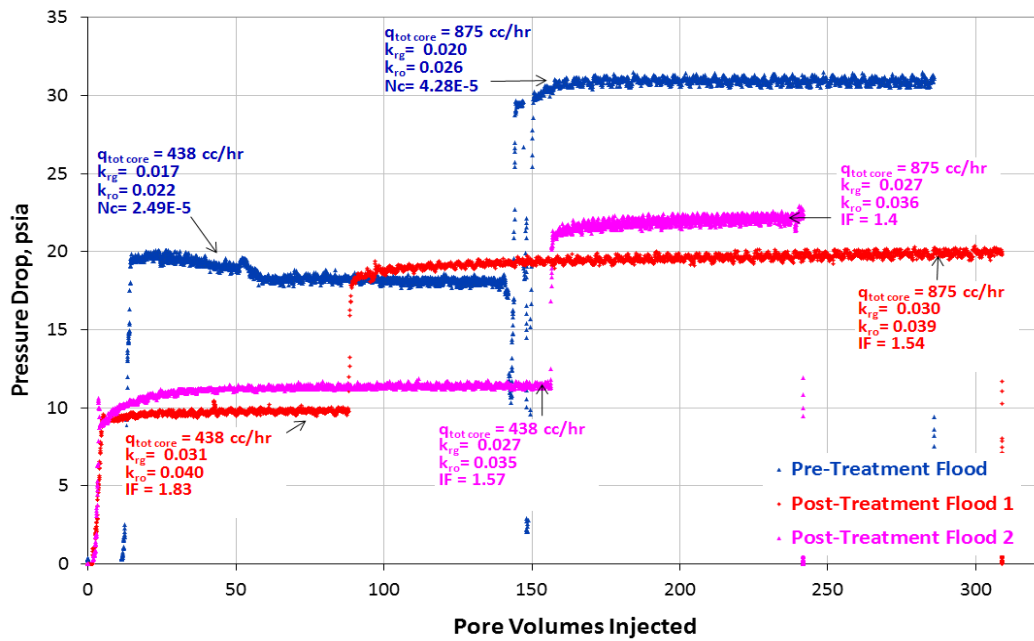


Figure 5.8 Pre and post-treatment pressure drop during two-phase volatile oil floods at two different flow rates (Experiment # 192)

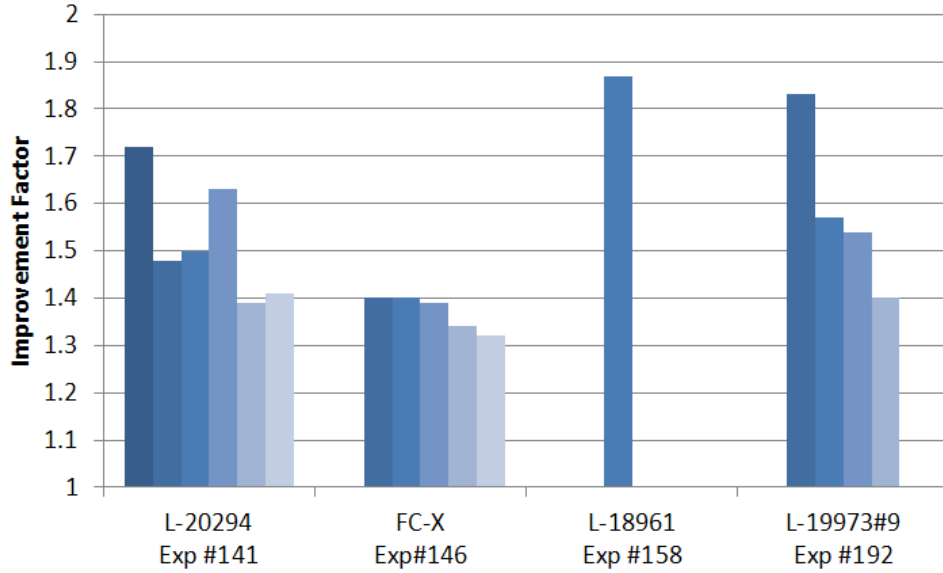


Figure 5.9 Improvement factor achieved for different volatile oil floods (batches) on treated Berea sandstone with selected fluorinated surfactants (Experiments #141, #146, #158 & #192)

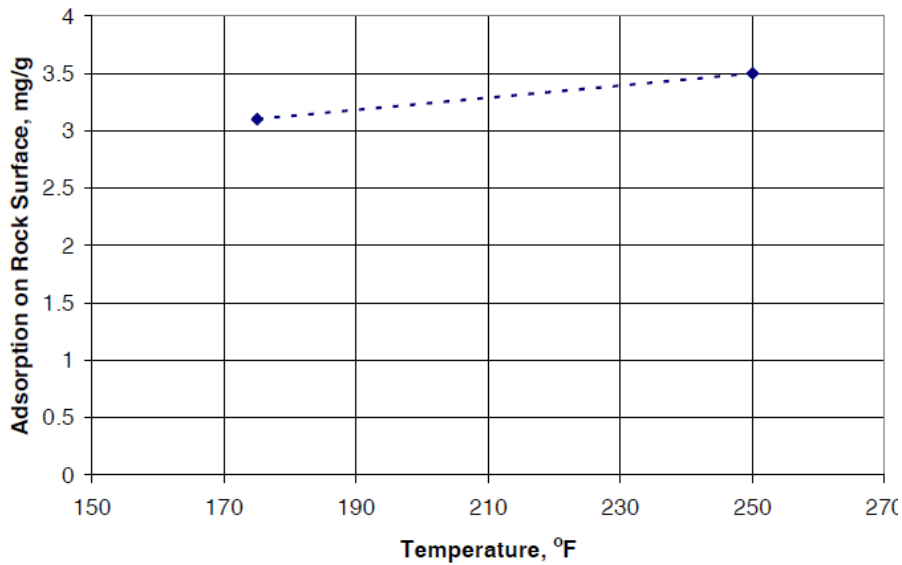


Figure 5.10 Effect of temperature on surfactant adsorption on Berea sandstone surface for treatment solution containing 2 wt% FC-X (Bang 2007)

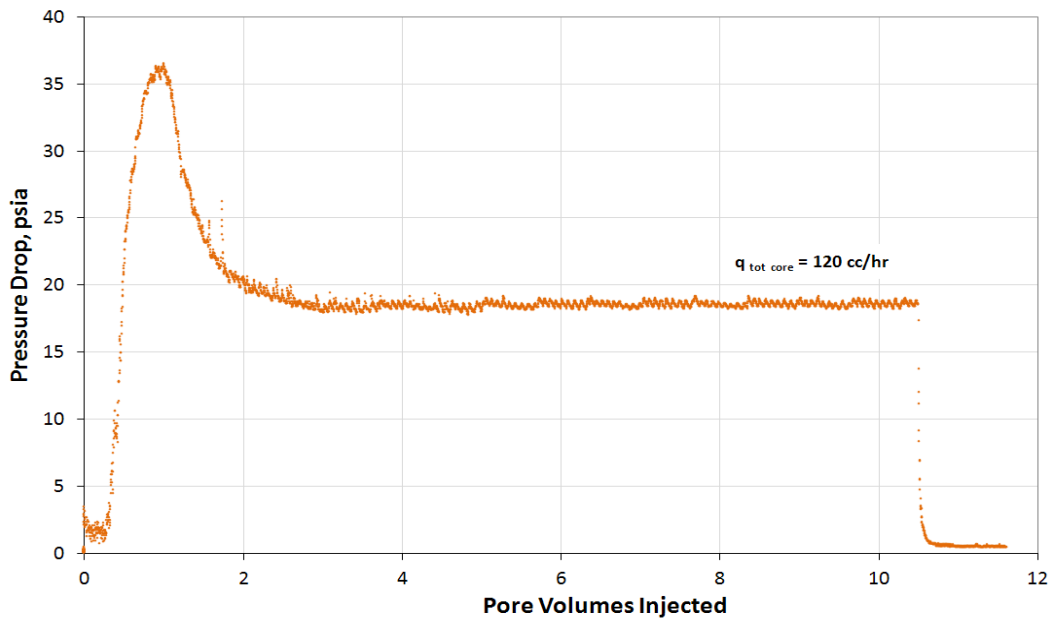


Figure 5.11 Pressure drop across the core during injection of chemical treatment 3 (Experiment # 176)

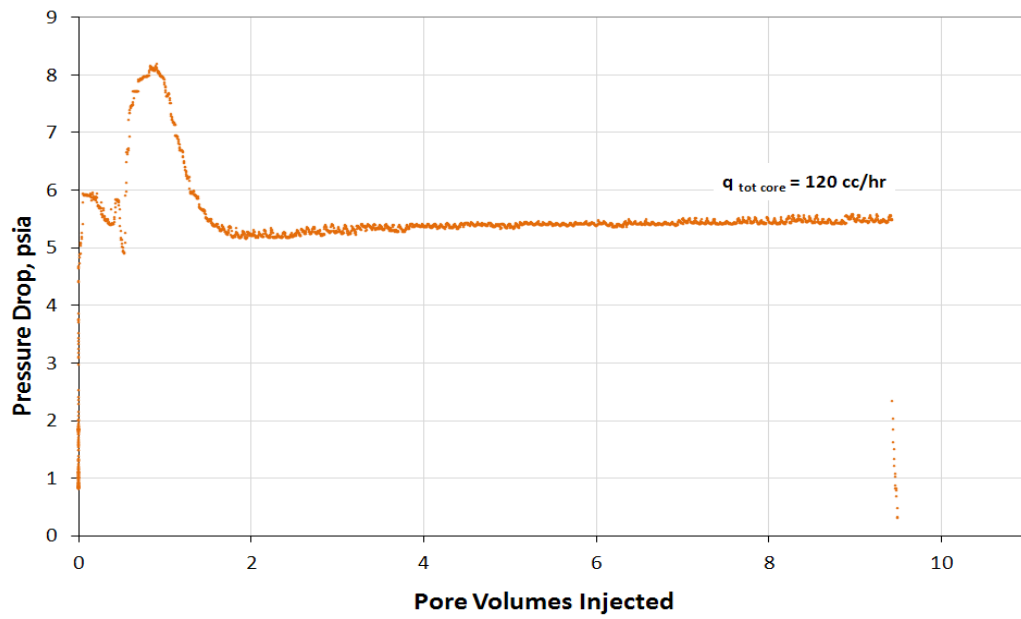


Figure 5.12 Pressure drop across the core during injection of chemical treatment 3 (Experiment # 189)

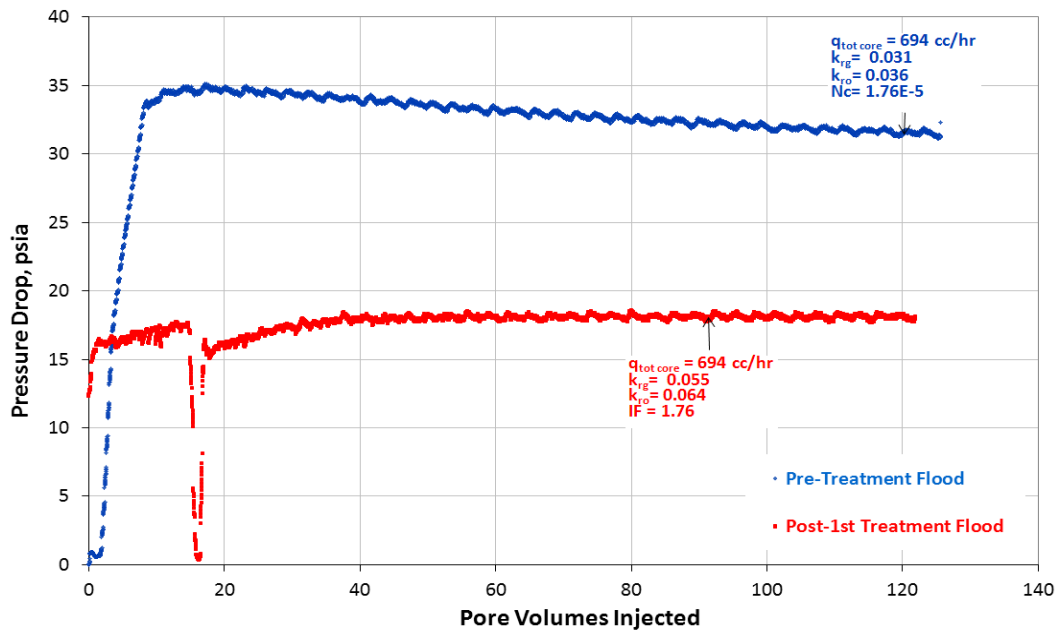


Figure 5.13 Pre and post-treatment pressure drop during two-phase volatile oil floods (Experiment # 176)

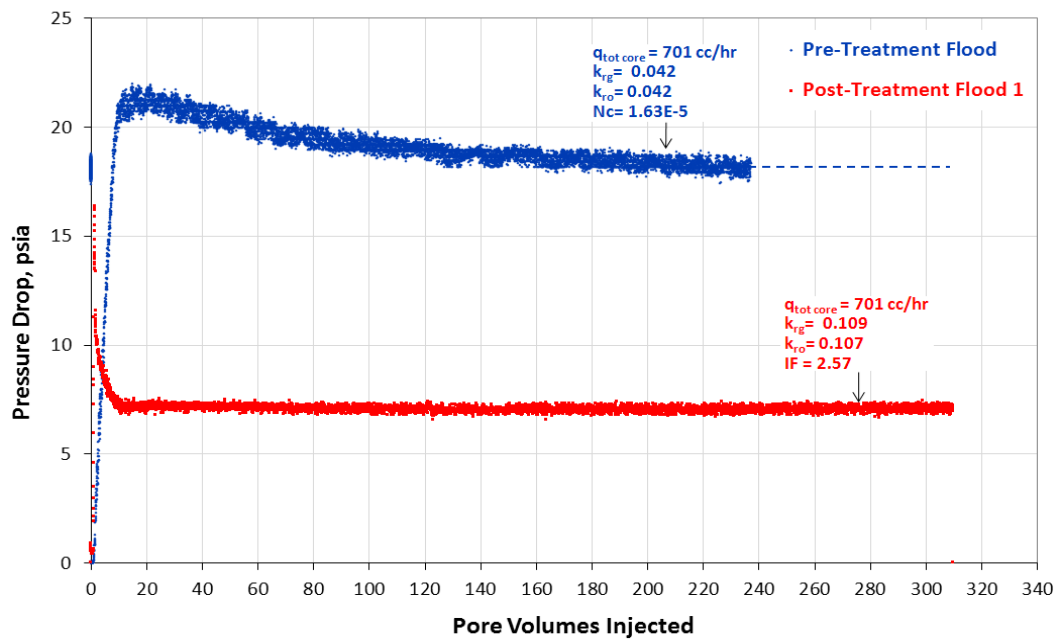


Figure 5.14 Pre and post-treatment pressure drop during two-phase volatile oil floods (Experiment # 189)

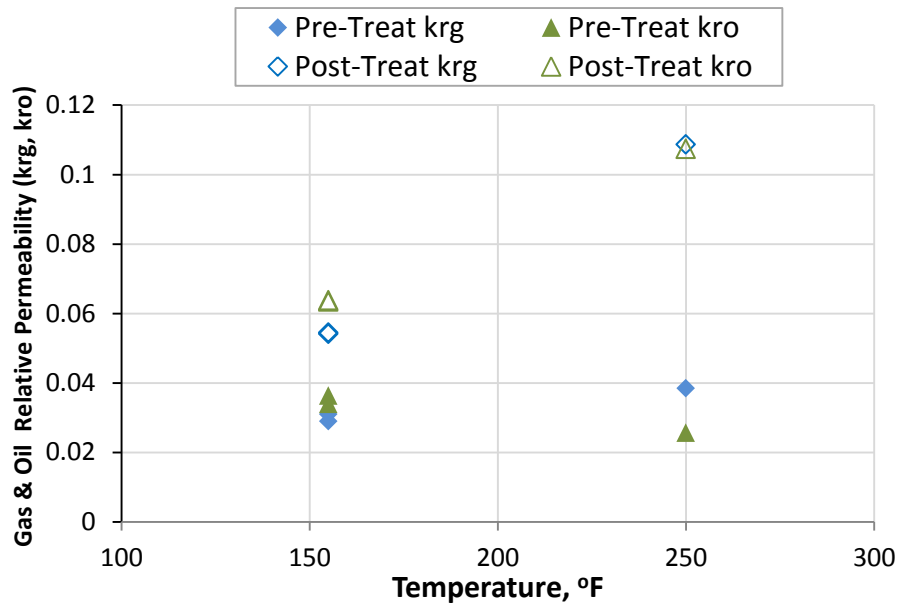


Figure 5.15 Pre and post-treatment gas and oil relative permeabilities versus temperature for Exp # 158, #176 and #189 treated with 1 wt% L-18961

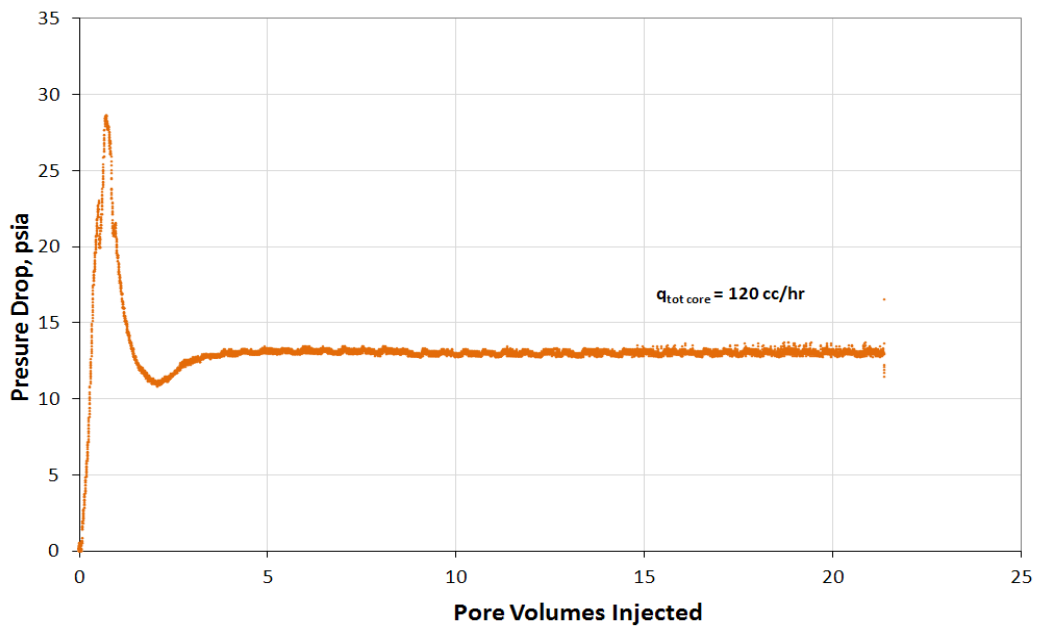


Figure 5.16 Pressure drop across the core during injection of chemical treatment 1 (Experiment # 210)

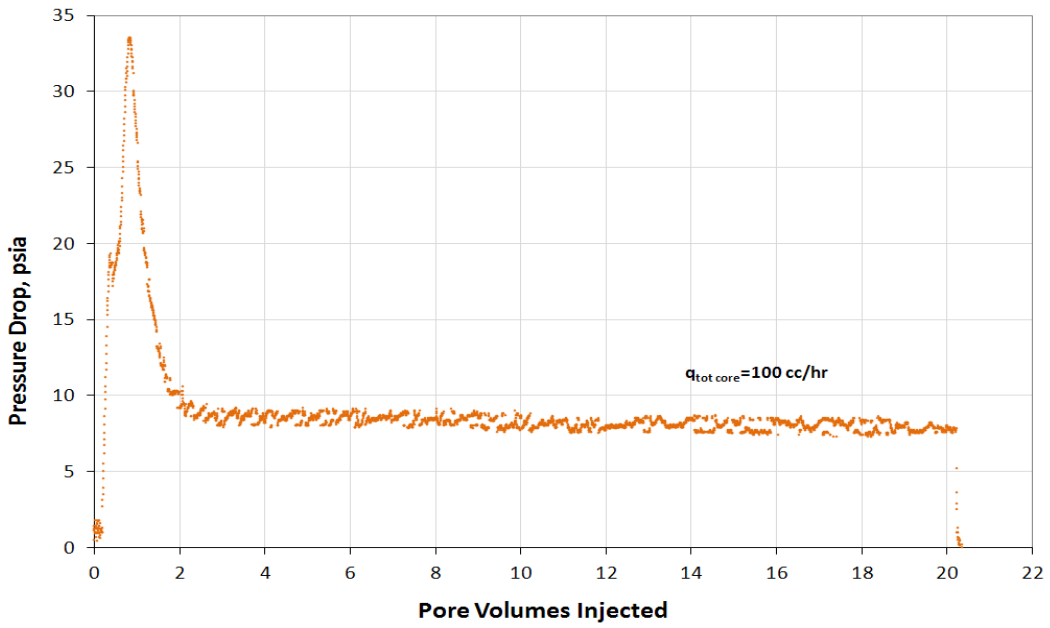


Figure 5.17 Pressure drop across the core during injection of chemical treatment 1 (Experiment # 228)

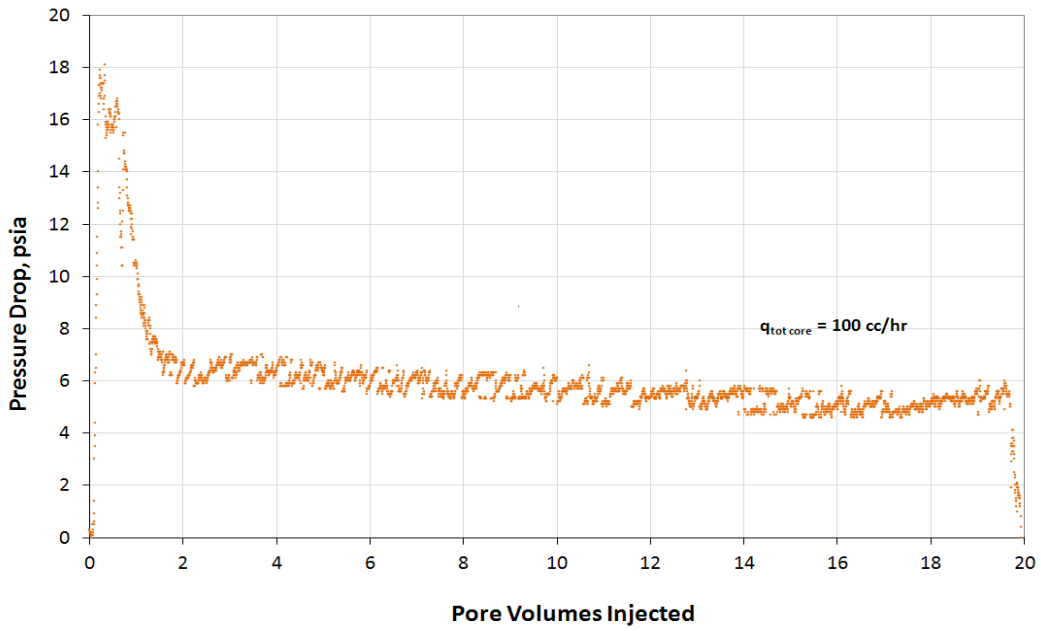


Figure 5.18 Pressure drop across the core during injection of chemical treatment 1 (Experiment # 229)

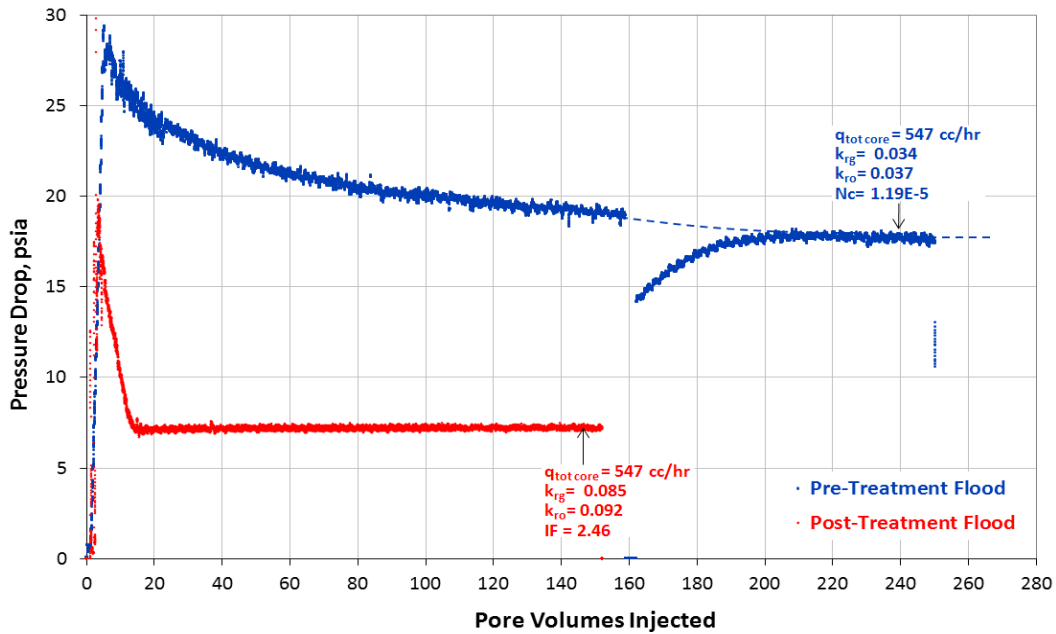


Figure 5.19 Pre and post-treatment pressure drop during two-phase volatile oil floods (Experiment # 210)

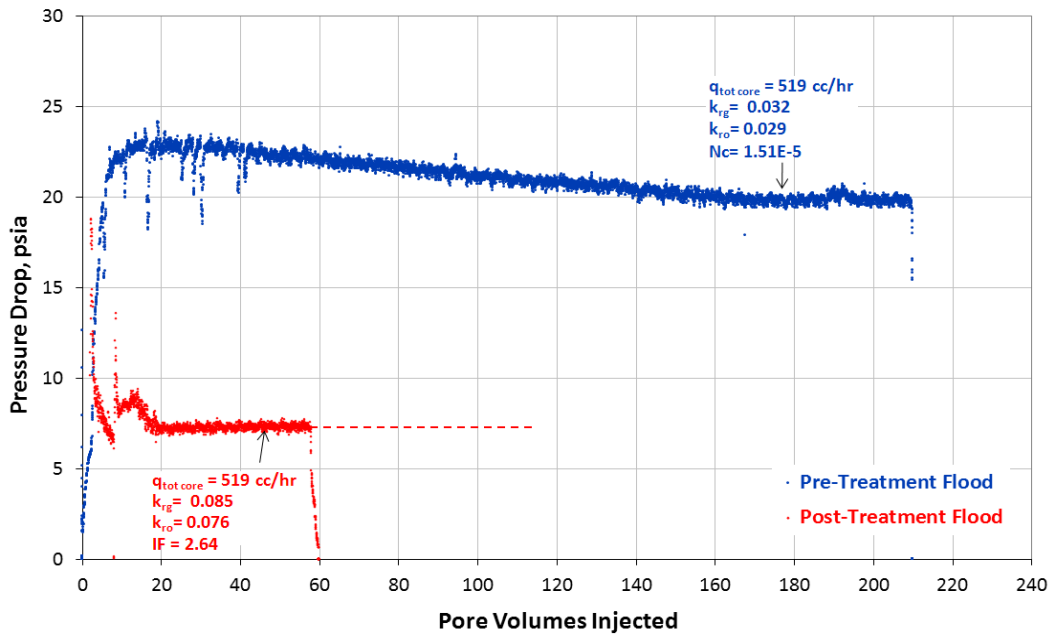


Figure 5.20 Pre and post-treatment pressure drop during two-phase volatile oil floods (Experiment # 228)

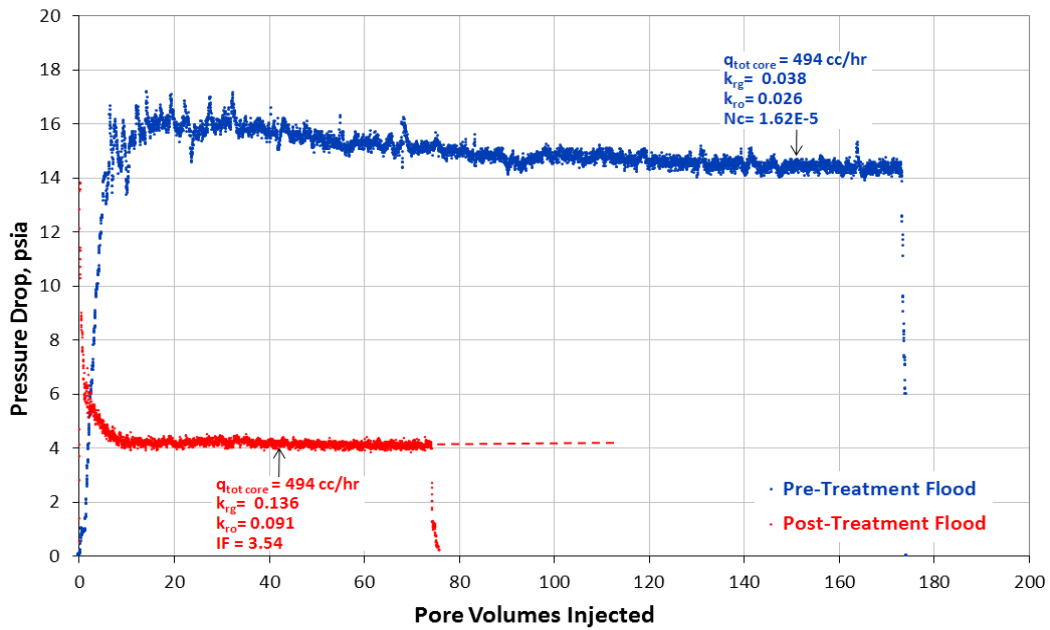


Figure 5.21 Pre and post-treatment pressure drop during two-phase volatile oil floods (Experiment # 229)

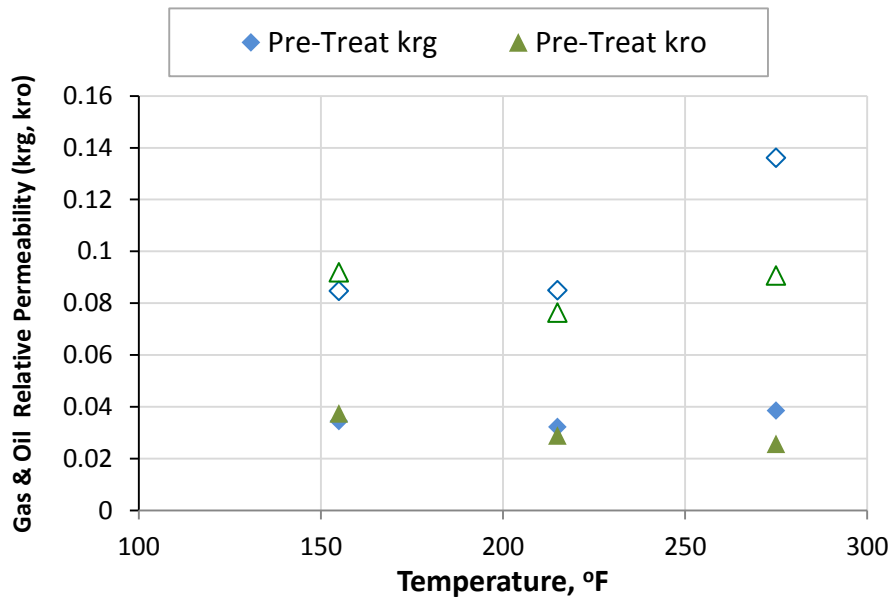


Figure 5.22 Pre and post-treatment gas and oil relative permeabilities versus temperature for Exp #210, #228 and #229 treated with 2 wt% FC-X

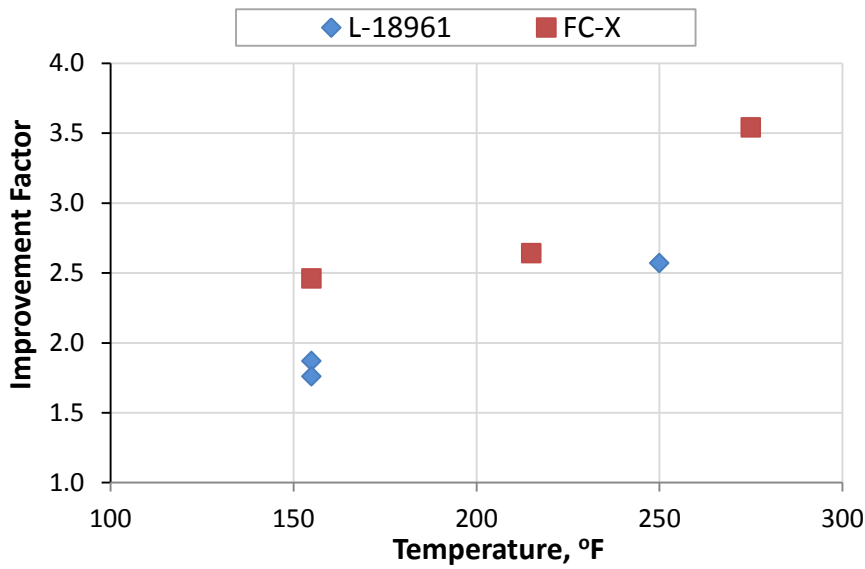


Figure 5.23 Temperature effect on improvement factor

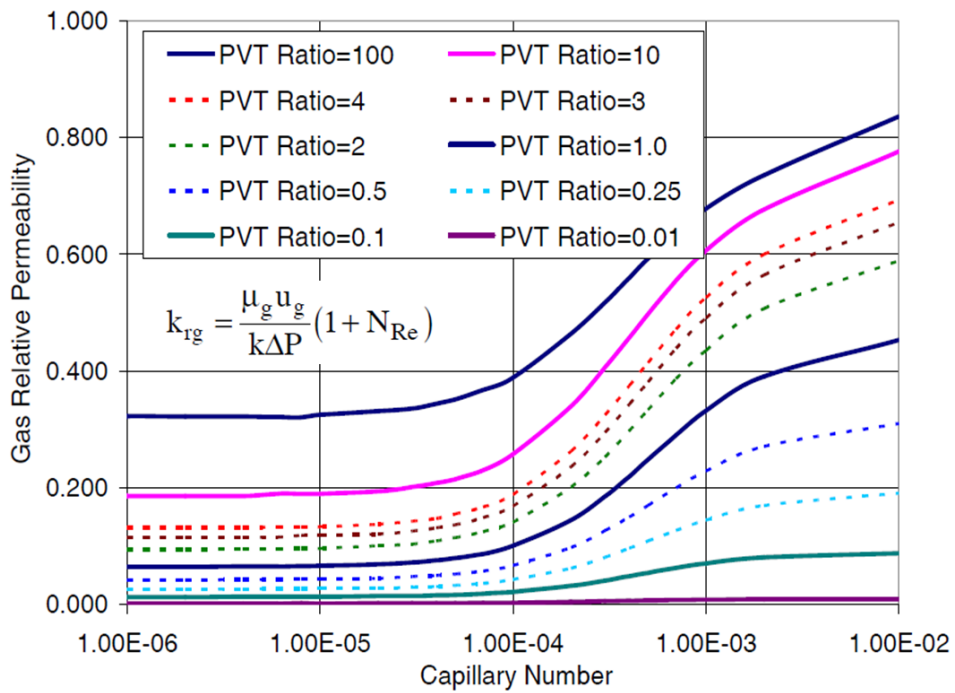


Figure 5.24 Gas relative permeability as a function of Nc (Bang 2007)

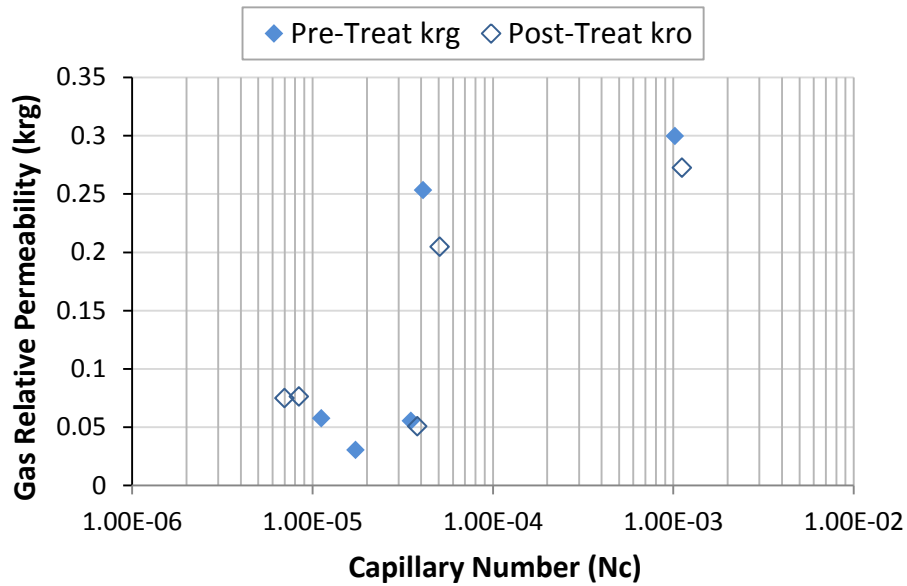


Figure 5.25 Capillary number effect on gas relative permeability before and after chemical treatment 2 wt% L-20294 (Experiment #148)

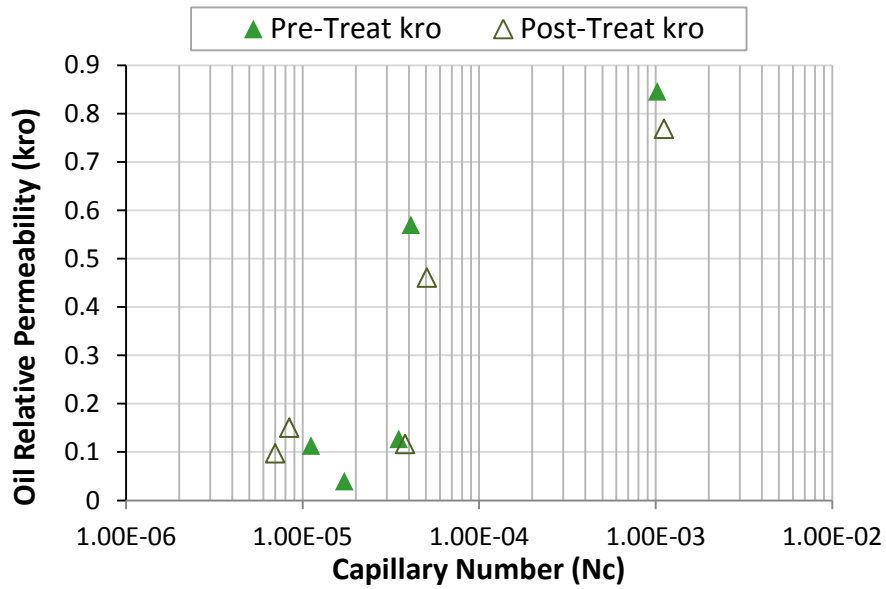


Figure 5.26 Capillary number effect on gas relative permeability before and after chemical treatment 2 wt% L-20294 (Experiment #148)

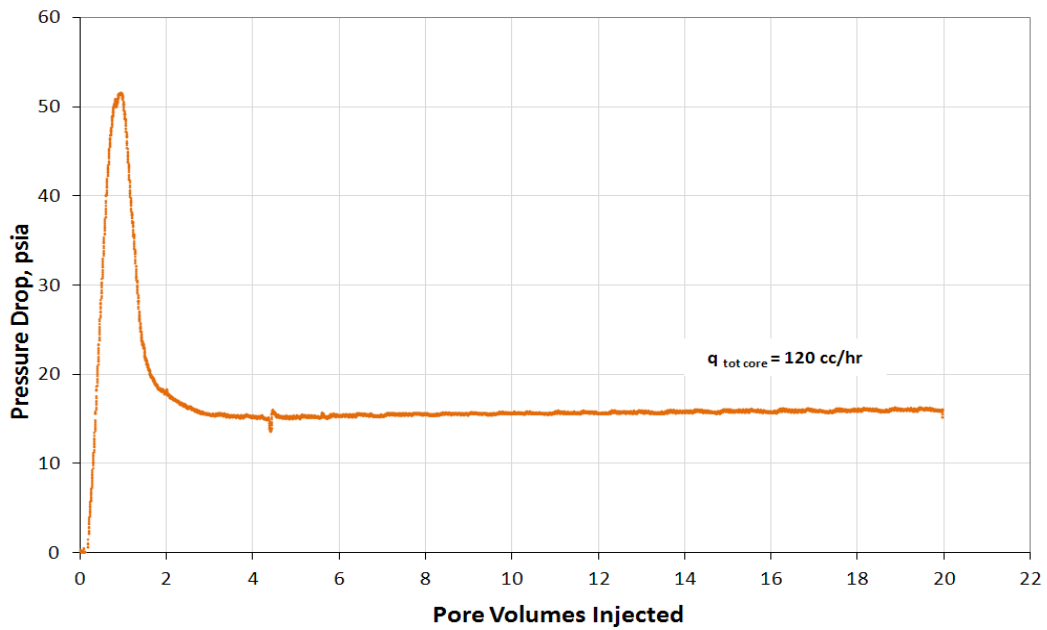


Figure 5.27 Pressure drop across the core during injection of chemical treatment 2 (Experiment # 148)

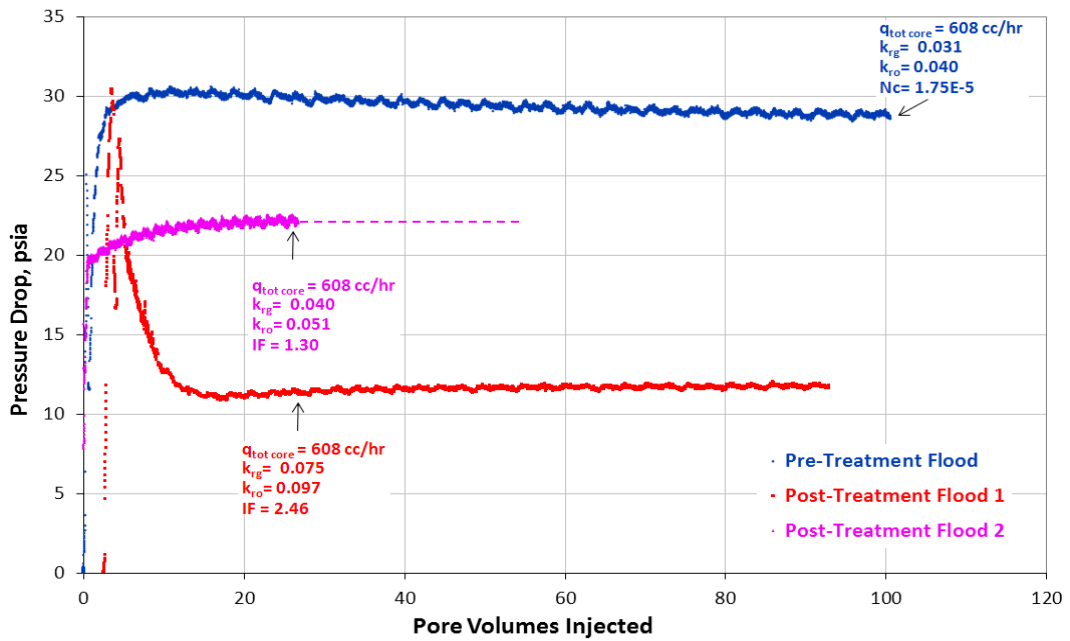


Figure 5.28 Pre and post-treatment pressure drop during two-phase volatile oil floods at 900 psig core pressure (Experiment # 148)

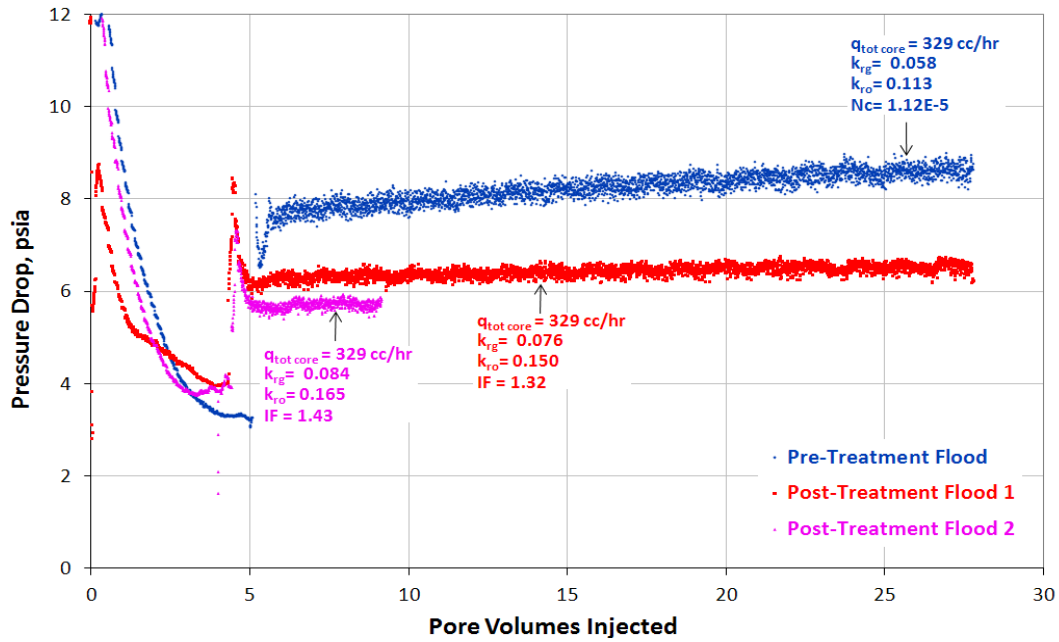


Figure 5.29 Pre and post-treatment pressure drop during two-phase volatile oil floods at 1600 psig core pressure (Experiment # 148)

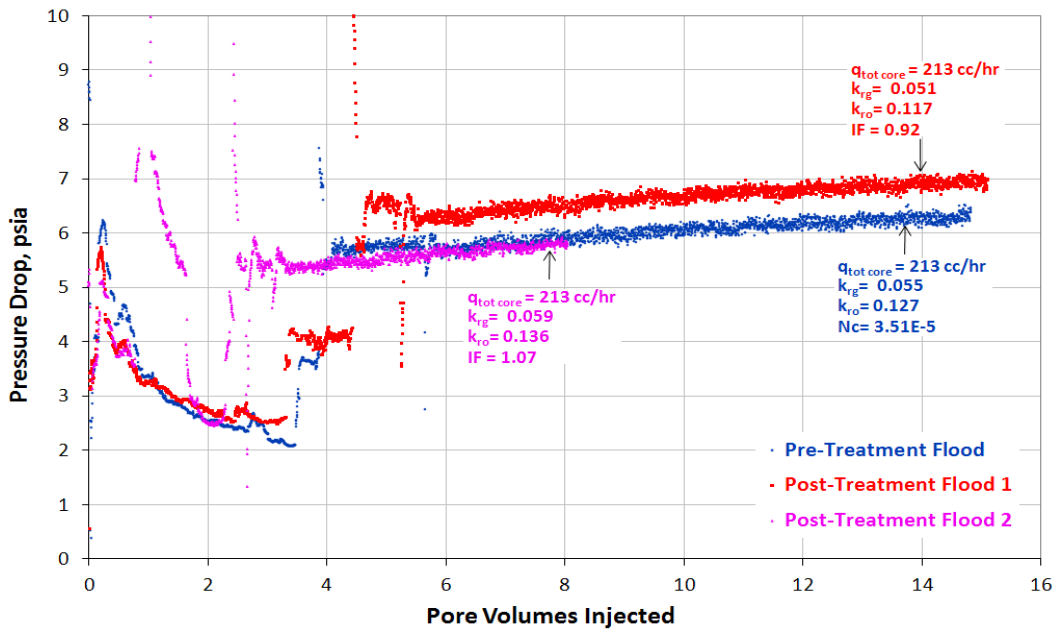


Figure 5.30 Pre and post-treatment pressure drop during two-phase volatile oil floods at 2500 psig core pressure (Experiment # 148)

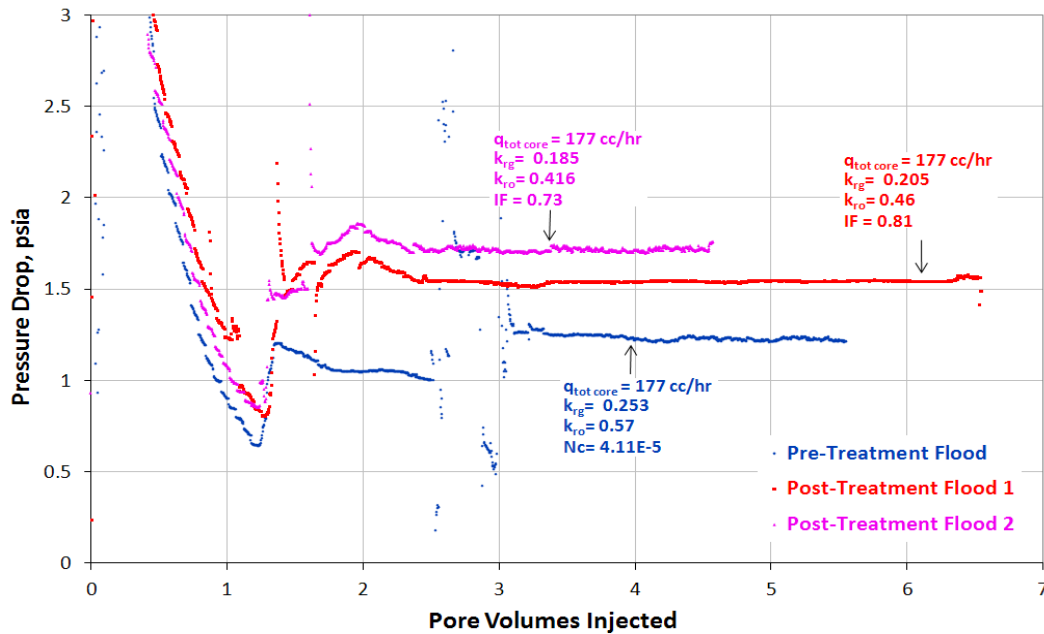


Figure 5.31 Pre and post-treatment pressure drop during two-phase volatile oil floods at 3100 psig core pressure (Experiment # 148)

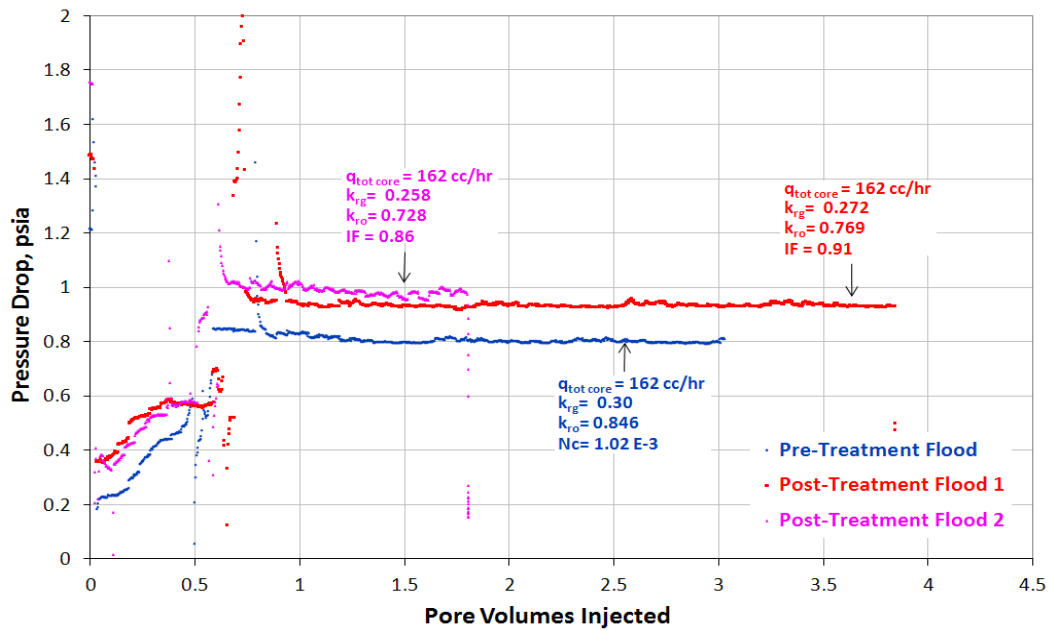


Figure 5.32 Pre and post-treatment pressure drop during two-phase volatile oil floods at 3500 psig core pressure (Experiment # 148)

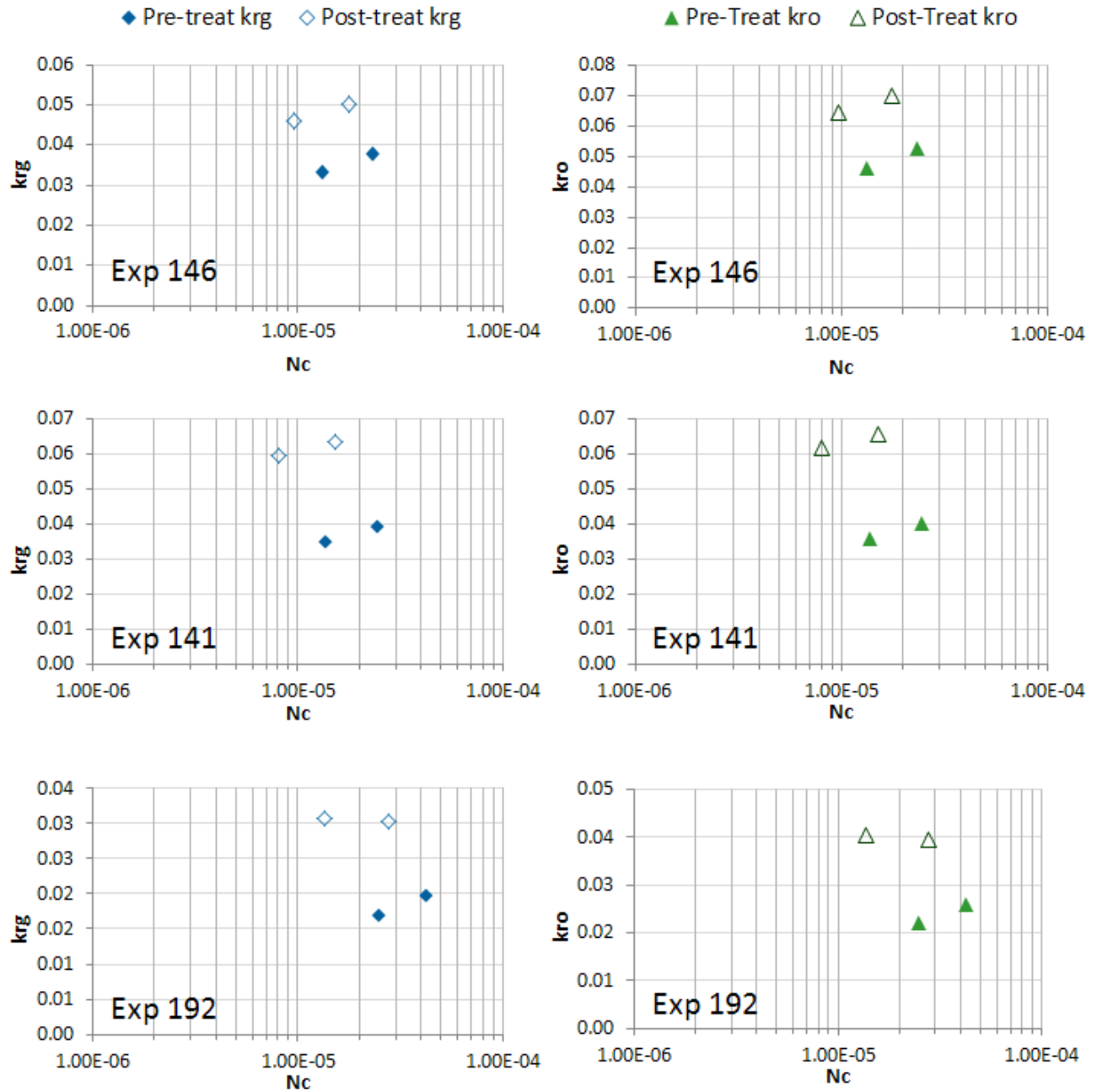


Figure 5.33 Capillary number effect on gas relative permeability before and after chemical treatment (Experiment #146, #141 & #192)

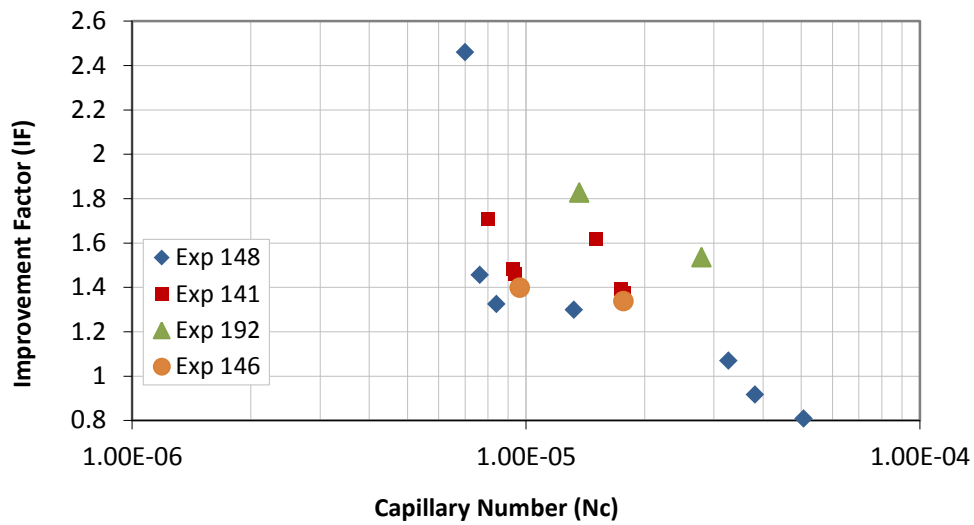


Figure 5.34 Capillary number effect on improvement factor (Experiment #141, #146, #148 and #192)

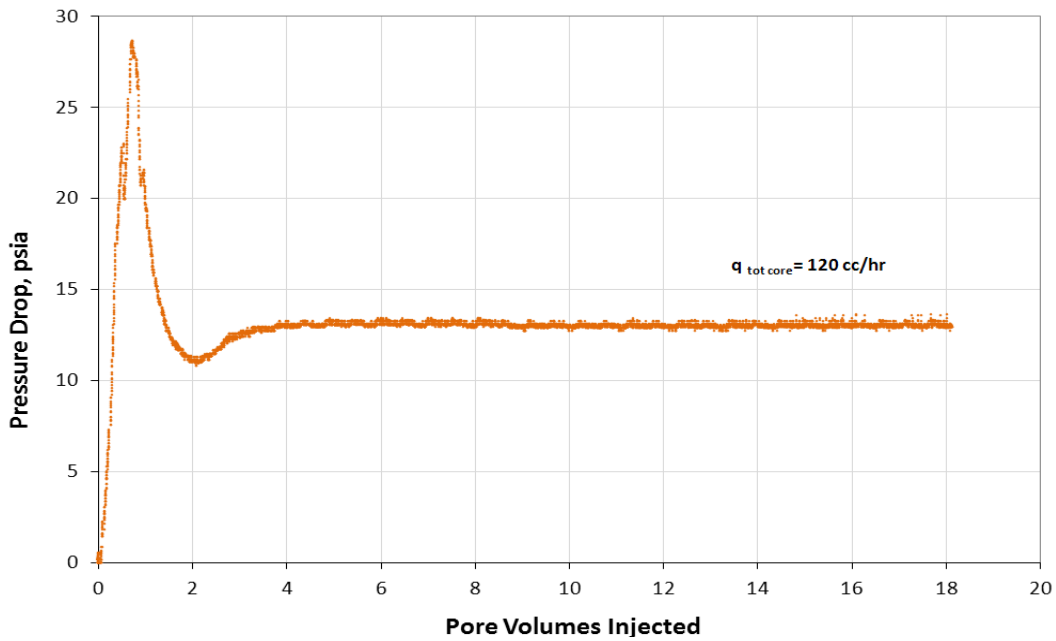


Figure 5.35 Pressure drop across the core during injection of chemical treatment 1 (Experiment # 210)

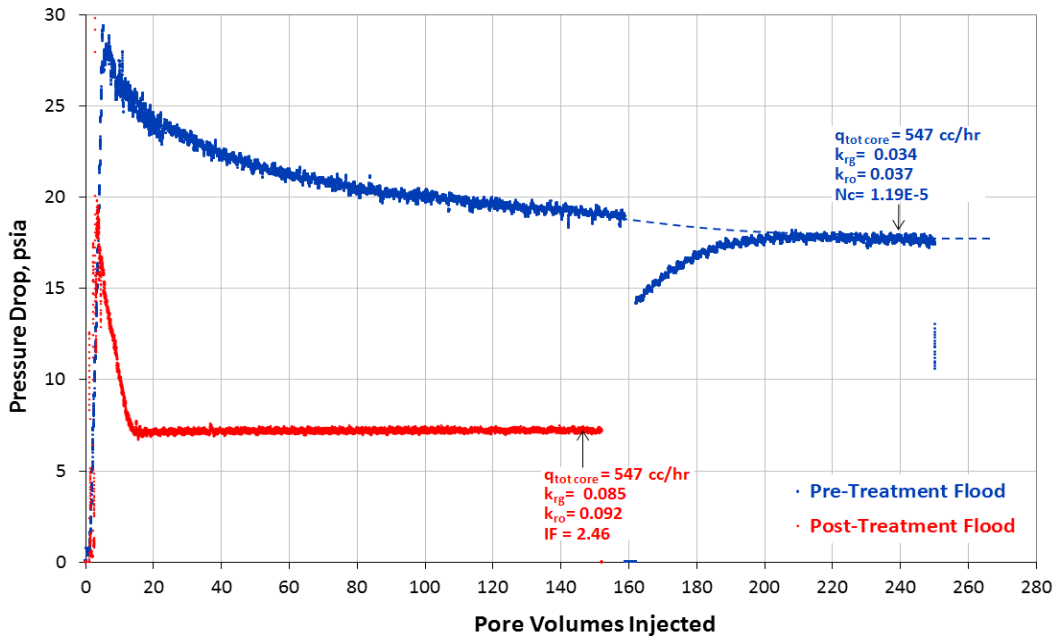


Figure 5.36 Pre and post-treatment pressure drop during two-phase volatile oil floods at 800 psig core pressure (Experiment # 210)

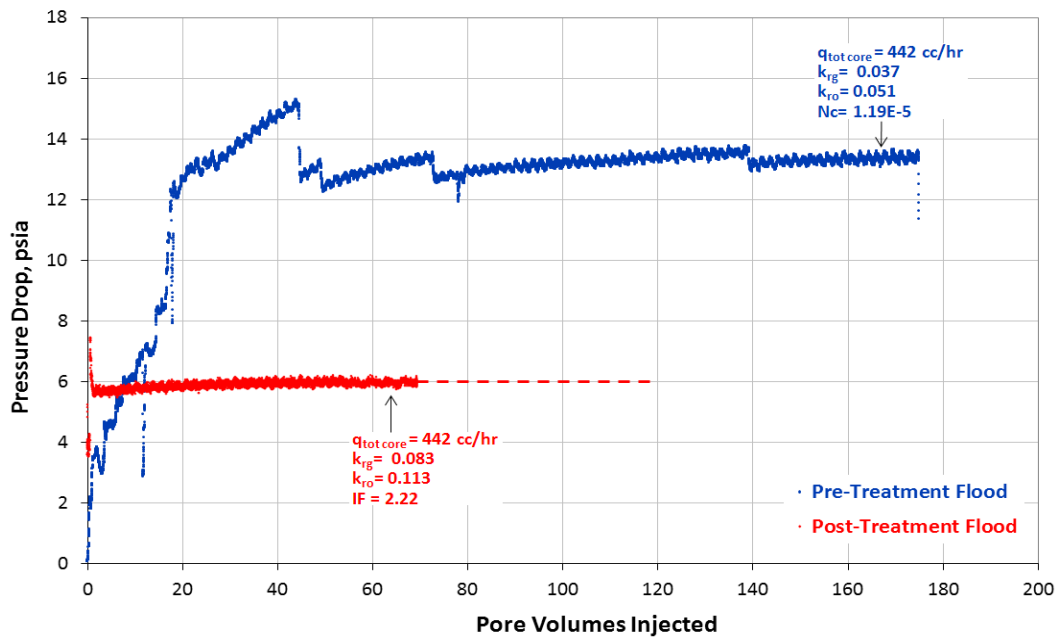


Figure 5.37 Pre and post-treatment pressure drop during two-phase volatile oil floods at 1100 psig core pressure (Experiment # 210)

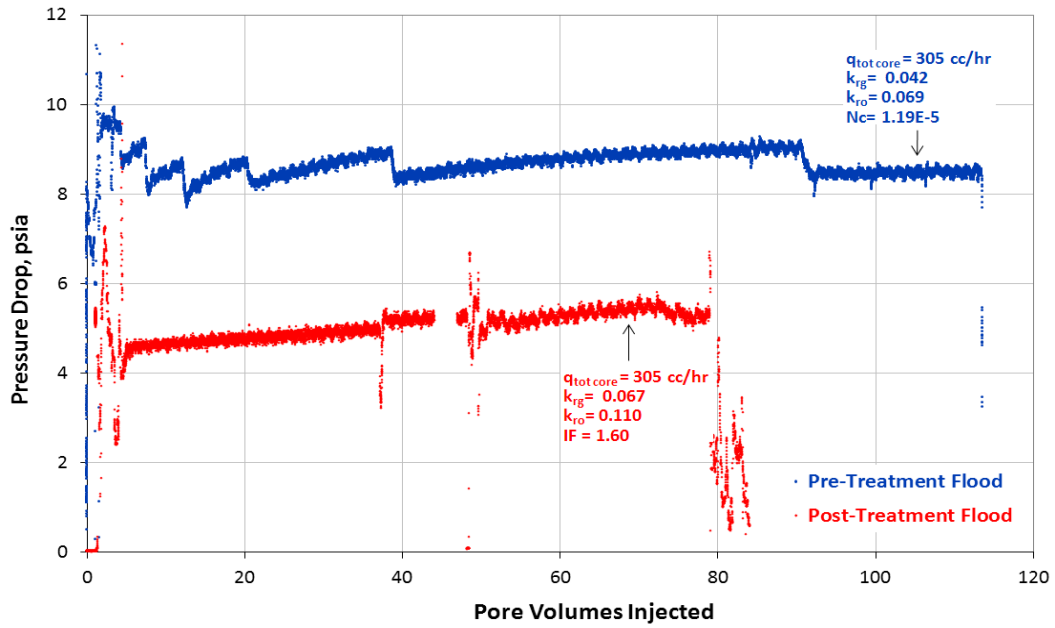


Figure 5.38 Pre and post-treatment pressure drop during two-phase volatile oil floods at 1500 psig core pressure (Experiment # 210)

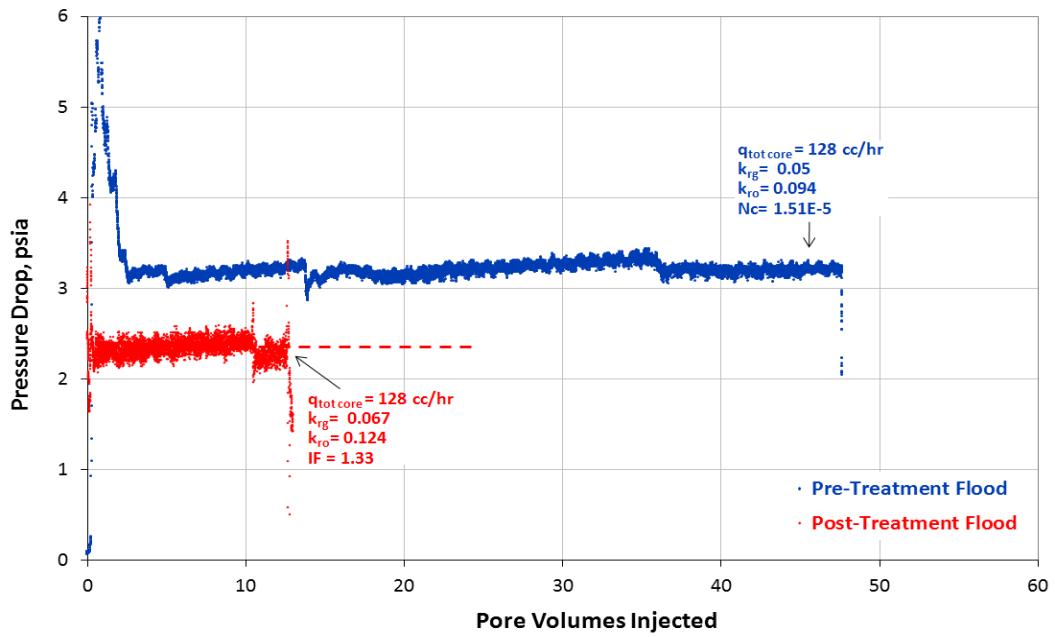


Figure 5.39 Pre and post-treatment pressure drop during two-phase volatile oil floods at 2200 psig core pressure (Experiment # 210)

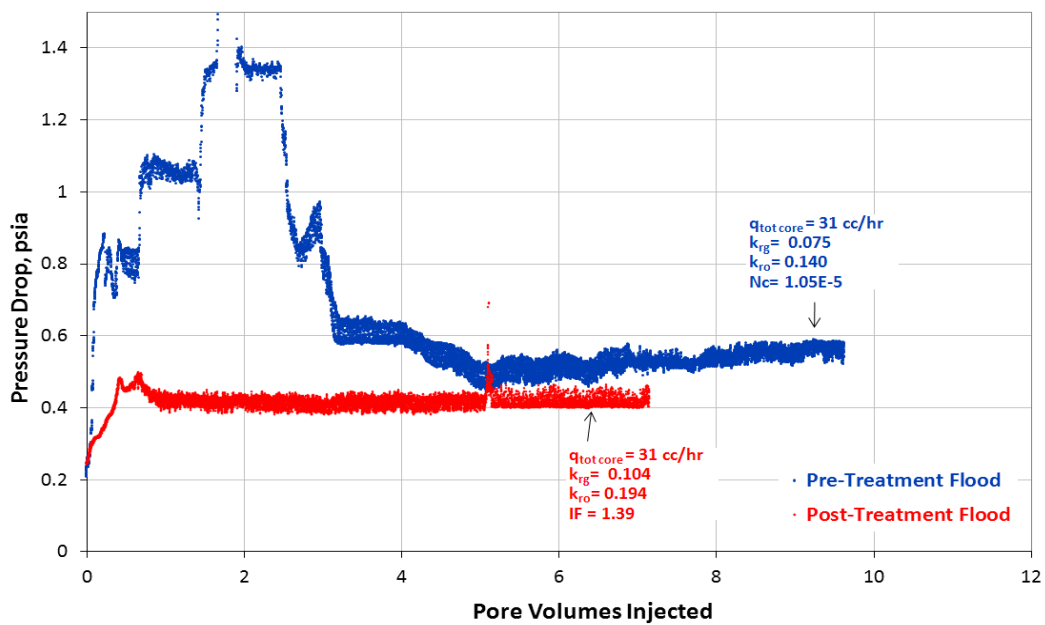


Figure 5.40 Pre and post-treatment pressure drop during two-phase volatile oil floods at 2900 psig core pressure (Experiment # 210)

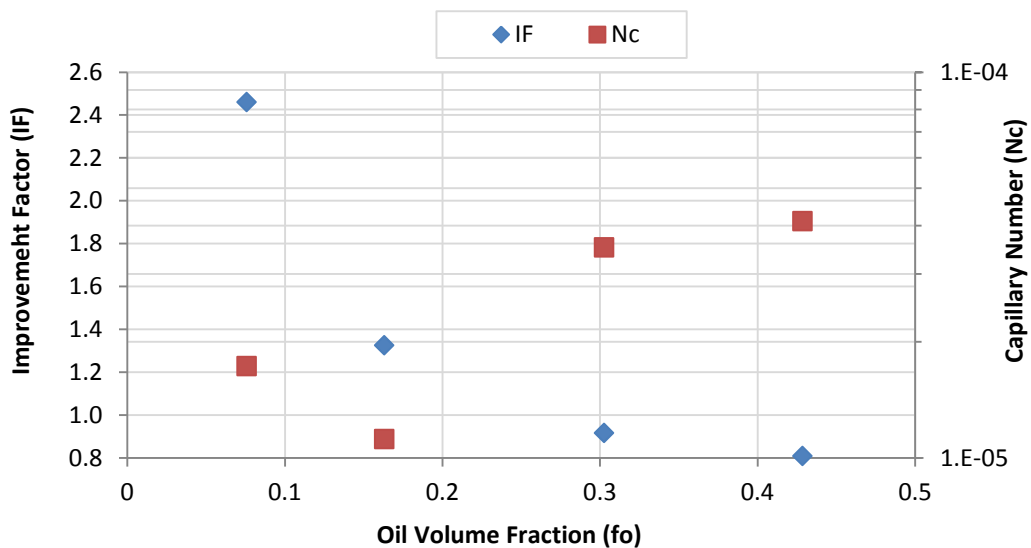


Figure 5.41 Observed improvement factors and capillary numbers for different oil volume fractions (Experiment #148)

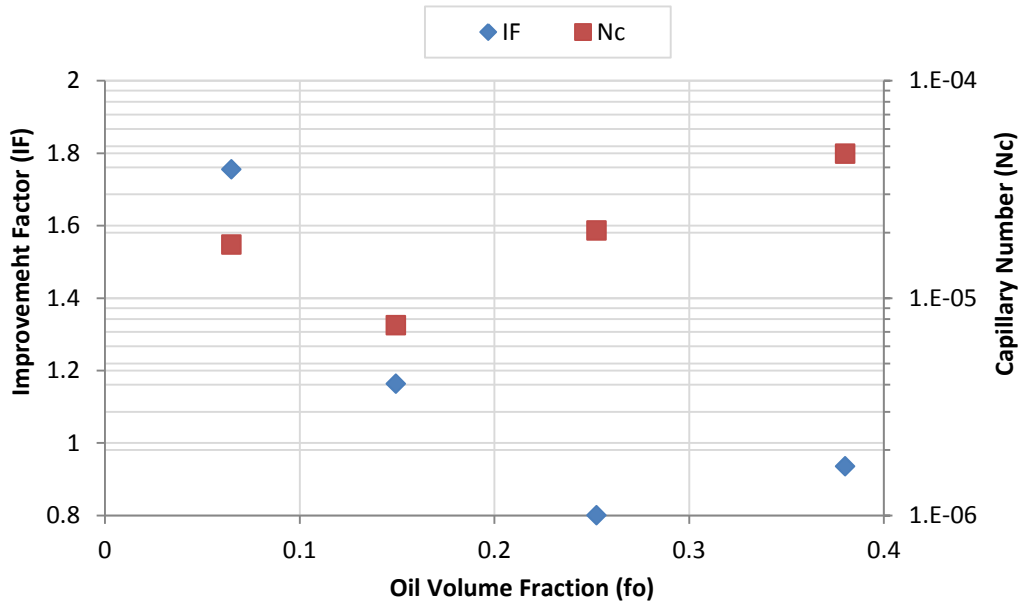


Figure 5.42 Observed improvement factors and capillary numbers for different oil volume fractions (Experiment #176)

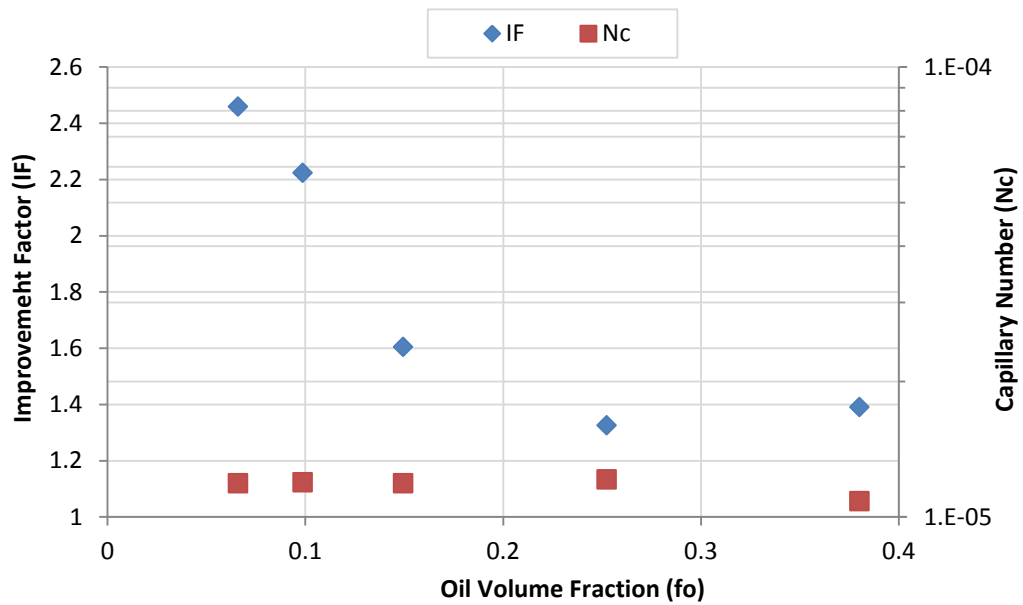


Figure 5.43 Observed improvement factors and capillary numbers for different oil volume fractions (Experiment #210)

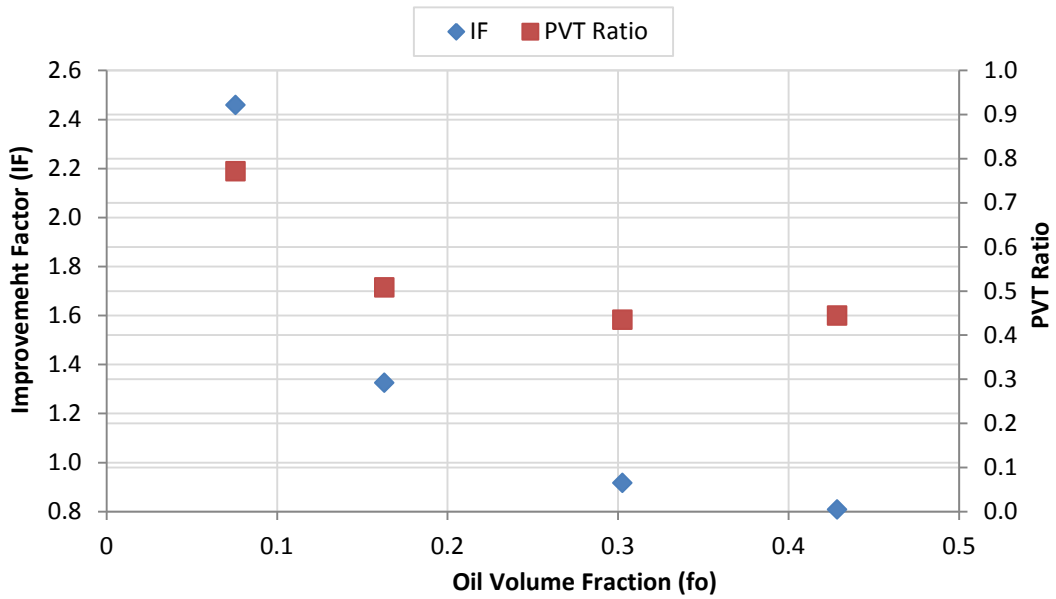


Figure 5.44 Observed improvement factors and PVT ratios for different oil volume fractions (Experiment #148)

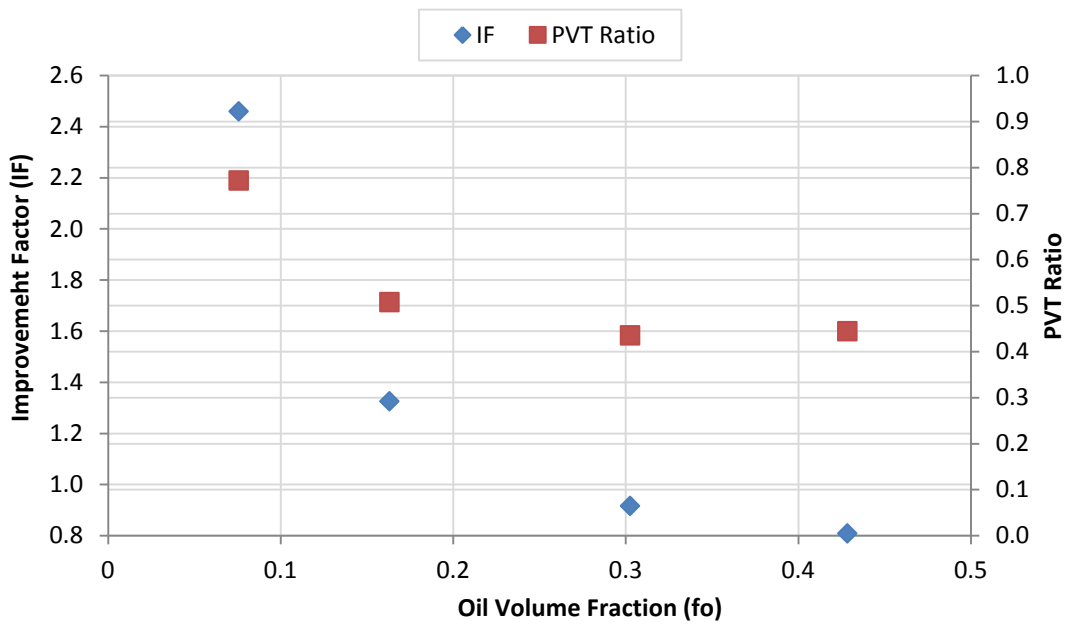


Figure 5.45 Observed improvement factors and PVT ratios for different oil volume fractions (Experiment #176)

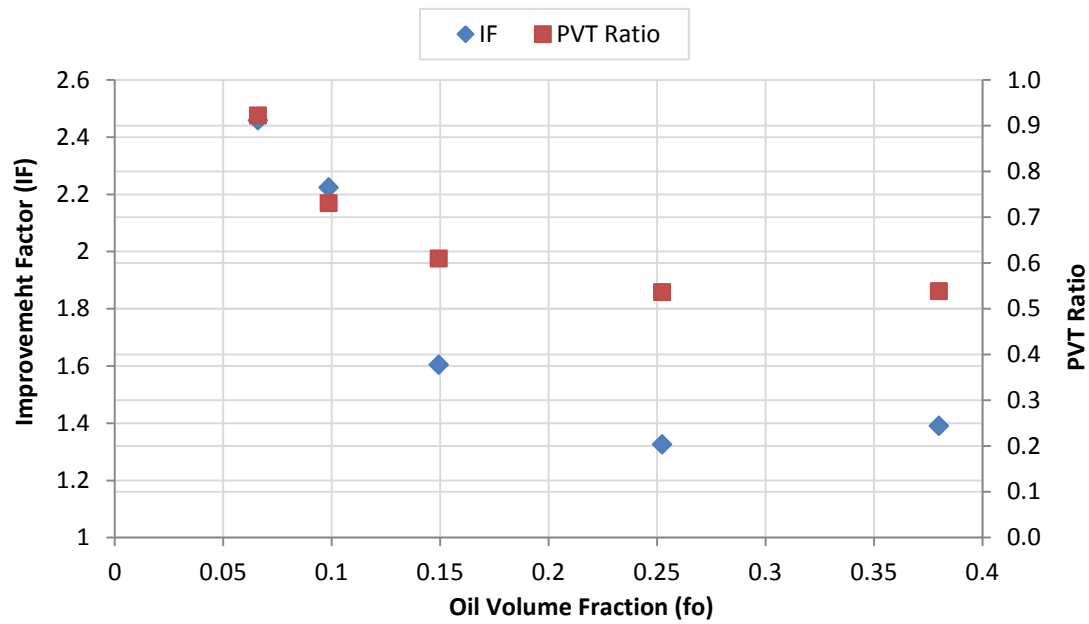


Figure 5.46 Observed improvement factors and PVT ratios for different oil volume fractions (Experiment #210)

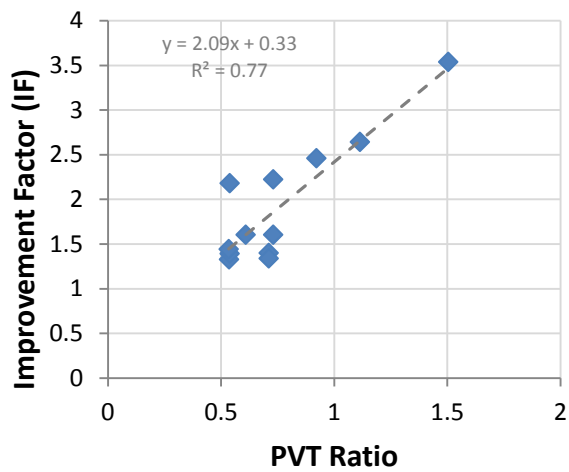


Figure 5.47 IF vs PVT ratio for experiments treated with 2 wt% FC-X

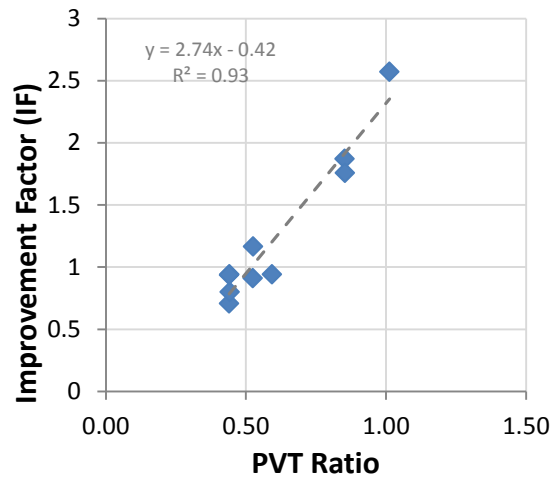


Figure 5.48 IF vs PVT ratio for experiments treated with 1 wt% L-18961

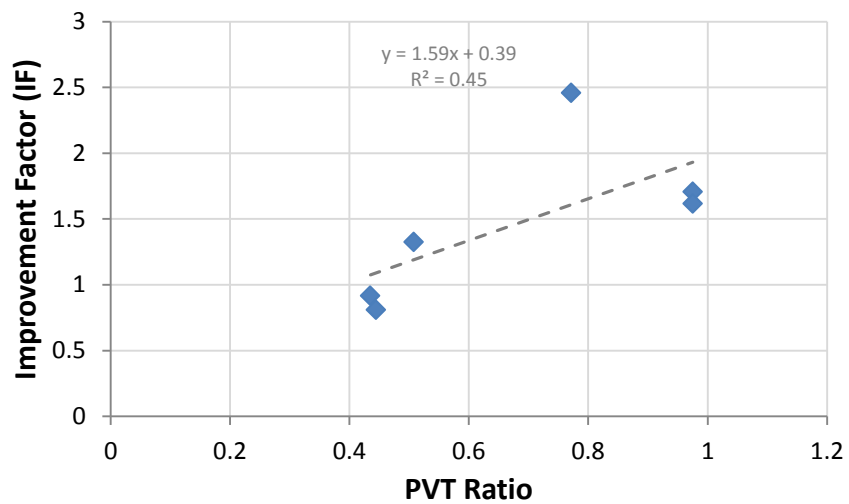


Figure 5.49 IF vs PVT ratio for experiments treated with 2 wt% L-20294

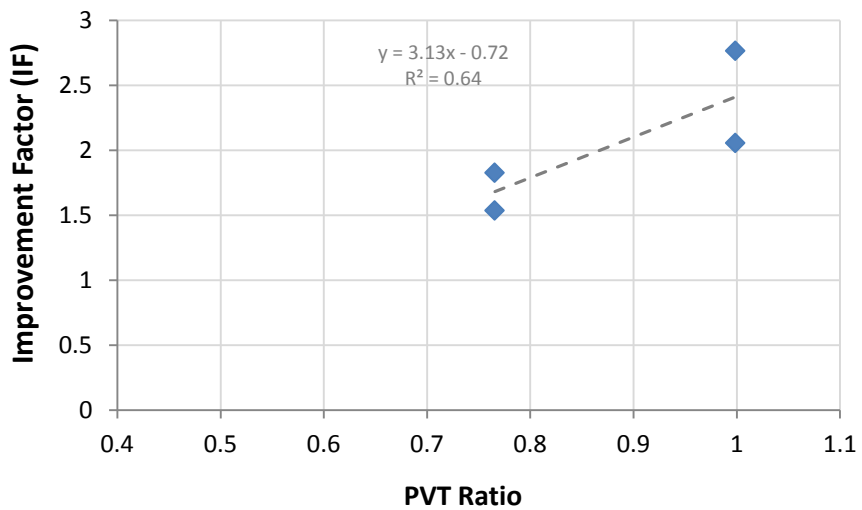


Figure 5.50 IF vs PVT ratio for experiments treated with 2 wt% L-19973#9

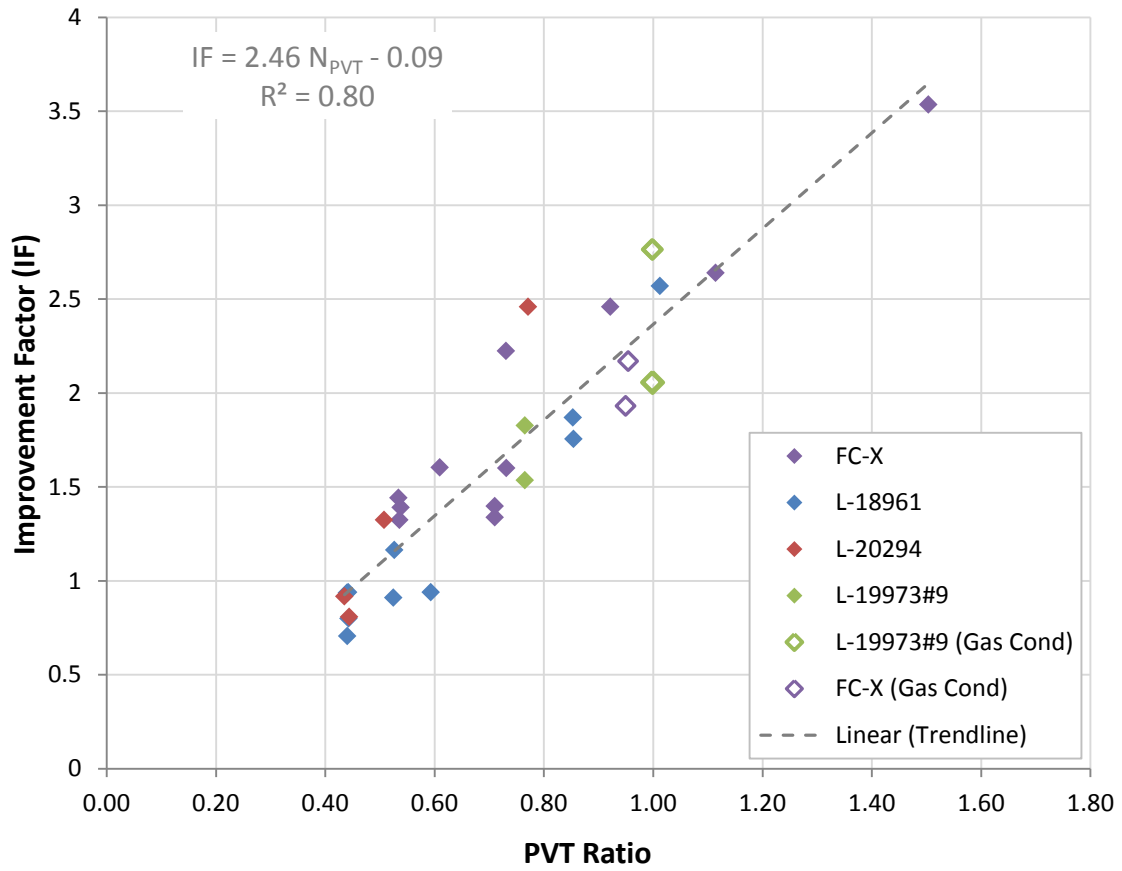


Figure 5.51 Improvement factor - PVT ratio correlation for Berea sandstones treated with C₄ fluorinated surfactants (initial improvement factor)

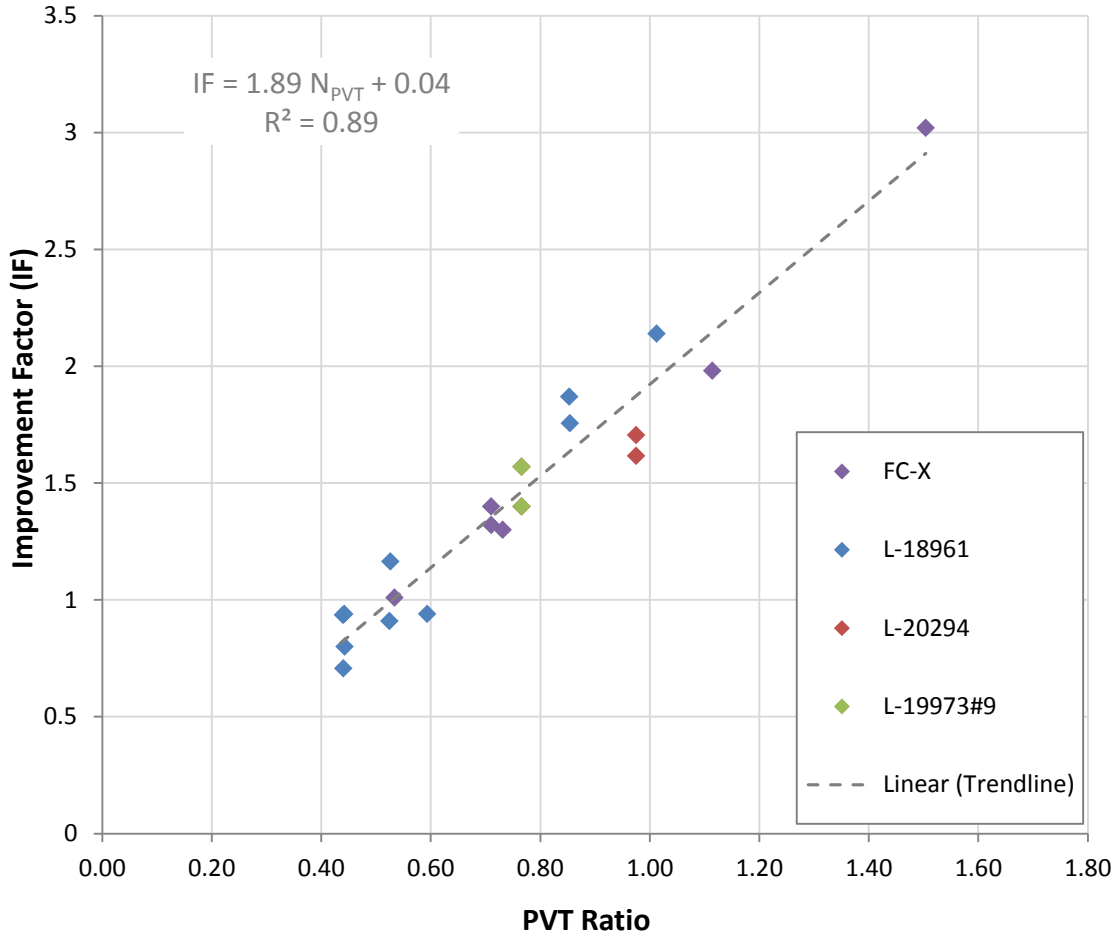


Figure 5.52 Improvement factor - PVT ratio correlation for Berea sandstones treated with C₄ fluorinated surfactants (final improvement factor)

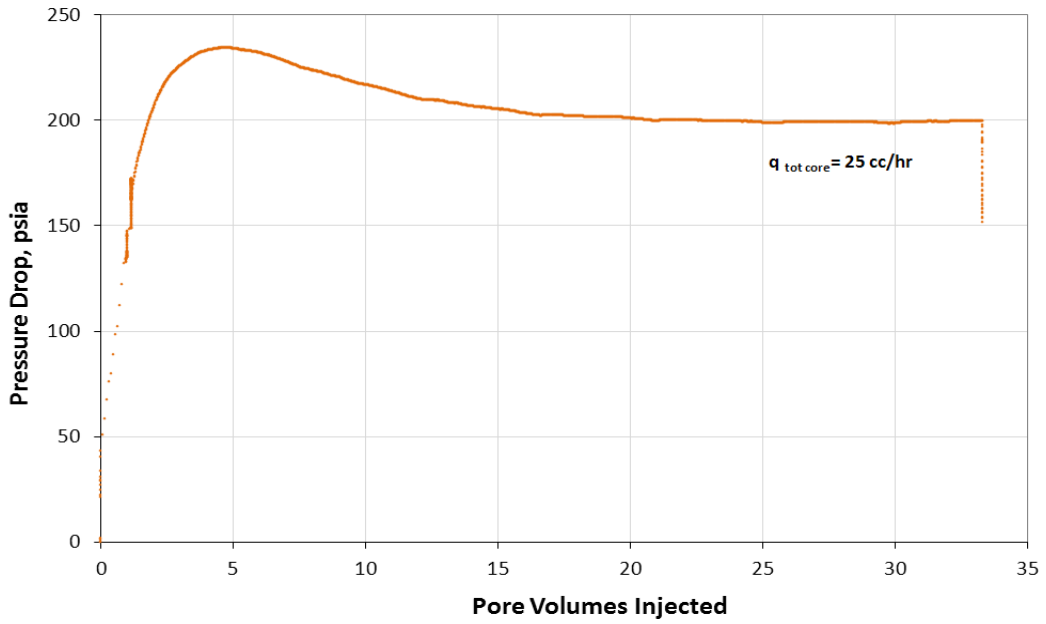


Figure 5.53 Pressure drop across the core during injection of chemical treatment 4 (Experiment # 196)

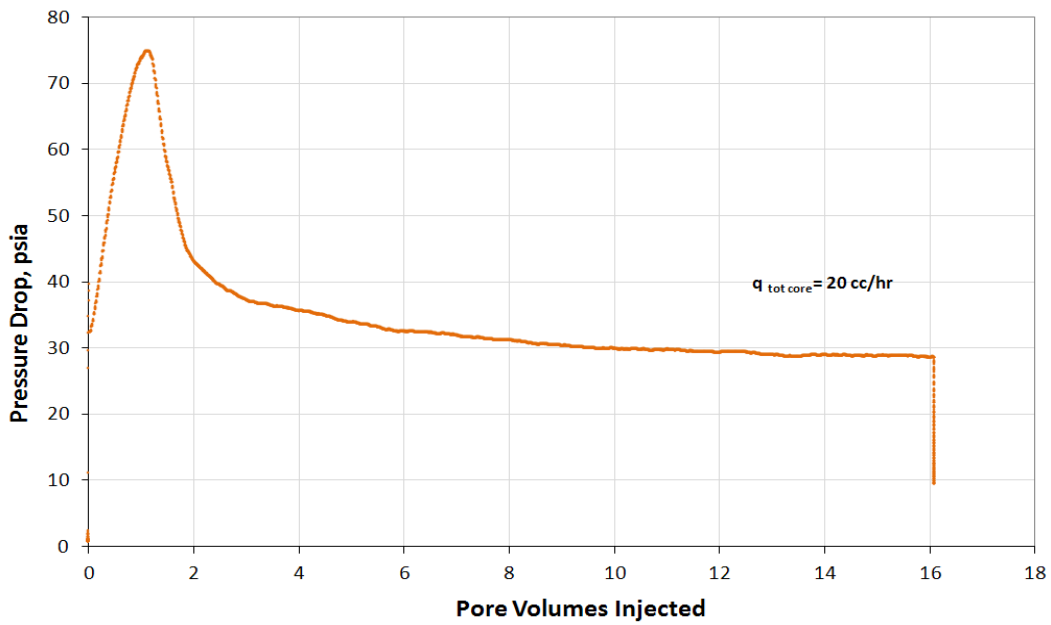


Figure 5.54 Pressure drop across the core during injection of chemical treatment 4 (Experiment # 198)

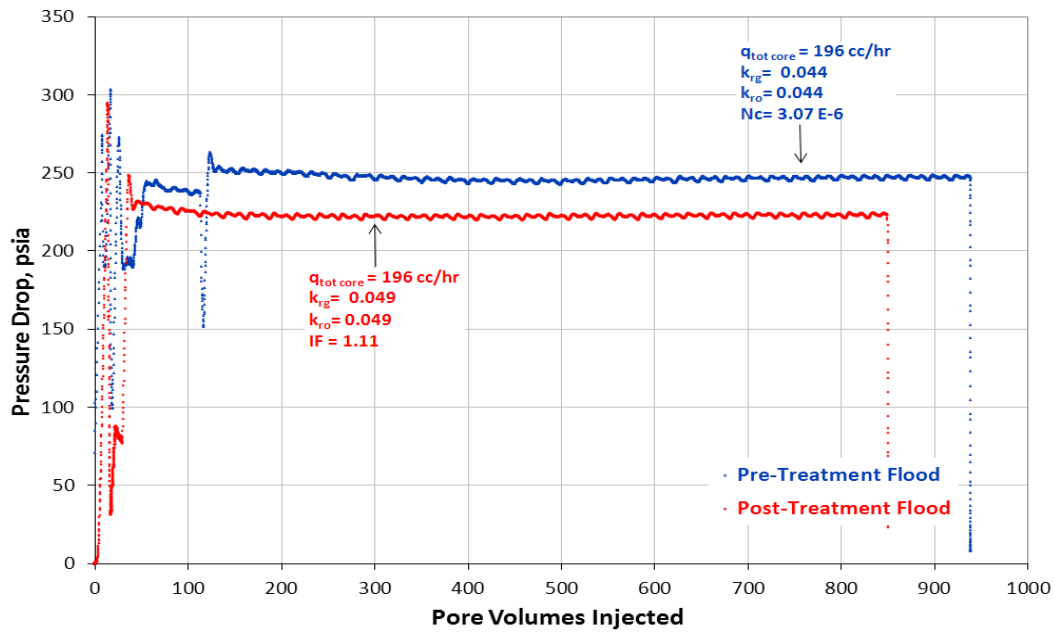


Figure 5.55 Pre and post-treatment pressure drop during two-phase volatile oil floods (Experiment # 196)

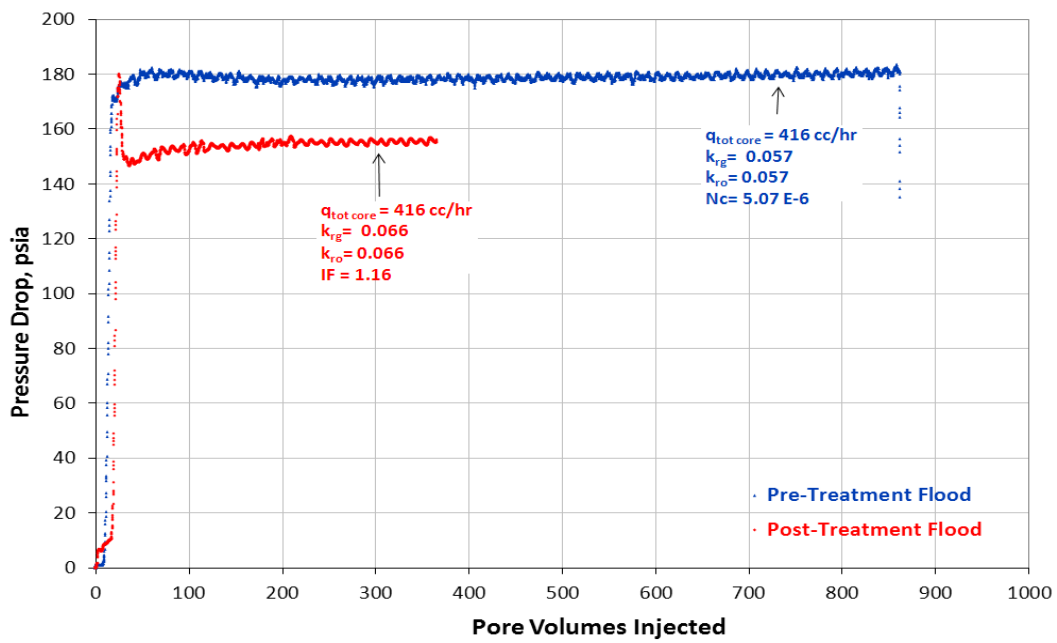


Figure 5.56 Pre and post-treatment pressure drop during two-phase volatile oil floods (Experiment # 198)

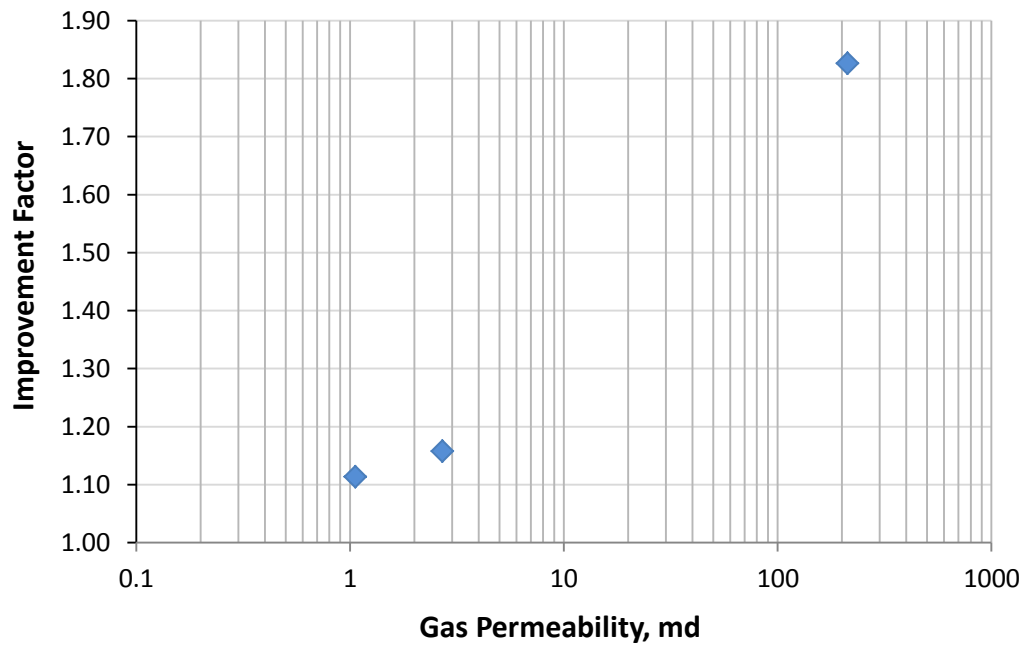


Figure 5.57 Effect of low permeability on improvement factor – results for chemical treatment 4, surfactant L-19973#9 (Experiments # 192, #196 and #198)

Chapter 6: Chemical Treatment of Carbonate Rocks

For this research, the use of fluorinated chemical treatments to mitigate “gas blocking” effect in volatile oil reservoirs was mainly focused on sandstone rocks. However, in an effort to extend the application of these chemical treatments to carbonate rocks, HPHT core flood experiments using Texas cream limestone (TCL) cores were also done. For TCL rocks the use of fluorinated chemical treatments has been studied before but only for gas condensate fluids.

To mitigate condensate accumulation near wellbore (also known as “condensate blocking”) in gas condensate reservoirs, Bang (2007) performed HPHT core flood experiments using various non-ionic fluorinated chemical treatments on TCL cores over a temperature range of 145°F to 250°F. No significant improvements in condensate and gas relative permeabilities were observed for any of the chemicals tested. The highest reported improvement factor reported was 1.3 but no discussion on durability of the treatments was addressed.

Also for gas condensates, a more rigorous study of on the application of fluorinated chemical treatments to carbonate rocks was performed by Ahmadi (2010). Carbonates such as TCL cores and Silurian Dolomite cores were treated with ionic and non-ionic surfactants over a temperature range of 175°F to 275°F. Two-step chemical treatments, using either an amine primer or a nano-solution primer, were suggested to increase the surfactant adsorption. The use of the amine primer increased the observed improvement factor and durability of the treatment, but the use of the nano-solution primer was limited since the improvement factors were low at low concentrations and at high concentrations it damaged the core. Without the aid of a primer, all of the surfactants tested prove to be non-effective, effective but non-durable.

The treatment of carbonate rocks with fluorinated chemical treatments for volatile oil reservoirs has been preliminary addressed in this work and it is discussed below. The use of non-ionic surfactants was not pursued because they had been used in previous experiments (Ahmadi 2010) and failed to produce a significant improvement. Only one surfactant was tested and it was anionic.

6.1 EFFECT OF ANIONIC SURFACTANT

The idea of using an anionic fluorinated surfactant was driven by the positive zeta potential on carbonate surfaces at reservoir pH conditions. The zeta potential indicates the degree of repulsion between adjacent, similarly charged particles, and from it the electrostatic-interaction force between rock surface and ionic surfactant could be calculated. In reservoir minerals, zeta potential can vary broadly. For the case of sandstones, quartz surfaces (commonly the dominant mineral) are negatively charged, and aluminosilicate minerals (feldspars and clays) may exhibit positive or negative charges according to the pH primarily determined by the brine. However, the zeta-potential determination for carbonate minerals is less direct. Carbonates surface charge is mainly defined by the brine-divalent and carbonate-ion contents. Under the presence of sufficient calcium ion, calcite (the most stable polymorph of CaCO_3) there will be a positive charge (Dubey and Doe 1993).

Thus, the use of the ionic fluorinated surfactant L-19446#1 whose functional group is calcium carboxylate $\text{Ca}(\text{RCOO})_2$, an ionic calcium salt, was thought to have potential for the treatment of carbonates. The negative charge of the carboxylate ion (RCOO^-) could provide adequate interaction with the surface of the TCL cores, ensured by the presence of the dissociated calcium ions (Ca^{2+}) from the surfactant, from the calcium chloride (CaCl_2) present in the brine, and from the carbonate rock itself.

The screening tests for surfactant L-19946#1 and the formulation of chemical treatment 5 has been explained in detail in Chapter 4. The formulation is summarized in Table 4.15. Brine 2, composed of 25,000 ppm of sodium chloride (NaCl) and 250 ppm of calcium chloride (CaCl₂), was used for the following experiments. The CaCl₂ was added to Brine 2, mainly to avoid ionic exchange between the carbonate surface and the brine, which could potentially result in core damage.

Experiment #181 and #185 were performed using chemical treatment 5. A detailed description of the HTHP core flood experimental setup used for the experiments was previously discussed in Chapter 3 and a schematic of the experimental system is shown in Figure 3.1. The two experiments were run at 155°F, at an initial water saturation of 20%. The hydrocarbon used was synthetic volatile oil mixture 2 given in Table 3.3. Detailed experimental procedure for each of the experiments is described in Appendix A.7 and A.8.

For experiment #181, the TCL core absolute permeability was 11 md and core pressures of 800 psi, 1500 psi, 2200 psi and 2900 psi were used. Table 6.1 summarizes the experimental conditions. Twenty pore volumes of chemical treatment 5 were injected at 100 cc/hr and the pressure drop across the core was 200 psi, the data is shown in Figure 6.1. No plugging or unusual behavior during treatment injection was observed. Figure 6.2 and Figure 6.5 show the pre and post-treatment two-phase volatile oil injection pressure drop data for each of the core pressures. The pre-treatment capillary numbers for increasing core pressures ranged from 6.5×10^{-6} to 3.9×10^{-5} and the PVT ratio ranged from 0.94 to 0.53. At a PVT ratio of 0.94, three volatile oil floods were performed and the IF ranged from 1.4 to 1.3. For lower PVT ratios, 0.61 to 0.53, the IF ranged from 1.4 to 0.9. It was thought that a possible reason for these low improvement factors was insufficient surfactant mass. In carbonates, the surface area is generally significantly

greater than for sandstones, therefore they may require higher amounts of surfactants to be adequately treated. The core was then re-treated and 20 PV more of chemical treatment 5 at 50 cc/hr were injected. The treatment rate was dropped to avoid the high pressure drop observed for the first treatment. Figure 6.6 shows the pressure drop across the core for the second-treatment injection. For the post-second-treatment two-phase volatile oil flood, the improvement factor came out to be similar to the one obtained after the first chemical treatment (Figure 6.7). This confirmed that the rock had been fully treated within the first chemical treatment. The results for this experiment are summarized in Table 6.2.

For Experiment #185, the TCL core absolute permeability was 25 md and the core pressure was 790 psi. Table 6.3 summarizes the experimental conditions. About 20 PV of chemical treatment 5 were injected at 50 cc/hr and no plugging or unusual behavior was observed, the data is given in Figure 6.8. Multiple injection flow rates were used and the pre and post-treatment two-phase volatile oil floods are shown in Figure 6.9. For the multiple injection flow rates, the pre-treatment capillary number ranged from 1.7×10^{-6} to 5.3×10^{-6} and PVT ratio was kept constant at 0.94. The calculated improvement factors ranged from 1.9 to 1.6. The drop in improvement factor is similar to what has been previously observed for the experiments conducted using sandstone cores. The results for this experiment are summarized in Table 6.4.

6.2 EFFECT OF CAPILLARY NUMBER

Figure 6.10 and Figure 6.11 show the pre and post-treatment gas and oil relative permeabilities for increasing capillary number calculated for Experiment #181. It can be seen that for capillary numbers above 1×10^{-5} the oil and gas relative permeability significantly increase and no improvement factor was achieved. This indicates that at this point is where viscous forces exceed the capillary forces as previously discussed in

Section 5.3. Figure 6.12 shows the improvement factors versus capillary number for Experiments #181 and #185. An improvement factor greater than 1.0 was only observed at low capillary numbers.

6.3 EFFECT OF PVT RATIO

The effect of the PVT ratio on carbonates treated with fluorinated chemical treatments is shown in Figure 6.13. For experiment #185 only the improvement factor for the higher capillary number 5×10^{-6} was considered since for Experiment #186 all the capillary numbers are high. Below PVT ratios of 0.5, no IF was observed.

It is difficult to establish a specific correlation between IF and PVT ratio on TCL rocks due to the small amount of data and the differences between absolute core permeabilities and capillary number ranges. However, as is the case with sandstones, the trend of higher improvement factors with increasing PVT ratio in carbonate rocks is also evident.

6.4 EFFECT OF LOW PERMEABILITY

Figure 6.14 compares the improvement factors for two TCL cores with different absolute permeabilities (Experiment #181 and #185). Although the two permeabilities are not significantly different, the core with the lower permeability had the lower IF. This result is similar to what was observed for low permeability sandstone cores.

6.5 SUMMARY AND CONCLUSIONS

Texas cream limestone cores were treated with the anionic fluorinated surfactant L-19446#1 to mitigate the effect of “gas blocking” in volatile oil reservoirs. Under reservoir conditions and in the presence of connate water, the chemical treatment improved the oil and gas relative permeability by a factor of 1.3 to 1.9. This indicates that the surfactant did modify the wettability of the carbonate surface.

The wettability alteration, due to chemical treatment seems to be durable and the sustained IF values are in agreement with those for gas condensate reported by Ahmadi (2010) where TCL cores were treated with the same treatment at 175°F (Exp #182). However, the number of experiments performed on carbonates is low and the reproducibility of such experiments needs confirmation.

The effects of capillary number, PVT ratio, and core absolute permeability on improvement factor were in agreement with what had been observed in treated sandstones. The chemical treatment was not tested for temperature effects.

Table 6.1 Summary of conditions for Experiment # 181

	Exp# 181
<i>Rock type</i>	TCL
k_g , md	11.3
S_{wi} %	20
<i>Brine Salinity NaCl - CaCl₂</i> , ppm	25000 - 250
<i>Temperature</i> , °F	155
<i>Single-Phase Vol. Oil Pressure (BPR-1)</i> , psig	4320
<i>Two-Phase Vol. Oil Pressure (BPR-2)</i> , psig	800, 1500, 2200, 2900
<i>Volatile Oil Mixture</i>	2
<i>Chemical Treatment</i>	5
<i>Surfactant</i>	L-19446#1

Table 6.2 Summary of results for Experiment # 181

	Exp# 181			
<i>Core pressure</i> , psia	800	1500	2200	2900
q_{tot} core, cc/hr	461	235	159	124
q_g , cc/hr	431	199	119	76
q_o , cc/hr	30	35	41	49
<i>PVT Ratio</i>	0.94	0.61	0.54	0.53
<i>Viscosity Ratio</i> μ_g/μ_o	0.07	0.11	0.19	0.34
<i>Liquid Fraction</i>	6.5%	15.1%	25.6%	39.0%
<i>Capillary Nc</i>	6.50E-06	9.78E-06	1.39E-05	3.90E-05
k_{rg} Before Treatment	0.053	0.040	0.057	0.092
k_{ro} Before Treatment	0.057	0.065	0.105	0.172
k_{rg} After 1st Treatment	0.067	0.054	0.054	0.084
k_{ro} After 1st Treatment	0.071	0.088	0.101	0.158
<i>Initial Improvement Factor</i>	1.4	*	*	*
<i>PV of Vol Oil Injected</i>			~ 400	
<i>Final Improvement Factor</i>	1.3	1.4	1.0	0.9
k_{rg} After 2nd Treatment	0.071	0.054	*	*
k_{ro} After 2nd Treatment	0.076	0.087	*	*
<i>Initial Improvement Factor</i>	1.3	1.3	*	*
<i>PV of Vol Oil Injected</i>			~ 200	

* Data not measured

Table 6.3 Summary of conditions for Experiment # 185

	Exp# 185
<i>Rock type</i>	TCL
k_g , md	24.8
S_{wi} %	20
<i>Brine Salinity NaCl - CaCl₂, ppm</i>	25000 - 250
<i>Temperature, °F</i>	155
<i>Single-Phase Vol. Oil Pressure (BPR-1), psig</i>	4260
<i>Two-Phase Vol. Oil Pressure (BPR-2), psig</i>	790
<i>Volatile Oil Mixture</i>	2
<i>Chemical Treatment</i>	5
<i>Surfactant</i>	L-19446#1

Table 6.4 Summary of results for Experiment # 185

	Exp# 185		
<i>Core pressure, psia</i>	790		
$q_{tot\ core}$, cc/hr	140	280	467
q_g , cc/hr	131	262	437
q_o , cc/hr	9	18	30
<i>PVT Ratio</i>	0.94		
<i>Viscosity Ratio μ_g/μ_o</i>	0.06		
<i>Liquid Fraction</i>	6.4%		
<i>Capillary Nc</i>	1.68E-06	3.34E-06	5.25E-06
k_{rg} Before Treatment	0.062	0.062	0.066
k_{ro} Before Treatment	0.065	0.066	0.070
k_{rg} After Treatment	0.112	0.116	0.114
k_{ro} After Treatment	0.119	0.123	0.121
<i>Initial Improvement Factor</i>	1.8	1.9	1.7
<i>PV of Vol Oil Injected</i>	~ 390		
<i>Final Improvement Factor</i>	1.6	1.7	1.7

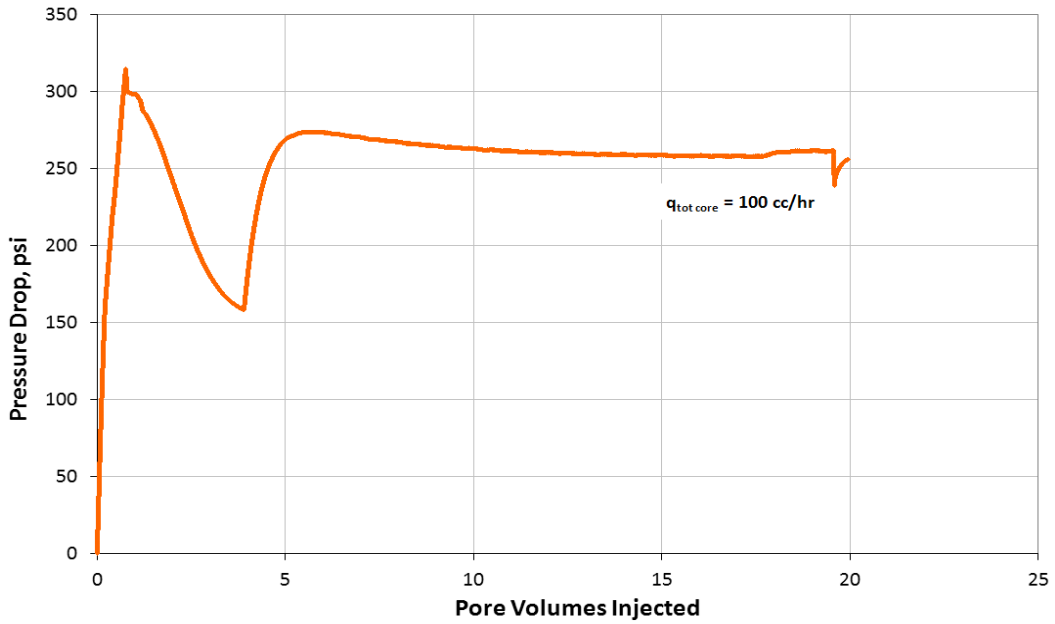


Figure 6.1 Pressure drop across the core during injection of chemical treatment 5 (Experiment # 181)

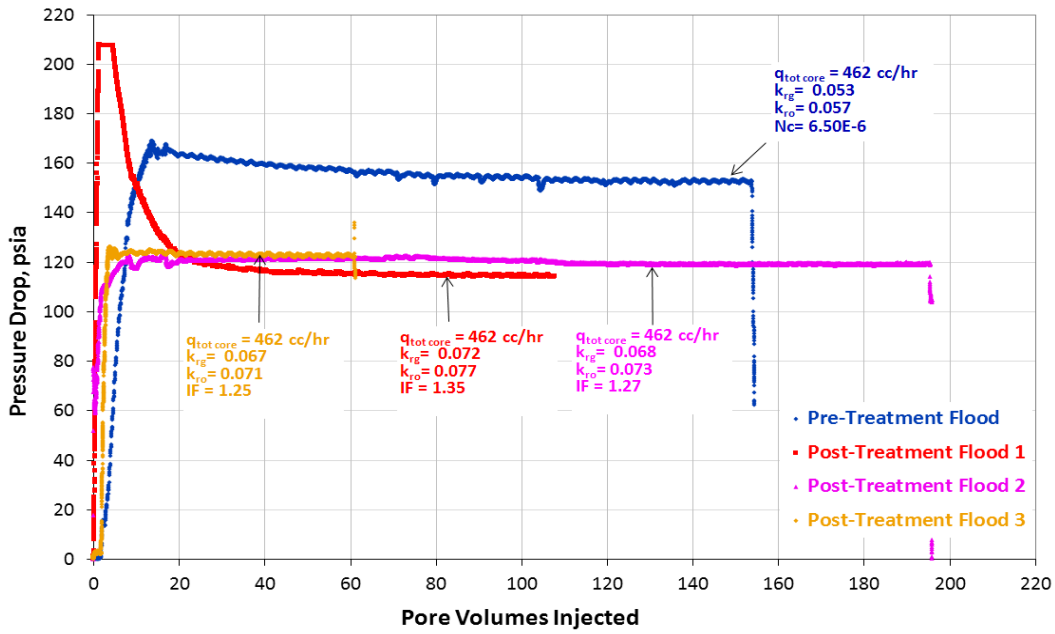


Figure 6.2 Pre and post-treatment pressure drop during two-phase volatile oil floods at 800 psi core pressure (Experiment # 181)

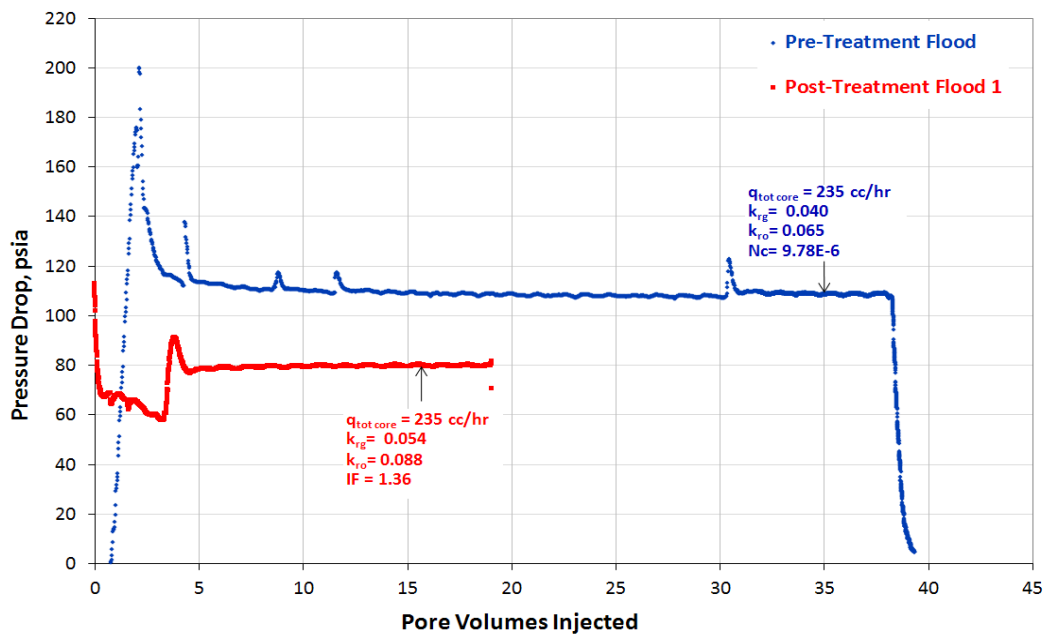


Figure 6.3 Pre and post-treatment pressure drop during two-phase volatile oil floods at 1500 psi core pressure (Experiment # 181)

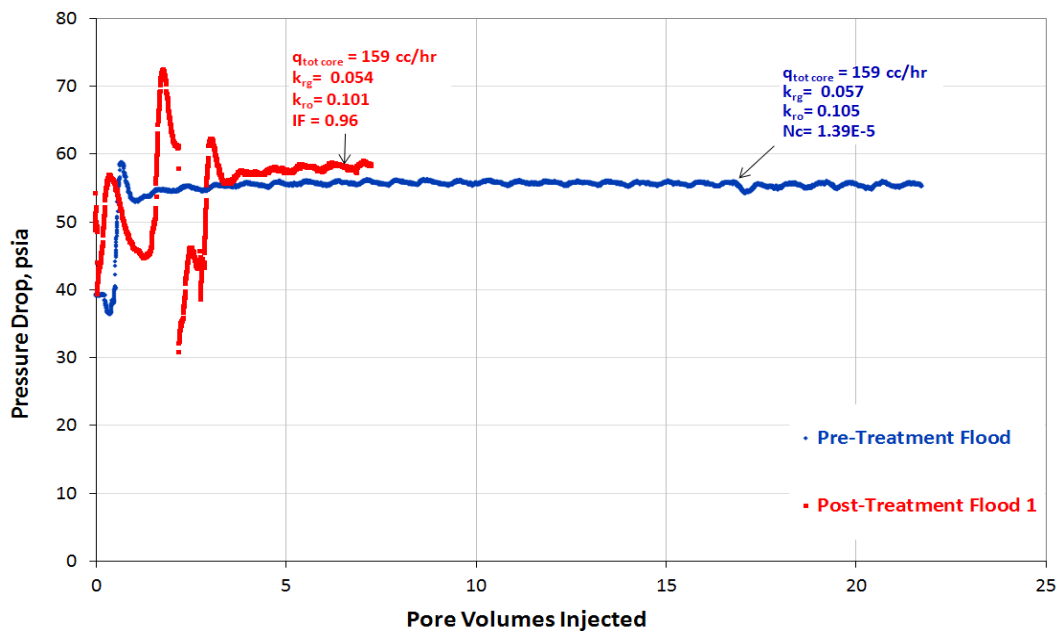


Figure 6.4 Pre and post-treatment pressure drop during two-phase volatile oil floods at 2200 psi core pressure (Experiment # 181)

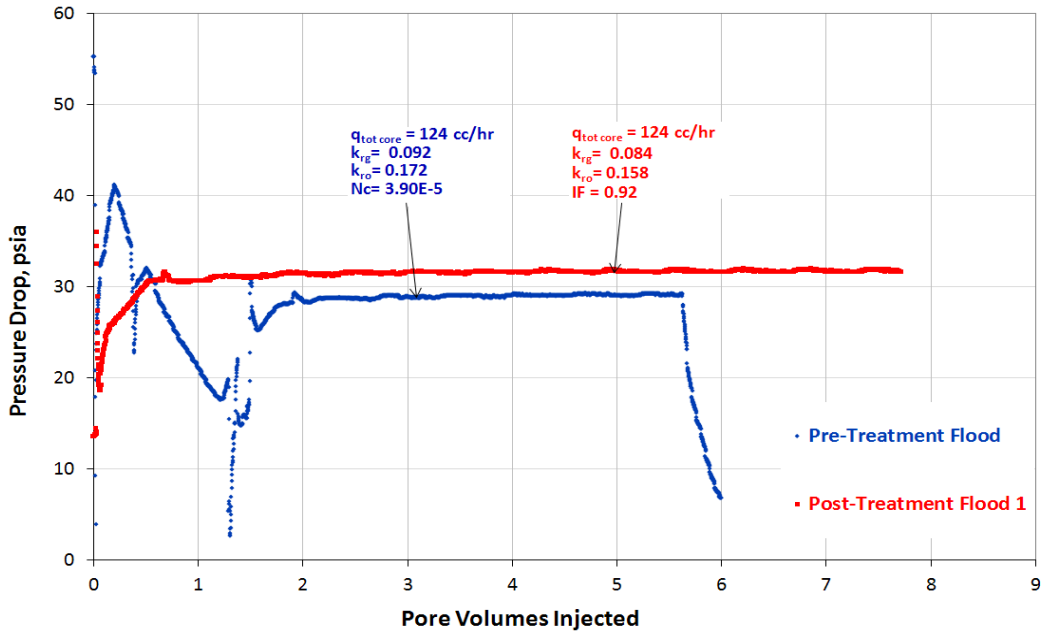


Figure 6.5 Pre and post-treatment pressure drop during two-phase volatile oil floods at 2900 psi core pressure (Experiment # 181)

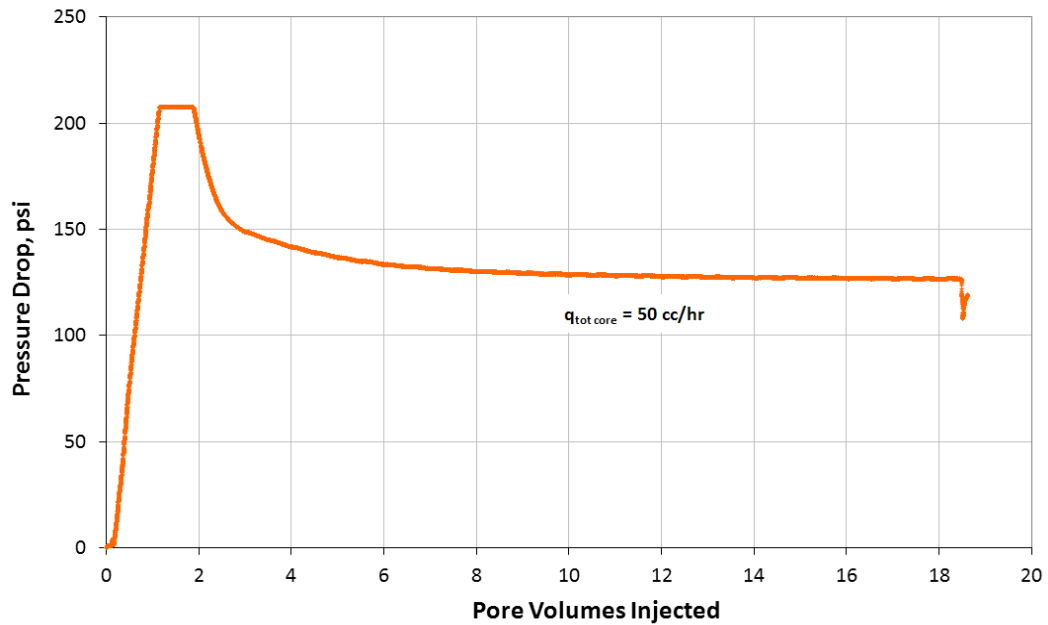


Figure 6.6 Pressure drop across the core during injection of second chemical treatment 5 (Experiment # 181)

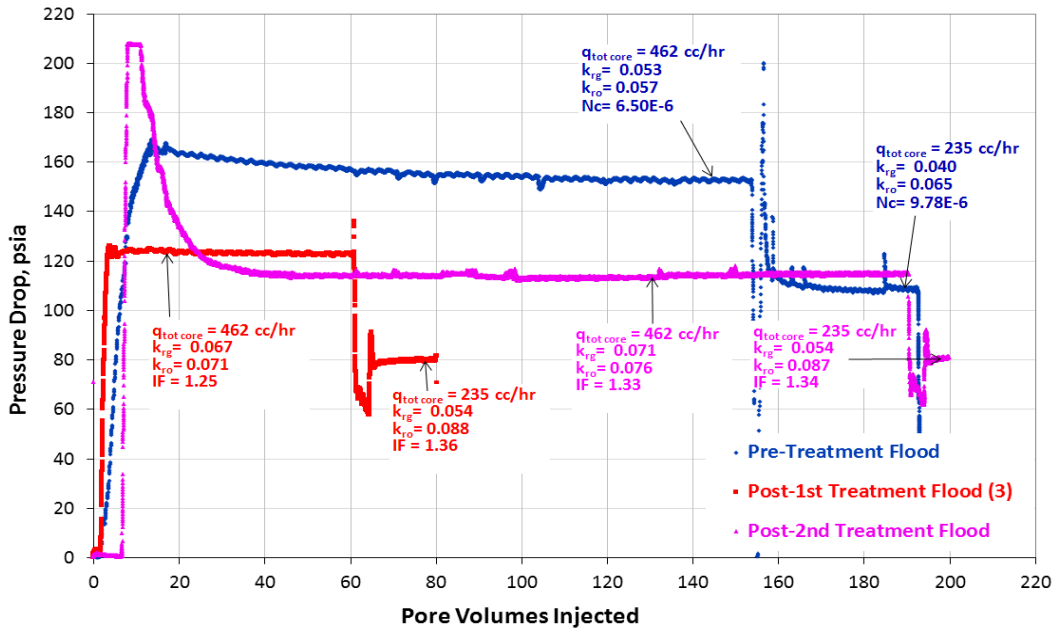


Figure 6.7 Pre and post-treatment pressure drop during two-phase volatile oil floods for 1st and 2nd chemical treatment at 800 psi and 1500 psi core pressures (Experiment # 181)

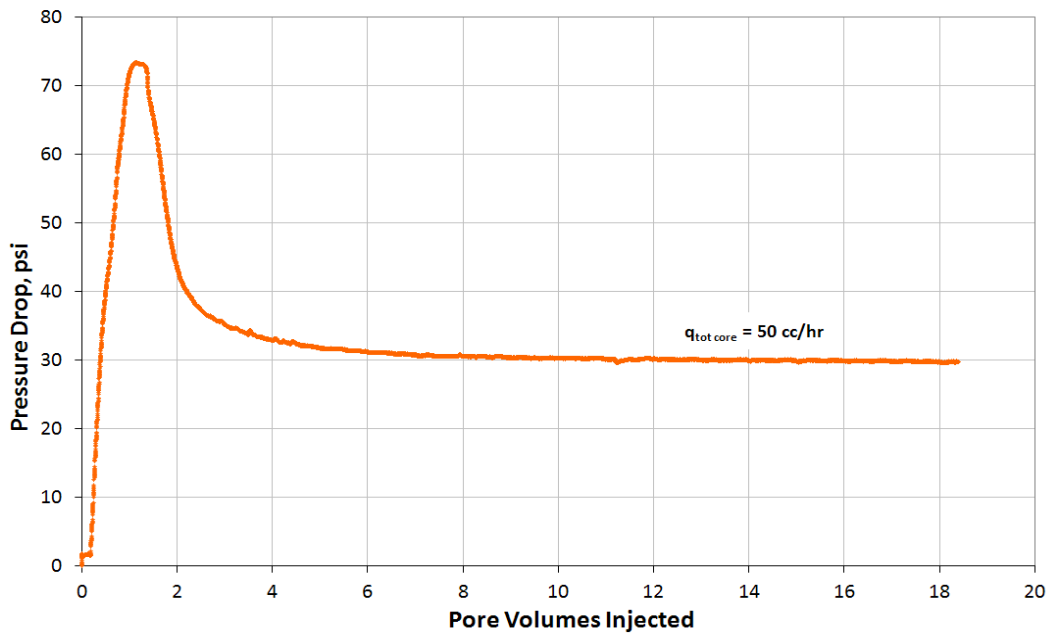


Figure 6.8 Pressure drop across the core during injection of chemical treatment 5 (Experiment # 185)

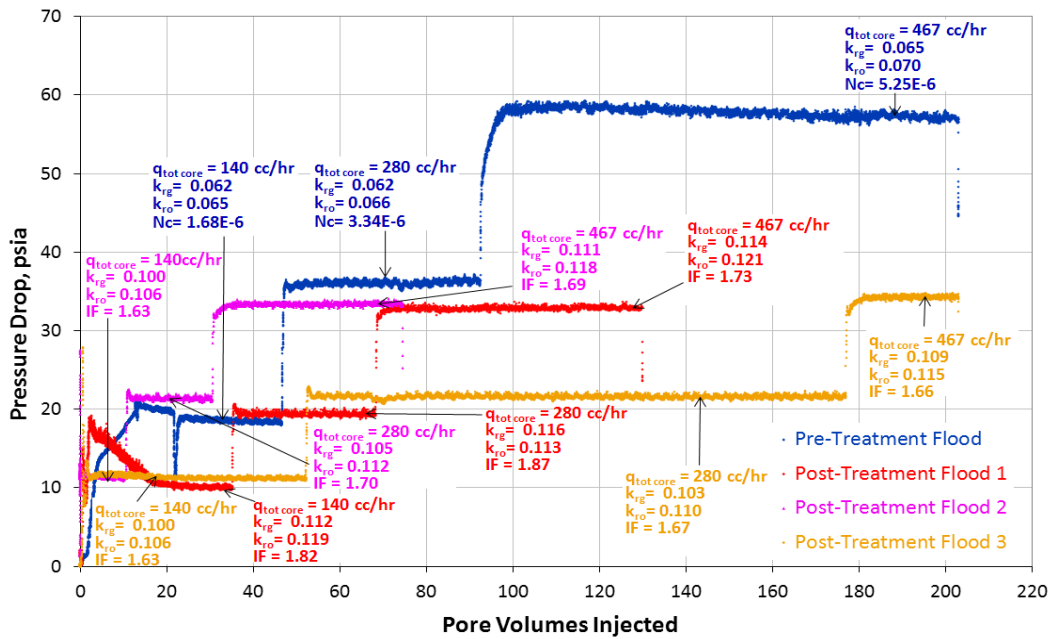


Figure 6.9 Pre and post-treatment pressure drop during two-phase volatile oil floods at three different flow rates (Experiment # 185)

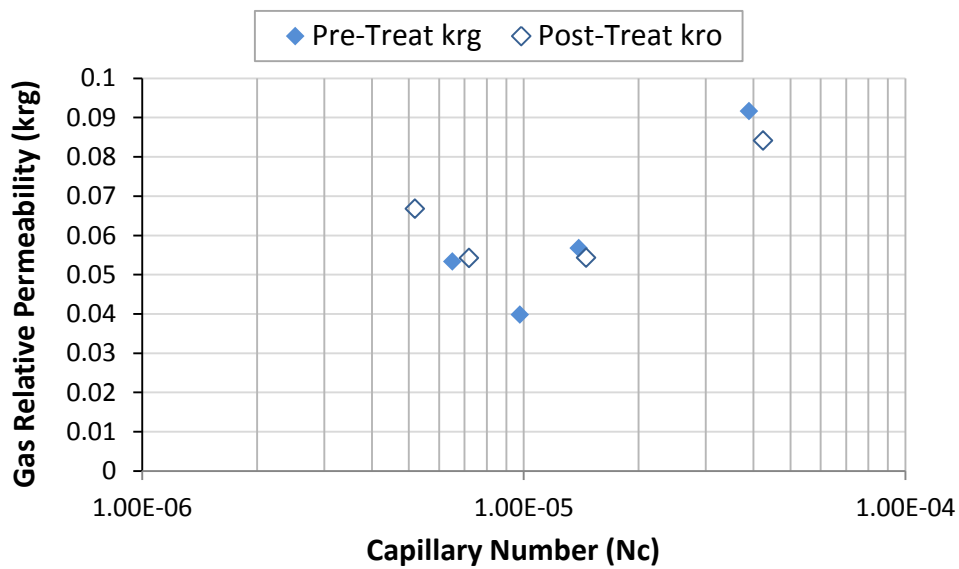


Figure 6.10 Capillary number effect on pre and post-treatment gas relative permeability (Experiment # 181)

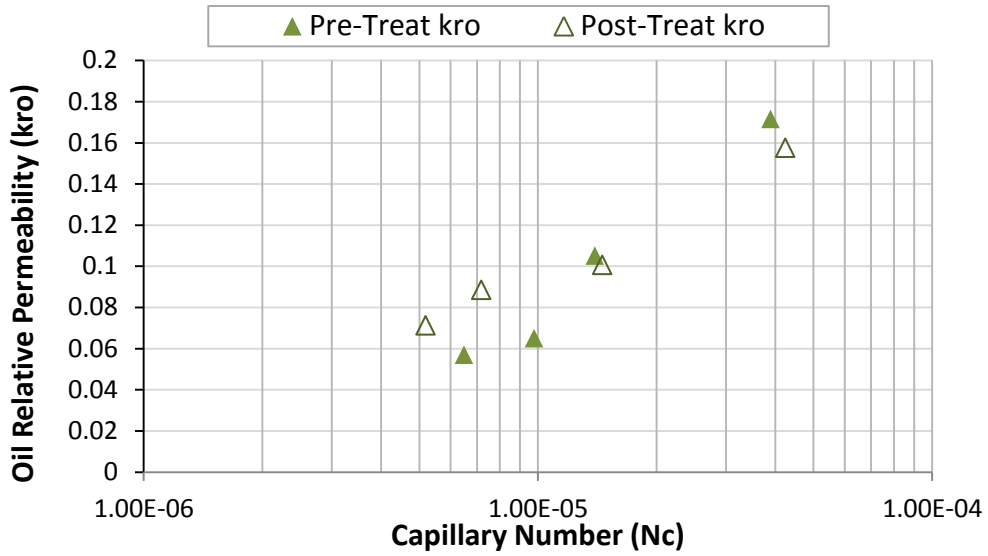


Figure 6.11 Capillary number effect on pre and post-treatment oil relative permeability (Experiment # 181)

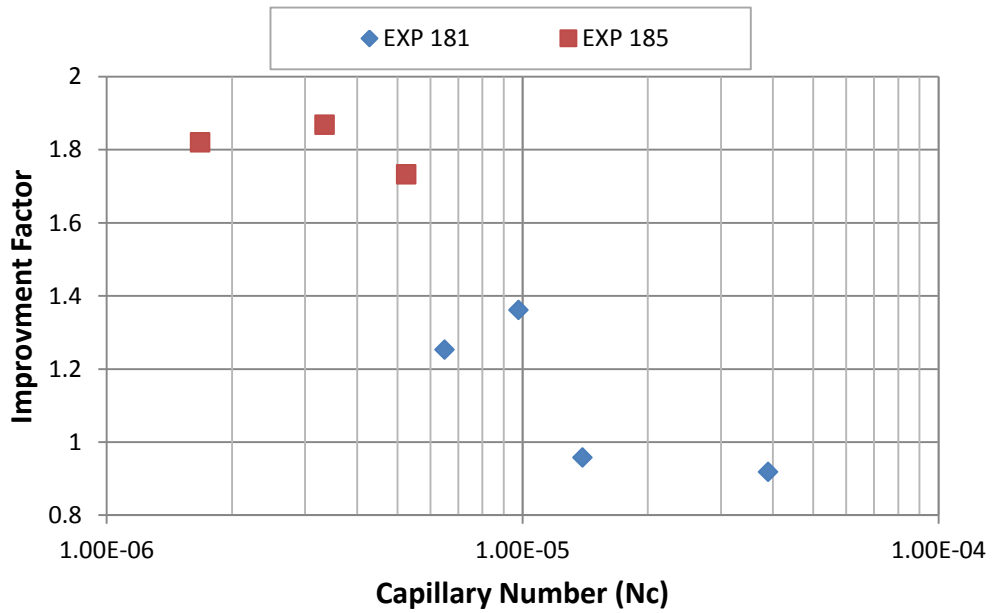


Figure 6.12 Capillary number effect on improvement factor (Experiments #181 & # 185)

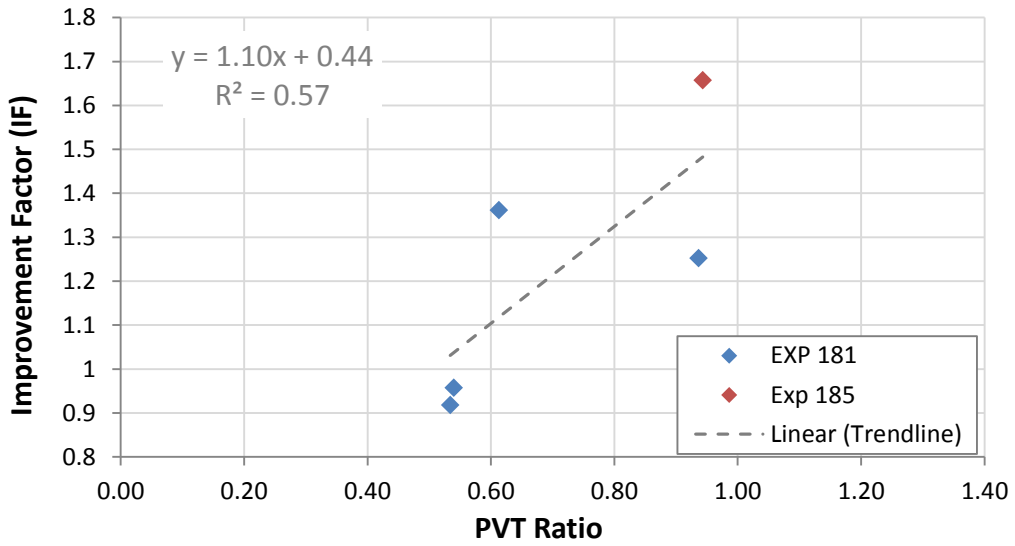


Figure 6.13 Effect of PVT ratio on improvement factor for carbonate cores

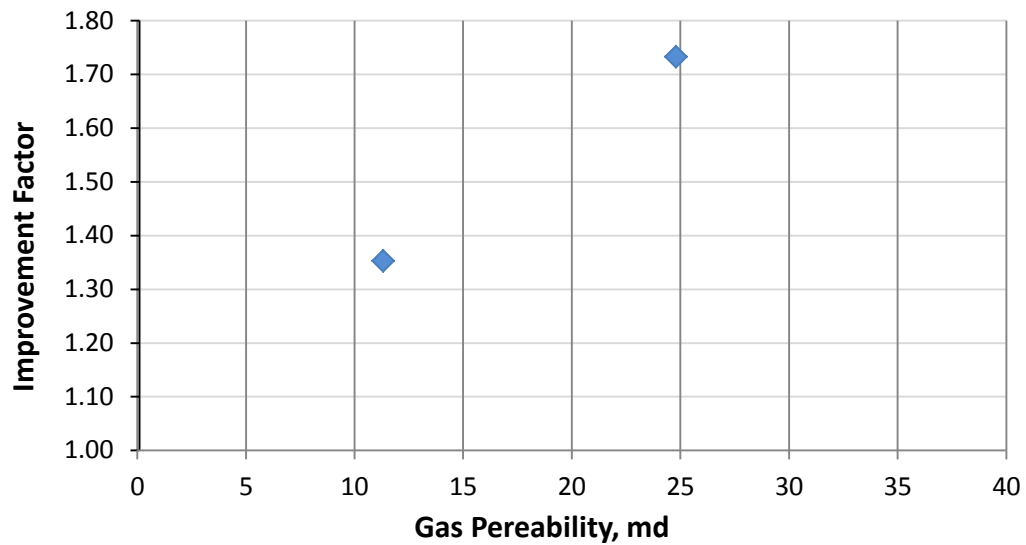


Figure 6.14 Effect of core absolute permeability on improvement factor for carbonate cores

Chapter 7: Evaluation of the Chemical Treatment Performance

The performance of fluorinated chemical treatments was mainly evaluated with HPHT core flood experiments, as discussed in Chapter 5 and 6. The treatments and the effects that they have on the volatile oil phases, gas and oil, were also studied with the aid of various analytical techniques to better understand the behavior. The analyses performed were; X-ray photoelectron spectroscopy (XPS) for fluorine measurements on treated cores, high-performance liquid chromatography (HPLC) for surfactant adsorption and desorption measurements, and computerized axial tomography (CT Scan) for fluid saturation measurements in core flood experiments.

Analytical procedures, calculations and results obtained from these analytical techniques are discussed below.

7.1 X-RAY PHOTOELECTRON SPECTROSCOPY FOR FLUORINE MEASUREMENTS

The use of X-ray photoelectron spectroscopy (XPS) for surface fluorine analysis has already been described in section 4.2.2. X-ray photoelectron spectroscopy is a surface chemical analysis technique that can be used to measure the elemental composition, chemical state and electronic state of the elements that exist within a material surface. A schematic of the operating principle of XPS was given in Figure 4.1.

The use of XPS for rock surface fluorine measurement was not only valuable for screening potential surfactants for wettability alteration, but also for core analysis after HPHT core flood experiments were completed. As discussed before, the fluorine present in the surfactant was used to qualitatively measure the presence of the surfactant in the treated rock surface.

7.1.2 Analytical procedure

The x-ray photoelectron spectrometer used for the fluorine measurements was manufactured by Kratos Analytical Company. The parameters used for XPS analysis have been shown in Table 4.2. and the analyzed elements according to the type of rock in Table 4.3.

Fluorine content measurements were performed longitudinally along cores treated in HTHP core flood experiments to obtain a profile of fluorine content along the core. To make these core measurements, a core was cut into two-inch sections and for each section a sample of each side was taken for XPS analysis.

To avoid surface alteration during core cutting, the following procedure was followed;

- Sampling spots were marked longitudinally along the core
- For a given spot, the core was cut half way through perpendicular to its length using a blade and then manually cracked. This allowed for a cross sectional section to exist which was untouched by the blade.
- Another complete cut was made to obtain a 2 mm slice having the cracked portion on one of the faces. This was repeated for every sampling spot.

After cutting and before XPS analysis, samples were dried over night at about 100°F and no rinsing or washing procedure was applied to avoid surface alteration.

During core flood experiments, two cases for the flow direction of injected fluids were used. For case 1, both fluids, chemical treatment and volatile oil, were injected from the same core end, and for case 2 they were injected from opposite ends. For future reference the core inlet will be referred to as the fluid injection end.

Figure 7.1 and 7.2 show schematics of the core sectional cuts and sampling spots, and the direction of fluid injection for case 1 and case 2 respectively.

7.1.2 Fluorine content along treated cores

Eight sandstone cores and one carbonate core from HTHP core flood experiments were analyzed for fluorine content. Sandstone cores correspond to experiments #141, #148, #176, #189, #224, #225, #228 and #229 where the surfactants used were L-20294, L-18961 and FC-X. The carbonate core corresponds to experiment #185 where the surfactant used was L-19446#1. Each of these experiments is described in appendix A.

For the cores from earlier experiments only three spots were analyzed for fluorine measurements: inlet, middle, outlet; and for the later ones a sample was taken every 2 inches for a total of seven samples. The XPS measurements are summarized in

Table 7.1

The results for the Berea cores are shown in Figure 7.3. In this figure the fluorine mass percentages are illustrated from inlet to outlet of the core with respect to the direction of the chemical treatment flood. It was observed that the highest levels of fluorine are for the end surface of the core which faces the inlet. Then, after only 0.25 inches from the inlet, the fluorine content significantly decreased to a level that remained almost constant throughout the core. The amount of fluorine content, excluding the inlet and outlet measurement, ranged from 0.5 wt% to 11 wt%. A probable reason for the observed initial high fluorine levels may be because the entire analyzed surfaced has been exposed to the chemical treatment compared to the other analyzed spots where only the surface of the interconnected pores has been treated. Another possibility is surfactant buildup before entering the pores. The results show that for Berea cores exposed to different treatments, experimental conditions, amounts of hydrocarbon injected and flood direction, the trend of constant fluorine levels throughout the core is similar. For experiment # 176 the core had been treated three times and the levels of fluorine were

higher than those for experiment # 189 which had been treated only once with the same chemical treatment.

A quick test was performed to study the increment of fluorine content with multiple treatments. In experiment #226, four Berea sandstone cores with similar permeability were treated with 20, 40, 60 and 80 pore volumes. Chemical treatment 1 was used and the treatment temperature was 155°F. The cores were not aged with the chemical treatment and no pre or post-treatment volatile oil fluids were injected. The four treated cores were analyzed for fluorine content and the results are shown in Figure 7.4. There was no significant difference in the fluorine content measured for the four treated cores. The mass of treatment injected seemed to have no effect on the fluorine mass measured on the cores internal surface.

In Figure 7.5 the fluorine measurements for experiments #141, #148, #189 & #224 are compared and the outer core faces were not included. All the cores had been treated only once, at 155°F, the direction of the floods were the same (case 1) but the chemical treatment was different. The observed fluorine contents are in agreement with what had been observed in Figure 4.2 for surfactant screening, where the highest fluorine contents of the selected surfactant were those for L-20294 and the lowest for FC-X.

For experiments #225, #228 & #229 that had been treated with chemical treatment 1 (2 wt% FC-X), under similar conditions and where the only variable had been the temperature (155°F, 215°F and 275°F, respectively) the fluorine measurements were compared in Figure 7.6. The analyses indicate that the fluorine content decreases at higher temperatures while increasing improvement factors with temperature had been observed. However, the levels of fluorine are low at all temperatures and the differences among the results are not significantly enough to draw a conclusion.

The measured fluorine contents for the carbonate core are shown in Figure 7.7. This core was the TCL core from experiment #185 and was treated with chemical treatment 5, the anionic surfactant L-19446#1 at 155°F. As observed for the sandstone cores, the highest fluorine content was at the inlet of the core and then the fluorine content was significantly less at all of the other points analyzed. The fluorine content ranged from 20 wt% to 5 wt% throughout the core. Only three samples along the core were analyzed, which was not enough to provide a defined profile of fluorine content.

Correlating XPS measured fluorine contents with improvement factors was not possible since the number of analyzed cores was low and the experimental conditions among experiments varied considerably (rock permeability, temperature, PVT ratio and capillary number) and the effect of these differences in experimental conditions on the IF is significant. Nevertheless, Gilani (2010) compared XPS measured fluorine contents of the inlet of treated cores in HPHT gas-condensate and volatile-oil core flood experiments with the improvement factor. He found that there is a positive relationship between the amounts of fluorine measured with the improvement factor.

7.2 HIGH-PERFORMANCE LIQUID CHROMATOGRAPHY FOR SURFACTANT ADSORPTION AND DESORPTION MEASUREMENTS

High-performance liquid chromatography (HPLC) is a commonly used chromatographic technique for analysis of liquid samples. HPLC separates a mixture of compounds into individual components. A detector provides a characteristic signal and retention time for the detected components and by doing this it is possible to identify and quantify them. When surfactants are involved, HPLC is commonly used to trace them and to calculate surfactant adsorption and desorption.

Adsorption of fluorinated surfactants, specifically for the case of FC-X, was studied by Bang (2007). Adsorption of the surfactant was obtained by measuring the

concentration of surfactant in the effluent coming out of the core during injection of chemical treatment. The methods he used to measure surfactant concentration were gravimetric analysis and high-performance liquid chromatography (HPLC). The amount of surfactant adsorbed on the rock surface was determined from the difference between the mass of surfactant injected and the mass produced. Both techniques reported for Berea rocks surfactant adsorption ranging from 3 to 3.5 mg/gr of rock. For treatment concentrations of 2 wt% FC-X, complete adsorption was observed within the first 5 PV; the number of pore volumes for complete adsorption increased for lower surfactant concentrations. He observed that for the amount of surfactant adsorption there is no significant change in improvement factor. No measurement for surfactant desorption were made.

In this work, a preliminary study for the surfactant desorption has been done and for Experiment #224 sample collection of chemical treatment and post-treatment volatile oil effluents was done. These samples were analyzed for surfactant concentration using HPLC. The amount of surfactant desorbed was determined from the difference between the mass of surfactant injected and the cumulative mass traced in the produced volatile oil effluent. The analytical procedure and results are discussed below.

7.2.1 Analytical procedure

For experiment #224 effluent samples for chemical treatment and post-treatment two-phase volatile oil floods were collected for HPLC analysis. Samples were collected with a frequency of 20 minutes for chemical treatment and 80 minutes for volatile oil. This represented a sample every 1.8 and 12.1 pore volumes of fluid injected respectively. The measurements were taken using a Dionex HPLC-UltiMate 3000™ equipped with a Dionex Acclaim® Surfactant column and light-scattering detector (ELSD).

To measure surfactant concentrations in the effluents and in post-treatment volatile oil effluents in order to calculate surfactant adsorption and desorption, a calibration plot for FC-X surfactant was built. Figure 7.8 illustrates the HPLC calibration plot for identification of surfactant FC-X. This plot was built with samples of surfactant FC-X diluted in methanol with a concentration range of 10 to 10,000 ppm. Then, the chemical treatment and volatile oil effluent samples were also pre-diluted in methanol for HPLC analysis. Table 7.2 summarizes the results for HPLC measurements.

7.2.2 Adsorption and desorption of the surfactant

The concentration measured in the chemical treatment effluents is shown in Figure 7.9. After the first 3 pore volumes of chemical treatment, the fluorine concentration was similar to the original concentration. This is in agreement with what had been observed before (Bang 2007) indicating that it is during the first couple of pore volumes of treatment injection that most of the adsorption takes place. Using a mass balance a surfactant adsorption of 2.6 mg-surfactant/gr-rock was calculated from these measurements. This result is similar to the reported adsorption value of 3 mg-surfactant/gr-rock for FC-X and Berea sandstone by Bang (2007). Thus, the mass of surfactant adsorbed was 585 mg.

The mass of surfactant found in the post-treatment volatile oil effluent is shown in Figure 7.10. These values were used to calculate the mass of surfactant desorbed. For sample #1, the desorbed mass was recalculated using the fitted data for the rest of the samples. Cumulative mass versus pore volumes of volatile oil are shown in Figure 7.11. For the last two figures, the increase in surfactant mass of sample # 17 corresponding to accumulator 3, resulted from the time left in between injection of accumulators 2 and 3 which led to a building up of surfactant concentration in the volatile oil left in the core indicating that the rate of desorption is driven by kinetics. This could explain the

observed decline in improvement factor commonly observed in between floods. After injection of about 290 PV of post-treatment volatile oil injection, the amount of surfactant FC-X desorbed from the treated Berea sandstone core was 27 mg which represents approximately 5% of the mass adsorbed initially. The final surfactant concentration in the effluents was approximately 1 ppm.

7.3 COMPUTERIZED AXIAL TOMOGRAPHY FOR FLUID SATURATION MEASUREMENTS

Computerized axial tomography (CT Scan or also CAT Scan) was used to study the effect of wettability alteration using fluorinated chemical treatments on the saturation of oil and gas. Using x-rays to create cross sectional views of a analyzed structure, CT Scan has proved its effectiveness for measuring oil, gas and water saturations along porous structures such as cores or sandpacks (Vizika and Lombard 1996; Sahni et al. 1998; DiCarlo et al. 2000; Dehghanpour et al. 2010).

In this work, a modified medical CT scanner manufactured by Universal System model HD-350E, was used to measure oil and gas saturations during pre and post-treatment two-phase volatile oil floods as well as residual oil and gas saturations. Experiment #231, #234 and #235 were the core flood experiments for which CT Scan was performed. For them, an aluminum core holder wrapped with carbon fiber was used and they followed the general core flood experimental procedure described in Section 3.2. No initial water saturation was used to avoid having three-phase saturations. Table 7.3 shows the experimental conditions. Pre and post-treatment two-phase volatile oil floods were performed at 75°F and chemical treatment at 155°F. Chemical treatment 1 (2 wt% FC-X) was used. PVT ratio was of about 0.7, capillary number was approximately $1.2E-5$ and the observed improvement factor was 3.4 for experiment #231, 2.1 for experiment #234 and 1.7 for experiment #235. Table 7.4 summarizes the results and Appendix A.22, A.23 and A.24 respectively describe each of the experiments.

The high pressure and temperatures used in this type of core flood experiment did not allowed the performance of the floods in the CT Scan set up therefore the core had to be moved back and forth from core flood set up to the CT Scan facility.

7.3.1 Analytical procedure and calculations

For the two-phase oil-gas system, the single energy technique (Sharma et al. 1997) was used to calculate the saturations. According to this technique, for each voxel of the sample the following equation can be used to describe the X-ray attenuation due to the combined effect of oil, gas and rock matrix.

$$CT_g S_g + CT_o S_o = CT_{go} \quad (7.1)$$

Where CT_g is the CT number of 100% gas saturated core, CT_o is the CT number of 100% oil saturated core, CT_{go} is the CT number of two-phase fluid saturated core, S_g is the gas saturation and S_o is the oil saturation.

Since $S_g + S_o = 1$ then oil saturation can be calculated as follows

$$S_o = \frac{CT_{go} - CT_g}{CT_o - CT_g} \quad (7.2)$$

Thus, for two-phase saturation measurements for the HTHP core flood experiments, two calibration scans were required for both gas and oil. The dry core was flooded with a gas phase and then scanned to produce a gas calibration. For the oil calibration, vacuum was induced to remove the gas and then the core was flooded with 5 PV of an oil phase assuming complete saturation of the pores. Table 7.5 shows the compositions for saturated gas and oil phases used at the experimental temperature and pressure.

After obtaining the calibration scans, the core was then cleaned of oil by flooding 5 PV of toluene, followed by 5 PV of a mixture of toluene-methanol (50/50), followed by

5PV of methanol and then dried with pressurized air overnight. Once the core was clean and dry, the core flood proceeded as usual.

Before and after chemical treatment, the two-phase saturation measurements were taken by performing the usual two-phase volatile oil flood and after reaching pseudo-state the flood was stopped and the core was immediately scanned.

After a two-phase volatile oil flood and for measurement of oil residual saturation, the core was accordingly flooded with several pore volumes of single-phase gas until pseudo steady state was reached. The flood was then stopped and the core was scanned. Then a similar procedure was used to measure residual gas saturation flooding the core with single-phase oil. Oil and gas residual saturation were measured before and after treatment.

Once the core flood experiment was finished, the core was again cleaned and dried following the procedure described above. Then it was saturated with gas and scanned for final gas saturation. The final gas saturation helped to confirm the effectiveness of the cleaning process to remove oil.

The CT scans images were taken perpendicular to the length of the core, for consecutive slices with a thickness of 5 mm (index), and using an energy level of 130 kV. Each image contains 512 by 512 CT attenuation number representing the density of material inside a voxel of 0.23 mm \times 0.23 mm \times 5 mm (that is the index). Every image was processed using MATLAB by first selecting the CT numbers corresponding to the core voxels and then calculating their average. Average CT numbers were used because the core was moved back and forth from the core flood set up to CT Scan facility changing the voxel positions between scans. Average CT numbers were independent of possible core rotation only taking into account the scanning position of the axes parallel to the length of the core.

7.3.2 Oil and gas saturations

For experiment #231, the calculated oil saturation before and after treatment is shown in Figure 7.12. Before treatment the oil saturation was about 59% and it was rather constant throughout the core. After treatment no IF was observed and the oil saturation was the same. After the chemical treatment flood, dry nitrogen was used to flush the treatment left in the core and in the lines. This could have been the reason why no IF was observed but it is not well understood why. Thus, the core was retreated and three floods of two-phase volatile oil followed; no nitrogen flush was used this time. Figure 7.13 show the results. After the second treatment, the oil saturation increased to about 73% where the calculated IF was 3.4. Oil saturation decreased for every flood as well as the improvement factor, and by the third flood no improvement factor was observed and S_o was the same as before treatment. The higher oil saturation and consequent lower gas saturation after chemical treatment indicates that treatment does mitigate “gas blocking”, allowing the oil to flow more easily but in particular the gas. In other words, the residual gas saturation drops. The higher oil and gas mobility led to pressure drop reduction, reduction of gas saturation (the non-wetting phase), increase of oil saturation (the wetting phase) and the consequent increase of oil and gas relative permeability. The residual oil saturation was also measured. Oil phase was taken to residual by flooding the core with gas (saturated) after the two-phase volatile oil flood. The results are shown in Figure 7.14. The residual oil saturation was about 20% and no significant change was observed before and after first and second chemical treatments. For the first inch of the core it was observed that the gas flood stripped out the oil. The injected gas had not been equilibrated with the oil and thus apparently was not fully saturated with the heavier components in the oil. Also, for the last inch of the core the oil saturation slightly increased because of capillary end effects which are inherent to this

type of experiment. The near zero oil saturation after core cleaning and drying the core indicated the complete removal of the oil and the effectiveness of the procedure.

For experiment #234 similar results were observed as for experiment #231. However, for this experiment the flow rate for the injection of the volatile oil was not kept constant before and after treatment, instead pressure drop was kept constant by adjusting the flow rate of injection. The injection flow rate for single-phase volatile oil (this is before BPR-1 or flashing) went from 485 cc/hr before treatment to 1,011 cc/hr after treatment. Figure 7.15 shows the results for pre and post-treatment oil saturations along the length of the core. For this experiment the core was treated only once and no nitrogen flush was used. The pre-treatment oil saturation was approximately 56% and the post-treatment approximately 69% with a corresponding IF of 2.1. Figure 7.16 shows the results for residual oil saturation and oil saturation after final core cleaning. S_{or} was about 16% and after final core cleaning S_{or} was zero.

For experiment #235 one more saturation measurement was done; residual gas saturation. Saturations were measured in the following order: two-phase volatile oil saturation followed by residual oil saturation followed by residual gas saturation. For pre and post-treatment two-phase volatile oil saturation the results are shown in Figure 7.17. The pre-treatment oil saturation was of about 57% and the post-treatment oil saturation was about 66% with a corresponding IF of 1.7. The results for residual oil saturation and oil saturation after final core cleaning are shown in Figure 7.18. S_{or} was about 19% and the oil saturation after cleaning the core was zero. The residual gas saturation results are shown in Figure 7.19. For the first 3 inches of the core the gas saturation did not exceed 2% and then the gas saturation increased significantly. Such an increase may be due to incomplete gas displacement or simply phase separation of the saturated oil used to displace the gas due to pressure drop towards the outlet of the core. Before treatment gas

saturation increased up to 36% towards the outlet of the core but after treatment it only increased up to 10%.

7.3.3 Changes in oil and gas relative permeability

In previous work, the relative permeability was measured as a function of pressure and the fractional flows were known, but the saturations were not known. Now saturations from the CT Scans are available to relate to the measured relative permeability values for experiment #235. Table 7.6 shows the relative permeabilities and saturations. Oil relative permeability at residual oil saturation is by definition zero and similarly at residual gas saturation gas relative permeability is zero. The residual oil saturation and end-point gas relative permeability did not significantly change after treatment. However, the residual gas saturation and oil relative permeability end point did change significantly. The end-point oil relative permeability increased from 0.45 before treatment to 0.81 after treatment. The residual gas saturation used was the average value observed though out the core and went from 10% before treatment to 3.3% after treatment.

The experimental results for relative permeabilities and oil and gas saturations were plotted and fitted with a trend line using the Corey equations:

$$k_{rg} = k_{rg}^o \frac{S_g - S_{gr}}{1 - S_{lr} - S_{gr}}^{n_g} \quad (7.4)$$

$$k_{ro} = k_{ro}^o \frac{1 - S_{lr} - S_g}{1 - S_{lr}}^{n_o} \quad (7.5)$$

where S_{gr} is the residual gas saturation, S_{lr} is the total residual liquid saturation ($S_{lr} = S_{or} + S_{wr}$), k_{rg}^o and k_{ro}^o are the end points of the respective relative permeability curves

for gas and oil at the corresponding end point saturations, and n_o and n_g are exponents for oil and gas, also known as Corey exponents.

The trend lines for oil and gas relative permeability curves before and after treatment are shown in Figure 7.20. Here, $S_{wr} = 0$ and before treatment $n_o = 3.4$ and $n_g = 5.5$ and after treatment $n_o = 5.0$ and $n_g = 3.4$. The results indicate that the effect of fluorinated chemical treatment improves the gas relative permeability for all saturations. However, the oil relative permeability does not change very much except at high oil saturation. For steady state flow of gas and oil, both the gas and oil relative permeability increase after treatment because the PVT ratio (and thus k_{rg}/k_{ro}) must be the same as before treatment. This can happen because the steady state oil saturation after treatment is greater than its value before treatment.

7.4 SUMMARY AND CONCLUSIONS

Three analytical techniques were used to better understand the behavior of fluorinated chemical treatments and their impact on remediating the “gas blocking” problem present in volatile oil reservoirs. These techniques were X-ray photoelectron spectroscopy (XPS), high-performance liquid chromatography (HPLC), and computerized axial tomography (CAT Scan).

XPS analysis was used to measure the fluorine content on eight sandstone cores and one carbonate core from HTHP core flood experiments #141, #148, #176, #189, #224, #225, #228 #229 and #185. Different measurements were done along the length of the cores and the results were compared by type of chemical treatment type, temperature and mass of treatment. For Berea cores treated with non-ionic surfactants L-20294, L-18961 and FC-X a rather uniform fluorine distribution was observed throughout the porous medium of the core and fluorine levels as high as 11 wt% were measured. The

highest levels of fluorine were for cores treated with surfactant L-20294. For a carbonate rock treated with anionic surfactant L-19446#1 the observed fluorine level was 10 wt%.

HPLC was used for surfactant adsorption and desorption measurements. The analysis was performed for the chemical treatment effluents and the post-treatment volatile oil effluents of experiment #224. Adsorption and desorption of the surfactant were studied using the measured surfactant concentrations in the effluents, then the mass of surfactant adsorbed and desorbed were calculated. For a Berea sandstone core treated with surfactant FC-X a adsorption value of 2.6 mg-surfactant/gr-rock was calculated. It was observed that complete adsorption happened within the first couple pore volumes of treatment injected and final concentrations of desorbed surfactant as low as 1 ppm were measured.

CT Scanning was used for gas and oil saturation measurements in core flood experiments. For Berea sandstone cores treated with surfactant FC-X the oil saturation increased from about 55% before treatment to about 70% after treatment. The residual oil saturation did not exhibit significant change but the residual gas saturation did change significantly. Using the data for oil and gas saturations as well as relative permeabilities calculated for flood experiments, relative permeability curves were matched to the experimental data.

Some conclusions for this chapter are:

- XPS, HPLC and CT Scanning proved to be adequate techniques providing a more robust analysis of the results obtained with HTHP core flood experiments.
- Different fluorinated C₄ surfactants exhibit similar low fluorine levels throughout treated Berea sandstones.

- The adsorption of the fluorinated surfactants is rather fast and happens within the first couple of pore volumes of chemical treatment.
- The desorption of surfactant FC-X from Berea sandstone cores is rather low and concentrations in the order of 10 ppm or less are to be expected in volatile oil effluents.
- The low amounts of final desorption indicates that the final improvement factor observed in the HTHP core flood experiments should be a good approximation of the steady IF value.
- For two-phase flow (oil and gas), fluorinated chemical treatments lead to lower gas saturations.
- Fluorinated chemical treatments increase the gas relative permeability for all oil saturations and increase the oil relative permeability only for high oil saturations ($S_o > 75\%$).

Table 7.1 XPS Fluorine content analysis along the core for core flood experiments

<i>Distance from the core's inlet, in</i>	<i>Fluorine content, wt%</i>								
	L-20294		L-18961		FC-X				L-19446#1
	Experiment #		Experiment #		Experiment #				Experiment #
	141	148	176**	189	224	225***	228***	229***	185****
0	12.97	20.56	33.12	*	7.21	10.57	4.24	14.9	19.54
0.25	*	*	*	3.68	2.02	2.01	1.63	0.48	*
2	*	*	*	*	1.79	1.99	0.72	0.52	*
4	11	7.06	4.94	1.95	2.54	1.98	1.11	0.5	9.93
6	*	*	*	*	2.35	1.78	1.05	0.98	*
7.75	4.63	4.22	4.17	1.58	1.87	1.96	2.24	1.12	4.68
8	*	*	*	*	1.84	4.15	2.23	3.08	*
<i>Avg F% without ends</i>	7.82	5.64	4.56	2.40	2.11	1.94	1.35	0.72	11.38
<i>Temp °F</i>	155	155	155	250	155	155	215	275	155
<i>IF</i>	1.7	2.5	3.5	2.6	2.2	2.6	2.6	3.5	1.8

* Data not available

** Core treated three times

*** Case 2 for flood direction

**** TCL core

Table 7.2 HPLC Measurements

Calibration Plot Sample #	Raw Area mAU-min	Surfactant Concentration ppm
0.001% Surfactant	0.234	10
0.01% Surfactant	1.040	100
0.05% Surfactant	8.588	500
0.1% Surfactant	28.085	1001
0.2% Surfactant	76.415	2004
0.3% Surfactant	131.330	3009
0.4% Surfactant	206.203	4016
0.5% Surfactant	276.147	5025
1.0% Surfactant	739.859	10101

Table 7.2 continuation...

Chem. Treat. Effluent Sample #	Dilution Factor	Raw Area mAU-min	Surfactant concentration ppm
1	3	132.194	8654
2	3	376.258	19304
3	3	387.906	19747
4	3	370.404	19080
5	3	379.736	19437
6	3	351.448	18342
7	3	440.561	21672
8	3	363.914	18829
9	3	366.518	18930
10	3	468.755	22652
11	3	480.669	23056
Volatile Oil Effluent Sample #	Dilution Factor	Raw Area mAU-min	Surfactant concentration ppm
1	3.00	213.063	12474
2	0.4	5.787	144
3	0.4	2.599	69
4	0.4	3.173	83
5	0.4	2.395	63
6	0.4	6.386	157
7	0.4	0.843	23
8	0.4	1.603	43
9	0.4	1.017	28
10	0.4	1.731	46
11	0.4	0.738	20
12	0.4	0.407	11
13	0.4	0.501	14
14	0.4	-0.021	0
15	0.4		
16	0.4	0.146	4
17	0.4	23.475	386
18	0.4		
19	0.4	-0.020	0
20	0.4	0.506	14
21	0.4	0.253	7
22	0.4		
23	0.4		
24	0.4	0.024	1

Table 7.3 Summary of conditions for Experiments #231, #234 and #235

	Exp# 231	Exp# 234	Exp# 235
<i>Rock type</i>	Berea	Berea	Berea
<i>k_g, md</i>	184	186	170
<i>Temperature, °F</i>	155	155	155
<i>Single-Phase Vol. Oil Pressure (BPR-1), psig</i>	3790	3820	3890
<i>Two-Phase Vol. Oil Pressure (BPR-2), psig</i>	850	850	855
<i>Volatile Oil Mixture</i>	1	1	1
<i>Chemical Treatment</i>	1	1	1
<i>Surfactant</i>	FC-X	FC-X	FC-X

Table 7.4 Summary of results for Experiment #231, #234 and #235

	Exp# 231	Exp# 234	Exp# 235
<i>Core pressure, psia</i>	850	850	855
<i>q_{gtot core}, cc/hr</i>	482	485	484
<i>q_g, cc/hr</i>	448	451	449
<i>q_o, cc/hr</i>	35	34	35
<i>PVT Ratio</i>	0.73	0.75	0.73
<i>Viscosity Ratio μ_g/μ_o</i>	0.06	0.06	0.06
<i>Liquid Fraction</i>	7.2%	7.0%	7.2%
<i>Capillary Nc</i>	1.17E-05	1.21E-05	1.25E-05
<i>k_{rg} Before Treatment</i>	0.030	0.029	0.028
<i>k_{ro} Before Treatment</i>	0.041	0.038	0.038
<i>k_{rg} After Treatment</i>	0.101*	0.059	0.046
<i>k_{ro} After Treatment</i>	0.137*	0.079	0.063
<i>Initial Improvement Factor</i>	3.4*	2.1	1.7
<i>PV of Vol Oil Injected</i>	~ 300	~ 290	~ 190

* Results for 2nd chemical treatment

Table 7.5 Gas and oil phase composition for volatile oil mixture 1 at 75°F and 850 psia

	<i>Total</i>	<i>Gas Phase</i>	<i>Oil Phase</i>
	<i>Mole %</i>		
Methane (C ₁)	78	90.5	25.3
Propane (C ₃)	13	9.2	28.9
n-Heptane (nC ₇)	6	0.2	30.2
n-Decane (nC ₁₀)	3	0.0	15.6

Table 7.6 Saturations and relative permeabilities for Experiment # 235

Before Treatment		
S _o	K _{ro}	K _{rg}
16.3%	0.000	0.980
56.0%	0.038	0.028
99.0%	0.450	0.000
After Treatment		
S _o	K _{ro}	K _{rg}
19.0%	0.000	0.980
66.4%	0.063	0.046
99.1%	0.810	0.000

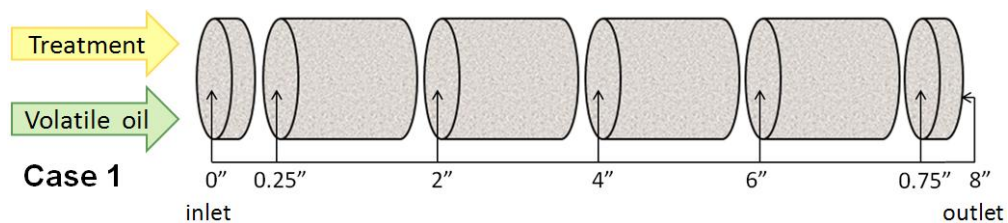


Figure 7.1 Core cuts for XPS analysis & direction of flood performance for case 1

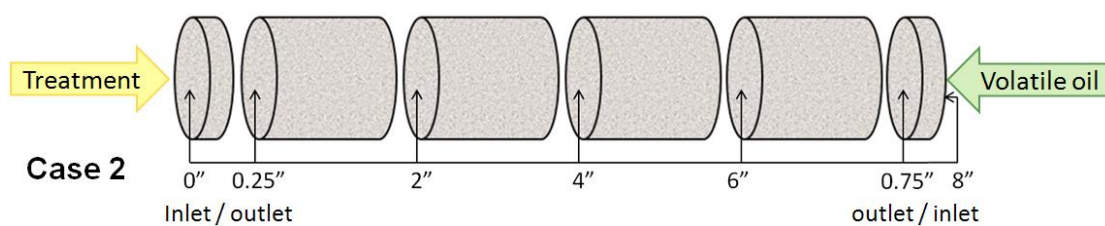


Figure 7.2 Core cuts for XPS analysis & direction of flood performance for case 2

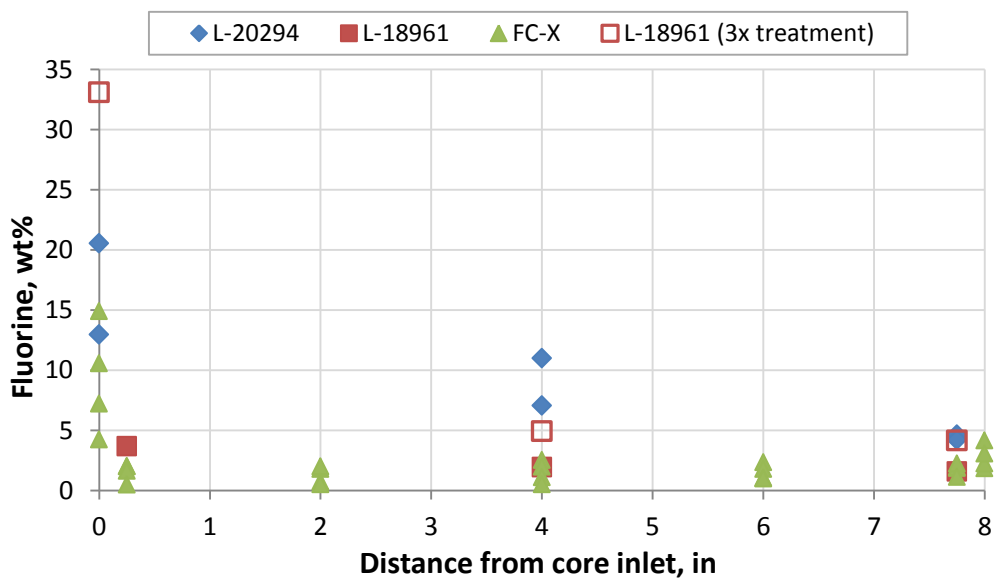


Figure 7.3 Fluorine content along Berea sandstone cores treated with different chemical treatments and experimental conditions

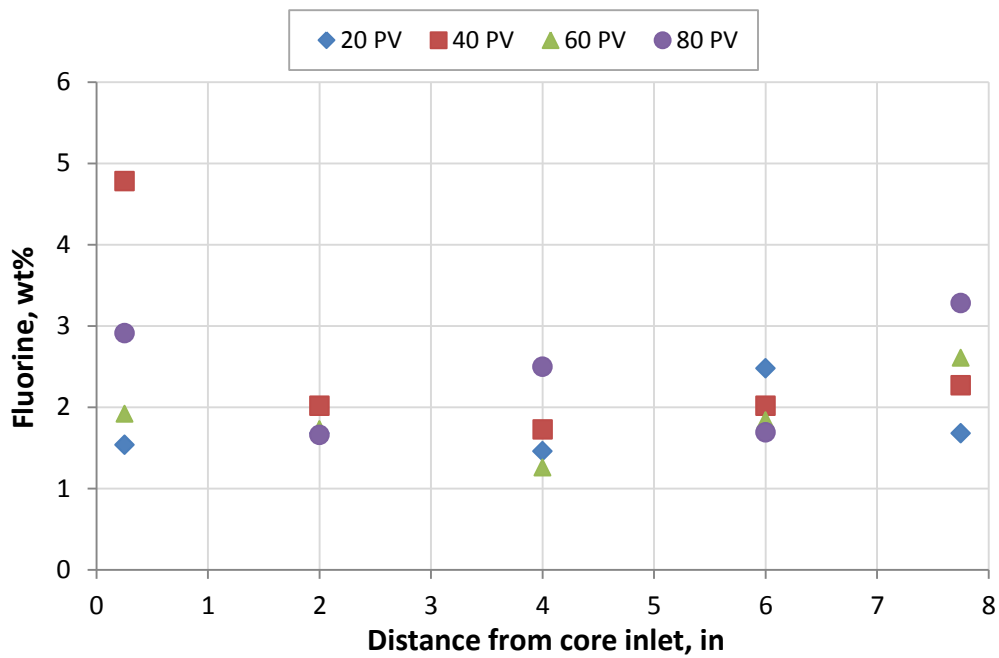


Figure 7.4 Fluorine content along Bera sandstone cores treated with different amounts of chemical treatment 1 (2 wt% FC-X) at 155°F temp (Exp #226)

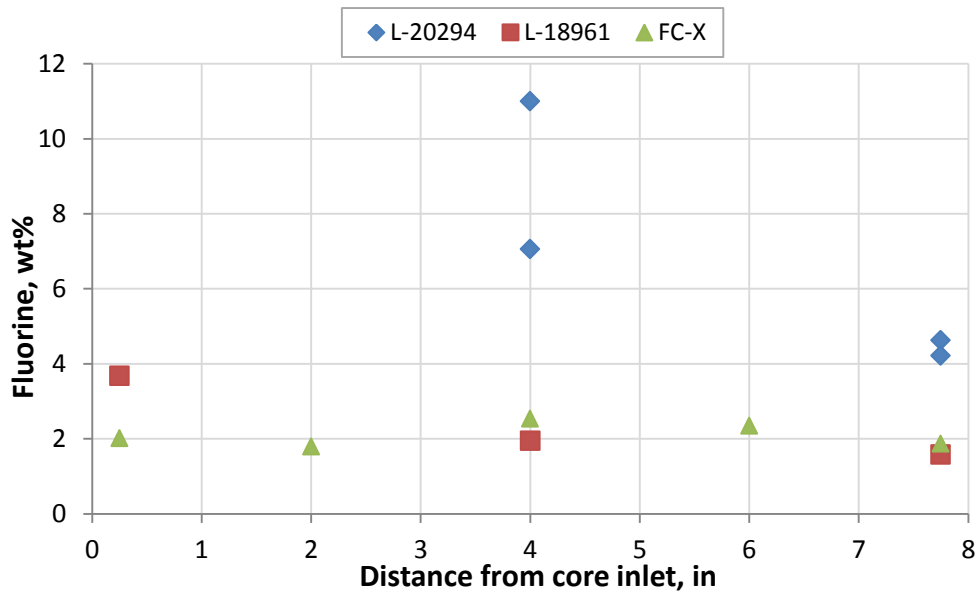


Figure 7.5 Fluorine content along Bera sandstone cores treated with different chemical treatments at 155°F and case 1 for flood direction (Exp #141, #148, #189 & #224)

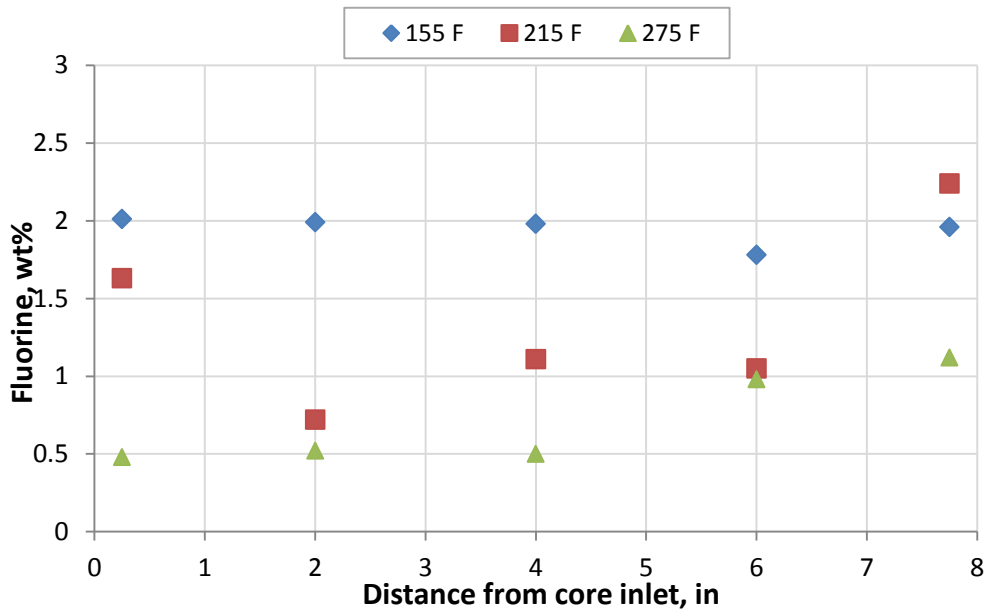


Figure 7.6 Fluorine content along Berea sandstone cores treated w/ chemical treatment 1 (2 wt% FC-X) at different temp and case 2 for flood direction (Exp #225, #228 & #229)

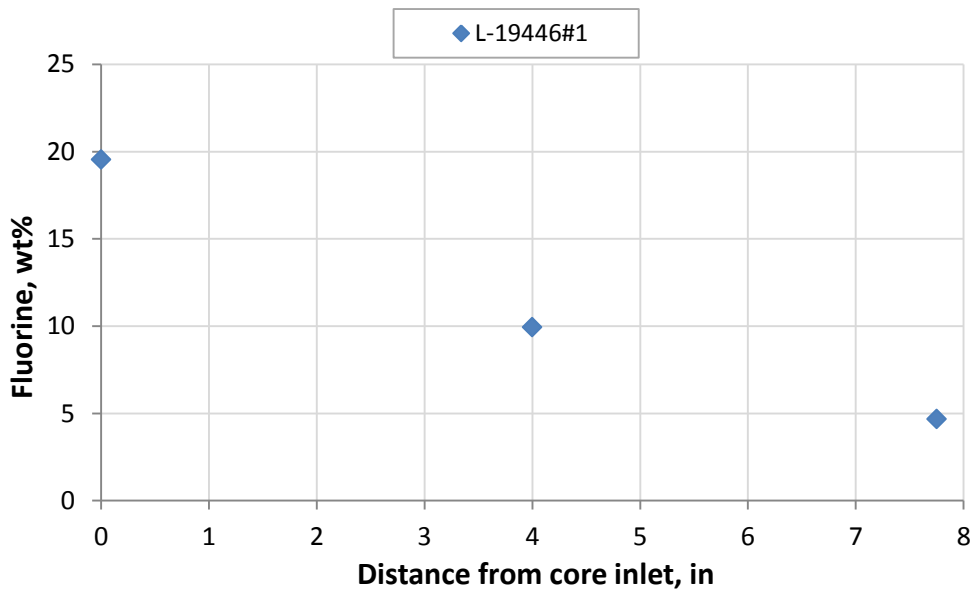


Figure 7.7 Fluorine content a along TCL core treated with chemical treatment 5 (2 wt% L-19446#1) at 155°F and case 2 for flood direction (Exp #185)

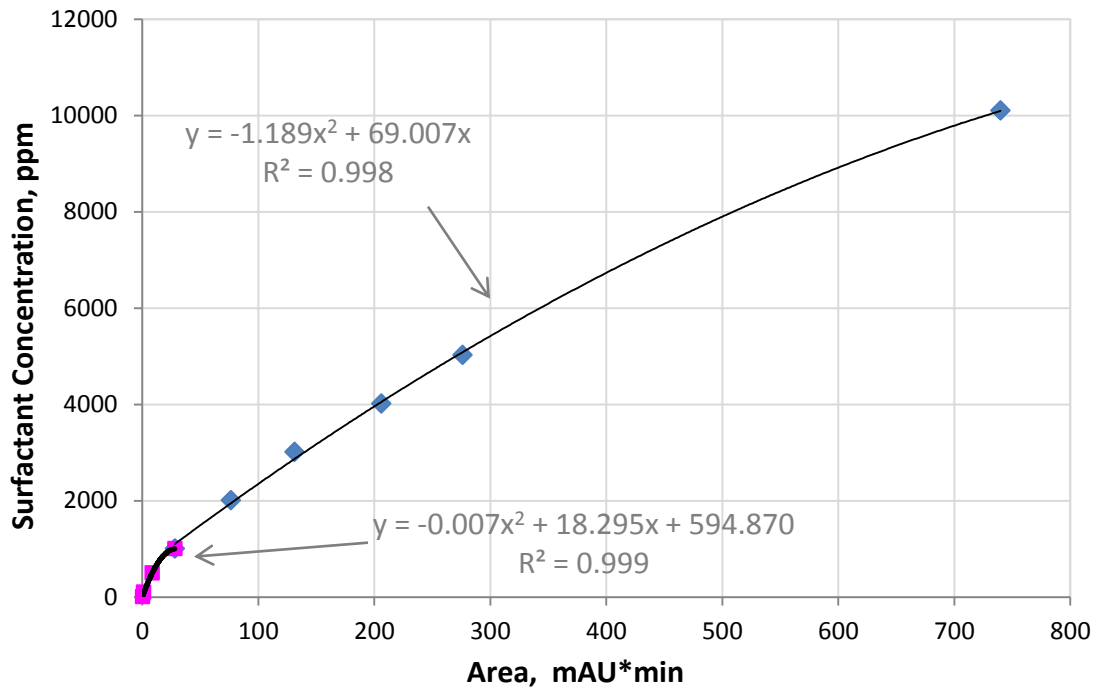


Figure 7.8 HPLC calibration curve for surfactant concentration

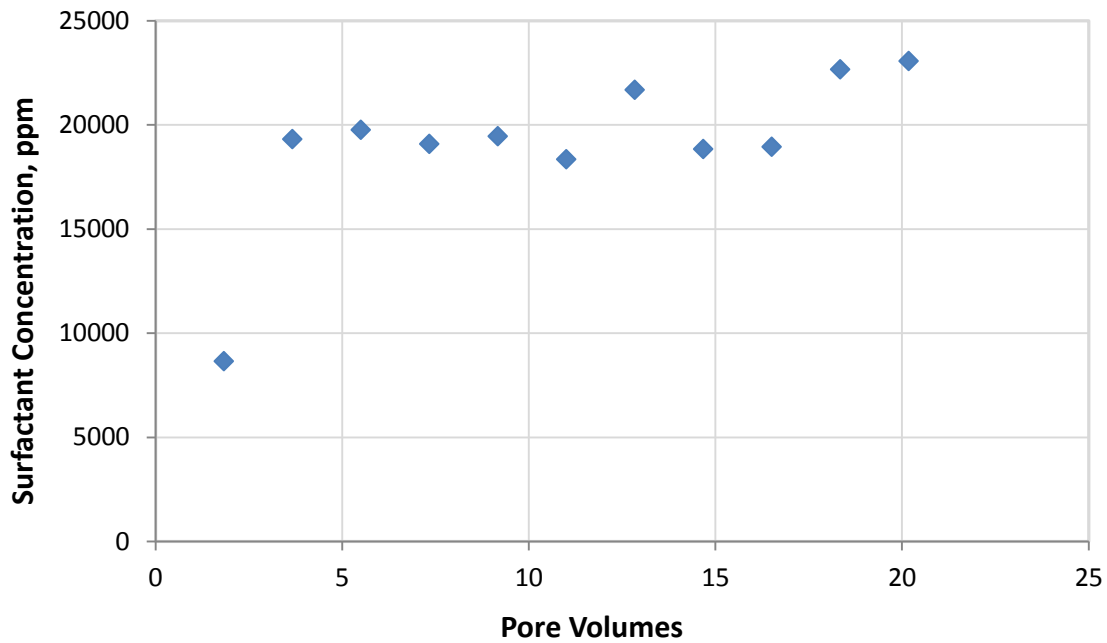


Figure 7.9 Surfactant concentration in chemical treatment effluent (Experiment # 224)

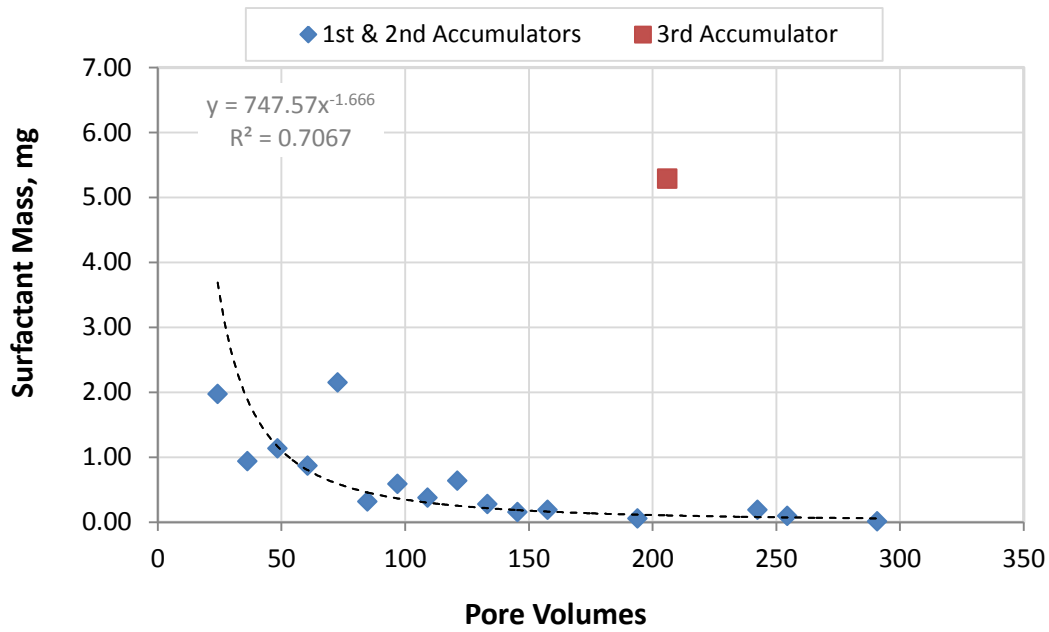


Figure 7.10 Surfactant mass in post-treatment volatile oil effluent (Experiment # 224)

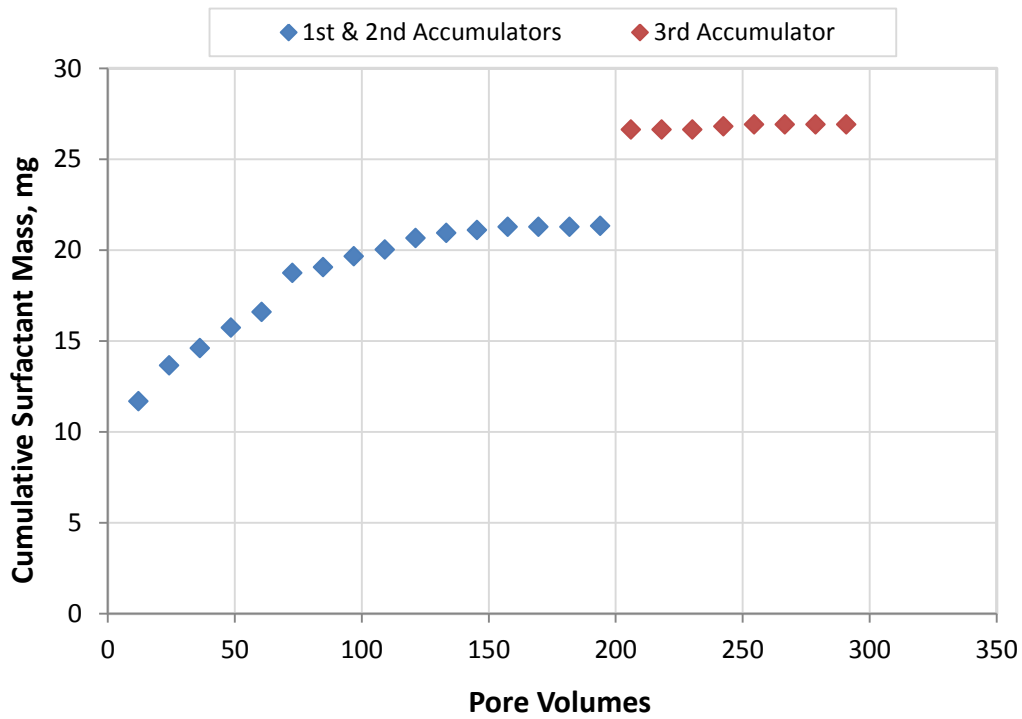


Figure 7.11 Cumulative surfactant mass in post-treatment volatile oil effluent (Experiment #224)

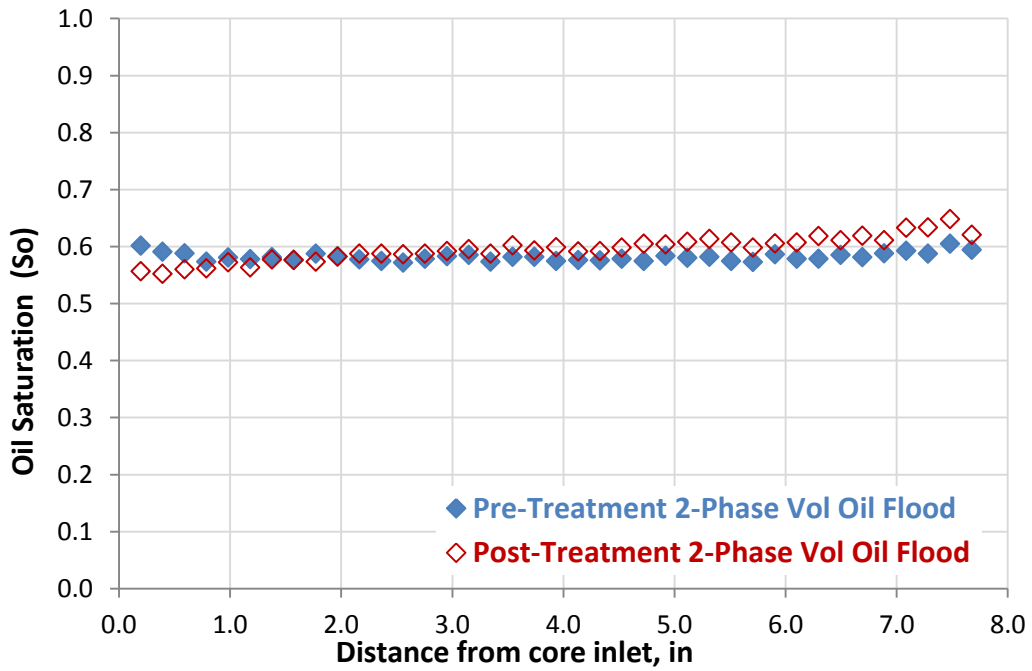


Figure 7.12 Oil saturation (S_o) profile before and after treatment (Experiment #231)

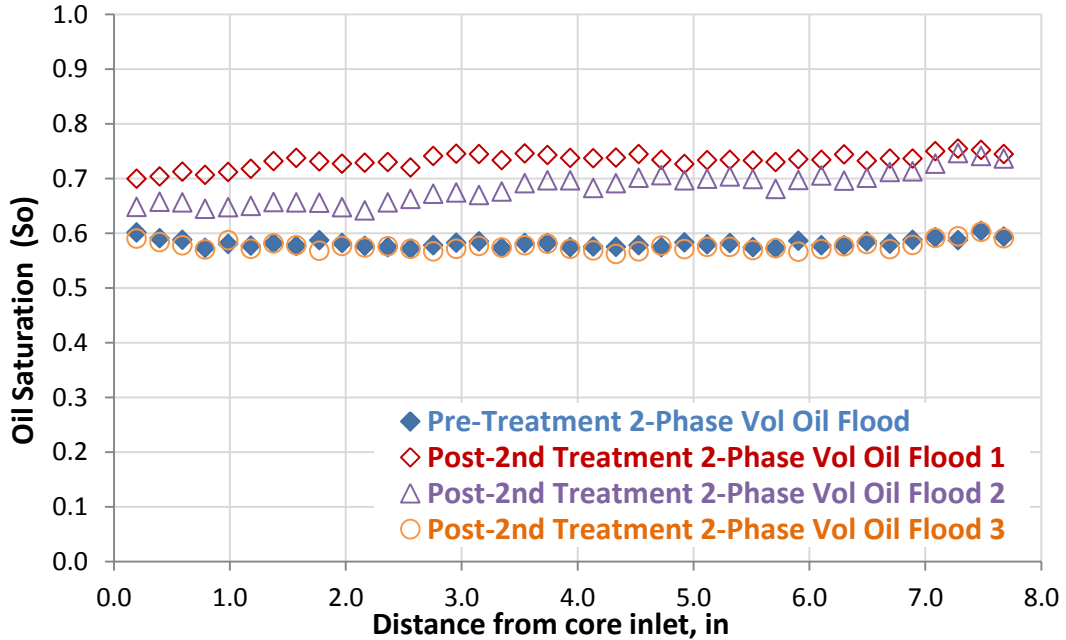


Figure 7.13 Oil saturation (S_o) profile before and after 2nd treatment (Experiment #231)

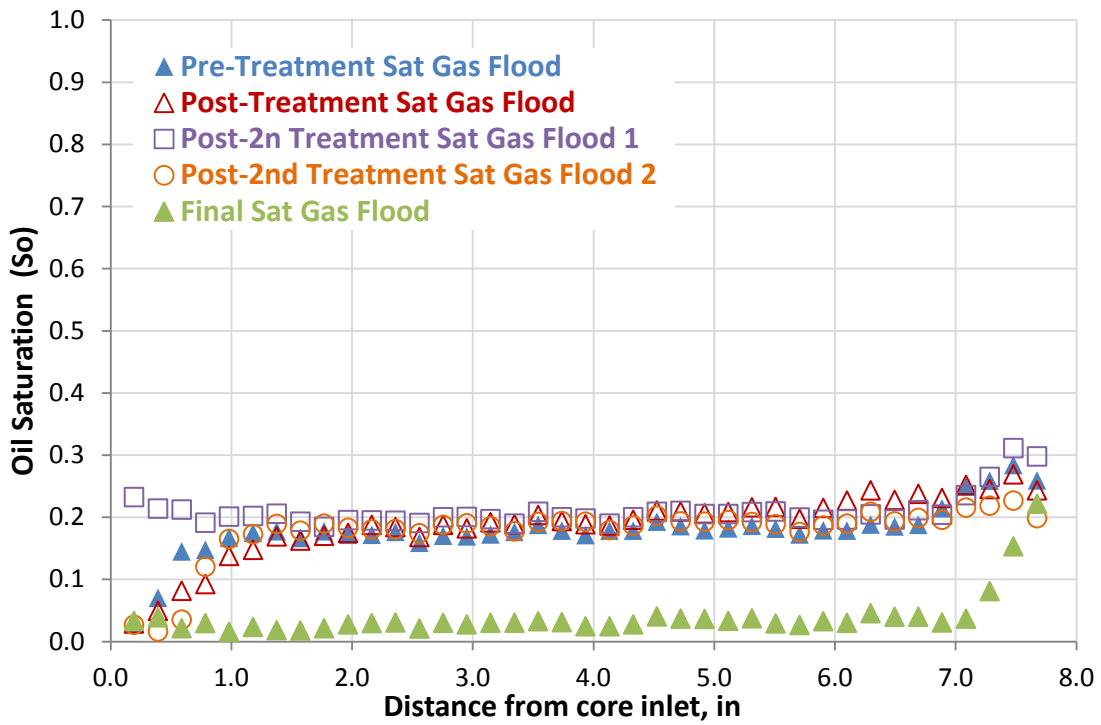


Figure 7.14 Residual oil saturation (S_{or}) profile before and after 1st & 2nd treatment (Experiment #231)

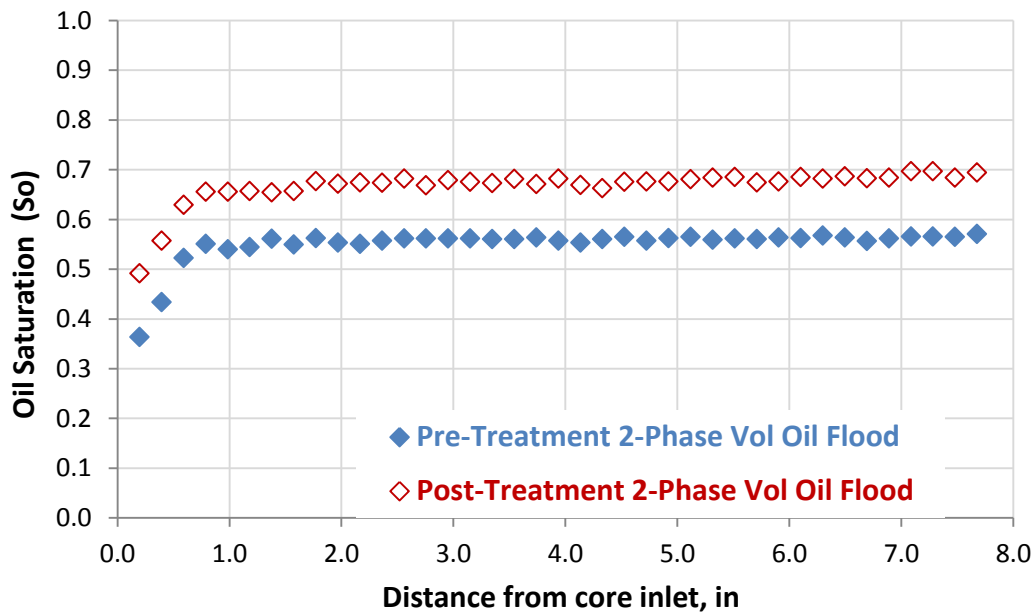


Figure 7.15 Oil saturation (S_o) profile before and after treatment (Experiment #234)

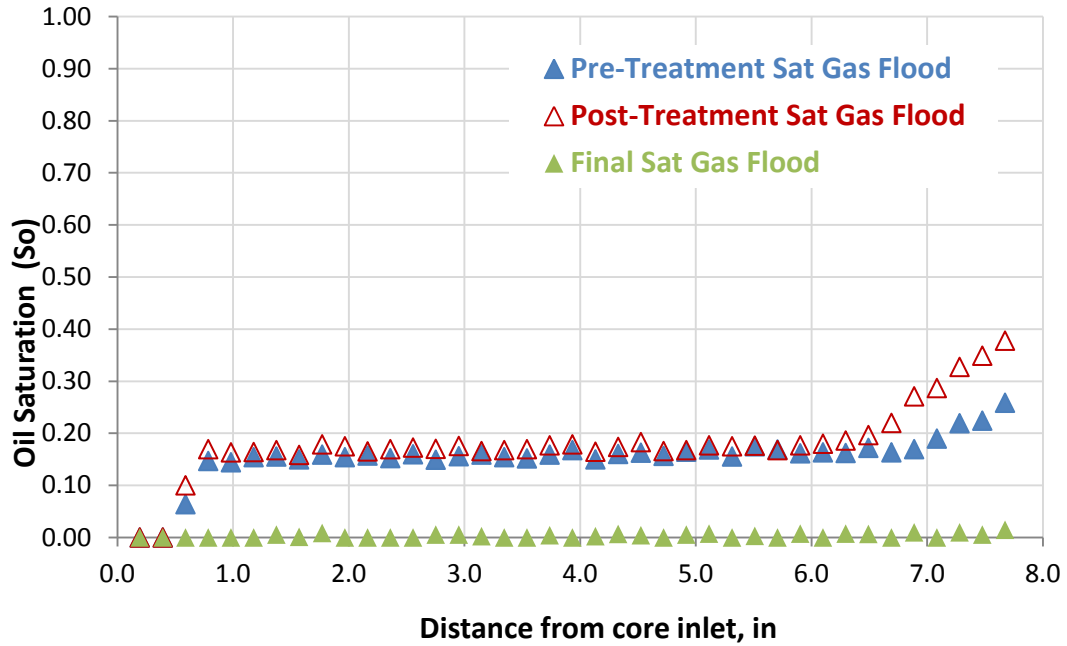


Figure 7.16 Residual oil saturation (S_{or}) profile before and after treatment (Exp #234)

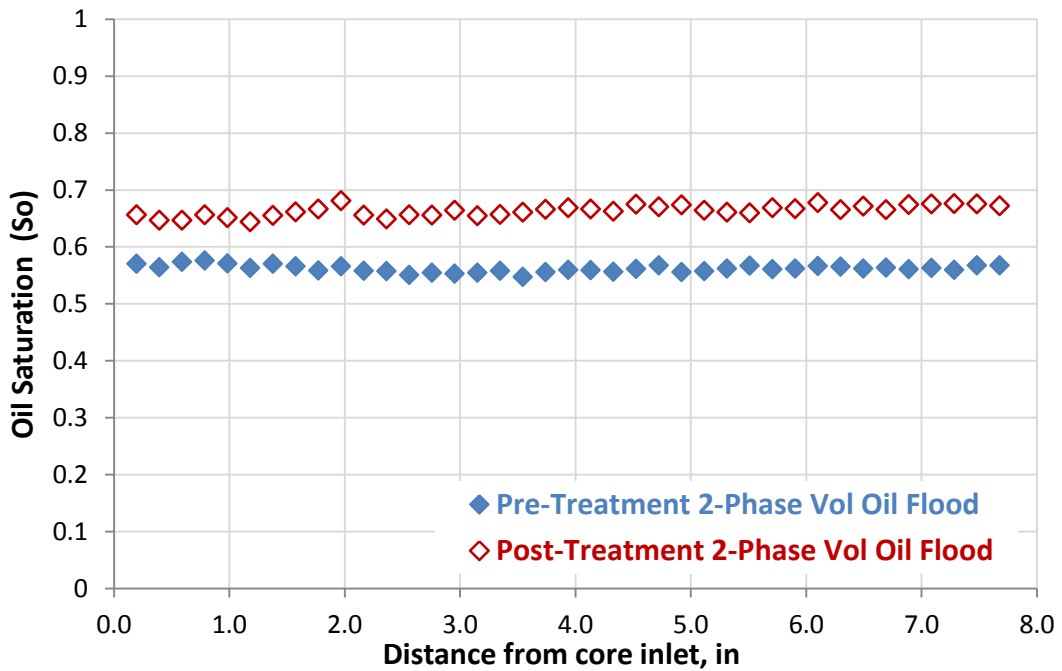


Figure 7.17 Oil saturation (S_o) profile before and after treatment (Experiment #235)

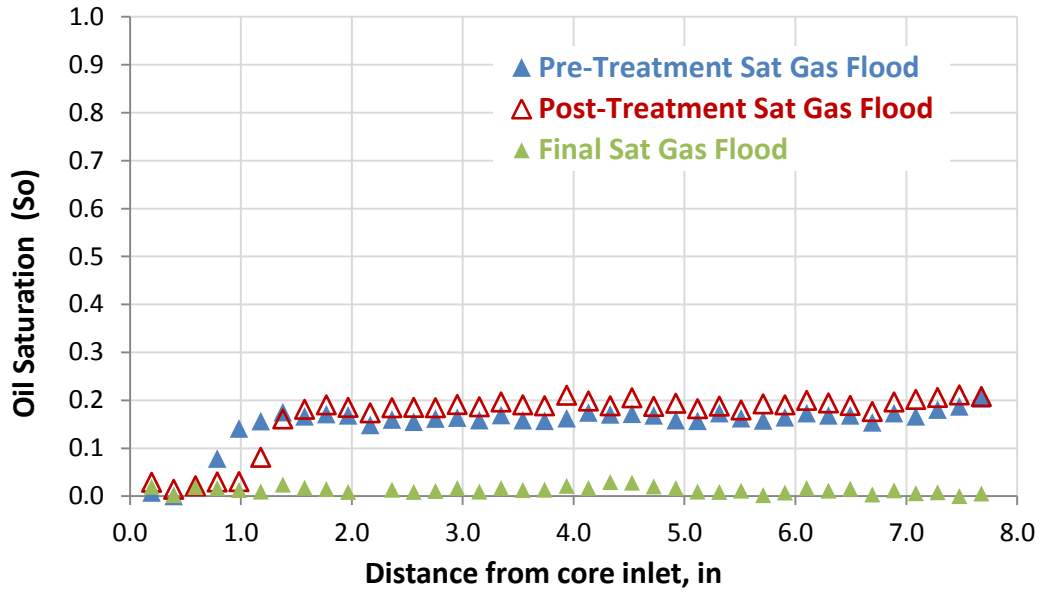


Figure 7.18 Residual oil saturation (S_{or}) profile before and after treatment (Exp #235)

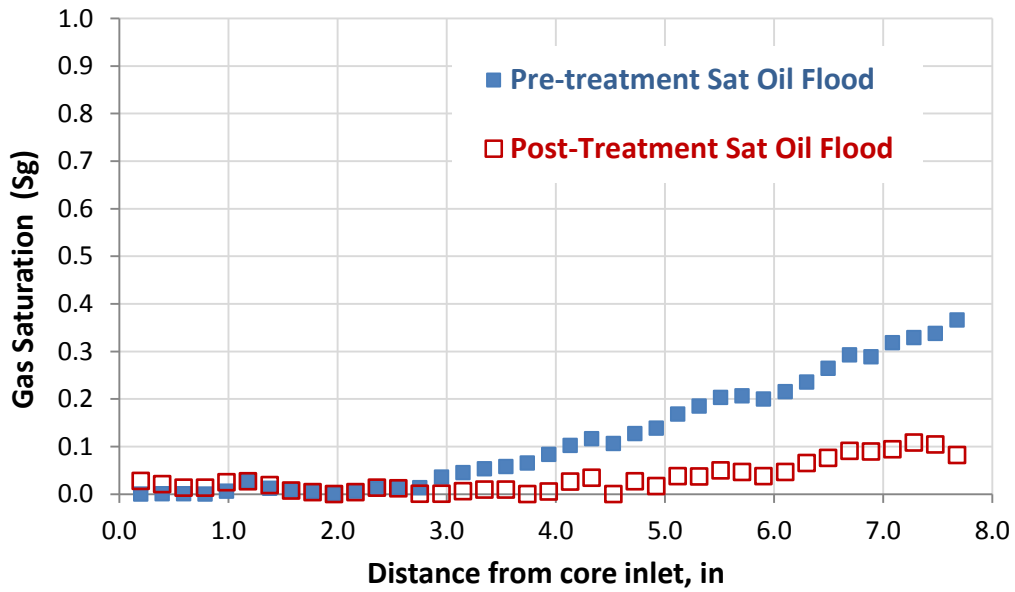


Figure 7.19 Residual gas saturation (S_{gr}) profile before and after treatment (Exp #235)

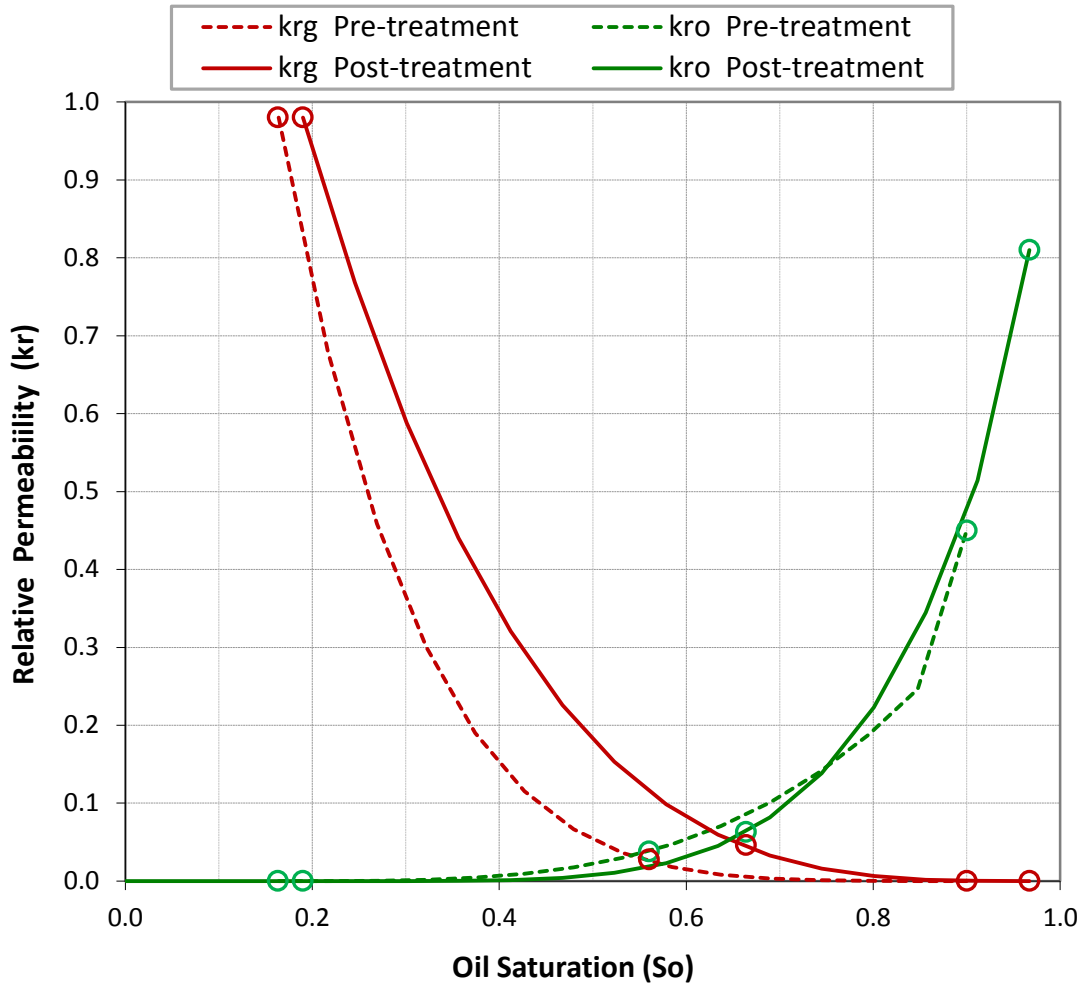


Figure 7.20 Pre and post-treatment oil and gas relative permeability curves

Chapter 8: Numerical Simulations of Volatile Oil Reservoirs Treated with Fluorinated Chemical Treatments

Predicting the productivity of a volatile oil well is a complex problem, especially when the reservoir fluids are undergoing phase changes. The accumulation of gas near the well leads to oil saturation changes that consequently alter relative permeability and capillary pressure. The well performance following chemical treatment is even more complicated to predict since the rock wettability of a treated zone will differ from the untreated zone affecting also relative permeability.

This chapter presents a short preliminary study for the prediction of well deliverability in a volatile oil reservoir treated with fluorinated chemical treatments. The primary goal of this simulation exercise was to demonstrate the benefit of the lab measured increase in gas and oil relative permeability in a typical wellbore geometry. This was done using numerical simulations and relative permeability data obtained from experimentation. Simulations for five different radii of treatment were performed and compared to the base case model in which no treatment was performed and the results for pressure depletion, oil and gas production, and productivity index are discussed below. Appendix B shows the code used.

8.1 STARS RESERVOIR SIMULATOR

Steam, thermal, and advanced processes reservoir simulator (STARS) is a simulator developed by Computer Modeling Group LTD (CMG). STARS is a thermal, k-value compositional, chemical reaction and geomechanics reservoir simulator used for modeling the flow of three-phases, multi-component fluids with the capability of modeling recovery processes involving the injection of steam, solvents, air and chemicals. This simulator was used to simulate effect of fluorinated chemical treatments

on volatile oil wells producing above and below the bubble point pressure because it is capable of simulating the gas and oil phase changes which occur during reservoir depletion.

8.2 RESERVOIR MODEL

The reservoir model consisted of a cylindrical reservoir with a single vertical well located at the center. The drainage radius was set to be 3,743 ft, the reservoir thickness of 100 ft, and the radius of the well 0.708 ft. The grid was cylindrical, and consisted of 53 grid blocks in the radial direction, and one layer in the vertical direction. To better account for the near wellbore fluid behavior refined grids adjacent to the wellbore in the radial direction were used. Table 8.1 shows the length of the grid in the radial direction. The cylindrical reservoir model is shown in Figure 8.1.

The reservoir rock permeability was set at 186 md with a ratio of horizontal to vertical permeability of 10. Porosity was set to 19%. These permeability and porosity values are representative of rock permeabilities reported for the Berea sandstone cores used for the core flood experiments described in previous chapters. Table 8.2 summarizes the reservoir parameters.

8.3 FLUID CHARACTERIZATION

The simulation fluid used in this study was volatile oil mixture 2 the composition was given in table 3.3. CMG's pre-processor for phase behavior calculation WINPROP was used to develop the fluid characteristics and the results were exported to STARS which features k-value tables for the various pressure and temperature of each component. The EOS parameters including critical temperature, critical temperature, critical volume, binary interaction coefficients, viscosity, and acentric factors were tuned in WINPROP for heavier components C_7 and C_{10} . This was done to match the PVT

results previously obtained with PVT Sim for volatile oil mixture 2 using PR78-Peneloux EOS. Table 8.3 shows the parameters used. Figure 8.2 shows the P-T diagram and Figure 8.3 the liquid volume percentage and the generated gas for different pressures for a constant volume depletion process (CVD) calculated with WINPROP.

8.4 ROCK-FLUID PROPERTIES MODEL

The relative permeability model used was based on the relative permeability curves obtained in Section 7.3.3. Where using the saturation exponent method, oil and gas relative permeability curves were fitted to experimentally measured oil and gas relative permeabilities and saturations. The model includes the oil and gas relative permeability curves for non-treated and treated rock shown in Figure 7.21. These curves correspond to a Berea sandstone rock flooded with volatile oil mixture 1 (Table 3.3) at 75°F and treated with chemical treatment 1 (2 wt% FC-X) at 155°F. It was assumed that for volatile oil mixture 2 at 155°F, which are used in the simulations, the relative permeability curves would apply.

8.5 INITIALIZATION

The initial condition for reservoir pressure was 4000 psi which is above the bubble point pressure (3550 psi) of the volatile oil mixture used. The reservoir temperature was assumed to be constant at 155°F. A near zero initial water saturation of 0.1% was used since the relative permeability curves were made from experimental data where no connate water was present. The initial oil saturation was assumed to be 99.89%. The initialization parameters are summarized in Table 8.4.

Five cases using different radii of treated zone and one base case without a treated zone were simulated. For the treated zone, near wellbore, different rock-fluid properties (relative permeabilities) were set, however all other reservoir properties were the same

for the treated and non-treated zones. The five radii used for the treated zone were 5, 10, 20, 30 and 55 feet. The injection chemical treatment process was not simulated.

8.6 SIMULATION RESULTS

The results for the simulations of a base case model and five cases of treated zones are discussed below.

8.6.1 Base case model

The base case model represented the original behavior for the depletion reservoir model. A near wellbore zone treated with fluorinated chemical treatment was not used. The simulation was run under a constant oil production of 1000 bbl/day and was simulated for a 60 year period (2000-2060). The simulation results for well-bottom hole, reservoir pressure at the boundary and oil and gas production rates are shown in Figure 8.1. For the first five years of production, the well bottom-hole pressure decreased linearly and after reaching the bubble point pressure of 3650 psi the pressure decline was damped by the produced gas phase. For about fifty years the oil production remained constant. The initial gas production was 3.2 MMscf/bbl for near thirty years exponentially increasing after that.

The well deliverability was expressed using the productivity index (PI) which shows the ability of the reservoir to deliver fluids to the wellbore. The PI was calculated as follows,

$$PI = \frac{q_o}{P_e - P_{wf}} \quad (8.1)$$

Where q_o is the oil production rate at standard conditions in bbl/day, P_e is the reservoir pressure at the boundary in psi, and P_{wf} is the well bottom-hole pressure in psi. This definition of PI is different from the typical one as the boundary pressure was used in the place of the average reservoir pressure.

The PI profile calculated for the base case is shown in Figure 8.5. The effect of “gas blocking” on PI was clearly observed after the fifth year of production when the PI decreased from approximately 24 bbl/day/psi to less than 10 bbl/day/psi in about six months.

8.6.2 Effect of the treated near wellbore zone volume

For the five cases with different treatment volumes corresponding to treated radii of 5, 10, 20, 30 and 55 feet the results from the simulated reservoir depletion were compared with the base case. As mentioned previously, the simulations used the modified oil and gas relative permeability curves obtained from experiment #235 for the treated zone. The calculated improvement factor was 1.7 for this experiment.

The simulation results for the well bottom-hole pressure for each case and the reference case are shown in Figure 8.6. Using chemical treatment, the well bottom-hole pressure remains slightly higher than without chemical treatment for the same cumulative oil production indicating that the pressure drop in the near wellbore region has been reduced. The volume used for the treated zone does not have significant effect on the well bottom-hole pressure.

Figure 8.7 shows how the rate of the produced gas significantly increased as the well bottom-hole pressure decreased when a chemical treatment was used. The volume treated mainly impacted the gas rate. Gas rate increased as much as 10 MMscf/day for the same bottom-hole pressure. The effect of treatment on oil production rate was not studied.

Figure 8.8 shows the cumulative oil produced with respect to well bottom-hole pressure. As mentioned before, the reduced pressure drop resulting from the chemical treatment kept well bottom-hole pressure higher for a longer period of time and, therefore, for well bottom-hole pressures below the bubble point pressure the cumulative

oil production increases. For a given bottom-hole pressure of 3,100 psi an increase of about 800,000 barrels of oil produced was observed for a treated zone with a radius of 55 ft. Similar behavior was observed for the case of cumulative gas produced where for the same well bottom-hole pressure of 3,100 psi the gas produced increased by 2.34 Bscf for the treated zone with radius of 55 ft. The results of cumulative gas are shown in Figure 8.9.

For the case where the treated zone had a radius of 20 ft, the oil saturation profile was compared for different times during reservoir depletion. The results are shown in Figure 8.10. Soon after the bubble point pressure is passed, a gas phase quickly developed in the near wellbore region. The gas saturation significantly changes from the non-treated zone to the treated one. The treated zone exhibited lower gas saturation, resulting in less “gas blocking”, maintaining oil and gas production. The lower gas saturation and therefore higher oil saturation resembles what is observed in core flood experiments when analyzed for oil saturation before and after treatment.

Productivity index profiles for the five treated cases were calculated and compared with the base case. Figure 8.11 shows the results. Higher productivity indexes were observed for all times, before and after passing the bubble point pressure, for the treated cases. This was the result of the drawdown of the pressure drop for the treated cases. The PI increased particularly for the early times of production. The PI increased for higher volumes of treated zone, and for the treated radius of 55 ft, PI increased as much as 10 bbl of oil/day/psi. In Figure 8.12 the PI obtained after seven years of production for all cases is compared with respect to radius of treatment. The most significant increase in PI is observed within 10 feet of the well bore.

8.7 SUMMARY AND CONCLUSIONS

Using the compositional simulator STARS from CMG, the oil and gas production of a single –layer, single-well cylindrical volatile oil reservoir with two zones, a treated near-wellbore zone and a non-treated zone, was simulated for six cases. The treated zone corresponded to a zone treated with fluorinated chemical treatments. The simulation cases were: one base case where the radius of treated zone was zero and five cases with increasing volume of zone treated; 5, 10, 20, 30 and 55 feet of treated radius. The simulations were conducted at a constant oil production of 1000 bbl/day, for a reservoir at 155°F and using modified relative permeabilities for the treated zone.

The results for well bottom-hole pressure, production gas rate, and oil cumulative production were studied and the well productivity index profile for each case was calculated.

The use of fluorinated chemical treatments resulted in lower pressure drawdown near the wellbore, especially after producing below bubble point pressure. This resulted in high well bottom-hole pressures for a longer time. The treatment provided an increase in the gas production rate and for a treated radius of 55ft it produced as much as 10 MMscf/day. Cumulative oil and gas produced increased for similar well bottom-hole pressures. For the treated zone of radius of 55 ft and for the given bottom-hole pressure of 3,100 psi, cumulative oil increased about 800,000 barrels and the gas produced increased by 2.34 Bscf. The PI increased for all times and increased as much as 10 bbl of oil/day/psi. The PI increased was more significant for the area within 10 ft of the treated radius, but the greater treatment volumes resulted in greater PIs.

These preliminary simulations showed the potential of fluorinated chemical treatments if used for treating the near wellbore area of volatile oil reservoirs and their capability for mitigating “gas blocking”. Further simulation studies should be undertaken,

including cases where the chemical treatment is injected once production is below bubble point pressure. Also, injection of the chemical treatment and flow back of the solvents should be simulated. STARS seems to be an adequate simulator for this process because it is able to account for thermal changes caused by the injection of chemical treatment.

Table 8.1 Reservoir grid length in the radial direction

Grid Length, ft										
<i>Layer 1-10</i>	0.35	0.41	0.47	0.54	0.62	0.71	0.81	0.93	1.07	1.23
<i>Layer 11-20</i>	1.42	1.63	1.87	2.15	2.47	2.84	3.26	3.75	4.31	4.95
<i>Layer 21-30</i>	5.69	6.54	7.51	8.63	9.92	11.40	13.10	15.05	17.30	19.87
<i>Layer 31-40</i>	22.84	26.24	30.16	34.65	39.82	45.76	52.58	60.43	69.44	79.79
<i>Layer 41-50</i>	91.69	105.36	121.08	139.13	159.88	183.72	211.12	242.60	278.78	320.35
<i>Layer 51-53</i>	368.12	423.02	486.10							

Table 8.2 Reservoir model parameters

<i>Permeability</i>	186 md
<i>Ratio of horizontal to vertical permeability</i>	10
<i>Porosity</i>	19.04 %
<i>Thickness</i>	100 ft
<i>Reservoir radius</i>	3743 ft
<i>Wellbore radius</i>	0.708 ft

Table 8.3 EOS parameters used in WINPROP

<i>Component</i>	C1	C3	C7	C10
<i>Mole %</i>	75	12	9	4
<i>SG</i>	0.300	0.507	0.727	0.782
<i>T_b, °F</i>	-258.61	-43.69	199.13	330.53
<i>P_c, atm</i>	45.40	41.90	30.97	25.01
<i>V_c, m³/kgmole</i>	0.099	0.203	0.381	0.521
<i>T_c</i>	190.6	369.8	543.2	622.1
<i>MW, gr/mol</i>	16.043	44.097	96.000	134.000
<i>Z_{RA}</i>	28.760	27.630	26.642	25.967
<i>ω_A</i>	0.4572	0.4572	0.4572	0.4572
<i>ω_B</i>	0.0778	0.0778	0.0778	0.0778
<i>P_{chor}</i>	77.0	150.3	278.4	382.9

Table 8.4 Initialization reservoir parameters

<i>Bubble point pressure</i>	3650 psi
<i>Initial pressure</i>	4000 psi
<i>Temperature</i>	155 °F
S_{oi}	99.89%
S_{wi}	0.10%

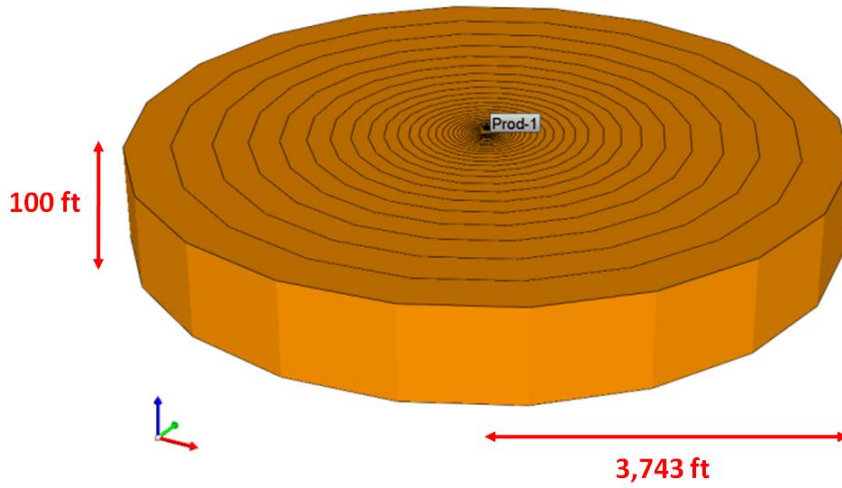


Figure 8.1 Cylindrical reservoir model with refined grids near wellbore

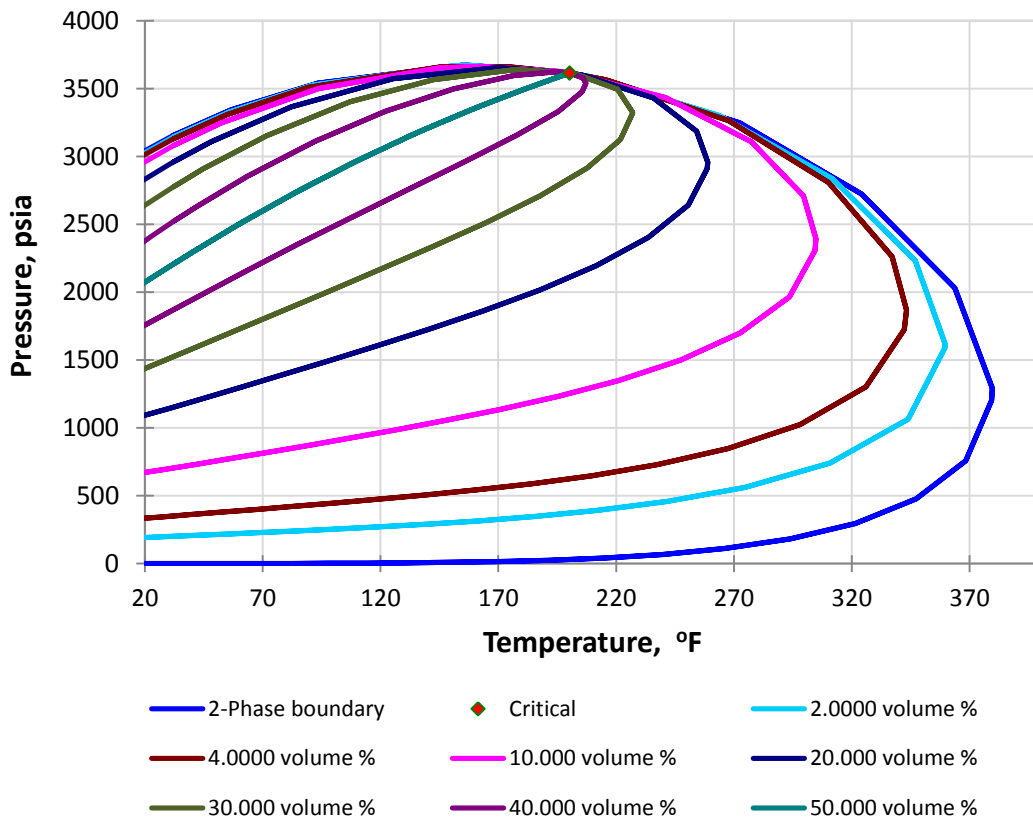


Figure 8.2 P-T diagram for volatile oil mixture 2 generated with WINPROP

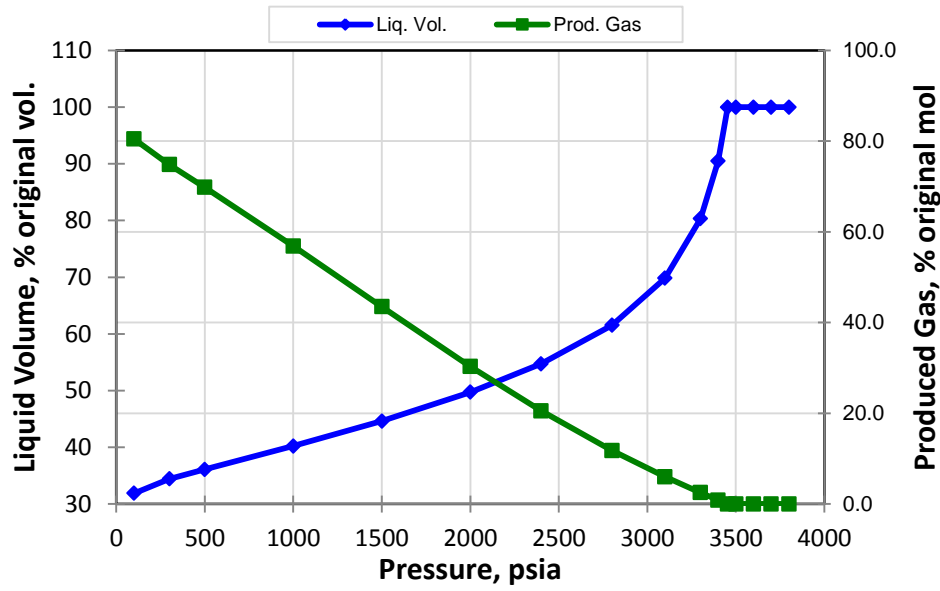


Figure 8.3 Liquid volume and produced gas with respect to pressure- CVD calculations using WINPROP

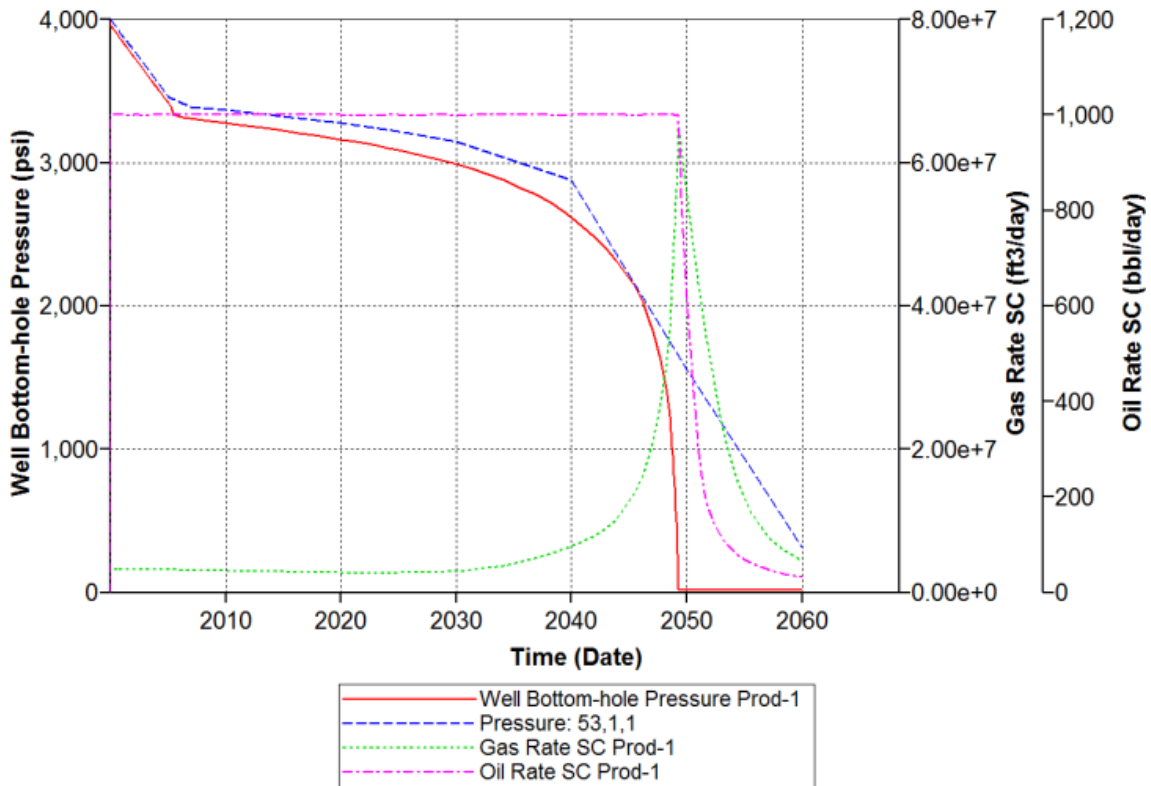


Figure 8.4 Simulation results for the reservoir depletion of the base case

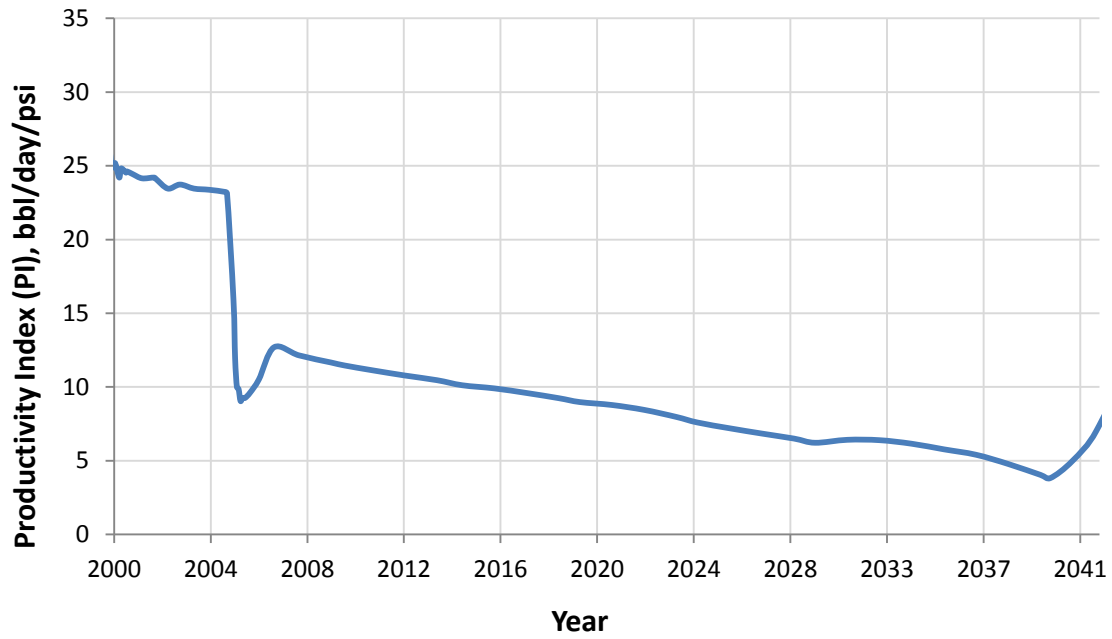


Figure 8.5 Productivity index profile for the base case

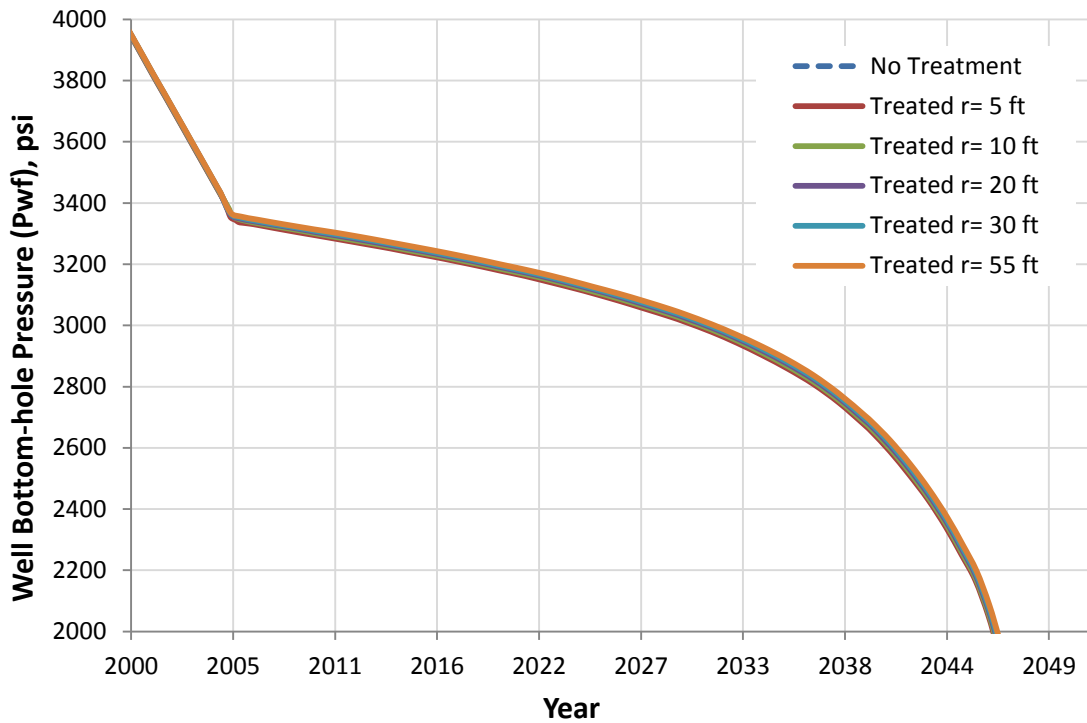


Figure 8.6 Well bottom-hole pressure profile for non-treated and treated cases

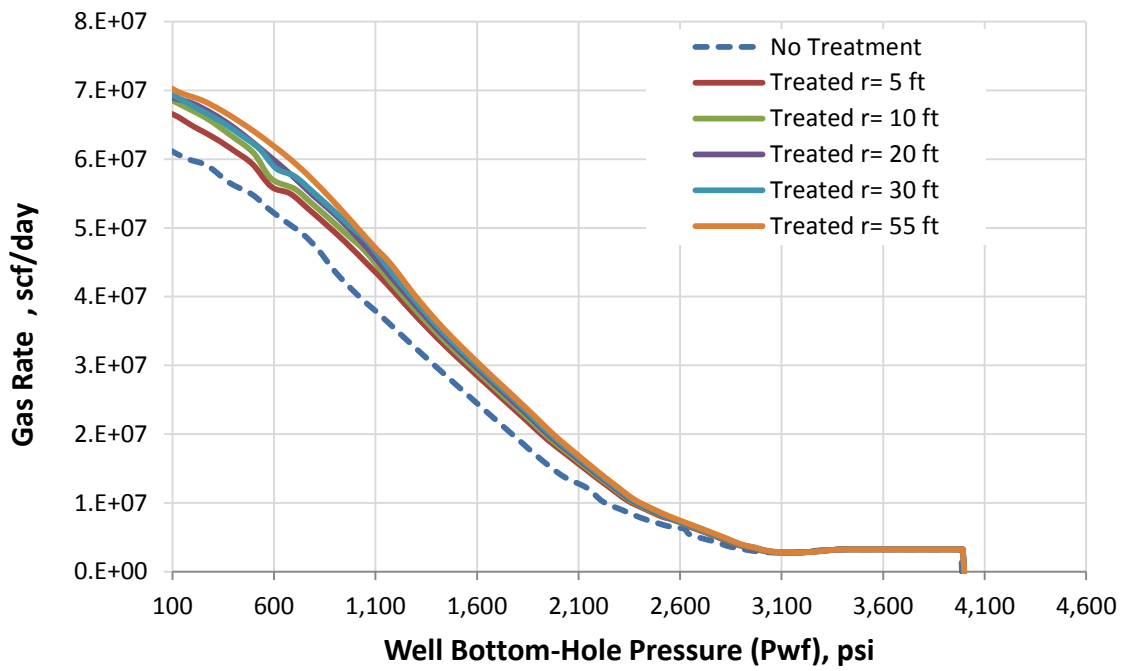


Figure 8.7 Rate of produced gas versus well bottom-hole pressure for non-treated and treated cases

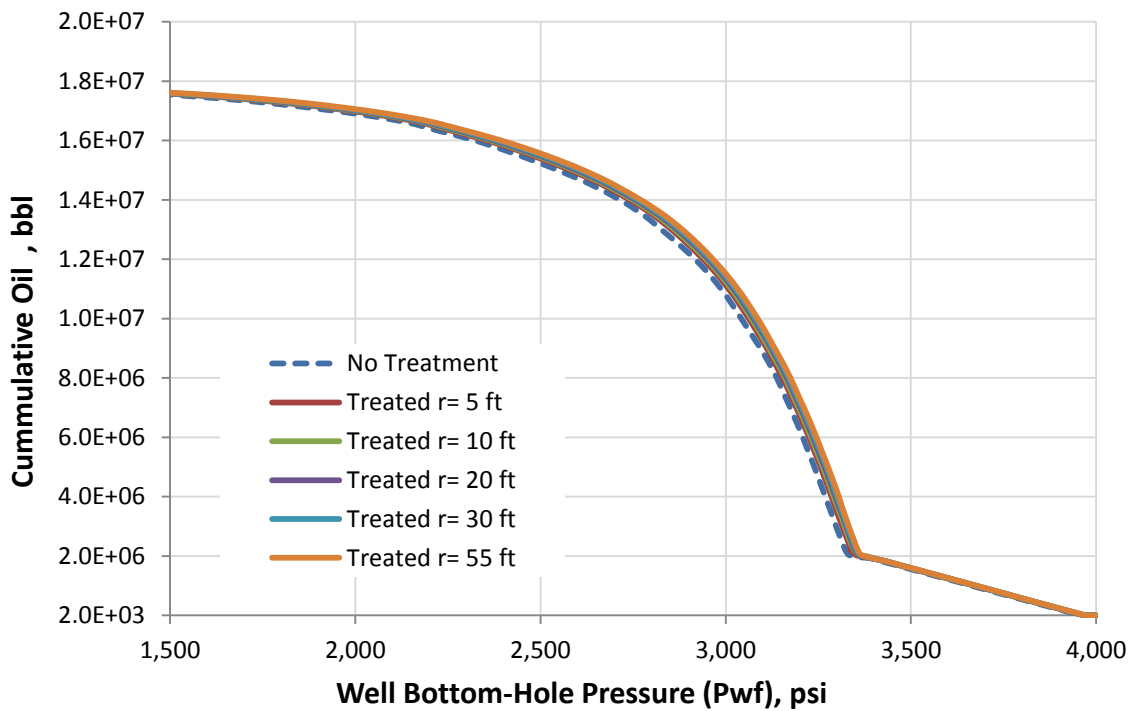


Figure 8.8 Cumulative oil vs. well-bottom hole pressure for non-treated and treated cases

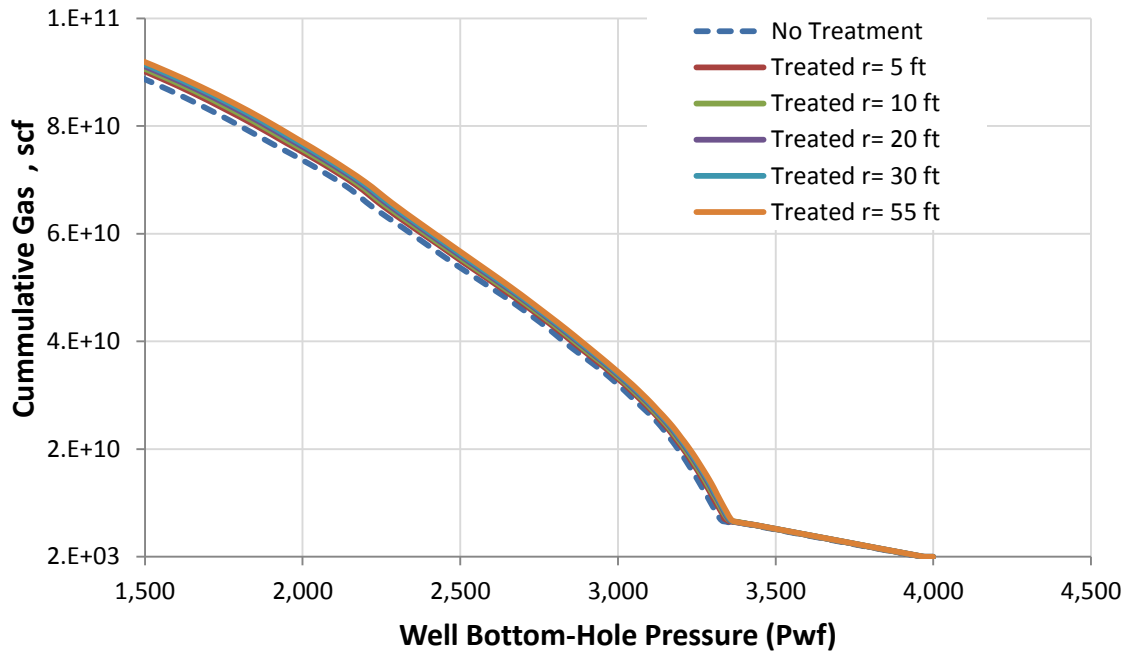


Figure 8.9 Cumulative gas vs. well-bottom hole pressure for non-treated and treated cases

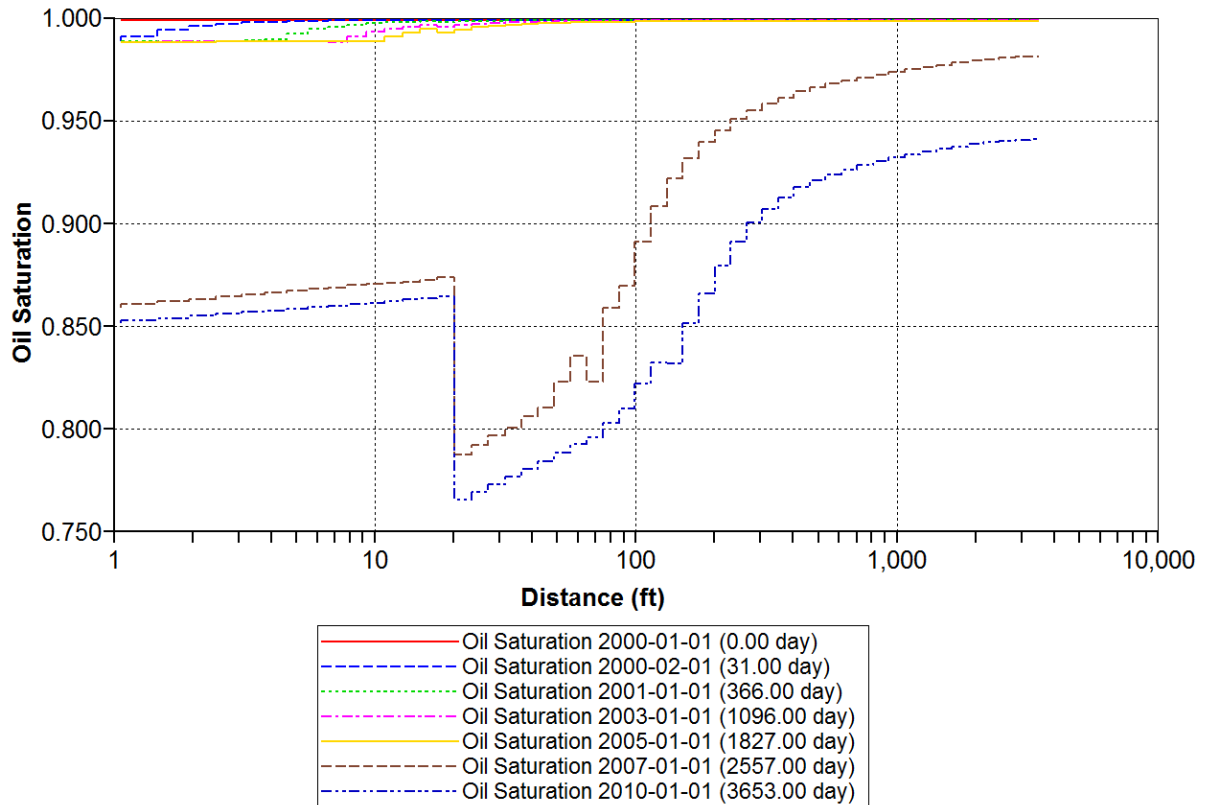


Figure 8.10 Oil Saturation profiles during reservoir depletion for a treated radius of 20 ft

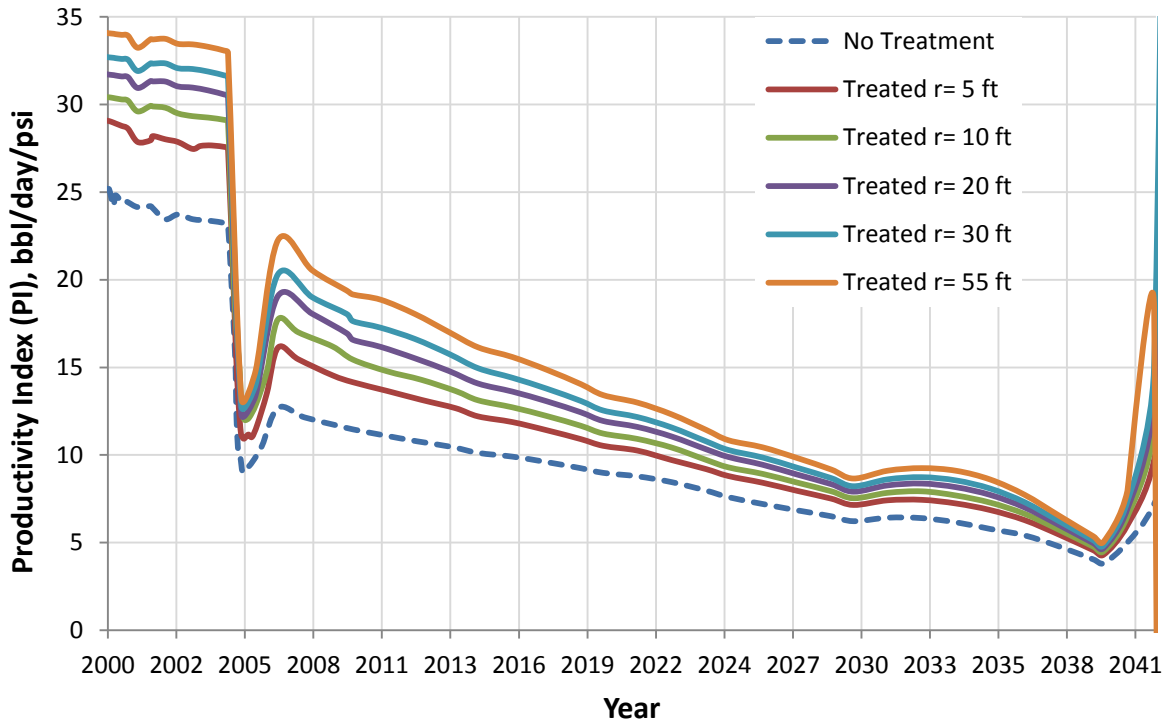


Figure 8.11 Productivity index profile for the non-treated and treated cases

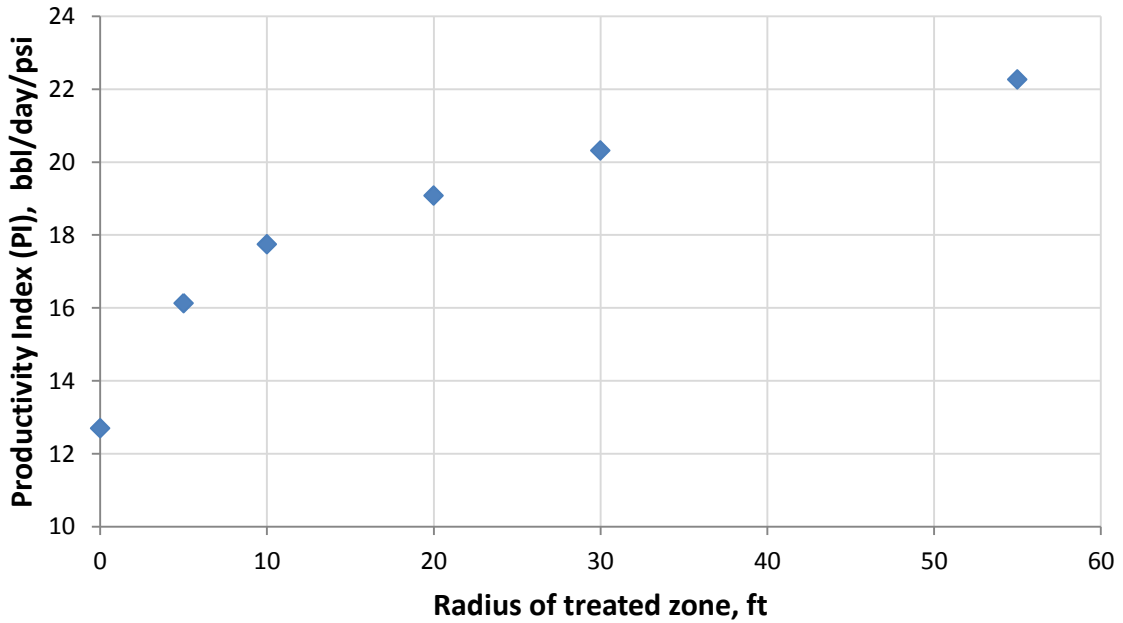


Figure 8.12 Productivity index for different radius of treated zone after 7 years of production

Chapter 9: Summary, Conclusions, and Future work

9.1 SUMMARY

The main objective of this research was to develop a chemical technique to improve and/or restore the productivity of volatile oil wells undergoing "gas blocking". The technique developed had to be effective, durable and have no adverse environmental impact. These goals were accomplished using fluorinated surfactants to alter the wettability of the rock surface.

The research goals were attained and tested by performing high-temperature high-pressure (HTHP) core flood experiments under simulated reservoir conditions. Analytical tools such as X-ray photoelectron spectroscopy (XPS), high-performance liquid chromatography (HPLC) and computerized axial tomography (CT Scan), as well as the use of numerical simulations were also used to interpret the experimental results.

Fluorinated surfactants have the ability to change the water and oil wettability of the formation from water/oil wet to neutral wet allowing oil, gas, and even water to flow more easily. Wettability alterations were indirectly observed as changes in oil and gas relative permeability.

To successfully alter rock wettability a chemical treatment had to be developed which could deliver the chemical so that it would bond to the rock surface. This required the selection of both a fluorinated surfactant and a solvent solution. Surfactants and solvent solutions were first screened to select potential formulations. Candidate surfactants were selected based on their ability to provide good repellency to oil and water. Two main features were sought in the molecular structure of a potential surfactant: a functional group to provide a bond to the rock surface and a fluorinated tail to provide repellency to oil and water. Only chemicals with fluorinated tails $\leq C_4$ were

considered because they have been shown to be environmentally acceptable. Candidate solvents were selected based on screening experiments where surfactant solubility, temperature stability, and brine compatibility were assessed. All candidate formulations were assessed using, drop tests, imbibition rate tests and XPS analysis to provide a qualitative, assessment of the behavior of the chemical treatment formulation. The selected surfactants for sandstones were FC-X is a fluorinated surfactant containing polymeric ethylene oxide, L-20294 is an epoxide, L-18961 a silane and L-19973#9 a cationic carboxylate. For treatment of carbonates L-19446#1 an anionic calcium carboxylate was chosen. The solvents used to deliver the surfactants were mixtures of 2-butoxyethanol and ethanol and in one case also isopropyl alcohol. The composition of the selected chemical treatment formulations are given in Chapter 4.

HTHP core flood experiments provided the most meaningful evaluation of the performance of fluorinated chemical treatments because the actual change in relative permeabilities were directly observed. Several HTHP core flood experiments were performed using two types of sandstones cores, Berea and Torrey Buff. Experiments were conducted with initial water saturations under diverse reservoir conditions. Steady-state gas and oil relative permeabilities were measured for pre and post-treatment two-phase volatile oil floods using measured steady state pressure drops. For sandstones, coreflood experimental results showed that fluorinated surfactant treatments can improve the relative permeability of both oil and gas by factors as high as 3.5. These results were obtained at low capillary numbers on the order of 1×10^{-5} to 1×10^{-6} and for PVT ratios greater than 0.5. Experimental temperatures were in the range of 155°F to 275°F for volatile oils with GOR's in the range of 4000 to 13,000 scf/STB.

Two HTHP core flood experiments were performed using Texas cream limestone cores, in the presence of connate water. The chemical treatment improved the oil and gas

relative permeability by a factor of 1.3 to 1.9. This indicates that the surfactant did modify the wettability of the carbonate surface.

XPS was used to measure the fluorine content in eight sandstone cores and one carbonate core from HTHP core flood experiments #141, #148, #176, #189, #224, #225, #228 #229 and #185. Measurements were made along the length of the cores and the results were compared by chemical treatment type, temperature and mass of treatment injected. For Berea cores treated with non-ionic surfactants L-20294, L-18961 and FC-X a rather uniform fluorine distribution was observed throughout the core and fluorine levels as high as 11wt% were measured. The highest levels of fluorine were for cores treated with the surfactant L-20294. For a carbonate rock treated with anionic surfactant L-19446#1 the observed fluorine level was 10 wt%.

HPLC was used for surfactant adsorption and desorption measurements. The analysis was performed for the chemical treatment effluents and the post-treatment volatile oil effluents of experiment #224. For a Berea sandstone core treated with surfactant FC-X, an adsorption of 2.6 gr-surfactant/gr-rock was measured. It was also observed that complete adsorption happened within the first three pore volumes of treatment injected. The final concentrations of surfactant desorbed in the volatile oil effluents were in the order of 10 ppm or less.

CT scanning was used to measure gas and oil saturation along the length of the core for core flood experiments. For Berea sandstone cores treated with surfactant FC-X the oil saturation increased from about 55% before treatment to about 70% after treatment. The residual oil saturation did not exhibit a significant change. The residual gas saturation varied from 10% before treatment to 3.3% after treatment. Using the data for oil and gas saturations as well as relative permeabilities calculated for flood experiments, relative permeability curves were plotted from the experimental data.

To predict the behavior of fluorinated chemical treatments in volatile oil reservoirs, the compositional simulator, STARS from CMG, was used to simulate the oil and gas production of a single –layer single-well cylindrical volatile oil reservoir with two zones, a treated near-wellbore zone and a non-treated zone. The treated zone corresponded to a zone treated with fluorinated chemical treatments. The simulation cases were: one base case where the radius of treated zone was zero and five cases with increasing volume of zone treated; 5, 10, 20, 30 and 55 feet of treated radius. The simulations were conducted at a constant oil production of 1000 bbl/day, for a reservoir at 155°F and using modified relative permeabilities for the treated zone. From the simulations it was observed that the use of fluorinated chemical treatments resulted in lower pressure drawdown near the wellbore, especially after producing below the bubble point pressure. This resulted in high well bottom-hole pressures for a longer period of time for the treated cases. The treatment provided an increase in the gas production rate and for a treated radius of 55 ft it produced as much as 10 MMscf/day. Cumulative oil and gas produced increased for well bottom-hole pressures. For a treated zone of radius 55 ft and bottom-hole pressure of 3,100 psi, cumulative oil increased about 800,000 barrels and the gas produced increased by 2.3 Bscf. The productivity index (PI) increased for all times and increased as much as 10 bbl of oil/day/psi. The PI increased was more significant for the area within 10 ft of the treated radius, but the greater treatment volumes resulted in greater PIs.

9.2 CONCLUSIONS

Specific conclusions from this study are as follows:

- C₄ fluorinated surfactants with non-ionic and ionic functional groups were shown to increase oil and gas relative permeabilities by altering the wettability of both sandstone and carbonate rocks from water-wet to neutral-wet cores.

- Fluorinated chemical treatments with surfactant concentrations ranging from 1 to 2 wt% using a 2-butoxyethanol/ethanol solvent improved the gas and oil relative permeabilities in the presence of connate water from about 1.1 to 3.5 depending on the PVT ratio, capillary number, rock permeability and surfactant.
- Surfactant L-20294 showed the best improvement factors among the surfactants tested and FC-X showed the least improvement.
- The treatment proved to be effective and stable at temperatures as high as 275°F with better results at higher temperatures.
- Fluorinated chemical treatments proved to be effective at capillary numbers on the order of 1×10^{-5} to 1×10^{-6} and PVT ratios greater than 0.5, but no improvement was seen for capillary numbers above 1×10^{-5} or for PVT ratios less than 0.5.
- For two-phase flow of oil and gas, fluorinated chemical treatments lead to lower gas saturations (CT-scan data).
- Fluorinated chemical treatments increased the gas relative permeability for all oil saturations and increased the oil relative permeability for oil saturations greater than 75%.
- The improvement factor increased linearly for PVT ratios above 0.5. Higher PVT ratios correspond to higher gas saturations where the gas blocking effect is greatest.
- The chemical treatment appears to be less effective in tighter cores with improvement factors of only about 1.2. This may be due to the difficulty in removing the solvent from the pore space of low permeability rocks. The use of more volatile solvents may help resolve this issue.

- The gas permeability measured at the end of each coreflood showed that the treatment solutions used did not damage the core.
- XPS analysis is a convenient tool to screen surfactants. This saves time and effort and complements the contact angle and imbibition rate tests also used to screen surfactants.
- XPS, HPLC and CT scanning proved to be helpful techniques providing a more robust analysis of the results obtained with HTHP core flood experiments.
- Different fluorinated C₄ surfactants exhibit similar fluorine levels throughout treated Berea sandstones.
- The adsorption of the fluorinated surfactants occurs within the first few pore volumes of chemical treatment.
- Surfactant FC-X desorbs from Berea sandstone cores on the order of 10 ppm during the post treatment two-phase volatile oil and gas flow.
- More work needs to be done on carbonates. There is no a formulation ready for field testing yet.
- Numerical simulations using the measured relative permeability data were used to estimate the gain in productivity for treated wells. These simulations suggest that the proposed fluorinated chemical treatments could be used as a preventive treatment or for a damaged well that has already been producing below the bubble point to increase gas and oil production rates and recoverable reserves.

9.3 FUTURE WORK

To better understand the behavior of fluorinate chemical treatments and improve their applicability the following work is suggested:

- Studies on the interaction mechanisms occurring at a molecular level between surfactant molecule and type of rock surface in the presence of solvents, hydrocarbons, and brine.
- More experimentation in different kinds of carbonate rocks over a wide range of conditions such as high temperature.
- Alternate solvent systems, more volatile and less viscous such as hydro-fluorocarbons.
- Core flood experiments for three phase floods gas-oil-water.
- Test the applicability of the chemical treatments on tight rocks with permeability less than 1 md.
- More studies on adsorption and desorption of fluorinated surfactants.
- Use electron microscopy techniques to analyze the rock surface and measure pore size before and after treatment to look for possible pore reduction due to surfactant interaction to better understand if there are structural changes that may lead to understand why the chemical does not work in some experiments.
- Further simulation studies should be undertaken, including cases where the chemical treatment is injected once production is below bubble point pressure. Also, injection of the chemical treatment and flow back of the solvents should be simulated.
- Field trials and rigorous studies of the resulting data obtained.

Appendix A

This appendix summarizes all the core flood experiments performed to evaluate the fluorinated chemical treatments by measuring changes in the oil and gas relative permeability before and after treatment caused by wettability alteration. This appendix also includes the core flood experiments performed to measure oil and gas saturation along the core using CT scanning.

Appendix A.1: EXPERIMENT #134

Objective:

The objective of this experiment was to investigate the effectiveness of chemical treatment 1 using non-ionic polymeric fluoro-surfactant FC-X in improving the oil and gas relative permeability. This was done for a volatile oil mixture below the bubble point pressure on a Berea sandstone core in the presence of initial water saturation. The experiment was performed at 155°F.

Experimental Procedure and Results:

A Berea core was prepared for the experiment following the standard procedure described Section 3.2.1.1. The initial core measurements and assumed properties can be found in Table A.1.1.

The gas permeability in the dry core was calculated for nitrogen at 75°F and for methane at 155°F. Nitrogen and methane were flowed through the core using five flow rates and the pressure drop across the core for each flow rate was recorded. Using this data, the fluid properties and accounting for non-Darcy effects the calculated gas permeability was 169 md for nitrogen and 154 md for methane. Table A.1.2 summarizes the flood conditions and fluid properties and Table A.1.3 the results for nitrogen flood and Table A.1.4 and Table A.1.5 show the flood conditions, fluid properties, and results for the methane flood. Figure A.1.1 shows the pressure drop measured across the core during the nitrogen flood. Figure A.1.2 shows the pressure drop measured across the core during the methane flood.

The initial gas permeability at initial water saturation was calculated next. Using synthetic brine 1 (25,000 ppm NaCl) an initial water saturation of 20% was established. This was done by applying vacuum to the core first and then injecting 3.6 ml of brine.

The core was shut in for 1 hour, allowing the brine to distribute through the core. Methane at 155°F was then flowed through the core using five flow rates and the pressure drop across the core for each flow rate was recorded. The calculated gas permeability was 122 md. The flood conditions and results are shown in

Table A.1.6 and Table A.1.7 respectively. Figure A.1.3 shows the pressure drop measured across the core during the methane flood.

Synthetic volatile oil mixture 2 (Table 3.3) was used for the two-phase flow measurements. The mixture was allowed a minimum of 12 hours to equilibrate to a single phase at 4200 psi and 155°F. The initial flood was conducted with the upstream backpressure regulator (BPR-1) set at 4243 psi and the downstream back pressure regulator (BPR-2) set at 690 psi. Volatile oil was injected at a total core flow rate of 673cc/hr and 1345 cc/hr. Table A.1.8 gives the fluid properties of the synthetic fluid calculated using the Peng-Robinson EOS at the flowing core pressure. Figure A.1.4 shows the pressure drop measured across the core during the initial two-phase volatile oil flood.

The core was then treated using chemical treatment 1 (Table 4.15). The solution was heated for at least 3 hours at 155°F. BPR1 was kept at 690 psi. The core was flooded with 20 pore volumes of the treatment solution at a flow rate of 120 cc/hr. The core was then shut in for 15 hours. Figure A.1.5 shows the measured pressure drop across the core during the treatment flood.

Post-treatment two-phase volatile oil flood was conducted under the same conditions as the initial two-phase flow. Figure A.1.6 shows the pressure drop measured across the core during the post-treatment two-phase volatile oil flood. A minimal improvement factor was observed; therefore the core was treated again.

The core was re-treated using the same procedure and treatment solution as before. Figure A.1.7 show the second chemical treatment flood injection. Then, another post-treatment two-phase volatile oil flood was conducted. Figure A.1.8 shows the post-2nd treatment two-phase volatile oil flood injection.

The final gas permeability was calculated using the procedure for the initial gas permeability using methane at 155°F. The calculated gas permeability was 133 md. The flood conditions and results are shown in Table A.1.9 and Table A.1.10 respectively.

For every two-phase volatile oil flood, oil and gas relative permeabilities k_{rg} and k_{ro} were calculated using the measured pressure drop across the core under steady state conditions and then improvement factors were calculated. Table A. 1.11 summarizes the experimental results.

Table A.1.1 Core properties (Exp #134)

<i>Length, in</i>	8.06
<i>Diameter, in</i>	0.998
<i>Mass Core, gr</i>	226.5
<i>Grain Density, gr/cc</i>	2.65
<i>Porosity (ϕ)</i>	17.28 %

Table A.1.2 Fluid properties and conditions for nitrogen gas permeability (Exp #134)

		<i>Density, gr/cc</i>
<i>Gas</i>	Nitrogen	
<i>Temperature, °F</i>	75	
<i>BPR 1-pressure, psi</i>	2900	0.2138
<i>BPR 2-pressure, psi</i>	1000	7.85E-02
<i>Gas Viscosity, cp</i>	0.0195	

Table A.1.3 Nitrogen flood results (Exp #134)

<i>q_{core}, cc/hr</i>	<i>ΔP, psi</i>	<i>k_g, md</i>
1362	2.760	159.32
2179	4.560	154.29
2724	5.930	148.31
3268	7.250	145.57
4085	9.350	141.09
<i>Corrected Permeability (k_g), md</i>		169.1

Table A.1.4 Fluid properties and conditions for methane gas permeability (Exp #134)

		<i>Density, gr/cc</i>
<i>Gas</i>	Methane	
<i>Temperature, °F</i>	155	
<i>BPR 1-pressure, psi</i>	3065	0.1283
<i>BPR 2-pressure, psi</i>	1125	4.72E-02
<i>Gas Viscosity, cp</i>	0.0141	

Table A.1.5 Methane flood results (Exp #134)

q_{core} , cc/hr	ΔP , psi	k_g , md
1362	2.19	145
2179	3.61	141
2724	4.58	139
3268	5.62	136
4085	7.2	132
<i>Corrected Permeability (k_g), md</i>		154.3

Table A.1.6 Fluid properties and conditions for methane gas permeability at S_{wi} (Exp #134)

		<i>Density, gr/cc</i>
<i>Gas</i>	Methane	
<i>Temperature, °F</i>	155	
<i>BPR 1-pressure, psi</i>	3065	0.1283
<i>BPR 2-pressure, psi</i>	1125	4.72E-02
<i>Gas Viscosity, cp</i>	0.0141	

Table A.1.7 Methane flood results at S_{wi} (Exp #134)

q_{core} , cc/hr	ΔP , psi	k_g , md
1362	2.660	119.30
2175	4.400	115.40
2718	5.670	111.94
3262	7.000	108.80
4077	8.780	108.43
<i>Corrected Permeability (k_g), md</i>		122.3

Table A.1.8 Volatile oil properties at BPR-1 and BPR-2 pressures (Exp #134)

<i>BPR 1-pressure, psi</i>	4243	
<i>BPR 2- pressure, psi</i>	690	
<i>Density at BPR 1-pressure, gr/cc</i>	0.3665	
Properties at BPR 2-pressure, psi	Gas Phase	Oil Phase
<i>Density, gr/cc</i>	0.0371	0.6124
<i>Viscosity (μ), cp</i>	0.0133	0.2411
<i>Volume Fraction</i>	0.9461	0.0539
<i>IFT, dyne/cm</i>	9.876	

Table A.1.9 Fluid properties and conditions for final methane gas permeability (Exp #134)

		<i>Density, gr/cc</i>
<i>Gas</i>	Methane	
<i>Temperature, °F</i>	155	
<i>BPR 1-pressure, psi</i>	4187	0.1659
<i>BPR 2-pressure, psi</i>	690	0.0283
<i>Gas Viscosity, cp</i>	0.0134	

Table A.1.10 Final methane flood results (Exp #134)

<i>q_{core}, cc/hr</i>	<i>ΔP, psi</i>	<i>k_g, md</i>
4690	8.700	119.61
5862	11.100	117.19
7034	13.700	113.94
8793	17.800	109.62
<i>Corrected Permeability (k_g), md</i>		132.81

Table A. 1.11 Pre and post-treatment volatile oil flood results and measured improvement factors (Exp #134)

	Exp#134	
<i>q_{gtot core}, cc/hr</i>	673	1345
<i>q_g, cc/hr</i>	636	1273
<i>q_o, cc/hr</i>	36	73
<i>PVT Ratio</i>	0.97	
<i>Viscosity Ratio μ_g/μ_o</i>	0.06	
<i>Capillary Nc</i>	1.44E-05	2.52E-05
<i>k_{rg} Before Treatment</i>	0.033	0.037
<i>k_{ro} Before Treatment</i>	0.034	0.039
<i>k_{rg} After Treatment</i>	0.038	0.043
<i>k_{ro} After Treatment</i>	0.039	0.044
<i>Initial Improvement Factor</i>	1.2	1.1
<i>PV of Vol Oil Injected</i>	~320	
<i>Final Improvement Factor</i>	1.0	1.0

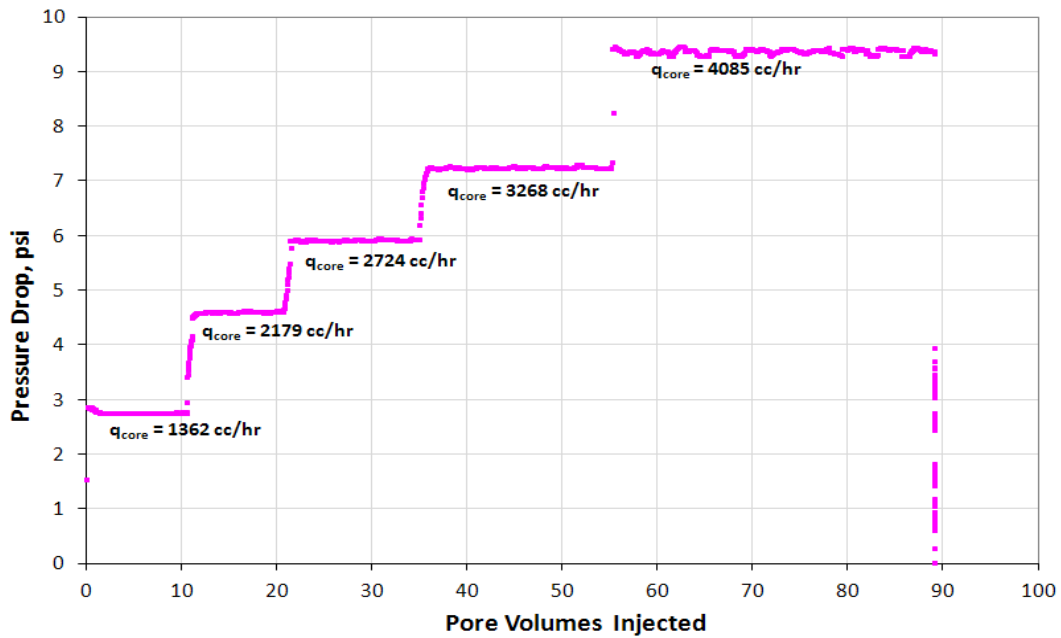


Figure A.1.1 Pressure drop across the core during the initial nitrogen flood at 75°F (Exp #134)

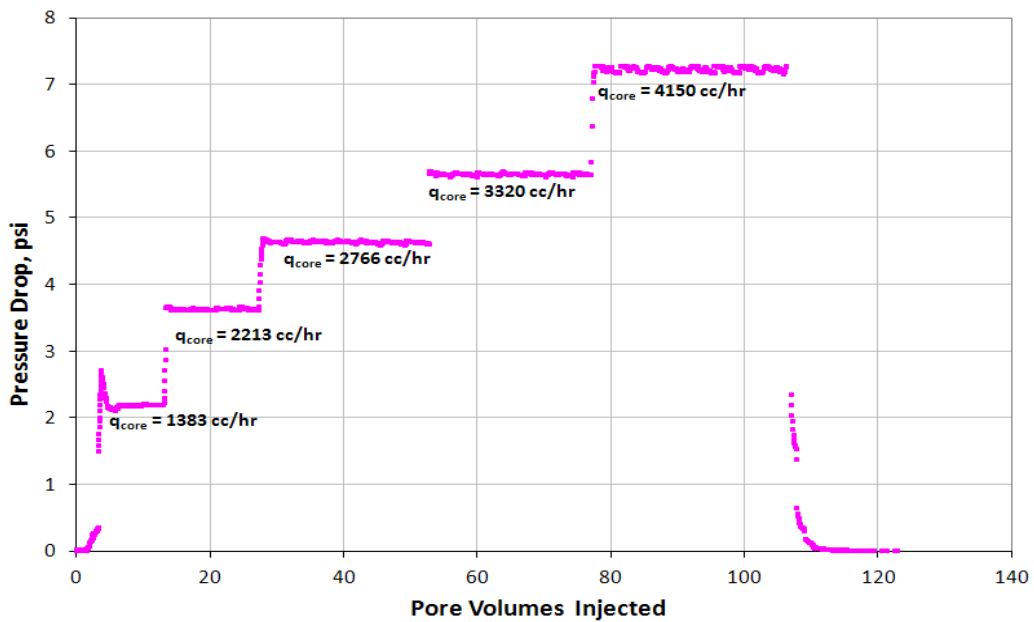


Figure A.1.2 Pressure drop across the core during the initial methane flood at 155°F (Exp #134)

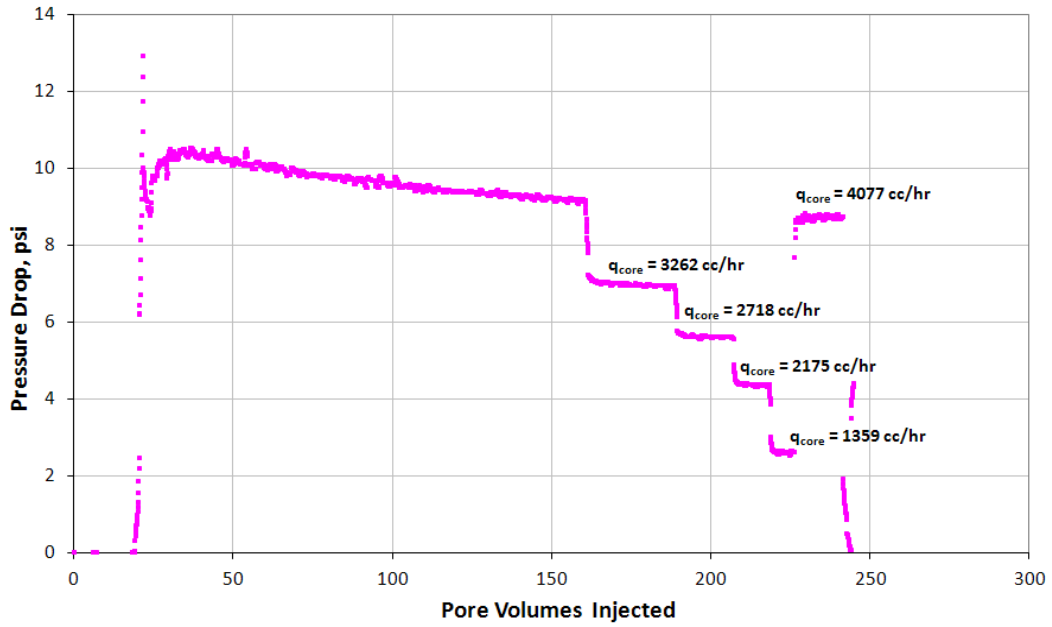


Figure A.1.3 Pressure drop across the core during the methane flood at S_{wi} 20% (Exp #134)

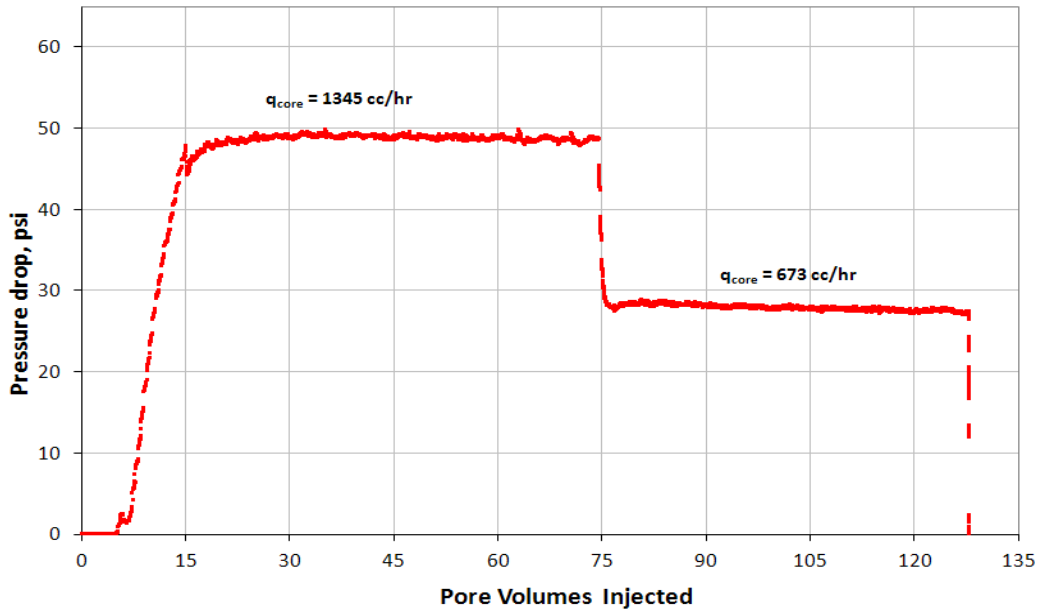


Figure A.1.4 Pressure drop across the core during the pre-treatment two-phase volatile oil flood (Exp #134)

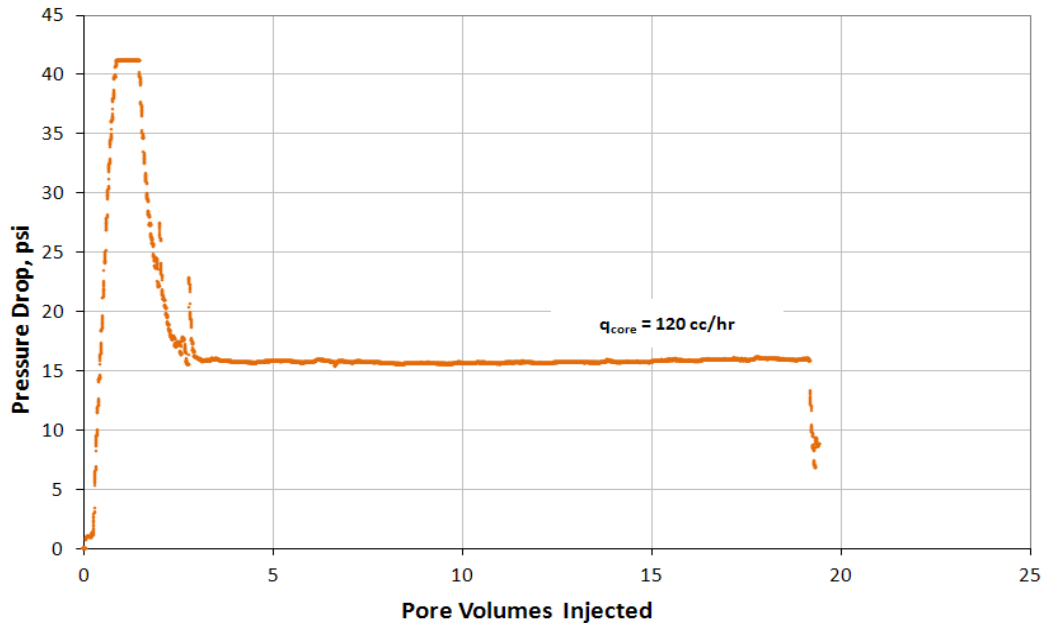


Figure A.1.5 Pressure drop across the core during injection of chemical treatment 1 (Exp # 134)

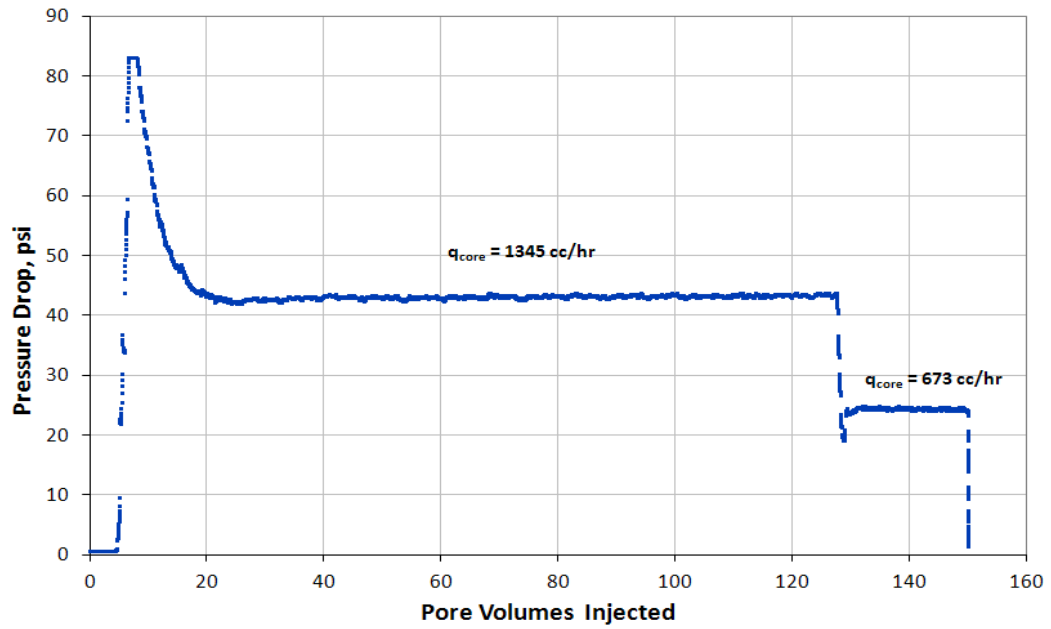


Figure A.1.6 Pressure drop across the core during the post-treatment two-phase volatile oil flood (Exp #134)

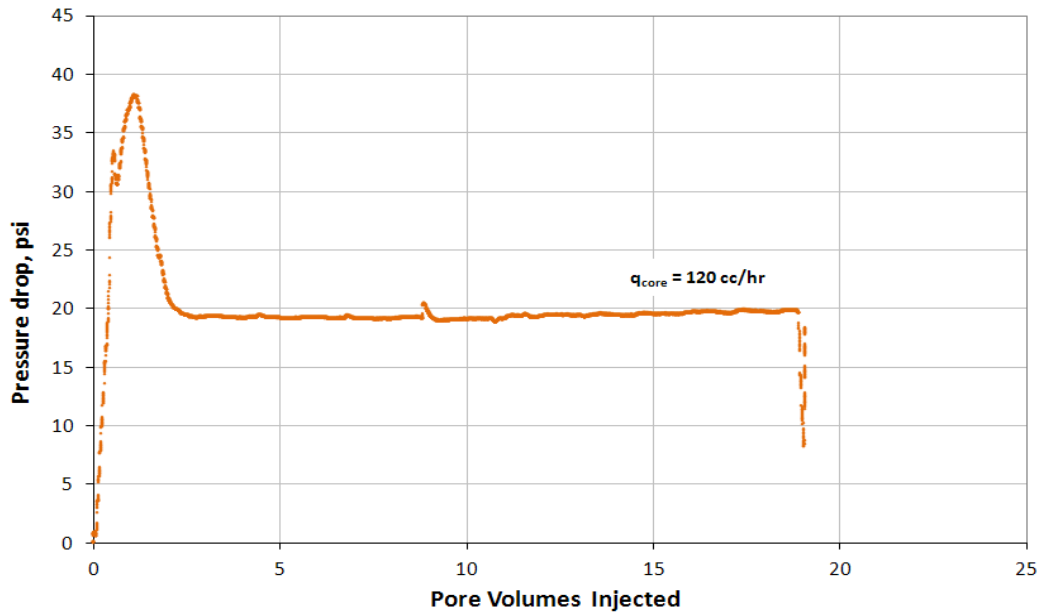


Figure A.1.7 Pressure drop across the core during injection of 2nd chemical treatment 1 (Exp # 134)

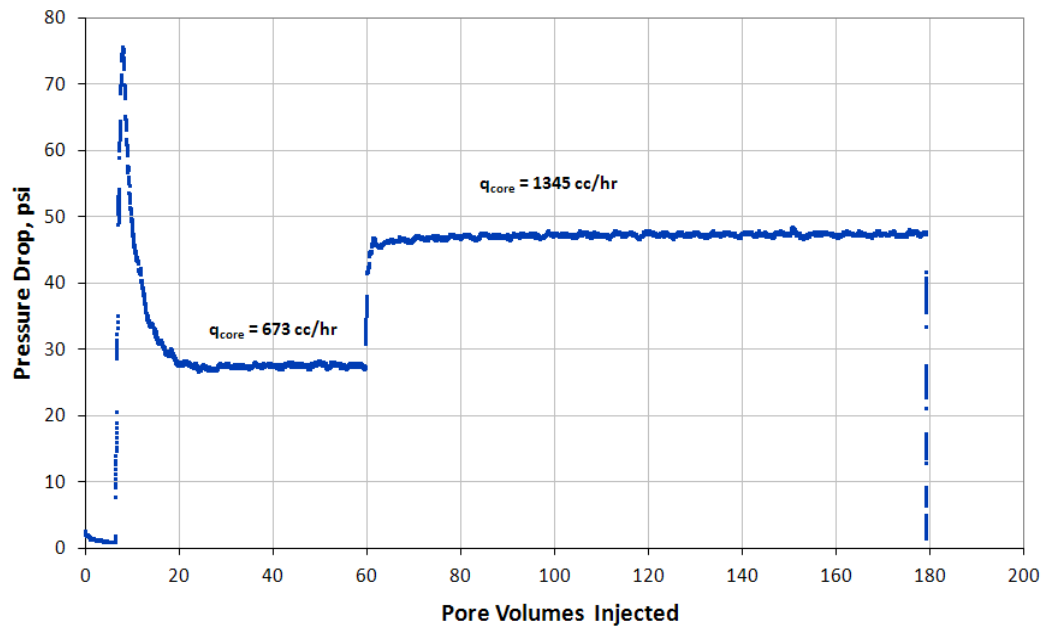


Figure A.1.8 Pressure drop across the core during the post-2nd treatment two-phase volatile oil flood (Exp #134)

Appendix A.2: EXPERIMENT #141

Objective:

The objective of this experiment was to investigate the effectiveness of chemical treatment 2 using non-ionic fluoro-surfactant L-20294 in improving the oil and gas relative permeability. This was done for a volatile oil mixture below the bubble point pressure on a Berea sandstone core and in the presence of initial water saturation. The experiment was performed at 155°F.

Experimental Procedure and Results:

A Berea core was prepared for the experiment following the standard procedure described Section 3.2.1.1. The initial core measurements and assumed properties can be found in Table A.2.1.

The initial gas permeability was calculated using methane at 155°F. Methane was flowed through the core using five flow rates and the pressure drop across the core for each flow rate was recorded. Using this data, the fluid properties and accounting for non-Darcy effects the calculated gas permeability was 189 md.

Table A.2.2 summarizes the flood conditions and fluid properties and

Table A.2.3 shows the results. Figure A.2.1 shows the pressure drop measured across the core during the methane flood.

The initial gas permeability at initial water saturation was calculated next. Using synthetic brine 1 (25,000 ppm NaCl) an initial water saturation of 20% was established. This was done by applying vacuum to the core first and then injecting 3.7 ml of brine. The core was shut in for 1 hour, allowing the brine to distribute through the core.

Methane at 155°F was then flowed through the core using five flow rates and the pressure drop across the core for each flow rate was recorded. The calculated gas permeability was 130 md. The flood conditions and results are shown in Table A.2.4 and Table A.2.5 respectively. Figure A.2.2 shows the pressure drop measured across the core during the methane flood at S_{wi} .

Synthetic volatile oil mixture 2 (Table 3.3) was used for the two-phase flow measurements. The mixture was allowed a minimum of 12 hours to equilibrate to a single phase at 4200 psi and 155°F. The initial flood was conducted with the upstream backpressure regulator (BPR-1) set at 4475 psi and the downstream back pressure regulator (BPR-2) set at 698 psi. Volatile oil was injected at a total core flow rate of 680 cc/hr and 1359 cc/hr. Table A.2.6 gives the fluid properties of the synthetic fluid calculated using the Peng-Robinson EOS at the flowing core pressure. Figure A.2.3 shows the pressure drop measured across the core during the initial two-phase volatile oil flood.

The core was then treated using chemical treatment 2 (Table 4.15). The solution was heated for at least 3 hours at 155°F. BPR1 was kept at 690 psi. The core was flooded with 20 pore volumes of the treatment solution at a flow rate of 120 cc/hr. The core was then shut in for 15 hours. Figure A.2.4 shows the measured pressure drop across the core during the treatment flood.

Post-treatment two-phase volatile oil flood was conducted under the same conditions as the initial two-phase flow. Figure A.2.5 shows the pressure drop measured across the core during the post-treatment two-phase volatile oil flood. A improvement factor of 1.7 and 1.6 was observed for low and high flow rate respectively. Then, two more volatile oil floods were performed to observe the durability of the treatment. For floods 2 and 3 the improvement factor remained almost constant at 1.5 and 1.4 for low

and high flow rate respectively. Figure A.2.6 and Figure A.2.7 show the pressure drop across the core for post-treatment volatile oil flood 2 and 3 respectively.

The final gas permeability was calculated using the procedure for the initial gas permeability using methane at 155°F. The calculated gas permeability was 133 md. The flood conditions and results are shown in Table A.2.7 and Table A.2.8 respectively. Figure A.2.8 shows the pressure drop measured across the core during the final methane flood.

For every two-phase volatile oil flood, oil and gas relative permeabilities k_{rg} and k_{ro} were calculated using the measured pressure drop across the core under steady state conditions and then improvement factors were measured. Table A.2.9 summarizes the experimental results.

Table A.2.1 Core properties (Exp #141)

<i>Length, in</i>	8.012
<i>Diameter, in</i>	0.997
<i>Mass Core, gr</i>	222.88
<i>Grain Density, gr/cc</i>	2.65
<i>Porosity (ϕ)</i>	17.95 %

Table A.2.2 Fluid properties and conditions for initial gas permeability (Exp #141)

		<i>Density, gr/cc</i>
<i>Gas</i>	Methane	
<i>Temperature, °F</i>	155	
<i>BPR 1-pressure, psi</i>	3137	0.131
<i>BPR 2-pressure, psi</i>	1007	4.20E-02
<i>Gas Viscosity, cp</i>	0.0139	

Table A.2.3 Initial methane flood results (Exp #141)

<i>q_{core}, cc/hr</i>	<i>ΔP, psi</i>	<i>k_g, md</i>
1871	2.400	178.77
2495	3.260	175.48
3119	4.130	173.15
3743	5.050	169.92
4679	6.500	165.02
<i>Corrected Permeability (k_g), md</i>		188.9

Table A.2.4 Fluid properties and conditions for methane gas permeability at S_{wi} (Exp #141)

		<i>Density, gr/cc</i>
<i>Gas</i>	Methane	
<i>Temperature, °F</i>	155	
<i>BPR 1-pressure, psi</i>	3123	0.1305
<i>BPR 2-pressure, psi</i>	1001	4.17E-02
<i>Gas Viscosity, cp</i>	0.0138	

Table A.2.5 Methane flood results at S_{wi} (Exp #141)

q_{core} , cc/hr	ΔP , psi	k_g , md
1878	3.500	122.11
2504	4.620	123.35
3130	5.850	121.76
3755	7.100	120.39
4694	9.200	116.14
<i>Corrected Permeability (k_g), md</i>		130.4

Table A.2.6 Volatile oil properties at BPR-1 and BPR-2 pressures (Exp #141)

<i>BPR 1-pressure, psi</i>	4475	
<i>BPR 2- pressure, psi</i>	698	
<i>Density at BPR 1-pressure, gr/cc</i>	0.3724	
Properties at BPR 2-pressure, psi	Gas Phase	Oil Phase
<i>Density, gr/cc</i>	0.0375	0.6125
<i>Viscosity (μ), cp</i>	0.0134	0.2412
<i>Volume Fraction</i>	0.9461	0.0539
<i>IFT, dyne/cm</i>	9.842	

Table A.2.7 Fluid properties and conditions for final methane gas permeability (Exp #141)

	Gas	Methane	<i>Density, gr/cc</i>
<i>Temperature, °F</i>		155	
<i>BPR 1-pressure, psi</i>		3323	0.1377
<i>BPR 2-pressure, psi</i>		1090	0.0456
<i>Gas Viscosity, cp</i>		0.014	

Table A.2.8 Final methane flood results (Exp #141)

q_{core} , cc/hr	ΔP , psi	k_g , md
1812	2.790	149.96
2416	3.800	146.80
3020	4.800	145.27
3624	5.850	143.04
4530	7.500	139.46
<i>Corrected Permeability (k_g), md</i>		155.43

Table A.2.9 Pre and post-treatment volatile oil flood results and measured improvement factors (Exp #141)

	Exp# 141	
$q_{g\text{tot core, cc/hr}}$	680	1359
$q_g, \text{cc/hr}$	643	1286
$q_o, \text{cc/hr}$	37	73
<i>PVT Ratio</i>	0.98	
<i>Viscosity Ratio μ_g/μ_o</i>	0.06	
<i>Capillary Nc</i>	1.38E-05	2.46E-05
k_{rg} Before Treatment	0.035	0.039
k_{ro} Before Treatment	0.036	0.040
k_{rg} After Treatment	0.060	0.063
k_{ro} After Treatment	0.062	0.066
<i>Initial Improvement Factor</i>	1.7	1.6
<i>PV of Vol Oil Injected</i>	~ 730	
<i>Final Improvement Factor</i>	1.5	1.4

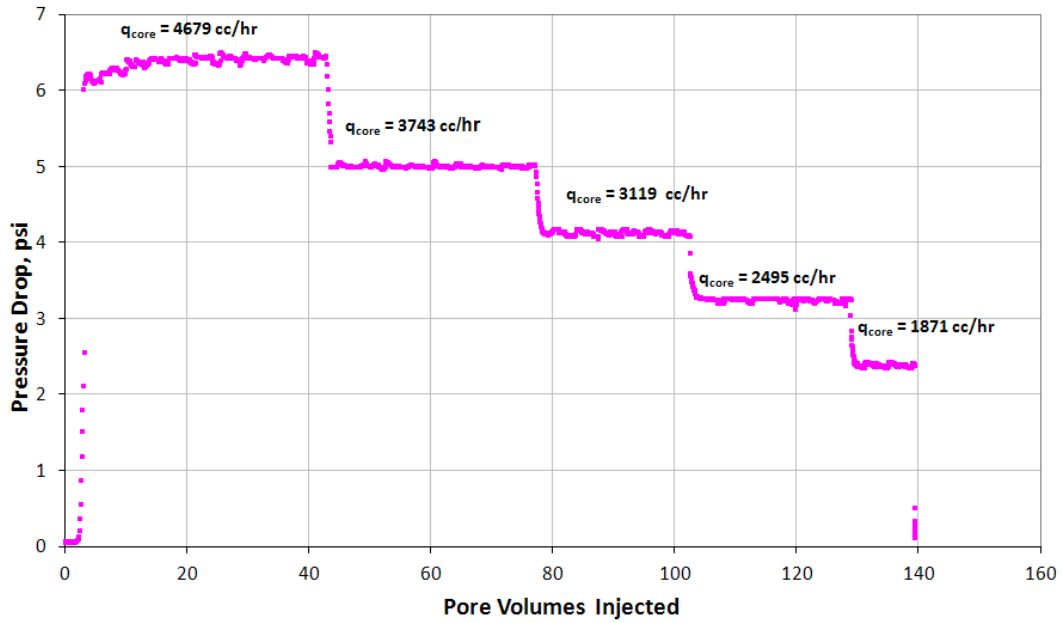


Figure A.2.1 Pressure drop across the core during the initial methane flood at 155°F (Exp #141)

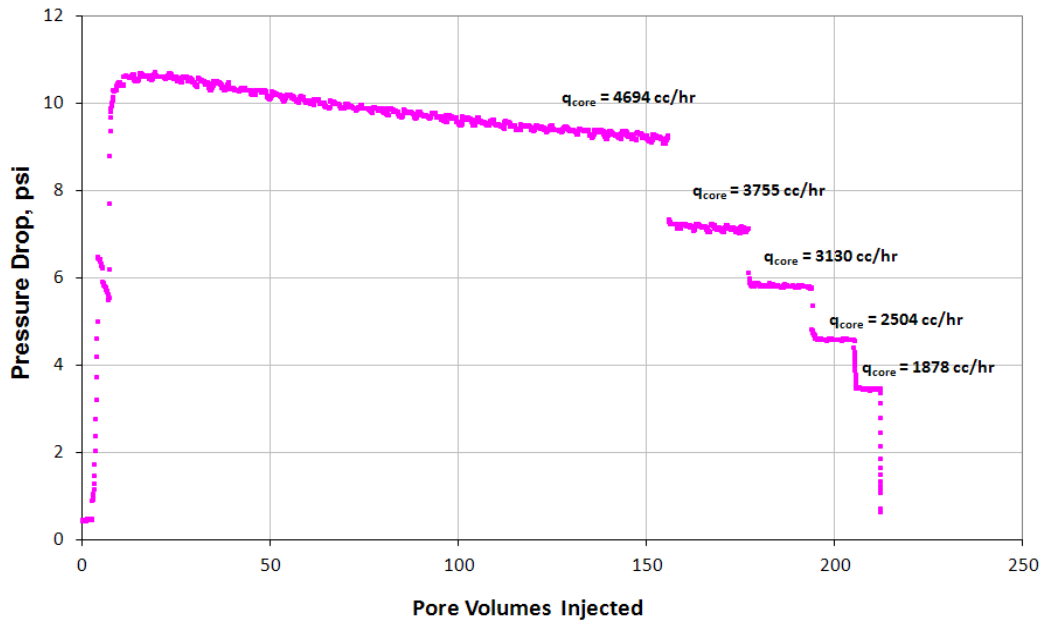


Figure A.2.2 Pressure drop across the core during the methane flood at S_{wi} of 20% (Exp #141)

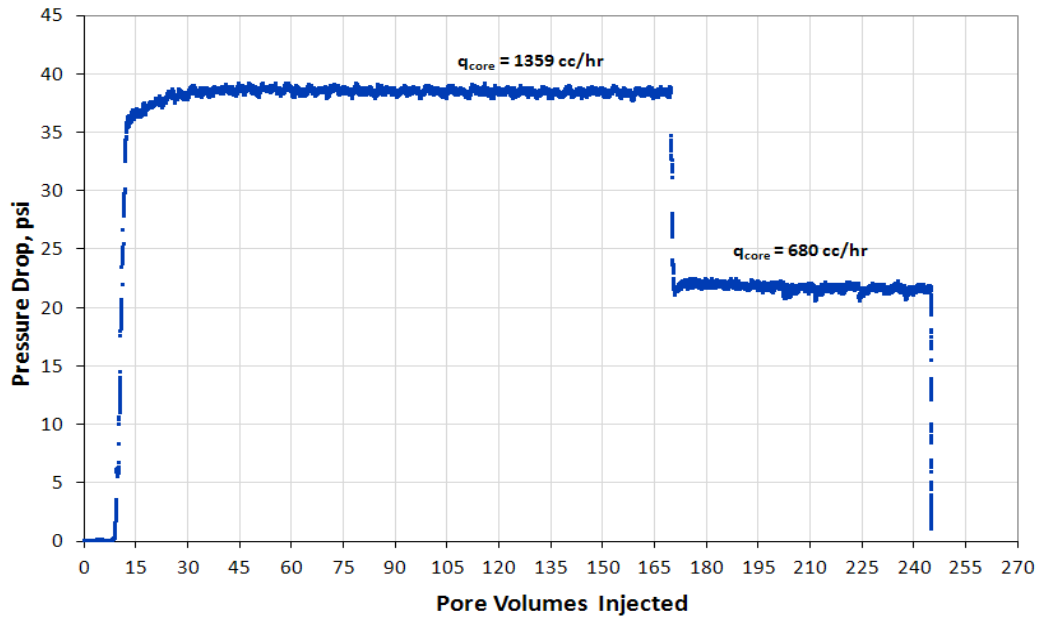


Figure A.2.3 Pressure drop across the core during the pre-treatment two-phase volatile oil flood (Exp #141)

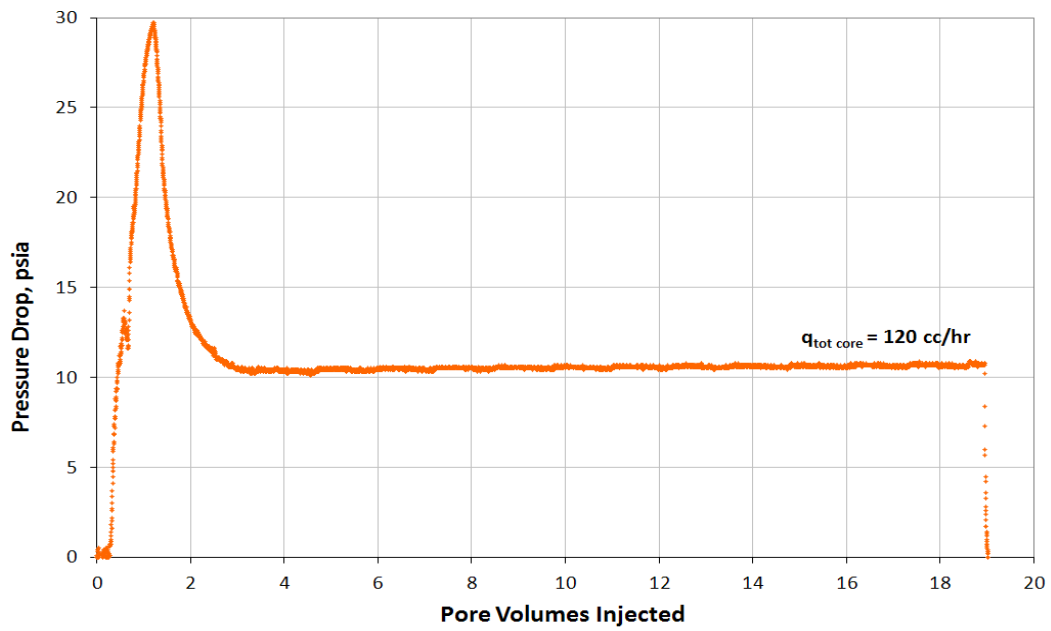


Figure A.2.4 Pressure drop across the core during injection of chemical treatment 2 (Exp #141)

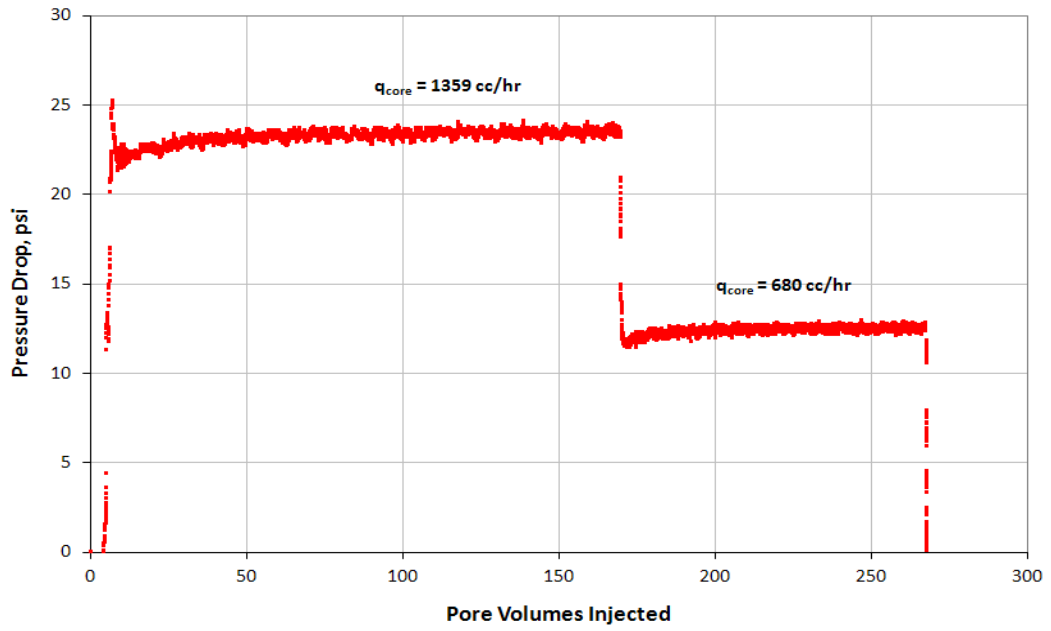


Figure A.2.5 Pressure drop across the core during the post-treatment two-phase volatile oil flood 1 (Exp #141)

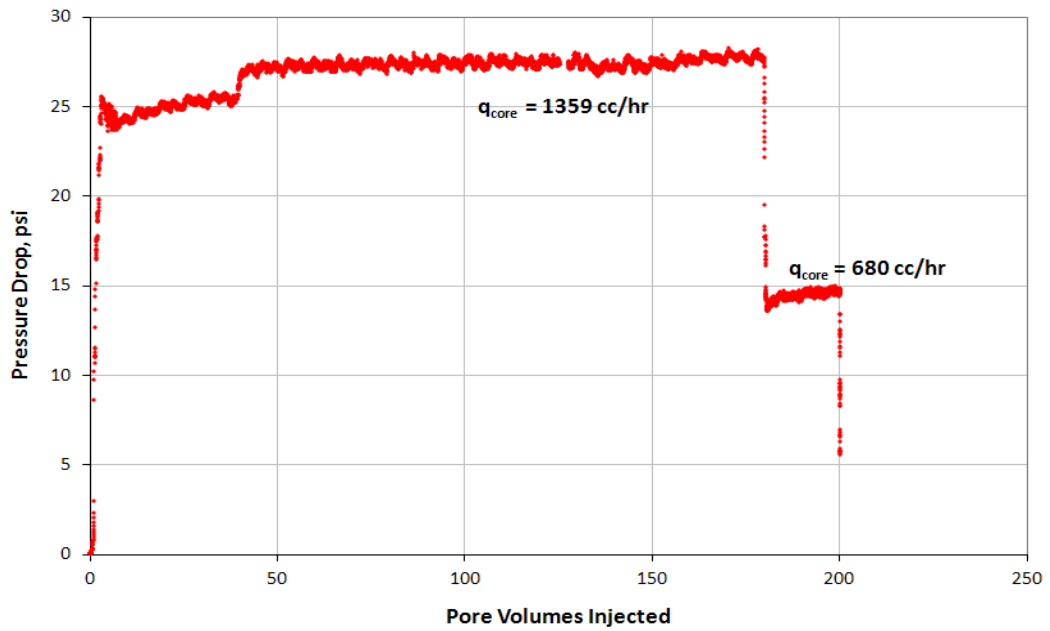


Figure A.2.6 Pressure drop across the core during the post-treatment two-phase volatile oil flood 2 (Exp #141)

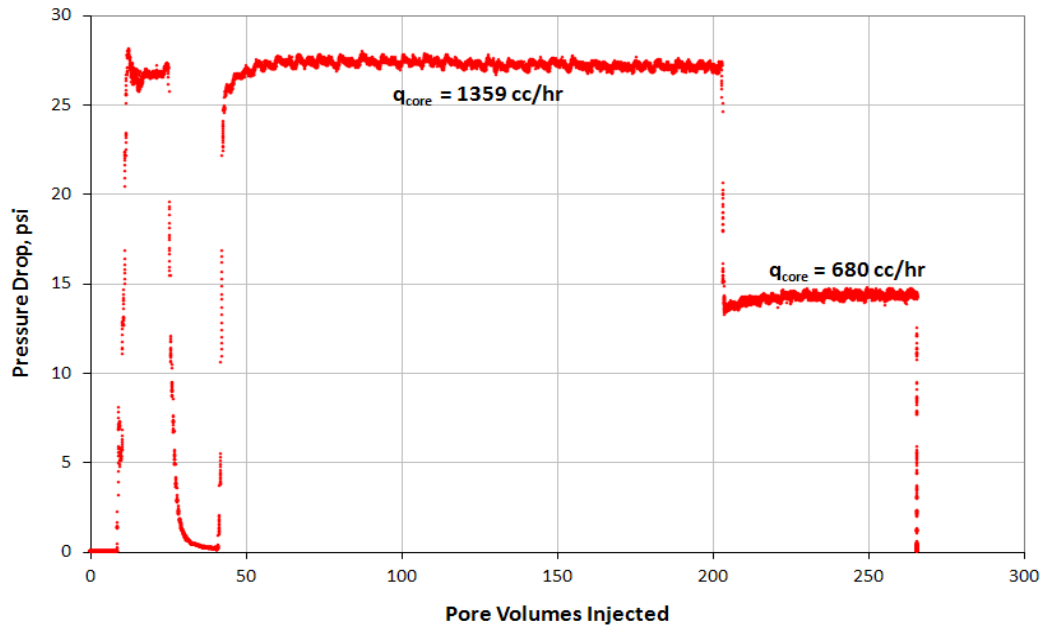


Figure A.2.7 Pressure drop across the core during the post-treatment two-phase volatile oil flood 3 (Exp #141)

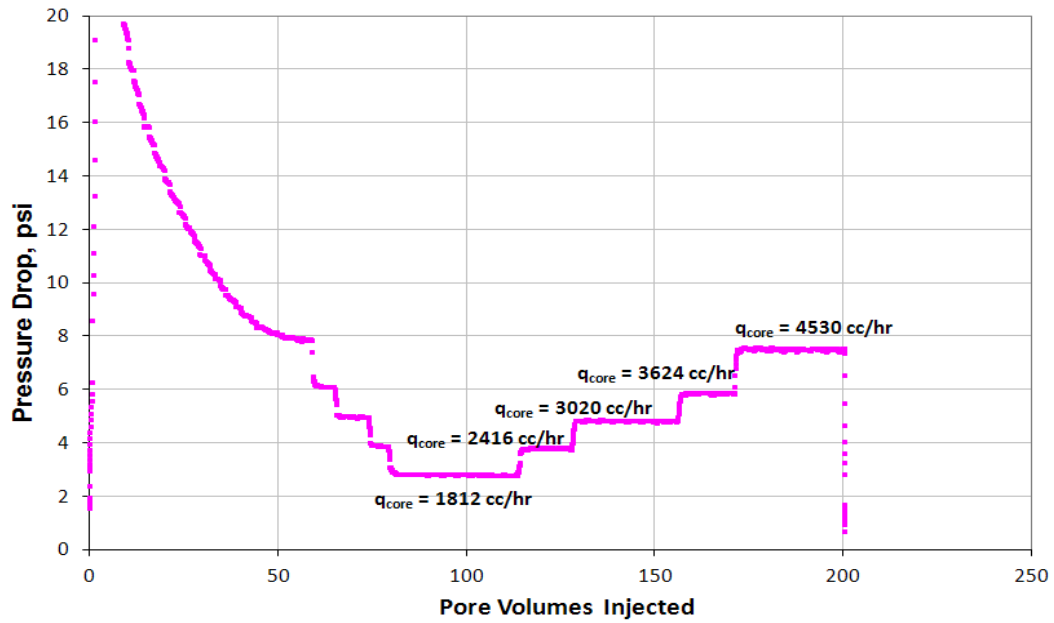


Figure A.2.8 Pressure drop across the core during the final methane flood (Exp #141)

Appendix A.3: EXPERIMENT#146

Objective:

The objective of this experiment was to investigate the effectiveness of chemical treatment 1 using non-ionic fluoro-surfactant FC-X in improving the oil and gas relative permeability and the durability of the treatment. This was done for a volatile oil mixture below the bubble point pressure on a Berea sandstone core and in the presence of initial water saturation. The experiment was performed at 155°F.

Experimental Procedure and Results:

A Berea core was prepared for the experiment following the standard procedure described Section 3.2.1.1. The initial core measurements and assumed properties can be found in Table A.3.1.

The initial gas permeability was calculated using methane at 155°F. Methane was flowed through the core using five flow rates and the pressure drop across the core for each flow rate was recorded. Using this data, the fluid properties and accounting for non-Darcy effects the calculated gas permeability was 113 md. Table A.3.2 summarizes the flood conditions and fluid properties and Table A. 3.3 shows the results. Figure A. 3.1 shows the pressure drop measured across the core during the methane flood.

The initial gas permeability at initial water saturation was calculated next. Using synthetic brine 1 (25,000 ppm NaCl) an initial water saturation of 20% was established. This was done by applying vacuum to the core first and then injecting 3.3 ml of brine. The core was shut in for 1 hour, allowing the brine to distribute through the core. Methane at 155°F was then flowed through the core using five flow rates and the pressure drop across the core for each flow rate was recorded. The calculated gas permeability

was 75 md. The flood conditions and results are shown in Table A.3.4 and Table A.3.5 respectively. Figure A. 3.2 shows the pressure drop measured across the core during the methane flood at S_{wi} .

Synthetic volatile oil mixture 2 (Table 3.3) was used for the two-phase flow measurements. The mixture was allowed a minimum of 12 hours to equilibrate to a single phase at 4200 psi and 155°F. The initial flood was conducted with the upstream backpressure regulator (BPR-1) set at 4436 psi and the downstream back pressure regulator (BPR-2) set at 994 psi. Volatile oil was injected at a total core flow rate of 460 cc/hr and 920 cc/hr. Table A.3.6 gives the fluid properties of the synthetic fluid calculated using the Peng-Robinson EOS at the flowing core pressure. Figure A. 3.3 shows the pressure drop measured across the core during the initial two-phase volatile oil flood.

The core was then treated using chemical treatment 1 (Table 4.15). The solution was heated for at least 3 hours at 155°F. BPR1 was kept at 994 psi. The core was flooded with approximately 23 pore volumes of the treatment solution at a flow rate of 120 cc/hr. The core was then shut in for 15 hours. Figure A.3.4 shows the measured pressure drop across the core during the treatment flood.

Post-treatment two-phase volatile oil flood was conducted under the same conditions as the initial two-phase flow. Figure A.3.5 shows the pressure drop measured across the core during the post-treatment two-phase volatile oil flood. An improvement factor of 1.4 was observed the high flow rate but not measurement was taken for the low flow rate. Thus, two more volatile oil floods were performed to observe the durability of the treatment and measure improvement factor for low and high flow rate. For floods 2 and 3 the improvement factor remained almost constant at 1.4 and 1.3 for low and high

flow rate respectively. Figure A.3.6 and Figure A.3.7 show the pressure drop across the core for post-treatment volatile oil flood 2 and 3 respectively.

The final gas permeability was calculated using the procedure for the initial gas permeability using methane at 155°F. The calculated gas permeability was 98 md. The flood conditions and results are shown in Table A.2.7, Table A.3.7 and Table A.3.8 respectively. Figure A.2.8, Figure A.3.8 shows the pressure drop measured across the core during the final methane flood.

For every two-phase volatile oil flood, oil and gas relative permeabilities k_{rg} and k_{ro} were calculated using the measured pressure drop across the core under steady state conditions and then improvement factors were measured. Table A.3.9 summarizes the experimental results.

Table A.3.1 Core properties (Exp #146)

<i>Length, in</i>	7.962
<i>Diameter, in</i>	0.996
<i>Mass Core, gr</i>	225.77
<i>Grain Density, gr/cc</i>	2.65
<i>Porosity (ϕ)</i>	16.19 %

Table A.3.2 Fluid properties and conditions for initial gas permeability (Exp #146)

		<i>Density, gr/cc</i>
<i>Gas</i>	Methane	
<i>Temperature, °F</i>	155	
<i>BPR 1-pressure, psi</i>	3123	0.1305
<i>BPR 2-pressure, psi</i>	994	4.14E-02
<i>Gas Viscosity, cp</i>	0.0138	

Table A. 3.3 Initial methane flood results (Exp #146)

<i>q_{core}, cc/hr</i>	<i>ΔP, psi</i>	<i>k_g, md</i>
1891	4.000	107.17
2522	5.490	104.11
3152	7.000	102.06
3783	8.600	99.69
4728	11.050	96.98
<i>Corrected Permeability (k_g), md</i>		113.3

Table A.3.4 Fluid properties and conditions for methane gas permeability at S_{wi} (Exp #146)

		<i>Density, gr/cc</i>
<i>Gas</i>	Methane	
<i>Temperature, °F</i>	155	
<i>BPR 1-pressure, psi</i>	3123	0.1305
<i>BPR 2-pressure, psi</i>	994	4.14E-02
<i>Gas Viscosity, cp</i>	0.0138	

Table A.3.5 Methane flood results at S_{wi} (Exp #146)

q_{core} , cc/hr	ΔP , psi	k_g , md
1891	6.200	69.14
2522	8.480	67.40
3152	10.850	65.85
3783	13.400	63.98
4729	17.400	61.59
Corrected Permeability (k_g), md		75.1

Table A.3.6 Volatile oil properties at BPR-1 and BPR-2 pressures (Exp #146)

BPR 1-pressure, psi	4436	
BPR 2- pressure, psi	994	
Density at BPR 1-pressure, gr/cc	0.3717	
Properties at BPR 2-pressure, psi	Gas Phase	Oil Phase
Density, gr/cc	0.0546	0.5902
Viscosity (μ), cp	0.0133	0.1769
Volume Fraction	0.9133	0.0867
IFT, dyne/cm	7.361	

Table A.3.7 Fluid properties and conditions for final gas permeability (Exp #146)

		Density, gr/cc
Gas	Methane	
Temperature, °F	155	
BPR 1-pressure, psi	3323	0.1377
BPR 2-pressure, psi	1090	0.0456
Gas Viscosity, cp	0.014	

Table A.3.8 Final methane flood results (Exp #146)

q_{core} , cc/hr	ΔP , psi	k_g , md
1812	2.790	149.96
2416	3.800	146.80
3020	4.800	145.27
3624	5.850	143.04
4530	7.500	138.87
Corrected Permeability (k_g), md		155.43

Table A.3.9 Pre and post-treatment volatile oil flood results and measured improvement factors (Exp #146)

	Exp# 146	
$q_{g\text{tot core, cc/hr}}$	460	920
$q_g, \text{cc/hr}$	420	840
$q_o, \text{cc/hr}$	40	80
<i>PVT Ratio</i>	0.79	
<i>Viscosity Ratio μ_g/μ_o</i>	0.06	
<i>Capillary Nc</i>	1.35E-05	2.36E-05
k_{rg} Before Treatment	0.031	0.036
k_{ro} Before Treatment	0.039	0.045
k_{rg} After Treatment	0.046	0.050
k_{ro} After Treatment	0.065	0.070
<i>Initial Improvement Factor</i>	*	1.4
<i>PV of Vol Oil Injected</i>	~600	
<i>Final Improvement Factor</i>	1.4	1.3

* Data not measured

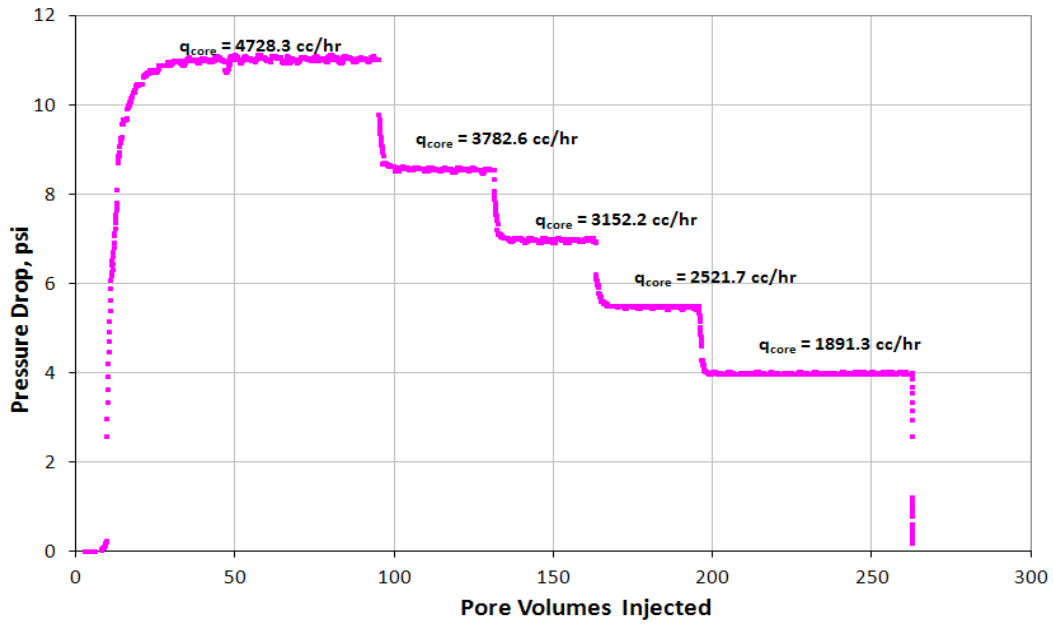


Figure A. 3.1 Pressure drop across the core during the initial methane flood at 155°F (Exp #146)

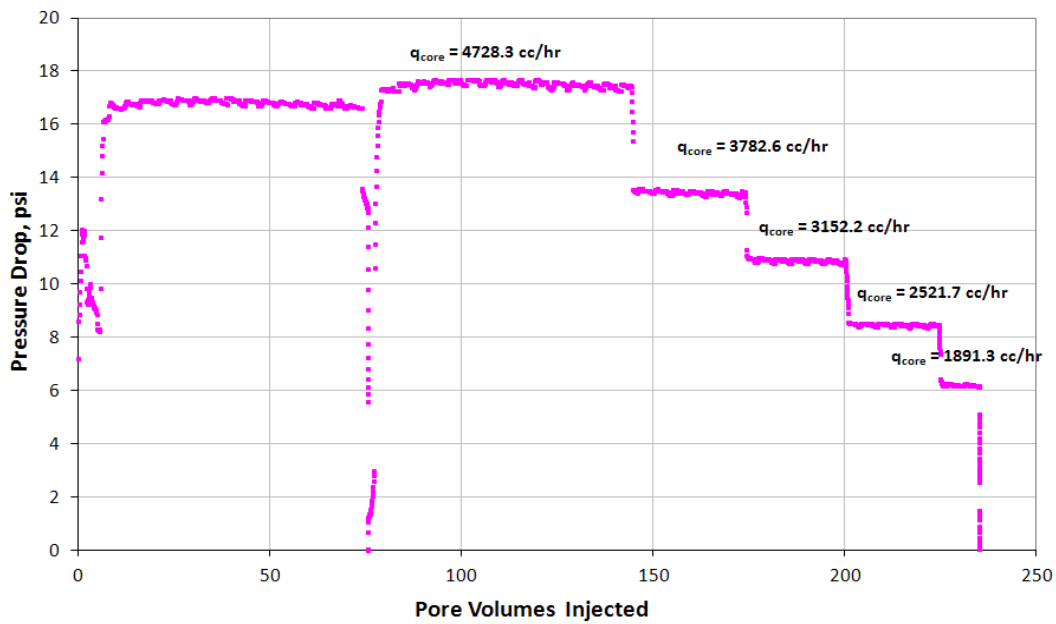


Figure A. 3.2 Pressure drop across the core during the methane flood at S_{wi} of 20% (Exp #146)

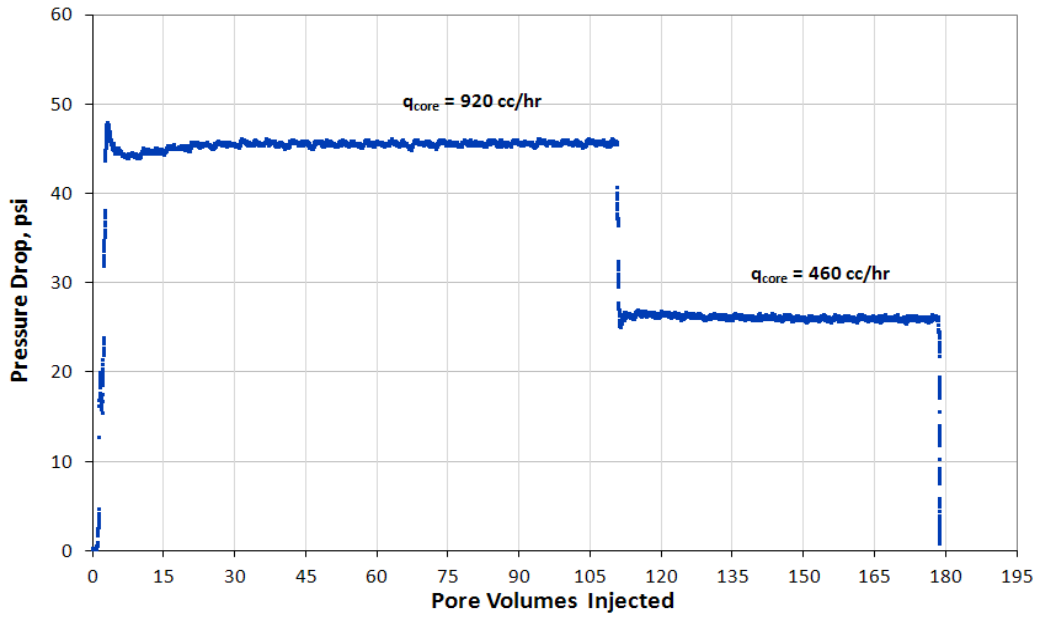


Figure A. 3.3 Pressure drop across the core during the pre-treatment two-phase volatile oil flood (Exp #146)

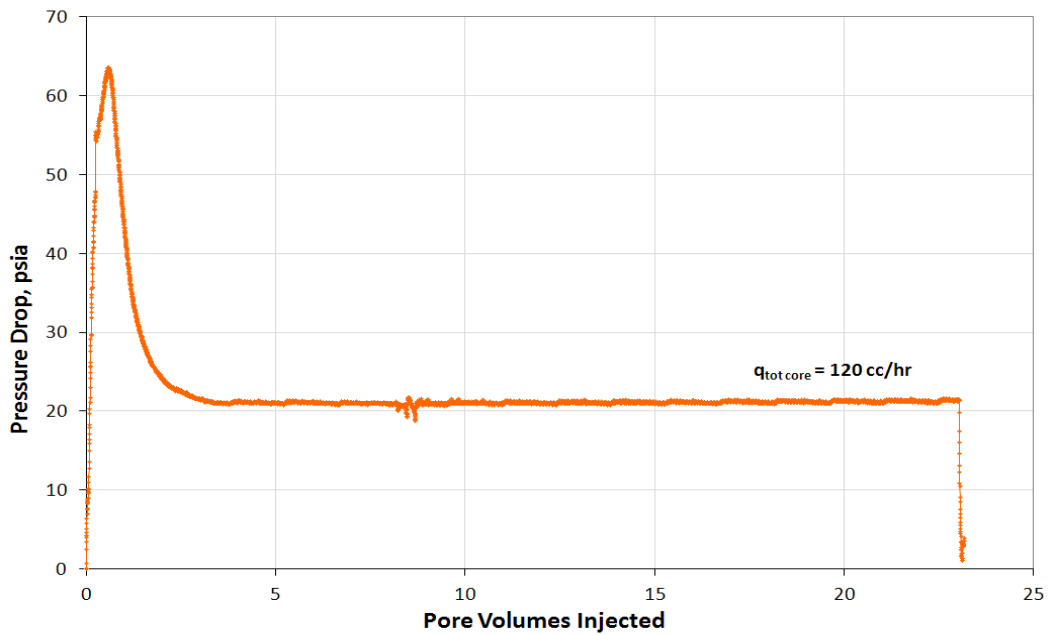


Figure A.3.4 Pressure drop across the core during injection of chemical treatment 1 (Exp # 146)

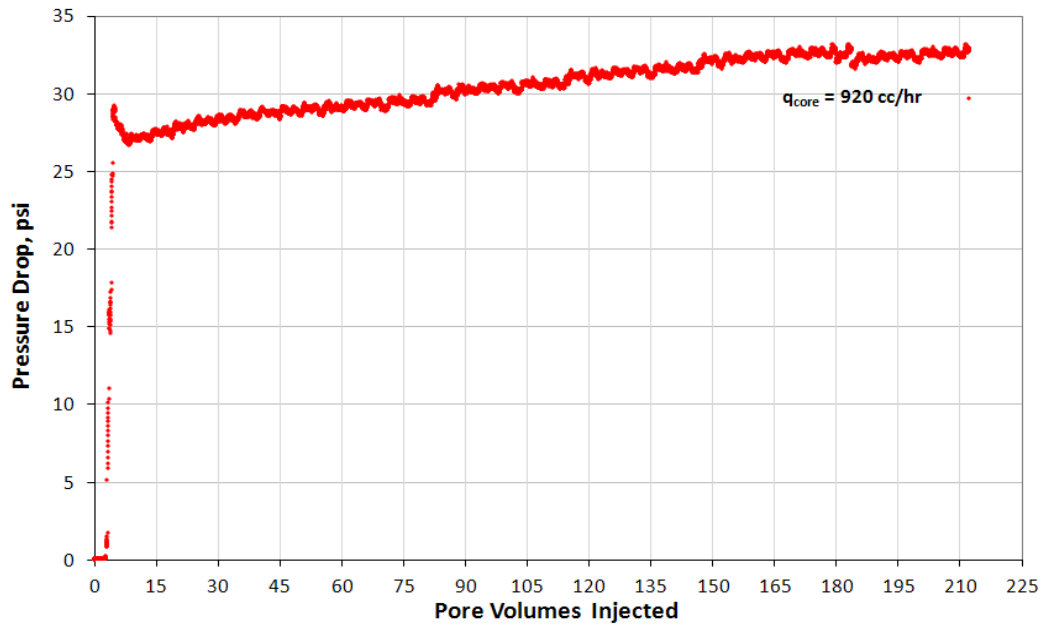


Figure A.3.5 Pressure drop across the core during the post-treatment two-phase volatile oil flood 1 (Exp #146)

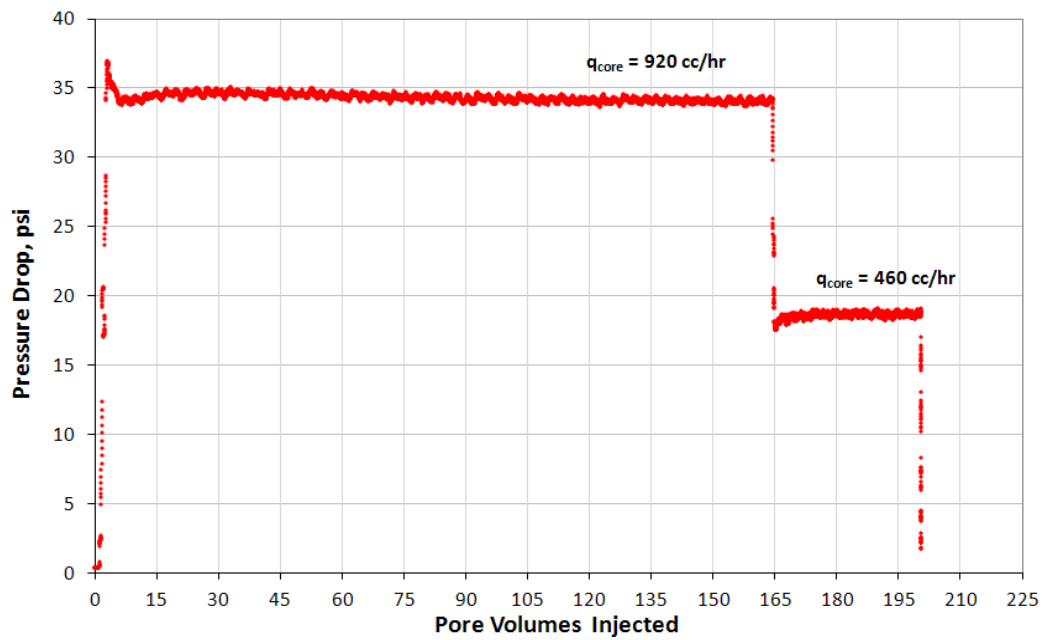


Figure A.3.6 Pressure drop across the core during the post-treatment two-phase volatile oil flood 2 (Exp #146)

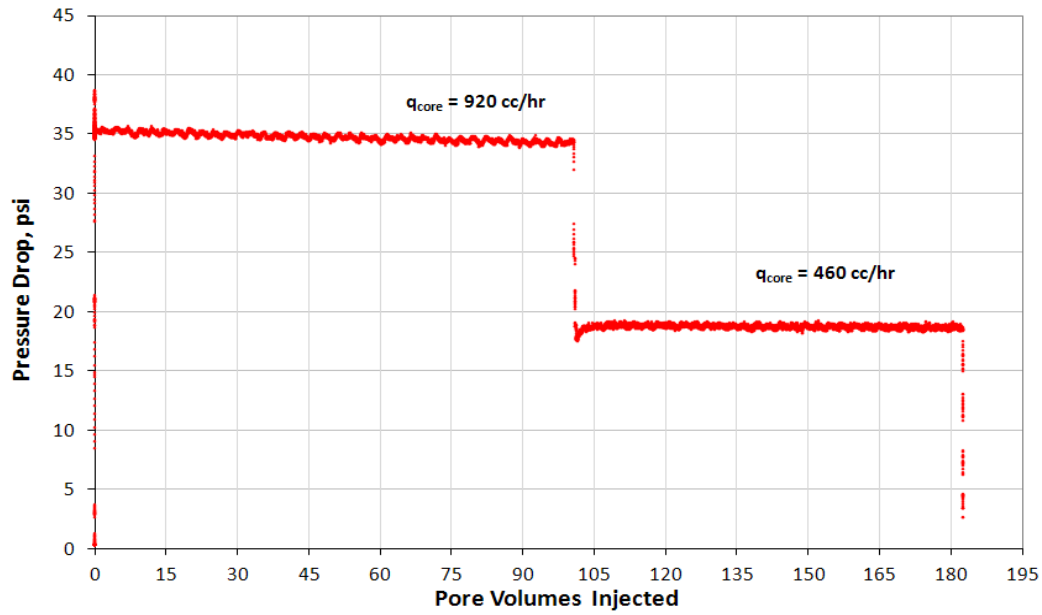


Figure A.3.7 Pressure drop across the core during the post-treatment two-phase volatile oil flood 3 (Exp #146)

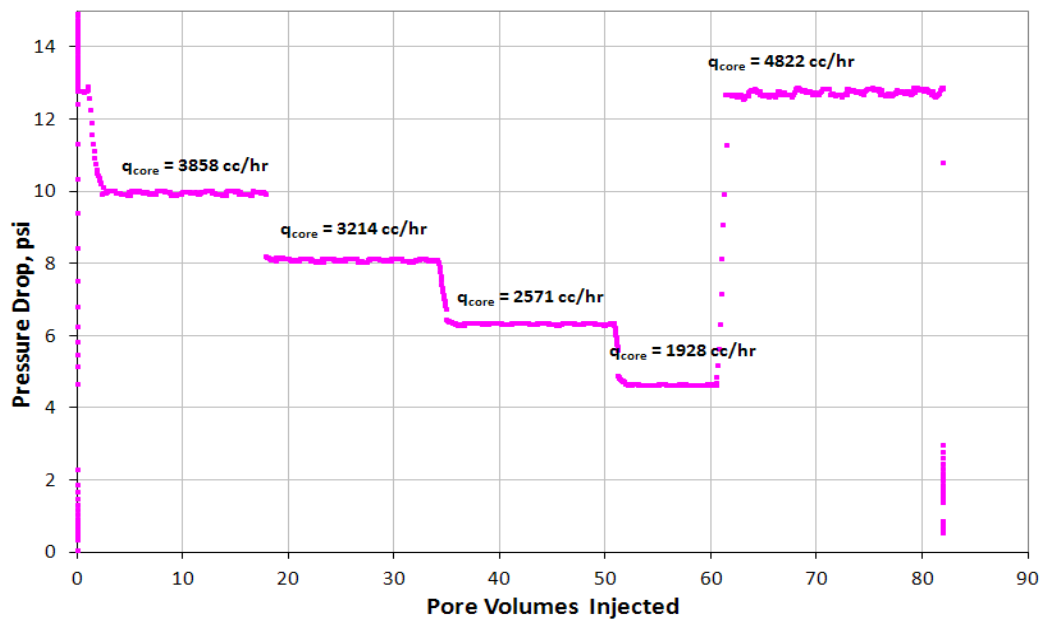


Figure A.3.8 Pressure drop across the core during the final methane flood at 155°F (Exp #146)

Appendix A.4: EXPERIMENT#148

Objective:

The objective of this experiment was to investigate the effectiveness of chemical treatment 2 using non-ionic fluoro-surfactant L-20294 in improving the oil and gas relative permeability at different PVT ratios and capillary numbers. This was done for a volatile oil mixture below the bubble point pressure on a Berea sandstone core and in the presence of initial water saturation. The experiment was performed at 155°F.

Experimental Procedure and Results:

A Berea core was prepared for the experiment following the standard procedure described Section 3.2.1.1. The initial core measurements and assumed properties can be found in Table A.4.1.

The initial gas permeability was calculated using methane at 155°F. Methane was flowed through the core using five flow rates and the pressure drop across the core for each flow rate was recorded. Using this data, the fluid properties and accounting for non-Darcy effects the calculated gas permeability was 144 md. Table A.4.2 summarizes the flood conditions and fluid properties and Table A.4.3 shows the results. Figure A.4.1 shows the pressure drop measured across the core during the methane flood.

The initial gas permeability at initial water saturation was calculated next. Using synthetic brine 1 (25,000 ppm NaCl) an initial water saturation of 20% was established. This was done by applying vacuum to the core first and then injecting 3.5 ml of brine. The core was shut in for 1 hour, allowing the brine to distribute through the core. Methane at 155°F was then flowed through the core using five flow rates and the pressure drop across the core for each flow rate was recorded. The calculated gas permeability

was 112 md. The flood conditions and results are shown in Table A.4.4 and Table A.4.5 respectively. Figure A.4.2 shows the pressure drop measured across the core during the methane flood at S_{wi} .

Synthetic volatile oil mixture 2 (Table 3.3) was used for the two-phase flow measurements. The mixture was allowed a minimum of 12 hours to equilibrate to a single phase at 4200 psi and 155°F. The initial flood was conducted with the upstream backpressure regulator (BPR-1) set at 4297 psi and the downstream back pressure regulator (BPR-2) set at 900 psi. Volatile oil was injected at an upstream BPR-1 flow rate of 150 cc/hr (this is for volatile oil at single liquid phase). Once steady state was observed the pressure drop across the core was measured. This procedure was repeated for BPR-2 pressures of 1600 psi, 2500 psi, 3100 psi and 3,500 psi. This allowed having different PVT ratios and capillary numbers. The PVT ratio ranged from 0.77 to 0.35 and capillary number from 7×10^{-6} to 1.1×10^{-3} . Table A.3.6 gives the fluid properties of the synthetic fluid calculated using the Peng-Robinson EOS at the flowing core pressures. Figure A.4.3 shows the pressure drop measured across the core during the initial two-phase volatile oil flood for the different BPR-2 pressures.

The core was then treated using chemical treatment 2 (Table 4.15). The solution was heated for at least 3 hours at 155°F. BPR1 was set at 695 psi. The core was flooded with 20 pore volumes of the treatment solution at a flow rate of 120 cc/hr. The core was then shut in for 15 hours. Figure A.4.4 shows the measured pressure drop across the core during the treatment flood.

Post-treatment two-phase volatile oil flood was conducted under the same conditions as the initial two-phase flow. Figure A.4.5 shows the pressure drop measured across the core during the post-treatment two-phase volatile oil flood. Improvement factor varied from 2.4 to 0.9 as the BPR-2 pressure increased. One more volatile oil

flood was performed to observe the durability of the treatment. Figure A.4.6 shows the pressure drop across the core for post-treatment volatile oil flood 2.

The final gas permeability was calculated following the procedure for the initial gas permeability using methane at 155°F. The calculated gas permeability was 127 md. The flood conditions and results are shown in Table A.2.7, Table A.4.7 and Table A.3.8 respectively. Figure A.2.8, Figure A.4.7 shows the pressure drop measured across the core during the final methane flood.

For every two-phase volatile oil flood, oil and gas relative permeabilities k_{rg} and k_{ro} were calculated using the measured pressure drop across the core under steady state conditions and then improvement factors were measured. Table A.3.9 summarizes the experimental results.

Table A.4.1 Core properties (Exp #148)

<i>Length, in</i>	7.948
<i>Diameter, in</i>	0.996
<i>Mass Core, gr</i>	221.95
<i>Grain Density, gr/cc</i>	2.65
<i>Porosity (ϕ)</i>	17.46 %

Table A.4.2 Fluid properties and conditions for initial gas permeability (Exp #148)

		<i>Density, gr/cc</i>
<i>Gas</i>	Methane	
<i>Temperature, °F</i>	155	
<i>BPR 1-pressure, psi</i>	4125	0.164
<i>BPR 2-pressure, psi</i>	2010	8.59E-02
<i>Gas Viscosity, cp</i>	0.0159	

Table A.4.3 Initial methane flood results (Exp #148)

<i>q_{core}, cc/hr</i>	<i>ΔP, psi</i>	<i>k_g, md</i>
1146	2.150	138.89
1527	2.880	138.25
1909	3.650	136.35
2291	4.470	133.61
2864	5.670	131.66
<i>Corrected Permeability (k_g), md</i>		144.4

Table A.4.4 Fluid properties and conditions for methane gas permeability at S_{wi} (Exp #148)

		<i>Density, gr/cc</i>
<i>Gas</i>	Methane	
<i>Temperature, °F</i>	155	
<i>BPR 1-pressure, psi</i>	3170	0.1322
<i>BPR 2-pressure, psi</i>	1050	4.39E-02
<i>Gas Viscosity, cp</i>	0.0139	

Table A.4.5 Methane flood results at S_{wi} (Exp #148)

q_{core} , cc/hr	ΔP , psi	k_g , md
1807	4.040	101.92
2409	5.500	99.82
3011	7.210	95.18
3614	8.860	92.95
4517	11.550	89.13
Corrected Permeability (k_g), md		112.2

Table A.4.6 Volatile oil properties at BPR-1 and BPR-2 pressures (Exp #148)

<i>BPR 1-pressure, psi</i>		4297								
<i>BPR 2- pressure, psi</i>		900	1600	2500	3100	3500				
<i>Density at BPR 1-pressure, gr/cc</i>		0.3677								
Properties of BPR 2-pressure, psi										
	900		1600		2500		3100		3500	
	Gas Phase	Oil Phase								
Density, gr/cc	0.0491	0.5979	0.0931	0.5501	0.1611	0.4861	0.22	0.4323	0.2831	0.372
Viscosity (μ), cp	0.0138	0.2181	0.0159	0.1607	0.0209	0.1107	0.0275	0.0825	0.0379	0.060
Volume Fraction	0.9242	0.0758	0.8369	0.1631	0.6974	0.3026	0.5714	0.4286	0.3609	0.639
IFT, dyne/cm	8.129		3.76		0.88		0.148		0.004	

Table A.4.7 Fluid properties and conditions for final gas permeability (Exp #148)

		<i>Density, gr/cc</i>
<i>Gas</i>	Methane	
<i>Temperature, °F</i>	155	
<i>BPR 1-pressure, psi</i>	4151	0.1648
<i>BPR 2-pressure, psi</i>	2023	0.0865
<i>Gas Viscosity, cp</i>	0.0159	

Table A.4.8 Final methane flood results (Exp #148)

$q_{core}, cc/hr$	$\Delta P, psi$	k_g, md
1143	2.530	117.78
1524	3.520	112.88
1905	4.580	108.44
2286	5.650	105.48
2858	7.350	101.36
<i>Corrected Permeability (k_g), md</i>		127.81

Table A.4.9 Pre and post-treatment volatile oil flood results and measured improvement factors (Exp #148)

	Exp# 148				
<i>BPR 2- pressure, psi</i>	900	1600	2500	3100	3500
$q_{tot\ core}, cc/hr$	608	329	213	177	162
$q_g, cc/hr$	562	275	148	101	58
$q_o, cc/hr$	46	54	64	76	104
<i>PVT Ratio</i>	0.77	0.51	0.44	0.44	0.35
<i>Viscosity Ratio μ_g/μ_o</i>	0.06	0.10	0.19	0.33	0.63
<i>Capillary Nc</i>	1.73E-05	1.12E-05	3.51E-05	4.11E-05	1.02E-03
k_{rg} Before Treatment	0.030	0.057	0.055	0.253	0.300
k_{ro} Before Treatment	0.040	0.113	0.127	0.570	0.846
k_{rg} After Treatment flood 1	0.075	0.076	0.051	0.205	0.272
k_{ro} After Treatment flood 1	0.097	0.150	0.117	0.460	0.769
k_{rg} After Treatment flood 2	0.040	0.082	0.059	0.185	0.258
k_{ro} After Treatment flood 2	0.051	0.162	0.136	0.416	0.728
<i>Initial Improvement Factor</i>	2.5	1.3	0.9	0.8	0.9
<i>PV of Vol Oil Injected</i>	~300				
<i>Final Improvement Factor</i>	1.3	1.4	1.1	0.7	0.9

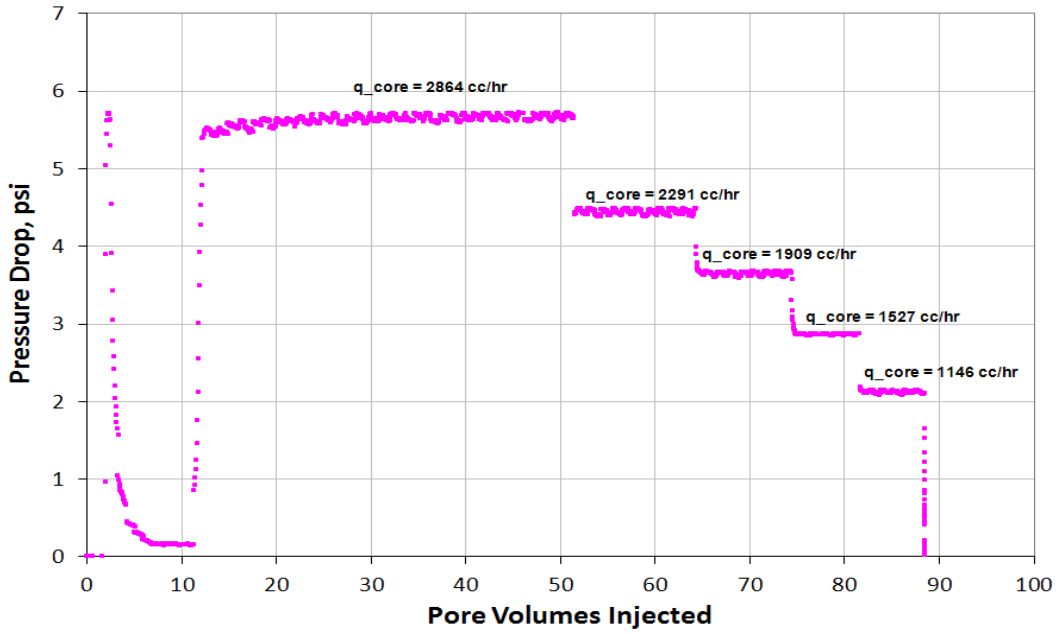


Figure A.4.1 Pressure drop across the core during the initial methane flood at 155°F (Exp #148)

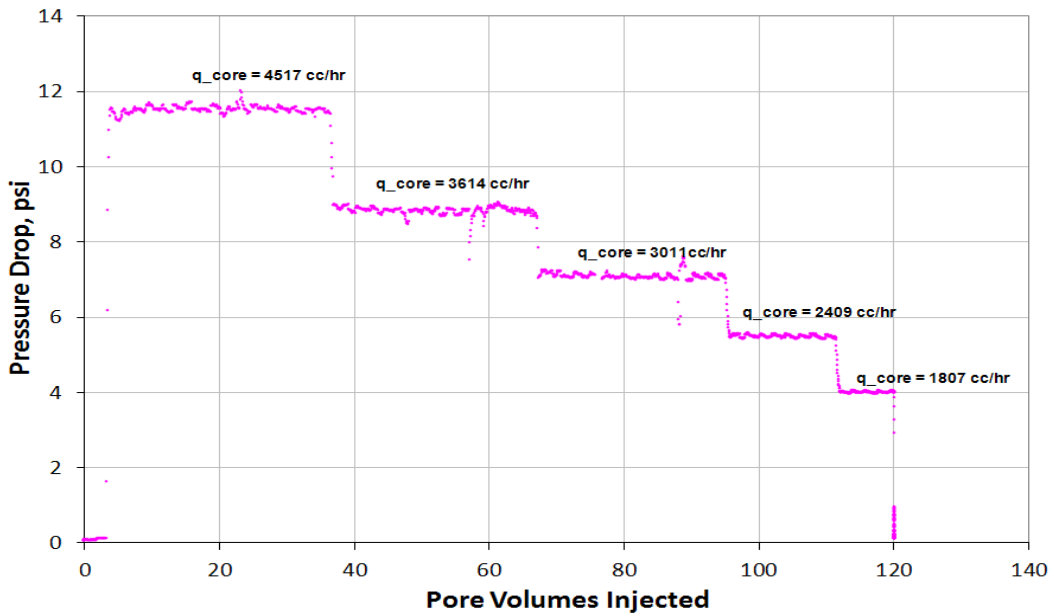


Figure A.4.2 Pressure drop across the core during the methane flood at S_{wi} of 20% (Exp #148)

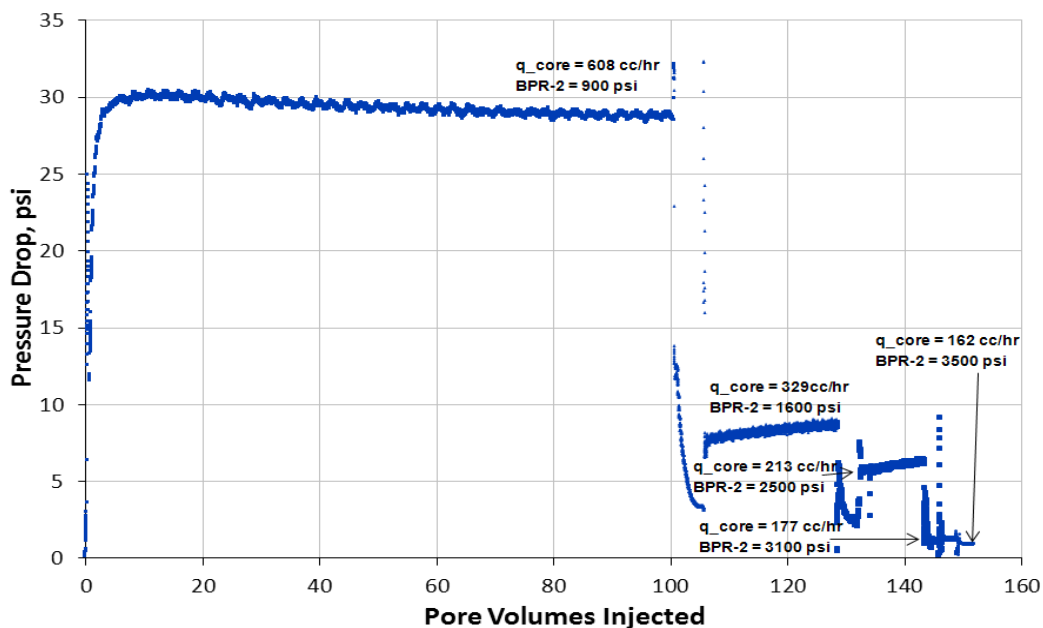


Figure A.4.3 Pressure drop across the core during the pre-treatment two-phase volatile oil flood (Exp #148)

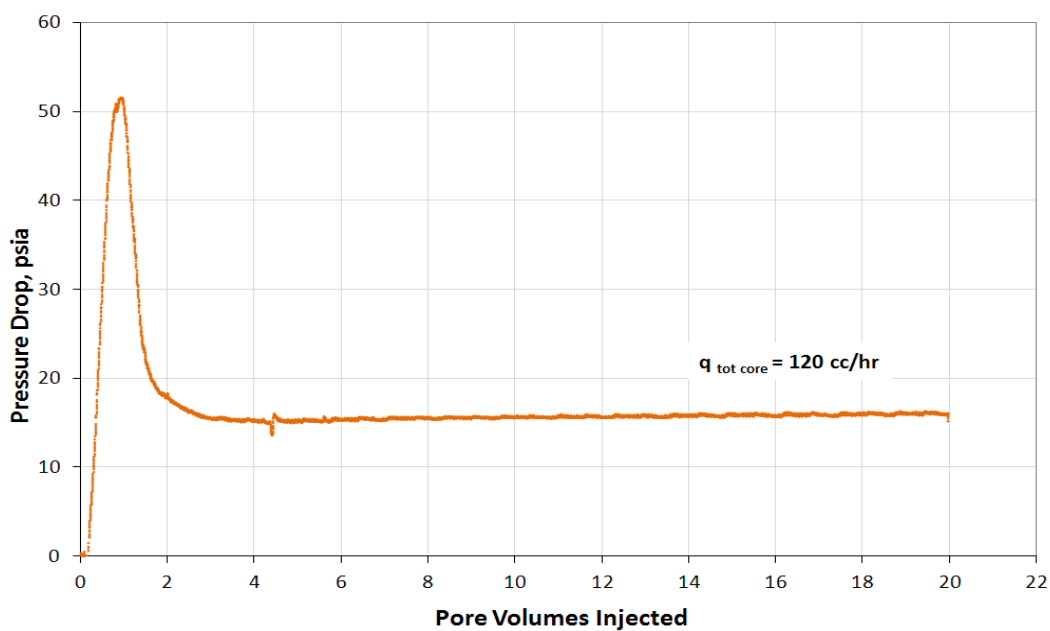


Figure A.4.4 Pressure drop across the core during injection of chemical treatment 2 (Exp # 148)

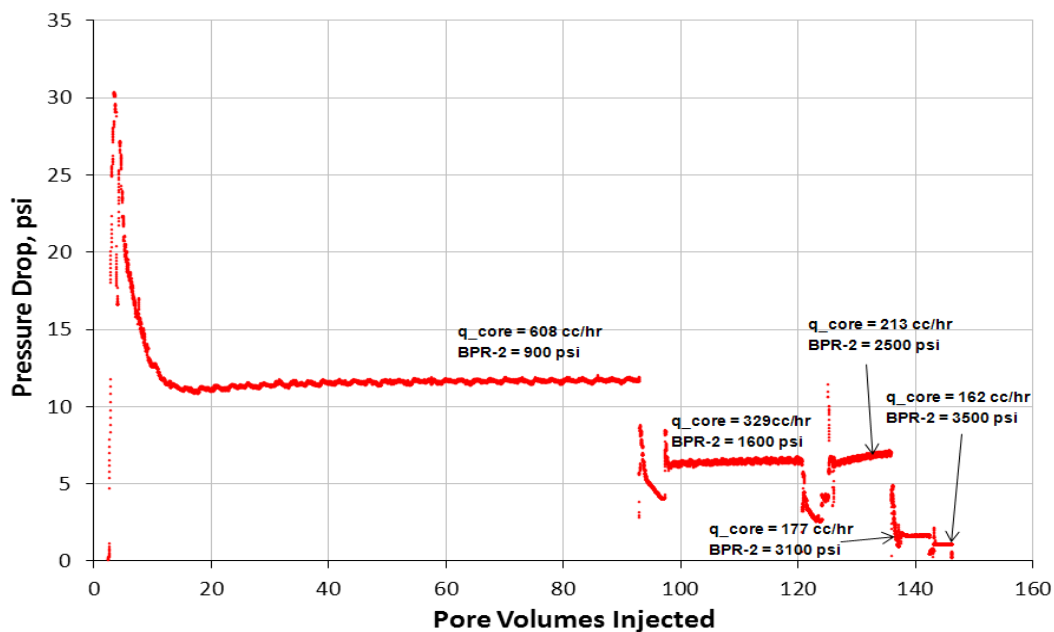


Figure A.4.5 Pressure drop across the core during the post-treatment two-phase volatile oil flood 1 (Exp #148)

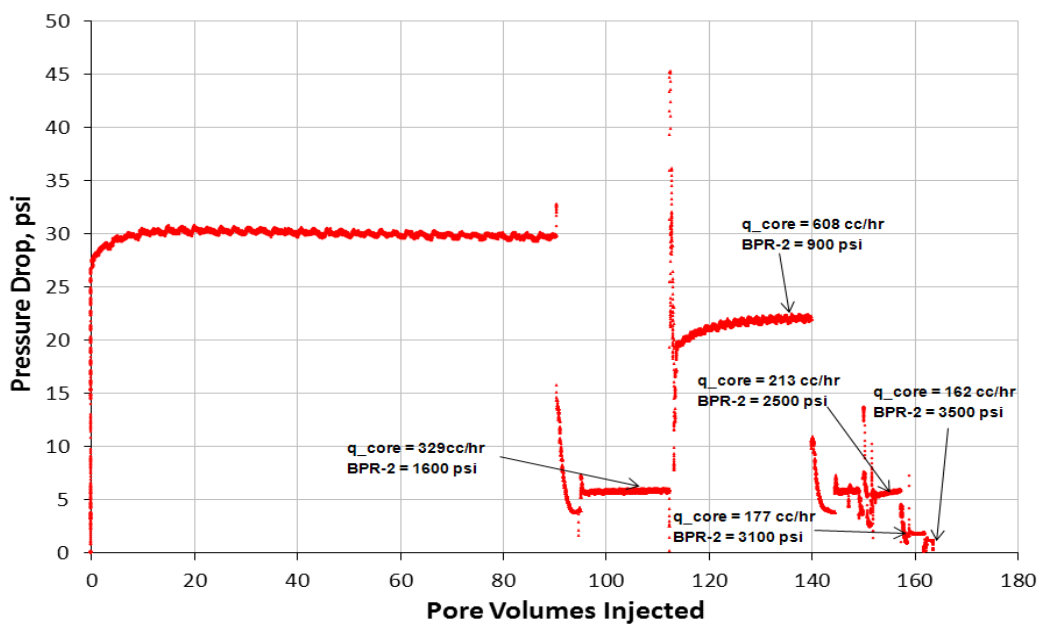


Figure A.4.6 Pressure drop across the core during the post-treatment two-phase volatile oil flood 2 (Exp #148)

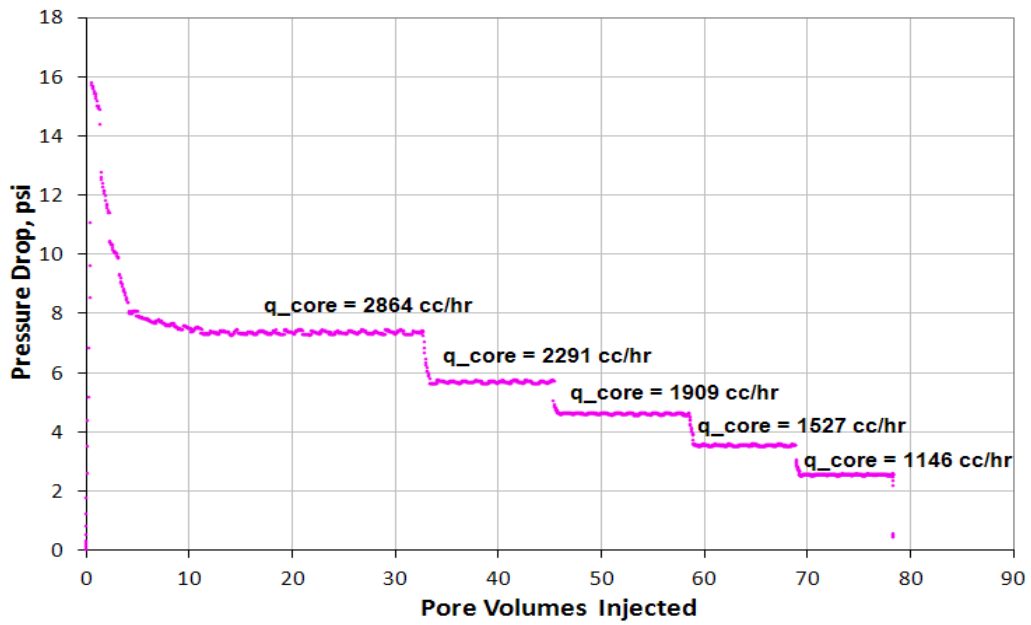


Figure A.4.7 Pressure drop across the core during the final methane flood at 155°F (Exp #148)

Appendix A.5: EXPERIMENT#158

Objective:

The objective of this experiment was to investigate the effectiveness of chemical treatment 3 using non-ionic fluoro-surfactant L-18961 in improving the oil and gas relative permeability at different PVT ratios and capillary numbers. This was done for a volatile oil mixture below the bubble point pressure on a Berea sandstone core and in the presence of initial water saturation. The experiment was performed at 155°F.

Experimental Procedure and Results:

A Berea core was prepared for the experiment following the standard procedure described Section 3.2.1.1. The initial core measurements and assumed properties can be found in Table A.5.1.

The initial gas permeability was calculated using methane at 155°F. Methane was flowed through the core using five flow rates and the pressure drop across the core for each flow rate was recorded. Using this data, the fluid properties and accounting for non-Darcy effects the calculated gas permeability was 217 md. Table A.5.2 summarizes the flood conditions and fluid properties and Table A.5.3 shows the results. Figure A.5.1 shows the pressure drop measured across the core during the methane flood.

The initial gas permeability at initial water saturation was calculated next. Using synthetic brine 1 (25,000 ppm NaCl) an initial water saturation of 20% was established. This was done by applying vacuum to the core first and then injecting 3.8 ml of brine. The core was shut in for 1 hour, allowing the brine to distribute through the core. Methane at 155°F was then flowed through the core using five flow rates and the pressure drop across the core for each flow rate was recorded. The calculated gas permeability

was 166 md. The flood conditions and results are shown in Table A.5.4 and Table A.4.5 respectively. Figure A.4.2 shows the pressure drop measured across the core during the methane flood at S_{wi} .

Synthetic volatile oil mixture 2 (Table 3.3) was used for the two-phase flow measurements. The mixture was allowed a minimum of 12 hours to equilibrate to a single phase at 4200 psi and 155°F. The initial flood was conducted with the upstream backpressure regulator (BPR-1) set at 4262 psi and the downstream back pressure regulator (BPR-2) set at 800 psi. Volatile oil was injected at an upstream BPR-1 flow rate of 150 cc/hr (this is for volatile oil at single liquid phase). Once steady state was observed the pressure drop across the core was measured. This procedure was repeated for BPR-2 pressures of 1,500 psi, 2,200 psi and 2,900 psi. This allowed having different PVT ratios and capillary numbers. The PVT ratio ranged from 0.85 to 0.44 and capillary number from 1.9×10^{-5} to 5.3×10^{-5} . Table A.3.6 gives the fluid properties of the synthetic fluid calculated using the Peng-Robinson EOS at the flowing core pressures. Figure A.4.3 shows the pressure drop measured across the core during the initial two-phase volatile oil flood for the different BPR-2 pressures.

The core was then treated using chemical treatment 3 (Table 4.15). The solution was heated for at least 3 hours at 155°F. BPR1 was set at 2200 psi. The core was flooded with 19 pore volumes of the treatment solution at a flow rate of 120 cc/hr. The core was then shut in for 15 hour. Figure A.4.4 shows the measured pressure drop across the core during the treatment flood.

Post-treatment two-phase volatile oil flood was conducted under the same conditions as the initial two-phase flow. Figure A.4.5 shows the pressure drop measured across the core during the post-treatment two-phase volatile oil flood. Improvement factor varied from 1.9 to 0.7 as the BPR-2 pressure increased.

The final gas permeability was calculated following the procedure for the initial gas permeability using methane at 155°F. The calculated gas permeability was 257 md. The flood conditions and results are shown in Table A.2.7, Table A.4.7 and Table A.3.8 respectively. Figure A.2.8 For every two-phase volatile oil flood, oil and gas relative permeabilities k_{rg} and k_{ro} were calculated using the measured pressure drop across the core under steady state conditions and then improvement factors were measured. Table A.3.9 summarizes the experimental results.

Table A.5.1 Core properties (Exp #158)

<i>Length, in</i>	7.93
<i>Diameter, in</i>	0.996
<i>Mass Core, gr</i>	218.58
<i>Grain Density, gr/cc</i>	2.65
<i>Porosity (ϕ)</i>	18.53 %

Table A.5.2 Fluid properties and conditions for initial gas permeability (Exp #158)

		<i>Density, gr/cc</i>
<i>Gas</i>	Methane	
<i>Temperature, °F</i>	155	
<i>BPR 1-pressure, psi</i>	4263	0.168
<i>BPR 2-pressure, psi</i>	1018	4.25E-02
<i>Gas Viscosity, cp</i>	0.0139	

Table A.5.3 Initial methane flood results (Exp #158)

<i>q_{core}, cc/hr</i>	<i>ΔP, psi</i>	<i>k_g, md</i>
2372	2.630	205.05
3162	3.600	199.73
3953	4.600	195.39
4744	5.640	191.23
5929	7.250	185.96
<i>Corrected Permeability (k_g), md</i>		216.9

Table A.5.4 Fluid properties and conditions for methane gas permeability at S_{wi} (Exp #158)

		<i>Density, gr/cc</i>
<i>Gas</i>	Methane	
<i>Temperature, °F</i>	155	
<i>BPR 1-pressure, psi</i>	4260	0.168
<i>BPR 2-pressure, psi</i>	1018	4.25E-02
<i>Gas Viscosity, cp</i>	0.0139	

Table A.5.5 Methane flood results at S_{wi} (Exp #158)

q_{core} , cc/hr	ΔP , psi	k_g , md
2372	3.830	140.80
3162	5.450	131.93
3953	7.100	126.59
4744	9.100	118.52
5929	12.00	112.35
Corrected Permeability (k_g), md		165.5

Table A.5.6 Volatile oil properties at BPR-1 and BPR-2 pressures (Exp #158)

BPR 1-pressure, psi		4262						
BPR 2- pressure, psi		801	1506	2205	2908			
Density at BPR 1-pressure, gr/cc		0.3668						
Properties of BPR 2-pressure, psi								
	801		1506		2205		2908	
	Gas Phase	Oil Phase						
Density, gr/cc	0.0433	0.605	0.0868	0.5564	0.1371	0.5082	0.199	0.4516
Viscosity (μ), cp	0.0136	0.2289	0.0155	0.167	0.0188	0.1254	0.0249	0.0915
Volume Fraction	0.9349	0.0651	0.8497	0.1503	0.7468	0.2532	0.6182	0.3818
IFT, dyne/cm	8.939		4.223		1.548		0.305	

Table A.5.7 Fluid properties and conditions for final gas permeability (Exp #158)

		Density, gr/cc
Gas	Methane	
Temperature, °F	155	
BPR 1-pressure, psi	4302	0.1693
BPR 2-pressure, psi	2014	0.0861
Gas Viscosity, cp	0.0159	

Table A.5.8 Final methane flood results (Exp #158)

q_{core} , cc/hr	ΔP , psi	k_g , md
1179.79	1.280	239.73
1573.05	1.780	229.85
1966.32	2.270	225.30
2359.58	2.800	219.18
2949.48	3.630	211.33
<i>Corrected Permeability (k_g), md</i>		256.91

Table A.5.9 Pre and post-treatment volatile oil flood results and measured improvement factors (Exp #158)

	Exp#158			
<i>BPR 2- pressure, psi</i>	801	1506	2205	2908
$q_{g_{tot\ core}}$, cc/hr	689	350	238	186
q_g , cc/hr	644	297	178	115
q_o , cc/hr	45	53	60	71
<i>PVT Ratio</i>	0.85	0.52	0.44	0.44
<i>Viscosity Ratio μ_g/μ_o</i>	0.06	0.09	0.15	0.27
<i>Capillary Nc</i>	1.87E-05	7.03E-06	1.47E-05	5.26E-05
k_{rg} Before Treatment	0.029	0.086	0.081	0.099
k_{ro} Before Treatment	0.034	0.163	0.184	0.224
k_{rg} After Treatment	0.054	0.078	0.076	0.070
k_{ro} After Treatment	0.063	0.149	0.173	0.158
<i>Initial Improvement Factor</i>	1.9	0.9	0.9	0.7
<i>PV of Vol Oil Injected</i>	~ 130			
<i>Final Improvement Factor</i>	*	*	*	*

* Data not measured

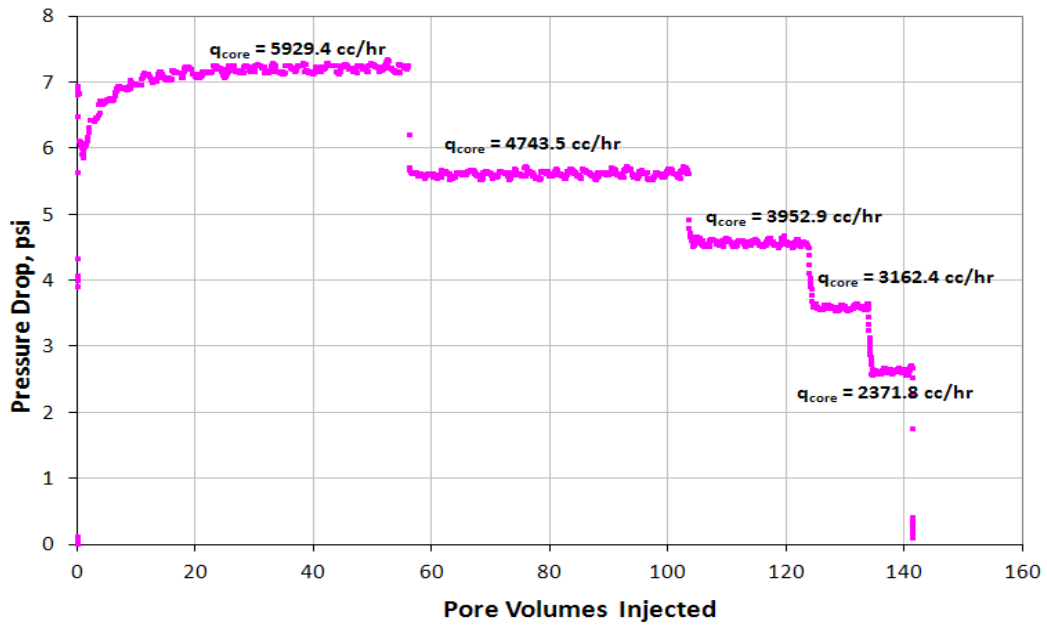


Figure A.5.1 Pressure drop across the core during the initial methane flood at 155°F (Exp #158)

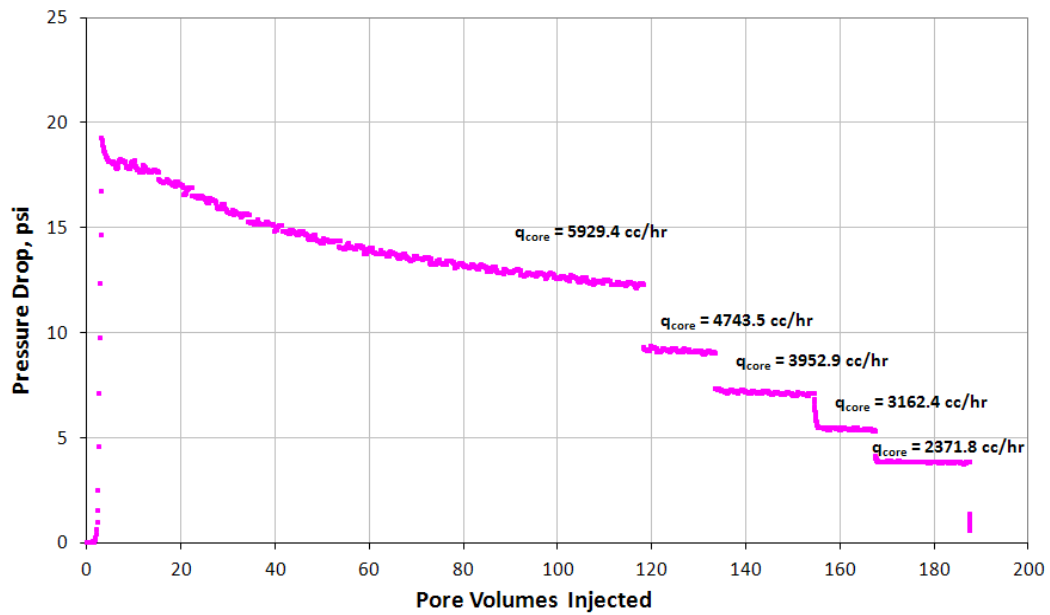


Figure A.5.2 Pressure drop across the core during the methane flood at S_{wi} of 20% (Exp #158)

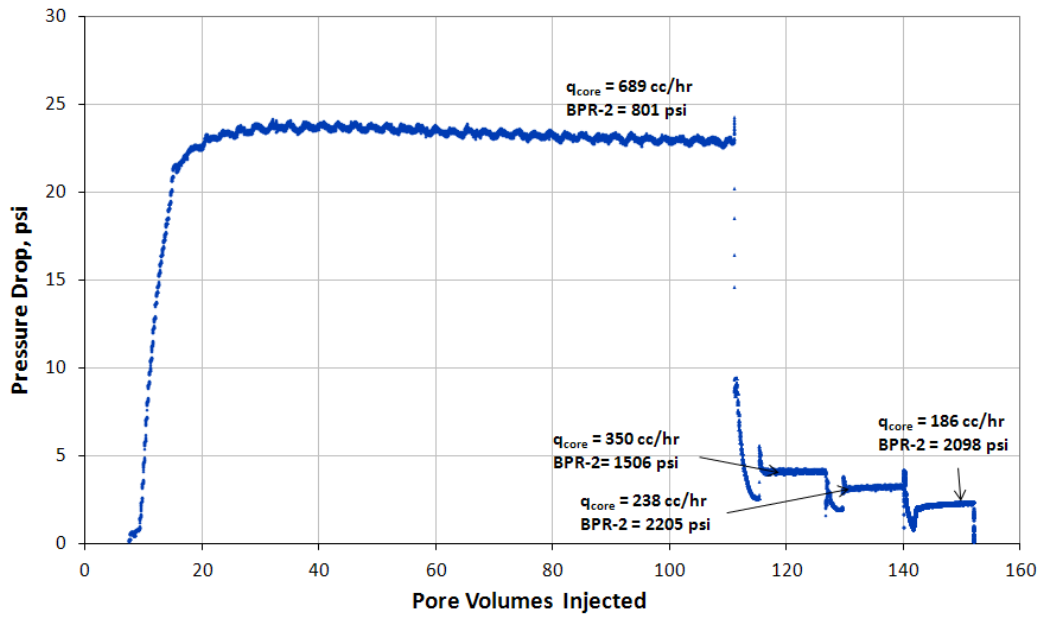


Figure A.5.3 Pressure drop across the core during the pre-treatment two-phase volatile oil flood (Exp #158)

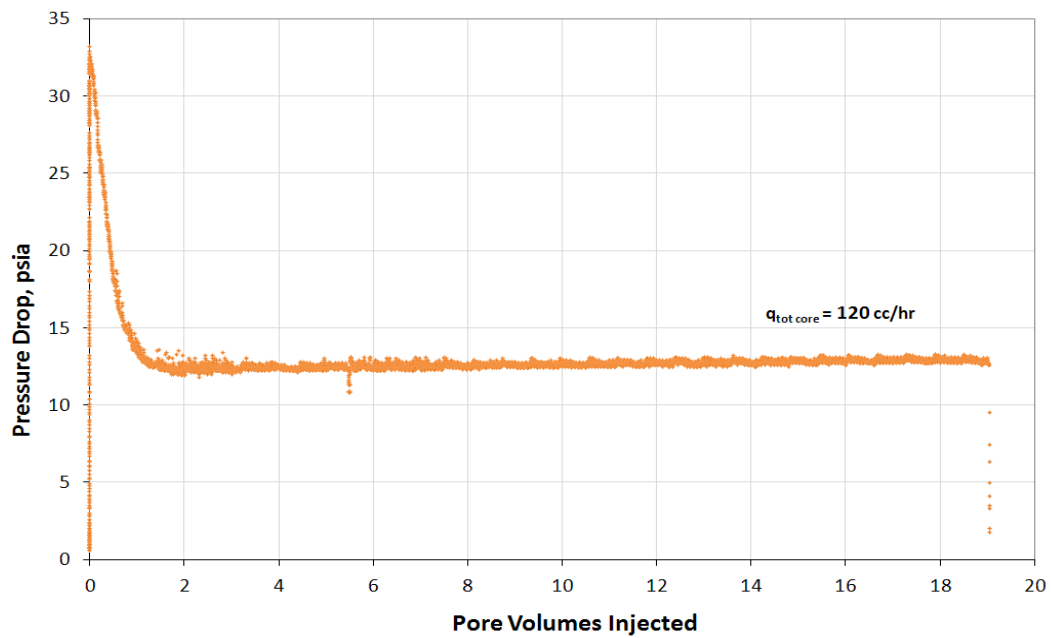


Figure A.5.4 Pressure drop across the core during injection of chemical treatment 3 (Exp #158)

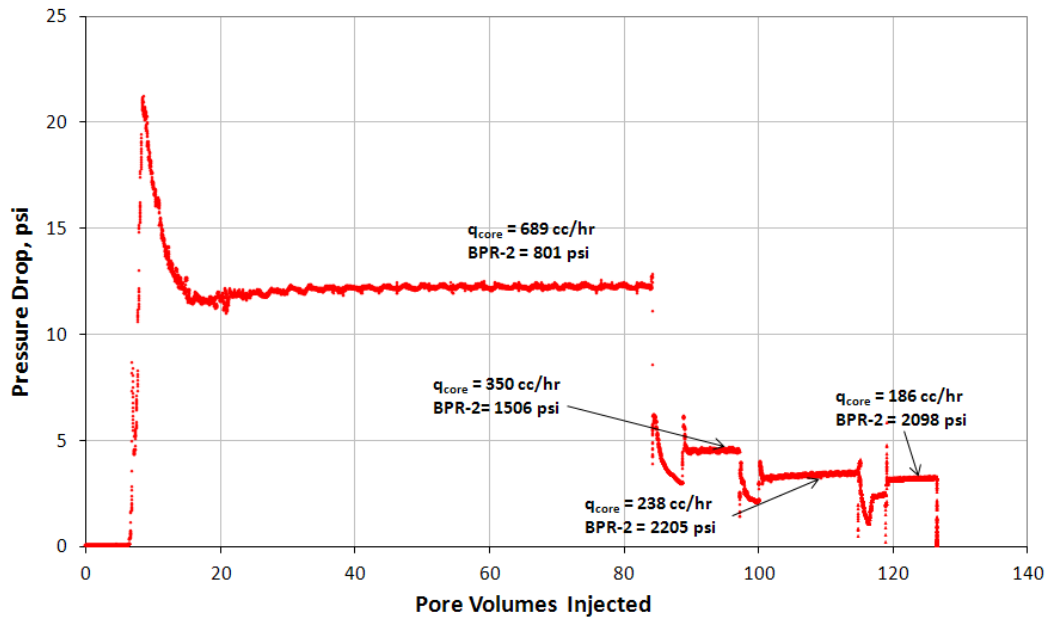


Figure A.5.5 Pressure drop across the core during the post-treatment two-phase volatile oil flood (Exp #158)

Appendix A.6: EXPERIMENT#176

Objective:

The objective of this experiment was to investigate the effectiveness of chemical treatment 3 using non-ionic fluoro-surfactant L-18961 in improving the oil and gas relative permeability at different PVT ratios and capillary numbers, and multiple treatment times. This was done for a volatile oil mixture below the bubble point pressure on a Berea sandstone core and in the presence of initial water saturation. The experiment was performed at 155°F.

Experimental Procedure and Results:

A Berea core was prepared for the experiment following the standard procedure described Section 3.2.1.1. The initial core measurements and assumed properties can be found in Table A.5.1.

The initial gas permeability was calculated using methane at 155°F. Methane was flowed through the core using five flow rates and the pressure drop across the core for each flow rate was recorded. Using this data, the fluid properties and accounting for non-Darcy effects the calculated gas permeability was 149 md. Table A.5.2 summarizes the flood conditions and fluid properties and Table A.5.3 shows the results. Figure A.6.1 shows the pressure drop measured across the core during the methane flood.

The initial gas permeability at initial water saturation was calculated next. Using synthetic brine 1 (25,000 ppm NaCl) an initial water saturation of 20% was established. This was done by applying vacuum to the core first and then injecting 3.5 ml of brine. The core was shut in for 1 hour, allowing the brine to distribute through the core. Methane at 155°F was then flowed through the core using five flow rates and the pressure

drop across the core for each flow rate was recorded. The calculated gas permeability was 141 md. The flood conditions and results are shown in Table A.5.4 and Table A.4.5 respectively. Figure A.4.2 shows the pressure drop measured across the core during the methane flood at S_{wi} .

Synthetic volatile oil mixture 2 (Table 3.3) was used for the two-phase flow measurements. The mixture was allowed a minimum of 12 hours to equilibrate to a single phase at 4200 psi and 155°F. The initial flood was conducted with the upstream backpressure regulator (BPR-1) set at 4350 psi and the downstream back pressure regulator (BPR-2) set at 805 psi. Volatile oil was injected at an upstream BPR-1 flow rate of 150 cc/hr (this is for volatile oil at single liquid phase). Once steady state was observed the pressure drop across the core was measured. This procedure was repeated for BPR-2 pressures of 1,500 psi, 2,200 psi and 2,900 psi. This allowed having different PVT ratios and capillary numbers. The PVT ratio ranged from 0.85 to 0.44 and capillary number from 1.8×10^{-5} to 4.6×10^{-5} . Table A.3.6 gives the fluid properties of the synthetic fluid calculated using the Peng-Robinson EOS at the flowing core pressures. Figure A.4.3 shows the pressure drop measured across the core during the initial two-phase volatile oil flood for the different BPR-2 pressures.

The core was then treated using chemical treatment 3 (Table 4.15). The solution was heated for at least 3 hours at 155°F. BPR1 was set at 2170 psi. The core was flooded with approximately 10 pore volumes of the treatment solution at a flow rate of 120 cc/hr. The core was then shut in for 1 hour. Figure A.4.4 shows the measured pressure drop across the core during the treatment flood.

Post-treatment two-phase volatile oil flood was conducted under the same conditions as the initial two-phase flow. Figure A.4.5 shows the pressure drop measured

across the core during the post-treatment two-phase volatile oil flood. Improvement factor varied from 1.8 to 0.9 as the BPR-2 pressure increased.

The core was retreated for a second time with 10 PV of the chemical treatment 3 and a volatile oil flood followed. The improvement factor increased and ranged from 3.2 to 0.8 for increasing pressures. The core was then retreated for a third time with 10 PV of chemical treatment 3 followed by a series of volatile oil floods. The improvement factor increased and ranged from 3.5 to 0.8 for increasing pressures. Figure A.6.6 to Figure A.6.9 show the second and third chemical treatments and the volatile oil floods that followed them.

The final gas permeability was calculated following the procedure for the initial gas permeability using methane at 155°F. The calculated gas permeability was 131 md. The flood conditions and results are shown in Table A.2.7, Table A.4.7 and Table A.3.8 respectively. Figure A.2.8 For every two-phase volatile oil flood, oil and gas relative permeabilities k_{rg} and k_{ro} were calculated using the measured pressure drop across the core under steady state conditions and then improvement factors were measured. Table A.3.9 summarizes the experimental results and Figure A.6.10 shows the pressure drop across the core for the final methane flood.

Table A.6.1 Core properties (Exp #176)

<i>Length, in</i>	8.025
<i>Diameter, in</i>	0.995
<i>Mass Core, gr</i>	224.86
<i>Grain Density, gr/cc</i>	2.65
<i>Porosity (ϕ)</i>	17.02%

Table A.6.2 Fluid properties and conditions for initial gas permeability (Exp #176)

		<i>Density, gr/cc</i>
<i>Gas</i>	Methane	
<i>Temperature, °F</i>	155	
<i>BPR 1-pressure, psi</i>	4223	0.1669
<i>BPR 2-pressure, psi</i>	1000	4.17E-02
<i>Gas Viscosity, cp</i>	0.0138	

Table A.6.3 Initial methane flood results (Exp #176)

<i>q_{core}, cc/hr</i>	<i>ΔP, psi</i>	<i>k_g, md</i>
2401	3.920	140.23
3202	5.380	136.23
4002	6.850	133.75
4803	8.350	131.66
6004	10.860	126.54
<i>Corrected Permeability (k_g), md</i>		149.2

Table A.6.4 Fluid properties and conditions for methane gas permeability at S_{wi} (Exp #176)

		<i>Density, gr/cc</i>
<i>Gas</i>	Methane	
<i>Temperature, °F</i>	155	
<i>BPR 1-pressure, psi</i>	4228	0.1669
<i>BPR 2-pressure, psi</i>	1003	4.17E-02
<i>Gas Viscosity, cp</i>	0.0138	

Table A.6.5 Methane flood results at S_{wi} (Exp #176)

q_{core} , cc/hr	ΔP , psi	k_g , md
2401	4.500	122.15
3202	6.400	114.52
4002	8.400	109.07
4803	10.500	104.70
6004	14.000	98.16
<i>Corrected Permeability (k_g), md</i>		141.4

Table A.6.6 Volatile oil properties at BPR-1 and BPR-2 pressures (Exp #176)

<i>BPR 1-pressure, psi</i>		4350						
<i>BPR 2- pressure, psi</i>		805	1500	2200	2900			
<i>Density at BPR 1-pressure, gr/cc</i>		0.3691						
Properties of BPR 2-pressure, psi								
	805		1500		2200		2900	
	Gas Phase	Oil Phase						
Density, gr/cc	0.0433	0.605	0.0864	0.5569	0.1367	0.5086	0.1982	0.4523
Viscosity (μ), cp	0.0136	0.229	0.0155	0.1675	0.0188	0.1257	0.0248	0.0919
Volume Fraction	0.935	0.065	0.8505	0.1495	0.7476	0.2524	0.6199	0.3801
IFT, dyne/cm	8.947		4.254		1.561		0.313	

Table A.6.7 Fluid properties and conditions for final gas permeability (Exp #176)

		<i>Density, gr/cc</i>
<i>Gas</i>	<i>Methane</i>	
<i>Temperature, °F</i>	155	
<i>BPR 1-pressure, psi</i>	4350	0.1707
<i>BPR 2-pressure, psi</i>	1003	0.0417
<i>Gas Viscosity, cp</i>	0.0138	

Table A.6.8 Final methane flood results (Exp #176)

$q_{core}, cc/hr$	$\Delta P, psi$	k_g, md
2456	4.600	122.22
3275	6.250	119.94
4094	8.100	115.68
4912	9.800	114.74
6140	12.800	109.81
<i>Corrected Permeability (k_g), md</i>		130.87

Table A.6.9 Pre and post-treatment volatile oil flood results and measured improvement factors (Exp #176)

	Exp# 176			
<i>BPR 2- pressure, psi</i>	805	1500	2200	2900
$q_{gtot\ core}, cc/hr$	694	353	240	188
$q_g, cc/hr$	649	300	180	116
$q_o, cc/hr$	45	53	61	71
<i>PVT Ratio</i>	0.85	0.53	0.44	0.44
<i>Viscosity Ratio μ_g/μ_o</i>	0.06	0.09	0.15	0.27
<i>Capillary Nc</i>	1.00E-05	6.44E-06	2.55E-05	4.93E-05
k_{rg} Before Treatment	0.031	0.081	0.059	0.111
k_{ro} Before Treatment	0.036	0.154	0.132	0.251
k_{rg} After Treatment	0.054	0.094	0.047	0.104
k_{ro} After Treatment	0.064	0.179	0.106	0.235
<i>Initial Improvement Factor</i>	1.8	1.2	0.8	0.9
k_{rg} After 2 nd Treatment	0.100	0.076	0.080	0.084
k_{ro} After 2 nd Treatment	0.117	0.145	0.180	0.192
<i>Initial Improvement Factor</i>	3.2	0.9	1.4	0.8
k_{rg} After 3 rd Treatment	0.109	0.091	0.072	0.093
k_{ro} After 3 rd Treatment	0.128	0.172	0.163	0.211
<i>Initial Improvement Factor</i>	3.5	1.1	1.2	0.8

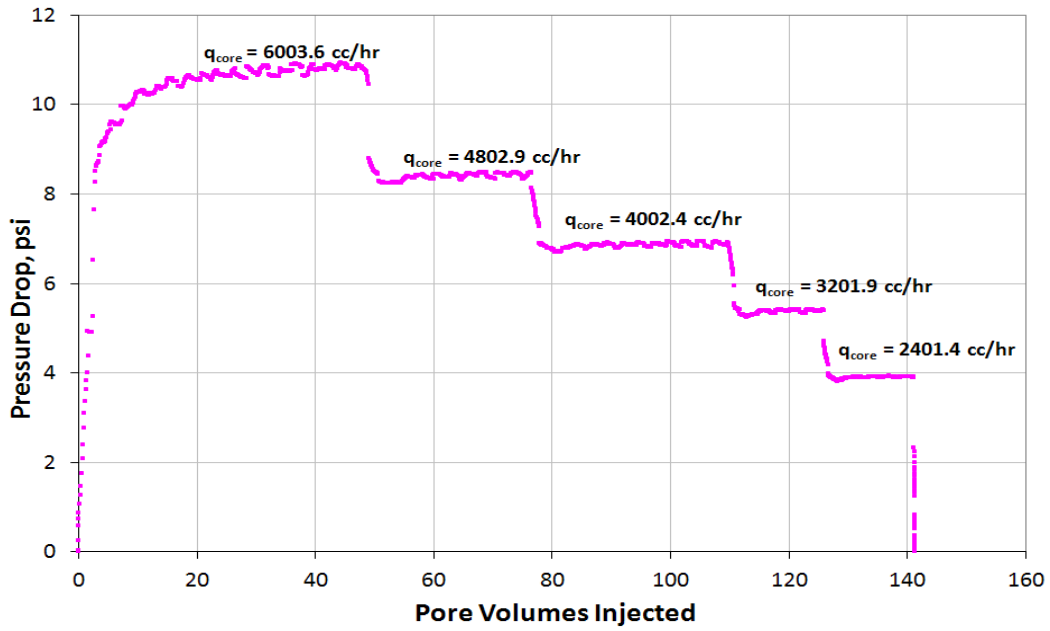


Figure A.6.1 Pressure drop across the core during the initial methane flood at 155°F (Exp #176)

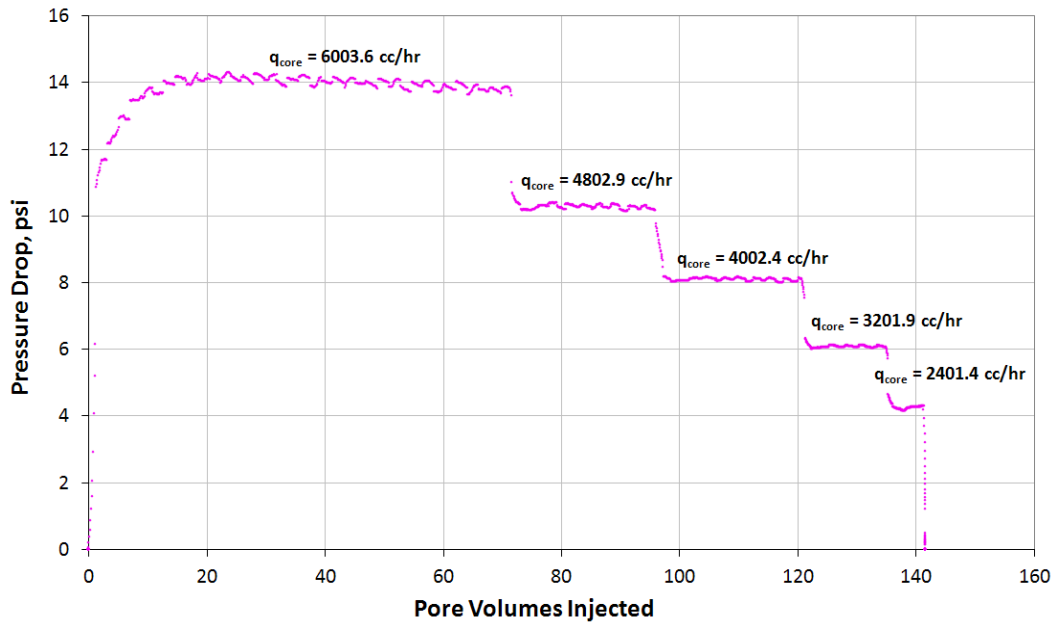


Figure A.6.2 Pressure drop across the core during the methane flood at S_{wi} of 20% (Exp #176)

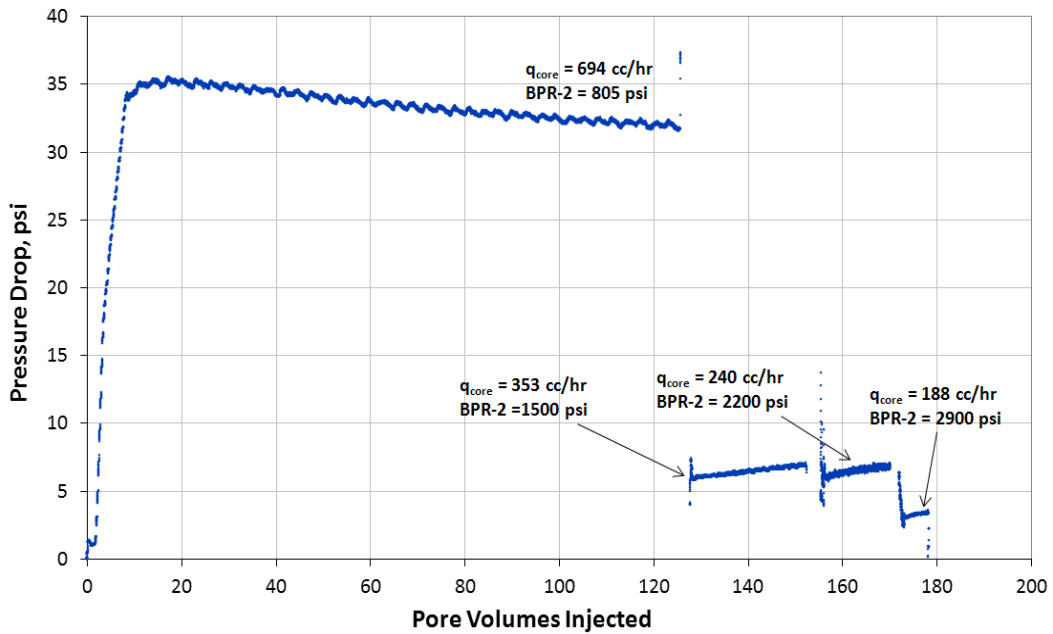


Figure A.6.3 Pressure drop across the core during the pre-treatment two-phase volatile oil flood (Exp #176)

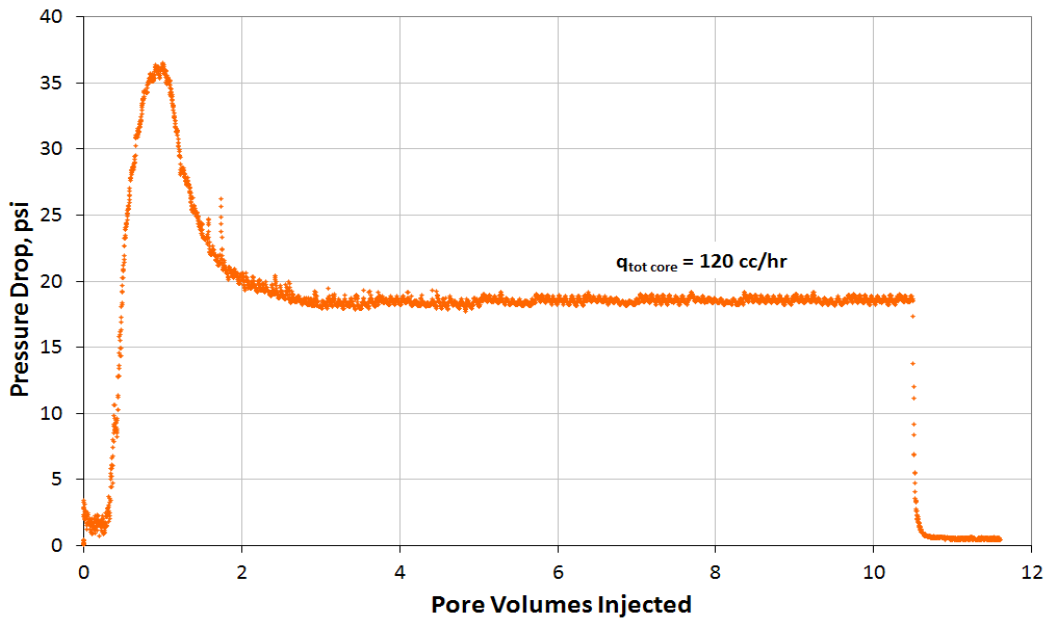


Figure A.6.4 Pressure drop across the core during injection of chemical treatment 3 (Exp # 176)

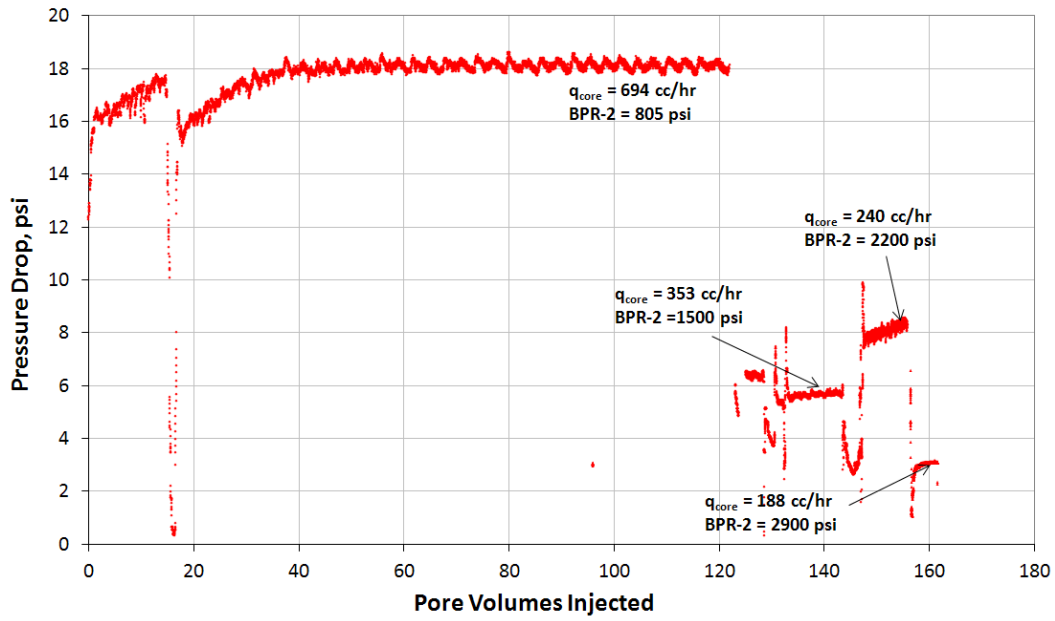


Figure A.6.5 Pressure drop across the core during the post-treatment two-phase volatile oil flood (Exp #176)

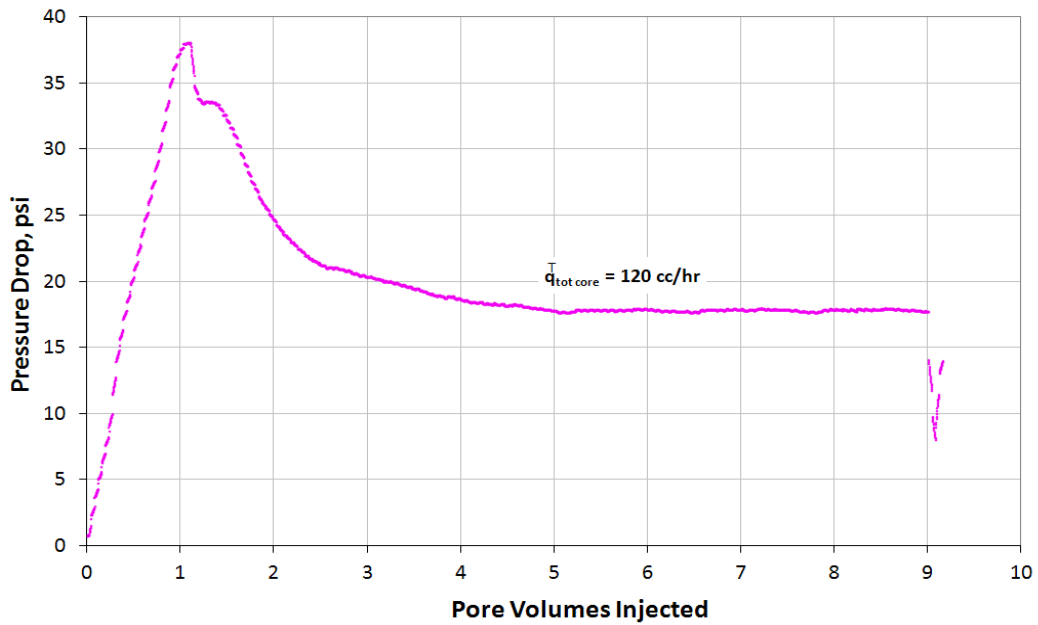


Figure A.6.6 Pressure drop across the core during injection of 2nd chemical treatment 3 (Exp # 176)

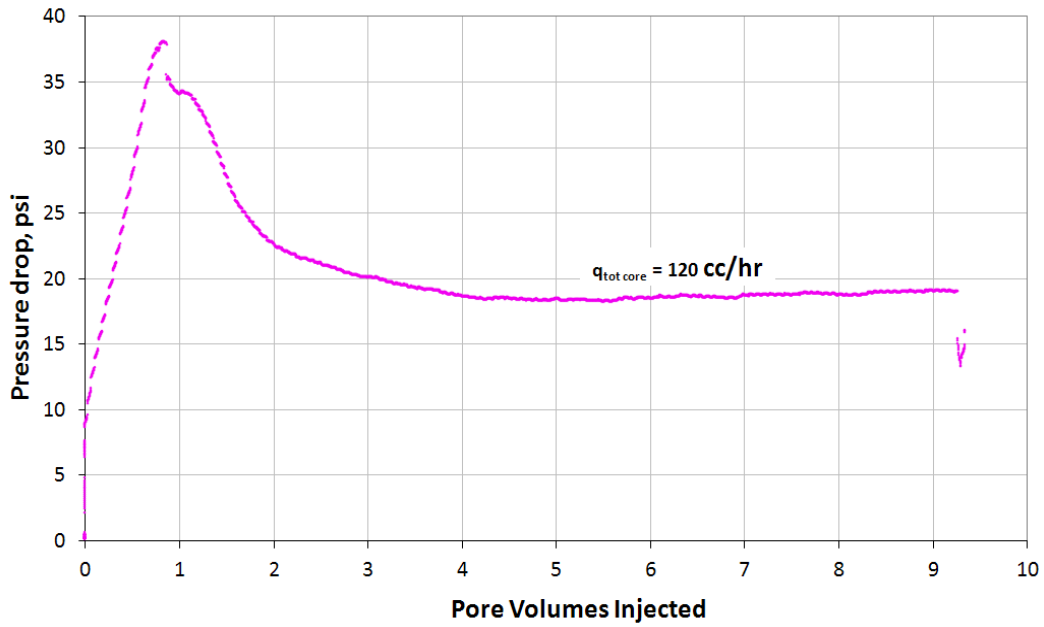


Figure A.6.7 Pressure drop across the core during injection of 3rd chemical treatment 3 (Exp # 176)

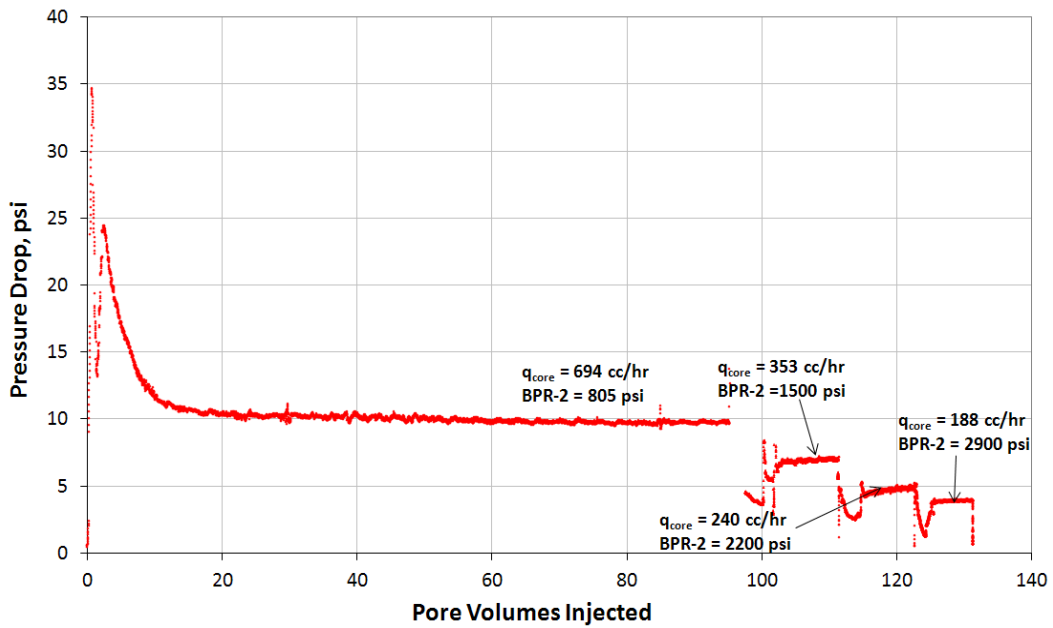


Figure A.6.8 Pressure drop across the core during the post-2nd treatment two-phase volatile oil flood (Exp #176)

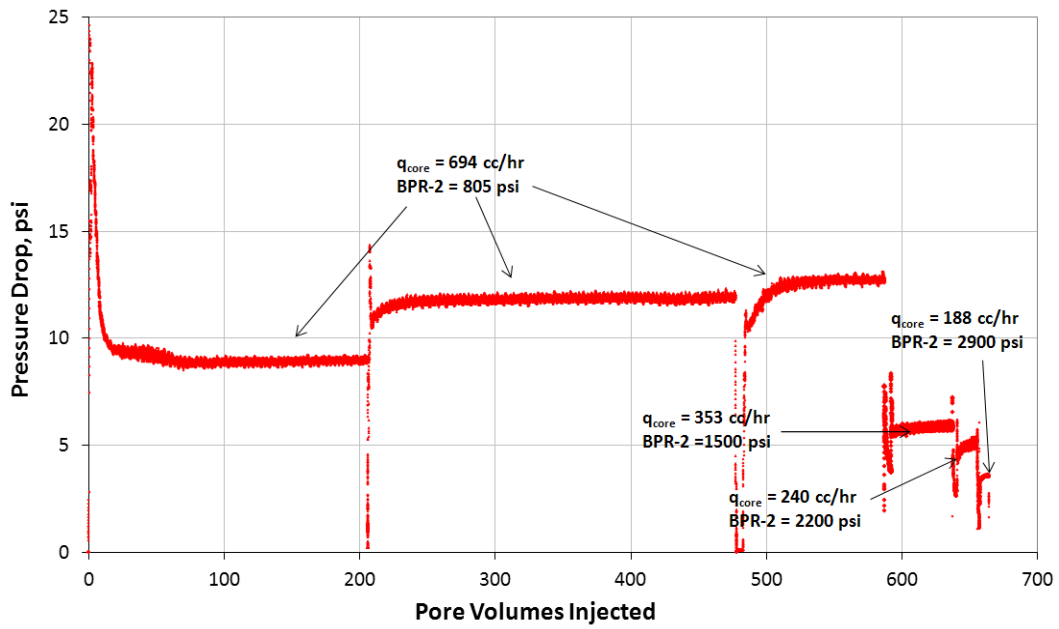


Figure A.6.9 Pressure drop across the core during the post-3rd treatment two-phase volatile oil flood (Exp #176)

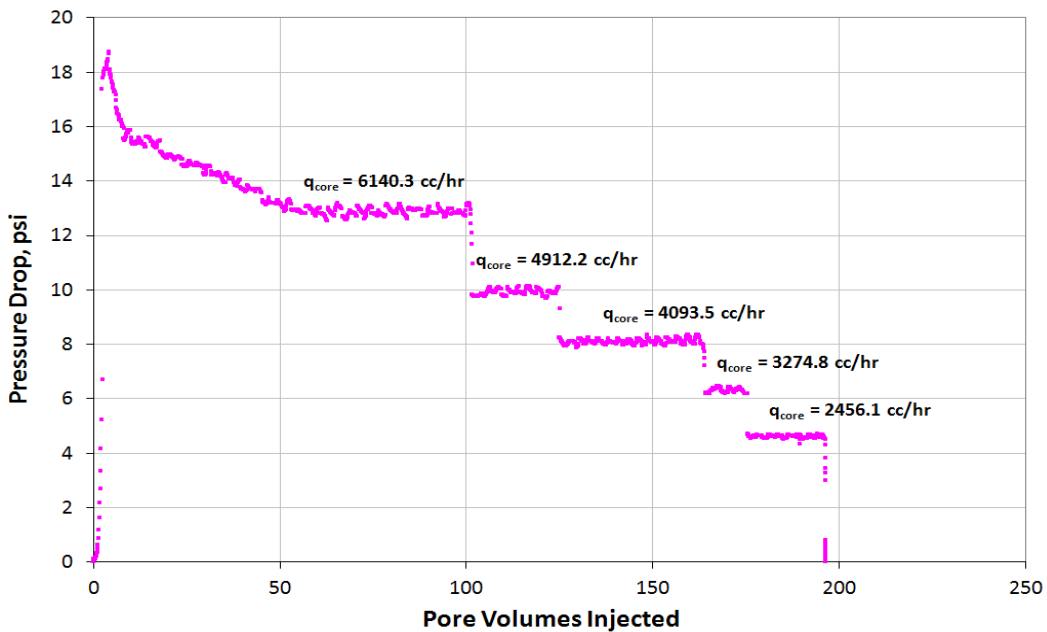


Figure A.6.10 Pressure drop across the core during the final methane flood at 155°F (Exp #176)

Appendix A.7: EXPERIMENT #181

Objective:

The objective of this experiment was to investigate the effectiveness of chemical treatment 5 using the anionic fluoro-surfactant L-19446#1 in improving the oil and gas relative permeability at different PVT ratios and capillary numbers, and multiple treatments. This was done for a volatile oil mixture below the bubble point pressure on a Texas cream limestone core and in the presence of initial water saturation. The experiment was performed at 155°F.

Experimental Procedure and Results:

A TCL core was prepared for the experiment following the standard procedure described Section 3.2.1.1. The initial core measurements and assumed properties can be found in Table A. 7.1.

The initial gas permeability was calculated using methane at 155°F. Methane was flowed through the core using four flow rates and the pressure drop across the core for each flow rate was recorded. Using this data, the fluid properties and accounting for non-Darcy effects the calculated gas permeability was 11 md. Table A.5.2 summarizes the flood conditions and fluid properties and Table A.5.3 shows the results. Figure A.6.1 shows the pressure drop measured across the core during the methane flood.

The initial gas permeability at initial water saturation was calculated next. Using synthetic brine 2 (25,000 ppm NaCl and 250 ppm CaCl₂) an initial water saturation of 20% was established. This was done by applying vacuum to the core first and then injecting 4.6 ml of brine. The core was shut in for 1 hour, allowing the brine to distribute through the core. Methane at 155°F was then flowed through the core using four flow

rates and the pressure drop across the core for each flow rate was recorded. The calculated gas permeability was 7 md. The flood conditions and results are shown in Table A.5.4 and Table A.4.5 respectively. Figure A.4.2 shows the pressure drop measured across the core during the methane flood at S_{wi} .

Synthetic volatile oil mixture 2 (Table 3.3) was used for the two-phase flow measurements. The mixture was allowed a minimum of 12 hours to equilibrate to a single phase at 4200 psi and 155°F. The initial flood was conducted with the upstream backpressure regulator (BPR-1) set at 4320 psi and the downstream back pressure regulator (BPR-2) set at 800 psi. Volatile oil was injected at an upstream BPR-1 flow rate of 100 cc/hr (this is for volatile oil at single liquid phase). Once steady state was observed the pressure drop across the core was measured. This procedure was repeated for BPR-2 pressures of 1,500 psi, 2,200 psi and 2,900 psi. This allowed having different PVT ratios and capillary numbers. The PVT ratio ranged from 0.94 to 0.53 and capillary number from 6.5×10^{-6} to 3.9×10^{-5} . Table A.3.6 gives the fluid properties of the synthetic fluid calculated using the Peng-Robinson EOS at the flowing core pressures. Figure A.4.3 shows the pressure drop measured across the core during the initial two-phase volatile oil flood for the different BPR-2 pressures.

The core was then treated using chemical treatment 5 (Table 4.15). The solution was heated for at least 3 hours at 155°F. BPR1 was set at 1100 psi. The core was flooded with approximately 20 pore volumes of the treatment solution at a flow rate of 100 cc/hr. The core was then shut in for 2 hour. Figure A.4.4 shows the measured pressure drop across the core during the treatment flood.

Post-treatment two-phase volatile oil flood was conducted under the same conditions as the initial two-phase flow. Figure A.4.5 shows the pressure drop measured

across the core during the post-treatment two-phase volatile oil flood. Improvement factor varied from 1.3 to 0.9 as the BPR-2 pressure increased.

The core was retreated for a second time with 19 PV of the chemical treatment 5 at a rate of 50 cc/hr. A volatile oil flood followed. The improvement factor remained at 1.3. Figure A.6.6 and Figure A.7.7 show the second chemical treatment and the volatile oil flood that followed.

The final gas permeability was calculated following the procedure for the initial gas permeability using methane at 155°F. The calculated gas permeability was 5.7 md. The flood conditions and results are shown in Table A.2.7, Table A.4.7 and Table A.3.8 respectively. Figure A.2.8 For every two-phase volatile oil flood, oil and gas relative permeabilities k_{rg} and k_{ro} were calculated using the measured pressure drop across the core under steady state conditions and then improvement factors were measured. Table A.3.9 summarizes the experimental results and Figure A.6.10 shows the pressure drop across the core for the final methane flood.

Table A. 7.1 Core properties (Exp #181)

<i>Length, in</i>	8.002
<i>Diameter, in</i>	0.994
<i>Mass Core, gr</i>	188.64
<i>Grain Density, gr/cc</i>	2.4
<i>Porosity (ϕ)</i>	22.76%

Table A.7.2 Fluid properties and conditions for initial gas permeability (Exp #181)

		<i>Density, gr/cc</i>
<i>Gas</i>	Methane	
<i>Temperature, °F</i>	155	
<i>BPR 1-pressure, psi</i>	4300	0.1692
<i>BPR 2-pressure, psi</i>	1200	5.05E-02
<i>Gas Viscosity, cp</i>	0.0142	

Table A.7.3 Initial methane flood results (Exp #181)

<i>q_{core}, cc/hr</i>	ΔP , psi	<i>k_g, md</i>
670	14.050	11.22
1005	21.250	11.13
1340	28.270	11.16
1675	35.950	10.97
<i>Corrected Permeability (k_g), md</i>		11.3

Table A.7.4 Fluid properties and conditions for methane gas permeability at S_{wi} (Exp #181)

		<i>Density, gr/cc</i>
<i>Gas</i>	Methane	
<i>Temperature, °F</i>	155	
<i>BPR 1-pressure, psi</i>	4300	0.1692
<i>BPR 2-pressure, psi</i>	1200	5.05E-02
<i>Gas Viscosity, cp</i>	0.0142	

Table A.7.5 Methane flood results at S_{wi} (Exp #181)

q_{core} , cc/hr	ΔP , psi	k_g , md
670	22.900	6.89
1005	34.700	6.82
1340	47.080	6.70
1675	60.000	6.57
<i>Corrected Permeability (k_g), md</i>		7.1

Table A.7.6 Volatile oil properties at BPR-1 and BPR-2 pressures (Exp #181)

<i>BPR 1-pressure, psi</i>		4320				
<i>BPR 2- pressure, psi</i>		800	1500	2200		
<i>Density at BPR 1-pressure, gr/cc</i>		0.3686				
Properties of BPR 2-pressure, psi						
	800		1500		2200	
	Gas Phase	Oil Phase	Gas Phase	Oil Phase	Gas Phase	Oil Phase
Density, gr/cc	0.0433	0.6042	0.0865	0.5551	0.137	0.5055
Viscosity (μ), cp	0.0129	0.1974	0.0148	0.1363	0.0182	0.0981
Volume Fraction	0.9348	0.0652	0.8495	0.1505	0.7443	0.2557
IFT, dyne/cm	8.905		4.201		1.513	

Table A.7.7 Fluid properties and conditions for final gas permeability (Exp #181)

		<i>Density, gr/cc</i>
<i>Gas</i>	Methane	
<i>Temperature, °F</i>	155	
<i>BPR 1-pressure, psi</i>	4315	0.1697
<i>BPR 2-pressure, psi</i>	1210	0.0509
<i>Gas Viscosity, cp</i>	0.0137	

Table A.7.8 Final methane flood results (Exp #181)

$q_{core}, cc/hr$	$\Delta P, psi$	k_g, md
1000	41.000	5.54
1334	55.000	5.51
1667	70.000	5.41
<i>Corrected Permeability (k_g), md</i>		5.71

Table A.7.9 Pre and post-treatment volatile oil flood results and measured improvement factors (Exp #181)

	Exp# 181			
<i>Core pressure, psia</i>	800	1500	2200	1900
$q_{gtot\ core}, cc/hr$	461	235	159	124
$q_g, cc/hr$	431	199	119	76
$q_o, cc/hr$	30	35	41	49
<i>PVT Ratio</i>	0.94	0.61	0.54	0.53
<i>Viscosity Ratio μ_g/μ_o</i>	0.07	0.11	0.19	0.34
<i>Liquid Fraction</i>	6.5%	15.1%	25.6%	39.0%
<i>Capillary Nc</i>	6.50E-06	9.78E-06	1.39E-05	3.90E-05
k_{rg} Before Treatment	0.053	0.040	0.057	0.092
k_{ro} Before Treatment	0.057	0.065	0.105	0.172
k_{rg} After 1st Treatment	0.067	0.054	0.054	0.084
k_{ro} After 1st Treatment	0.071	0.088	0.101	0.158
<i>Initial Improvement Factor</i>	1.4	*	*	*
<i>PV of Vol Oil Injected</i>	~ 400			
<i>Final Improvement Factor</i>	1.3	1.4	1.0	0.9
k_{rg} After 2nd Treatment	0.071	0.054	*	*
k_{ro} After 2nd Treatment	0.076	0.087	*	*
<i>Initial Improvement Factor</i>	1.3	1.3	*	*
<i>PV of Vol Oil Injected</i>	~ 200			

* Data not measured

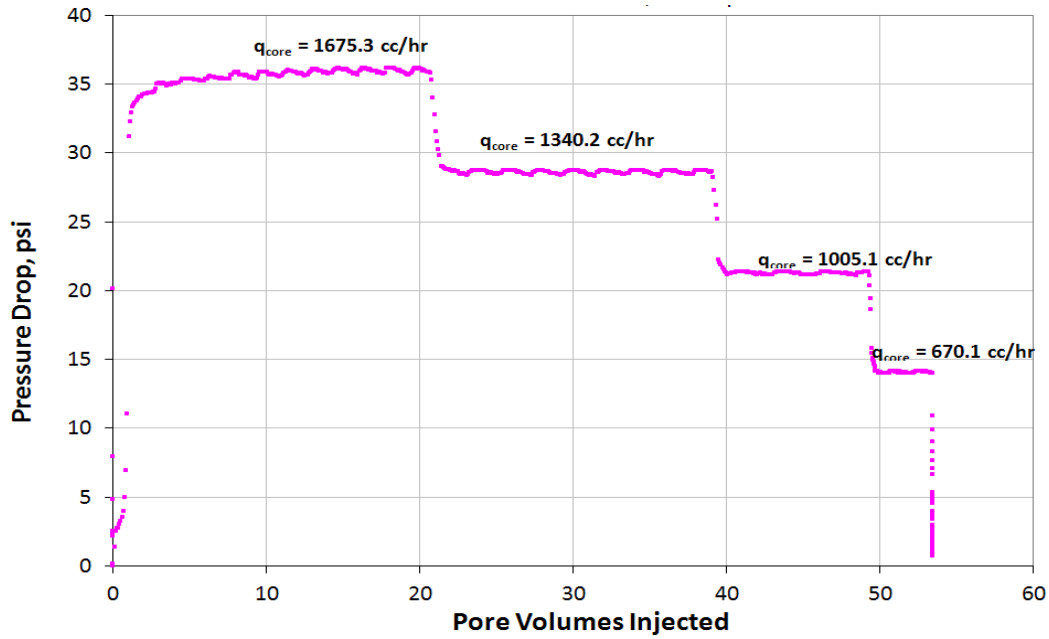


Figure A.7.1 Pressure drop across the core during the initial methane flood at 155°F (Exp #181)

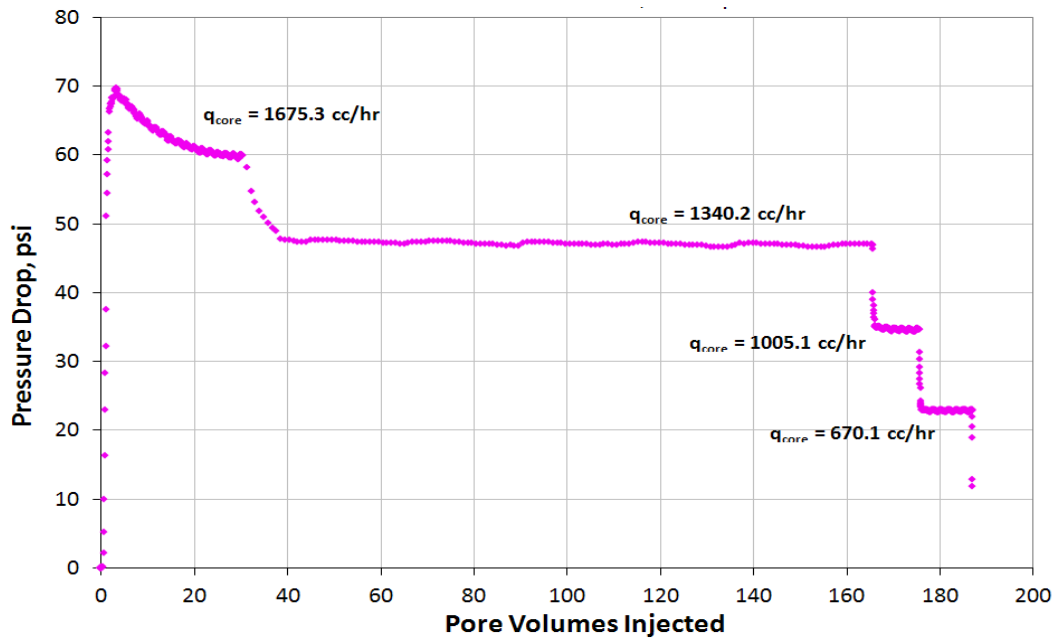


Figure A.7.2 Pressure drop across the core during the methane flood at S_{wi} of 20% (Exp #181)

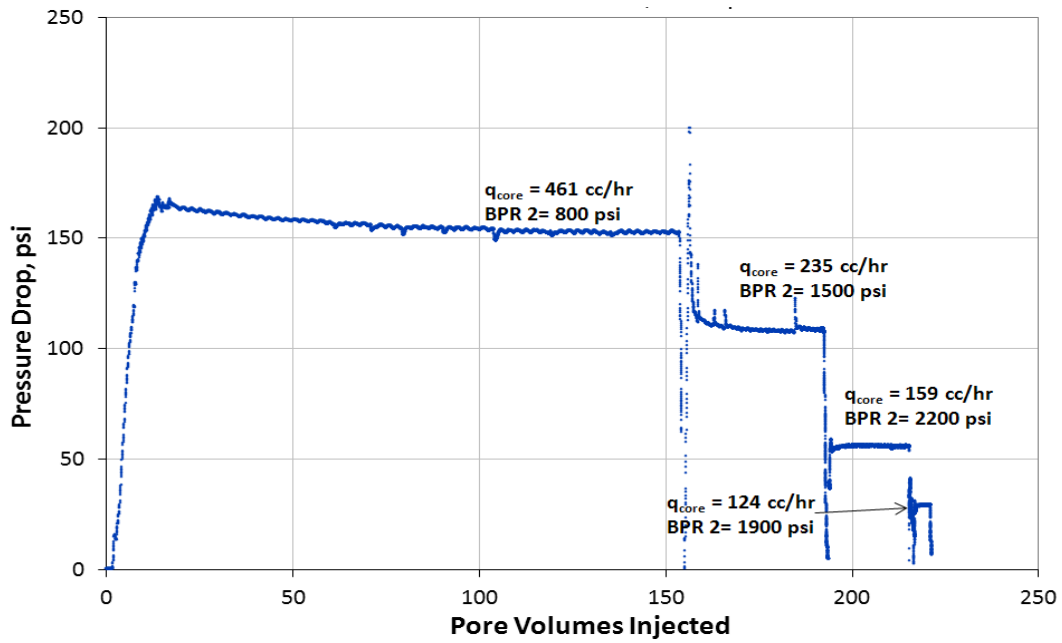


Figure A.7.3 Pressure drop across the core during the pre-treatment two-phase volatile oil flood (Exp #181)

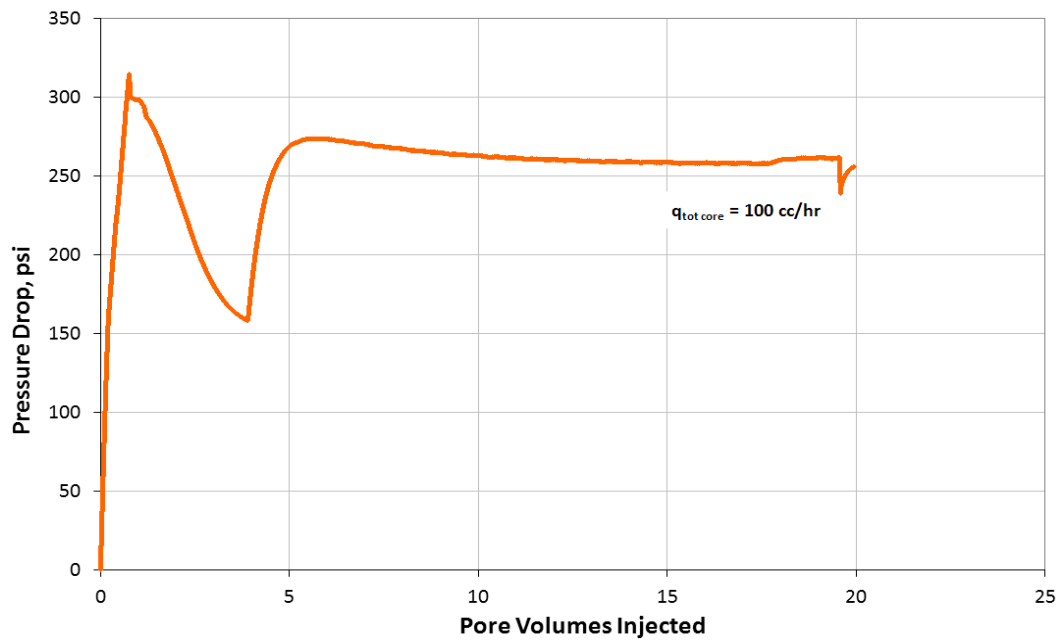


Figure A.7.4 Pressure drop across the core during injection of chemical treatment 5 (Exp #181)

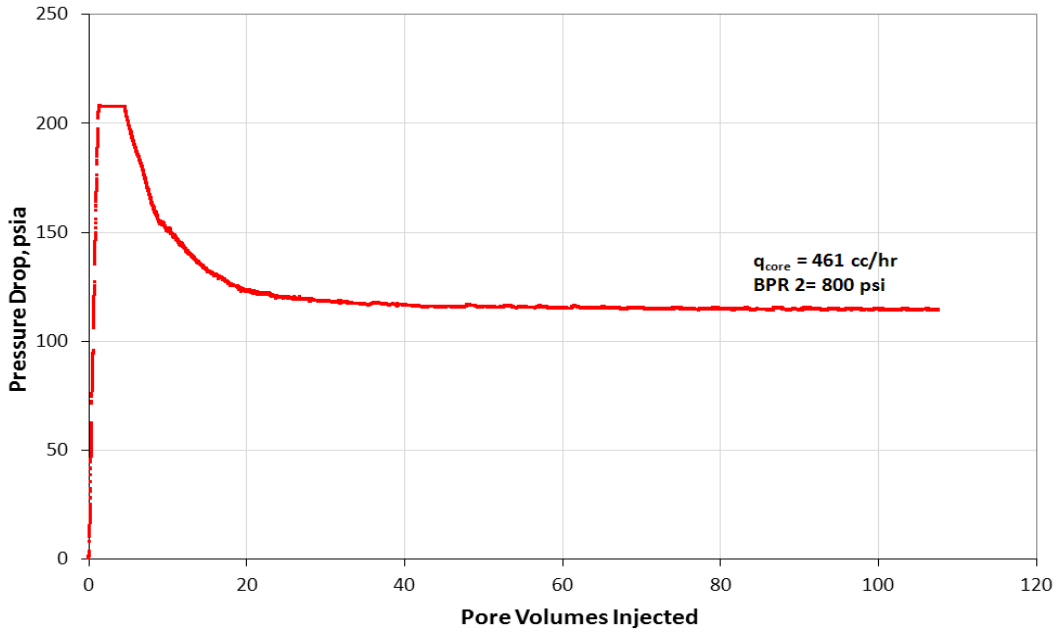


Figure A.7.5 Pressure drop across the core during the post-treatment two-phase volatile oil flood (Exp #181)

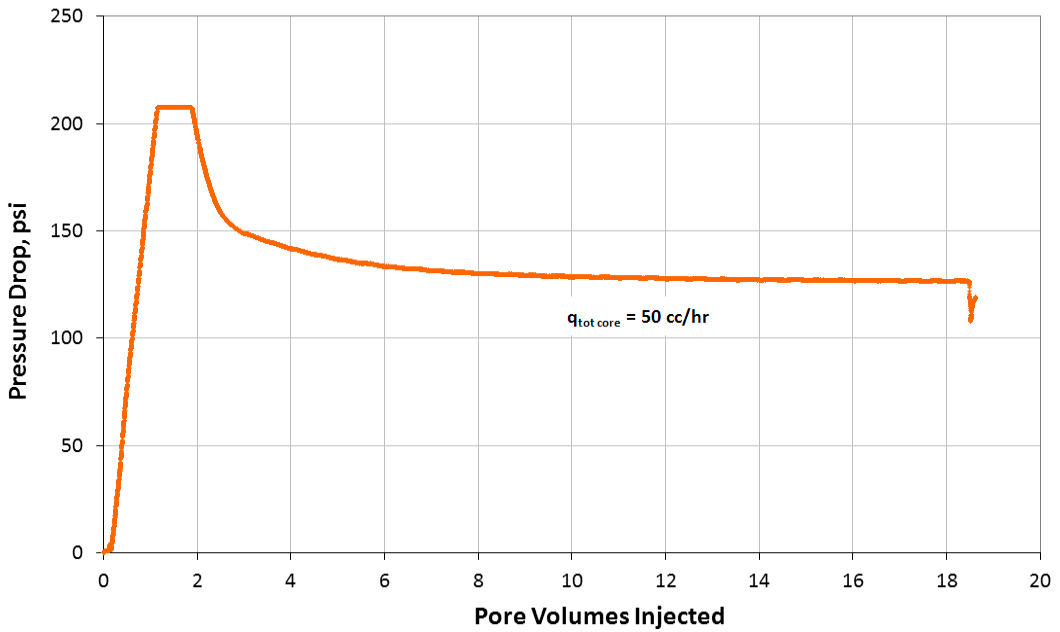


Figure A.7.6 Pressure drop across the core during injection of 2nd chemical treatment 5 (Exp # 181)

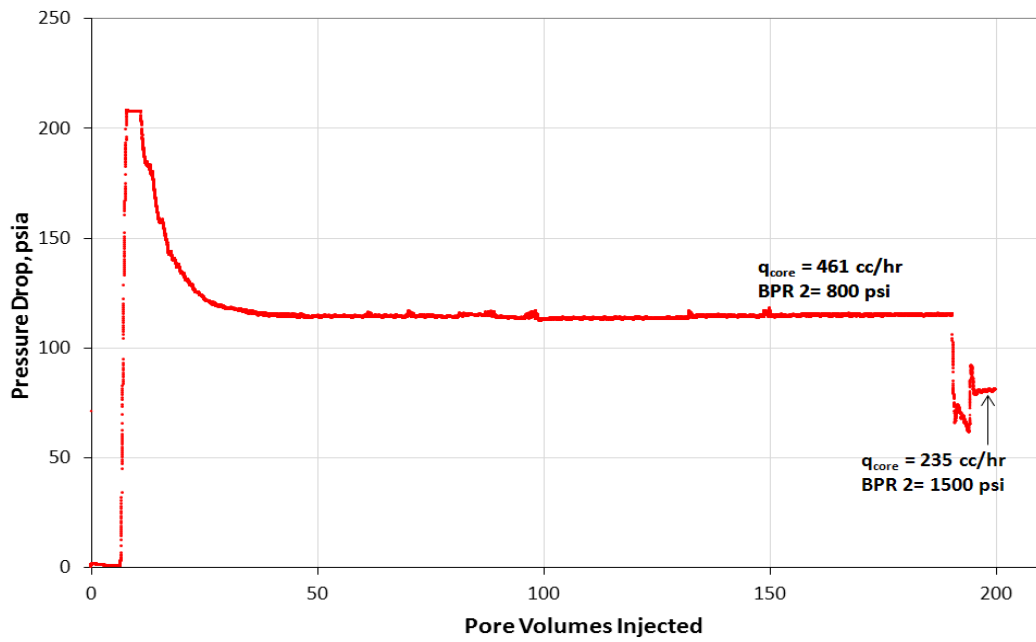


Figure A.7.7 Pressure drop across the core during the post-2nd treatment two-phase volatile oil flood (Exp #181)

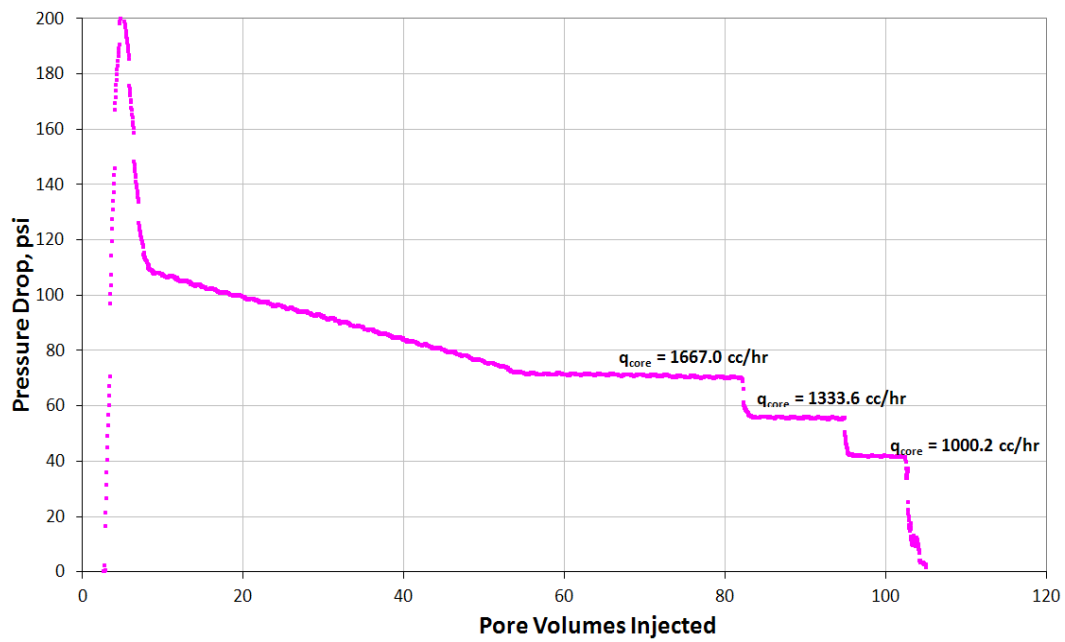


Figure A.7.8 Pressure drop across the core during the final methane flood at 155°F (Exp #181)

Appendix A.8: EXPERIMENT #185

Objective:

The objective of this experiment was to investigate the effectiveness of chemical treatment 5 using the anionic fluoro-surfactant L-19446#1 in improving the oil and gas relative permeability at different capillary numbers. This was done for a volatile oil mixture below the bubble point pressure on a Texas cream limestone core and in the presence of initial water saturation. The experiment was performed at 155°F.

Experimental Procedure and Results:

A TCL core was prepared for the experiment following the standard procedure described Section 3.2.1.1. The initial core measurements and assumed properties can be found in Table A. 7.1.

The initial gas permeability was calculated using methane at 155°F. Methane was flowed through the core using four flow rates and the pressure drop across the core for each flow rate was recorded. Using this data, the fluid properties and accounting for non-Darcy effects the calculated gas permeability was 25 md. Table A.5.2 summarizes the flood conditions and fluid properties and Table A.5.3 shows the results. Figure A.6.1 shows the pressure drop measured across the core during the methane flood.

The initial gas permeability at initial water saturation was calculated next. Using synthetic brine 2 (25,000 ppm NaCl and 250 ppm CaCl₂) an initial water saturation of 20% was established. This was done by applying vacuum to the core first and then injecting 4.6 ml of brine. The core was shut in for 1 hour, allowing the brine to distribute through the core. Methane at 155°F was then flowed through the core using four flow rates and the pressure drop across the core for each flow rate was recorded. The

calculated gas permeability was 22 md. The flood conditions and results are shown in Table A.5.4 and Table A.4.5 respectively. Figure A.4.2 shows the pressure drop measured across the core during the methane flood at S_{wi} .

Synthetic volatile oil mixture 2 (Table 3.3) was used for the two-phase flow measurements. The mixture was allowed a minimum of 12 hours to equilibrate to a single phase at 4200 psi and 155°F. The initial flood was conducted with the upstream backpressure regulator (BPR-1) set at 4260 psi and the downstream back pressure regulator (BPR-2) set at 788 psi. Volatile oil was injected at an upstream BPR-1 flow rate of 30 cc/hr (this is for volatile oil at single liquid phase). Once steady state was observed the pressure drop across the core was measured. This procedure was repeated for upstream BPR-1 flow rates of 60 cc/hr, and 100 cc/hr. This allowed having different capillary numbers with constant PVT ratio. The capillary number from 2.2×10^{-6} to 6.4×10^{-6} and the PVT ratio was 0.94. Table A.3.6 gives the fluid properties of the synthetic fluid calculated using the Peng-Robinson EOS at the flowing core pressures. Figure A.4.3 shows the pressure drop measured across the core during the initial two-phase volatile oil flood for the different flow rates.

The core was then treated using chemical treatment 5 (Table 4.15). The solution was heated for at least 3 hours at 155°F. BPR1 was set at 790 psi. The core was flooded with approximately 20 pore volumes of the treatment solution at a flow rate of 50 cc/hr. The core was then shut in for 2 hour. Figure A.4.4 shows the measured pressure drop across the core during the treatment flood.

Post-treatment two-phase volatile oil flood was conducted under the same conditions as the initial two-phase flow. Figure A.4.5 shows the pressure drop measured across the core during the post-treatment two-phase volatile oil flood. Improvement factor was of about 2.

Two more batches of post-treatment volatile oil flood followed. The improvement factor remained at about 1.8. Figure A.6.6 and Figure A.7.7 show the second and third post-treatment volatile oil floods.

The final gas permeability was calculated following the procedure for the initial gas permeability using methane at 155°F. The calculated gas permeability was 22 md. The flood conditions and results are shown in Table A.4.7 and Table A.3.8 respectively. Figure A.6.10 shows the pressure drop across the core for the final methane flood.

For every two-phase volatile oil flood, oil and gas relative permeabilities k_{rg} and k_{ro} were calculated using the measured pressure drop across the core under steady state conditions and then improvement factors were measured. Table A.3.9 summarizes the experimental results.

Table A. 8.1 Core properties (Exp #185)

<i>Length, in</i>	8.00
<i>Diameter, in</i>	0.994
<i>Mass Core, gr</i>	188.01
<i>Grain Density, gr/cc</i>	2.4
<i>Porosity (ϕ)</i>	23.00%

Table A.8.2 Fluid properties and conditions for initial gas permeability (Exp #185)

		<i>Density, gr/cc</i>
<i>Gas</i>	Methane	
<i>Temperature, °F</i>	155	
<i>BPR 1-pressure, psi</i>	4091	0.1692
<i>BPR 2-pressure, psi</i>	968	4.04E-02
<i>Gas Viscosity, cp</i>	0.0133	

Table A.8.3 Initial methane flood results (Exp #185)

<i>q_{core}, cc/hr</i>	<i>ΔP, psi</i>	<i>k_g, md</i>
838	7.600	24.29
1256	11.460	24.16
1675	15.450	23.89
2094	19.650	23.48
<i>Corrected Permeability (k_g), md</i>		24.8

Table A.8.4 Fluid properties and conditions for methane gas permeability at S_{wi} (Exp #185)

		<i>Density, gr/cc</i>
<i>Gas</i>	Methane	
<i>Temperature, °F</i>	155	
<i>BPR 1-pressure, psi</i>	4097	0.1692
<i>BPR 2-pressure, psi</i>	970	4.04E-02
<i>Gas Viscosity, cp</i>	0.0133	

Table A.8.5 Methane flood results at S_{wi} (Exp #185)

q_{core} , cc/hr	ΔP , psi	k_g , md
838	8.600	21.46
1256	13.050	21.22
1675	17.780	20.76
2094	22.450	20.55
<i>Corrected Permeability (k_g), md</i>		21.9

Table A.8.6 Volatile oil properties at BPR-1 and BPR-2 pressures (Exp #185)

<i>BPR 1-pressure, psi</i>	4260	
<i>BPR 2- pressure, psi</i>	788	
<i>Density at BPR 1-pressure, gr/cc</i>	0.367	
Properties at BPR 2-pressure, psi		
	Gas Phase	Oil Phase
<i>Density, gr/cc</i>	0.0426	0.6051
<i>Viscosity (μ), cp</i>	0.0128	0.1988
<i>Volume Fraction</i>	0.9361	0.0639
<i>IFT, dyne/cm</i>	9.008	

Table A.8.7 Fluid properties and conditions for final gas permeability (Exp #185)

		<i>Density, gr/cc</i>
<i>Gas</i>	Methane	
<i>Temperature, °F</i>	155	
<i>BPR 1-pressure, psi</i>	4225	0.167
<i>BPR 2-pressure, psi</i>	782	0.0323
<i>Gas Viscosity, cp</i>	0.0135	

Table A.8.8 Final methane flood results (Exp #185)

q_{core} , cc/hr	ΔP , psi	k_g , md
1551	16.500	21.03
2068	22.100	20.93
2585	28.500	20.29
<i>Corrected Permeability (k_g), md</i>		22.3

Table A.8.9 Pre and post-treatment volatile oil flood results and measured improvement factors (Exp #185)

	Exp# 185		
<i>Core pressure, psia</i>	790		
<i>q_{gtot core}, cc/hr</i>	140	280	467
<i>q_g, cc/hr</i>	131	262	437
<i>q_o, cc/hr</i>	9	18	30
<i>PVT Ratio</i>	0.94		
<i>Viscosity Ratio μ_g/μ_o</i>	0.06		
<i>Liquid Fraction</i>	6.4%		
<i>Capillary Nc</i>	1.68E-06	3.34E-06	5.25E-06
<i>k_{rg} Before Treatment</i>	0.062	0.062	0.066
<i>k_{ro} Before Treatment</i>	0.065	0.066	0.070
<i>k_{rg} After Treatment</i>	0.112	0.116	0.114
<i>k_{ro} After Treatment</i>	0.119	0.123	0.121
<i>Initial Improvement Factor</i>	1.8	1.9	1.7
<i>PV of Vol Oil Injected</i>	~ 390		
<i>Final Improvement Factor</i>	1.6	1.7	1.7

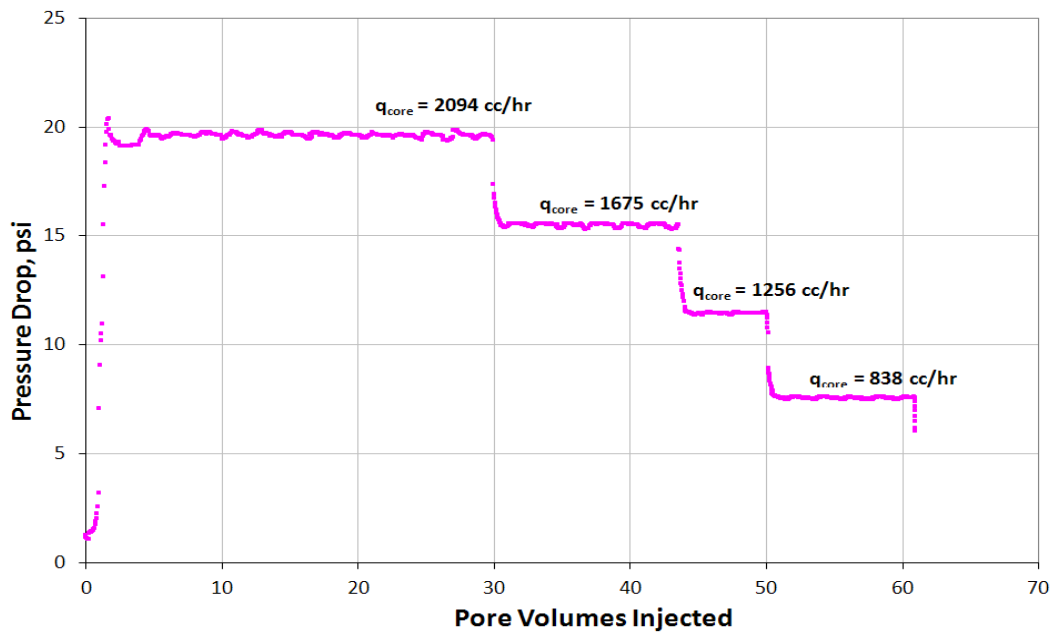


Figure A.8.1 Pressure drop across the core during the initial methane flood at 155°F (Exp #185)

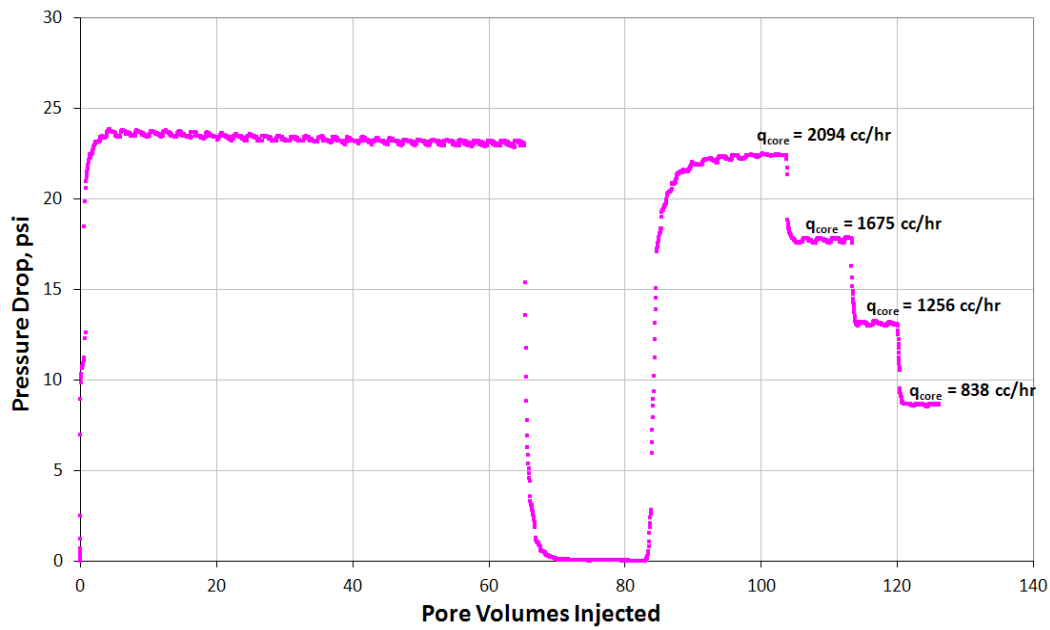


Figure A.8.2 Pressure drop across the core during the methane flood at S_{wi} of 20% (Exp #185)

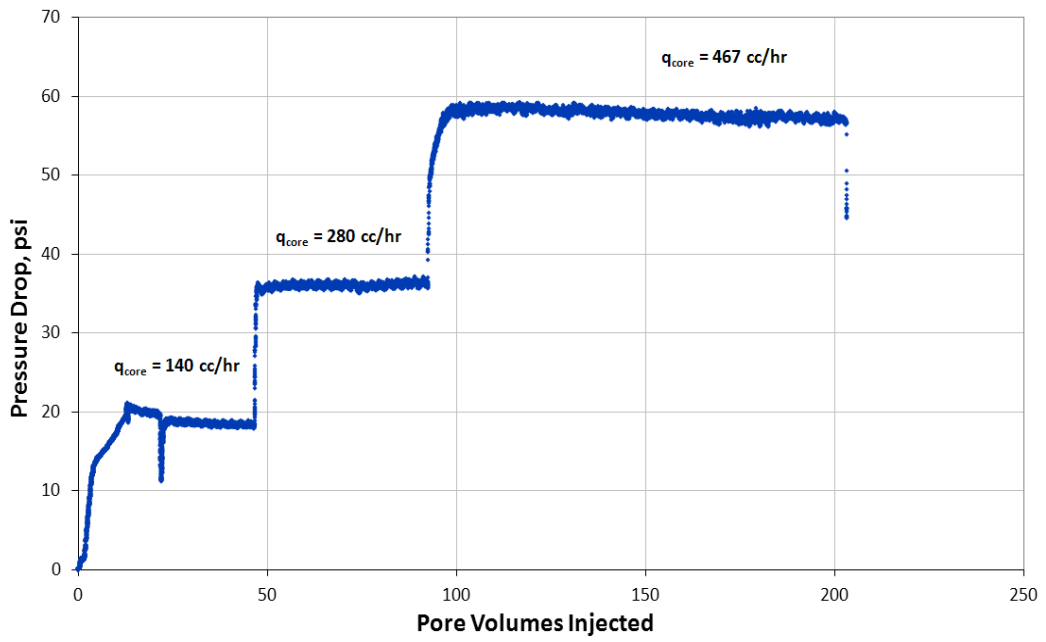


Figure A.8.3 Pressure drop across the core during the pre-treatment two-phase volatile oil flood (Exp #185)

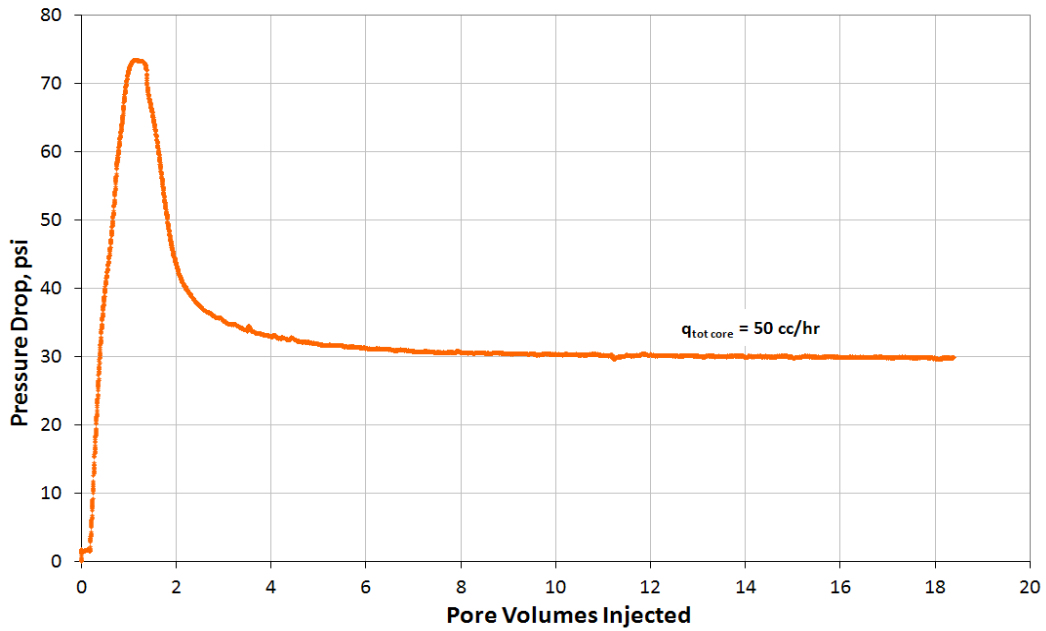


Figure A.8.4 Pressure drop across the core during injection of chemical treatment 5 (Exp #185)

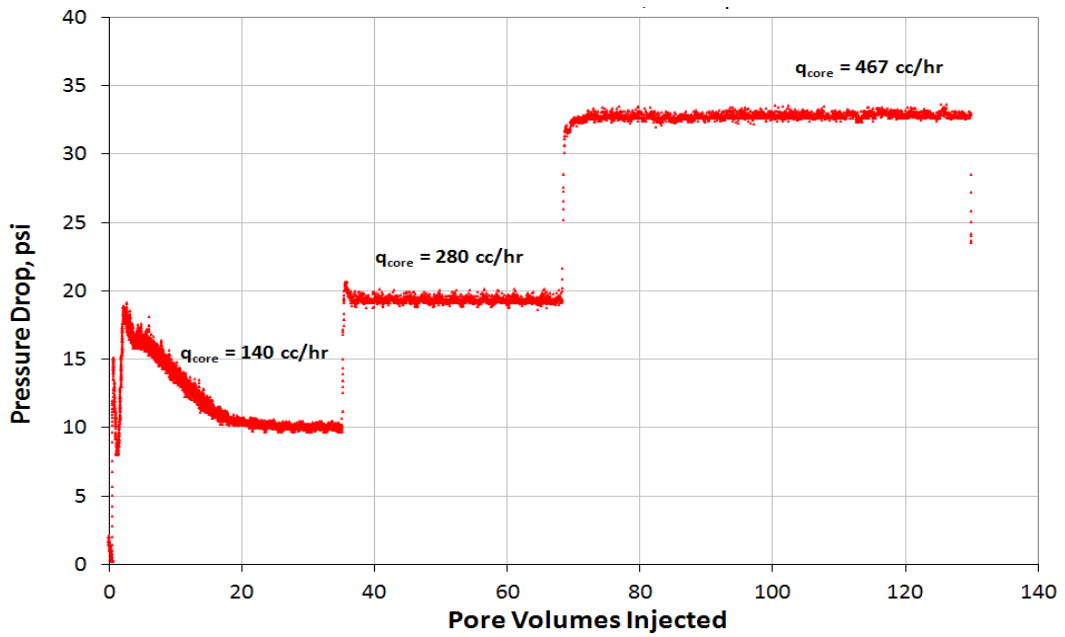


Figure A.8.5 Pressure drop across the core during the post-treatment two-phase volatile oil flood (Exp #185)

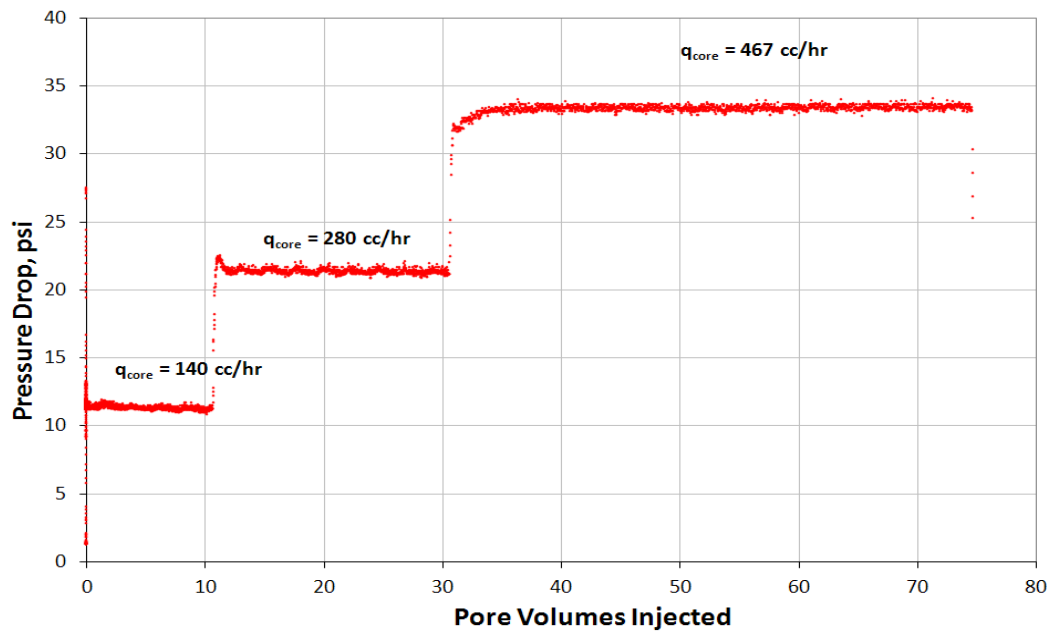


Figure A.8.6 Pressure drop across the core during the post-treatment two-phase volatile oil flood 2 (Exp #185)

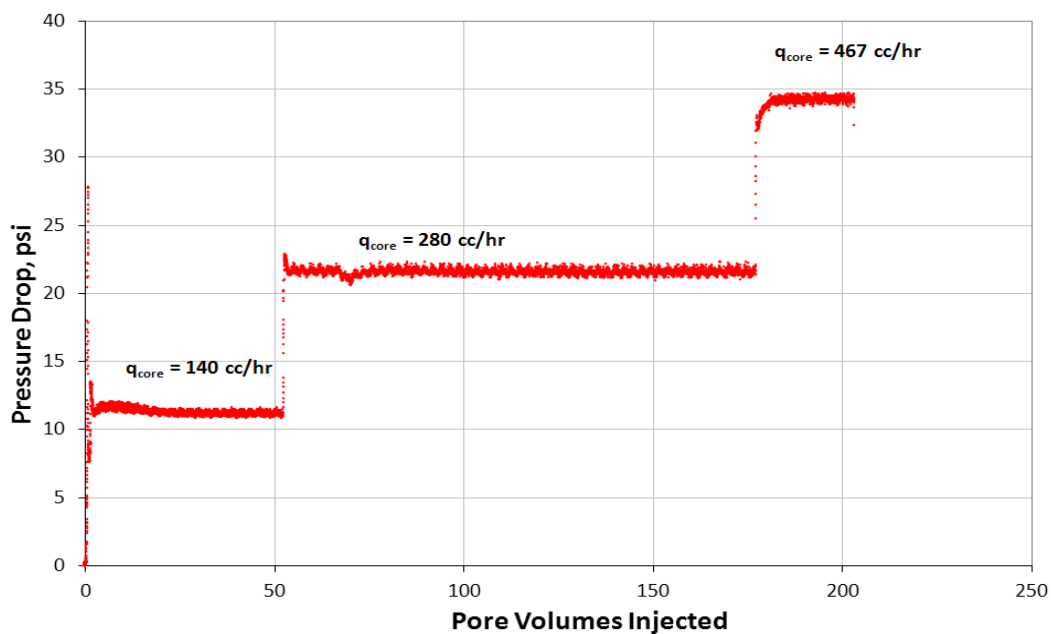


Figure A.8.7 Pressure drop across the core during the post-treatment two-phase volatile oil flood 3 (Exp #185)

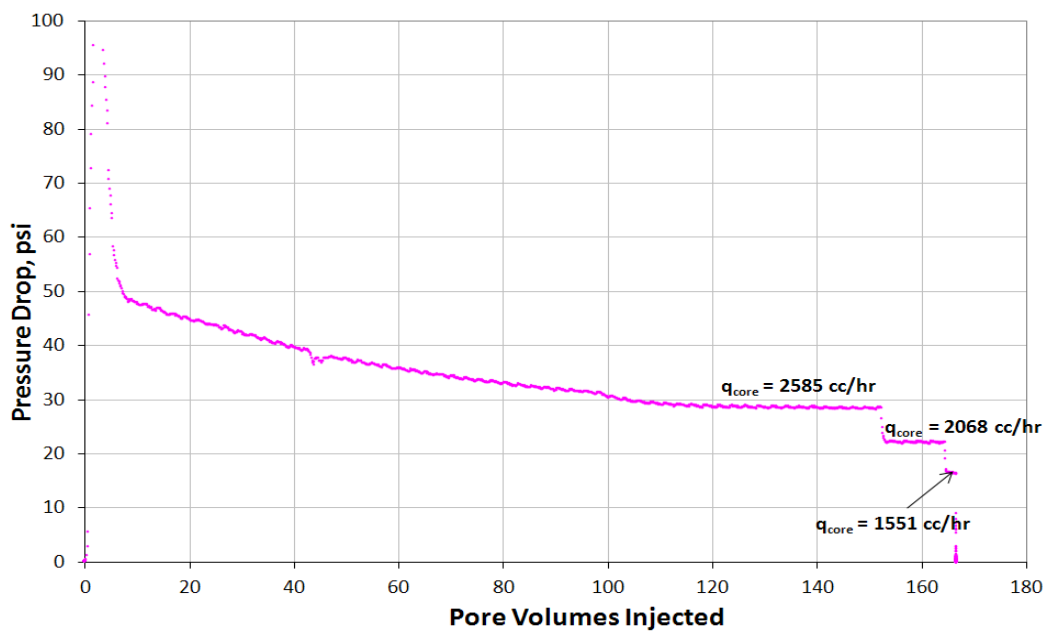


Figure A.8.8 Pressure drop across the core during the final methane flood at 155°F (Exp #185)

Appendix A.9: EXPERIMENT #189

Objective:

The objective of this experiment was to investigate the effectiveness of chemical treatment 3 using the fluoro-surfactant L-18961 in improving the oil and gas relative permeability at high temperature. This was done for a volatile oil mixture below the bubble point pressure on a Berea sandstone core and in the presence of initial water saturation. The experiment was performed at 250°F.

Experimental Procedure and Results:

A Berea sandstone core was prepared for the experiment following the standard procedure described Section 3.2.1.1. The initial core measurements and assumed properties can be found in Table A. 7.1.

The initial gas permeability was calculated using methane at 250°F. Methane was flowed through the core using five flow rates and the pressure drop across the core for each flow rate was recorded. Using this data, the fluid properties and accounting for non-Darcy effects the calculated gas permeability was 212 md. Table A.5.2 summarizes the flood conditions and fluid properties and Table A.5.3 shows the results. Figure A.6.1 shows the pressure drop measured across the core during the methane flood.

The initial gas permeability at initial water saturation was calculated next. Using synthetic brine 1 (25,000 ppm NaCl) an initial water saturation of 20% was established. This was done by applying vacuum to the core first and then injecting 3.7 ml of brine. The core was shut in for 1 hour, allowing the brine to distribute through the core. Methane at 250°F was then flowed through the core using five flow rates and the pressure drop across the core for each flow rate was recorded. The calculated gas permeability

was 192 md. The flood conditions and results are shown in Table A.5.4 and Table A.4.5 respectively. Figure A.4.2 shows the pressure drop measured across the core during the methane flood at S_{wi} .

Synthetic volatile oil mixture 4 (Table 3.3) was used for the two-phase flow measurements. The mixture was allowed a minimum of 12 hours to equilibrate to a single phase at 4200 psi and 155°F. The initial flood was conducted with the upstream backpressure regulator (BPR-1) set at 4280 psi and the downstream back pressure regulator (BPR-2) set at 780 psi. Volatile oil was injected at an upstream BPR-1 flow rate of 30 cc/hr (this is for volatile oil at single liquid phase). Once steady state was observed the pressure drop across the core was measured. This procedure was repeated for a BPR-2 pressure of 1460 psi. This allowed having different capillary numbers and PVT ratios. The capillary number ranged from 1.6×10^{-5} to 6.8×10^{-6} and the PVT ratio from 1.0 to 0.59. Table A.3.6 gives the fluid properties of the synthetic fluid calculated using the Peng-Robinson EOS at the flowing core pressures. Figure A.4.3 shows the pressure drop measured across the core during the initial two-phase volatile oil flood for the different BPR-2 pressures.

The core was then treated using chemical treatment 3 (Table 4.15). The solution was heated for at least 1 hour at 250°F. BPR1 was set at 1460 psi. The core was flooded with approximately 10 pore volumes of the treatment solution at a flow rate of 120 cc/hr. The core was then shut in for 2 hour. Figure A.4.4 shows the measured pressure drop across the core during the treatment flood.

Post-treatment two-phase volatile oil flood was conducted under the same conditions as the initial two-phase flow. Figure A.4.5 shows the pressure drop measured across the core during the post-treatment two-phase volatile oil flood. Initial improvement factor was 2.6.

One more batch of post-treatment volatile oil flood followed. The improvement factor was 2.1. Figure A.6.6 shows the second post-treatment volatile oil flood.

The final gas permeability was calculated following the procedure for the initial gas permeability using methane at 250°F. The calculated gas permeability was 174 md. The flood conditions and results are shown in Table A.4.7 and Table A.3.8 respectively. Figure A.6.10 shows the pressure drop across the core for the final methane flood.

For every two-phase volatile oil flood, oil and gas relative permeabilities k_{rg} and k_{ro} were calculated using the measured pressure drop across the core under steady state conditions and then improvement factors were measured. Table A.3.9 summarizes the experimental results.

Table A. 9.1 Core properties (Exp #189)

<i>Length, in</i>	8.023
<i>Diameter, in</i>	0.994
<i>Mass Core, gr</i>	221.56
<i>Grain Density, gr/cc</i>	2.65
<i>Porosity (ϕ)</i>	18.05%

Table A.9.2 Fluid properties and conditions for initial gas permeability (Exp #189)

		<i>Density, gr/cc</i>
<i>Gas</i>	Methane	
<i>Temperature, °F</i>	250	
<i>BPR 1-pressure, psi</i>	3156	0.1075
<i>BPR 2-pressure, psi</i>	785	2.72E-02
<i>Gas Viscosity, cp</i>	0.0149	

Table A.9.3 Initial methane flood results (Exp #189)

<i>q_{core}, cc/hr</i>	<i>ΔP, psi</i>	<i>k_g, md</i>
2371	2.880	203.86
3162	3.940	198.68
3952	5.060	193.38
4743	6.200	189.39
5928	7.880	186.26
<i>Corrected Permeability (k_g), md</i>		211.5

Table A.9.4 Fluid properties and conditions for methane gas permeability at S_{wi} (Exp #189)

		<i>Density, gr/cc</i>
<i>Gas</i>	Methane	
<i>Temperature, °F</i>	250	
<i>BPR 1-pressure, psi</i>	3120	0.1064
<i>BPR 2-pressure, psi</i>	785	2.72E-02
<i>Gas Viscosity, cp</i>	0.0149	

Table A.9.5 Methane flood results at S_{wi} (Exp #189)

q_{core} , cc/hr	ΔP , psi	k_g , md
2347	3.150	184.47
3129	4.370	177.30
3912	5.420	178.69
4694	6.700	173.46
5868	8.590	169.12
<i>Corrected Permeability (k_g), md</i>		191.8

Table A.9.6 Volatile oil properties at BPR-1 and BPR-2 pressures (Exp #189)

<i>BPR 1-pressure, psi</i>		4280		
<i>BPR 2- pressure, psi</i>		780	1460	
<i>Density at BPR 1-pressure, gr/cc</i>		0.359		
Properties of BPR 2-pressure, psi				
	780		1460	
	Gas Phase	Oil Phase	Gas Phase	Oil Phase
Density, gr/cc	0.0402	0.5905	0.0773	0.5451
Viscosity (μ), cp	0.0149	0.2059	0.0165	0.1573
Volume Fraction	0.9333	0.0667	0.8498	0.1502
IFT, dyne/cm	7.851		3.991	

Table A.9.7 Fluid properties and conditions for final gas permeability (Exp #189)

<i>Gas</i>	<i>Methane</i>	<i>Density, gr/cc</i>
<i>Temperature, °F</i>	250	
<i>BPR 1-pressure, psi</i>	4337	0.141
<i>BPR 2-pressure, psi</i>	1440	0.0503
<i>Gas Viscosity, cp</i>	0.0158	

Table A.9.8 Final methane flood results (Exp #189)

$q_{core}, cc/hr$	$\Delta P, psi$	k_g, md
1682	2.700	163.54
2243	3.500	168.22
2803	4.360	168.79
3364	5.320	166.00
4205	6.890	160.22
<i>Corrected Permeability (k_g), md</i>		174.18

Table A.9.9 Pre and post-treatment volatile oil flood results and measured improvement factors (Exp #189)

	Exp# 189	
$q_{g_{tot\ core}}, cc/hr$	701	365
$q_g, cc/hr$	654	311
$q_o, cc/hr$	47	55
<i>PVT Ratio</i>	1.01	0.59
<i>Viscosity Ratio μ_g/μ_o</i>	0.07	0.10
<i>Capillary Nc</i>	1.63E-05	6.81E-06
k_{rg} Before Treatment	0.042	0.105
k_{ro} Before Treatment	0.042	0.176
k_{rg} After Treatment	0.109	0.098
k_{ro} After Treatment	0.107	0.165
<i>Initial Improvement Factor</i>	2.6	*
<i>PV of Vol Oil Injected</i>	~490	
<i>Final Improvement Factor</i>	2.1	0.9

* Data not measured

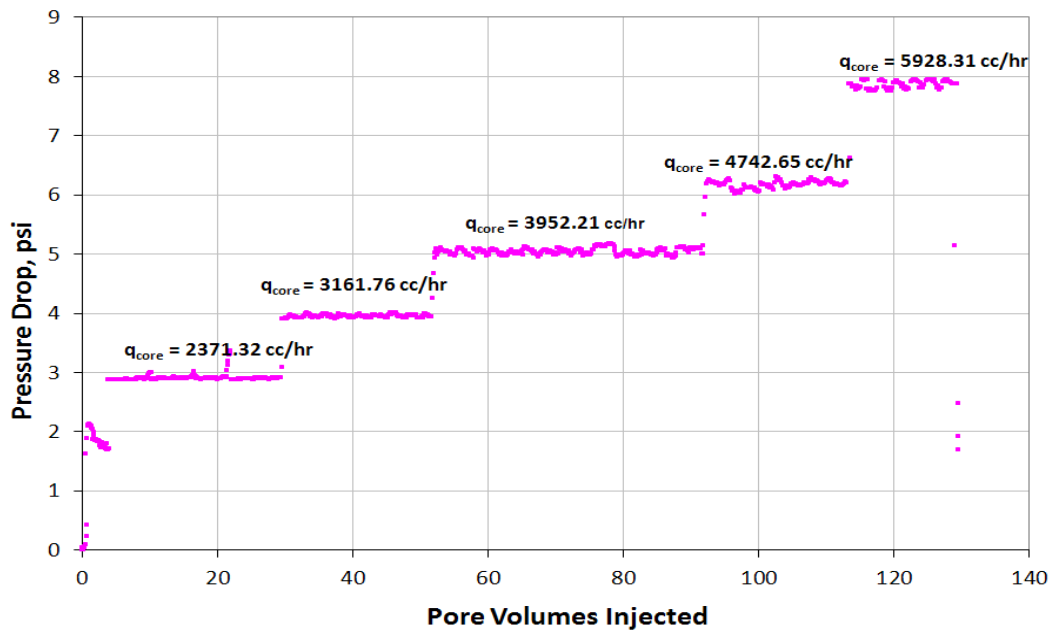


Figure A.9.1 Pressure drop across the core during the initial methane flood at 250°F (Exp #189)

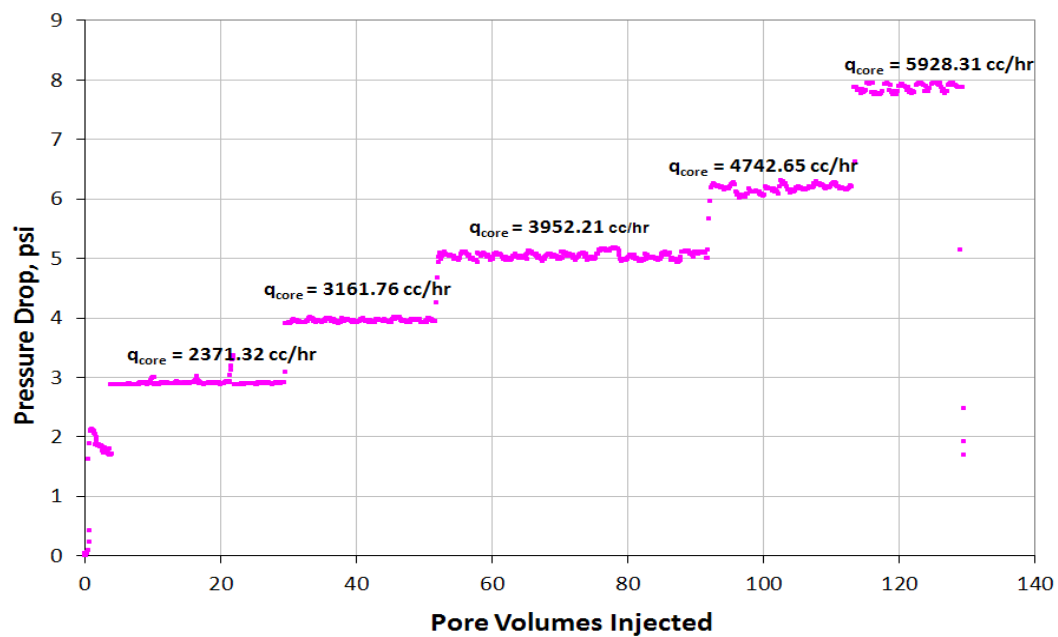


Figure A.9.2 Pressure drop across the core during the methane flood at S_{wi} of 20% (Exp #189)

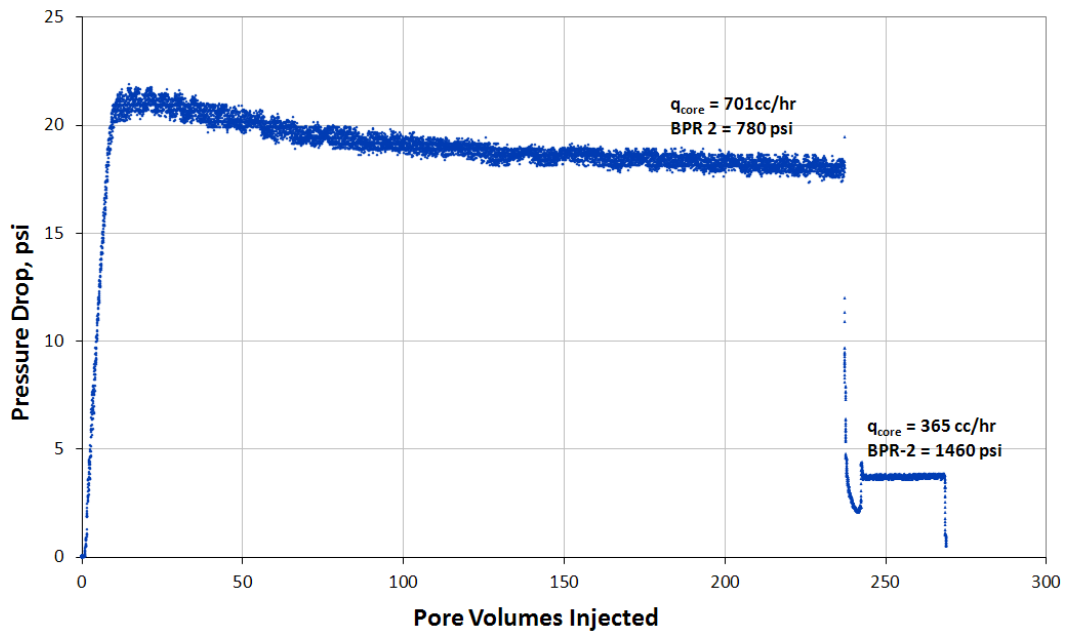


Figure A.9.3 Pressure drop across the core during the pre-treatment two-phase volatile oil flood (Exp #189)

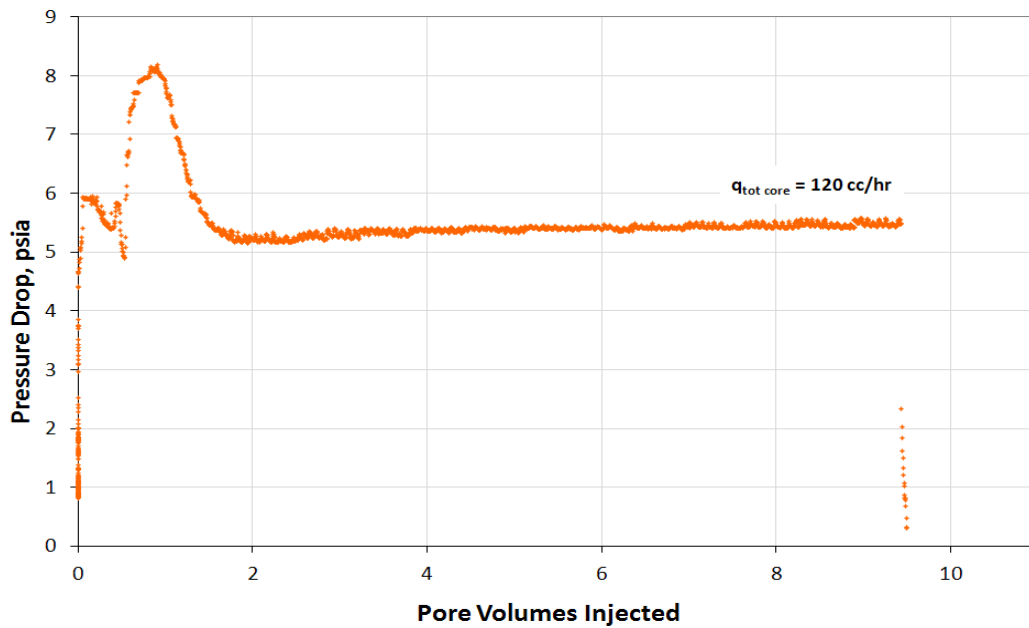


Figure A.9.4 Pressure drop across the core during injection of chemical treatment 3 (Exp # 189)

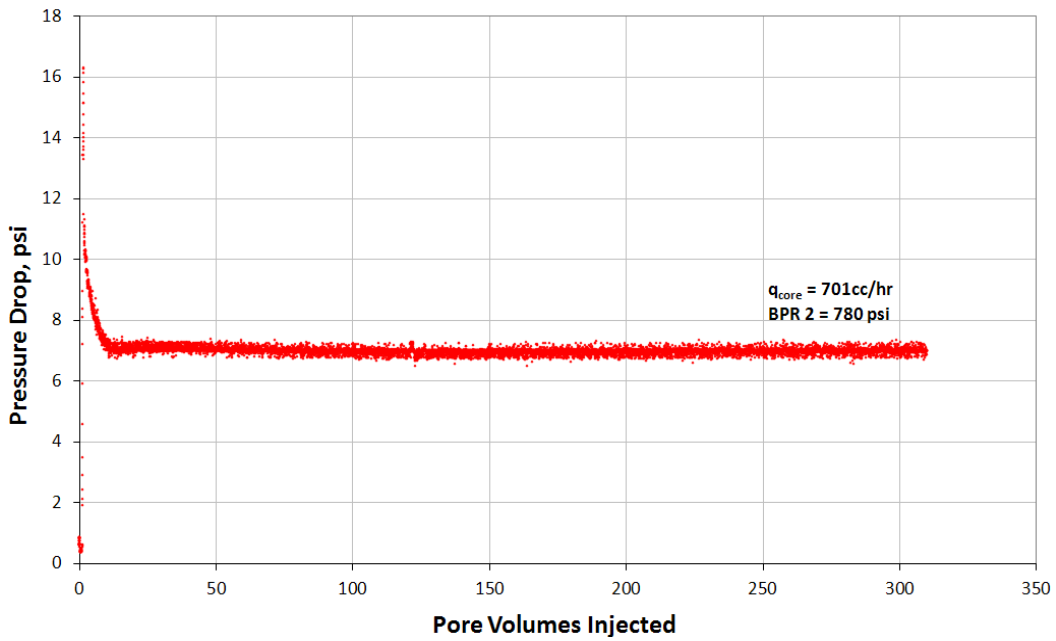


Figure A.9.5 Pressure drop across the core during the post-treatment two-phase volatile oil flood (Exp #189)

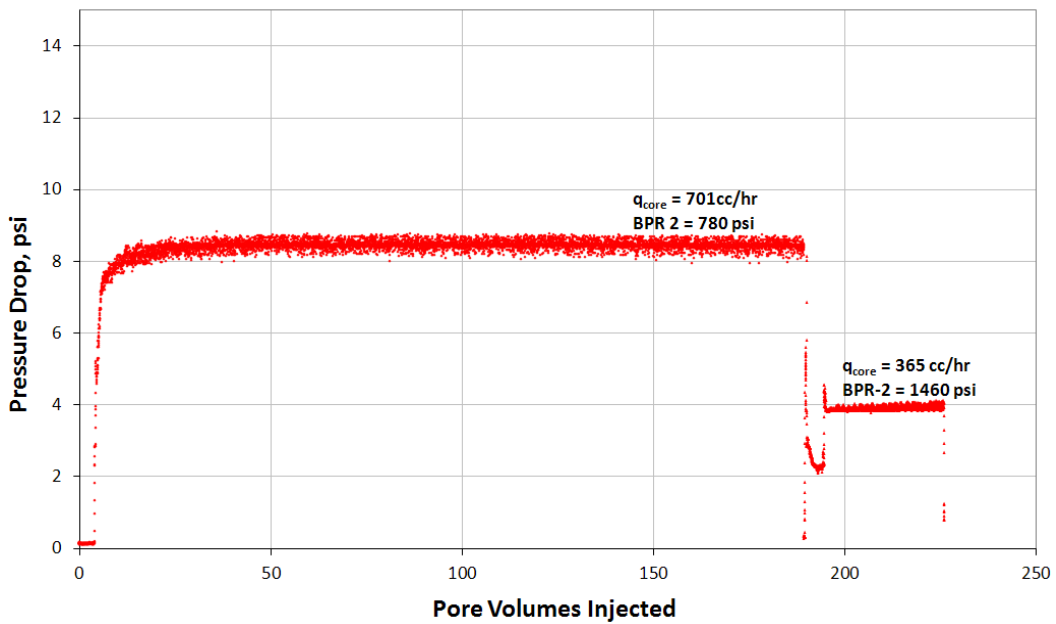


Figure A.9.6 Pressure drop across the core during the post-treatment two-phase volatile oil flood 2 (Exp #189)

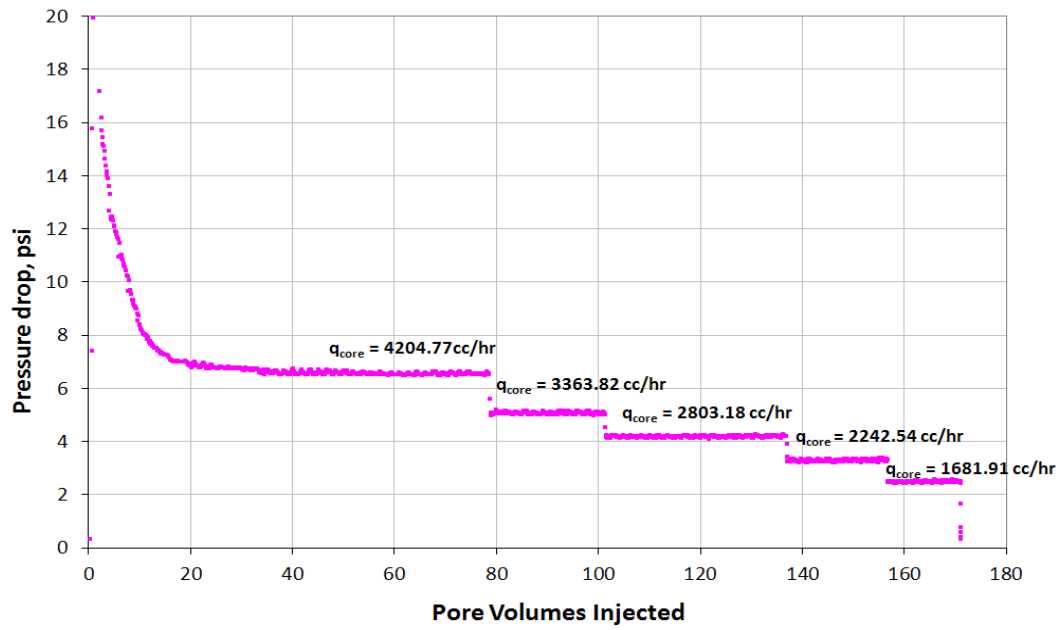


Figure A.9.7 Pressure drop across the core during the final methane flood at 250°F (Exp #189)

Appendix A.10: EXPERIMENT #192

Objective:

The objective of this experiment was to investigate the effectiveness of chemical treatment 4 using the cationic fluoro-surfactant L-19773#9 in improving the oil and gas relative permeability. This was done for a volatile oil mixture below the bubble point pressure on a Berea sandstone core and in the presence of initial water saturation. The experiment was performed at 155°F.

Experimental Procedure and Results:

A Berea sandstone core was prepared for the experiment following the standard procedure described Section 3.2.1.1. The initial core measurements and assumed properties can be found in Table A. 7.1.

The initial gas permeability was calculated using methane at 155°F. Methane was flowed through the core using five flow rates and the pressure drop across the core for each flow rate was recorded. Using this data, the fluid properties and accounting for non-Darcy effects the calculated gas permeability was 205 md. Table A.5.2 summarizes the flood conditions and fluid properties and Table A.5.3 shows the results. Figure A.6.1 shows the pressure drop measured across the core during the methane flood.

The initial gas permeability at initial water saturation was calculated next. Using synthetic brine 1 (25,000 ppm NaCl) an initial water saturation of 20% was established. This was done by applying vacuum to the core first and then injecting 2.4 ml of brine. The core was shut in for 1 hour, allowing the brine to distribute through the core. Methane at 155°F was then flowed through the core using five flow rates and the pressure drop across the core for each flow rate was recorded. The calculated gas permeability

was 123 md. The flood conditions and results are shown in Table A.5.4 and Table A.4.5 respectively. Figure A.4.2 shows the pressure drop measured across the core during the methane flood at S_{wi} .

Synthetic volatile oil mixture 2 (Table 3.3) was used for the two-phase flow measurements. The mixture was allowed a minimum of 12 hours to equilibrate to a single phase at 4200 psi and 155°F. The initial flood was conducted with the upstream backpressure regulator (BPR-1) set at 4454 psi and the downstream back pressure regulator (BPR-2) set at 1042 psi. Volatile oil was injected at an upstream BPR-1 flow rate of 125 cc/hr (this is for volatile oil at single liquid phase). Once steady state was observed the pressure drop across the core was measured. This procedure was repeated for an upstream BPR-1 flow rate of 250 cc/hr. This allowed having different capillary numbers. The capillary number ranged from 2.5×10^{-5} to 4.3×10^{-5} and the PVT ratio was 0.77. Table A.3.6 gives the fluid properties of the synthetic fluid calculated using the Peng-Robinson EOS at the flowing core pressures. Figure A.4.3 shows the pressure drop measured across the core during the initial two-phase volatile oil flood for the different BPR-2 pressures.

The core was then treated using chemical treatment 4 (Table 4.15). The solution was heated for at least 1 hour at 155°F. BPR1 was set at 1040 psi. The core was flooded with approximately 18 pore volumes of the treatment solution at a flow rate of 120 cc/hr. The core was then shut in for 12 hours. Figure A.4.4 shows the measured pressure drop across the core during the treatment flood.

Post-treatment two-phase volatile oil flood was conducted under the same conditions as the initial two-phase flow. Figure A.4.5 shows the pressure drop measured across the core during the post-treatment two-phase volatile oil flood. Initial improvement factor was approximately 1.8.

A second batch of post-treatment volatile oil flood followed. The improvement factor ranged from 1.6 to 1.4. Figure A.6.6 shows the second post-treatment volatile oil flood.

The final gas permeability was calculated following the procedure for the initial gas permeability using methane at 155°F. The calculated gas permeability was 86 md. The flood conditions and results are shown in Table A.4.7 and Table A.3.8 respectively. Figure A.6.10 shows the pressure drop across the core for the final methane flood.

For every two-phase volatile oil flood, oil and gas relative permeabilities k_{rg} and k_{ro} were calculated using the measured pressure drop across the core under steady state conditions and then improvement factors were measured. Table A.3.9 summarizes the experimental results.

Table A. 10.1 Core properties (Exp #192)

<i>Length, in</i>	5.617
<i>Diameter, in</i>	0.994
<i>Mass Core, gr</i>	157.82
<i>Grain Density, gr/cc</i>	2.65
<i>Porosity (ϕ)</i>	16.62%

Table A.10.2 Fluid properties and conditions for initial gas permeability (Exp #192)

		<i>Density, gr/cc</i>
<i>Gas</i>	Methane	
<i>Temperature, °F</i>	155	
<i>BPR 1-pressure, psi</i>	2610	0.1108
<i>BPR 2-pressure, psi</i>	1045	4.36E-02
<i>Gas Viscosity, cp</i>	0.0134	

Table A.10.3 Initial methane flood results (Exp #192)

<i>q_{core}, cc/hr</i>	<i>ΔP, psi</i>	<i>k_g, md</i>
1525	1.380	172.24
2033	2.010	157.67
2541	2.700	146.72
3050	3.400	139.82
3812	4.550	130.60
<i>Corrected Permeability (k_g), md</i>		204.9

Table A.10.4 Fluid properties and conditions for methane gas permeability at S_{wi} (Exp #192)

		<i>Density, gr/cc</i>
<i>Gas</i>	Methane	
<i>Temperature, °F</i>	155	
<i>BPR 1-pressure, psi</i>	2600	0.1104
<i>BPR 2-pressure, psi</i>	1040	4.34E-02
<i>Gas Viscosity, cp</i>	0.017	

Table A.10.5 Methane flood results at S_{wi} (Exp #192)

q_{core} , cc/hr	ΔP , psi	k_g , md
1526		
2035	3.670	109.66
2544	4.690	107.27
3053	5.710	105.73
3816	7.510	100.48
<i>Corrected Permeability (k_g), md</i>		122.6

Table A.10.6 Volatile oil properties at BPR-1 and BPR-2 pressures (Exp #192)

<i>BPR 1-pressure, psi</i>	4454	
<i>BPR 2- pressure, psi</i>	1042	
<i>Density at BPR 1-pressure, gr/cc</i>	0.3722	
Properties at BPR 2- pressure, psi		
	Gas Phase	Oil Phase
<i>Density, gr/cc</i>	0.0575	0.5868
<i>Viscosity (μ), cp</i>	0.0134	0.1723
<i>Volume Fraction</i>	0.9078	0.0922
<i>IFT, dyne/cm</i>	7.01	

Table A.10.7 Fluid properties and conditions for final gas permeability (Exp #192)

		<i>Density, gr/cc</i>
<i>Gas</i>	Methane	
<i>Temperature, °F</i>	155	
<i>BPR 1-pressure, psi</i>	2705	0.1146
<i>BPR 2-pressure, psi</i>	1040	0.0434
<i>Gas Viscosity, cp</i>	0.0134	

Table A.10.8 Final methane flood results (Exp #192)

q_{core} , cc/hr	ΔP , psi	k_g , md
1584	3.000	82.33
2112	3.950	83.37
2641	4.950	83.16
3169	6.050	81.65
3961	7.710	80.08
<i>Corrected Permeability (k_g), md</i>		85.61

Table A.10.9 Pre and post-treatment volatile oil flood results and measured improvement factors (Exp #192)

	Exp# 192	
$q_{g_{tot\ core}}$, cc/hr	438	875
q_g , cc/hr	397	795
q_o , cc/hr	40	81
<i>PVT Ratio</i>	0.77	
<i>Viscosity Ratio μ_g/μ_o</i>	0.08	
<i>Capillary Nc</i>	2.49E-05	4.28E-05
k_{rg} Before Treatment	0.017	0.020
k_{ro} Before Treatment	0.022	0.026
k_{rg} After Treatment	0.031	0.030
k_{ro} After Treatment	0.040	0.039
<i>Initial Improvement Factor</i>	1.8	1.5
<i>PV of Vol Oil Injected</i>	~ 550	
<i>Final Improvement Factor</i>	1.6	1.4

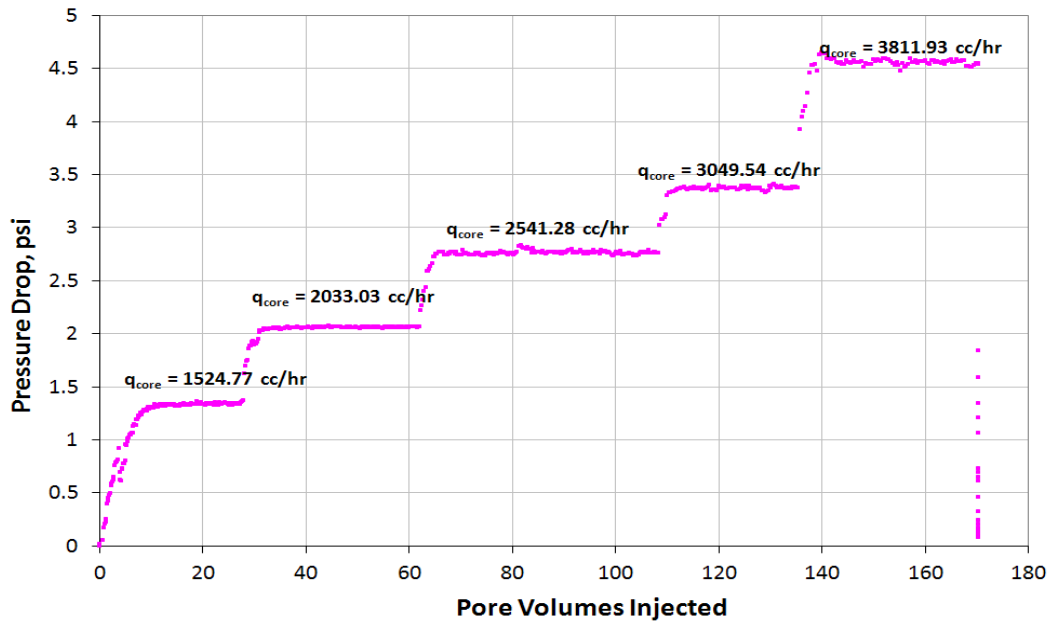


Figure A.10.1 Pressure drop across the core during the initial methane flood at 155°F (Exp #192)

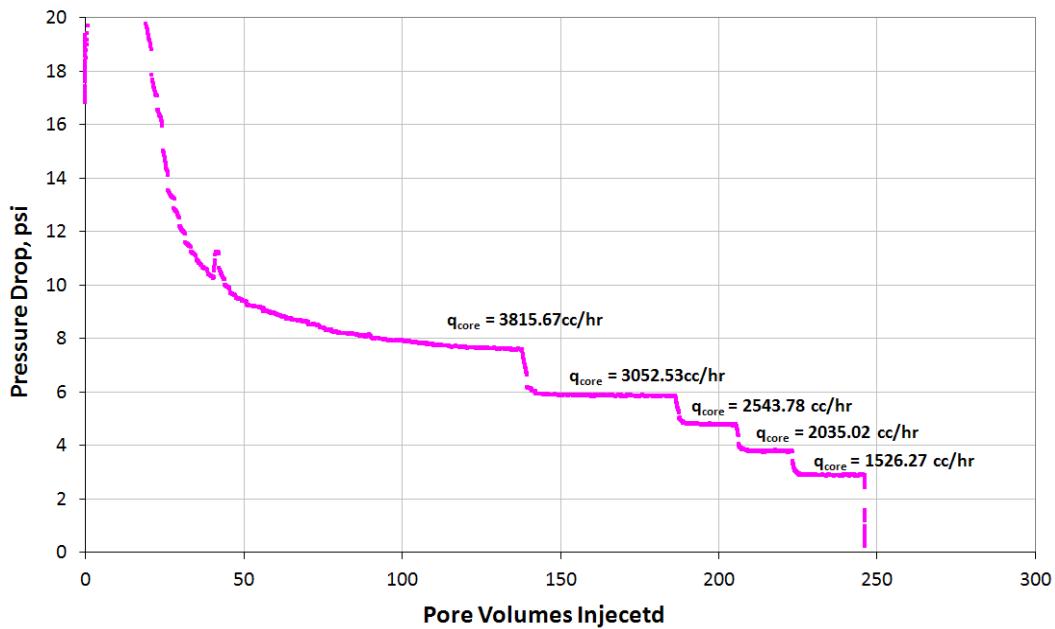


Figure A.10.2 Pressure drop across the core during the methane flood at S_{wi} of 20% (Exp #192)

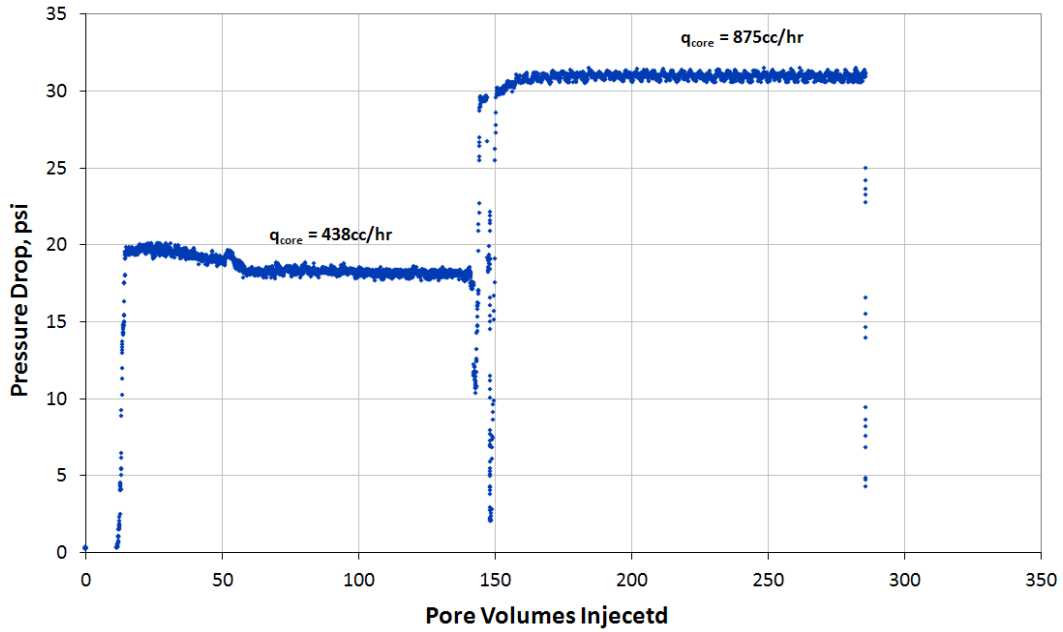


Figure A.10.3 Pressure drop across the core during the pre-treatment two-phase volatile oil flood (Exp #192)

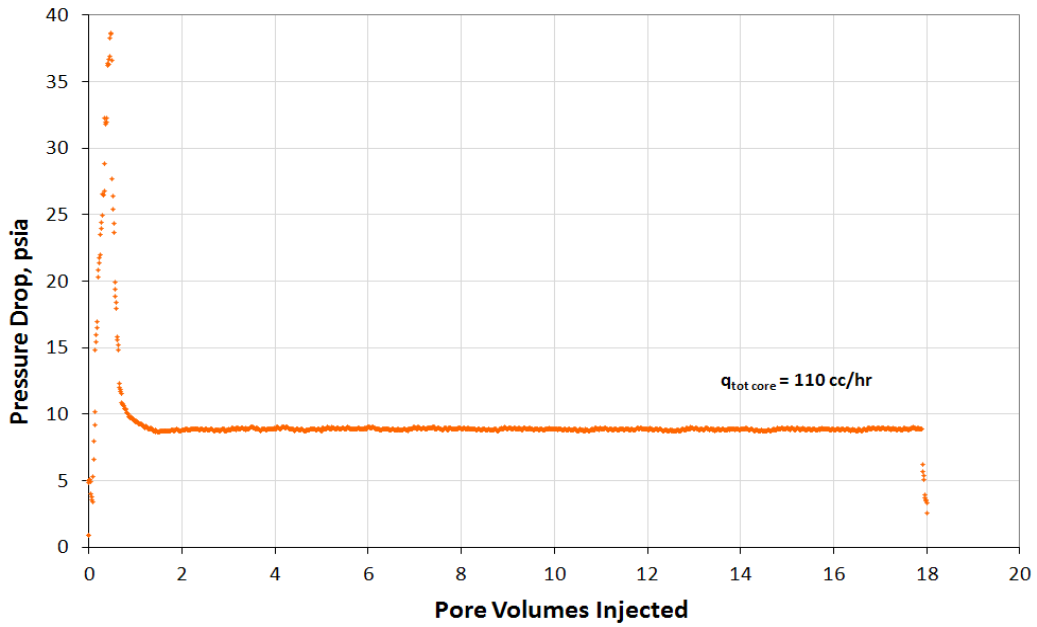


Figure A.10.4 Pressure drop across the core during injection of chemical treatment 4 (Exp # 192)

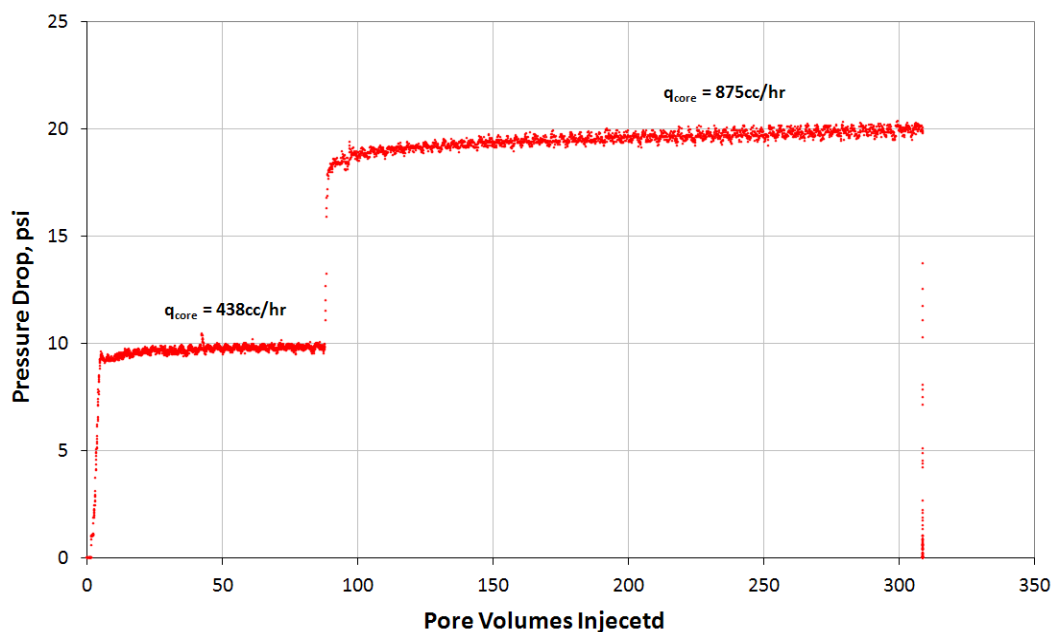


Figure A.10.5 Pressure drop across the core during the post-treatment two-phase volatile oil flood (Exp #192)

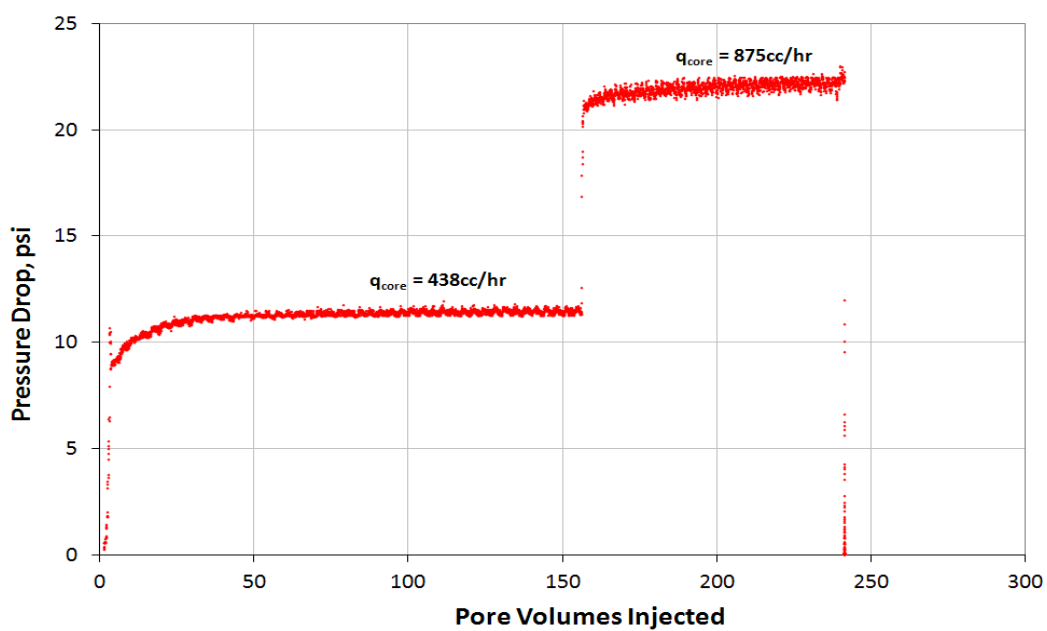


Figure A.10.6 Pressure drop across the core during the post-treatment two-phase volatile oil flood 2 (Exp #192)

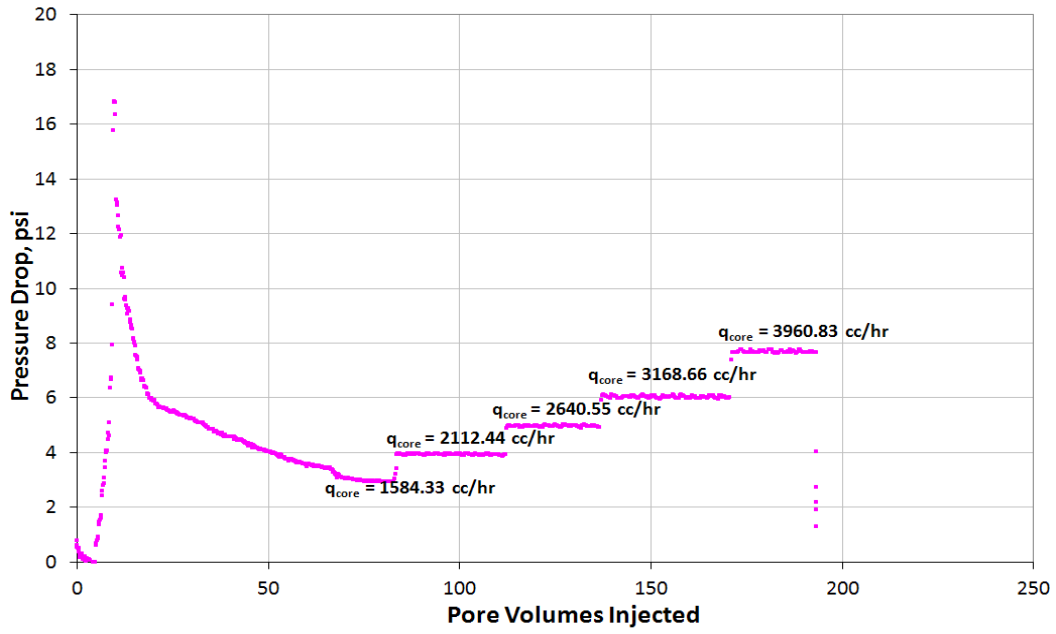


Figure A.10.7 Pressure drop across the core during the final methane flood at 155°F (Exp #192)

Appendix A.11: EXPERIMENT #196

Objective:

The objective of this experiment was to investigate the effectiveness of chemical treatment 4 using the cationic fluoro-surfactant L-19773#9 in improving the oil and gas relative permeability in low permeability cores. This was done for a volatile oil mixture below the bubble point pressure on a Torrey Buff sandstone core and in the presence of initial water saturation. The experiment was performed at 155°F.

Experimental Procedure and Results:

A Torrey Buff sandstone core was prepared for the experiment following the standard procedure described Section 3.2.1.1. The initial core measurements and assumed properties can be found in Table A. 7.1.

The initial gas permeability was calculated using methane at 155°F. Methane was flowed through the core using four flow rates and the pressure drop across the core for each flow rate was recorded. Using this data, the fluid properties and accounting for non-Darcy effects the calculated gas permeability was 1.1 md. Table A.5.2 summarizes the flood conditions and fluid properties and Table A.5.3 shows the results. Figure A.6.1 shows the pressure drop measured across the core during the methane flood.

The initial gas permeability at initial water saturation was calculated next. Using synthetic brine 1 (25,000 ppm NaCl) an initial water saturation of 20% was established. This was done by applying vacuum to the core first and then injecting 1 ml of brine. The core was shut in for 1 hour, allowing the brine to distribute through the core. Methane at 155°F was then flowed through the core using four flow rates and the pressure drop across the core for each flow rate was recorded. The calculated gas permeability was 0.8

md. The flood conditions and results are shown in Table A.5.4 and Table A.4.5 respectively. Figure A.4.2 shows the pressure drop measured across the core during the methane flood at S_{wi} .

Synthetic volatile oil mixture 2 (Table 3.3) was used for the two-phase flow measurements. The mixture was allowed a minimum of 12 hours to equilibrate to a single phase at 4200 psi and 155°F. The initial flood was conducted with the upstream backpressure regulator (BPR-1) set at 4400 psi and the downstream back pressure regulator (BPR-2) set at 672 psi. Volatile oil was injected at an upstream BPR-1 flow rate of 35 cc/hr (this is for volatile oil at single liquid phase). Once steady state was observed the pressure drop across the core was measured. Capillary number was 3.1×10^{-6} and the PVT ratio was 0.99. Table A.3.6 gives the fluid properties of the synthetic fluid calculated using the Peng-Robinson EOS at the flowing core pressures. Figure A.4.3 shows the pressure drop measured across the core during the initial two-phase volatile oil flood for the different BPR-2 pressures.

The core was then treated using chemical treatment 4 (Table 4.15). The solution was heated for at least 1 hour at 155°F. BPR-2 was set at 700 psi. The core was flooded with approximately 33 pore volumes of the treatment solution at a flow rate of 25 cc/hr. The core was then shut in for 12 hours. Figure A.4.4 shows the measured pressure drop across the core during the treatment flood.

Post-treatment two-phase volatile oil flood was conducted under the same conditions as the initial two-phase flow. Figure A.4.5 shows the pressure drop measured across the core during the post-treatment two-phase volatile oil flood. The improvement factor was approximately 1.1.

The final gas permeability was calculated following the procedure for the initial gas permeability using methane at 155°F. The calculated gas permeability was 0.6 md.

The flood conditions and results are shown in Table A.4.7 and Table A.3.8 respectively. Figure A.6.10 shows the pressure drop across the core for the final methane flood.

For every two-phase volatile oil flood, oil and gas relative permeabilities k_{rg} and k_{ro} were calculated using the measured pressure drop across the core under steady state conditions and then improvement factors were measured. Table A.3.9 summarizes the experimental results.

Table A. 11.1 Core properties (Exp #196)

<i>Length, in</i>	2.261
<i>Diameter, in</i>	0.997
<i>Mass Core, gr</i>	64.65
<i>Grain Density, gr/cc</i>	2.72
<i>Porosity (ϕ)</i>	17.83%

Table A.11.2 Fluid properties and conditions for initial gas permeability (Exp #196)

		<i>Density, gr/cc</i>
<i>Gas</i>	Methane	
<i>Temperature, °F</i>	155	
<i>BPR 1-pressure, psi</i>	3450	0.1421
<i>BPR 2-pressure, psi</i>	840	3.48E-02
<i>Gas Viscosity, cp</i>	0.0136	

Table A.11.3 Initial methane flood results (Exp #196)

<i>q_{core}, cc/hr</i>	<i>ΔP, psi</i>	<i>k_g, md</i>
408	25.700	1.01
613	40.600	0.95
817	55.700	0.96
1021	71.500	0.90
<i>Corrected Permeability (k_g), md</i>		1.1

Table A.11.4 Fluid properties and conditions for methane gas permeability at S_{wi} (Exp #196)

		<i>Density, gr/cc</i>
<i>Gas</i>	Methane	
<i>Temperature, °F</i>	155	
<i>BPR 1-pressure, psi</i>	2530	0.1088
<i>BPR 2-pressure, psi</i>	690	2.83E-02
<i>Gas Viscosity, cp</i>	0.0134	

Table A.11.5 Methane flood results at S_{wi} (Exp #196)

q_{core} , cc/hr	ΔP , psi	k_g , md
384	30.100	0.80
577	45.270	0.79
769	59.500	0.81
961	73.850	0.81
<i>Corrected Permeability (k_g), md</i>		0.8

Table A.11.6 Volatile oil properties at BPR-1 and BPR-2 pressures (Exp #196)

<i>BPR 1-pressure, psi</i>	4400	
<i>BPR 2- pressure, psi</i>	672	
<i>Density at BPR 1-pressure, gr/cc</i>	0.3705	
Properties at BPR 2- pressure, psi		
	Gas Phase	Oil Phase
<i>Density, gr/cc</i>	0.036	0.6145
<i>Viscosity (μ), cp</i>	0.0133	0.2446
<i>Volume Fraction</i>	0.9481	0.0519
<i>IFT, dyne/cm</i>	10.08	

Table A.11.7 Fluid properties and conditions for final gas permeability (Exp #196)

		<i>Density, gr/cc</i>
<i>Gas</i>	Methane	
<i>Temperature, °F</i>	155	
<i>BPR 1-pressure, psi</i>	2705	0.173
<i>BPR 2-pressure, psi</i>	1040	0.0441
<i>Gas Viscosity, cp</i>	0.0139	

Table A.11.8 Final methane flood results (Exp #196)

q_{core} , cc/hr	ΔP , psi	k_g , md
392	39.600	0.64
588	59.800	0.64
785	79.400	0.64
981	99.500	0.64
<i>Corrected Permeability (k_g), md</i>		0.64

Table A.11.9 Pre and post-treatment volatile oil flood results and measured improvement factors (Exp #196)

	Exp# 196
$q_{gtot\ core}, cc/hr$	196
$q_g, cc/hr$	186
$q_o, cc/hr$	10
<i>PVT Ratio</i>	0.99
<i>Viscosity Ratio μ_g/μ_o</i>	0.05
<i>Capillary Nc</i>	3.07E-06
k_{rg} Before Treatment	0.044
k_{ro} Before Treatment	0.044
k_{rg} After Treatment	0.049
k_{ro} After Treatment	0.049
<i>Initial Improvement Factor</i>	1.1
<i>PV of Vol Oil Injected</i>	~850
<i>Final Improvement Factor</i>	*

* A second batch of a volatile oil was not injected

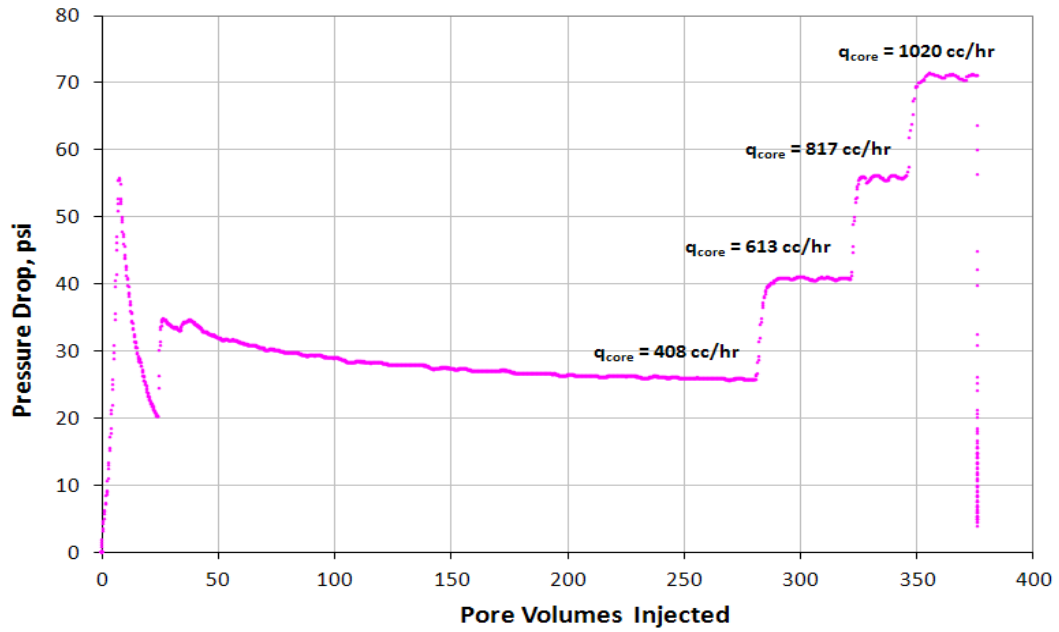


Figure A.11.1 Pressure drop across the core during the initial methane flood at 155°F (Exp #196)

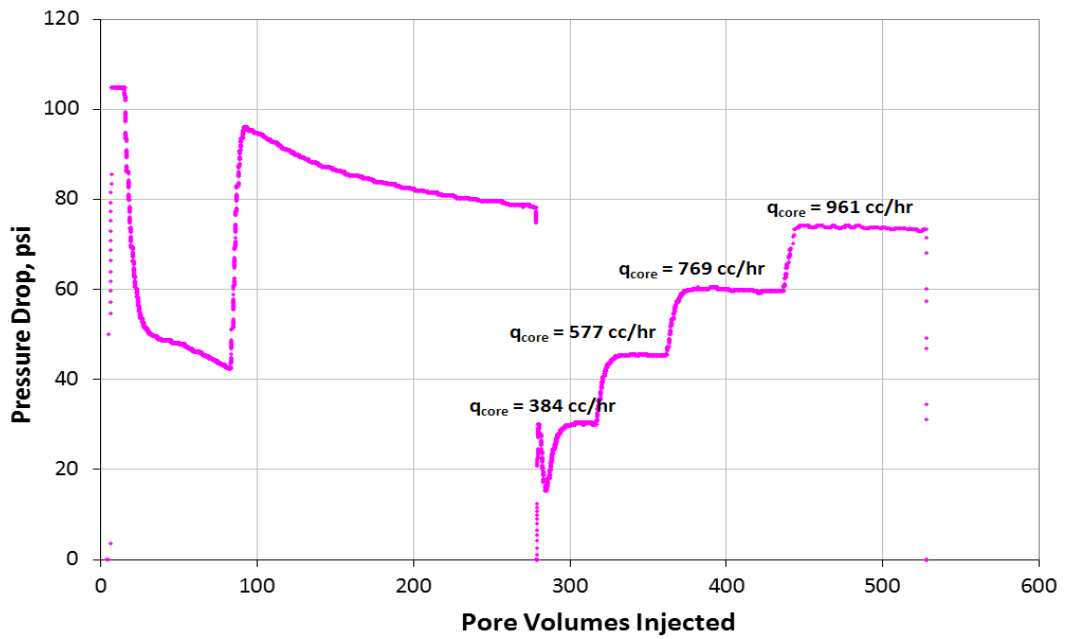


Figure A.11.2 Pressure drop across the core during the methane flood at S_{wi} of 20% (Exp #196)

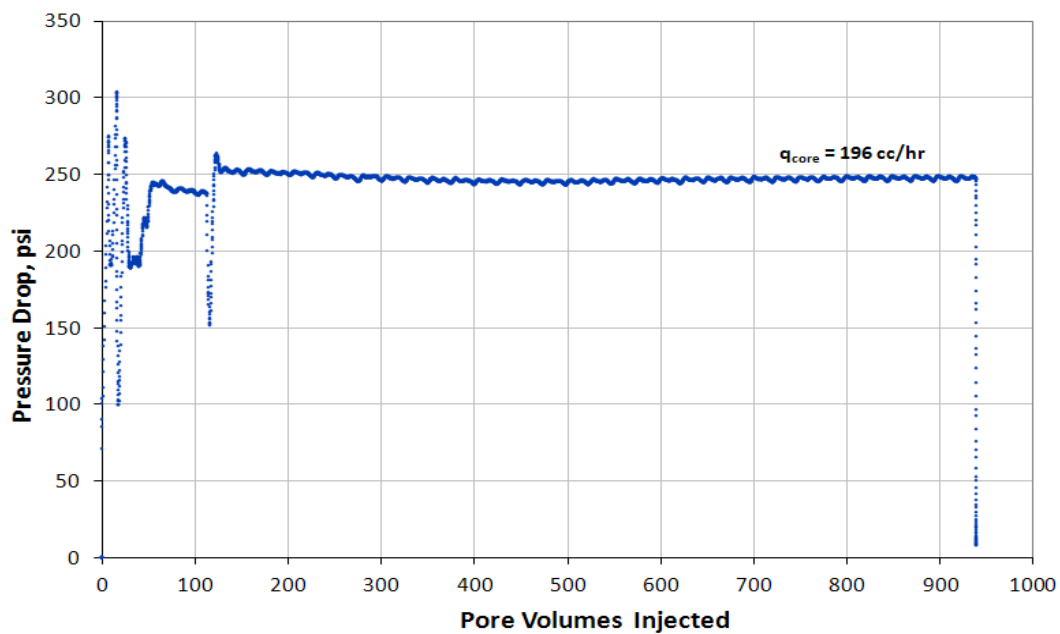


Figure A.11.3 Pressure drop across the core during the pre-treatment two-phase volatile oil flood (Exp #196)

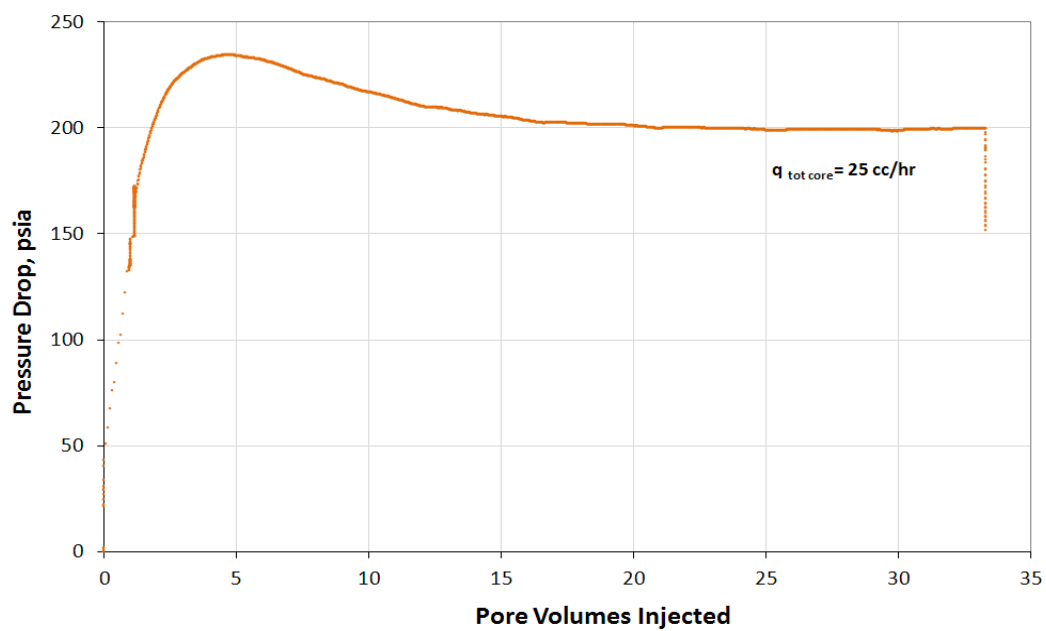


Figure A.11.4 Pressure drop across the core during injection of chemical treatment 4 (Exp # 196)

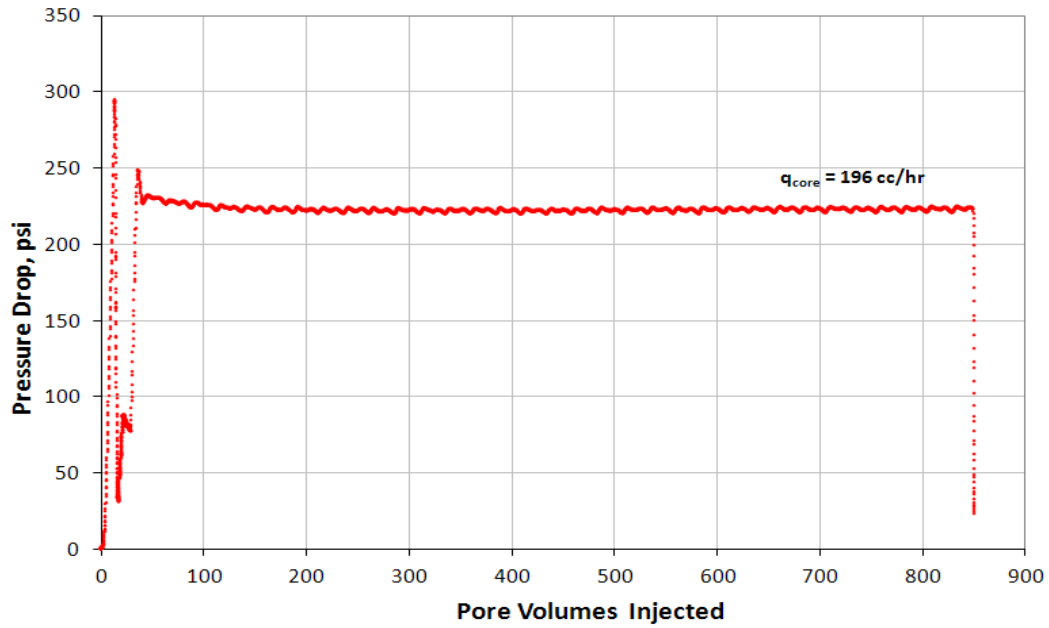


Figure A.11.5 Pressure drop across the core during the post-treatment two-phase volatile oil flood (Exp #196)

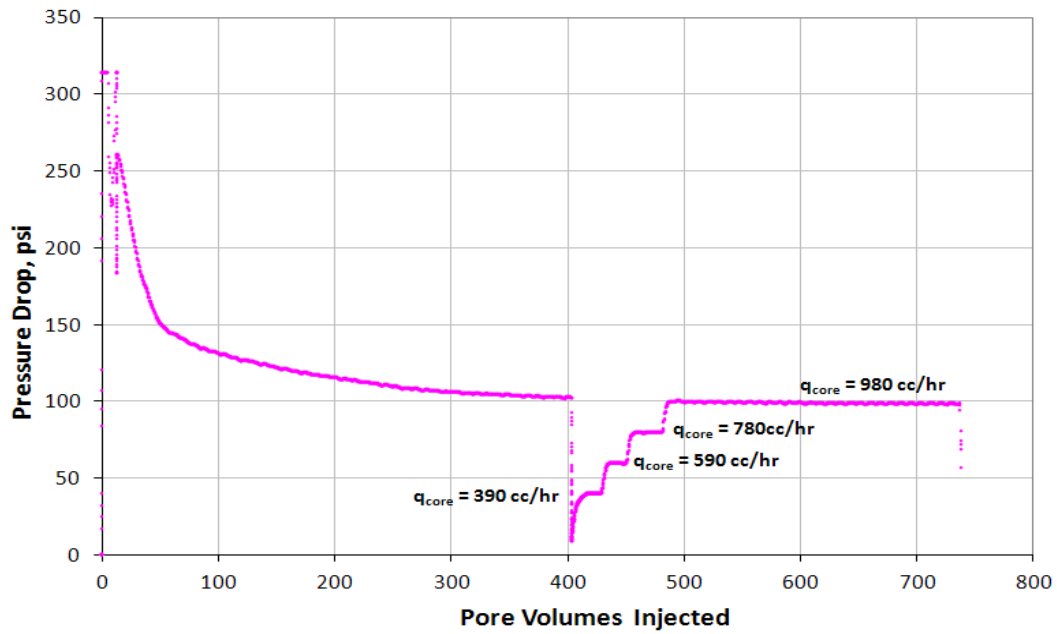


Figure A.11.6 Pressure drop across the core during the final methane flood at 155°F (Exp #196)

Appendix A.12: EXPERIMENT #198

Objective:

The objective of this experiment was to investigate the effectiveness of chemical treatment 4 using the cationic fluoro-surfactant L-19773#9 in improving the oil and gas relative permeability in low permeability cores. This was done for a volatile oil mixture below the bubble point pressure on a Torrey Buff sandstone core and in the presence of initial water saturation. The experiment was performed at 155°F.

Experimental Procedure and Results:

A Torrey Buff sandstone core was prepared for the experiment following the standard procedure described Section 3.2.1.1. The initial core measurements and assumed properties can be found in Table A. 7.1.

The initial gas permeability was calculated using methane at 155°F. Methane was flowed through the core using four flow rates and the pressure drop across the core for each flow rate was recorded. Using this data, the fluid properties and accounting for non-Darcy effects the calculated gas permeability was 2.7 md. Table A.5.2 summarizes the flood conditions and fluid properties and Table A.5.3 shows the results. Figure A.6.1 shows the pressure drop measured across the core during the methane flood.

The initial gas permeability at initial water saturation was calculated next. Using synthetic brine 1 (25,000 ppm NaCl) an initial water saturation of 20% was established. This was done by applying vacuum to the core first and then injecting 1.2 ml of brine. The core was shut in for 1 hour, allowing the brine to distribute through the core. Methane at 155°F was then flowed through the core using four flow rates and the pressure drop across the core for each flow rate was recorded. The calculated gas

permeability was 2.3 md. Flood conditions and results are shown in Table A.5.4 and Table A.4.5 respectively. Figure A.4.2 shows the pressure drop measured across the core during the methane flood at S_{wi} .

Synthetic volatile oil mixture 2 (Table 3.3) was used for the two-phase flow measurements. The mixture was allowed a minimum of 12 hours to equilibrate to a single phase at 4200 psi and 155°F. The initial flood was conducted with the upstream backpressure regulator (BPR-1) set at 4380 psi and the downstream back pressure regulator (BPR-2) set at 670 psi. Volatile oil was injected at an upstream BPR-1 flow rate of 74 cc/hr (this is for volatile oil at single liquid phase). Once steady state was observed the pressure drop across the core was measured. Capillary number was 5.1×10^{-6} and the PVT ratio was 1.0. Table A.3.6 gives the fluid properties of the synthetic fluid calculated using the Peng-Robinson EOS at the flowing core pressures. Figure A.4.3 shows the pressure drop measured across the core during the initial two-phase volatile oil flood for the different BPR-2 pressures.

The core was then treated using chemical treatment 4 (Table 4.15). The solution was heated for at least 1 hour at 155°F. BPR-2 was set at 700 psi. The core was flooded with approximately 16 pore volumes of the treatment solution at a flow rate of 20 cc/hr. The core was then shut in for 12 hours. Figure A.4.4 shows the measured pressure drop across the core during the treatment flood.

Post-treatment two-phase volatile oil flood was conducted under the same conditions as the initial two-phase flow. Figure A.4.5 shows the pressure drop measured across the core during the post-treatment two-phase volatile oil flood. The improvement factor was approximately 1.2.

The final gas permeability was calculated following the procedure for the initial gas permeability using methane at 155°F. The calculated gas permeability was 2.2 md.

Flood conditions and results are shown in Table A.4.7 and Table A.3.8 respectively. Figure A.6.10 shows the pressure drop across the core for the final methane flood.

For every two-phase volatile oil flood, oil and gas relative permeabilities k_{rg} and k_{ro} were calculated using the measured pressure drop across the core under steady state conditions and then improvement factors were measured. Table A.3.9 summarizes the experimental results.

Table A. 12.1 Core properties (Exp #198)

<i>Length, in</i>	2.527
<i>Diameter, in</i>	0.994
<i>Mass Core, gr</i>	71.04
<i>Grain Density, gr/cc</i>	2.72
<i>Porosity (ϕ)</i>	18.72%

Table A.12.2 Fluid properties and conditions for initial gas permeability (Exp #198)

		<i>Density, gr/cc</i>
<i>Gas</i>	Methane	
<i>Temperature, °F</i>	155	
<i>BPR 1-pressure, psi</i>	2410	0.1027
<i>BPR 2-pressure, psi</i>	960	3.99E-02
<i>Gas Viscosity, cp</i>	0.0138	

Table A.12.3 Initial methane flood results (Exp #198)

<i>q_{core}, cc/hr</i>	<i>ΔP, psi</i>	<i>k_g, md</i>
257	6.810	2.73
515	14.100	2.64
772	21.500	2.59
1030	28.900	2.57
<i>Corrected Permeability (k_g), md</i>		2.7

Table A.12.4 Fluid properties and conditions for methane gas permeability at S_{wi} (Exp #198)

		<i>Density, gr/cc</i>
<i>Gas</i>	Methane	
<i>Temperature, °F</i>	155	
<i>BPR 1-pressure, psi</i>	2410	0.1027
<i>BPR 2-pressure, psi</i>	960	3.99E-02
<i>Gas Viscosity, cp</i>	0.0138	

Table A.12.5 Methane flood results at S_{wi} (Exp #198)

q_{core} , cc/hr	ΔP , psi	k_g , md
257	7.980	2.33
515	16.200	2.30
772	24.200	2.30
1030	32.400	2.30
<i>Corrected Permeability (k_g), md</i>		2.3

Table A.12.6 Volatile oil properties at BPR-1 and BPR-2 pressures (Exp #198)

<i>BPR 1-pressure, psi</i>	4382	
<i>BPR 2- pressure, psi</i>	669	
<i>Density at BPR 1-pressure, gr/cc</i>	0.3699	
Properties at BPR 2- pressure, psi		
	Gas Phase	Oil Phase
<i>Density, gr/cc</i>	0.0359	0.6147
<i>Viscosity (μ), cp</i>	0.0133	0.245
<i>Volume Fraction</i>	0.9484	0.0516
<i>IFT, dyne/cm</i>	10.108	

Table A.12.7 Fluid properties and conditions for final gas permeability (Exp #198)

		<i>Density, gr/cc</i>
<i>Gas</i>	Methane	
<i>Temperature, °F</i>	155	
<i>BPR 1-pressure, psi</i>	3110	0.13
<i>BPR 2-pressure, psi</i>	665	0.0272
<i>Gas Viscosity, cp</i>	0.0133	

Table A.12.8 Final methane flood results (Exp #198)

q_{core} , cc/hr	ΔP , psi	k_g , md
478	14.760	2.25
956	29.500	2.26
1434	44.800	2.23
1912	59.400	2.24
<i>Corrected Permeability (k_g), md</i>		2.22

Table A.12.9 Pre and post-treatment volatile oil flood results and measured improvement factors (Exp #198)

	Exp# 198
$q_{g\text{tot core, cc/hr}}$	416
$q_g, \text{cc/hr}$	395
$q_o, \text{cc/hr}$	21
<i>PVT Ratio</i>	1.00
<i>Viscosity Ratio μ_g/μ_o</i>	0.05
<i>Capillary Nc</i>	5.07E-06
k_{rg} Before Treatment	0.057
k_{ro} Before Treatment	0.057
k_{rg} After Treatment	0.066
k_{ro} After Treatment	0.066
<i>Initial Improvement Factor</i>	1.2
<i>PV of Vol Oil Injected</i>	~380
<i>Final Improvement Factor</i>	*

* A second batch of a volatile oil was not injected

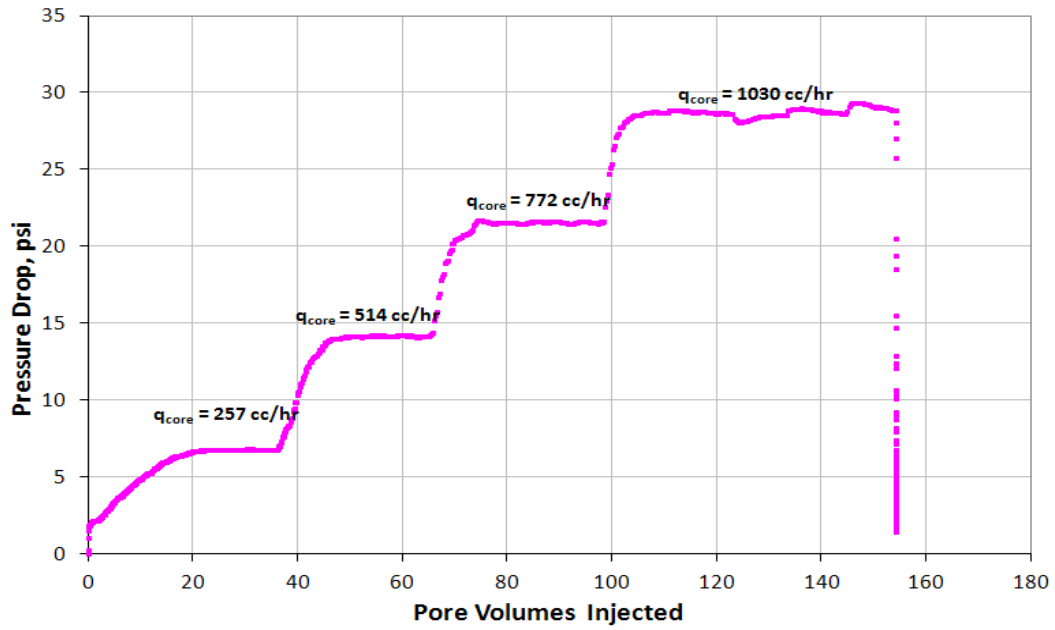


Figure A.12.1 Pressure drop across the core during the initial methane flood at 155°F (Exp #198)

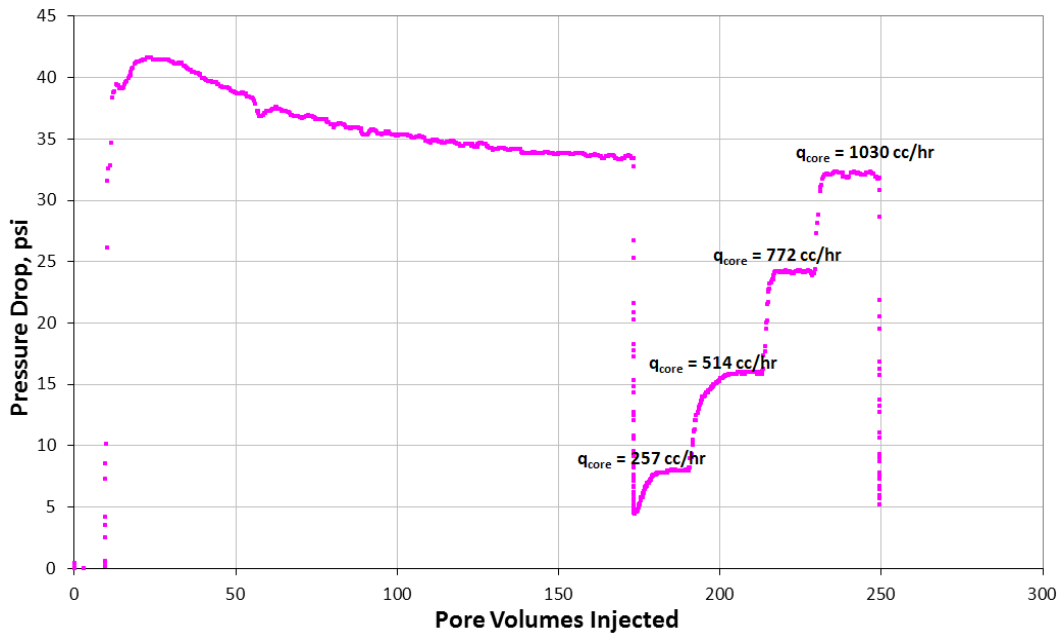


Figure A.12.2 Pressure drop across the core during the methane flood at S_{wi} of 20% (Exp #198)

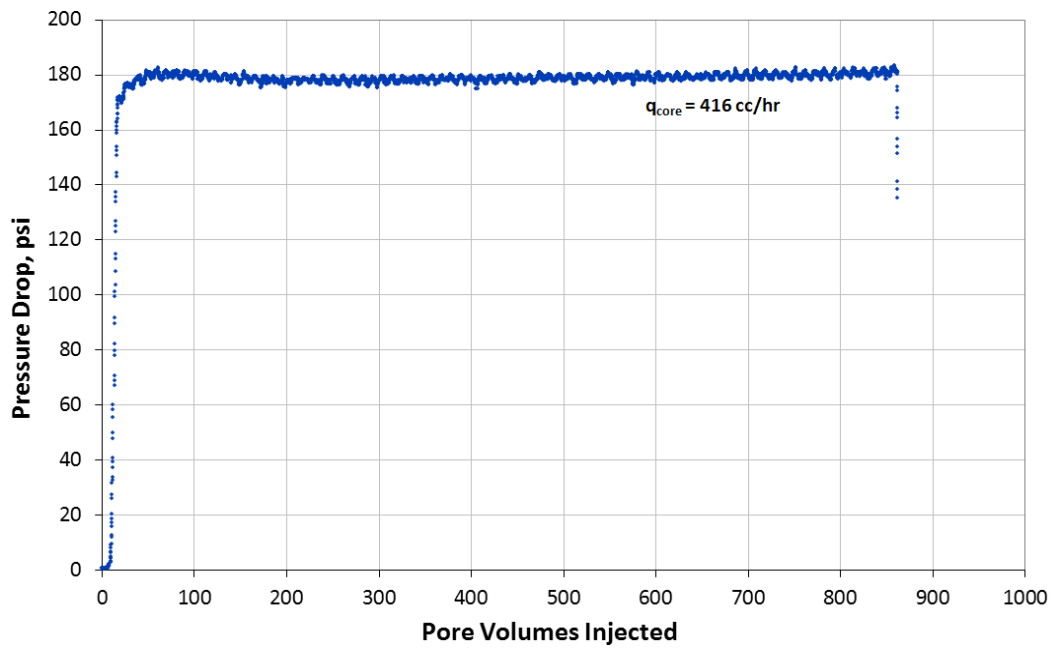


Figure A.12.3 Pressure drop across the core during the pre-treatment two-phase volatile oil flood (Exp #198)

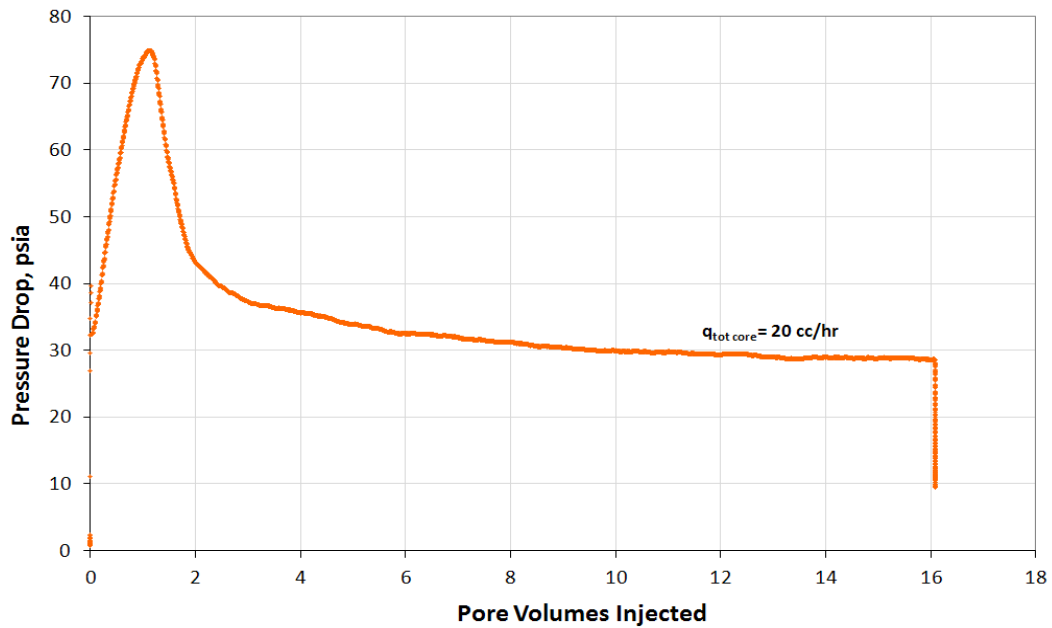


Figure A.12.4 Pressure drop across the core during injection of chemical treatment 4 (Exp # 198)

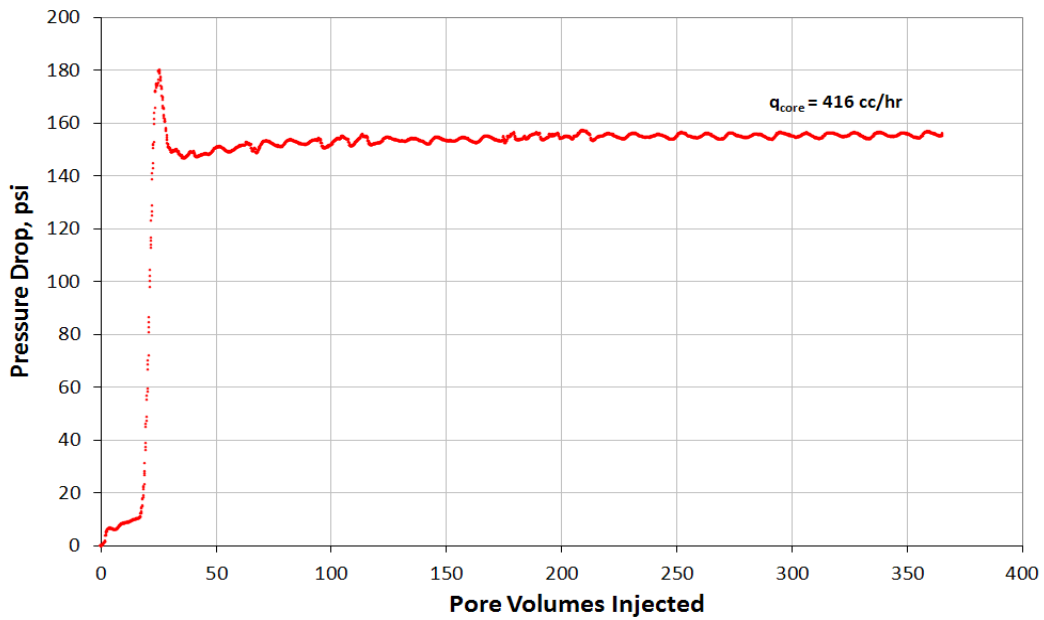


Figure A.12.5 Pressure drop across the core during the post-treatment two-phase volatile oil flood (Exp #198)

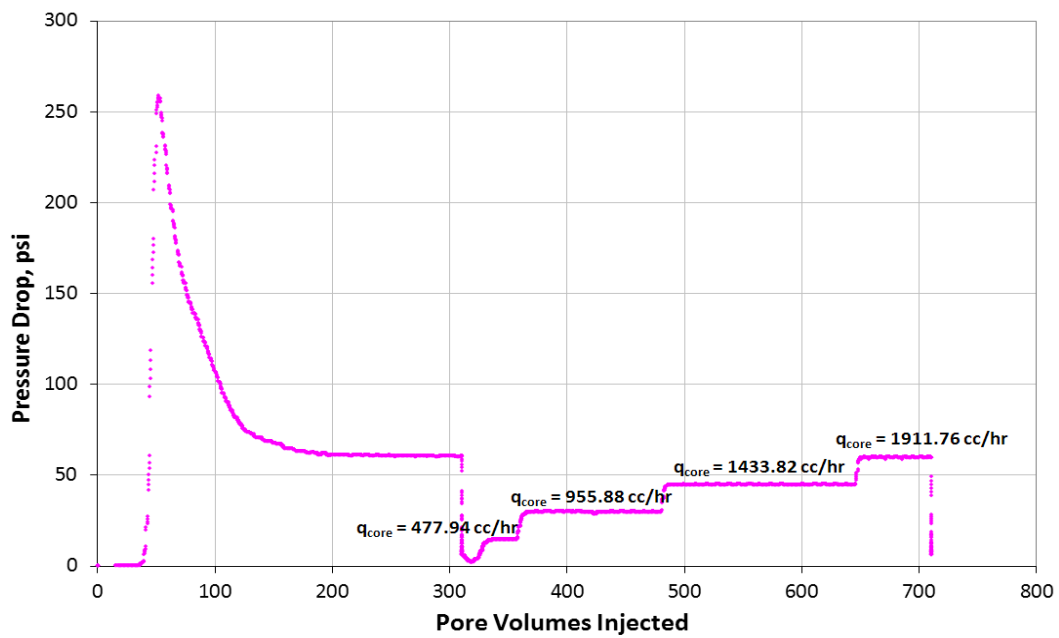


Figure A.12.6 Pressure drop across the core during the final methane flood at 155°F (Exp #198)

Appendix A.13: EXPERIMENT #200

Objective:

The objective of this experiment was to investigate the effectiveness of chemical treatment 3 using non-ionic fluoro-surfactant L-18961 in improving the oil and gas relative permeability at different PVT ratios and constant capillary number. This was done for a volatile oil mixture below the bubble point pressure on a Berea sandstone core and in the presence of initial water saturation. The experiment was performed at 155°F.

Experimental Procedure and Results:

A Berea core was prepared for the experiment following the standard procedure described Section 3.2.1.1. The initial core measurements and assumed properties can be found in Table A.5.1.

The initial gas permeability was calculated using methane at 155°F. Methane was flowed through the core using five flow rates and the pressure drop across the core for each flow rate was recorded. Using this data, the fluid properties and accounting for non-Darcy effects the calculated gas permeability was 366 md. Table A.5.2 summarizes the flood conditions and fluid properties and Table A.5.3 shows the results. Figure A.6.1 shows the pressure drop measured across the core during the methane flood.

The initial gas permeability at initial water saturation was calculated next. Using synthetic brine 1 (25,000 ppm NaCl) an initial water saturation of 20% was established. This was done by applying vacuum to the core first and then injecting 4.2 ml of brine. The core was shut in for 1 hour, allowing the brine to distribute through the core. Methane at 155°F was then flowed through the core using five flow rates and the pressure drop across the core for each flow rate was recorded. The calculated gas permeability

was 316 md. Flood conditions and results are shown in Table A.5.4 and Table A.4.5 respectively. Figure A.4.2 shows the pressure drop measured across the core during the methane flood at S_{wi} .

Synthetic volatile oil mixture 2 (Table 3.3) was used for the two-phase flow measurements. The mixture was allowed a minimum of 12 hours to equilibrate to a single phase at 4200 psi and 155°F. The initial flood was conducted with the upstream backpressure regulator (BPR-1) set at 4340 psi and the downstream back pressure regulator (BPR-2) set at 800 psi. Volatile oil was injected at an upstream BPR-1 flow rate of 120 cc/hr (this is for volatile oil at single liquid phase) corresponding to a flow regime with a capillary number of approximately 2×10^{-5} . Once steady state was observed the pressure drop across the core was measured. This procedure was repeated for BPR-2 pressures of 1,500 psi, 2,200 psi and 2,900 psi. This allowed having different PVT ratios and the capillary number was kept constant. The PVT ratio ranged from 0.94 to 0.53. Table A.3.6 gives the fluid properties of the synthetic fluid calculated using the Peng-Robinson EOS at the flowing core pressures. Figure A.4.3 shows the pressure drop measured across the core during the initial two-phase volatile oil flood for the different BPR-2 pressures.

The core was then treated using chemical treatment 3 (Table 4.15). The solution was heated for at least 3 hours at 155°F. BPR2 was set at 1013 psi. The core was flooded with approximately 11 pore volumes of the treatment solution at a flow rate of 100 cc/hr. The core was then shut in for 1 hour. Figure A.4.4 shows the measured pressure drop across the core during the treatment flood.

Post-treatment two-phase volatile oil flood was conducted under the same conditions as the initial two-phase flow. Figure A.4.5 shows the pressure drop measured

across the core during the post-treatment two-phase volatile oil flood. Improvement factor varied from 1.3 to 0.7.

The final gas permeability was calculated following the procedure for the initial gas permeability using methane at 155°F. The calculated gas permeability was 275 md. Flood conditions and results are shown in Table A.4.7 and Table A.3.8 respectively. Figure A.13.6 shows the pressure drop across the core for the final methane flood.

For every two-phase volatile oil flood, oil and gas relative permeabilities k_{rg} and k_{ro} were calculated using the measured pressure drop across the core under steady state conditions and then improvement factors were measured. Table A.3.9 summarizes the experimental results.

Table A.13.1 Core properties (Exp #200)

<i>Length, in</i>	7.91
<i>Diameter, in</i>	0.996
<i>Mass Core, gr</i>	211.82
<i>Grain Density, gr/cc</i>	2.65
<i>Porosity (ϕ)</i>	20.90%

Table A.13.2 Fluid properties and conditions for initial gas permeability (Exp #200)

		<i>Density, gr/cc</i>
<i>Gas</i>	Methane	
<i>Temperature, °F</i>	155	
<i>BPR 1-pressure, psi</i>	3940	0.1583
<i>BPR 2-pressure, psi</i>	1000	4.17E-02
<i>Gas Viscosity, cp</i>	0.0134	

Table A.13.3 Initial methane flood results (Exp #200)

<i>q_{core}, cc/hr</i>	<i>ΔP, psi</i>	<i>k_g, md</i>
5694	4.000	311.45
6833	4.980	300.19
7592	5.650	293.99
8352	6.300	290.03
9490	7.400	280.58
<i>Corrected Permeability (k_g), md</i>		366.4

Table A.13.4 Fluid properties and conditions for methane gas permeability at S_{wi} (Exp #200)

		<i>Density, gr/cc</i>
<i>Gas</i>	Methane	
<i>Temperature, °F</i>	155	
<i>BPR 1-pressure, psi</i>	4000	0.1602
<i>BPR 2-pressure, psi</i>	1000	4.17E-02
<i>Gas Viscosity, cp</i>	0.0134	

Table A.13.5 Methane flood results at S_{wi} (Exp #200)

q_{core} , cc/hr	ΔP , psi	k_g , md
5763	6.100	206.68
6915	7.700	196.48
7683	8.950	187.82
8452	10.300	179.52
9604	12.400	169.46
<i>Corrected Permeability (k_g), md</i>		315.9

Table A.13.6 Volatile oil properties at BPR-1 and BPR-2 pressures (Exp #200)

<i>BPR 1-pressure, psi</i>		4340						
<i>BPR 2- pressure, psi</i>		800	1500	2200	2900			
<i>Density at BPR 1-pressure, gr/cc</i>		0.3692						
Properties of BPR 2-pressure, psi								
	800		1500		2200		2900	
	Gas Phase	Oil Phase						
Density, gr/cc	0.0433	0.6042	0.0865	0.5551	0.137	0.5055	0.1997	0.0433
Viscosity (μ), cp	0.0129	0.1974	0.0148	0.1363	0.0182	0.0981	0.024	0.0129
Volume Fraction	0.9348	0.0652	0.8495	0.1505	0.7443	0.2557	0.6097	0.9348
IFT, dyne/cm	8.905		4.201		1.513		0.283	8.905

Table A.13.7 Fluid properties and conditions for final gas permeability (Exp #200)

<i>Gas</i>	<i>Methane</i>	<i>Density, gr/cc</i>
<i>Temperature, °F</i>	155	
<i>BPR 1-pressure, psi</i>	3192	0.133
<i>BPR 2-pressure, psi</i>	1004	4.17E-02
<i>Gas Viscosity, cp</i>	0.0134	

Table A.13.8 Final methane flood results (Exp #200)

$q_{core}, cc/hr$	$\Delta P, psi$	k_g, md
4784	4.500	232.60
5741	5.650	222.31
6379	6.400	218.06
7017	7.150	214.71
7974	8.400	207.68
<i>Corrected Permeability (k_g), md</i>		274.58

Table A.13.9 Pre and post-treatment volatile oil flood results and measured improvement factors (Exp #200)

	Exp#200			
$q_{gtot\ core}, cc/hr$	555	611	176	50
$q_g, cc/hr$	519	519	131	30
$q_o, cc/hr$	36	92	45	19
<i>PVT Ratio</i>	0.94	0.61	0.54	0.53
<i>Viscosity Ratio μ_g/μ_o</i>	0.07	0.11	0.19	0.34
<i>Capillary Nc</i>	1.97E-05	2.03E-05	2.13E-05	2.32E-05
k_{rg} Before Treatment	0.021	0.050	0.041	0.061
k_{ro} Before Treatment	0.022	0.081	0.076	0.115
k_{rg} After Treatment	0.027	0.041	0.029	0.068
k_{ro} After Treatment	0.029	0.066	0.055	0.127
<i>Initial Improvement Factor</i>	1.3	0.8	0.7	1.1
<i>PV of Vol Oil Injected</i>	~200			
<i>Final Improvement Factor</i>	*	*	*	*

* A second batch of a volatile oil was not injected

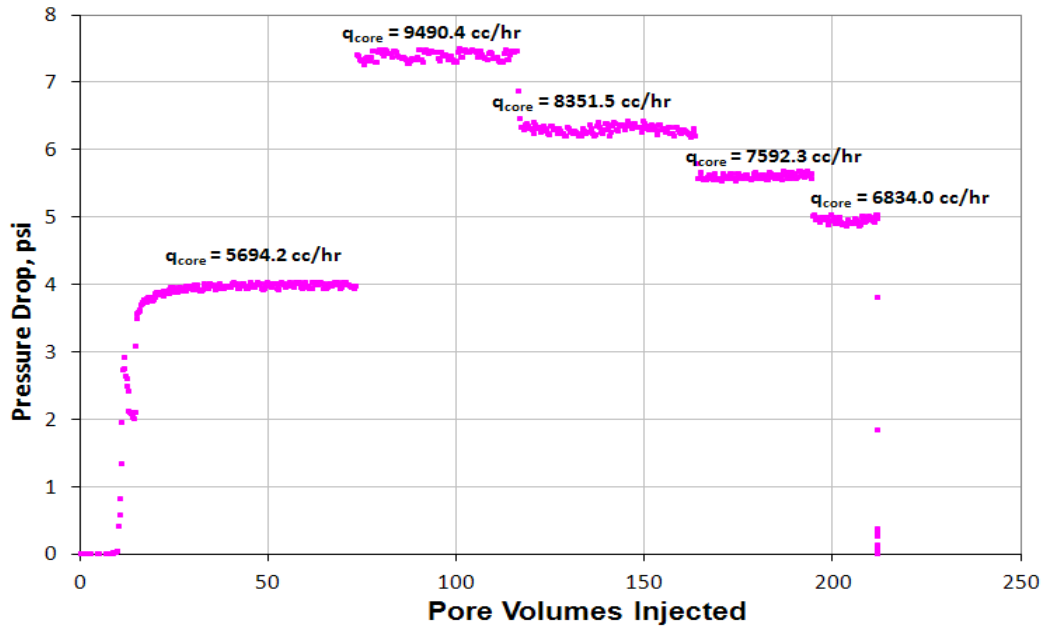


Figure A.13.1 Pressure drop across the core during the initial methane flood at 155°F (Exp #200)

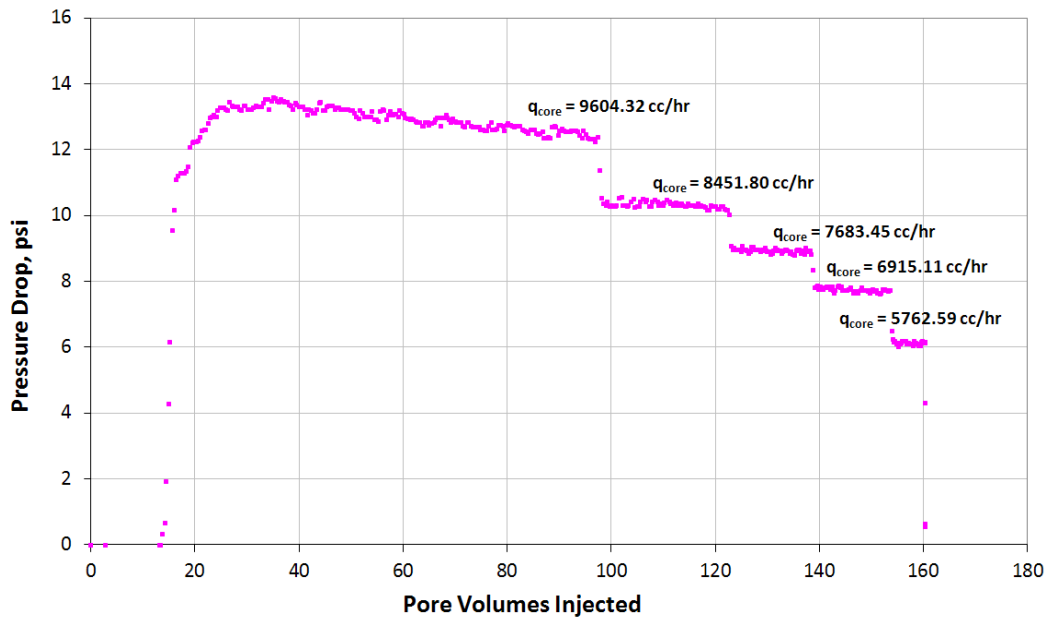


Figure A.13.2 Pressure drop across the core during the methane flood at S_{wi} of 20% (Exp #200)

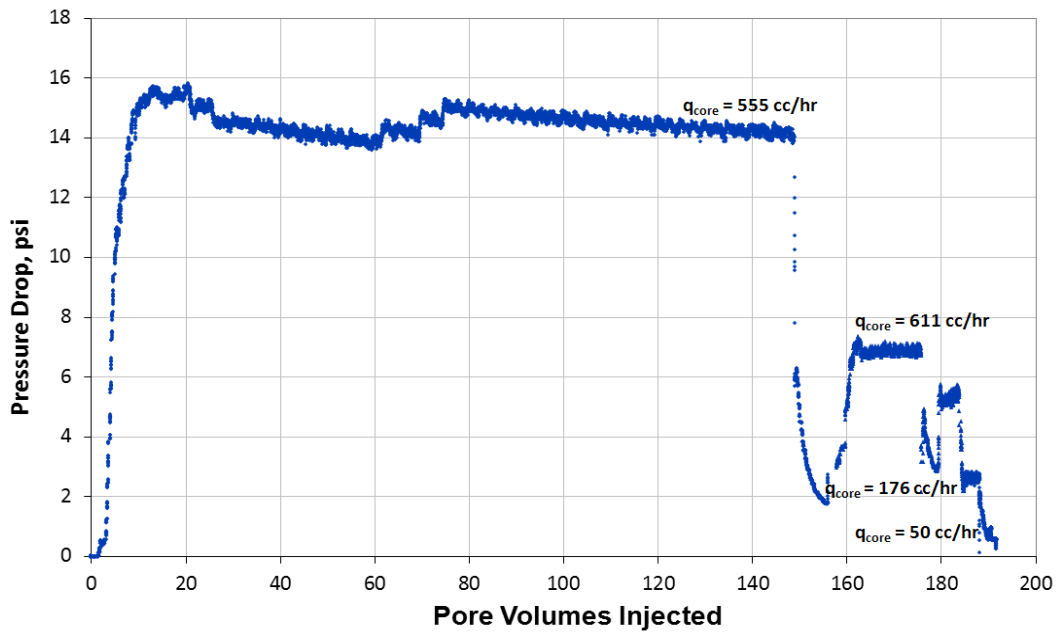


Figure A.13.3 Pressure drop across the core during the pre-treatment two-phase volatile oil flood (Exp #200)

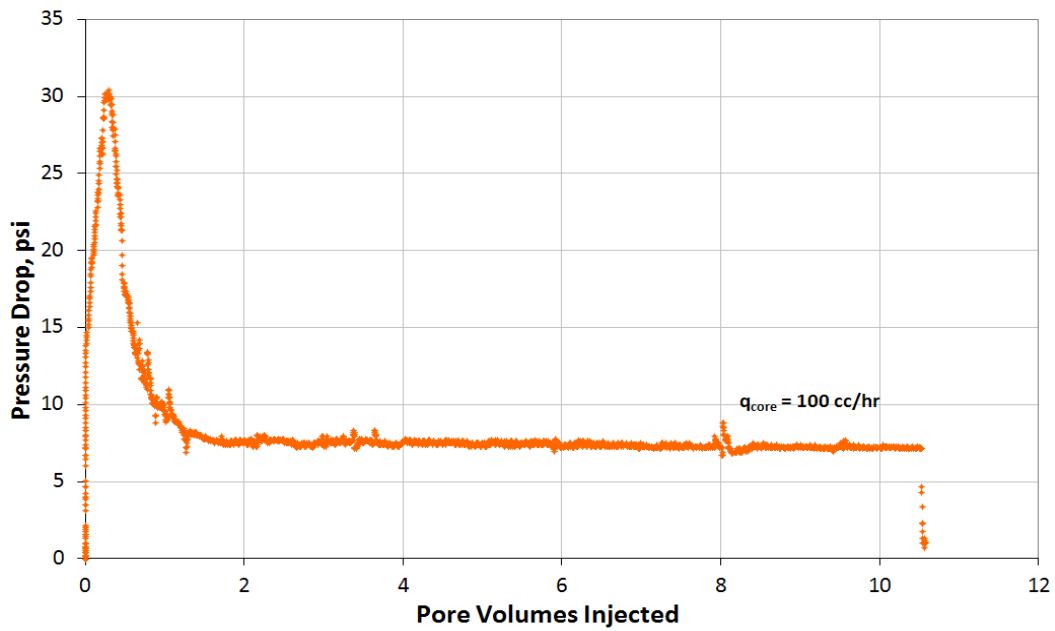


Figure A.13.4 Pressure drop across the core during injection of chemical treatment 3 (Exp # 200)

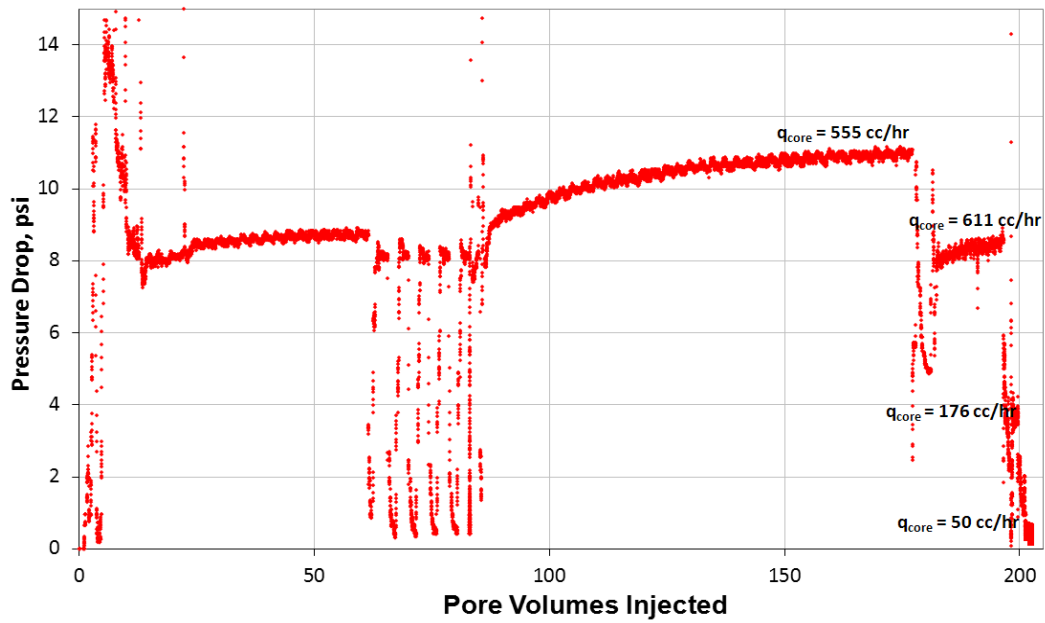


Figure A.13.5 Pressure drop across the core during the post-treatment two-phase volatile oil flood (Exp #200)

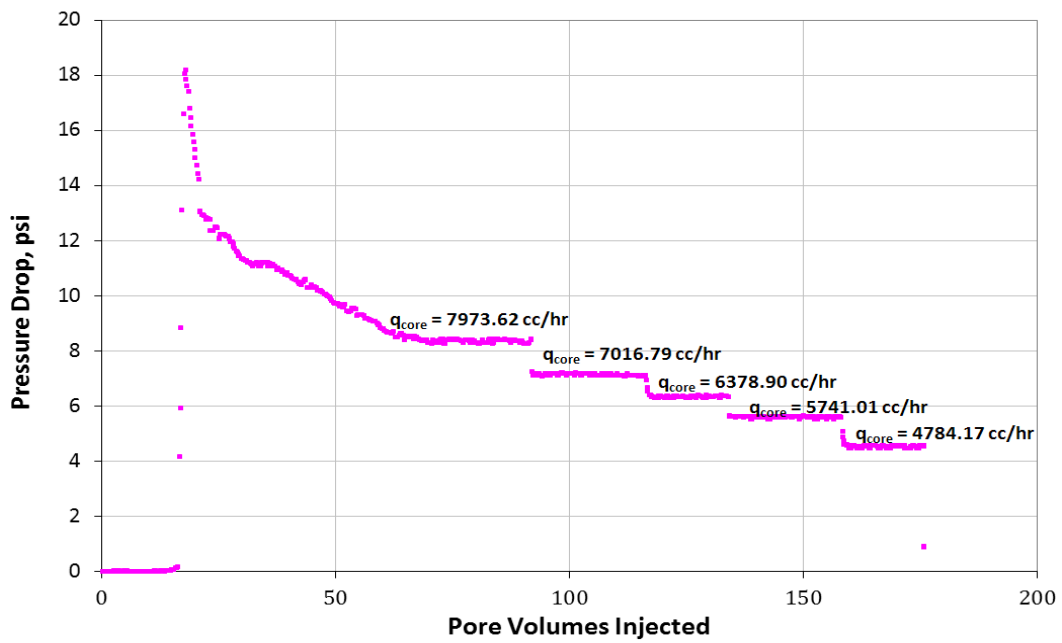


Figure A.13.6 Pressure drop across the core during the final methane flood at 155°F (Exp #200)

Appendix A.14: EXPERIMENT #210

Objective:

The objective of this experiment was to investigate the effectiveness of chemical treatment 1 using non-ionic fluoro-surfactant FC-X in improving the oil and gas relative permeability at different PVT ratios and constant capillary number. This was done for a volatile oil mixture below the bubble point pressure on a Berea sandstone core and in the presence of initial water saturation. The experiment was performed at 155°F.

Experimental Procedure and Results:

A Berea core was prepared for the experiment following the standard procedure described Section 3.2.1.1. The initial core measurements and assumed properties can be found in Table A.5.1.

The initial gas permeability was calculated using methane at 155°F. Methane was flowed through the core using five flow rates and the pressure drop across the core for each flow rate was recorded. Using this data, the fluid properties and accounting for non-Darcy effects the calculated gas permeability was 178 md. Table A.5.2 summarizes the flood conditions and fluid properties and Table A.5.3 shows the results. Figure A.6.1 shows the pressure drop measured across the core during the methane flood.

The initial gas permeability at initial water saturation was calculated next. Using synthetic brine 1 (25,000 ppm NaCl) an initial water saturation of 20% was established. This was done by applying vacuum to the core first and then injecting 4.3 ml of brine. The core was shut in for 1 hour, allowing the brine to distribute through the core. Methane at 155°F was then flowed through the core using five flow rates and the pressure drop across the core for each flow rate was recorded. The calculated gas permeability

was 164 md. Flood conditions and results are shown in Table A.5.4 and Table A.4.5 respectively. Figure A.4.2 shows the pressure drop measured across the core during the methane flood at S_{wi} .

Synthetic volatile oil mixture 2 (Table 3.3) was used for the two-phase flow measurements. The mixture was allowed a minimum of 12 hours to equilibrate to a single phase at 4200 psi and 155°F. The initial flood was conducted with the upstream backpressure regulator (BPR-1) set at 4320 psi and the downstream back pressure regulator (BPR-2) set at 810 psi. Volatile oil was injected at an upstream BPR-1 flow rate of 120 cc/hr (this is for volatile oil at single liquid phase) corresponding to a capillary number of approximately 1.2×10^{-5} . Once steady state was observed the pressure drop across the core was measured. This procedure was repeated for BPR-2 pressures of 1,100 psi, 1,500 psi, 2,200 psi and 2,900 psi. This allowed having different PVT ratios and the capillary number was kept constant. The PVT ratio ranged from 0.92 to 0.54. Table A.3.6 gives the fluid properties of the synthetic fluid calculated using the Peng-Robinson EOS at the flowing core pressures. Figure A.4.3 shows the pressure drop measured across the core during the initial two-phase volatile oil flood for the different BPR-2 pressures.

The core was then treated using chemical treatment 1 (Table 4.15). The solution was heated for at least 3 hours at 155°F. BPR2 was set at 790 psi. The core was flooded with approximately 18 pore volumes of the treatment solution at a flow rate of 120 cc/hr. The core was then shut in for 12 hour. Figure A.4.4 shows the measured pressure drop across the core during the treatment flood.

Post-treatment two-phase volatile oil flood was conducted under the same conditions as the initial two-phase flow. Figure A.14.5 shows the pressure drop measured

across the core during the post-treatment two-phase volatile oil flood. Improvement factor varied from 2.5 to 1.3.

A second batch of post-treatment two phase volatile oil flood followed. Improvement factor ranged from 2.4 to 1.0

The final gas permeability was calculated following the procedure for the initial gas permeability using methane at 155°F. The calculated gas permeability was 309 md. Flood conditions and results are shown in Table A.4.7 and Table A.3.8 respectively. Figure A.14.6 shows the pressure drop across the core for the final methane flood.

For every two-phase volatile oil flood, oil and gas relative permeabilities k_{rg} and k_{ro} were calculated using the measured pressure drop across the core under steady state conditions and then improvement factors were measured. Table A.3.9 summarizes the experimental results.

Table A.14.1 Core properties (Exp #210)

<i>Length, in</i>	8.005
<i>Diameter, in</i>	0.998
<i>Mass Core, gr</i>	214.66
<i>Grain Density, gr/cc</i>	2.65
<i>Porosity (ϕ)</i>	21.06%

Table A.14.2 Fluid properties and conditions for initial gas permeability (Exp #210)

		<i>Density, gr/cc</i>
<i>Gas</i>	Methane	
<i>Temperature, °F</i>	155	
<i>BPR 1-pressure, psi</i>	3740	0.1519
<i>BPR 2-pressure, psi</i>	1020	4.26E-02
<i>Gas Viscosity, cp</i>	0.0134	

Table A.14.3 Initial methane flood results (Exp #210)

<i>q_{core}, cc/hr</i>	<i>ΔP, psi</i>	<i>k_g, md</i>
5349	9.150	128.82
6418	11.500	123.00
7131	13.250	118.62
7855	14.900	116.03
8914	18.000	109.14
<i>Corrected Permeability (k_g), md</i>		177.7

Table A.14.4 Fluid properties and conditions for methane gas permeability at S_{wi} (Exp #210)

		<i>Density, gr/cc</i>
<i>Gas</i>	Methane	
<i>Temperature, °F</i>	155	
<i>BPR 1-pressure, psi</i>	3730	0.1516
<i>BPR 2-pressure, psi</i>	1020	4.26E-02
<i>Gas Viscosity, cp</i>	0.0134	

Table A.14.5 Methane flood results at S_{wi} (Exp #210)

q_{core} , cc/hr	ΔP , psi	k_g , md
5338	11.900	98.86
6406	15.300	92.27
7117	18.000	87.14
7829	21.000	82.16
8897	25.000	78.43
<i>Corrected Permeability (k_g), md</i>		164.0

Table A.14.6 Volatile oil properties at BPR-1 and BPR-2 pressures (Exp #210)

<i>BPR 1-pressure, psi</i>		4320								
<i>BPR 2- pressure, psi</i>		810	1100	1500	2200	2900				
<i>Density at BPR 1-pressure, gr/cc</i>		0.3683								
Properties of BPR 2-pressure, psi										
	810		1100		1500		2200		2900	
	Gas Phase	Oil Phase								
Density, gr/cc	0.0438	0.6043	0.061	0.5839	0.0864	0.5569	0.1367	0.5086	0.1982	0.4523
Viscosity (μ), cp	0.0129	0.1977	0.0135	0.1687	0.0148	0.1381	0.0181	0.1	0.0239	0.0724
Volume Fraction	0.9339	0.0661	0.9013	0.0987	0.8505	0.1495	0.7476	0.2524	0.6199	0.3801
IFT, dyne/cm	8.863		6.649		4.254		1.561		0.313	

Table A.14.7 Fluid properties and conditions for final gas permeability (Exp #210)

		<i>Density, gr/cc</i>
<i>Gas</i>	<i>Methane</i>	
<i>Temperature, °F</i>	155	
<i>BPR 1-pressure, psi</i>	4140	0.1645
<i>BPR 2-pressure, psi</i>	810	3.34E-02
<i>Gas Viscosity, cp</i>	0.0131	

Table A.14.8 Final methane flood results (Exp #210)

$q_{core}, cc/hr$	$\Delta P, psi$	k_g, md
7388	8.500	187.26
8866	10.600	180.19
9850	12.400	171.15
10835	14.500	161.00
12313	17.500	151.59
<i>Corrected Permeability (k_g), md</i>		309.63

Table A.14.9 Pre and post-treatment volatile oil flood results and measured improvement factors (Exp #210)

	Exp# 210				
$q_{g\text{tot core}}, cc/hr$	547	442	305	128	31
$q_g, cc/hr$	511	398	260	96	19
$q_o, cc/hr$	36	44	46	32	12
<i>PVT Ratio</i>	0.92	0.73	0.61	0.54	0.54
<i>Viscosity Ratio μ_g/μ_o</i>	0.07	0.08	0.11	0.18	0.33
<i>Capillary Nc</i>	1.19E-05	1.19E-05	1.19E-05	1.21E-05	1.08E-05
k_{rg} Before Treatment	0.034	0.037	0.042	0.050	0.075
k_{ro} Before Treatment	0.037	0.051	0.069	0.094	0.140
k_{rg} After Treatment	0.085	0.083	0.067	0.067	0.104
k_{ro} After Treatment	0.092	0.113	0.110	0.124	0.194
<i>Initial Improvement Factor</i>	2.5	2.2	1.6	1.3	1.4
<i>PV of Vol Oil Injected</i>	~330				
<i>Final Improvement Factor</i>	2.4	2.1	1.0	1.0	1.0

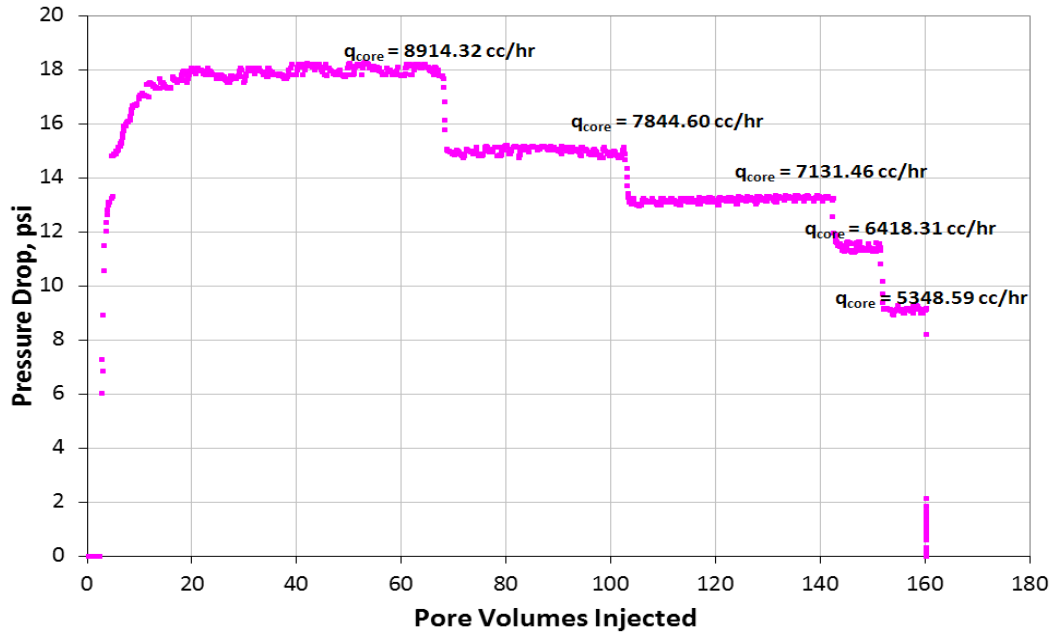


Figure A.14.1 Pressure drop across the core during the initial methane flood at 155°F (Exp #210)

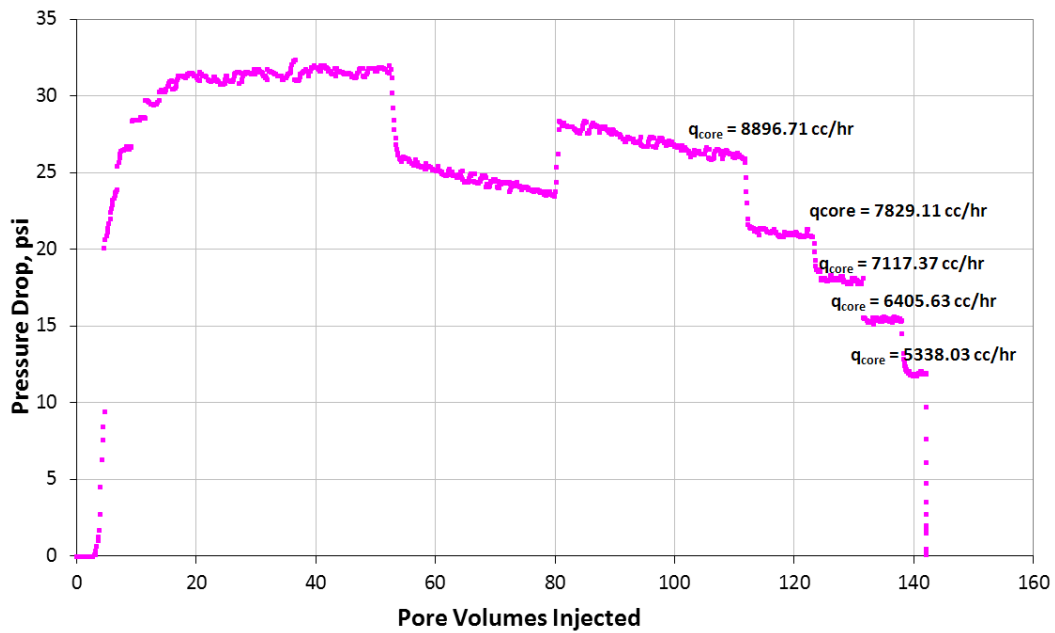


Figure A.14.2 Pressure drop across the core during the methane flood at S_{wi} of 20% (Exp #210)

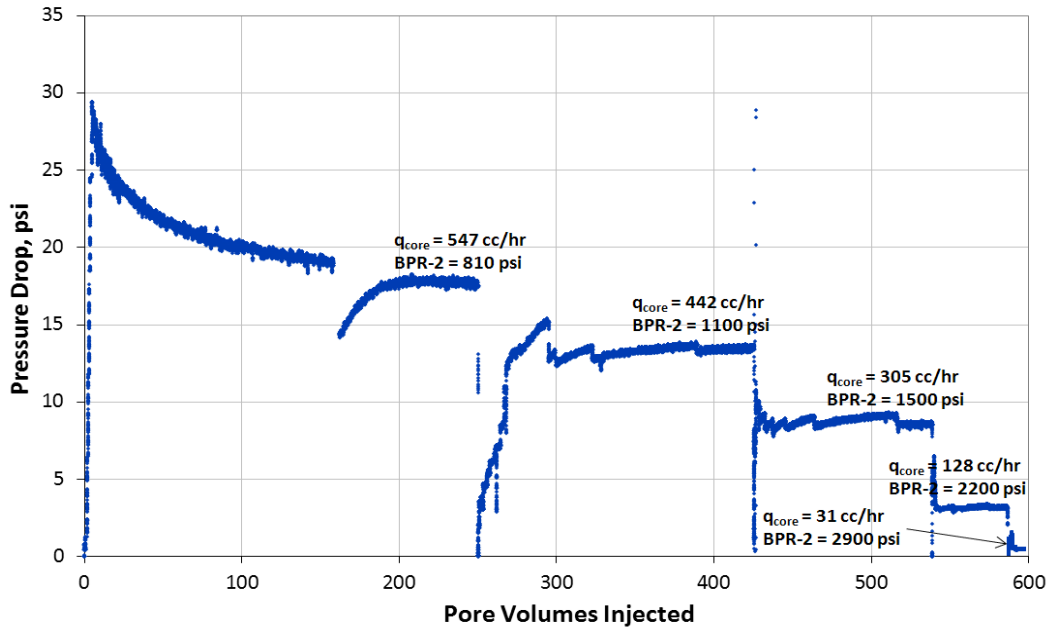


Figure A.14.3 Pressure drop across the core during the pre-treatment two-phase volatile oil flood (Exp #210)

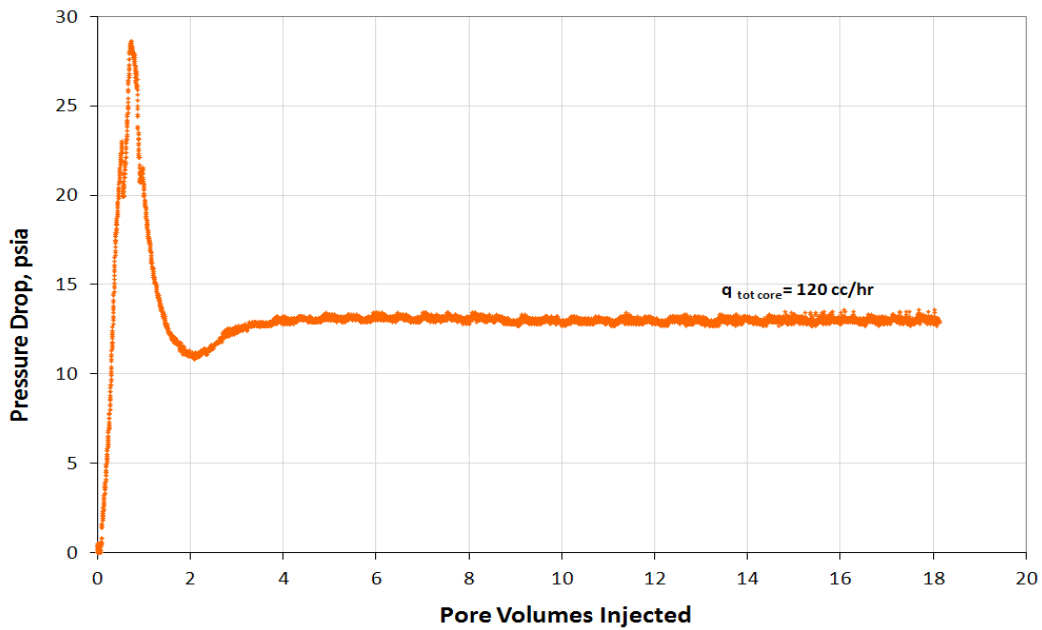


Figure A.14.4 Pressure drop across the core during injection of chemical treatment 1 (Exp #210)

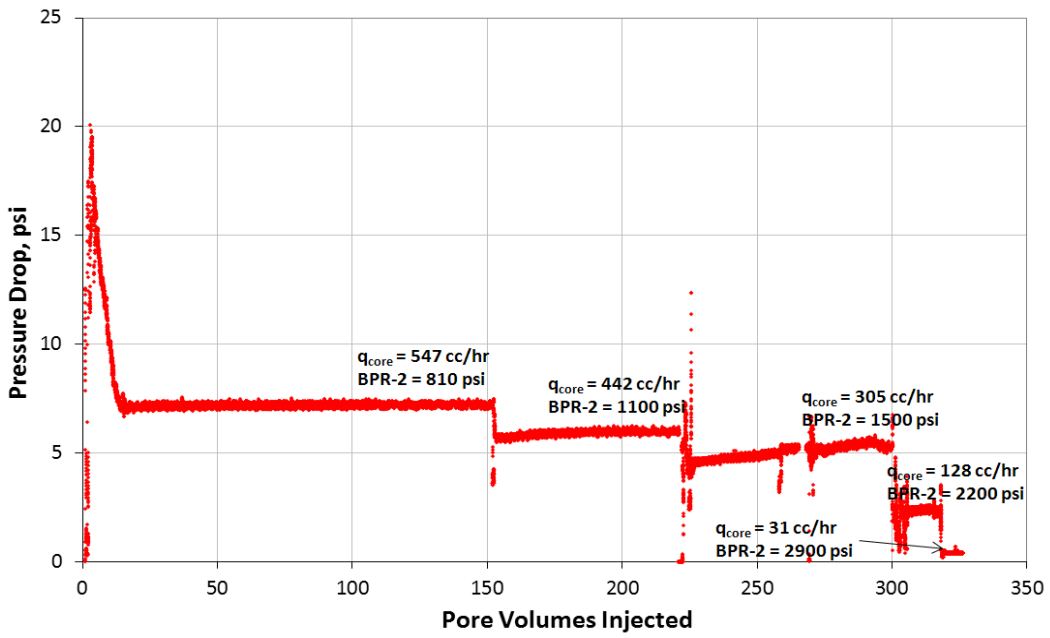


Figure A.14.5 Pressure drop across the core during the post-treatment two-phase volatile oil flood (Exp #210)

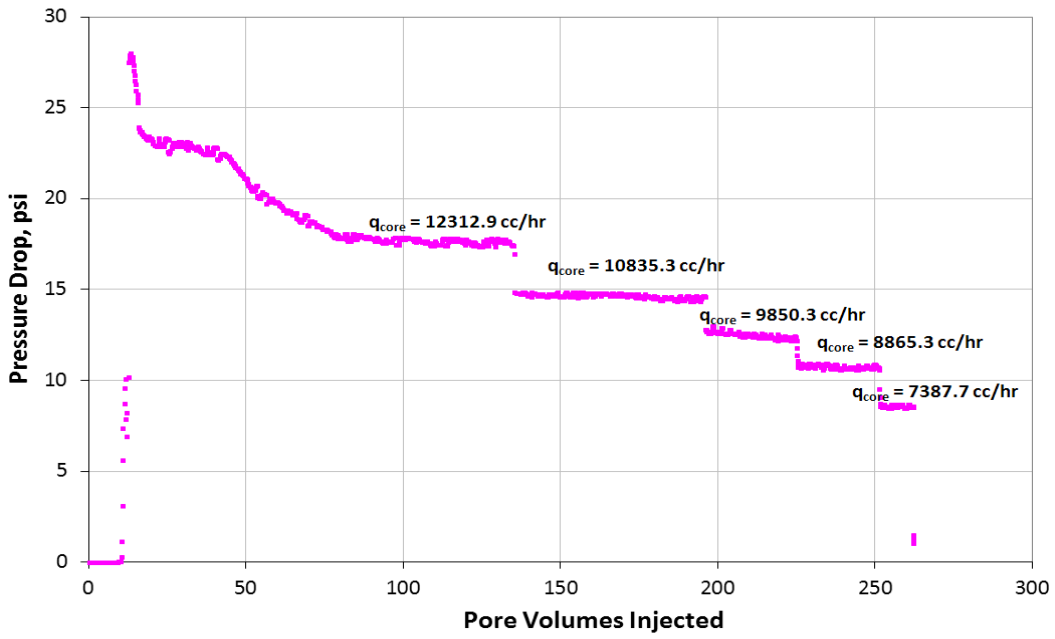


Figure A.14.6 Pressure drop across the core during the final methane flood at 155°F (Exp #210)

Appendix A.15: EXPERIMENT #221

Objective:

The objective of this experiment was to investigate the effectiveness of chemical treatment 1 using non-ionic fluoro-surfactant FC-X in improving the oil and gas relative permeability at high liquid fraction. This was done for a volatile oil mixture below the bubble point pressure on a Berea sandstone core and in the presence of initial water saturation. The experiment was performed at 155°F.

Experimental Procedure and Results:

A Berea core was prepared for the experiment following the standard procedure described Section 3.2.1.1. The initial core measurements and assumed properties can be found in Table A.5.1.

The initial gas permeability was calculated using methane at 155°F. Methane was flowed through the core using five flow rates and the pressure drop across the core for each flow rate was recorded. Using this data, the fluid properties and accounting for non-Darcy effects the calculated gas permeability was 93 md. Table A.5.2 summarizes the flood conditions and fluid properties and Table A.5.3 shows the results. Figure A.6.1 shows the pressure drop measured across the core during the methane flood.

The initial gas permeability at initial water saturation was calculated next. Using synthetic brine 1 (25,000 ppm NaCl) an initial water saturation of 20% was established. This was done by applying vacuum to the core first and then injecting 3.4 ml of brine. The core was shut in for 1 hour, allowing the brine to distribute through the core. Methane at 155°F was then flowed through the core using five flow rates and the pressure drop across the core for each flow rate was recorded. The calculated gas permeability

was 70 md. Flood conditions and results are shown in Table A.5.4 and Table A.4.5 respectively. Figure A.4.2 shows the pressure drop measured across the core during the methane flood at S_{wi} .

Synthetic volatile oil mixture 2 (Table 3.3) was used for the two-phase flow measurements. The mixture was allowed a minimum of 12 hours to equilibrate to a single phase at 4200 psi and 155°F. The initial flood was conducted with the upstream backpressure regulator (BPR-1) set at 4325 psi and the downstream back pressure regulator (BPR-2) set at 2915 psi. Volatile oil was injected at an upstream BPR-1 flow rate of 25 cc/hr (this is for volatile oil at single liquid phase) corresponding to a capillary number of approximately 2.1×10^{-5} . Once steady state was observed the pressure drop across the core was measured. The PVT ratio was 0.53. Table A.3.6 gives the fluid properties of the synthetic fluid calculated using the Peng-Robinson EOS at the flowing core pressures. Figure A.4.3 shows the pressure drop measured across the core during the initial two-phase volatile oil flood for the different BPR-2 pressures.

The core was then treated using chemical treatment 1 (Table 4.15). The solution was heated for at least 3 hours at 155°F. BPR2 was set at 2918 psi. The core was flooded with approximately 18 pore volumes of the treatment solution at a flow rate of 100 cc/hr. The core was then shut in for 12 hour. Figure A.4.4 shows the measured pressure drop across the core during the treatment flood.

Post-treatment two-phase volatile oil flood was conducted under the same conditions as the initial two-phase flow. Figure A.4.5 shows the pressure drop measured across the core during the post-treatment two-phase volatile oil flood. Improvement factor was 1.4.

A second batch of post-treatment two phase volatile oil flood followed. Figure A.6.10 shows the pressure drop measured across the core during the post-treatment two-phase volatile oil flood 2. Improvement factor was 1.0

The final gas permeability was not calculated since water passed through the core at the end of post-treatment volatile oil flood 2 due to piston failure.

For every two-phase volatile oil flood, oil and gas relative permeabilities k_{rg} and k_{ro} were calculated using the measured pressure drop across the core under steady state conditions and then improvement factors were measured. Table A.3.9 summarizes the experimental results.

Table A.15.1 Core properties (Exp #221)

<i>Length, in</i>	7.935
<i>Diameter, in</i>	0.993
<i>Mass Core, gr</i>	221.42
<i>Grain Density, gr/cc</i>	2.65
<i>Porosity (ϕ)</i>	17.03%

Table A.15.2 Fluid properties and conditions for initial gas permeability (Exp #221)

		<i>Density, gr/cc</i>
<i>Gas</i>	Methane	
<i>Temperature, °F</i>	155	
<i>BPR 1-pressure, psi</i>	4248	0.1674
<i>BPR 2-pressure, psi</i>	958	0.0398
<i>Gas Viscosity, cp</i>	0.0133	

Table A.15.3 Initial methane flood results (Exp #221)

<i>q_{core}, cc/hr</i>	<i>ΔP, psi</i>	<i>k_g, md</i>
6309	16.300	84.77
7571	20.000	82.91
8412	22.500	81.88
9253	25.200	80.42
10515	29.000	79.41
<i>Corrected Permeability (k_g), md</i>		92.9

Table A.15.4 Fluid properties and conditions for methane gas permeability at S_{wi} (Exp #221)

		<i>Density, gr/cc</i>
<i>Gas</i>	Methane	
<i>Temperature, °F</i>	155	
<i>BPR 1-pressure, psi</i>	4235	0.1677
<i>BPR 2-pressure, psi</i>	956	3.98E-02
<i>Gas Viscosity, cp</i>	0.0133	

Table A.15.5 Methane flood results at S_{wi} (Exp #221)

q_{core} , cc/hr	ΔP , psi	k_g , md
6320	21.200	65.29
7584	26.600	62.45
8427	29.300	62.99
9270	33.300	60.97
10534	39.200	58.85
Corrected Permeability (k_g), md		70.3

Table A.15.6 Volatile oil properties at BPR-1 and BPR-2 pressures (Exp #221)

BPR 1-pressure, psi	4325	
BPR 2- pressure, psi	2915	
Density at BPR 1-pressure, gr/cc	0.3688	
Properties at BPR 2- pressure		
	Gas Phase	Oil Phase
Density, gr/cc	0.2013	0.4454
Viscosity (μ), cp	0.0242	0.0697
Volume Fraction	0.6061	0.3939
IFT, dyne/cm	0.268	

Table A.15.7 Pre and post-treatment volatile oil flood results and measured improvement factors (Exp #221)

	Exp #221
$q_{gtot\ core}$, cc/hr	31
q_g , cc/hr	19
q_o , cc/hr	12
PVT Ratio	0.53
Viscosity Ratio μ_g/μ_o	0.35
Capillary Nc	2.14E-05
k_{rg} Before Treatment	0.044
k_{ro} Before Treatment	0.082
k_{rg} After Treatment	0.063
k_{ro} After Treatment	0.119
Initial Improvement Factor	1.4
PV of Vol Oil Injected	~60
Final Improvement Factor	1.01

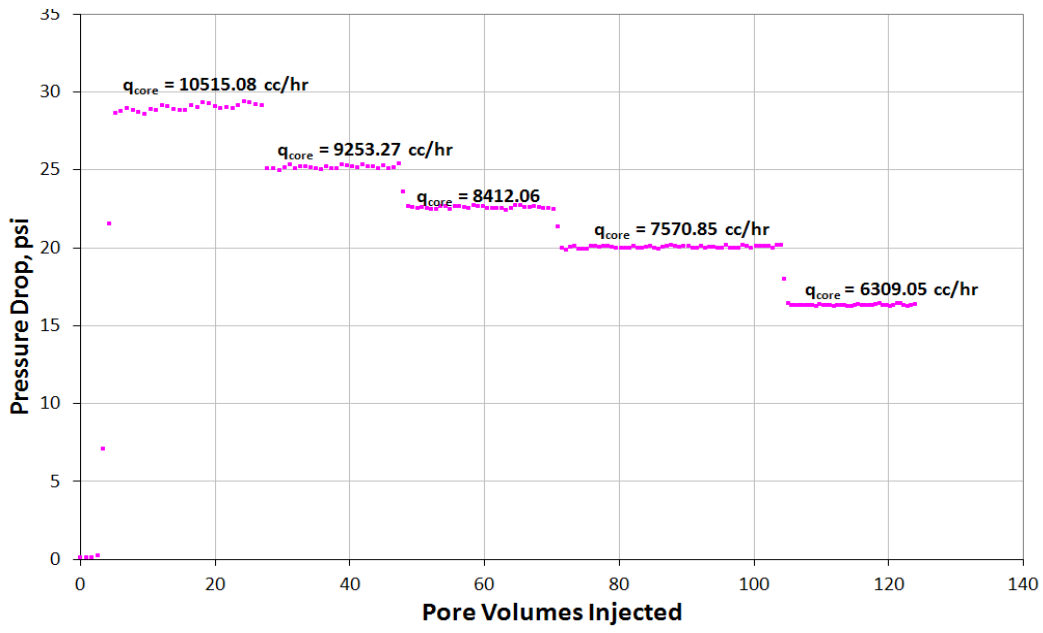


Figure A.15.1 Pressure drop across the core during the initial methane flood at 155°F (Exp #221)

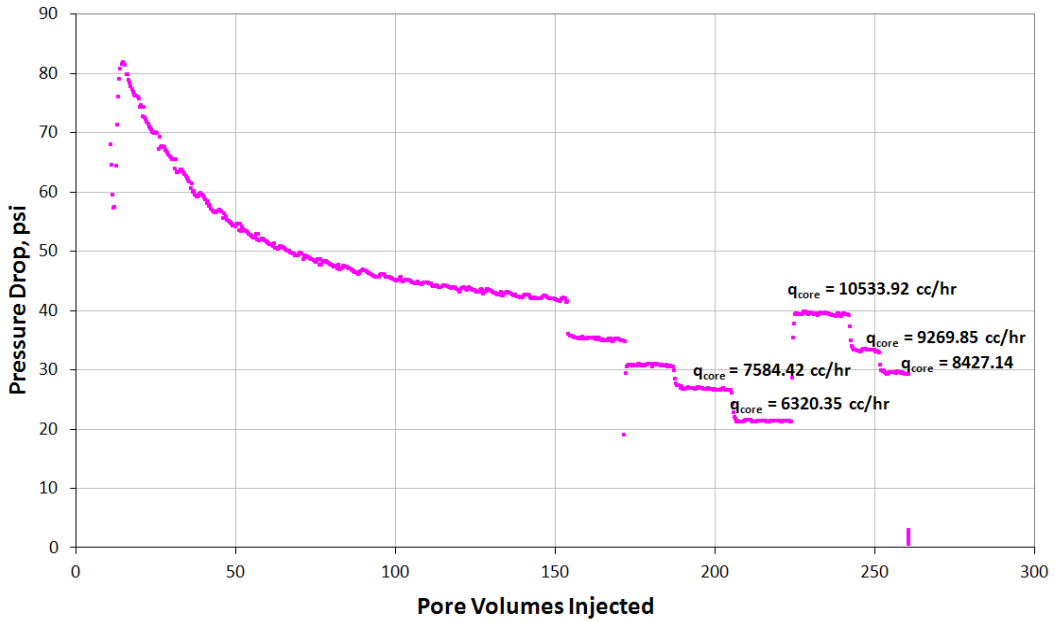


Figure A.15.2 Pressure drop across the core during the methane flood at S_{wi} of 20% (Exp #221)

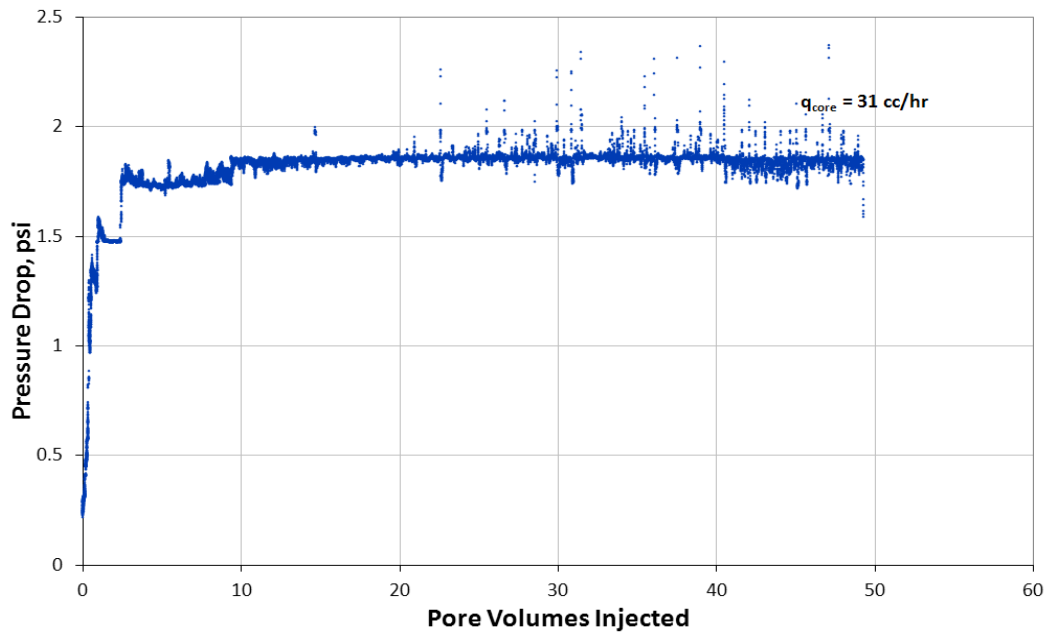


Figure A.15.3 Pressure drop across the core during the pre-treatment two-phase volatile oil flood (Exp #221)

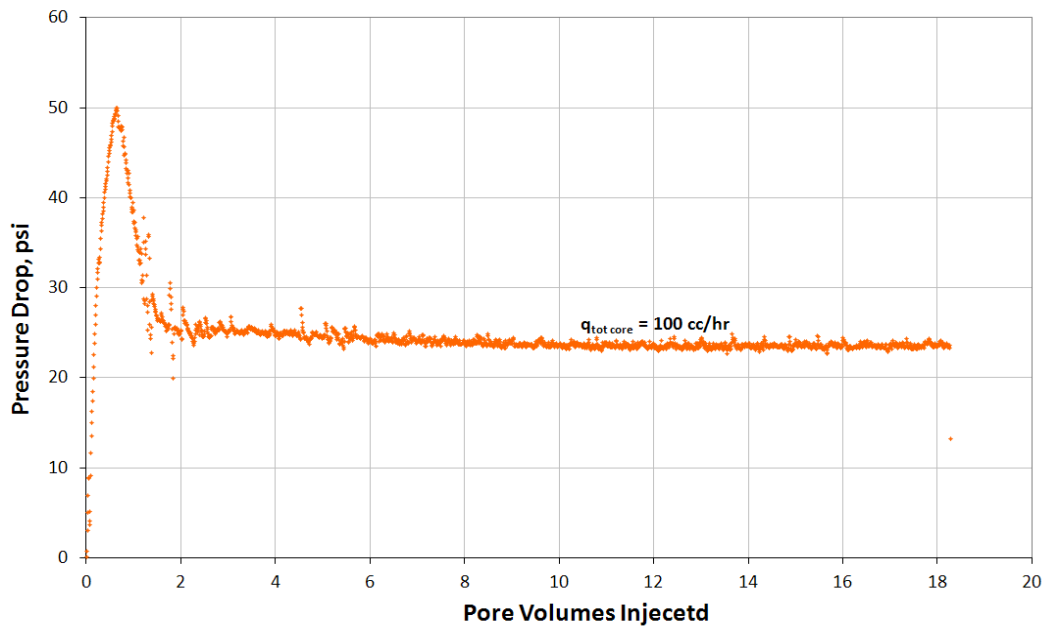


Figure A.15.4 Pressure drop across the core during injection of chemical treatment 1 (Exp # 221)

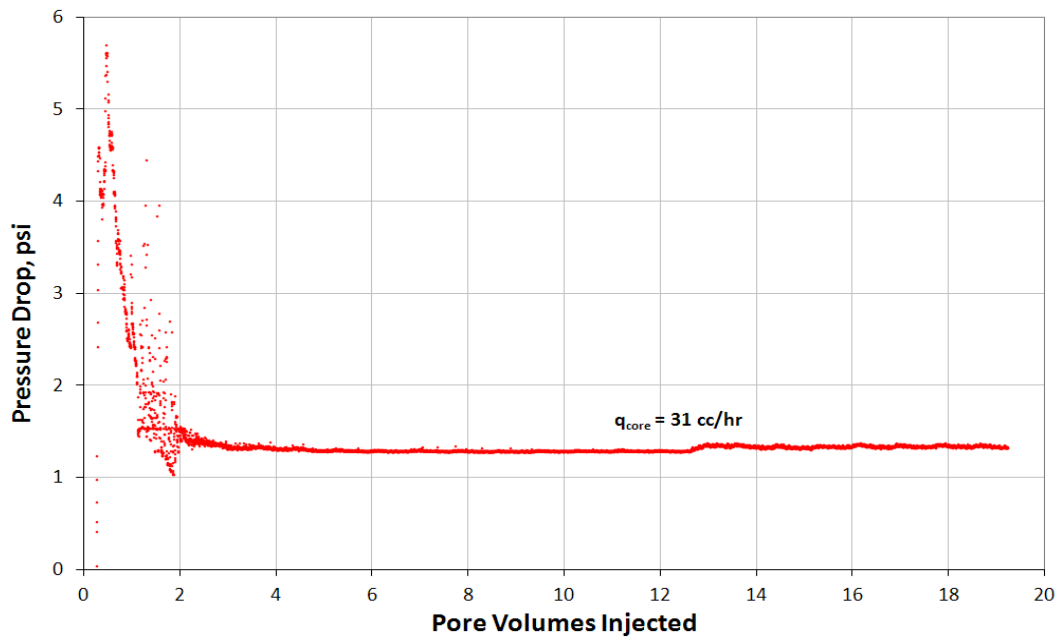


Figure A.15.5 Pressure drop across the core during the post-treatment two-phase volatile oil flood (Exp #221)

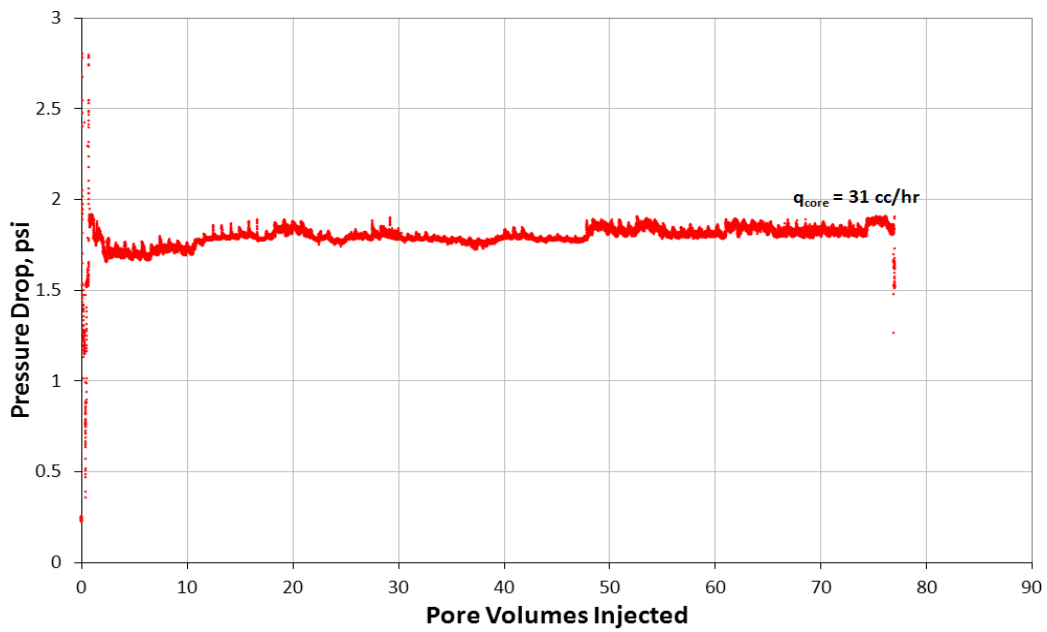


Figure A.15.6 Pressure drop across the core during the post-treatment two-phase volatile oil flood 2 (Exp #221)

Appendix A.16: EXPERIMENT #224

Objective:

The objective of this experiment was to investigate the effectiveness of chemical treatment 1 using non-ionic fluoro-surfactant FC-X in improving the oil and gas relative permeability at high liquid fraction. This was done for a volatile oil mixture below the bubble point pressure on a Berea sandstone core and in the presence of initial water saturation. The experiment was performed at 155°F.

Experimental Procedure and Results:

A Berea core was prepared for the experiment following the standard procedure described Section 3.2.1.1. The initial core measurements and assumed properties can be found in Table A.5.1.

The initial gas permeability was calculated using methane at 155°F. Methane was flowed through the core using five flow rates and the pressure drop across the core for each flow rate was recorded. Using this data, the fluid properties and accounting for non-Darcy effects the calculated gas permeability was 134 md. Table A.5.2 summarizes the flood conditions and fluid properties and Table A.5.3 shows the results. Figure A.6.1 shows the pressure drop measured across the core during the methane flood.

The initial gas permeability at initial water saturation was calculated next. Using synthetic brine 1 (25,000 ppm NaCl) an initial water saturation of 20% was established. This was done by applying vacuum to the core first and then injecting 3.6 ml of brine. The core was shut in for 1 hour, allowing the brine to distribute through the core. Methane at 155°F was then flowed through the core using five flow rates and the pressure drop across the core for each flow rate was recorded. The calculated gas permeability

was 111 md. Flood conditions and results are shown in Table A.5.4 and Table A.4.5 respectively. Figure A.4.2 shows the pressure drop measured across the core during the methane flood at S_{wi} .

Synthetic volatile oil mixture 2 (Table 3.3) was used for the two-phase flow measurements. The mixture was allowed a minimum of 12 hours to equilibrate to a single phase at 4200 psi and 155°F. The initial flood was conducted with the upstream backpressure regulator (BPR-1) set at 4230 psi and the downstream back pressure regulator (BPR-2) set at 2220 psi. Volatile oil was injected at an upstream BPR-1 flow rate of 105 cc/hr (this is for volatile oil at single liquid phase) corresponding to a capillary number of approximately 3×10^{-5} . Once steady state was observed the pressure drop across the core was measured. The PVT ratio was 0.54. Table A.3.6 gives the fluid properties of the synthetic fluid calculated using the Peng-Robinson EOS at the flowing core pressures. Figure A.4.3 shows the pressure drop measured across the core during the initial two-phase volatile oil flood for the different BPR-2 pressures.

The core was then treated using chemical treatment 1 (Table 4.15). The solution was heated for at least 3 hours at 155°F. BPR2 was set at 2230 psi. The core was flooded with approximately 19 pore volumes of the treatment solution at a flow rate of 100 cc/hr. The core was then shut in for 12 hour. Figure A.4.4 shows the measured pressure drop across the core during the treatment flood.

Post-treatment two-phase volatile oil flood was conducted under the same conditions as the initial two-phase flow. Figure A.4.5 shows the pressure drop measured across the core during the post-treatment two-phase volatile oil flood. Improvement factor was 2.2.

A second batch of post-treatment two phase volatile oil flood followed. Figure A.6.10 shows the pressure drop measured across the core during the post-treatment two-phase volatile oil flood 2. Improvement factor was 1.6

The final gas permeability was calculated following the procedure for the initial gas permeability using methane at 155°F. The calculated gas permeability was 102 md. Flood conditions and results are shown in Table A.4.7 and Table A.3.8 respectively. Figure A.6.10 shows the pressure drop across the core for the final methane flood.

For every two-phase volatile oil flood, oil and gas relative permeabilities k_{rg} and k_{ro} were calculated using the measured pressure drop across the core under steady state conditions and then improvement factors were measured. Table A.16.9 summarizes the experimental results.

Table A.16.1 Core properties (Exp #224)

<i>Length, in</i>	7.91
<i>Diameter, in</i>	0.989
<i>Mass Core, gr</i>	219.21
<i>Grain Density, gr/cc</i>	2.65
<i>Porosity (ϕ)</i>	16.93%

Table A.16.2 Fluid properties and conditions for initial gas permeability (Exp #224)

		<i>Density, gr/cc</i>
<i>Gas</i>	Methane	
<i>Temperature, °F</i>	155	
<i>BPR 1-pressure, psi</i>	3975	0.2354
<i>BPR 2-pressure, psi</i>	1018	0.0677
<i>Gas Viscosity, cp</i>	0.0203	

Table A.16.3 Initial methane flood results (Exp #224)

<i>q_{core}, cc/hr</i>	<i>ΔP, psi</i>	<i>k_g, md</i>
5216	12.050	145.40
6259	14.850	141.58
6954	16.750	139.47
7650	18.700	137.42
8693	21.750	134.26
<i>Corrected Permeability (k_g), md</i>		161.9

Table A.16.4 Fluid properties and conditions for methane gas permeability at S_{wi} (Exp #224)

		<i>Density, gr/cc</i>
<i>Gas</i>	Methane	
<i>Temperature, °F</i>	155	
<i>BPR 1-pressure, psi</i>	3973	0.2354
<i>BPR 2-pressure, psi</i>	1018	6.77E-02
<i>Gas Viscosity, cp</i>	0.0203	

Table A.16.5 Methane flood results at S_{wi} (Exp #224)

q_{core} , cc/hr	ΔP , psi	k_g , md
5216	14.400	121.67
6259	18.000	116.81
6954	20.630	113.24
7650	23.300	110.29
8693	26.400	110.61
<i>Corrected Permeability (k_g), md</i>		136.4

Table A.16.6 Volatile oil properties at BPR-1 and BPR-2 pressures (Exp #224)

<i>BPR 1-pressure, psi</i>	4230	
<i>BPR 2- pressure, psi</i>	2220	
<i>Density at BPR 1-pressure, gr/cc</i>	0.3662	
Properties at BPR 2- pressure, psi		
	Gas Phase	Oil Phase
<i>Density, gr/cc</i>	0.1386	0.504
<i>Viscosity (μ), cp</i>	0.0183	0.0972
<i>Volume Fraction</i>	0.741	0.259
<i>IFT, dyne/cm</i>	1.46	

Table A.16.7 Fluid properties and conditions for final gas permeability (Exp #224)

<i>Gas</i>	<i>Nitrogen</i>	<i>Density, gr/cc</i>
<i>Temperature, °F</i>	155	
<i>BPR 1-pressure, psi</i>	4266	0.2473
<i>BPR 2-pressure, psi</i>	2223	1.42E-01
<i>Gas Viscosity, cp</i>	0.0222	

Table A.16.8 Final methane flood results (Exp #224)

q_{core} , cc/hr	ΔP , psi	k_g , md
2612	10.700	89.69
3135	13.200	87.25
3483	14.900	85.88
3831	16.700	84.29
4354	19.400	82.45
<i>Corrected Permeability (k_g), md</i>		102.22

Table A.16.9 Pre and post-treatment volatile oil flood results and measured improvement factors (Exp #224)

	Exp #224
$q_{gtot\ core}, cc/hr$	165
$q_g, cc/hr$	122
$q_o, cc/hr$	43
<i>PVT Ratio</i>	0.54
<i>Viscosity Ratio μ_g/μ_o</i>	0.19
<i>Capillary Nc</i>	3.00E-05
$k_{rg\ Before\ Treatment}$	0.028
$k_{ro\ Before\ Treatment}$	0.053
$k_{rg\ After\ Treatment}$	0.062
$k_{ro\ After\ Treatment}$	0.115
<i>Initial Improvement Factor</i>	2.18
<i>PV of Vol Oil Injected</i>	~280
<i>Final Improvement Factor</i>	1.59

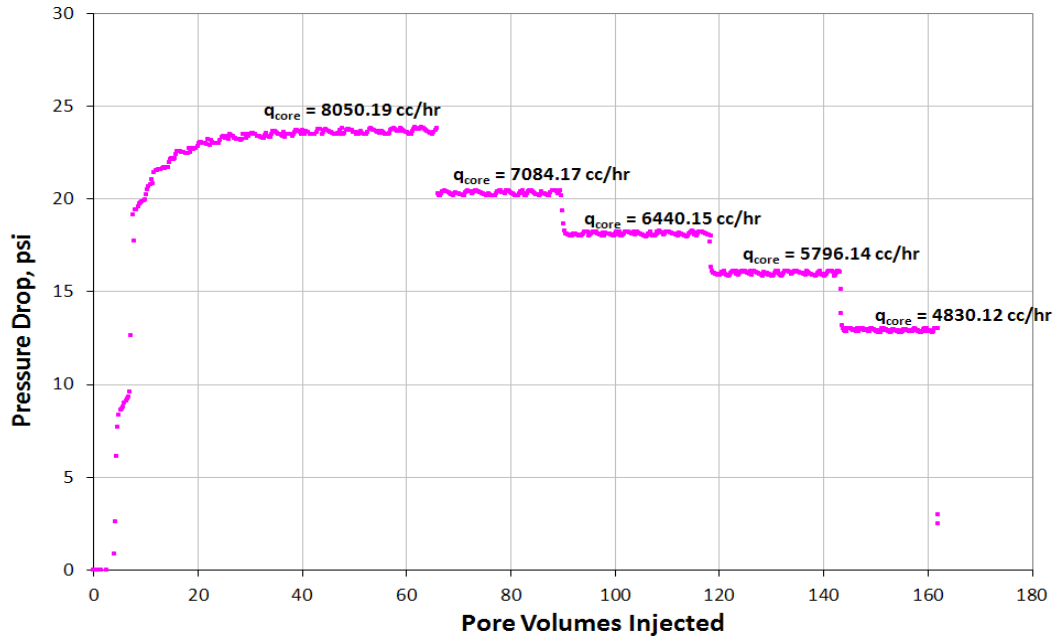


Figure A.16.1 Pressure drop across the core during the initial methane flood at 155°F (Exp #224)

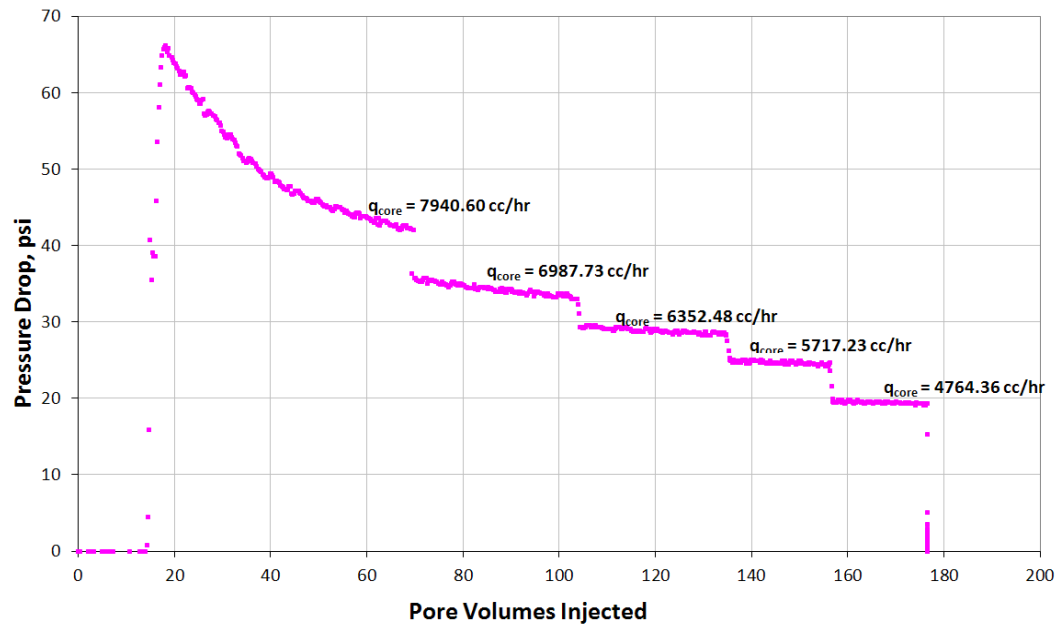


Figure A.16.2 Pressure drop across the core during the methane flood at S_{wi} of 20% (Exp #224)

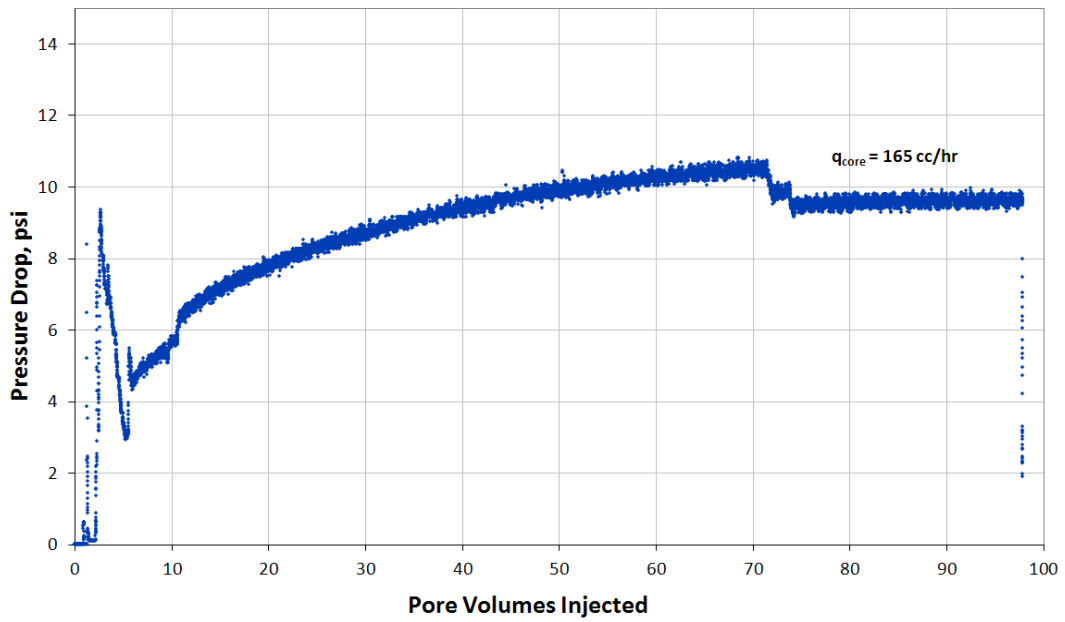


Figure A.16.3 Pressure drop across the core during the pre-treatment two-phase volatile oil flood (Exp #224)

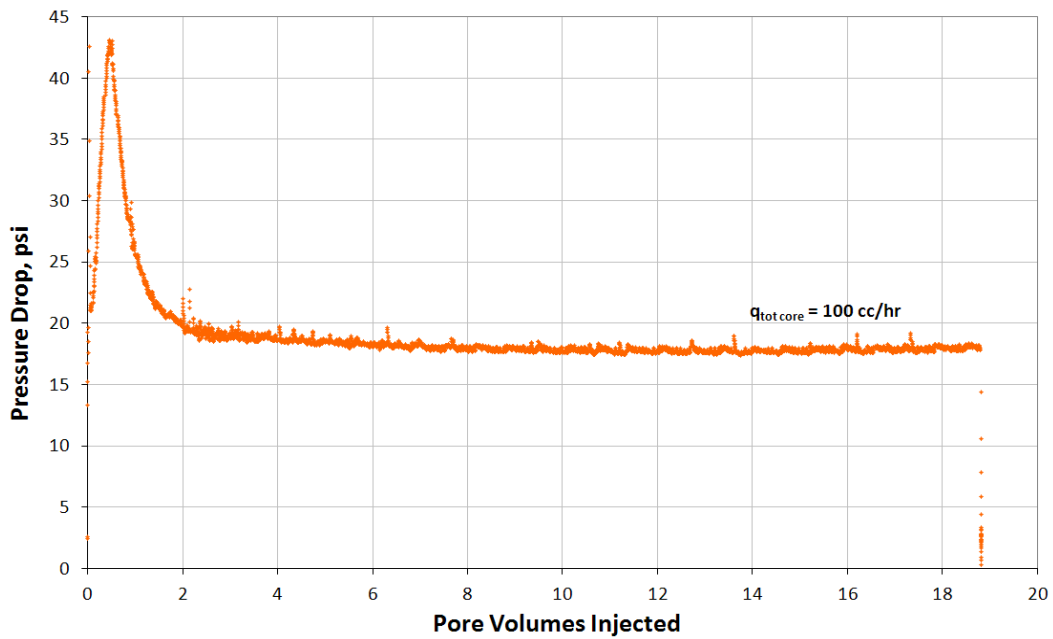


Figure A.16.4 Pressure drop across the core during injection of chemical treatment 1 (Exp # 224)

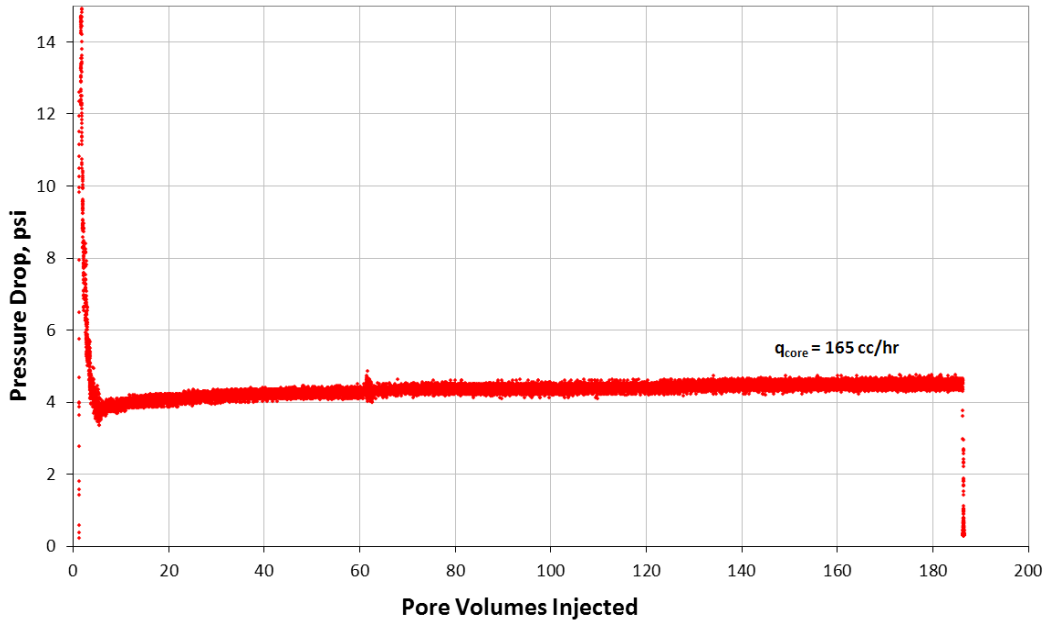


Figure A.16.5 Pressure drop across the core during the post-treatment two-phase volatile oil flood (Exp #224)

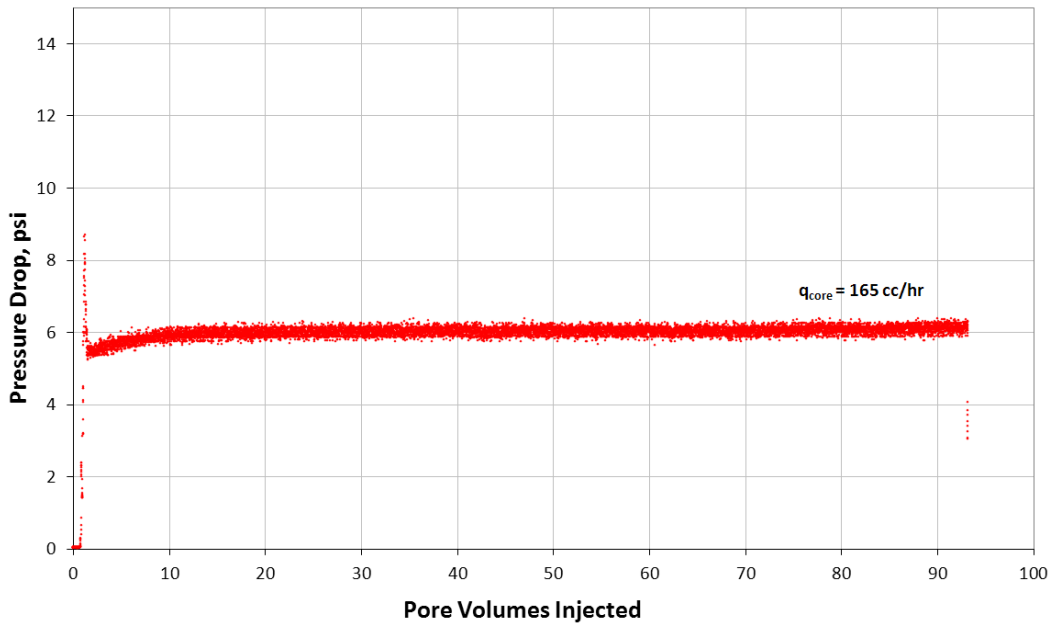


Figure A.16.6 Pressure drop across the core during the post-treatment two-phase volatile oil flood 2 (Exp #224)

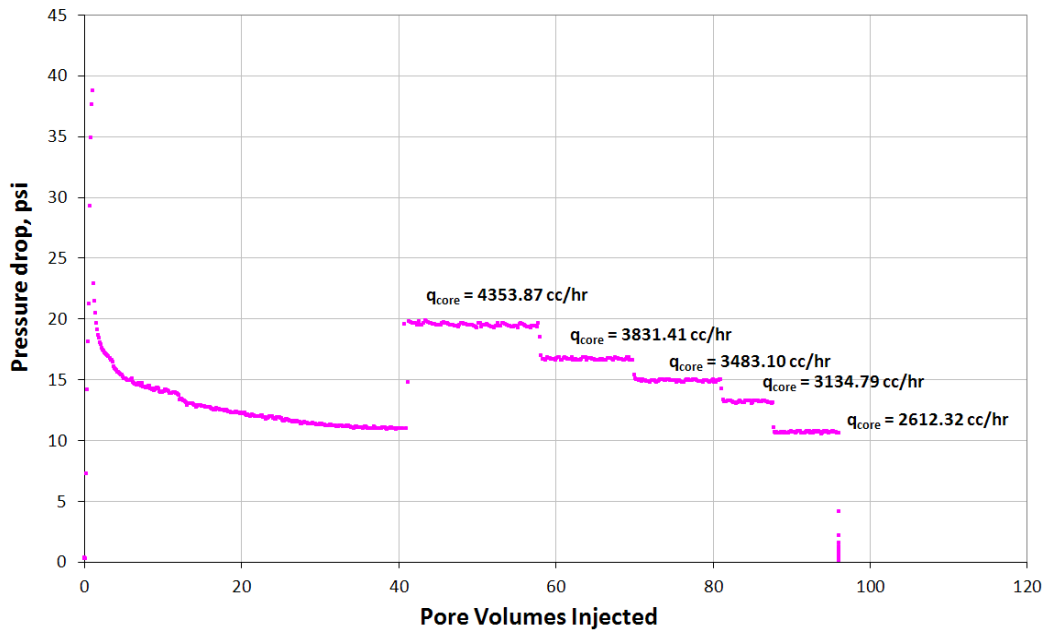


Figure A.16.7 Pressure drop across the core during the final methane flood at 155°F (Exp #224)

Appendix A.17: EXPERIMENT #225

Objective:

The objective of this experiment was to investigate the effectiveness of chemical treatment 1 using non-ionic fluoro-surfactant FC-X in improving the oil and gas relative permeability at low liquid fraction. This was done for a volatile oil mixture below the bubble point pressure on a Berea sandstone core and in the presence of initial water saturation. The experiment was performed at 155°F.

Experimental Procedure and Results:

A Berea core was prepared for the experiment following the standard procedure described Section 3.2.1.1. The initial core measurements and assumed properties can be found in Table A.5.1.

The initial gas permeability was calculated using nitrogen at 75°F. Nitrogen was flowed through the core using five flow rates and the pressure drop across the core for each flow rate was recorded. Using this data, the fluid properties and accounting for non-Darcy effects the calculated gas permeability was 132 md. Table A.5.2 summarizes the flood conditions and fluid properties and Table A.5.3 shows the results. Figure A.6.1 shows the pressure drop measured across the core during the methane flood.

The initial gas permeability at initial water saturation was calculated next. Using synthetic brine 1 (25,000 ppm NaCl) an initial water saturation of 20% was established. This was done by applying vacuum to the core first and then injecting 3.8 ml of brine. The core was shut in for 1 hour, allowing the brine to distribute through the core. Nitrogen at 155°F was then flowed through the core using five flow rates and the pressure drop across the core for each flow rate was recorded. The calculated gas

permeability was 112 md. Flood conditions and results are shown in Table A.5.4 and Table A.4.5 respectively. Figure A.4.2 shows the pressure drop measured across the core during the methane flood at S_{wi} .

Synthetic volatile oil mixture 2 (Table 3.3) was used for the two-phase flow measurements. The mixture was allowed a minimum of 12 hours to equilibrate to a single phase at 4200 psi and 155°F. The initial flood was conducted with the upstream backpressure regulator (BPR-1) set at 4240 psi and the downstream back pressure regulator (BPR-2) set at 717 psi. Volatile oil was injected at an upstream BPR-1 flow rate of 150 cc/hr (this is for volatile oil at single liquid phase) corresponding to a capillary number of approximately 2×10^{-5} . Once steady state was observed the pressure drop across the core was measured. The PVT ratio was 1.02. Table A.3.6 gives the fluid properties of the synthetic fluid calculated using the Peng-Robinson EOS at the flowing core pressures. Figure A.4.3 shows the pressure drop measured across the core during the initial two-phase volatile oil flood for the different BPR-2 pressures.

The core was then treated using chemical treatment 1 (Table 4.15). The solution was heated for at least 3 hours at 155°F. BPR2 was set at 720 psi. The core was flooded with approximately 20 pore volumes of the treatment solution at a flow rate of 100 cc/hr. The core was then shut in for 12 hour. Figure A.4.4 shows the measured pressure drop across the core during the treatment flood.

Post-treatment two-phase volatile oil flood was conducted under the same conditions as the initial two-phase flow. Figure A.4.5 shows the pressure drop measured across the core during the post-treatment two-phase volatile oil flood. Improvement factor was 2.6.

A second batch of post-treatment two phase volatile oil flood followed. Figure A.17.6 shows the pressure drop measured across the core during the post-treatment two-phase volatile oil flood 2. Improvement factor was 1.9.

The final gas permeability was calculated following the procedure for the initial gas permeability using nitrogen at 155°F. The calculated gas permeability was 94 md. Flood conditions and results are shown in Table A.4.7 and Table A.3.8 respectively. Figure A.16.7 shows the pressure drop across the core for the final methane flood.

For every two-phase volatile oil flood, oil and gas relative permeabilities k_{rg} and k_{ro} were calculated using the measured pressure drop across the core under steady state conditions and then improvement factors were measured. Table A.16.9 summarizes the experimental results.

Table A.17.1 Core properties (Exp #225)

<i>Length, in</i>	7.955
<i>Diameter, in</i>	0.997
<i>Mass Core, gr</i>	219.85
<i>Grain Density, gr/cc</i>	2.65
<i>Porosity (ϕ)</i>	18.48%

Table A.17.2 Fluid properties and conditions for initial gas permeability (Exp #225)

		<i>Density, gr/cc</i>
<i>Gas</i>	Nitrogen	
<i>Temperature, °F</i>	75	
<i>BPR 1-pressure, psi</i>	3460	0.2479
<i>BPR 2-pressure, psi</i>	991	0.0785
<i>Gas Viscosity, cp</i>	0.0187	

Table A.17.3 Initial nitrogen flood results (Exp #225)

<i>q_{core}, cc/hr</i>	<i>ΔP, psi</i>	<i>k_g, md</i>
4737	12.400	116.99
5684	15.100	115.28
6316	17.100	113.11
6948	19.100	111.39
7895	22.150	109.15
<i>Corrected Permeability (k_g), md</i>		131.6

Table A.17.4 Fluid properties and conditions for nitrogen gas permeability at S_{wi} (Exp #225)

		<i>Density, gr/cc</i>
<i>Gas</i>	Nitrogen	
<i>Temperature, °F</i>	155	
<i>BPR 1-pressure, psi</i>	4090	0.2433
<i>BPR 2-pressure, psi</i>	1170	7.82E-02
<i>Gas Viscosity, cp</i>	0.0205	

Table A.17.5 Methane flood results at S_{wi} (Exp #225)

q_{core} , cc/hr	ΔP , psi	k_g , md
4666.88	23.800	65.83
5600.26	30.200	62.26
6222.51	35.100	59.52
6844.76	40.700	56.46
7778.13	49.800	52.44
Corrected Permeability (k_g), md		112.2

Table A.17.6 Volatile oil properties at BPR-1 and BPR-2 pressures (Exp #225)

BPR 1-pressure, psi	4240	
BPR 2- pressure, psi	717	
Density at BPR 1-pressure, gr/cc	0.3665	
Properties at BPR 2- pressure		
	Gas Phase	Oil Phase
Density, gr/cc	0.0386	0.6104
Viscosity (μ), cp	0.0127	0.2074
Volume Fraction	0.9434	0.0566
IFT, dyne/cm	9.631	

Table A.17.7 Fluid properties and conditions for final gas permeability (Exp #225)

		Density, gr/cc
Gas	Nitrogen	
Temperature, °F	155	
BPR 1-pressure, psi	4235	0.2477
BPR 2-pressure, psi	710	4.76E-02
Gas Viscosity, cp	0.02	

Table A.17.8 Final nitrogen flood results (Exp #225)

q_{core} , cc/hr	ΔP , psi	k_g , md
7806	33.700	75.86
9367	42.000	73.05
10408	47.400	71.92
11448	53.600	69.96

13009	63.500	67.10
<i>Corrected Permeability (k_g), md</i>		93.81

Table A.17.9 Pre and post-treatment volatile oil flood results and measured improvement factors (Exp #225)

	Exp #225
$q_{g\text{tot core}}$, cc/hr	774.69
q_g , cc/hr	730.84
q_o , cc/hr	43.85
<i>PVT Ratio</i>	1.02
<i>Viscosity Ratio μ_g/μ_o</i>	0.06
<i>Capillary Nc</i>	1.96E-05
k_{rg} Before Treatment	0.0270
k_{ro} Before Treatment	0.0265
k_{rg} After Treatment	0.0704
k_{ro} After Treatment	0.0690
<i>Initial Improvement Factor</i>	2.60
<i>PV of Vol Oil Injected</i>	~550
<i>Final Improvement Factor</i>	1.88

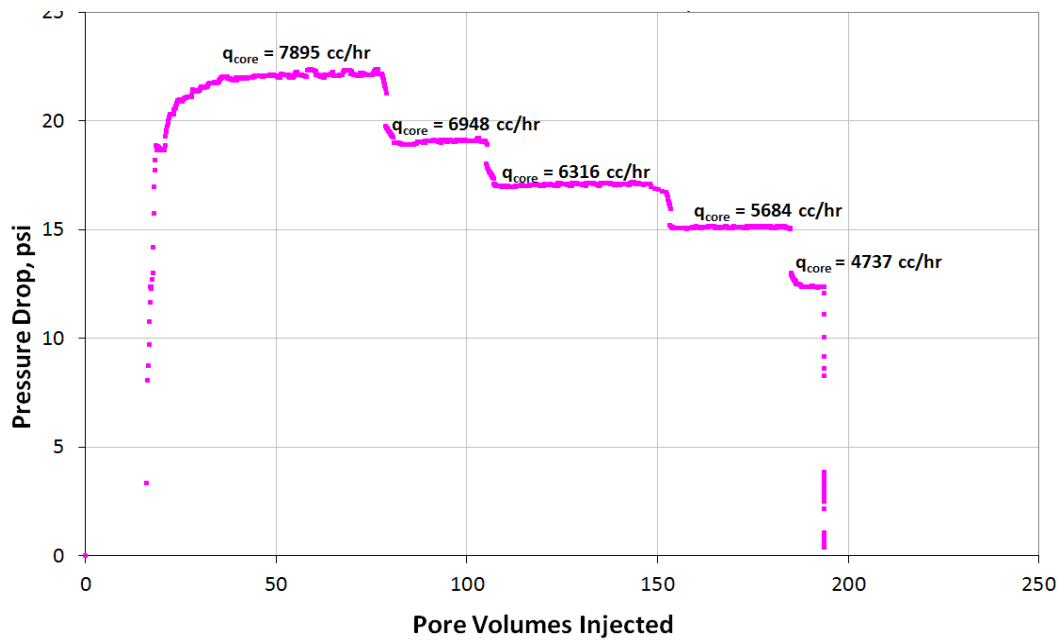


Figure A.17.1 Pressure drop across the core during the initial nitrogen flood at 75°F (Exp #225)

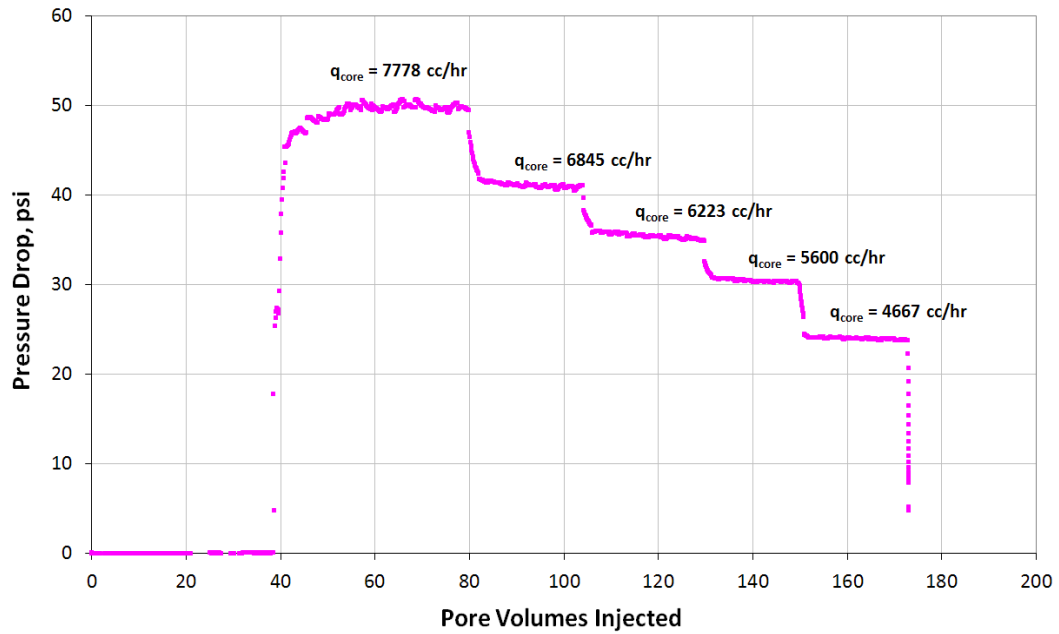


Figure A.17.2 Pressure drop across the core during the nitrogen flood at S_{wi} of 20% (Exp #225)

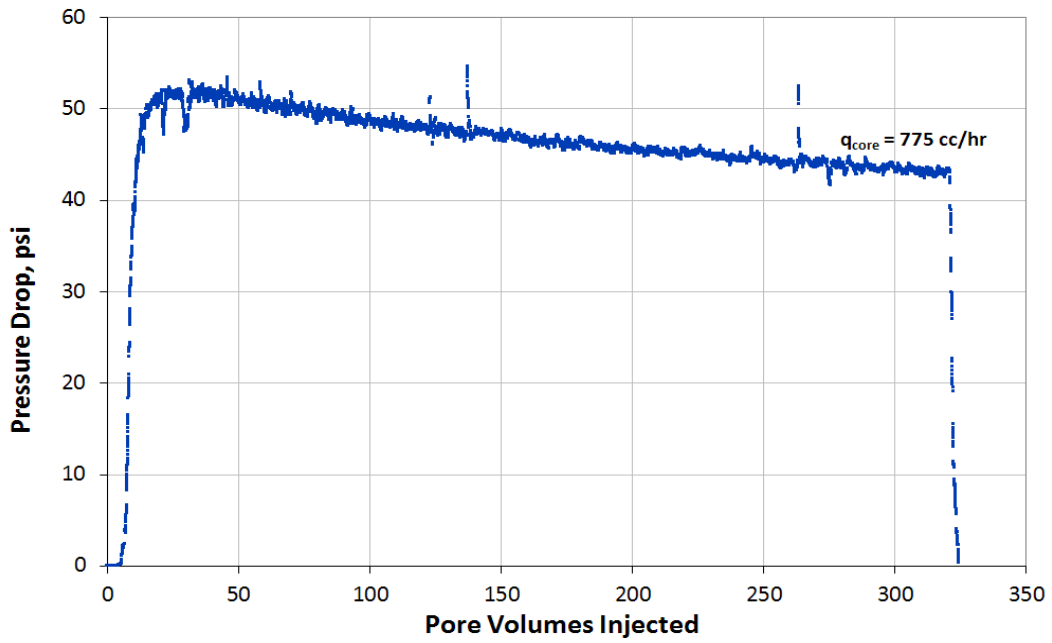


Figure A.17.3 Pressure drop across the core during the pre-treatment two-phase volatile oil flood (Exp #225)

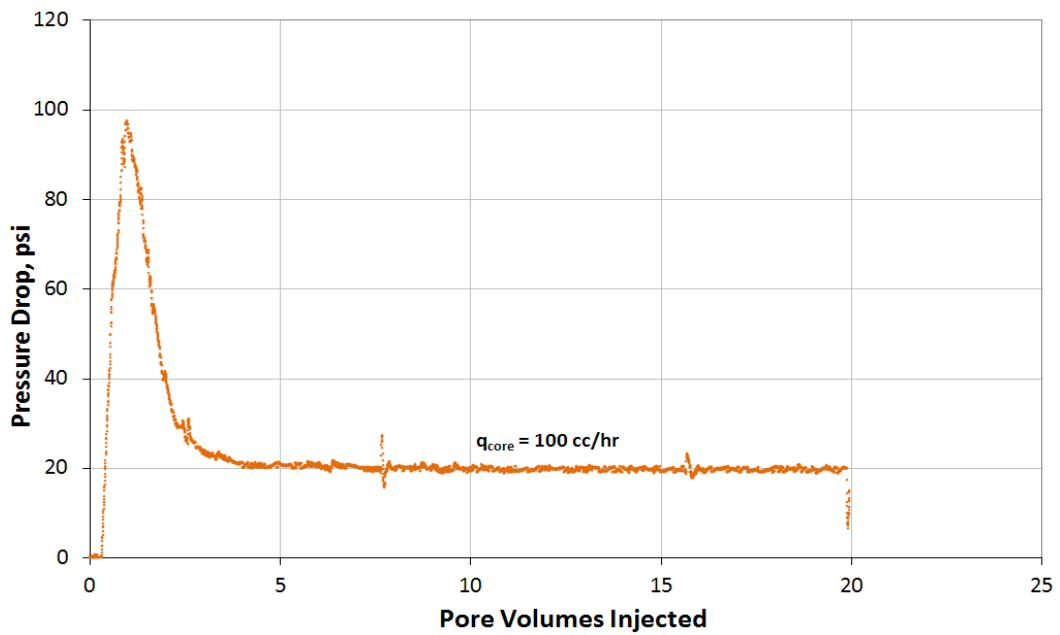


Figure A.17.4 Pressure drop across the core during injection of chemical treatment 1 (Exp # 225)

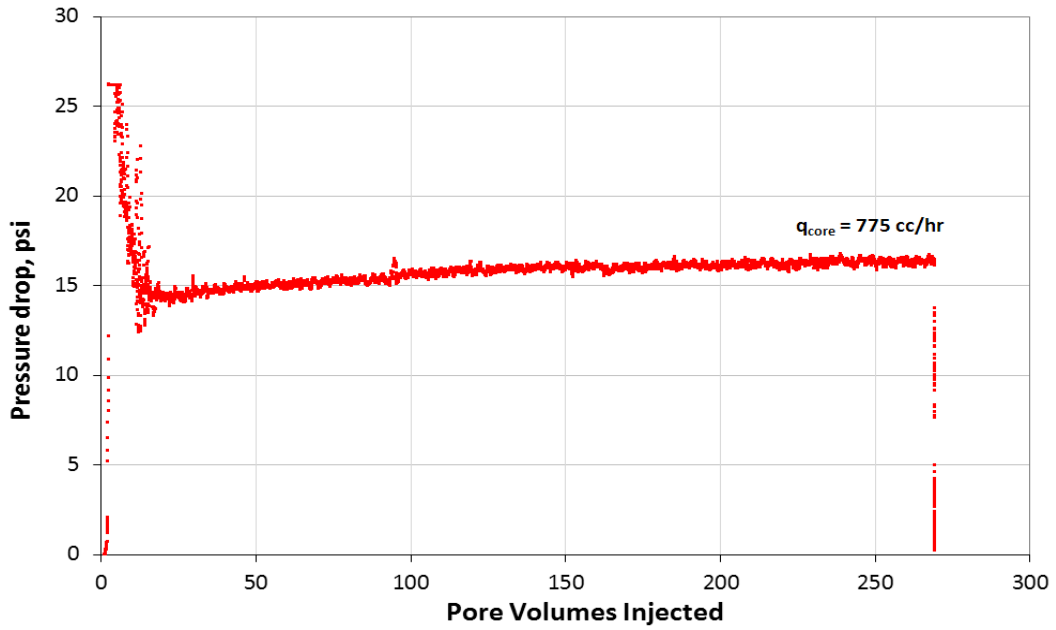


Figure A.17.5 Pressure drop across the core during the post-treatment two-phase volatile oil flood (Exp #225)

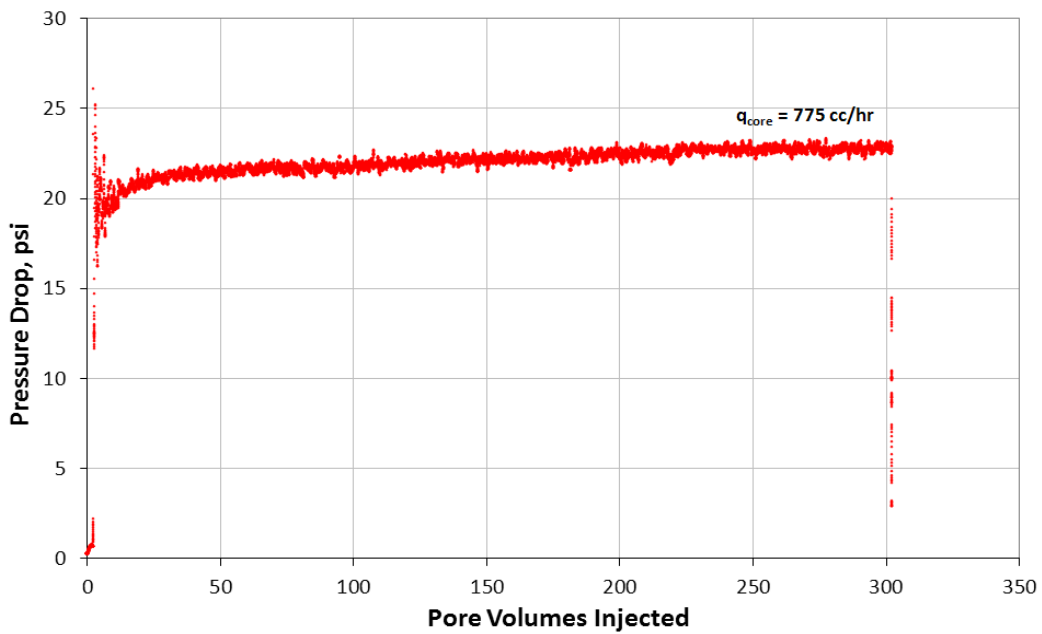


Figure A.17.6 Pressure drop across the core during the post-treatment two-phase volatile oil flood 2 (Exp #225)

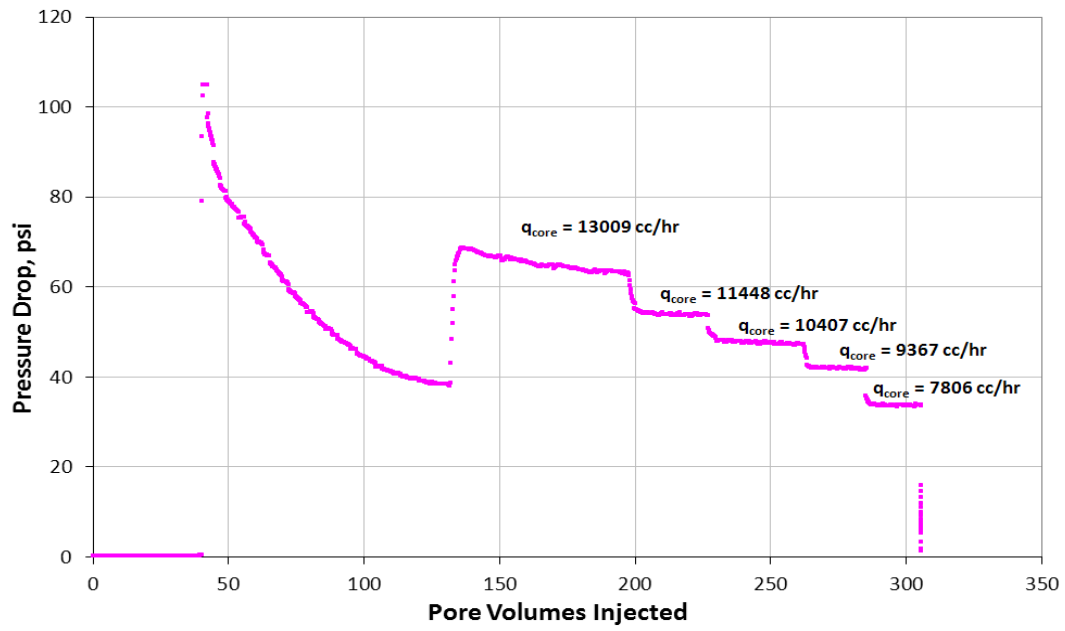


Figure A.17.7 Pressure drop across the core during the final nitrogen flood at 155°F (Exp #225)

Appendix A.18: EXPERIMENT #228

Objective:

The objective of this experiment was to investigate the effectiveness of chemical treatment 1 using non-ionic fluoro-surfactant FC-X in improving the oil and gas relative permeability at high temperature. This was done for a volatile oil mixture below the bubble point pressure on a Berea sandstone core and in the presence of initial water saturation. The experiment was performed at 215°F.

Experimental Procedure and Results:

A Berea core was prepared for the experiment following the standard procedure described Section 3.2.1.1. The initial core measurements and assumed properties can be found in Table A.5.1.

The initial gas permeability was calculated using nitrogen at 75°F. Nitrogen was flowed through the core using five flow rates and the pressure drop across the core for each flow rate was recorded. Using this data, the fluid properties and accounting for non-Darcy effects the calculated gas permeability was 170 md. Table A.5.2 summarizes the flood conditions and fluid properties and Table A.5.3 shows the results. Figure A.6.1 shows the pressure drop measured across the core during the methane flood.

The initial gas permeability at initial water saturation was calculated next. Using synthetic brine 1 (25,000 ppm NaCl) an initial water saturation of 20% was established. This was done by applying vacuum to the core first and then injecting 3.7 ml of brine. The core was shut in for 1 hour, allowing the brine to distribute through the core. Nitrogen at 75°F was then flowed through the core using five flow rates and the pressure drop across the core for each flow rate was recorded. The calculated gas permeability

was 150 md. Flood conditions and results are shown in Table A.5.4 and Table A.4.5 respectively. Figure A.4.2 shows the pressure drop measured across the core during the methane flood at S_{wi} .

Synthetic volatile oil mixture 3 (Table 3.3) was used for the two-phase flow measurements. The mixture was allowed a minimum of 12 hours to equilibrate to a single phase at 4300 psi and 215°F. The initial flood was conducted with the upstream backpressure regulator (BPR-1) set at 4350 psi and the downstream back pressure regulator (BPR-2) set at 850 psi. Volatile oil was injected at an upstream BPR-1 flow rate of 120 cc/hr (this is for volatile oil at single liquid phase) corresponding to a capillary number of approximately 1.5×10^{-5} . Once steady state was observed the pressure drop across the core was measured. The PVT ratio was 1.11. Table A.3.6 gives the fluid properties of the synthetic fluid calculated using the Peng-Robinson EOS at the flowing core pressures. Figure A.4.3 shows the pressure drop measured across the core during the initial two-phase volatile oil flood for the different BPR-2 pressures.

The core was then treated using chemical treatment 1 (Table 4.15). The solution was heated for at least 3 hours at 215°F. BPR2 was set at 830 psi. The core was flooded with approximately 20 pore volumes of the treatment solution at a flow rate of 100 cc/hr. The core was then shut in for 12 hour. Figure A.4.4 shows the measured pressure drop across the core during the treatment flood.

Post-treatment two-phase volatile oil flood was conducted under the same conditions as the initial two-phase flow. Figure A.4.5 shows the pressure drop measured across the core during the post-treatment two-phase volatile oil flood. Improvement factor was 2.6.

A second batch of post-treatment two phase volatile oil flood followed. Figure A.6.10 shows the pressure drop measured across the core during the post-treatment two-phase volatile oil flood 2. Improvement factor was approximately 2.

The final gas permeability was calculated following the procedure for the initial gas permeability using methane at 215°F. The calculated gas permeability was 173 md. Flood conditions and results are shown in Table A.4.7 and Table A.3.8 respectively. Figure A.6.10 shows the pressure drop across the core for the final methane flood.

For every two-phase volatile oil flood, oil and gas relative permeabilities k_{rg} and k_{ro} were calculated using the measured pressure drop across the core under steady state conditions and then improvement factors were measured. Table A.16.9 summarizes the experimental results.

Table A.18.1 Core properties (Exp #228)

<i>Length, in</i>	7.966
<i>Diameter, in</i>	0.992
<i>Mass Core, gr</i>	218.56
<i>Grain Density, gr/cc</i>	2.65
<i>Porosity (ϕ)</i>	18.25 %

Table A.18.2 Fluid properties and conditions for initial gas permeability (Exp #228)

		<i>Density, gr/cc</i>
<i>Gas</i>	Nitrogen	
<i>Temperature, °F</i>	75	
<i>BPR 1-pressure, psi</i>	3766	0.2654
<i>BPR 2-pressure, psi</i>	1024	0.0803
<i>Gas Viscosity, cp</i>	0.0187	

Table A.18.3 Initial nitrogen flood results (Exp #228)

<i>q_{core}, cc/hr</i>	ΔP , psi	<i>k_g, md</i>
4958	10.780	142.46
5949	13.400	137.53
6610	15.250	134.27
7271	17.150	131.33
8262	20.100	127.34
<i>Corrected Permeability (k_g), md</i>		170.4

Table A.18.4 Fluid properties and conditions for nitrogen gas permeability at S_{wi} (Exp #228)

		<i>Density, gr/cc</i>
<i>Gas</i>	Nitrogen	
<i>Temperature, °F</i>	75	
<i>BPR 1-pressure, psi</i>	3766	0.2654
<i>BPR 2-pressure, psi</i>	1024	0.0803
<i>Gas Viscosity, cp</i>	0.0187	

Table A.18.5 Nitrogen flood results at S_{wi} (Exp #228)

q_{core} , cc/hr	ΔP , psi	k_g , md
4958	14.100	108.92
5949	17.730	103.94
6610	20.560	99.59
7271	23.400	96.26
8263	28.000	91.41
<i>Corrected Permeability (k_g), md</i>		150.0

Table A.18.6 Volatile oil properties at BPR-1 and BPR-2 pressures (Exp #228)

<i>BPR 1-pressure, psi</i>	4350	
<i>BPR 2- pressure, psi</i>	850	
<i>Density at BPR 1-pressure, gr/cc</i>	0.3577	
Properties at BPR 2- pressure, psi		
	Gas Phase	Oil Phase
<i>Density, gr/cc</i>	0.0442	0.5844
<i>Viscosity (μ), cp</i>	0.0136	0.159
<i>Volume Fraction</i>	0.9287	0.0713
<i>IFT, dyne/cm</i>	7.505	

Table A.18.7 Fluid properties and conditions for final gas permeability (Exp #228)

		<i>Density, gr/cc</i>
<i>Gas</i>	Methane	
<i>Temperature, °F</i>	215	
<i>BPR 1-pressure, psi</i>	3350	0.1214
<i>BPR 2-pressure, psi</i>	675	2.47E-02
<i>Gas Viscosity, cp</i>	0.0138	

Table A.18.8 Final methane flood results (Exp #228)

$q_{core}, cc/hr$	$\Delta P, psi$	k_g, md
7372	20.000	84.27
8847	25.000	80.90
9830	29.000	77.49
10813	34.800	71.03
12287	43.000	65.32
<i>Corrected Permeability (k_g), md</i>		173.21

Table A.18.9 Pre and post-treatment volatile oil flood results and measured improvement factors (Exp #228)

	Exp# 228
$q_{gtot\ core}, cc/hr$	519
$q_g, cc/hr$	482
$q_o, cc/hr$	37
<i>PVT Ratio</i>	1.11
<i>Viscosity Ratio μ_g/μ_o</i>	0.09
<i>Capillary Nc</i>	1.51E-05
k_{rg} Before Treatment	0.032
k_{ro} Before Treatment	0.029
k_{rg} After Treatment	0.085
k_{ro} After Treatment	0.076
<i>Initial Improvement Factor</i>	2.6
<i>PV of Vol Oil Injected</i>	~320
<i>Final Improvement Factor</i>	2

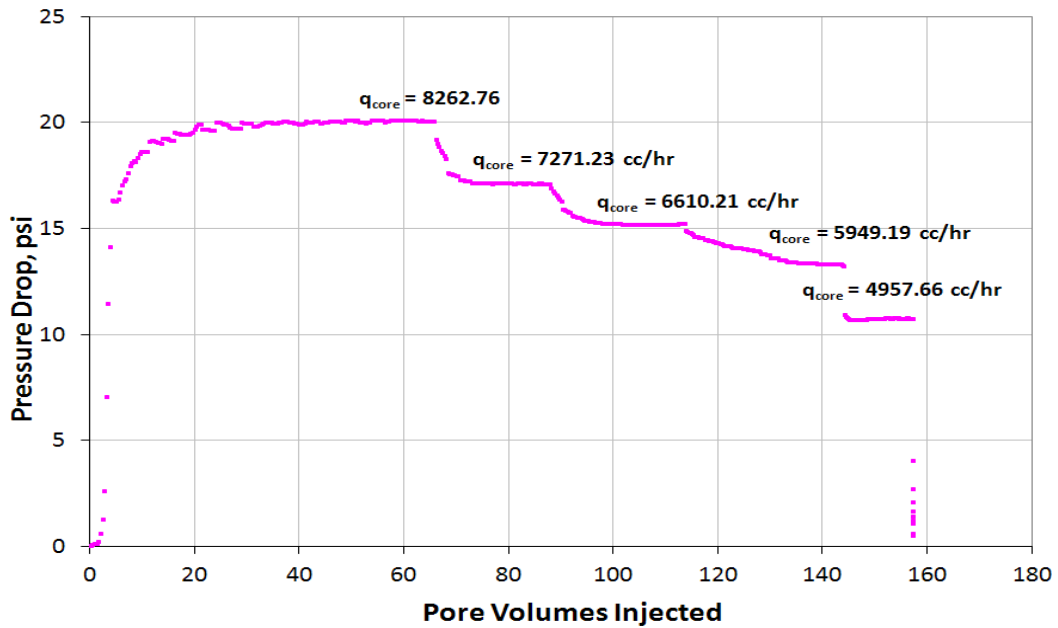


Figure A.18.1 Pressure drop across the core during the initial nitrogen flood at 75°F (Exp #228)

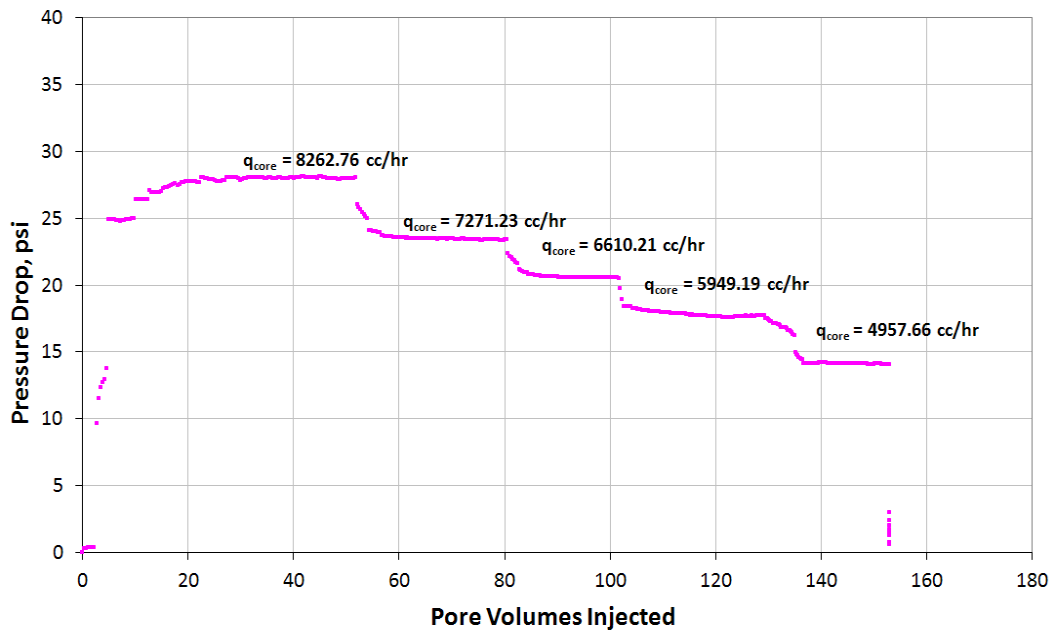


Figure A.18.2 Pressure drop across the core during the nitrogen flood at S_{wi} of 20% (Exp #228)

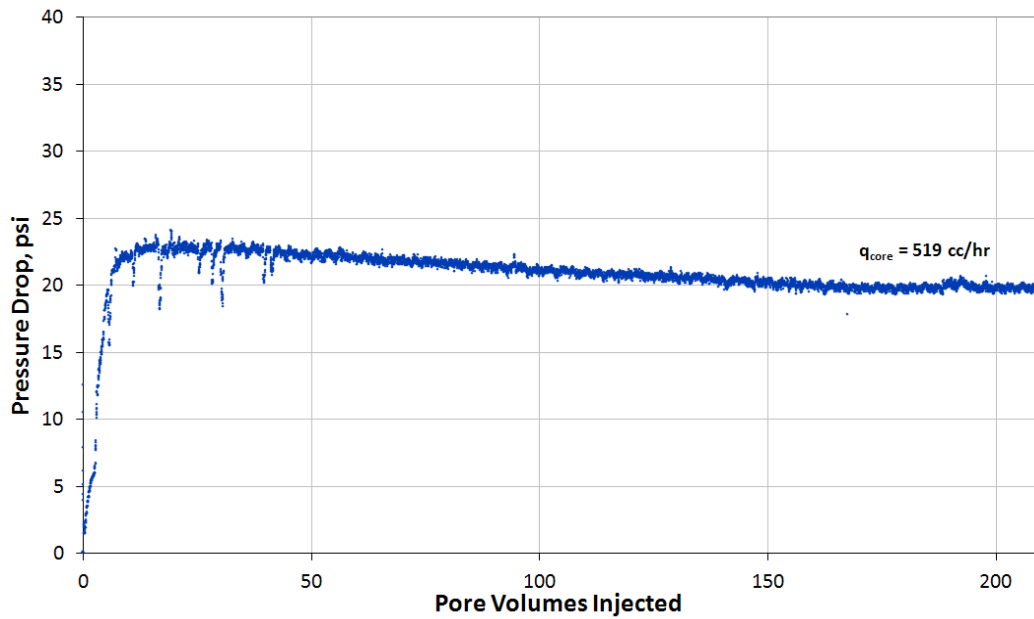


Figure A.18.3 Pressure drop across the core during the pre-treatment two-phase volatile oil flood (Exp #228)

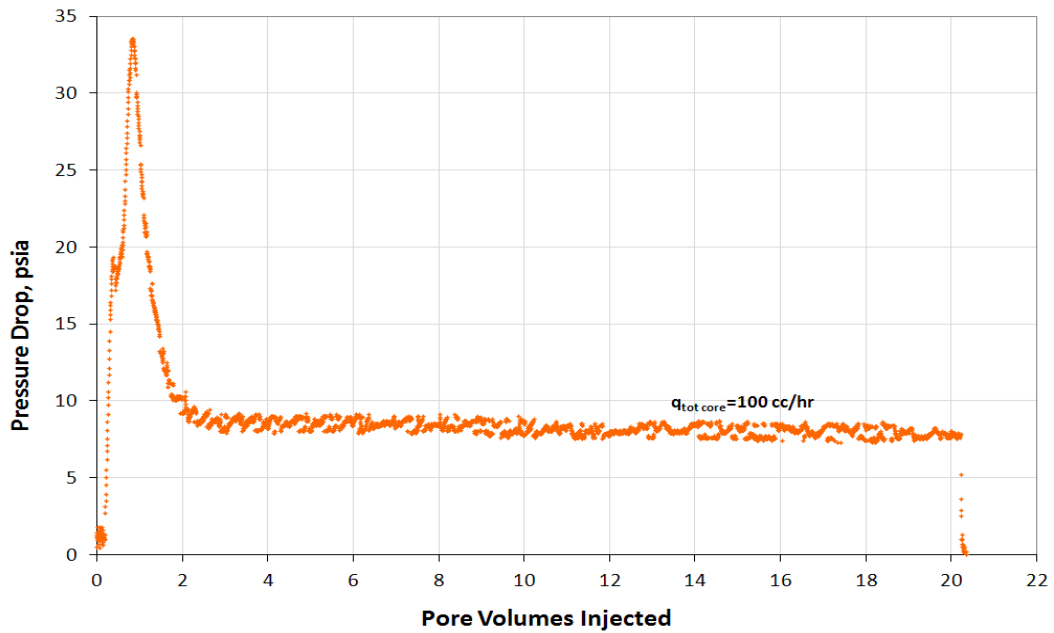


Figure A.18.4 Pressure drop across the core during injection of chemical treatment 1 (Exp # 228)

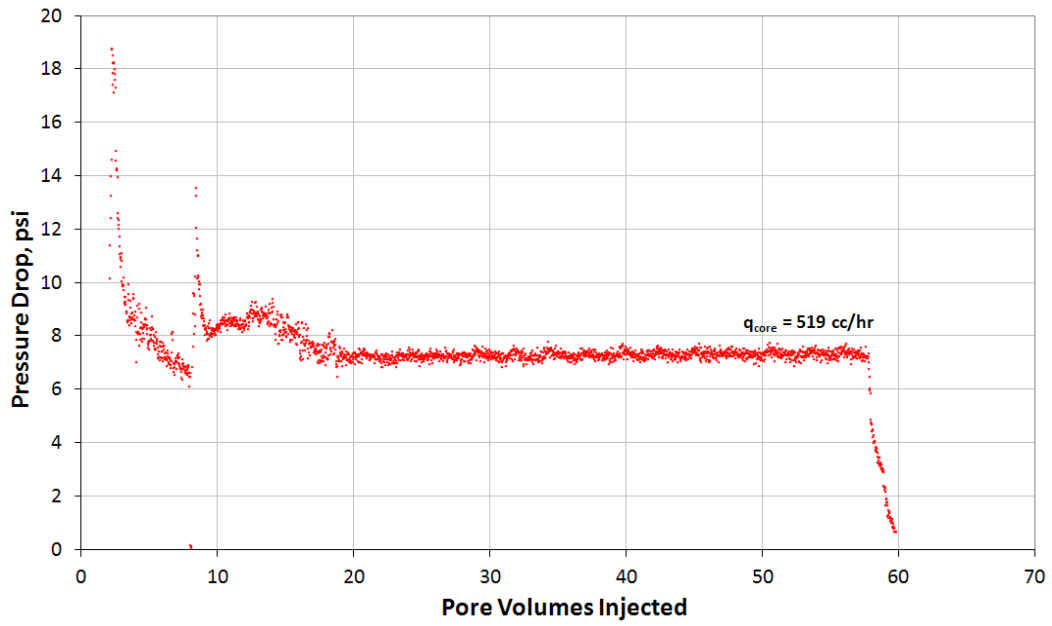


Figure A.18.5 Pressure drop across the core during the post-treatment two-phase volatile oil flood (Exp #228)

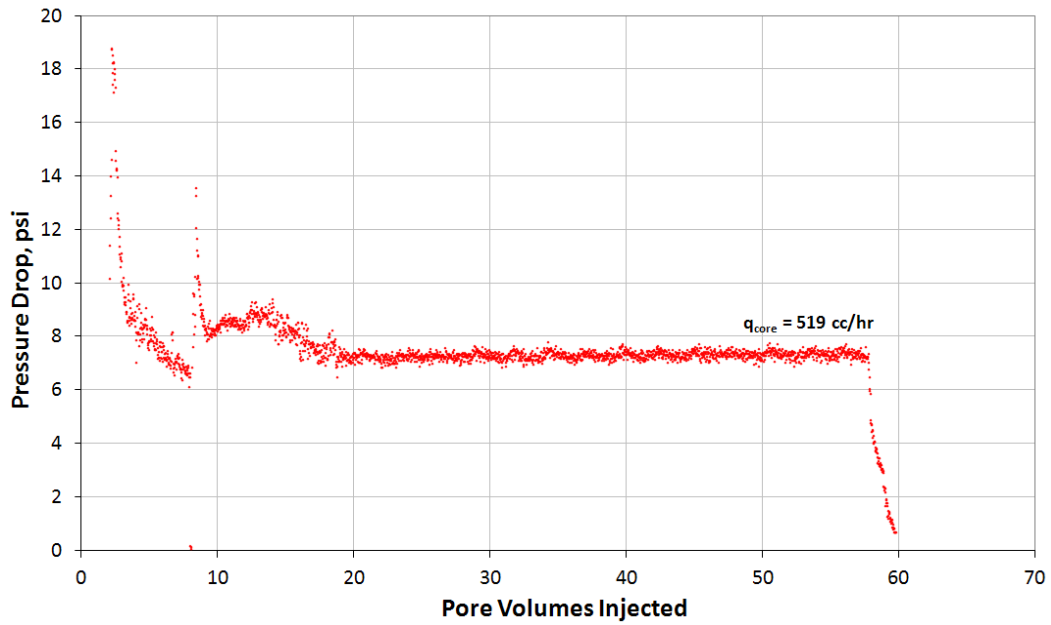


Figure A.18.6 Pressure drop across the core during the post-treatment two-phase volatile oil flood 2 (Exp #228)

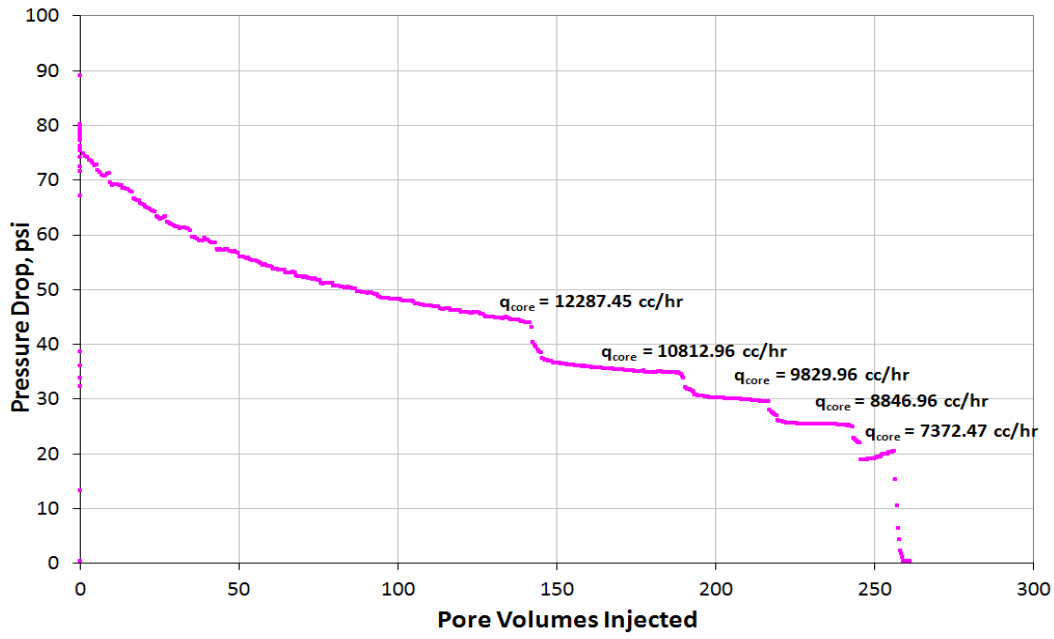


Figure A.18.7 Pressure drop across the core during the final methane flood at 215°F (Exp #228)

Appendix A.19: EXPERIMENT #229

Objective:

The objective of this experiment was to investigate the effectiveness of chemical treatment 1 using non-ionic fluoro-surfactant FC-X in improving the oil and gas relative permeability at high temperature. This was done for a volatile oil mixture below the bubble point pressure on a Berea sandstone core and in the presence of initial water saturation. The experiment was performed at 275°F.

Experimental Procedure and Results:

A Berea core was prepared for the experiment following the standard procedure described Section 3.2.1.1. The initial core measurements and assumed properties can be found in Table A.5.1.

The initial gas permeability was calculated using nitrogen at 75°F. Nitrogen was flowed through the core using five flow rates and the pressure drop across the core for each flow rate was recorded. Using this data, the fluid properties and accounting for non-Darcy effects the calculated gas permeability was 193 md. Table A.5.2 summarizes the flood conditions and fluid properties and Table A.5.3 shows the results. Figure A.6.1 shows the pressure drop measured across the core during the methane flood.

The initial gas permeability at initial water saturation was calculated next. Using synthetic brine 1 (25,000 ppm NaCl) an initial water saturation of 20% was established. This was done by applying vacuum to the core first and then injecting 3.7 ml of brine. The core was shut in for 1 hour, allowing the brine to distribute through the core. Nitrogen at 75°F was then flowed through the core using five flow rates and the pressure drop across the core for each flow rate was recorded. The calculated gas permeability

was 173 md. Flood conditions and results are shown in Table A.5.4 and Table A.4.5 respectively. Figure A.4.2 shows the pressure drop measured across the core during the methane flood at S_{wi} .

Synthetic volatile oil mixture 5 (Table 3.3) was used for the two-phase flow measurements. The mixture was allowed a minimum of 12 hours to equilibrate to a single phase at 4000 psi and 275°F. The initial flood was conducted with the upstream backpressure regulator (BPR-1) set at 4080 psi and the downstream back pressure regulator (BPR-2) set at 855 psi. Volatile oil was injected at an upstream BPR-1 flow rate of 120 cc/hr (this is for volatile oil at single liquid phase) corresponding to a capillary number of approximately 1.6×10^{-5} . Once steady state was observed the pressure drop across the core was measured. The PVT ratio was 1.5. Table A.3.6 gives the fluid properties of the synthetic fluid calculated using the Peng-Robinson EOS at the flowing core pressures. Figure A.4.3 shows the pressure drop measured across the core during the initial two-phase volatile oil flood for the different BPR-2 pressures.

The core was then treated using chemical treatment 1 (Table 4.15). The solution was heated for at least 3 hours at 275°F. BPR2 was set at 850 psi. The core was flooded with approximately 20 pore volumes of the treatment solution at a flow rate of 100 cc/hr. The core was then shut in for 12 hour. Figure A.4.4 shows the measured pressure drop across the core during the treatment flood.

Post-treatment two-phase volatile oil flood was conducted under the same conditions as the initial two-phase flow. Figure A.4.5 shows the pressure drop measured across the core during the post-treatment two-phase volatile oil flood. Improvement factor was 3.5.

A second batch of post-treatment two phase volatile oil flood followed. Figure A.18.6 shows the pressure drop measured across the core during the post-treatment two-phase volatile oil flood 2. Improvement factor was approximately 3.

The final gas permeability was calculated following the procedure for the initial gas permeability using nitrogen at 75°F. The calculated gas permeability was 205 md. Flood conditions and results are shown in Table A.4.7 and Table A.3.8 respectively. Figure A.16.7 shows the pressure drop across the core for the final nitrogen flood.

For every two-phase volatile oil flood, oil and gas relative permeabilities k_{rg} and k_{ro} were calculated using the measured pressure drop across the core under steady state conditions and then improvement factors were measured. Table A.16.9 summarizes the experimental results.

Table A.19.1 Core properties (Exp #229)

<i>Length, in</i>	7.936
<i>Diameter, in</i>	0.991
<i>Mass Core, gr</i>	216.25
<i>Grain Density, gr/cc</i>	2.65
<i>Porosity (ϕ)</i>	18.65 %

Table A.19.2 Fluid properties and conditions for initial gas permeability (Exp #229)

		<i>Density, gr/cc</i>
<i>Gas</i>	Nitrogen	
<i>Temperature, °F</i>	75	
<i>BPR 1-pressure, psi</i>	3285	0.2375
<i>BPR 2-pressure, psi</i>	810	0.0637
<i>Gas Viscosity, cp</i>	0.0184	

Table A.19.3 Initial nitrogen flood results (Exp #229)

<i>q_{core}, cc/hr</i>	<i>ΔP, psi</i>	<i>k_g, md</i>
5593	10.280	165.53
6711	12.710	160.66
7457	14.360	158.00
8203	16.100	155.01
9321	18.900	150.05
<i>Corrected Permeability (k_g), md</i>		192.9

Table A.19.4 Fluid properties and conditions for nitrogen gas permeability at S_{wi} (Exp #229)

		<i>Density, gr/cc</i>
<i>Gas</i>	Nitrogen	
<i>Temperature, °F</i>	75	
<i>BPR 1-pressure, psi</i>	3285	0.2375
<i>BPR 2-pressure, psi</i>	810	0.0637
<i>Gas Viscosity, cp</i>	0.0184	

Table A.19.5 Nitrogen flood results at S_{wi} (Exp #229)

q_{core} , cc/hr	ΔP , psi	k_g , md
5592.62	13.270	128.23
6711.15	16.690	122.34
7456.83	19.150	118.48
8202.51	22.000	113.44
9321.04	26.000	109.08
<i>Corrected Permeability (k_g), md</i>		173.3

Table A.19.6 Volatile oil properties at BPR-1 and BPR-2 pressures (Exp #229)

<i>BPR 1-pressure, psi</i>	4080	
<i>BPR 2- pressure, psi</i>	855	
<i>Density at BPR 1-pressure, gr/cc</i>	0.343	
Properties at BPR 2- pressure, psi		
	Gas Phase	Oil Phase
<i>Density, gr/cc</i>	0.0468	0.5552
<i>Viscosity (μ), cp</i>	0.0142	0.1221
<i>Volume Fraction</i>	0.9281	0.0719
<i>IFT, dyne/cm</i>	5.844	

Table A.19.7 Fluid properties and conditions for final gas permeability (Exp #229)

		<i>Density, gr/cc</i>
<i>Gas</i>	Nitrogen	
<i>Temperature, °F</i>	75	
<i>BPR 1-pressure, psi</i>	3245	0.2351
<i>BPR 2-pressure, psi</i>	730	5.74E-02
<i>Gas Viscosity, cp</i>	0.0183	

Table A.19.8 Final nitrogen flood results (Exp #229)

$q_{core}, cc/hr$	$\Delta P, psi$	k_g, md
6144	13.100	141.92
7372	16.200	137.71
8192	18.650	132.91
9011	21.100	129.23
10240	25.900	119.64
<i>Corrected Permeability (k_g), md</i>		205.56173.2193.81

Table A.19.9 Pre and post-treatment volatile oil flood results and measured improvement factors (Exp #229)

	Exp# 229
$q_{gtot\ core}, cc/hr$	494
$q_g, cc/hr$	458
$q_o, cc/hr$	36
<i>PVT Ratio</i>	1.50
<i>Viscosity Ratio μ_g/μ_o</i>	0.12
<i>Capillary Nc</i>	1.62E-05
k_{rg} Before Treatment	0.038
k_{ro} Before Treatment	0.026
k_{rg} After Treatment	0.136
k_{ro} After Treatment	0.091
<i>Initial Improvement Factor</i>	3.5
<i>PV of Vol Oil Injected</i>	~330
<i>Final Improvement Factor</i>	3

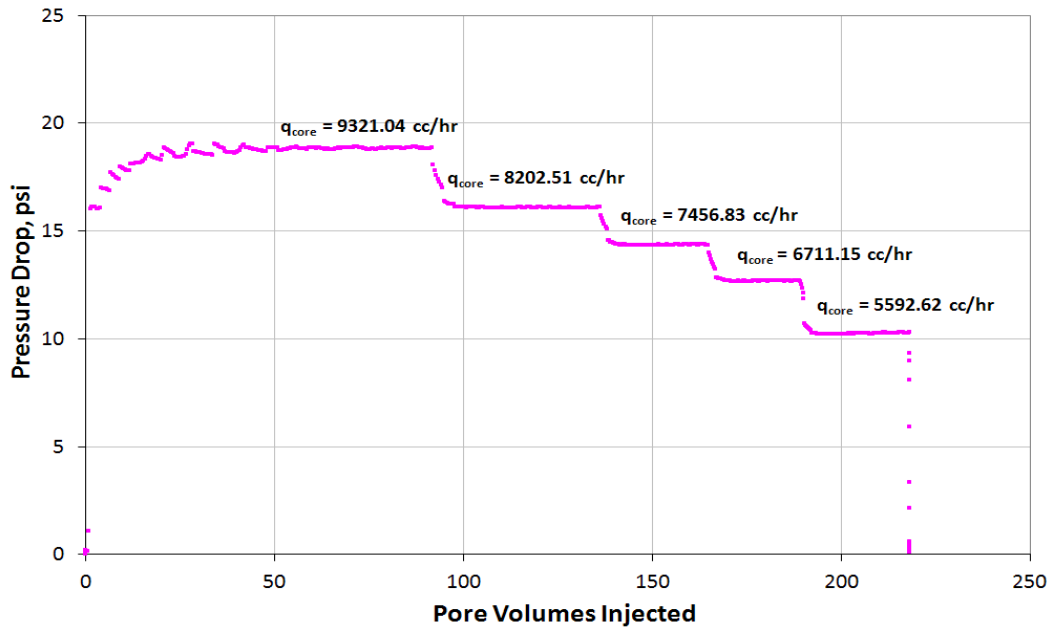


Figure A.19.1 Pressure drop across the core during the initial nitrogen flood at 75°F (Exp #229)

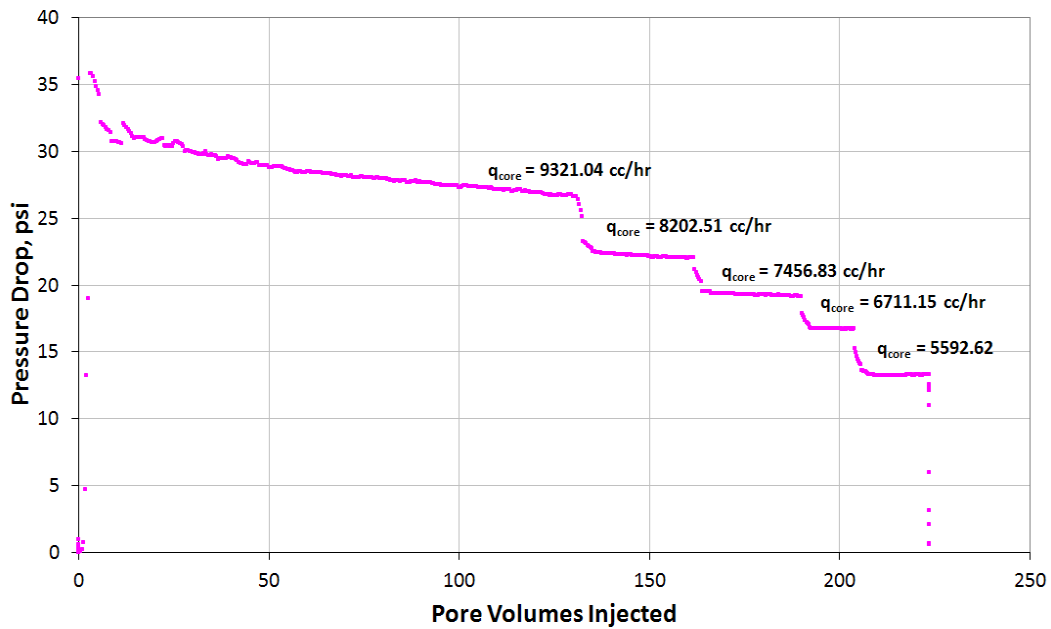


Figure A.19.2 Pressure drop across the core during the nitrogen flood at S_{wi} of 20% (Exp #229)

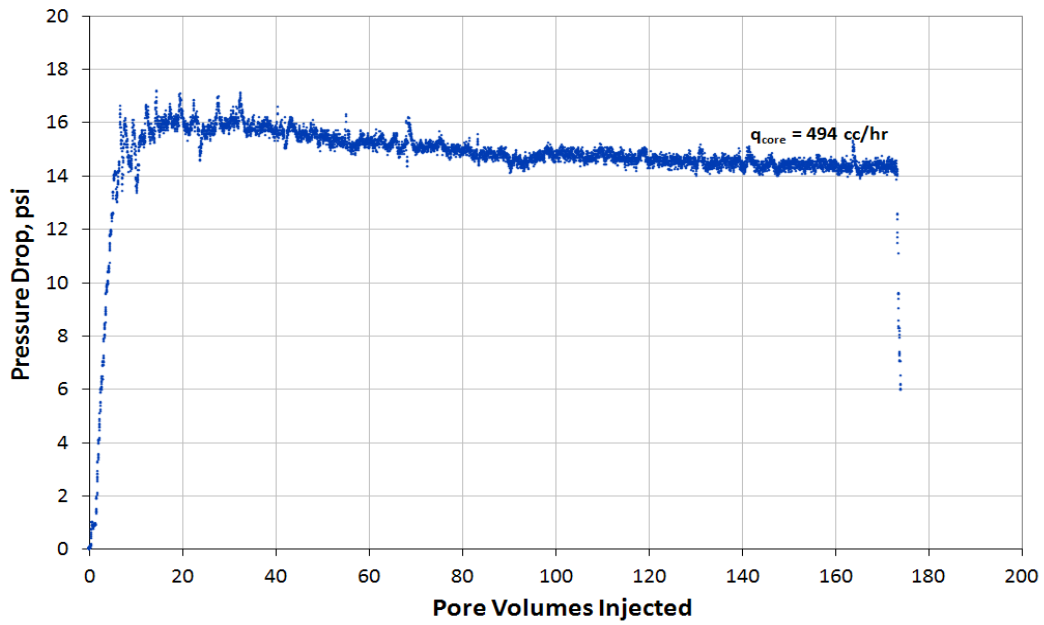


Figure A.19.3 Pressure drop across the core during the pre-treatment two-phase volatile oil flood (Exp #229)

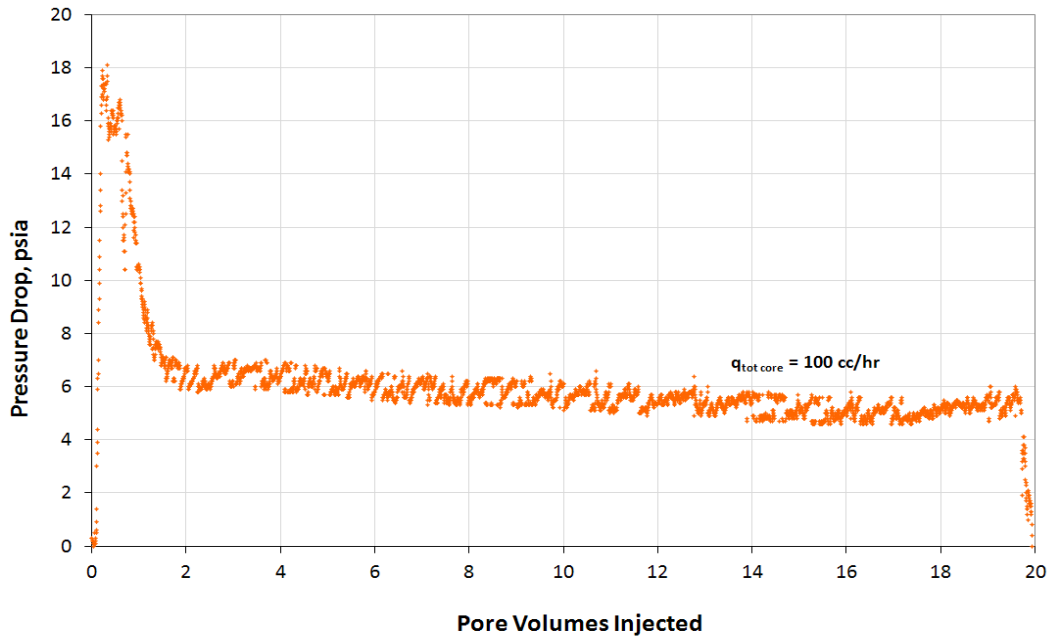


Figure A.19.4 Pressure drop across the core during injection of chemical treatment 1 (Exp # 229)

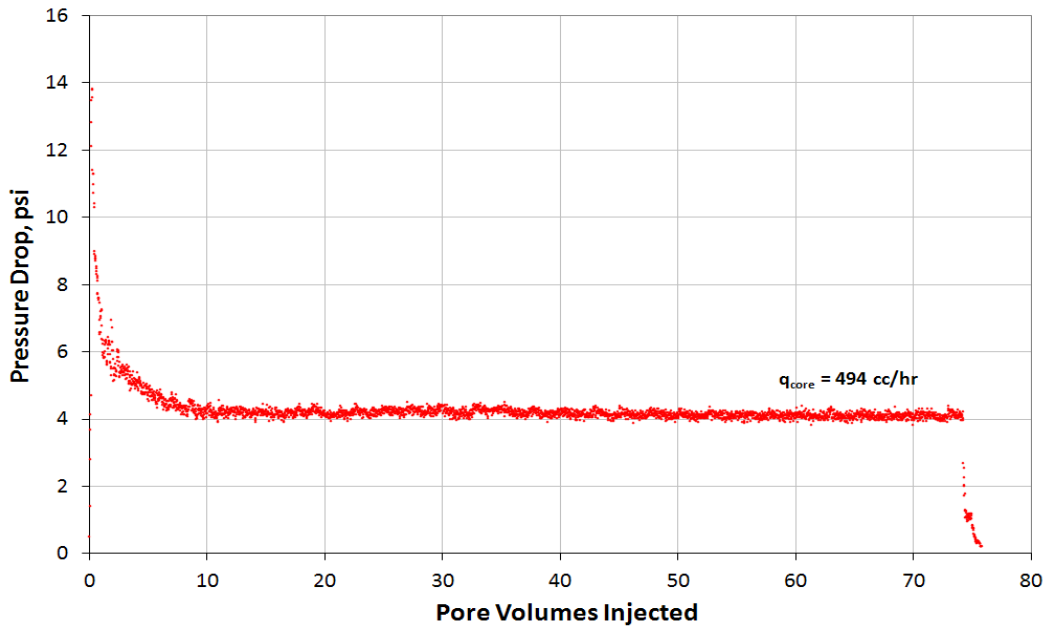


Figure A.19.5 Pressure drop across the core during the post-treatment two-phase volatile oil flood (Exp #229)

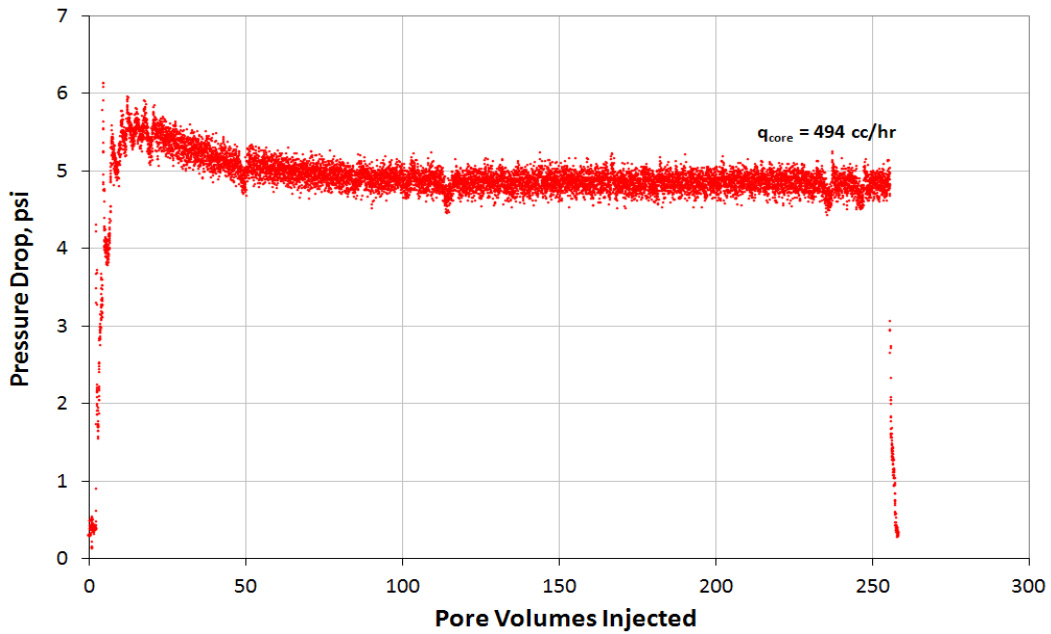


Figure A.19.6 Pressure drop across the core during the post-treatment two-phase volatile oil flood 2 (Exp #229)

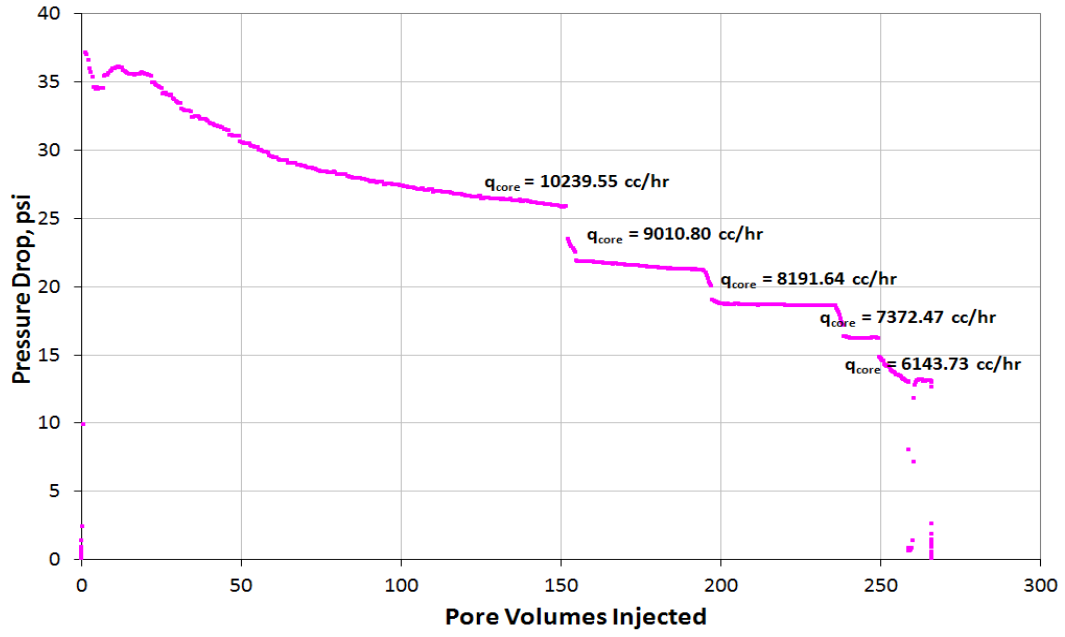


Figure A.19.7 Pressure drop across the core during the final nitrogen flood at 75°F (Exp #229)

Appendix A.20: EXPERIMENT #231

Objective:

The objective of this experiment was to determine the oil and gas saturation along a Berea sandstone core before and after treatment by using CT Scanning. The core was treated with chemical treatment 1 using non-ionic fluoro-surfactant FC-X to improve the oil and gas relative permeability at 155°F.

Experimental Procedure and Results:

A Berea core was prepared for the experiment following the standard procedure described Section 3.2.1.1. The initial core measurements and assumed properties can be found in Table A.5.1.

The initial gas permeability was calculated using nitrogen at 75°F. Nitrogen was flowed through the core using four flow rates and the pressure drop across the core for each flow rate was recorded. Using this data, the fluid properties and accounting for non-Darcy effects the calculated gas permeability was 184 md. Table A.5.2 summarizes the flood conditions and fluid properties and Table A.5.3 shows the results. Figure A.6.1 shows the pressure drop measured across the core during the methane flood.

The CT number for dry core was measured by flooding the core with a saturated gas mixture which composition is given in Table A.20.4 and then the core was scanned. This mixture represented the gas composition of the gas phase in the two phase flood when the gas fraction is ~ 93% by volume (850 psi) at 75°F.

The CT number for wet core was measured by flooding the core with a saturated liquid mixture which composition is given in Table A.20.5 and then the core was

scanned. This mixture represented the oil composition of the liquid phase in the two phase flood when the liquid fraction is ~ 7% by volume (850 psi) at 75°F.

After that the core was cleaned using 10 pore volumes of toluene, followed by 5 pore volumes of a mixture 50 vol% toluene- 50 vol% methanol, followed by 5 pore volumes of methanol. The core was then dried with air overnight at 150°F.

A post-cleaning dry permeability was measured using methane at 150°F and following the same procedure as for the initial permeability measurement. Table A.5.4 summarizes the flood conditions and fluid properties and Table A.4.5 shows the results. Figure A.4.2 shows the pressure drop measured across the core during the methane flood.

Synthetic volatile oil mixture 1 (Table 3.3) was used for the two-phase flow measurements. The mixture was allowed a minimum of 12 hours to equilibrate to a single phase at 3700 psi and 75°F. The initial flood was conducted at 75°F with the upstream backpressure regulator (BPR-1) set at 3785 psi and the downstream back pressure regulator (BPR-2) set at 850 psi. Volatile oil was injected at an upstream BPR-1 flow rate of 120 cc/hr (this is for volatile oil at single liquid phase). Once steady state was observed the pressure drop across the core was measured, the flow was stopped and the core holder was immediately taken to CT scanning to obtain the CT numbers for two-phase flood. PVT ratio was 0.73 and capillary number was 1.2×10^{-5} . Table A.3.6 gives the fluid properties of the synthetic fluid calculated using the Peng-Robinson EOS at the flowing core pressures. Figure A.4.3 shows the pressure drop measured across the core during the initial two-phase volatile oil flood.

The core was then flooded with saturated gas (Table A.20.4) to measure the pre-treatment residual oil saturation (S_{or}) along the core. Table A.20.9 shows the flood conditions and fluid properties and Table A.20.10 shows the flood results.

The temperature was then raised to 155°F and the core was treated using chemical treatment 1 (Table 4.15). The solution was heated for at least 3 hours at 155°F. BPR1 was set at 860 psi. The core was flooded with approximately 20 pore volumes of the treatment solution at a flow rate of 100 cc/hr. The core was then shut in for 12 hours. After that the chemical treatment was removed from core using saturated gas (Table A.20.4). Figure A.4.4 shows the measured pressure drop across the core during the treatment flood.

Post-treatment two-phase volatile oil flood was conducted under the same conditions as the initial two-phase flow. Figure A.4.5 shows the pressure drop measured across the core during the post-treatment two-phase volatile oil flood. No improvement factor was observed.

The core was retreated for a second time with 20 PV of the chemical treatment 1. This time the treatment was not removed with saturated gas. Figure A.20.6 shows the measured pressure drop across the core during the second treatment flood.

Two post-2nd treatment two-phase volatile oil floods were conducted under the same conditions as the initial two-phase flow. Figure A.20.7 shows the pressure drop measured across the core during the post-2nd treatment two-phase volatile oil floods 1 and 2. Improvement factor was 3.4 and 2.2 in that order.

The core was then flooded with saturated gas (Table A.20.4) to measure the post-treatment residual oil saturation (S_{or}) along the core. Table A.20.11 shows the flood conditions and fluid properties and Table A.20.12 shows the flood results.

After this, a third post-2nd treatment two-phase volatile oil floods was conducted. Figure A.4.5 Figure A.6.9 shows the pressure drop measured across the core during the post-2nd treatment two-phase volatile oil flood 3. Improvement factor was 1.

The core was again cleaned following the same procedure as before and the final gas permeability was calculated following the procedure for the initial gas permeability using nitrogen at 75°F. The calculated gas permeability was 181 md. The flood conditions and results are shown in Table A.4.7 and Table A.3.8 respectively. Figure A.6.10 shows the pressure drop across the core for the final methane flood.

For every two-phase volatile oil flood, oil and gas relative permeabilities k_{rg} and k_{ro} were calculated using the measured pressure drop across the core under steady state conditions and then improvement factors were measured. Table A.3.9 summarizes the experimental results.

The analytical procedure to calculate the oil and gas saturations along the core using the measured CT numbers, are explained in Section 7.3.1. Figure 7.12 to 7.14 show the results for the calculated oil saturations along the core before and after treatment.

Table A.20.1 Core properties (Exp #231)

<i>Length, in</i>	7.959
<i>Diameter, in</i>	0.986
<i>Mass Core, gr</i>	215.15
<i>Grain Density, gr/cc</i>	2.65
<i>Porosity (ϕ)</i>	18.47 %

Table A.20.2 Fluid properties and conditions for initial gas permeability (Exp #231)

		<i>Density, gr/cc</i>
<i>Gas</i>	Nitrogen	
<i>Temperature, °F</i>	75	
<i>BPR 1-pressure, psi</i>	3071	0.2245
<i>BPR 2-pressure, psi</i>	988	0.0776
<i>Gas Viscosity, cp</i>	0.0187	

Table A.20.3 Initial methane flood results (Exp #231)

<i>q_{core}, cc/hr</i>	<i>ΔP, psi</i>	<i>k_g, md</i>
5207	10.150	160.72
5786	11.500	157.62
6365	12.850	155.16
7233	14.950	151.56
<i>Corrected Permeability (k_g), md</i>		184.2

Table A.20.4 Composition of saturated gas (Exp #231)

<i>Component</i>	<i>Mole%</i>
Methane	90.54
Propane	9.46

Table A.20.5 Composition of saturated oil (Exp #231)

<i>Component</i>	<i>Mole%</i>
Methane	25.3
Propane	28.9
Heptane	30.2
Decane	15.6

Table A.20.6 Fluid properties and conditions for methane gas permeability after initial core cleaning (Exp #231)

		<i>Density, gr/cc</i>
<i>Gas</i>	Methane	
<i>Temperature, °F</i>	150	
<i>BPR 1-pressure, psi</i>	2940	0.1252
<i>BPR 2-pressure, psi</i>	970	4.08E-02
<i>Gas Viscosity, cp</i>	0.0133	

Table A.20.7 Methane flood results after initial core cleaning (Exp #231)

<i>q_{core}, cc/hr</i>	<i>ΔP, psi</i>	<i>k_g, md</i>
4602	6.500	157.78
5523	8.000	153.84
6137	9.000	151.94
6750	10.000	150.42
7671	11.600	147.35
<i>Corrected Permeability (k_g), md</i>		170.3

Table A.20.8 Volatile oil properties at BPR-1 and BPR-2 pressures (Exp #231)

<i>BPR 1-pressure, psi</i>	3785	
<i>BPR 2- pressure, psi</i>	853	
<i>Density at BPR 1-pressure, gr/cc</i>	0.3721	
Properties at BPR 2- pressure, psi		
	Gas Phase	Oil Phase
<i>Density, gr/cc</i>	0.0532	0.6035
<i>Viscosity (μ), cp</i>	0.0121	0.2141
<i>Volume Fraction</i>	0.9284	0.0716
<i>IFT, dyne/cm</i>	8.715	

Table A.20.9 Fluid properties and conditions for saturated gas flood to measure S_{or} before treatment (Exp #231)

		<i>Density, gr/cc</i>
<i>Gas</i>	Saturated Gas Mixture	
<i>Temperature, °F</i>	75	
<i>BPR 1-pressure, psi</i>	3765	0.2323
<i>BPR 2-pressure, psi</i>	853	5.26E-02
<i>Gas Viscosity, cp</i>	0.0121	

Table A.20.10 Saturated gas flood results before treatment (Exp #231)

<i>q_{core}, cc/hr</i>	<i>ΔP, psi</i>	<i>k_g, md</i>
767	1.750	88.86

Table A.20.11 Fluid properties and conditions for saturated gas flood to measure S_{or} after treatment (Exp #231)

		<i>Density, gr/cc</i>
<i>Gas</i>	Saturated Gas Mixture	
<i>Temperature, °F</i>	75	
<i>OBPR 1-pressure, psi</i>	3746	0.2316
<i>BPR 2-pressure, psi</i>	846	5.21E-02
<i>Gas Viscosity, cp</i>	0.0121	

Table A.20.12 Saturated gas flood results after treatment (Exp #231)

<i>q_{core}, cc/hr</i>	<i>ΔP, psi</i>	<i>k_g, md</i>
767	1.700	91.47

Table A.20.13 Fluid properties and conditions for final gas permeability (Exp #231)

		<i>Density, gr/cc</i>
<i>Gas</i>	Nitrogen	
<i>Temperature, °F</i>	75	
<i>BPR 1-pressure, psi</i>	3060	0.2238
<i>BPR 2-pressure, psi</i>	948	7.44E-02
<i>Gas Viscosity, cp</i>	0.0186	

Table A.20.14 Final nitrogen flood results (Exp #231)

<i>q_{core}, cc/hr</i>	<i>ΔP, psi</i>	<i>k_g, md</i>
4512.10	9.150	153.66
5414.52	11.350	148.65
6016.13	12.800	146.45
6617.74	14.400	143.20
7520.16	16.900	138.65
<i>Corrected Permeability (k_g), md</i>		181.29

Table A.20.15 Pre and post-treatment volatile oil flood results and measured improvement factors (Exp #231)

	Exp# 231
<i>BPR 2- pressure, psi</i>	850
<i>q_{gtot core}, cc/hr</i>	482.20
<i>q_g, cc/hr</i>	447.67
<i>q_o, cc/hr</i>	34.53
<i>PVT Ratio</i>	0.73
<i>Viscosity Ratio μ_g/μ_o</i>	0.06
<i>Capillary Nc</i>	1.17E-05
<i>k_{rg} Before Treatment</i>	0.0299
<i>k_{ro} Before Treatment</i>	0.0407
<i>k_{rg} After Treatment</i>	0.0294
<i>k_{ro} After Treatment</i>	0.0401
<i>Initial Improvement Factor</i>	1.0
<i>k_{rg} After 2nd Treatment</i>	0.1005
<i>k_{ro} After 2nd Treatment</i>	0.1372
<i>Initial Improvement Factor</i>	3.4
<i>Final Improvement Factor</i>	2.20

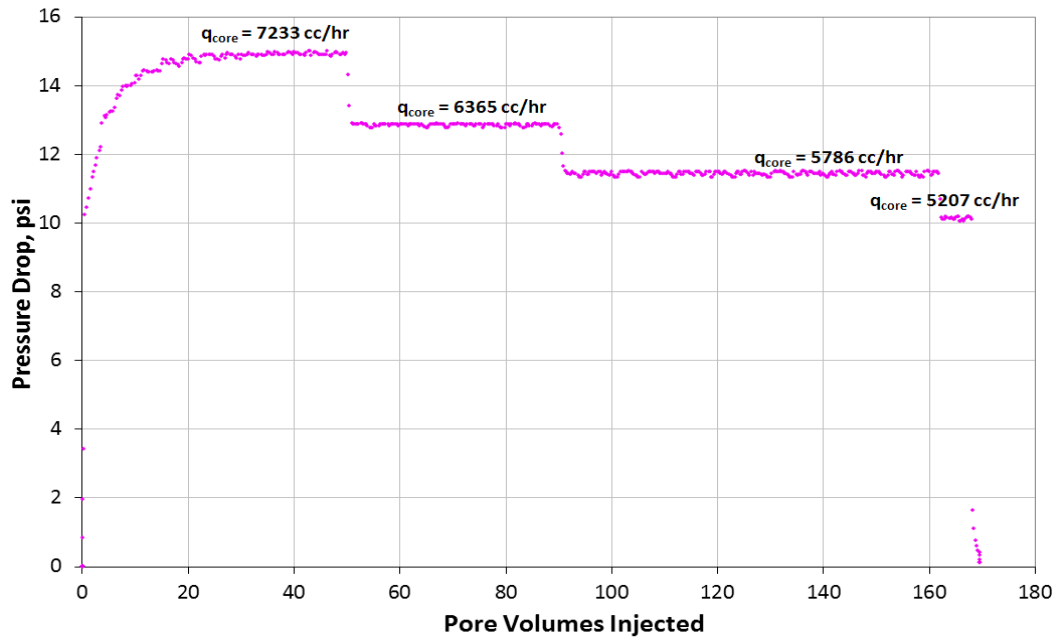


Figure A.20.1 Pressure drop across the core during the initial nitrogen flood at 75°F (Exp #231)

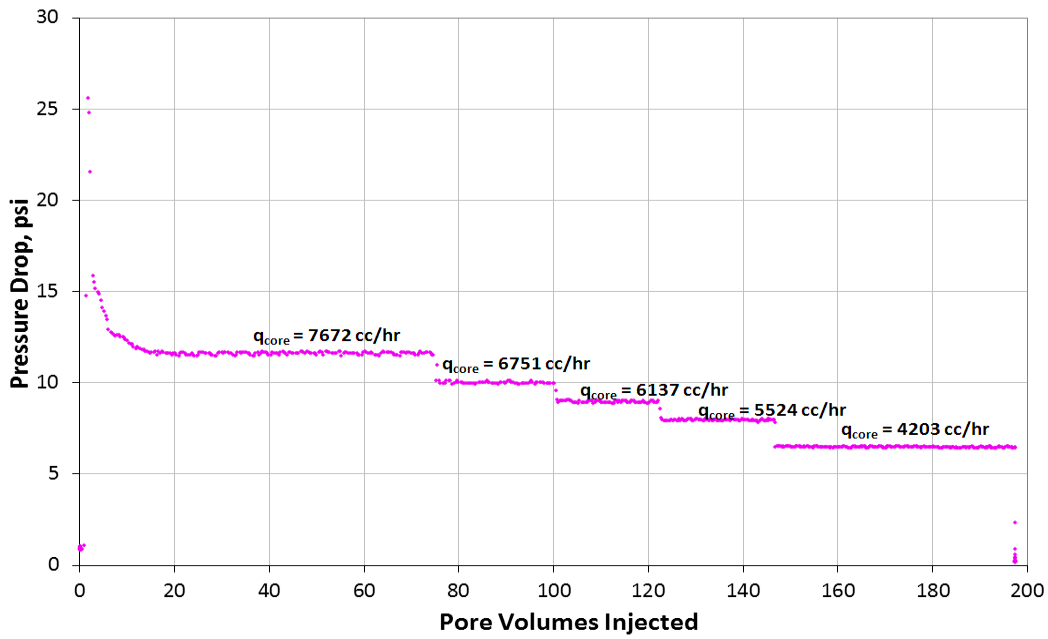


Figure A.20.2 Pressure drop across the core during the methane flood after initial core cleaning (Exp #231)

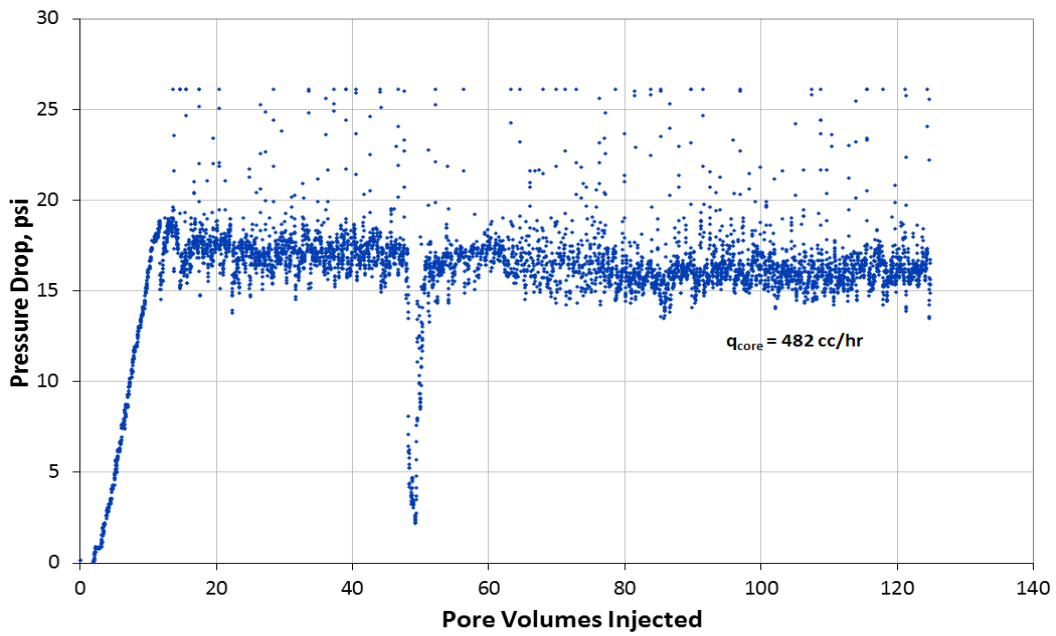


Figure A.20.3 Pressure drop across the core during the pre-treatment two-phase volatile oil flood (Exp #231)

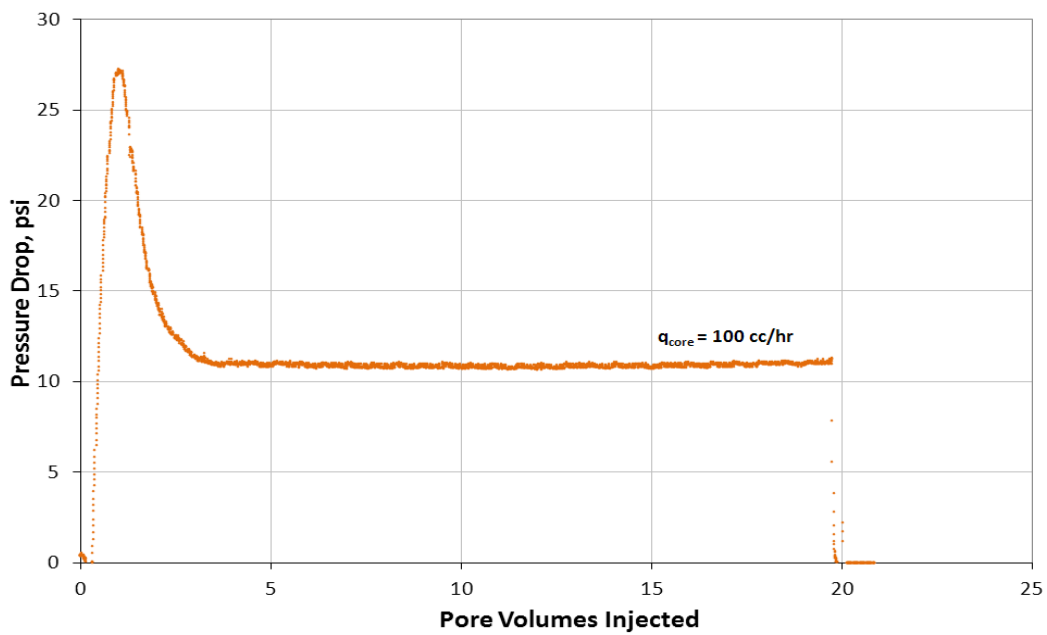


Figure A.20.4 Pressure drop across the core during injection of chemical treatment 1 (Exp # 231)

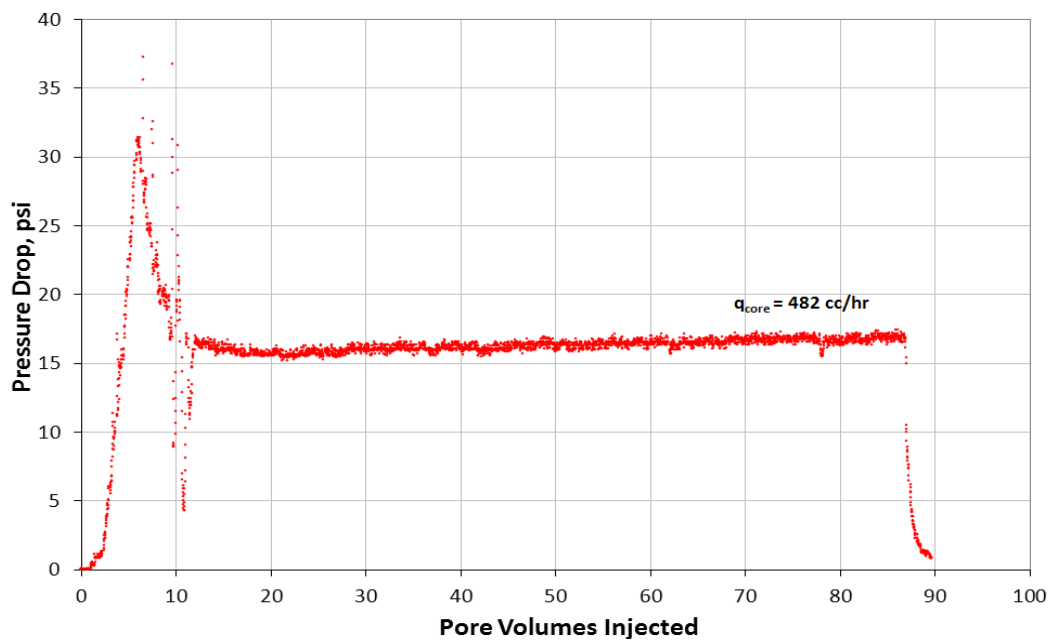


Figure A.20.5 Pressure drop across the core during the post-treatment two-phase volatile oil flood (Exp #231)

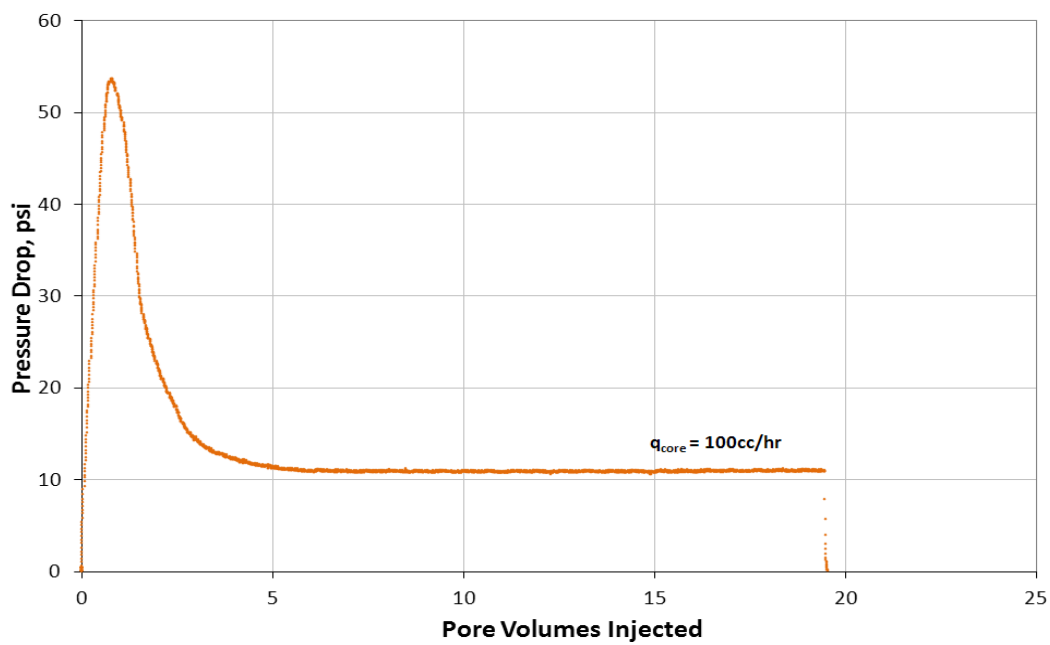


Figure A.20.6 Pressure drop across the core during injection of second chemical treatment 1 (Exp # 231)

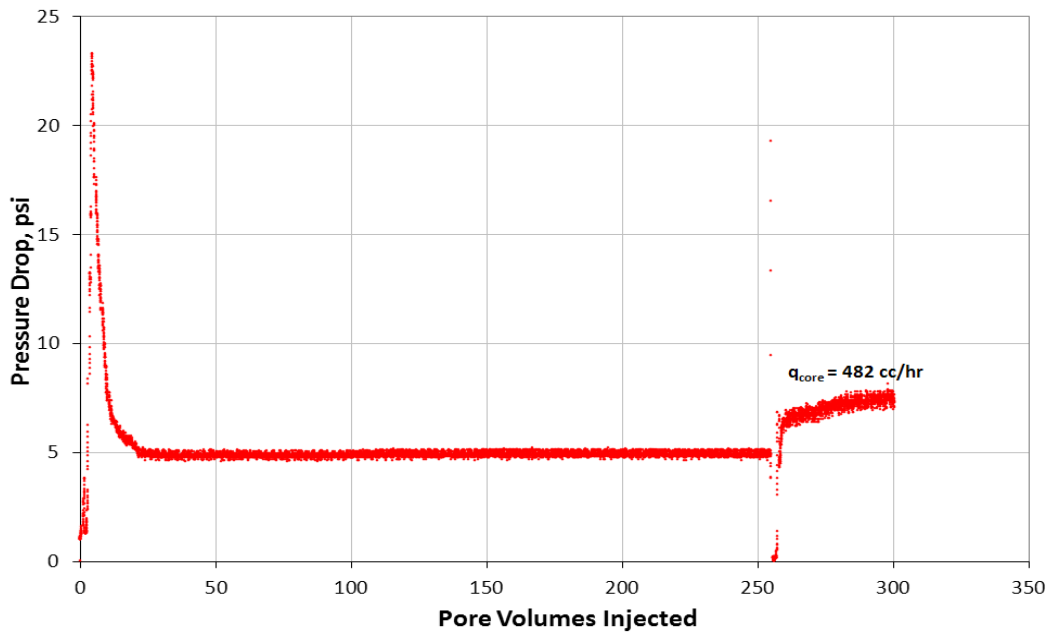


Figure A.20.7 Pressure drop across the core during the post-2nd treatment two-phase volatile oil flood 1 and 2 (Exp #231)

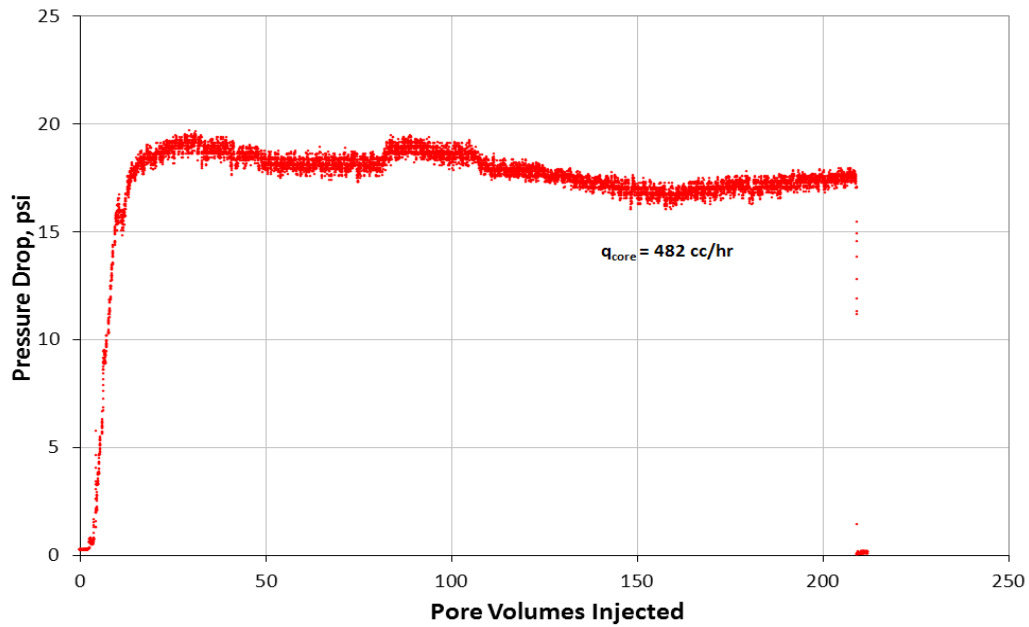


Figure A.20.8 Pressure drop across the core during the post-2nd treatment two-phase volatile oil flood 3 (Exp #231)

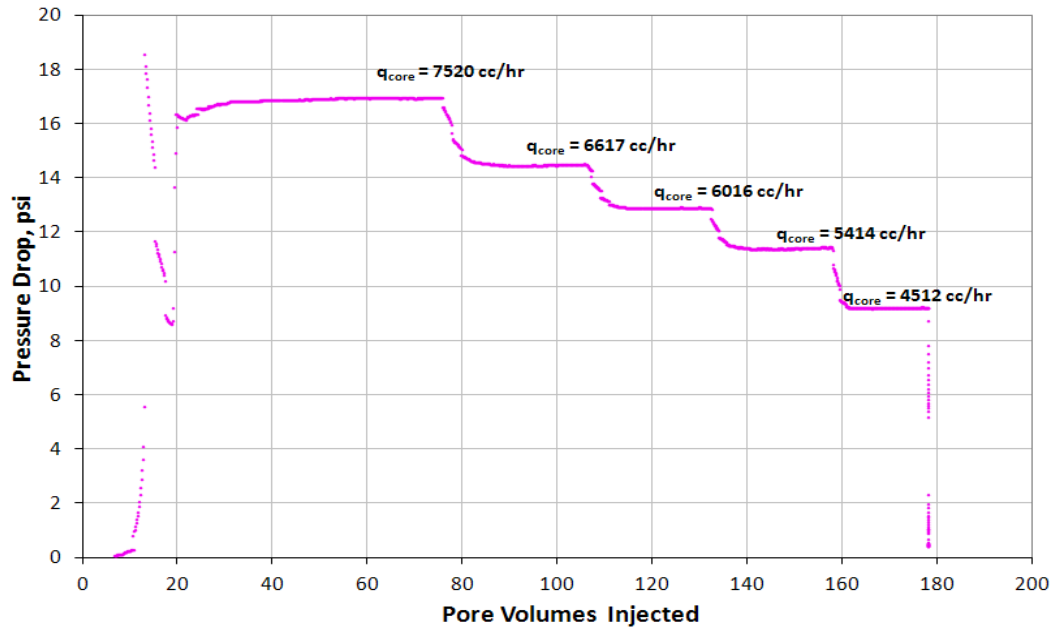


Figure A.20.9 Pressure drop across the core during the final nitrogen flood at 75°F (Exp #231)

Appendix A.21: EXPERIMENT #234

Objective:

The objective of this experiment was to determine the oil and gas saturation along a Berea sandstone core before and after treatment by using CT Scanning. The core was treated with chemical treatment 1 using non-ionic fluoro-surfactant FC-X to improve the oil and gas relative permeability at 155°F.

Experimental Procedure and Results:

A Berea core was prepared for the experiment following the standard procedure described Section 3.2.1.1. The initial core measurements and assumed properties can be found in Table A.5.1.

The initial gas permeability was calculated using nitrogen at 75°F. Nitrogen was flowed through the core using five flow rates and the pressure drop across the core for each flow rate was recorded. Using this data, the fluid properties and accounting for non-Darcy effects the calculated gas permeability was 186 md. Table A.5.2 summarizes the flood conditions and fluid properties and Table A.5.3 shows the results. Figure A.6.1 shows the pressure drop measured across the core during the methane flood.

The CT number for dry core was measured by flooding the core with a saturated gas mixture which composition is given in Table A.20.4 and then the core was scanned. This mixture represented the gas composition of the gas phase in the two phase flood when the gas fraction is ~ 93% by volume (850 psi) at 75°F.

The CT number for wet core was measured by flooding the core with a saturated liquid mixture which composition is given in Table A.20.5 and then the core was

scanned. This mixture represented the oil composition of the liquid phase in the two phase flood when the liquid fraction is ~ 7% by volume (850 psi) at 75°F.

After that the core was cleaned using 10 pore volumes of toluene, followed by 5 pore volumes of a mixture 50 vol% toluene- 50 vol% methanol, followed by 5 pore volumes of methanol. The core was then dried with air overnight at 75°F.

A post-cleaning dry permeability was measured using nitrogen at 75°F and following the same procedure as for the initial permeability measurement. Table A.5.4 summarizes the flood conditions and fluid properties and Table A.4.5 shows the results. Figure A.4.2 shows the pressure drop measured across the core during the methane flood.

Synthetic volatile oil mixture 1 (Table 3.3) was used for the two-phase flow measurements. The mixture was allowed a minimum of 12 hours to equilibrate to a single phase at 3700 psi and 75°F. The initial flood was conducted at 75°F with the upstream backpressure regulator (BPR-1) set at 3820 psi and the downstream back pressure regulator (BPR-2) set at 850 psi. Volatile oil was injected at an upstream BPR-1 flow rate of 120 cc/hr (this is for volatile oil at single liquid phase). Once steady state was observed the pressure drop across the core was measured, the flow was stopped and the core holder was immediately taken to CT scanning to obtain the CT numbers for two-phase flood. PVT ratio was 0.75 and capillary number was 1.2×10^{-5} . Table A.3.6 gives the fluid properties of the synthetic fluid calculated using the Peng-Robinson EOS at the flowing core pressures. Figure A.4.3 shows the pressure drop measured across the core during the initial two-phase volatile oil flood.

The core was then flooded with saturated gas (Table A.20.4) to measure the pre-treatment residual oil saturation (S_{or}) along the core. Table A.20.9 shows the flood conditions and fluid properties and Table A.20.10 shows the flood results.

The temperature was then raised to 155°F and the core was treated using chemical treatment 1 (Table 4.15). The solution was heated for at least 3 hours at 155°F. BPR1 was set at 860 psi. The core was flooded with approximately 20 pore volumes of the treatment solution at a flow rate of 100 cc/hr. The core was then shut in for 12 hours.

Post-treatment two-phase volatile oil flood was conducted under the same conditions as the initial two-phase flow but instead of using constant injection flow rate, this was adjusted to obtain the same pressure drop as before treatment. The new injection flow rate was used to calculate the improvement factor. Improvement factor was approximately 2. Figure A.4.5 shows the pressure drop measured across the core during the post-treatment two-phase volatile oil flood.

The core was then flooded with saturated gas (Table A.20.4) to measure the post-treatment residual oil saturation (S_{or}) along the core. Table A.20.11 shows the flood conditions and fluid properties and Table A.20.12 shows the flood results.

The core was again cleaned following the same procedure as before and the final gas permeability was calculated following the procedure for the initial gas permeability using nitrogen at 75°F. The calculated gas permeability was 163 md. The flood conditions and results are shown in Table A.4.7 and Table A.3.8 respectively. Figure A.6.10 shows the pressure drop across the core for the final methane flood.

For every two-phase volatile oil flood, oil and gas relative permeabilities k_{rg} and k_{ro} were calculated using the measured pressure drop across the core under steady state conditions and then improvement factors were measured. Table A.3.9 summarizes the experimental results.

The analytical procedure to calculate the oil and gas saturations along the core using the measured CT numbers, are explained in Section 7.3.1. Figure 7.15 and 7.16

show the results for the calculated oil saturations along the core before and after treatment.

Table A.21.1 Core properties (Exp #234)

<i>Length, in</i>	7.926
<i>Diameter, in</i>	0.993
<i>Mass Core, gr</i>	215.81
<i>Grain Density, gr/cc</i>	2.65
<i>Porosity (ϕ)</i>	19.04 %

Table A.21.2 Fluid properties and conditions for initial gas permeability (Exp #234)

		<i>Density, gr/cc</i>
<i>Gas</i>	Nitrogen	
<i>Temperature, °F</i>	75	
<i>BPR 1-pressure, psi</i>	2824	0.2089
<i>BPR 2-pressure, psi</i>	1007	0.0790
<i>Gas Viscosity, cp</i>	0.0187	

Table A.21.3 Initial nitrogen flood results (Exp #234)

<i>q_{core}, cc/hr</i>	<i>ΔP, psi</i>	<i>k_g, md</i>
3966	7.330	166.44
4760	9.020	162.31
5289	10.170	159.95
5817	11.350	157.66
<i>Corrected Permeability (k_g), md</i>		186.3

Table A.21.4 Composition of saturated gas (Exp #234)

<i>Component</i>	<i>Mole%</i>
Methane	90.54
Propane	9.46

Table A.21.5 Composition of saturated oil (Exp #234)

<i>Component</i>	<i>Mole%</i>
Methane	25.3
Propane	28.9
Heptane	30.2
Decane	15.6

Table A.21.6 Fluid properties and conditions for nitrogen gas permeability after initial core cleaning (Exp #234)

<i>Gas</i>	<i>Nitrogen</i>	<i>Density, gr/cc</i>
<i>Temperature, °F</i>	75	
<i>BPR 1-pressure, psi</i>	3040	0.2226
<i>BPR 2-pressure, psi</i>	850	6.68E-02
<i>Gas Viscosity, cp</i>	0.0185	

Table A.21.7 Nitrogen flood results after initial core cleaning (Exp #234)

<i>q_{core}, cc/hr</i>	<i>ΔP, psi</i>	<i>k_g, md</i>
4665.92	9.300	152.67
5599.10	11.470	148.54
6221.23	13.000	145.62
6843.35	14.500	143.62
7776.53	16.950	139.61
<i>Corrected Permeability (k_g), md</i>		187.4

Table A.21.8 Volatile oil properties at BPR-1 and BPR-2 pressures (Exp #234)

<i>BPR 1-pressure, psi</i>	3820	
<i>BPR 2- pressure, psi</i>	853	
<i>Density at BPR 1-pressure, gr/cc</i>	0.3708	
Properties at BPR 2- pressure, psi		
	Gas Phase	Oil Phase
<i>Density, gr/cc</i>	0.0529	0.6037
<i>Viscosity (μ), cp</i>	0.0121	0.2137
<i>Volume Fraction</i>	0.9296	0.0704
<i>IFT, dyne/cm</i>	8.72	

Table A.21.9 Fluid properties and conditions for saturated gas flood to measure S_{or} before treatment (Exp #234)

		<i>Density, gr/cc</i>
<i>Gas</i>	Saturated Gas Mixture	
<i>Temperature, °F</i>	75	
<i>BPR 1-pressure, psi</i>	3831	0.2323
<i>BPR 2-pressure, psi</i>	865	5.26E-02
<i>Gas Viscosity, cp</i>	0.0121	

Table A.21.10 Saturated gas flood results before treatment (Exp #234)

<i>q_{core}, cc/hr</i>	<i>ΔP, psi</i>	<i>k_g, md</i>
767	1.05	148.1

Table A.21.11 Fluid properties and conditions for saturated gas flood to measure S_{or} after treatment (Exp #234)

		<i>Density, gr/cc</i>
<i>Gas</i>	Saturated Gas Mixture	
<i>Temperature, °F</i>	75	
<i>OBPR 1-pressure, psi</i>	3838	0.2316
<i>BPR 2-pressure, psi</i>	850	5.21E-02
<i>Gas Viscosity, cp</i>	0.0121	

Table A.21.12 Saturated gas flood results after treatment (Exp #234)

<i>q_{core}, cc/hr</i>	<i>ΔP, psi</i>	<i>k_g, md</i>
767	1.75	91.47

Table A.21.13 Fluid properties and conditions for final gas permeability (Exp #234)

		<i>Density, gr/cc</i>
<i>Gas</i>	Nitrogen	
<i>Temperature, °F</i>	75	
<i>BPR 1-pressure, psi</i>	3054	0.2234
<i>BPR 2-pressure, psi</i>	841	6.61E-02
<i>Gas Viscosity, cp</i>	0.0184	

Table A.21.14 Final nitrogen flood results (Exp #234)

<i>q_{core}, cc/hr</i>	<i>ΔP, psi</i>	<i>k_g, md</i>
5069.59	12.950	118.48
6083.51	16.550	111.25
6759.46	19.000	107.67
7435.40	21.500	104.67
8449.32	25.800	99.12
<i>Corrected Permeability (k_g), md</i>		163

Table A.21.15 Pre and post-treatment volatile oil flood results and measured improvement factors (Exp #234)

	Exp# 234
<i>BPR 2- pressure, psi</i>	853
<i>q_{gtot core}, cc/hr</i>	485.36
<i>q_g, cc/hr</i>	451.19
<i>q_o, cc/hr</i>	34.17
<i>PVT Ratio</i>	0.75
<i>Viscosity Ratio μ_g/μ_o</i>	0.06
<i>Capillary Nc</i>	1.21E-05
<i>k_{rg} Before Treatment</i>	0.0288
<i>k_{ro} Before Treatment</i>	0.0385
<i>k_{rg} After Treatment</i>	0.0591
<i>k_{ro} After Treatment</i>	0.0790
<i>Initial Improvement Factor</i>	2.05
<i>Injected Pore Vol.</i>	~80

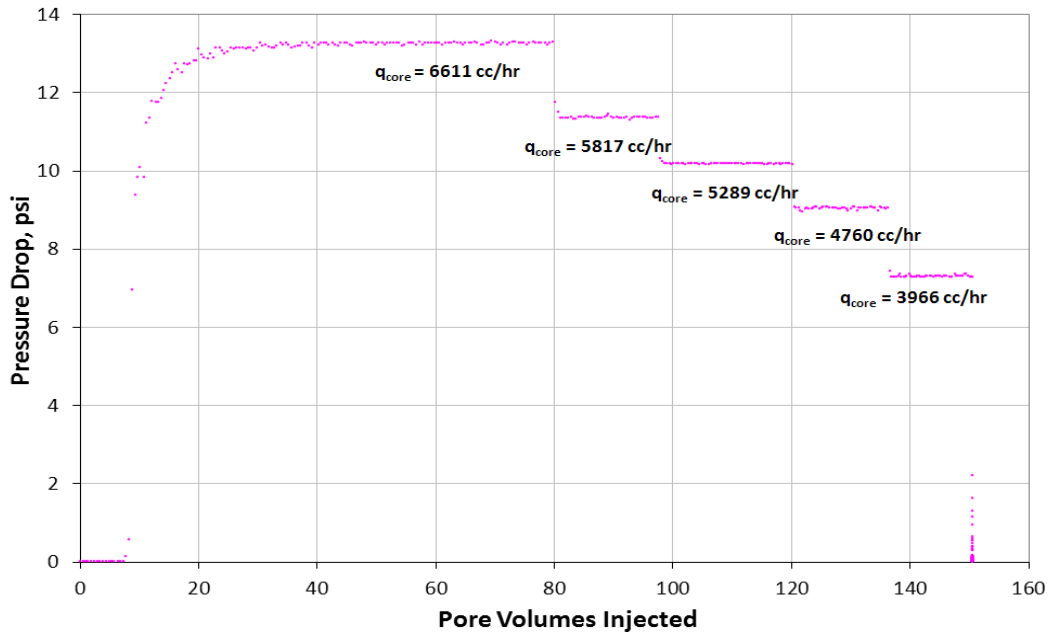


Figure A.21.1 Pressure drop across the core during the initial nitrogen flood at 75°F (Exp #234)

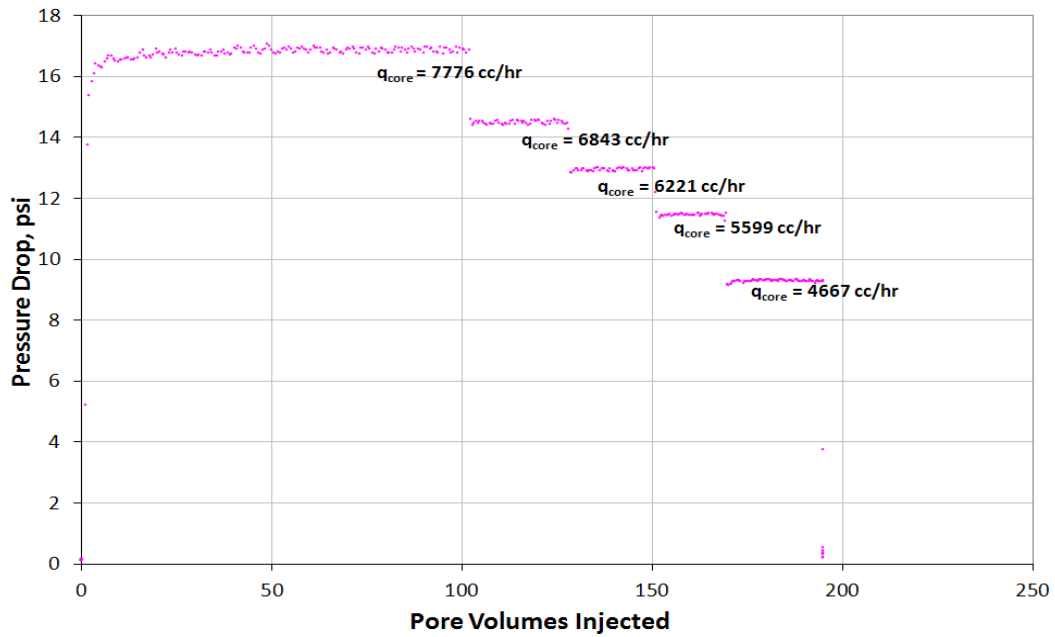


Figure A.21.2 Pressure drop across the core during the nitrogen flood after initial core cleaning (Exp #234)

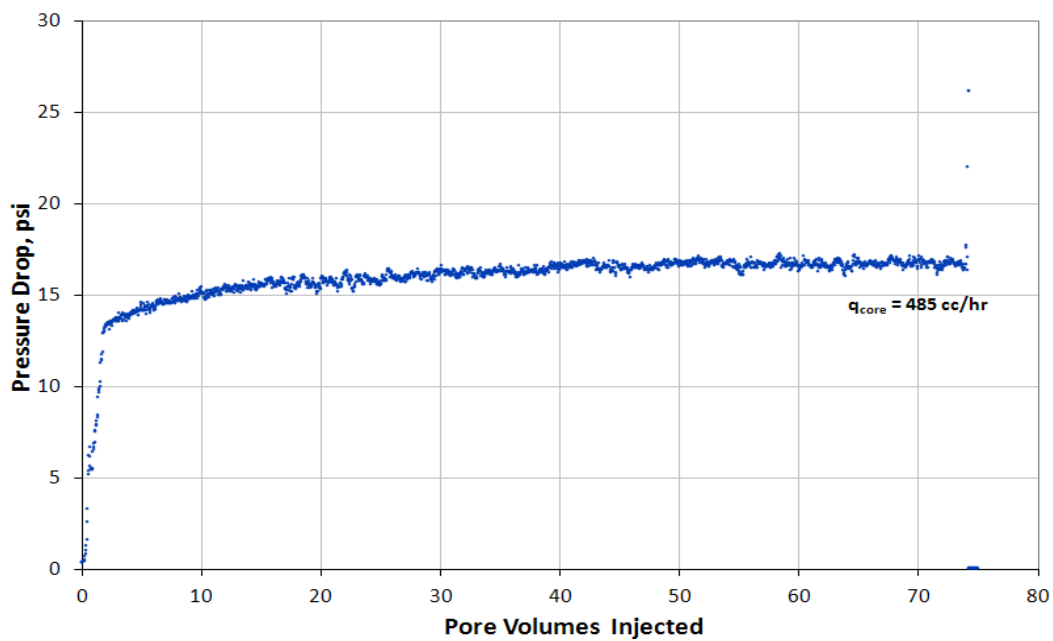


Figure A.21.3 Pressure drop across the core during the pre-treatment two-phase volatile oil flood (Exp #234)

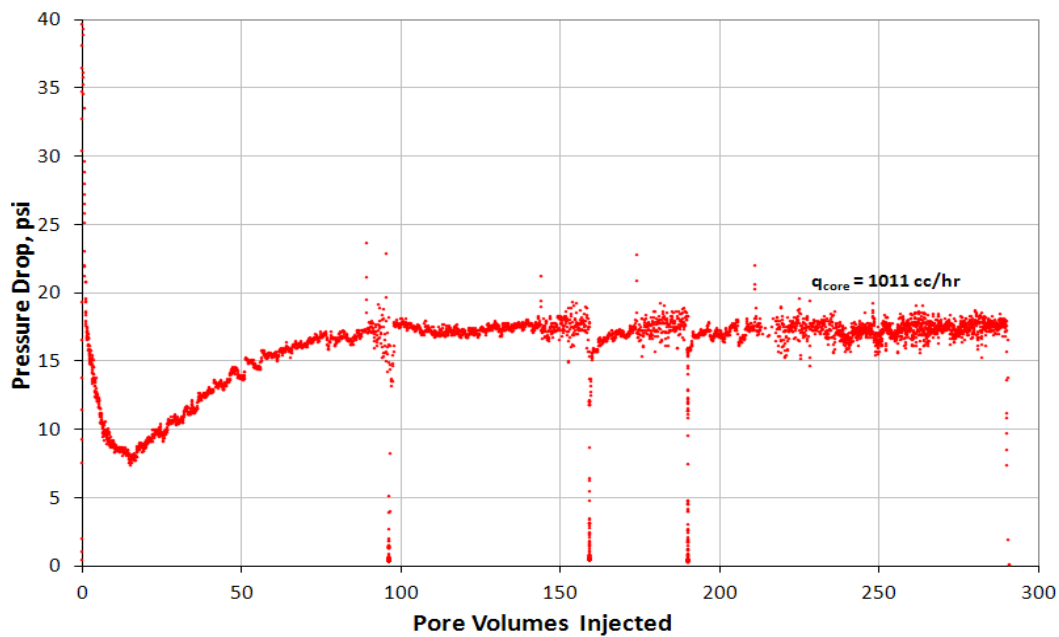


Figure A.21.4 Pressure drop across the core during the post-treatment two-phase volatile oil flood (Exp #234)

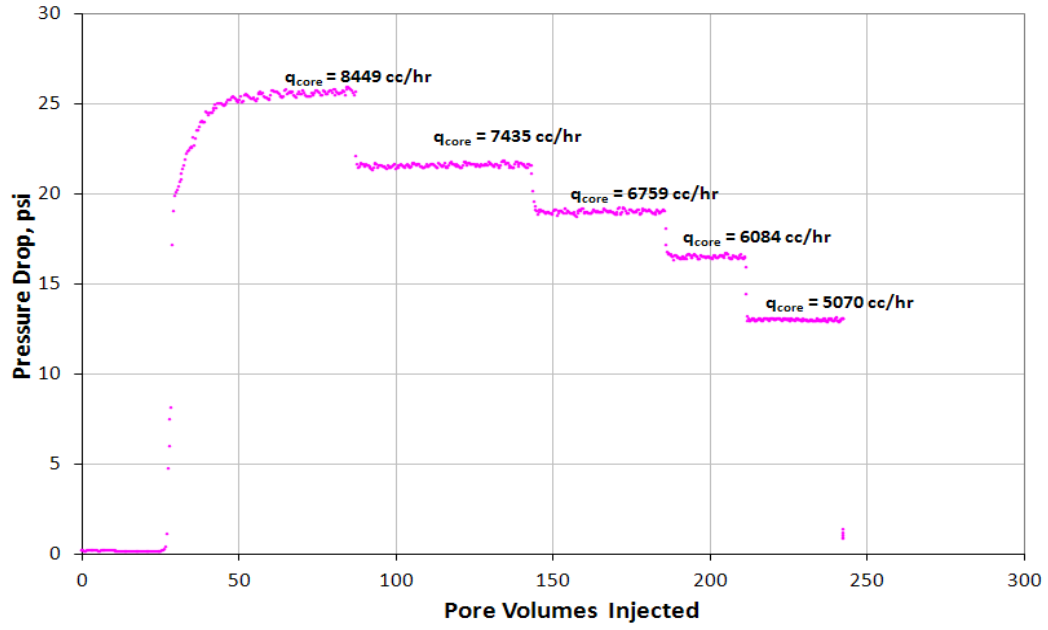


Figure A.21.5 Pressure drop across the core during the final nitrogen flood at 75°F (Exp #234)

Appendix A.22: EXPERIMENT #235

Objective:

The objective of this experiment was to determine the oil and gas saturation along a Berea sandstone core before and after treatment by using CT Scanning and to measure the oil and gas relative permeability before and after treatment. With the measured saturations and relative permeabilities experimental relative permeability curves were calculated. The core was treated with chemical treatment 1 using non-ionic fluoro-surfactant FC-X to improve the oil and gas relative permeability at 155°F.

Experimental Procedure and Results:

A Berea core was prepared for the experiment following the standard procedure described Section 3.2.1.1. The initial core measurements and assumed properties can be found in Table A.5.1.

The initial gas permeability was calculated using nitrogen at 75°F. Nitrogen was flowed through the core using five flow rates and the pressure drop across the core for each flow rate was recorded. Using this data, the fluid properties and accounting for non-Darcy effects the calculated gas permeability was 170 md. Table A.5.2 summarizes the flood conditions and fluid properties and Table A.5.3 shows the results. Figure A.6.1 shows the pressure drop measured across the core during the methane flood.

The CT number for dry core was measured by flooding the core with a saturated gas mixture which composition is given in Table A.20.4 and then the core was scanned. This mixture represented the gas composition of the gas phase in the two phase flood when the gas fraction is ~ 93% by volume (850 psi) at 75°F.

The CT number for wet core was measured by flooding the core with a saturated liquid mixture which composition is given in Table A.20.5 and then the core was scanned. This mixture represented the oil composition of the liquid phase in the two phase flood when the liquid fraction is ~ 7% by volume (850 psi) at 75°F.

After that the core was cleaned using 10 pore volumes of toluene, followed by 5 pore volumes of a mixture 50 vol% toluene- 50 vol% methanol, followed by 5 pore volumes of methanol. The core was then dried with air overnight at 75°F.

A post-cleaning dry permeability was measured using nitrogen at 75°F and following the same procedure as for the initial permeability measurement. Table A.5.4 summarizes the flood conditions and fluid properties and Table A.4.5 shows the results. Figure A.4.2 shows the pressure drop measured across the core during the nitrogen flood.

Synthetic volatile oil mixture 1 (Table 3.3) was used for the two-phase flow measurements. The mixture was allowed a minimum of 12 hours to equilibrate to a single phase at 3700 psi and 75°F. The initial flood was conducted at 75°F with the upstream backpressure regulator (BPR-1) set at 3887 psi and the downstream back pressure regulator (BPR-2) set at 855 psi. Volatile oil was injected at an upstream BPR-1 flow rate of 120 cc/hr (this is for volatile oil at single liquid phase). Once steady state was observed the pressure drop across the core was measured, the flow was stopped and the core holder was immediately taken to CT scanning to obtain the CT numbers for two-phase flood. PVT ratio was 0.73 and capillary number was 1.25×10^{-5} . Table A.3.6 gives the fluid properties of the synthetic fluid calculated using the Peng-Robinson EOS at the flowing core pressures. Figure A.4.3 shows the pressure drop measured across the core during the initial two-phase volatile oil flood.

The core was then flooded with saturated gas (Table A.20.4) and it was scanned to measure the pre-treatment residual oil saturation (S_{or}) along the core. Table A.20.9

shows the flood conditions and fluid properties and Table A.20.10 shows the flood results.

The core was then flooded with saturated liquid (Table A.20.5) and it was scanned to measure the pre-treatment residual gas saturation (S_{gr}) along the core. Table A.22.11 shows the flood conditions and fluid properties and Table A.22.12 shows the flood results.

The temperature was then raised to 155°F and the core was treated using chemical treatment 1 (Table 4.15). The solution was heated for at least 3 hours at 155°F. BPR1 was set at 850 psi. The core was flooded with approximately 20 pore volumes of the treatment solution at a flow rate of 100 cc/hr. The core was then shut in for 12 hours. Figure A.4.4 shows the measured pressure drop across the core during the treatment flood.

Post-treatment two-phase volatile oil flood was conducted under the same conditions as the initial two-phase flow. Figure A.4.5 shows the pressure drop measured across the core during the post-treatment two-phase volatile oil flood. Improvement factor was 1.7.

The core was then flooded with saturated gas (Table A.20.4) and it was scanned to measure the post-treatment residual oil saturation (S_{or}) along the core. Table A.20.11 shows the flood conditions and fluid properties and Table A.20.12 shows the flood results.

The core was then flooded with saturated liquid (Table A.20.5) and it was scanned to measure the post-treatment residual gas saturation (S_{gr}) along the core. Table A.22.15 shows the flood conditions and fluid properties and Table A.22.16 shows the flood results.

The core was again cleaned following the same procedure as before and the final gas permeability was calculated following the procedure for the initial gas permeability using nitrogen at 75°F. The calculated gas permeability was 183 md. The flood conditions and results are shown in Table A.4.7 and Table A.3.8 respectively. Figure A.6.10 shows the pressure drop across the core for the final methane flood.

For every single phase gas or oil flood, and two-phase volatile oil flood, oil and gas relative permeabilities k_{rg} and k_{ro} were calculated using the measured pressure drop across the core under steady state conditions and then improvement factors were measured and relative permeability curves were built. Table A.3.9 summarizes the experimental results.

The analytical procedure to calculate the oil and gas saturations along the core using the measured CT numbers, are explained in Section 7.3.1. Figure 7.12 to 7.14 show the results for the calculated oil saturations along the core before and after treatment. Section 7.3.3 explains how the relative permeability curves were calculated and Figure 7.20 illustrate the experimental relative permeability curves before and after treatment.

Table A.22.1 Core properties (Exp #235)

<i>Length, in</i>	7.979
<i>Diameter, in</i>	0.993
<i>Mass Core, gr</i>	219.04
<i>Grain Density, gr/cc</i>	2.65
<i>Porosity (ϕ)</i>	18.37 %

Table A.22.2 Fluid properties and conditions for initial gas permeability (Exp #235)

		<i>Density, gr/cc</i>
<i>Gas</i>	Nitrogen	
<i>Temperature, °F</i>	75	
<i>BPR 1-pressure, psi</i>	2895	0.2135
<i>BPR 2-pressure, psi</i>	1080	0.0847
<i>Gas Viscosity, cp</i>	0.0188	

Table A.22.3 Initial nitrogen flood results (Exp #235)

<i>q_{core}, cc/hr</i>	<i>ΔP, psi</i>	<i>k_g, md</i>
3781	7.780	151.29
4537	9.550	147.90
5041	10.800	145.31
5545	12.120	142.43
6301	14.010	140.02
<i>Corrected Permeability (k_g), md</i>		170.0

Table A.22.4 Composition of saturated gas (Exp #235)

<i>Component</i>	<i>Mole%</i>
Methane	90.54
Propane	9.46

Table A.22.5 Composition of saturated oil (Exp #235)

<i>Component</i>	<i>Mole%</i>
Methane	25.3
Propane	28.9
Heptane	30.2
Decane	15.6

Table A.22.6 Fluid properties and conditions for nitrogen gas permeability after initial core cleaning (Exp #235)

<i>Gas</i>	<i>Nitrogen</i>	<i>Density, gr/cc</i>
<i>Temperature, °F</i>	75	
<i>BPR 1-pressure, psi</i>	2955	0.2163
<i>BPR 2-pressure, psi</i>	865	6.80E-02
<i>Gas Viscosity, cp</i>	0.0185	

Table A.22.7 Nitrogen flood results after initial core cleaning (Exp #235)

<i>q_{core}, cc/hr</i>	<i>ΔP, psi</i>	<i>k_g, md</i>
4771.32	10.050	145.43
5725.59	12.400	141.45
6361.76	14.050	138.71
6997.94	15.750	136.11
7952.21	18.400	132.39
<i>Corrected Permeability (k_g), md</i>		168.7

Table A.22.8 Volatile oil properties at BPR-1 and BPR-2 pressures (Exp #235)

<i>BPR 1-pressure, psi</i>	3887	
<i>BPR 2- pressure, psi</i>	855	
<i>Density at BPR 1-pressure, gr/cc</i>	0.3747	
Properties at BPR 2- pressure, psi		
	Gas Phase	Oil Phase
<i>Density, gr/cc</i>	0.0533	0.6033
<i>Viscosity (μ), cp</i>	0.0121	0.2138
<i>Volume Fraction</i>	0.9281	0.0719
<i>IFT, dyne/cm</i>	8.695	

Table A.22.9 Fluid properties and conditions for saturated gas flood to measure S_{or} before treatment (Exp #235)

		<i>Density, gr/cc</i>
<i>Gas</i>	Saturated Gas Mixture	
<i>Temperature, °F</i>	75	
<i>BPR 1-pressure, psi</i>	3900	0.2371
<i>BPR 2-pressure, psi</i>	860	5.31E-02
<i>Gas Viscosity, cp</i>	0.0121	

Table A.22.10 Saturated gas flood results before treatment (Exp #235)

<i>q_{core}, cc/hr</i>	<i>ΔP, psi</i>	<i>k_g, md</i>
893.03	1.100	162.66
1113.31	1.900	117.40
1590.44	2.800	113.81
<i>Corrected Permeability (k_g), md</i>		167

Table A.22.11 Fluid properties and conditions for saturated oil flood to measure S_{gr} before treatment (Exp #235)

		<i>Density, gr/cc</i>
<i>Gas</i>	Saturated Oil Mixture	
<i>Temperature, °F</i>	75	
<i>BPR 1-pressure, psi</i>	3900	0.2371
<i>BPR 2-pressure, psi</i>	860	5.31E-02
<i>Gas Viscosity, cp</i>	0.0121	

Table A.22.12 Saturated oil flood results before treatment (Exp #235)

<i>q_{core}, cc/hr</i>	<i>ΔP, psi</i>	<i>k_g, md</i>
250	11.7	76.07

Table A.22.13 Fluid properties and conditions for saturated gas flood to measure S_{or} after treatment (Exp #235)

		<i>Density, gr/cc</i>
<i>Gas</i>	Saturated Gas Mixture	
<i>Temperature, °F</i>	75	
<i>OBPR 1-pressure, psi</i>	3900	0.2371
<i>BPR 2-pressure, psi</i>	860	5.31E-02
<i>Gas Viscosity, cp</i>	0.0121	

Table A.22.14 Saturated gas flood results after treatment (Exp #231)

<i>q_{core}, cc/hr</i>	ΔP , <i>psi</i>	<i>k_g, md</i>
1116.3	1.400	159.76

Table A.22.15 Fluid properties and conditions for saturated oil flood to measure S_{gr} after treatment (Exp #235)

		<i>Density, gr/cc</i>
<i>Gas</i>	Saturated Oil Mixture	
<i>Temperature, °F</i>	75	
<i>BPR 1-pressure, psi</i>	850	0.604
<i>BPR 2-pressure, psi</i>	850	6.04E-01
<i>Gas Viscosity, cp</i>	0.215	

Table A.22.16 Saturated oil flood results after treatment (Exp #235)

<i>q_{core}, cc/hr</i>	ΔP , <i>psi</i>	<i>k_g, md</i>
250	6.5	136.93

Table A.22.17 Fluid properties and conditions for final gas permeability (Exp #235)

		<i>Density, gr/cc</i>
<i>Gas</i>	Nitrogen	
<i>Temperature, °F</i>	75	
<i>BPR 1-pressure, psi</i>	2850	0.2106
<i>BPR 2-pressure, psi</i>	542	6.62E-02
<i>Gas Viscosity, cp</i>	0.0184	

Table A.22.18 Final nitrogen flood results (Exp #235)

$q_{core}, cc/hr$	$\Delta P, psi$	k_g, md
4771.90	10.110	143.81
5726.28	12.720	137.16
6362.54	14.560	133.14
6998.79	16.500	129.23
7953.17	19.450	124.58
<i>Corrected Permeability (k_g), md</i>		183.03

Table A.22.19 Pre and post-treatment volatile oil flood results and measured improvement factors (Exp #235)

	Exp# 235
<i>BPR 2- pressure, psi</i>	855
$q_{gtot\ core}, cc/hr$	484.29
$q_g, cc/hr$	449.47
$q_o, cc/hr$	34.82
<i>PVT Ratio</i>	0.73
<i>Viscosity Ratio μ_g/μ_o</i>	0.06
<i>Capillary Nc</i>	1.17E-05
k_{rg} Before Treatment	0.0279
k_{ro} Before Treatment	0.0382
k_{rg} After Treatment	0.0461
k_{ro} After Treatment	0.0630
<i>Initial Improvement Factor</i>	1.65
<i>Injected Pore Vol.</i>	~190

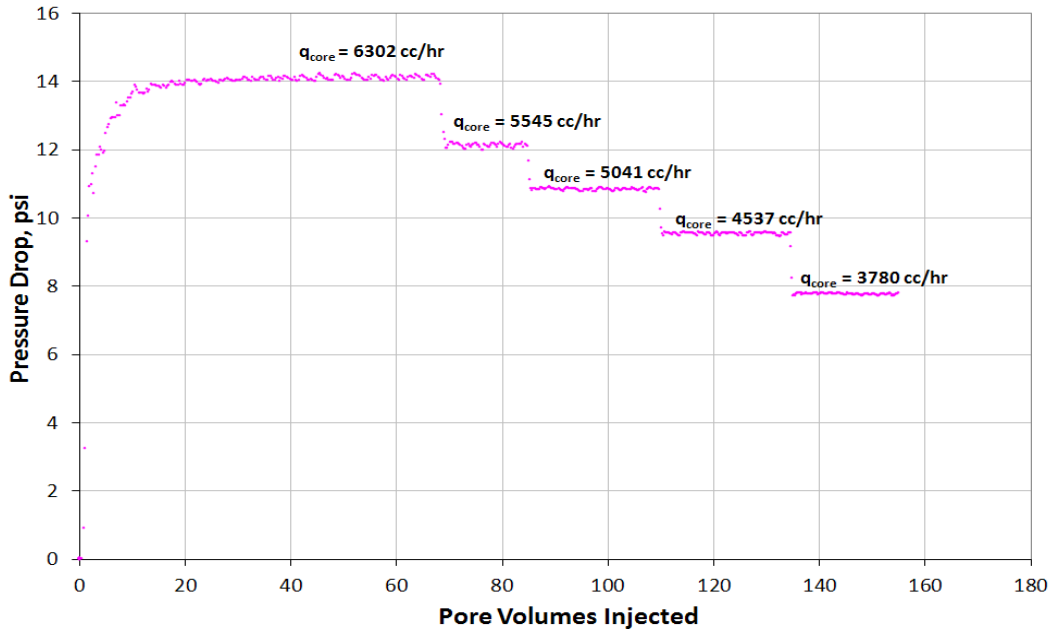


Figure A.22.1 Pressure drop across the core during the initial nitrogen flood at 75°F (Exp #235)

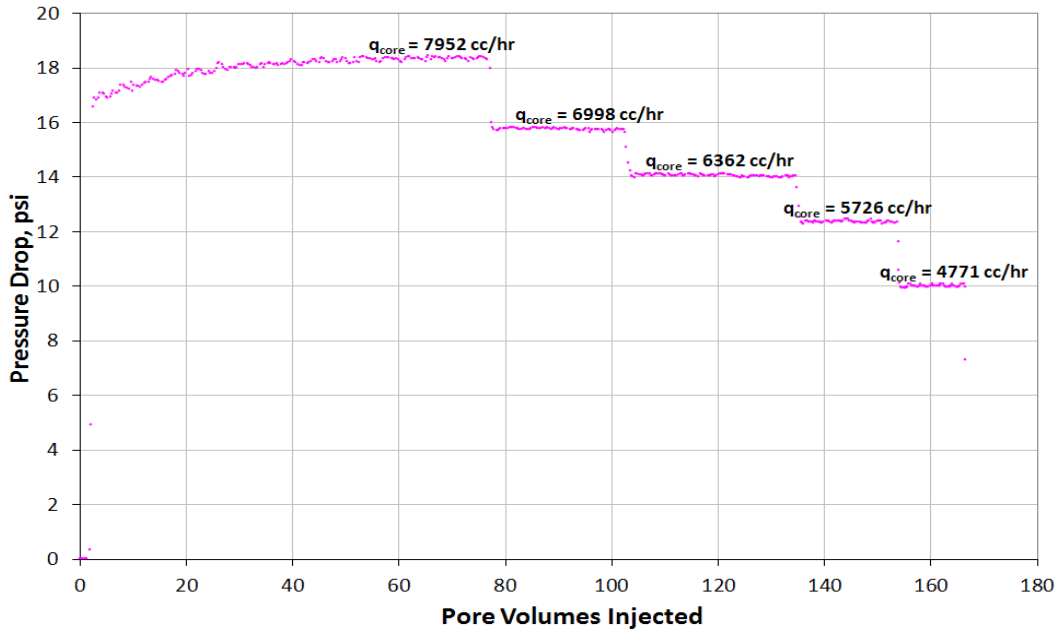


Figure A.22.2 Pressure drop across the core during the nitrogen flood after initial core cleaning (Exp #235)

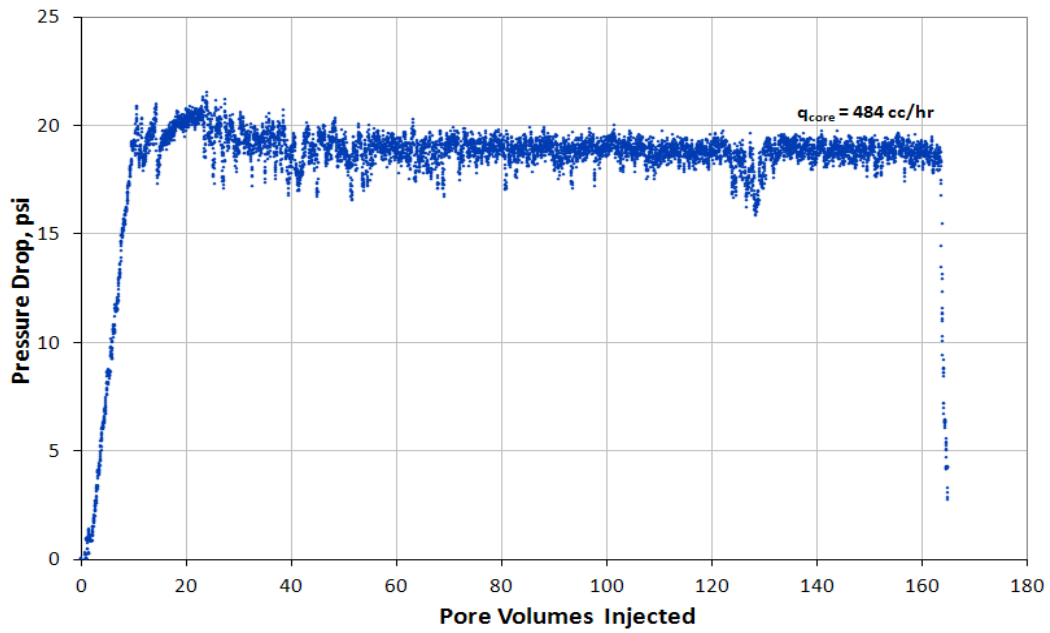


Figure A.22.3 Pressure drop across the core during the pre-treatment two-phase volatile oil flood (Exp #235)

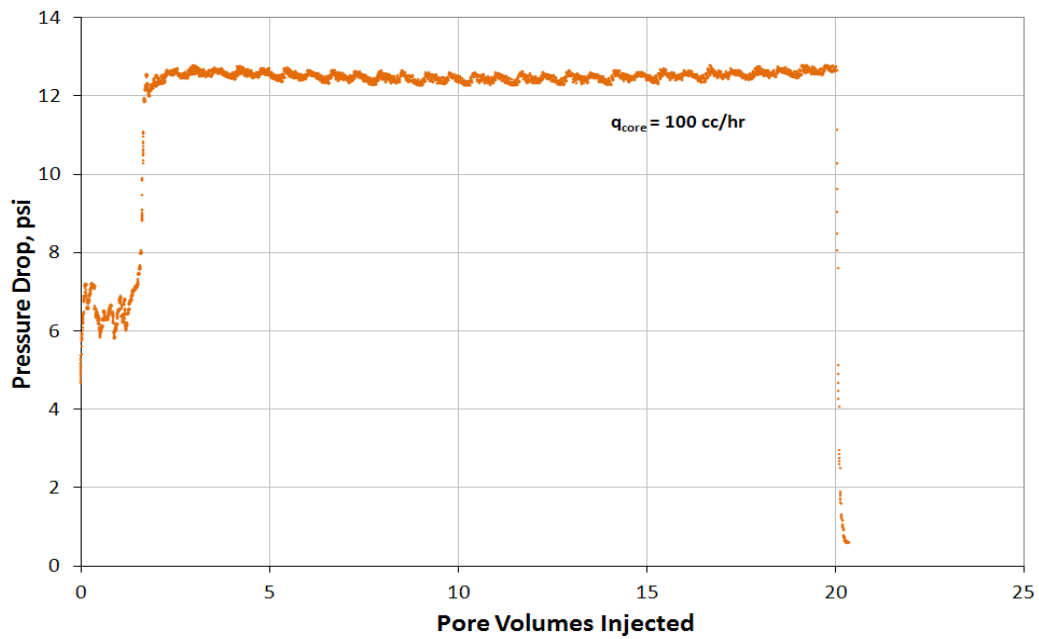


Figure A.22.4 Pressure drop across the core during injection of chemical treatment 1 (Exp #235)

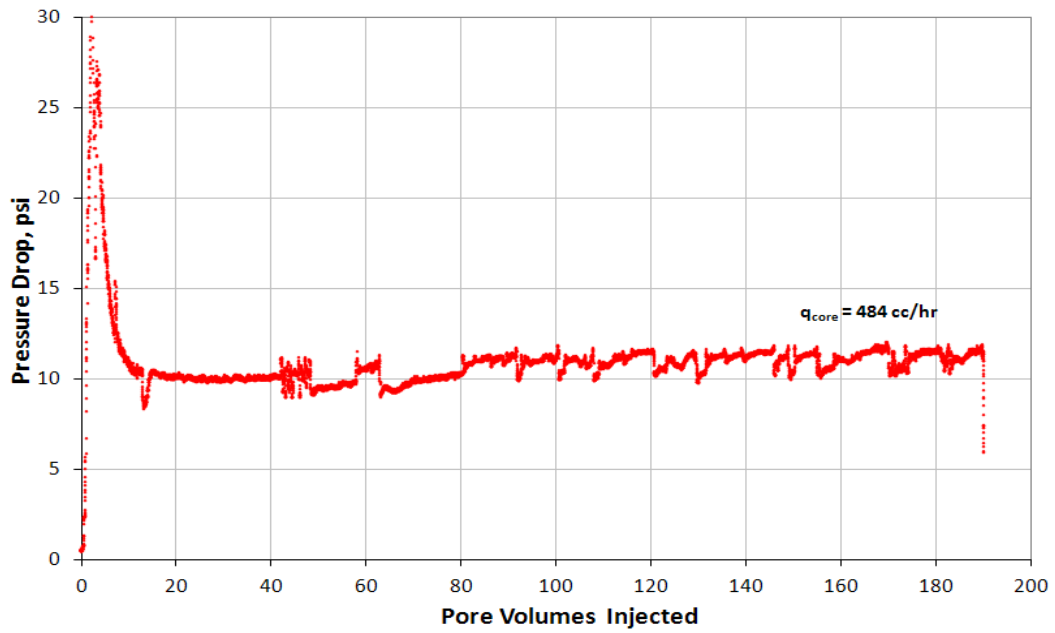


Figure A.22.5 Pressure drop across the core during the post-treatment two-phase volatile oil flood (Exp #235)

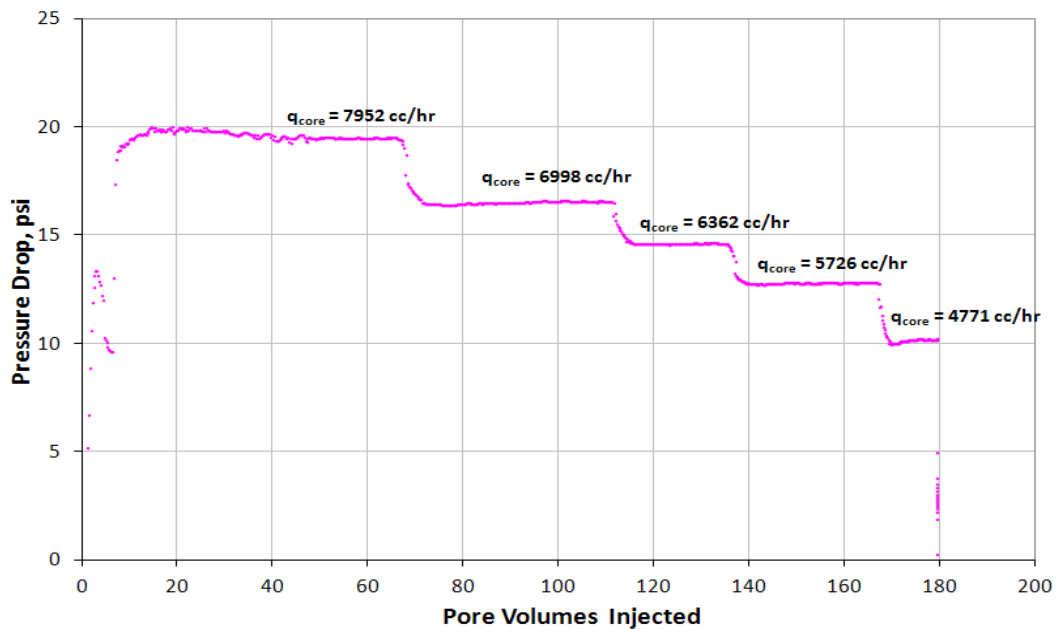


Figure A.22.6 Pressure drop across the core during the final nitrogen flood at 75°F (Exp #235)

Appendix B

This appendix show the code used for the numerical simulations performed in Chapter 8.. using the numerical simulator STARS from CMG.

```
RESULTS SIMULATOR STARS
INUNIT FIELD
WSRF GRID TIME
OUTSRF GRID PRES SG SO STRMLN SW TEMP VELOCRC
** ===== GRID WITH REFINEMENT =====
GRID RADIAL 53 1 1 RW 0.708
KDIR DOWN
DI IVAR
0.353 0.406 0.466 0.535 0.615
0.707 0.813 0.934 1.073 1.233
1.417 1.628 1.871 2.150 2.470
2.839 3.262 3.749 4.308 4.950
5.688 6.537 7.511 8.631 9.919
11.398 13.097 15.051 17.295 19.874
22.838 26.243 30.157 34.654 39.822
45.760 52.584 60.426 69.437 79.792
91.690 105.364 121.076 139.131 159.879
183.721 211.118 242.601 278.779 320.351
368.123 423.019 486.102
DJ JVAR 360
DK KVAR 100
DTOP 53*10000
NULL KVAR 1
POR CON 0.1904
PERMI CON 186
PERMJ CON 186
PERMK CON 18.6
PINCHOUTARRAY CON 1
END-GRID
ROCKTYPE 1
ROCKCP 35
THCONR 44
THCONW 8.6
THCONO 1.8
THCONG 1.0
HLOSSPROP OVERBUR 35 24 UNDERBUR 35 24

** ===== FLUID CHARACTERIZATION =====
MODEL 5 5 5 ** 5 components, with water (default) first
COMPNAME 'WATER' 'C1' 'C3' 'FC7' 'FC10'
**
CMM 0.0000 16.0430 44.0970 96.0000 134.0000
PCRIT 0.00 667.20 615.76 455.13 367.55
TCRIT 0.00 -116.59 205.97 518.09 660.11
```



```

*KVTABLE 'C3      '
**              Pressure,  psia

** T, deg F      2.0000E+02  1.0000E+03  1.8000E+03  2.6000E+03
3.4000E+03  4.2000E+03  5.0000E+03

** 60.000
<extrap.> <extrap.>
                6.4369E-01  2.8275E-01  3.5431E-01  5.1562E-01
8.1398E-01  8.1398E-01  8.1398E-01
** 90.000
<extrap.> <extrap.>
                9.2505E-01  3.6464E-01  4.0263E-01  5.3034E-01
7.6342E-01  7.6342E-01  7.6342E-01
** 120.000
<extrap.> <extrap.>
                1.2669E+00  4.5868E-01  4.6126E-01  5.6176E-01
7.5793E-01  7.5793E-01  7.5793E-01
** 150.000
<extrap.> <extrap.>
                1.6666E+00  5.6334E-01  5.2737E-01  6.0391E-01
7.7572E-01  7.7572E-01  7.7572E-01
** 180.000
<extrap.> <extrap.>
                2.1196E+00  6.7677E-01  5.9885E-01  6.5306E-01
8.0870E-01  8.0870E-01  8.0870E-01

*KVTABLE 'FC7      '
**              Pressure,  psia

** T, deg F      2.0000E+02  1.0000E+03  1.8000E+03  2.6000E+03
3.4000E+03  4.2000E+03  5.0000E+03

** 60.000
<extrap.> <extrap.>
                5.9760E-03  7.7398E-03  2.8156E-02  1.0888E-01
5.0339E-01  5.0339E-01  5.0339E-01
** 90.000
<extrap.> <extrap.>
                1.2504E-02  1.2658E-02  3.4661E-02  1.0765E-01
3.9397E-01  3.9397E-01  3.9397E-01
** 120.000
<extrap.> <extrap.>
                2.4000E-02  2.0000E-02  4.4515E-02  1.1664E-01
3.6855E-01  3.6855E-01  3.6855E-01
** 150.000
<extrap.> <extrap.>
                4.2844E-02  3.0522E-02  5.8088E-02  1.3355E-01
3.8189E-01  3.8189E-01  3.8189E-01
** 180.000
<extrap.> <extrap.>

```

7.1890E-02 4.5095E-02 7.6010E-02 1.5806E-01
4.2548E-01 4.2548E-01 4.2548E-01

*KVTABLE 'FC10'

** Pressure, psia

** T, deg F 2.0000E+02 1.0000E+03 1.8000E+03 2.6000E+03
3.4000E+03 4.2000E+03 5.0000E+03

** 60.000

<extrap.> <extrap.>
2.3297E-04 6.5767E-04 5.0655E-03 3.8306E-02
3.6491E-01 3.6491E-01 3.6491E-01

** 90.000

<extrap.> <extrap.>
6.3954E-04 1.2742E-03 6.6012E-03 3.6939E-02
2.5328E-01 2.5328E-01 2.5328E-01

** 120.000

<extrap.> <extrap.>
1.5654E-03 2.3671E-03 9.1880E-03 4.0703E-02
2.2794E-01 2.2794E-01 2.2794E-01

** 150.000

<extrap.> <extrap.>
3.4783E-03 4.2129E-03 1.3152E-02 4.8700E-02
2.3837E-01 2.3837E-01 2.3837E-01

** 180.000

<extrap.> <extrap.>
7.1126E-03 7.2021E-03 1.8996E-02 6.1343E-02
2.7781E-01 2.7781E-01 2.7781E-01

** ===== ROCK-FLUID PROPERTIES =====

ROCKFLUID

RPT 1

SWT

**\$	Sw	krw	krow
0.001	0.0000	0.4500	
0.062	0.0020	0.3224	
0.122	0.0082	0.2249	
0.183	0.0184	0.1520	
0.244	0.0327	0.0990	
0.304	0.0510	0.0616	
0.365	0.0735	0.0363	
0.426	0.1000	0.0199	
0.486	0.1306	0.0099	
0.547	0.1653	0.0044	
0.607	0.2041	0.0016	
0.668	0.2469	0.0004	
0.729	0.2939	0.0001	
0.789	0.3449	0.0000	
0.85	0.4000	0.0000	

SLT

**\$	S1	kr _g	kro _g
------	----	-----------------	------------------

0.164	0.9800	0.0000
0.223	0.6486	0.0001
0.282	0.4151	0.0006
0.341	0.2554	0.0025
0.400	0.1499	0.0066
0.459	0.0831	0.0142
0.518	0.0429	0.0263
0.577	0.0202	0.0444
0.636	0.0085	0.0700
0.695	0.0030	0.1044
0.754	0.0008	0.1494
0.813	0.0002	0.2066
0.872	0.000014	0.2777
0.931	0.000000	0.3646
0.99	0.000000	0.4500

RPT 2

SWT

**\$	Sw	krw	krow
0.001	0.00000	0.81000	
0.062	0.00204	0.55919	
0.122	0.00816	0.37476	
0.183	0.01837	0.24255	
0.244	0.03265	0.15061	
0.304	0.05102	0.08893	
0.365	0.07347	0.04935	
0.426	0.10000	0.02531	
0.486	0.13061	0.01171	
0.547	0.16531	0.00471	
0.607	0.20408	0.00154	
0.668	0.24694	0.00037	
0.729	0.29388	0.00005	
0.789	0.34490	0.00000	
0.850	0.40000	0.00000	

SLT

**\$	Sl	krq	krog
0.190	0.9800	0.0000	
0.247	0.7625	0.0000	
0.304	0.5786	0.0000	
0.361	0.4284	0.0004	
0.419	0.3082	0.0016	
0.476	0.2139	0.0050	
0.533	0.1421	0.0124	
0.590	0.0893	0.0268	
0.647	0.0521	0.0523	
0.704	0.0275	0.0944	
0.761	0.0125	0.1600	
0.819	0.0044	0.2579	
0.876	0.0010	0.3987	
0.933	0.0001	0.5953	
0.990	0.0000	0.81	

RTYPE IJK

1:53 1 1 1
1:23 1 1 2

** ===== INITIALIZATION =====

INITIAL
VERTICAL OFF
INITREGION 1
PRES CON 4000
SW CON 0.001
SO CON 0.9989
MFRAC_OIL 'C1 ' CON 2.1839E-01
MFRAC_OIL 'C3 ' CON 1.7711E-01
MFRAC_OIL 'FC7 ' CON 4.3259E-01
MFRAC_OIL 'FC10 ' CON 1.7191E-01

** ===== NUMERICAL CONTROL =====

NUMERICAL
DTMAX 500
DTMIN 1.E-06

** ===== RECURRENT DATA =====

RUN
DATE 2000 1 1
DTWELL 0.0001

WELL 'Prod-1'
PRODUCER 'Prod-1'
OPERATE MAX STO 1000 CONT
GEOMETRY K 0.708 0.249 1. 0.
PERF GEOA 'Prod-1'
1 1 1 1. OPEN FLOW-TO 'SURFACE' REFLAYER
DATE 2000 1 2
DATE 2000 1 5
DATE 2000 1 10
DATE 2000 2 1
DATE 2000 4 1
DATE 2000 7 1
DATE 2000 10 1
DATE 2001 1 1
DATE 2002 1 1
DATE 2003 1 1
DATE 2005 1 1
DATE 2007 1 1
DATE 2010 1 1
DATE 2015 1 1
DATE 2020 1 1
DATE 2025 1 1
DATE 2030 1 1
DATE 2040 1 1
DATE 2050 1 1
DATE 2060 1 1
STOP

References

- Afidick, D., Kaczorowski, N. and Bette, S. 1994. Production Performance of a Retrograde Gas Reservoir: A Case Study of the Arun Field. Paper SPE 28749 presented at the SPE Asia Pacific Oil and Gas Conference. Melbourne, Australia. 7-10 November.
- Ahmadi, M. 2010. Development of a Chemical Treatment for Condensate and Water Blocking in Carbonate Gas Reservoirs. PhD Dissertation. The University of Texas at Austin. Austin, Texas. U.S.A.
- Ahmadi, M., Sharma, M.M., Pope, G.A., Torres, D. E., McCulley, C. A., and Linnemeyer, H. 2010. Chemical Treatment to Mitigate Condensate and Water Blocking in Gas Wells in Carbonate Reservoirs. Paper SPE 133591 presented at the Western North America Regional Meeting, Anaheim, CA, USA, 26-30 May.
- Al-Anazi, Hamoud Ali. 2003. Experimental Measurements of Condensate Blocking and Treatments in Low and High Permeability Cores. PhD Dissertation. The University of Texas at Austin. Austin, Texas. U.S.A.
- Ali, J.K., McGauley, P.J., and Wilson, C.J. 1997. The Effects of High-Velocity Flow and PVT Changes Near the Wellbore on Condensate Well Performance. Paper SPE 38923-MS presented at the SPE Annual Technical Conference and Exhibition. San Antonio, Texas. 5-8 October.
- App, J. and Burger, J. 2009. Experimental Determination of Relative Permeabilities for a Rich Gas/Condensate System Using Live Fluid. SPE paper 109810-PA. Journal SPE Reservoir Evaluation & Engineering 12 (2) 263-269. April.
- Asar, H. and Lyman, H. 1988. Influence of Interfacial Tension on Gas/Oil Relative Permeability in a Gas-Condensate System. SPE paper 11740-PA. Journal *SPE Reservoir Engineering* 3 (1) 257-264. February.
- Ayyalasomayajula, P., Silpngarmlers, N. and Kamath, J. 2005. Well Deliverability Predictions for a Low-Permeability Gas/Condensate Reservoir. Paper SPE-95529-MS presented at the SPE Annual Technical Conference and Exhibition. Dallas, TX, USA, 9-12 Oct.
- Bang, Vishal. 2005. Phase Behavior Study of Hydrocarbon-Water-Alcohol Mixtures. M.S. Thesis. The University of Texas at Austin. Austin, Texas. U.S.A.
- Bang, V. 2007. Development of a Successful Chemical Treatment of Gas Wells with Condensate or Water Blocking Damage. PhD Dissertation. The University of Texas at Austin. Austin, Texas. U.S.A.

- Bang, V., Ayyalasomayajula, P., Kumar, V., Pope, G. and Sharma, M. 2006. Relative Permeability of Gas-Condensate Fluids: A General Correlation. SPE paper 102741-MS presented at *SPE Annual Technical Conference and Exhibition*. San Antonio, Texas, USA. 24-27 September.
- Bang, V., Yuan, C., Pope, G.A., Sharma, M.M., Baran, J.R., Skildum, J.D. and Linnemeyer, H.C. 2008. Improving Productivity of Hydraulically Fractured Gas Condensate Wells by Chemical Treatment. Paper OTC 19599, presented at the Offshore Technology Conference, Houston, TX. 5-8 May
- Bang, V., Pope, G., Sharma, M., Baran, J., and Ahmadi, M. 2008. A New Solution to Restore Productivity of Gas Wells With Condensate and Water Blocks. Paper SPE-116711-MS presented at the SPE Annual Technical Conference and Exhibition. Denver Colorado, USA, 21-24 Sep.
- Bang, V., Pope, G., Sharma, M. and Baran, J. 2009. Development of a Successful Chemical Treatment for Gas Wells with Water and Condensate Blocking Damage. Paper SPE-124977 presented at the SPE Annual Technical Conference and Exhibition., New Orleans, Louisiana, USA, 4-7 Oct.
- Blom, S., Jacques H. and Soetekouw, D. 2000. Relative Permeability at Near-Critical Conditions. Paper 62874-PA. *SPE Journal* 5 (2) 172-181. June.
- Briggs, D. and Seah, M. P. 1990. Practical Surface Analysis: Auger and X-ray photoelectron spectroscopy. Wiley.
- Brown, R. and Fatt, I. 1956. Measurements of Fractional Wettability of Oil Fields Rocks by the Nuclear Magnetic Relaxation Method. SPE paper 743-G presented at the *Fall Meeting of the Petroleum Branch of AIME*. Los Angeles, California. 14-17 October.
- Brundle, C. R. and Baker, A. D. 1977. Electron Spectroscopy: Theory, Techniques and Applications. London. Academic Press.
- Butler, M., Trueblood, J., Pope, G., Sharma, M., Baran, J. and Johnson, D. 2009. A Field Demonstration of a New Chemical Stimulation Treatment for Fluid-Blocked Gas Wells. Paper SPE-125077-MS presented at the SPE Annual Technical Conference and Exhibition. New Orleans, Louisiana, USA, 4-7 October.
- Chen, J., Hirasaki, G.J. and Flaum, M. 2004. Effects of OBM Invasion on Irreducible Water Saturation: Mechanisms and Modifications of NMR Interpretation. Paper 90141-MS presented at the SPE Annual Technical Conference and Exhibition. Houston, Texas. 26-29 September 2004.

- Chopra, A. and Carter, R. 1986. Proof of the Two-Phase Steady-State Theory for Flow Through Porous Media. Paper SPE 14472-PA. *Journal of Formation Evaluation* 1 (6) 603-608. December.
- Dehghanpour, H., DiCarlo, D., Aminzadeh, B. and Mirzaei, M. 2010. Two-Phase and Three-Phase Saturation Routes and Relative Permeability During Fast Drainage. Paper 129962-MS presented at the SPE Improved Oil Recovery Symposium. Tulsa, Oklahoma, USA, 24-28 April 2010.
- DiCarlo, D.A., Sahni, A, and Blunt, M.J. 2000. Three-Phase Relative Permeability of Water-Wet, Oil-Wet, and Mixed-Wet Sandpacks. Paper 60767-PA. *SPE Journal* 5 (1) 82-91. March.
- Du, L., Walker, J., Pope, G., Sharma, M. and Peng, W. 2000. Use of Solvents To Improve the Productivity of Gas Condensate Wells. Paper 62935-MS presented at the SPE Annual Technical Conference and Exhibition. Dallas, Texas, 1-4 October 2000.
- Dubey, S.T. and Doe, P.H. 1993. Base Number and Wetting Properties of Crude Oils. *SPE Reservoir Engineering* 8 (3) 195-200, August.
- Durand, C. and Beccat, P. 1998. Use of XPS for reservoir sandstone wettability evaluation. Application to kaolinite and illite. *Journal of Petroleum Science and Engineering* 20 (3-4) 259-265. June.
- Fahes, M. and Firoozabadi, A. 2005. Wettability Alteration to Intermediate Gas-Wetting in Gas/Condensate Reservoirs at High Temperatures. Paper SPE-96184 presented at the SPE Annual Technical Conference and Exhibition. Dallas, TX, USA, 9-12 Oct.
- Firoozabadi, A. and Katz, D. 1979. An Analysis of High-Velocity Gas Flow Through Porous Media. *Journal of Petroleum Technology* 31 (2) 211-216. February.
- Gilani, Syed Furqan Hassan. 2010. Correlating Wettability Alteration with Changes in Gas Permeability in Gas Condensate Reservoirs. M.S. Thesis. The University of Texas at Austin. Austin, Texas. U.S.A.
- Gravier, J.F., Lemouzy, P., Barroux, C. and Abed, A.F. 1986. Determination of Gas-Condensate Relative Permeability on Whole Cores Under Reservoir Conditions. *SPE Journal of Formation Evaluation* 1 (1) 9-15. February.

- Gringarten, A.C., Al-Lamki, A., Daungkaew, S., Mott, R. and Whittle, T.M. 2000. Well Test Analysis in Gas-Condensate Reservoirs. Paper 62920-MS presented at the *SPE Annual Technical Conference and Exhibition*. Dallas, Texas, 1-4 October.
- Haeshin, L., Dellatore, S.M., Miller, W.M. and Messersmith, P.B. 2007. Mussel-Inspired Surface Chemistry for Multifunctional Coatings. *Science* 318 (5849) 426 -430. October.
- Ham, J. and Eilerts, C. 1967. Effect of Saturation on Mobility of Low Liquid-Vapor Ratio Fluids. *Society of Petroleum Engineers Journal* 7 (1) 11-19. March.
- Haniff, M.S. and Ali, J.K. 1990. Relative Permeability and Low Tension Fluid Flow in Gas Condensate Systems. Paper 20917-MS presented at the European Petroleum Conference. The Hague, Netherlands. 21-24 October.
- Henderson, G.D., Danesh, A., Tehrani, D., Al-Shaidi, S. and Peden, J.M. 1998. Measurement and Correlation of Gas Condensate Relative Permeability by the Steady-State Method. *Journal SPE Reservoir Evaluation & Engineering* 1 (2) 134-140. April.
- Jadhunandan, P. and Morrow, N. 1995. Effect of Wettability on Waterflood Recovery for Crude-Oil/Brine/Rock Systems. Paper SPE 22597. *Journal SPE Reservoir Engineering* 10 (1) 40-46. February.
- Kalaydjian, F.J-M., Bourbiaux, B.J. and Lombard, J-M. 1996. Predicting gas-condensate reservoir performance: how flow parameters are altered when approaching production wells. Paper 36715-MS presented at the *SPE Annual Technical Conference and Exhibition*. Denver, Colorado. 6-9 October.
- Kissa, E. 2001. Fluorinated surfactants and repellents. CRC Press.
- Kumar, V. 2006. Chemical Stimulation of Gas Condensate Reservoirs an Experimental and Simulation Study. PhD Dissertation. The University of Texas at Austin. Austin, Texas. U.S.A.
- Kumar, V., Pope, G. and Sharma, M. 2006. Improving the Gas and Condensate Relative Permeability Using Chemical Treatments. Paper SPE-100529-MS presented at the *SPE Gas Technology Symposium*. Calgary, Alberta, Canada, 15-17 May.
- Kumar, V., Bang, V., Pope, G.A., Sharma, M.M., Ayyalasomayajula, P.S. and Kamath, J. 2006. Chemical Stimulation of Gas/Condensate Reservoirs. Paper SPE 102669 presented at the *SPE Annual Technical Conference and Exhibition*. San Antonio, TX. 24-27 September.

- Land, C. 1968. Calculation of Imbibition Relative Permeability for Two- and Three-Phase Flow From Rock Properties. Paper 1942-PA. Society of Petroleum Engineers Journal 8 (2) 149-156. June.
- Li, K. and Firoozabadi, A. 2000. Experimental Study of Wettability Alteration to Preferential Gas-Wetting in Porous Media and Its Effects. Paper SPE 62515. Journal SPE Reservoir Evaluation and Engineering 3 (2) 139-149. April.
- Li, K. and Firoozabadi, A. 2000. Phenomenological Modeling of Critical Condensate Saturation and Relative Permeabilities in Gas/Condensate Systems. SPE Journal 5 (2) 138-147. June.
- Lindeloff, N. and Michelsen, M. 2002. Phase Envelope Calculations for Hydrocarbon-Water Mixtures. Paper 77770-MS presented at the SPE Annual Technical Conference and Exhibition. San Antonio, Texas. 29 September - 2 October.
- Liu, Y., Zheng, H., Huang, G., Li, G. and Li, K. 2006. Improving Production in Gas/Condensate Reservoirs by Wettability Alteration to Gas Wetness. Paper 99739-MS presented at the SPE/DOE Symposium on Improved Oil Recovery. Tulsa, Oklahoma, USA. 22-26 April.
- Longeron, D.G. 1980. Influence of Very Low Interfacial Tensions on Relative Permeability. Paper 7609-PA. Society of Petroleum Engineers Journal 20 (5) 391-401. October.
- McCain, W.D. 1990. The Properties of Petroleum Fluids. 2nd ed. Tulsa, Oklahoma. PennWell Books.
- McCulley, C.A. 2011. Development of a Chemical Treatment for Condensate Blocking in Tight Gas Sandstone. M.S. Thesis. The University of Texas at Austin. Austin, Texas. U.S.A.
- Mitchell, A.G., Hazell, L.B. and Webb, K.J. 1990. Wettability Determination: Pore Surface Analysis. Paper 20505-MS presented at the SPE Annual Technical Conference and Exhibition. New Orleans, Louisiana. 23-26 September.
- Mohanty, S.C.J. 2007. X-Ray Photoelectron Spectroscopy. Vanivihar, Bhubaneswar: P.G. Department of Physics Utkal University.
- Mott, R., Cable, A. and Spearing, M. 1999. A New Method of Measuring Relative Permeabilities for Calculating Gas-Condensate Well Deliverability. Paper 56484-MS SPE Annual Technical Conference and Exhibition. Houston, Texas. 3-6 October.

- Mott, R., Cable, A. and Spearing, M. 2000. Measurements and Simulation of Inertial and High Capillary Number Flow Phenomena in Gas-Condensate Relative Permeability. Paper 62932-MS presented at the SPE Annual Technical Conference and Exhibition. Dallas, Texas. 1-4 October.
- Noh, M. and Firoozabadi, A. 2006. Effect of Wettability on High-Velocity Coefficient in Two-Phase Gas-Liquid Flow. Paper SPE-102773-MS presented at the SPE Annual Technical Conference and Exhibition. San Antonio, TX, USA, 24-27 September.
- Owolabi, O. and Watson, R. 1993. Effects of Rock-Pore Characteristics on Oil Recovery at Breakthrough and Ultimate Oil Recovery in Water-Wet Sandstones. Paper SPE-26935 presented at the SPE Eastern Regional Meeting. Pittsburg, Pennsylvania, USA, 2-4 November.
- Organization of the Petroleum Exporting Countries. 2010. World Oil Outlook 2010.
- Panga, M. Suzylawati, I., Pascal, C. and Mathew, S. 2007. Preventive Treatment for Enhancing Water Removal from Gas Reservoirs by Wettability Alteration. Paper SPE-105367-MS presented at the SPE Middle East Oil & Gas Show and Conference. Kingdom of Bahrain, 11-14 March.
- Panga, M., Yean, S., Pei, L., Keng, C., Philippe, E., Pascal, C. and Mathew, S. 2006. Wettability Alteration for Water-Block Prevention in High-Temperature Gas Wells. Paper SPE-100182-MS presented at the SPE Europec/EAGE Annual Conference and Exhibition. Vienna, Austria, 12-15 June.
- Pedersen, K. S. 2007. Phase Behavior of Petroleum Reservoir Fluids. Boca Raton. CRC/Taylor & Francis.
- Peters, E.J. Petrophysics. Austin, Texas. U.S.A.: Department of Geosystem and Petroleum Engineering, The University of Texas at Austin.
- Pope, G., Wu, W., Narayanaswamy, G., Delshad, M., Sharma, M. and Wang, P. 2000. Modeling Relative Permeability Effects in Gas-Condensate Reservoirs With a New Trapping Model. Paper 62497-PA. SPE Journal of Reservoir Evaluation & Engineering 3 (2) 171-178. April.
- Ramirez, W.F., Oen, A.C., Strobel J.F., Falconer, J.L. and Evans, H.E. 1986. Surface Composition of Berea Sandstone. Paper 11972-PA. SPE Journal of Formation Evaluation 1 (1) 23-30. February.
- Rosen, Milton J. 2004. Surfactants and Interfacial Phenomena. 3rd ed. Hoboken, N.J. Wiley-Interscience.

- Sahni, A., Burger, J. and Blunt, M. 1998. Measurement of Three Phase Relative Permeability during Gravity Drainage using CT Scanning. Paper 39655-MS presented at the SPE/DOE Improved Oil Recovery Symposium. Tulsa, Oklahoma. 19-22 April.
- Salathiel, R.A. 1973. Oil Recovery by Surface Film Drainage In Mixed-Wettability Rocks. *Journal of Petroleum Technology* 25 (10) 1216-1224. October.
- Sanni, M. and Gringarten, A. 2008. Application of Well Testing for Well Deliverability Forecasting in Volatile Oil Reservoirs. Paper SPE 118377 presented at the Abu Dhabi International Petroleum Exhibition and Conference. Abu Dhabi, UAE, 3-6 November.
- Sanni, M. and Gringarten, A. 2008. Well Test Analysis in Volatile Oil Reservoirs. Paper 116239-MS presented at the SPE Annual Technical Conference and Exhibition. Denver, Colorado, USA. 21-24 September.
- Sharifi, M. and Ahmadi, M. 2009. Two-Phase Flow in Volatile Oil Reservoir Using Two-Phase Pseudo-Pressure Well Test Method. Paper PETSOC-09-09-06-TN. *Journal of Canadian Petroleum Technology*, 48 (9) 6-11. September.
- Sharma, B C., Brigham, W.E. and Castanier, L.M. 1997. CT Imaging Techniques for Two-Phase and Three-Phase In-Situ Saturation Measurements. AUPRI TR 107 Report. Stanford University, June.
- Tang, G. and Firoozabadi, A. 2000. Relative Permeability Modification in Gas-Liquid Systems Through Wettability Alteration to Intermediate Gas-Wetting. Paper SPE 62934 presented at the SPE Annual Technical Conference and Exhibition. Dallas, TX, USA, 1-4 October.
- Thiebot, B. and Sakthikumar, S. 1991. Cycling Fractured Reservoirs Containing Volatile Oil: Laboratory Investigation of the Performance of Lean Gas or Nitrogen Injection. Paper SPE 21427 presented at the Middle East Oil Show, Bahrain, 16-19 Nov.
- Toledo, P.G., Araujo, Y.C. and Leon, V.V. 1996. Wettability of Oil-Producing Reservoir Rocks as Determined from X-ray Photoelectron Spectroscopy. *Journal of Colloid and Interface Science* 183 (2) 301-308. November.
- Treiber, L.E., and Owens, W.W. 1972. A Laboratory Evaluation of the Wettability of Fifty Oil-Producing Reservoirs. *Society of Petroleum Engineers Journal* 12 (6)531-540. December.

- U.S. Energy Information Administration. 2010. International Energy Outlook 2010. U.S. Department of Energy, July.
- Vizika, O. and Lombard, J-M. 1996. Wettability and Spreading: Two Key Parameters in Oil Recovery With Three-Phase Gravity Drainage. Paper 28613-PA. SPE Journal of Reservoir Engineering 11 (1) 54-60. February.
- Walker, J.G. 2000. Laboratory Evaluation of Alcohols and Surfactants to Increase Production from Gas-Condensate Reservoirs. M.S. Thesis. The University of Texas at Austin. Austin, Texas. U.S.A.
- Wang, X. and Mohanty, K. K. 1999. Critical Condensate Saturation in Porous Media. Journal of Colloid and Interface Science 214 (2) 416-426. June.
- Yan, W., Wang, L., Yang, L.Y. and Guo, T.M. 2001. A systematic experimental study on the phase behavior of complex fluid mixtures up to near-critical region. Fluid Phase Equilibria 190 (1-2) 159-178. November.
- Yang, T., Chen, W.D. and Guo, T.M. 1997. Phase behavior of a near-critical reservoir fluid mixture. Fluid Phase Equilibria 128 (1-2) 183-197. February.

Vita

David Enrique Torres Lopez completed his high school education at Colegio Anahuac Garibaldi, Guadalajara, Mexico in May 1999. After this he performed his undergrad studies in chemical engineering at the Instituto Tecnológico de Estudios Superiores de Occidente I.T.E.S.O., at Guadalajara, Jalisco Mexico and earned his Bachelors degree in December 2003. After some years of working experience, he started his graduate studies at The University of Texas at Austin in August 2006. He was awarded with a Masters degree in Chemical Engineering on December 2008. Then, he continued with his PhD studies in Chemical Engineering at the University of Texas at Austin and performed his research in the Gas Condensate and Volatile Oil Laboratory in the Petroleum Engineering Department. David Torres did summer internships with Total France Petrochemicals and ConocoPhillips during his graduate studies at the University of Texas at Austin.

\

Permanent address: Av. Nueva Galicia #1540 casa 314

Guadalajara, Jalisco, Mexico. C.P.45645

This dissertation was typed by the author.

